労災疾病臨床研究事業費補助金

悪性中皮腫に対するヒト化抗CD26抗体を基盤とする安全かつ有効な新規併用療法の確立

平成28年度　総括・分担研究報告書

研究代表者　森本　幾夫

平成29(2017)年3月

厚生労働科学研究費補助金
労災疾病臨床研究事業

悪性中皮腫に対するヒト化抗CD26抗体を基盤とする安全かつ有効な新規併用療法の確立

平成二十八年度　総括・分担研究報告書

目　次

Ⅰ．総括研究報告

悪性中皮腫に対するヒト化抗 CD26 抗体を基盤とする安全かつ有効な新規併用療法の確立・・・・1
研究代表者　森本　幾夫 順天堂大学大学院医学研究科　免疫病・がん先端治療学講座 客員教授

Ⅱ．分担研究報告

1. ヒト化 CD26 抗体と YB1 阻害アンチセンスとの併用療法の検討・・・・・・・・・・・・・・・13
研究代表者　森本　幾夫
順天堂大学大学院医学研究科免疫病・がん先端治療学講座 客員教授
研究協力者　岡本　俊博
順天堂大学大学院医学研究科免疫病・がん先端治療学講座 研究補助員
研究協力者　波多野　良
順天堂大学大学院医学研究科免疫病・がん先端治療学講座 博士研究員
研究協力者　山崎　裕人
順天堂大学大学院医学研究科免疫病・がん先端治療学講座 協力研究員
研究協力者　中野　賢二
九州大学 先端融合医療ﾚﾄﾞｯｸｽﾅﾋﾞ研究拠点 教授

2. 中皮腫におけるCD26およびYB-1発現について・・・・・・・・・・・・・・・・・・・・・・25
研究分担者　山田　健人
埼玉医科大学 病理学 教授

3. ヒト化 CD26 抗体の免疫チェックポイント阻害薬としての新たな可能性：CD26 共刺激シグナルによる IL-10, BTLA, LAG3 の発現誘導
・・・・・・・・・・・・・・・・・・・・・・・・・・・・・・・・31
研究代表者　森本　幾夫
順天堂大学大学院医学研究科免疫病・がん先端治療学講座 客員教授
研究分担者　山田　健人
埼玉医科大学病理学 教授
研究協力者　波多野　良
順天堂大学大学院医学研究科免疫病・がん先端治療学講座 博士研究員
研究協力者　大沼　圭
順天堂大学大学院医学研究科免疫病・がん先端治療学講座 准教授

4. 中皮腫治療における CD26 の役割：可溶性 CD26/DPPIVは治療奏効性判定のバイオマーカーか
・・・・・・・・・・・・・・・・・・・・・・・・・・・・・・・・43
研究代表者　森本　幾夫
順天堂大学大学院医学研究科免疫病・がん先端治療学講座 客員教授
研究協力者　大沼　圭
順天堂大学大学院医学研究科免疫病・がん先端治療学講座 准教授
研究協力者　金子　有太郎　Y's AC 株式会社

Ⅲ. 研究成果の刊行に関する一覧表・・・・・・・・・・・・・・・・・・・・・・・・・・・・51
Ⅳ. 研究成果の刊行物・別刷　・・・・・・・・・・・・・・・・・・・・・・・・・・・・・・57

Ⅰ．　総括研究報告

労災疾病臨床研究事業費補助金
総括研究報告書

悪性中皮腫に対するヒト化抗CD26抗体を基盤とする安全かつ有効な新規併用療法の確立

研究代表者　森本　幾夫　順天堂大学大学院医学研究科
免疫病・がん先端治療学講座客員教授

研究要旨

悪性胸膜中皮腫はアスベストばく露によって起こる胸膜中皮由来の難治性悪性腫瘍であり、現時点で満足できる治療法はなく、新たな治療法の確立が望まれる。我々は、新規治療標的分子として悪性胸膜中皮腫細胞に発現するCD26に着目し、ヒト化CD26抗体を開発しフランスにて第I相臨床試験を行った。安全性が確認されるとともに治療薬としての有効性を示唆する結果も得られ、平成29年春から国内での第I/II相臨床試験を予定している。しかしながら、CD26抗体単剤投与では、Stabilized Diseaseが認められるも完全寛解までは得られず、悪性胸膜中皮腫患者に完全寛解と肺機能改善をもたらす安全かつ有効なCD26抗体との革新的な併用療法の開発が望まれる。Y-box binding protein (YB-1)はがんの浸潤・転移促進に関与することから、有用な治療標的として着目されている分子であり、近年、共同研究者の中野賢二博士により良質なYB-1 antisense oligonucleotide (YB-1 AON)が開発された。In vitro及び in vivo study解析において、YB-1 AONとCD26抗体の併用の有用性が示唆されたが、そのメカニズムとして YB-1 AON 及び CD26 抗体それぞれはcyclophilin A発現を抑制し、さらに併用でより強くcyclophilin A発現が抑制することによる可能性が示唆された。

中皮腫検体におけるYB-1の発現評価方法および半定量的解析法を確立した。その結果、85%の症例においてCD26とYB-1の共発現が明らかとなり、細胞内局在においても細胞質内での共在が示された。

CD26抗体は免疫系にも影響する可能性が考えられる。CD26共刺激は健常者の末梢血CD4 T細胞に対して免疫チェックポイント分子であるBTLAとLAG3の高発現、IL-10の高産生を誘導し、CD8 T細胞に対してもCD28共刺激と比較してBTLAの発現を顕著に誘導する。がん細胞の周囲に多く存在すると考えられる免疫抑制性因子は様々な免疫チェックポイント分子の発現とともに、CD26の発現も増強させることが示唆された。特にBTLAの発現誘導に関しては、CD26共刺激に特徴的であることが示唆された。

SD、PD患者を識別できるバイオマーカーは存在しないかということで患者血清中の可溶性CD26/DPPⅣ酵素値に注目した。ヒト化CD26抗体の化学療法抵抗性悪性中皮腫及びその他CD26陽性悪性腫瘍をターゲットにしたフランスのFirst in Man第一相臨床試験から血清中の可溶性CD26/DPPⅣ酵素活性値がPD及びSDを識別できるバイオマーカーとなる可能性が示唆された。

研究分担者
岸本　卓巳：岡山労災病院・副院長
山田　健人：埼玉医科大学医学部
病理学 教授

研究協力者
青江　啓介：山口宇部医療センター
内科系診療部長
藤本　伸一：岡山労災病院
第二呼吸器内科部長
大沼　　圭：順天堂大学大学院医学研究科
免疫病・がん先端治療学講座
准教授
波多野　良：順天堂大学大学院医学研究科
免疫病・がん先端治療学講座
博士研究員
山崎　裕人：順天堂大学大学院医学研究科
免疫病・がん先端治療学講座
研究員
中野　賢二：九州大学先端融合医療レドックスナビ研究拠点教授

A. 研究目的

悪性中皮腫は､アスベストばく露により発生する難治性悪性腫瘍である。アスベストばく露から悪性中皮腫発生までの潜伏期間は約 30～50 年とされ本邦においても患者数は今後ますます増加すると予想されている。悪性胸膜中皮腫に対する治療法としては手術療法、放射線療法、化学療法などが施行されているが、いずれも満足できる治療成績ではない。更に化学療法の標準治療とされているアリムタ、シスプラチンなどの抗がん剤治療では日本人では副作用が強く、その治療を完遂できる患者は約半数に満たず、生存期間は約 1 年と極めて予後不良である。また悪性中皮腫はアスベストばく露により発症するため労災疾病行政上も病態解明と安全で有効な新規治療法開発が急務とされている。

CD26 分子は T 細胞共刺激分子で DPPⅣ 酵素活性を有し、研究代表者の森本らは CD26cDNA の単離から CD26 抗体の開発を世界に先駆けて行い当分野では最先端に位置している。CD26 は正常中皮には発現しないが上皮型悪性中皮腫では約 8 割に発現しており、中皮腫細胞の増殖・浸潤に重要な役割を果たすことから、抗腫瘍作用を有する良質なヒト化 CD26 抗体を開発し、悪性中皮腫の新規治療法として有効な可能性が示唆された。(Clin Cancer.Res.2007)

アリムタ､シスプラチンなど抗がん剤治療抵抗性の悪性中皮腫及びその他 CD26 陽性悪性腫瘍を対象に、フランスで本抗体の第 1 相臨床試験を施行し、その安全性が確認され、更に悪性中皮腫 19 例中 10 例が Stabilized Disease(SD)となり､その内 6 例で 3 ヶ月以上(5 例は 6 ヶ月以上)SD が継続し、その有効性が示唆され本邦でも 2017 年春から第 I 相臨床試験がスタートする。本臨床試験ではヒト化 CD26 抗体の単独投与のため完全寛解は得られず、症状緩和、肺の機能改善、治癒を目指す安全かつ有効な新規治療薬との併用療法の確立が望まれる。

Y-box binding protein-1(YB-1)は癌細胞の増殖、浸潤に関与する転写因子で悪性中皮腫でも高発現している(Oncology2014)。研究協力者九州大学中野賢二博士らは YB-1 発現を阻害する架橋型核酸アンチセンスを開発し、膵癌モデルの系で有効かつ毒性も低いことを報告した(特願

2012-89772)。更に中皮腫組織での CD26 陽性度評価がアリムタを含む化学療法剤の効果予測として有用なことを我々はすでに報告している(Clin Cancer Res 2012)。

本研究では⑴ヒト化 CD26 抗体と YB-1 アンチセンスとの併用による副作用の少ない安全で有効な悪性中皮腫の焦学的治療法の確立を目指すと伴に⑵悪性中皮腫における CD26 と YB-1 発現と治療反応性や予後を含む臨床パラメーターとの相関を明らかにする。また最近 CTLA-4 抗体や PD-1/PD-L1 抗体が免疫チェックポイント阻害薬として悪性黒色腫や肺癌治療薬として注目されつつあるが、CD26 抗体も免疫チェックポイント阻害薬として作用する可能性を示唆するデータも得られ(J.Immnnol.2015),⑶CD26 共刺激シグナルによる免疫チェックポイント分子の発現誘導及びその他のメカニズムを明らかにすること⑷フランスの検体を用いて SD、PD の認別するバイオマーカーを同定することを目的として研究を行った。

B. 研究方法

各分担研究報告書に著述

(倫理面への配慮)

ヒト化 CD26 抗体及び YB1-ASO の抗腫瘍効果を評価するためのマウスを用いた動物実験は、順天堂大学医学部実験動物委員会の審査を受け承認されている(承認番号 270138)。

患者検体などについては研究対象者に対する人権擁護上の配慮及び研究により研究対象者が受ける不利益、利益等の説明を患者及び遺族に対して行い、書面でのインフォームド・コンセントを得ている。また病理組織について免疫染色して CD26 発現を解析する研究については、慶應義塾大学医学部および埼玉医科大学の倫理委員会の審査にて承認されている(承認番号 20120100 および 734)。

成人健常者の末梢血を用いた研究については、順天堂大学医学部研究等倫理委員会の審査を受け承認されている(承認番号 2015008)。末梢血の提供を受ける際には、研究対象者に対する人的擁護上の配慮及び研究により研究対象者が受ける不利益、利益等の説明を行い、書面でのインフォームド・コンセントを得ている。

フランスで実施されたヒト化 CD26 抗体投与の第 I 相臨床試験における対象症例血清中の可溶性 CD26 及び DPPⅣ酵素活性の測定については順天堂大学倫理審査委員会の審査にて承認されている(順天医倫理第 2012076 及び 2012087)。試料を匿名化することで個人のプライバシーが漏れることのないように配慮した。

C. 研究結果

1. ヒト化CD26抗体とYB-1阻害アンチセンスとの併用療法の検討

Y-box binding protein (YB-1)はがんの浸潤・転移促進に関与することから、有用な治療標的として着目されている分子であり、共同研究者の中野賢二博士により良質な YB-1 antisense oligonucleotide (YB-1 AON)が開発された。昨年度に、in vitro 及び in vivo の結果から CD26 抗体と YB-1 AON との併用の有用性を示唆する成果が得られた。YB-1 AON 処理により YB1 の発現が減少するとともに CD26 の発現も

低下することが示された。CD26 ノックダウン及び CD26 抗体処理中皮腫細胞株の DNA マイクロアレイデータから、様々な癌で予後因子として知られる cyclophilin A を見出し、cyclophilin A の発現が CD26 抗体及び YB-1 AON それぞれ単剤で抑制され、両者の併用によりさらに抑制されることを示した。今後 cyclophilin A に着目して CD26 抗体と YB-1 AON の併用メカニズムの詳細を明らかにする。

2. 中皮腫における CD26 及び YB-1 発現について

悪性中皮腫の新規治療法として期待されるヒト化 CD26 抗体療法および YB-1 アンチセンス療法においては、腫瘍組織における CD26 および YB-1 分子の発現の適確な評価が重要である。本研究では、すでに確立された CD26 発現評価方法とともに、新たに YB-1 発現評価方法の確立を通じて、中皮腫検体における本分子群の免疫染色での発現評価法について検討した。その結果、73 症例において、CD26 および YB-1 は、それぞれ 60、68 症例で陽性であり、CD26 陰性 12 症例中では 4 症例で YB-1 陰性であった。また肉腫型中皮腫では CD26 発現頻度は低いが、YB-1 は高率に発現していることを見出した。これらの染色標本をデジタル画像とし、半定量的に発現量の解析を行い、CD26 の細胞内発現局在とその強度を半定量化しうることを見出すとともに、YB-1 については細胞質に 90%以上の発現が認められることを明らかにした。

3. ヒト化 CD26 抗体の免疫チェックポイント阻害薬としての新たな可能性：CD26 共刺激シグナルによる IL-10、BTLA、LAG3 の発現誘導

有効かつ安全な CD26 抗体との併用療法の開発とともに、CD26 抗体の抗腫瘍作用メカニズムの更なる解明は極めて重要である。CD26 は T 細胞に活性化シグナルを伝達する共刺激分子としても機能するため、CD26 抗体は免疫系にも影響する可能性が考えられる。昨年度に、CD26 シグナルによって免疫チェックポイント分子 BTLA と LAG3 の高発現、抑制性サイトカイン IL-10 高産生が誘導されることを報告した。今年度は、がん細胞周囲に多く存在するプロスタグランジンやアデノシン等の免疫抑制性因子が様々な免疫チェックポイント分子の発現とともに CD26 の発現も増強させること、BTLA の顕著な発現増強は CD26 共刺激に特徴的であることを明らかにした。このことから、CD26 抗体は T 細胞への CD26 シグナルの伝達をブロックし、特に IL-10 産生と BTLA の発現誘導を阻害する免疫チェックポイント阻害薬としても作用する可能性が示唆される。

4. 中皮腫治療における CD26 の役割：可溶性 CD26/DPPⅣは治療奏効性判定のバイオマーカーか

ヒト化 CD26 抗体の First in Man 第Ⅰ相臨床試験を化学療法抵抗性悪性中皮腫及びその他 CD26 陽性悪性腫瘍をターゲットに行なった。患者総計 33 例でヒト化 CD26 抗体投与 1 ヶ月後 2 週間後に modified RECIST 評価により 13 例が Progressive disease(PD)、13

例がStabilized disease(SD)、7例が評価出来ずであった。

特に悪性中皮腫症例においては評価可能例の19例中10例がSDと評価され、5例が6ヶ月以上、1例が3ヶ月以上SDが継続し、有効性を示唆するデータが得られた。ヒト化CD26抗体投与患者において血清中の可溶性CD26/DPPⅣ酵素値を測定したところ、ヒト化CD26抗体の投与量が増加するにつれて可溶性CD26/DPPⅣ値が低下する傾向にあった。PD、SD患者を識別できるバイオマーカーは存在しないかということでヒト化CD26抗体（YS110）投与後の患者血清中の可溶性CD26/DPPⅣ酵素値に注目して解析した。その結果SD患者はPD患者と比べて可溶性CD26/DPPⅣ酵素値ともに特にDay29ヒト化CD26抗体投与前において有意に低値（可溶性CD26：P=0.016、DPPⅣ値：P=0.0267）(Wilcoxon rank sum test)であった。これらの結果から血清可溶性CD26/DPPⅣ酵素値はヒト化CD26抗体投与によるPD及びSDを予測するバイオマーカーとなる可能性が示唆された。

D. 考察

YB-1 AONとCD26抗体は、それぞれ単独でもin vitroで中皮腫細胞の増殖と浸潤を抑制するが、両者を併用することで、それらの効果が増強された。さらにin vivoでの移植実験においても、YB-1 AONの増殖抑制効果は、CD26抗体の併用により増強された。その併用効果の分子メカニズムとして、YB-1 AON処理によってCD26のタンパク発現が低下したため、CD26ノックダウン及びCD26抗体処理後のDNAマイクロアレイ解析を行い、我々は候補分子の一つとしてcyclophilin Aに着目した。CD26抗体またはYB-1 －AONの処理により、それぞれ単剤でcyclophilin Aの発現が抑制されたが、両者を併用することにより強く抑制された。またcyclophilin Aのノックダウン実験により、cyclophilin Aは悪性中皮腫でも、増殖及び浸潤を促進している可能性が示唆された。したがって悪性中皮腫細胞においては、CD26抗体とYB-1 AONの併用による増殖及び浸潤抑制作用の分子メカニズムの一つとして、cyclophilin Aの関与が示唆された。cyclophilin Aは、癌細胞の増殖や浸潤を促進することが報告されている(Nat Med 21:572 2015; Nat Chem Biol 12:117 2016)。さらに、子宮内膜癌、食道扁平上皮癌、腎明細胞癌などにおいては、予後予測因子であることが報告されている (Mol Cell Proteomics 7:1810 2008; Genet Test Mol Biomarkers 19:182 2015; Cancer Biol Ther 11:535 2011)。今回、悪性中皮腫細胞株においてYB-1 AON及びCD26抗体が、cyclophilin Aの発現を抑制することが示されたが、悪性中皮腫においてcyclophilin Aが予後予測因子であれば、CD26抗体やYB-1 AONを悪性中皮腫の治療に用いる意義もさらに強くなると考えられる。そのため、悪性中皮腫病理組織でのcyclophilin Aの発現や、予後因子としての可能性の

検討も今後は必要になると予想される。

YB-1は、転写・翻訳に関わる分子であるが、興味深いことに免疫染色での観察では、YB-1タンパク質の主たる局在部位は細胞質であり、核の陽性像はほとんど得られていない。一方、CD26は、細胞膜貫通型の細胞表面に局在する糖蛋白質であるが、細胞内での局在は、細胞膜のみならず細胞質でのライソゾームや核内と広範囲である。これらの二つの分子のがん細胞における局在は重要な意味を持つが、免疫染色での観察では、CD26とYB-1が中皮腫細胞の細胞質において、類似した瀰漫性の局在を示すことは、これらの分子の相互作用の可能性がある。本研究課題では、CD26を標的とした抗体療法は、抗体による免疫学的細胞傷害やCD26機能の抑制が主体であり、腫瘍細胞の細胞表面CD26は抗体により細胞質内に内在化される。一方、YB-1を標的としたアンチセンス療法は、アンチセンスによるYB-1蛋白発現抑制が主体である。このように併用療法においては、抗体によりCD26は細胞質内での増加とその核内移行が惹起され、一方、YB-1蛋白はアンチセンスにより減少することが想像されるが、その場合に、中皮腫細胞における細胞増殖や細胞死の変化がどうなるか、さらなる検証が期待される。

ヒト化CD26抗体の抗腫瘍作用メカニズムの更なる解明を目的として、CD26抗体の免疫系への影響、特に新たながん治療法として近年非常に注目されている免疫チェックポイント阻害薬としても機能する可能性について昨年度に引き続き検討している。CD26の細胞内ドメインはわずか6アミノ酸で構成されており、フォスファターゼが会合することが知られているITIMやITSMと呼ばれる既存の配列は存在しない。このことから、CD26分子の細胞内ドメインを介して直接抑制性のシグナルが伝達する可能性は低いと考えられる。そのため、CD26分子を介して直接抑制性シグナルが伝達するのではなく、CD26シグナルによって抑制機能を有する免疫チェックポイント分子を誘導し、それらを介して免疫応答を負に制御する、すなわち免疫チェックポイント分子として機能する可能性を検討している。これまでの結果から、CD26共刺激はCD4 T細胞に対してBTLAとLAG3の高発現、IL-10の高産生を誘導し、CD8 T細胞に対してもCD28共刺激と比較してBTLAの発現を顕著に誘導することが示された。また、がん細胞周囲に多く存在すると考えられる免疫抑制性因子のうち、TGF-βはPD1のPGE_2、L-Kynurenine、AdenosineはTIM3のみならずCD26の発現を顕著に増強することが示唆され、がん細胞周囲に浸潤したT細胞はCD26の発現が増強している可能性が考えられる。ヒト化CD26抗体が免疫チェックポイント阻害薬としても機能して、腫瘍免疫を増強させることを直接的に証明するためには、がん抗原特異的なT細胞のエフェクター機能の解析が望まれるが、メラノーマのようによく研究されている

がんとは異なり、悪性中皮腫ではがん抗原が特定されていないうえ、腫瘍細胞塊の入手も難しいなど研究の遂行が難しい要素が多い。そこで、がん細胞に特異的なT細胞に特化しての解析ではないが、平成29年春から予定しているヒト化CD26抗体の国内第I/II相臨床試験で、ヒト化CD26抗体を投与した後の末梢血T細胞のエフェクター機能、IL-10産生能、チェックポイント分子の発現変化についても、特にBTLAとLAG3に着目して解析を行う予定である。また、悪性中皮腫患者における免疫チェックポイント分子の発現パターンを末梢血T細胞、胸水中T細胞、悪性中皮腫周囲に浸潤したT細胞を用いて解析する。

フランスの臨床試験において患者血清中の可溶性CD26/DPPⅣ酵素値がヒト化CD26抗体投与で低下していく傾向にあり、今までSLEやHIVにおいてこの値は活動性やウィルス価のバイオマーカーになる可能性を報告していることから可溶性CD26/DPPⅣ値に注目した。その結果血清中の可溶性CD26/DPPⅣ値はヒト化CD26抗体投与によるPD及びSDを識別するバイオマーカーとなる可能性が示唆された。Nature Immunology(2015)にDPPⅣ酵素と腫瘍免疫についての論文を発表した。

担癌マウスに現在糖尿病治療薬として用いられているシタグリプチンをエサに混ぜて食べさすことによりDPPⅣ酵素の基質CXCL10の不活性化を抑制し、その結果CXCR3陽性T細胞が腫瘍組織にリクルートされ、腫瘍を破壊していくというものである。免疫チェックポイント阻害薬のCTLA-4及びPD-1抗体にDPPⅣ酵素阻害薬を上乗せして投与することにより、その群では他群と比較してほとんど腫瘍は縮小した。このようにDPPⅣ酵素活性阻害は腫瘍免疫の促進に関与する可能性を示唆した。

フランスでの臨床検体の解析からヒト化CD26抗体投与SD患者において血清可溶性CD26/DPPⅣ酵素値がPD患者よりDay29pre時で有意に低いことはDPPⅣ酵素活性阻害が腫瘍免疫促進に関与していることを支持する結果であった。また、PD-1/PD-L1及びCTLA-4抗体との併用療法なども今後検討すべき課題と思われ、ヒト化CD26抗体の作用機序について免疫チェックポイント阻害以外の作用機序についても今後検討すべきと思われる。

E. 結論

1. in vitro及びin vivoの研究によりCD26抗体とYB-1－AONの併用効果が示唆された。そのメカニズムの1つとして両者ともに腫瘍細胞のcyclophilin Aの発現を抑制することが明らかとなった
2. 中皮腫検体において85%の症例においてCD26とYB-1の共発現が明らかとなり、細胞内局在においても細胞質での共在が示された。
3. CD26共刺激は健常者のCD4T細胞に対してBTLAとLAG3の高発現、IL-10の高産生を誘導し、CD8T細胞に対し

てもCD28共刺激と比較してBTLAの発現を顕著に誘導した。特にBTLAの発現誘導に関し、CD26共刺激に特徴的であることが示唆された。

4. ヒト化CD26抗体のフランスでのFirst in Man第1相臨床試験の結果から血清中の可溶性CD26/DPPⅣ酵素値がPD及びSDを識別できるバイオマーカーとなる可能性が示唆された。

F. 健康危険情報

現時点では、特記すべき健康危険情報はない。

G. 次年度以降の計画

1. cyclophilin AのCD26陽性細胞における役割、YB-1 AON及びCD26抗体によるcyclophilin Aの発現制御メカニズムを詳細に検討する。さらに、悪性中皮腫病理組織におけるcyclophilin Aの発現と予後因子としての可能性を検討する。
2. 前年度に引き続き、中皮腫組織（岡山労災病院20例、山口宇部医療センター13例）についてYB-1とCD26の発現を検討し、YB-1とCD26の発現レベルと臨床病理学的指標である、１）特異な浸潤増殖態度、２）遠隔転移、３）治療反応性、４）病期・生存期間、との関連を解析する。更にCD26シグナル系とYB-1シグナル系の標的遺伝子やシグナルのクロストークする中でバイオマーカーとなりうる分子について免疫染色にて発現を検討して、中皮腫の臨床病理学的指標との関連を解析する。
3. 悪性中皮腫自身やその周囲の細胞にBTLAやLAG3、そのリガンドであるHVEMやMHC class IIが発現しているか免疫組織染色で検討する。また、CD26共刺激に特徴的なBTLAの発現誘導に関わるシグナル伝達経路、及び転写因子についての解析を行う。本年度に引き続き、悪性中皮腫患者の末梢血T細胞、胸水T細胞、悪性中皮腫周囲に浸潤したT細胞を用いて、各種免疫チェックポイント分子の発現パターンやエフェクター分子、CD26の発現を解析するとともに、CD26抗体の国内第I/II相臨床試験検体を用いて、CD26抗体投与による血清中IL-10濃度、末梢血T細胞上のBTLA、LAG3の発現変動を経時的にモニタリングしていく。
4. フランスでの第1相臨床試験の解析からPD, SDの識別に血清可溶性CD26/DPPⅣ値が有用な可能性が示唆されたことから血清DPPⅣが腫瘍免疫亢進に働いている可能性を探るためフランスの検体及び本年春からスタートする本邦第1相臨床試験患者血清中のDPPⅣ酵素の基質であるCXCL10などケモカインの切断様式について解析する。

H. 研究発表

1. 論文発表

1) Angevin E, Isambert N, Trillet-Lenoir V, You B, Alexandre J, Zalcman G, Vielh P, Farace F, Valleix F, Podoll T, Kuramochi Y, Miyashita I, Hosono O, Dang NH, Ohnuma K, Yamada T, Kaneko Y,

Morimoto C. First-in-Human phase 1 of YS110, a monoclonal antibody directed against CD26 in advanced CD26-expressing cancers. Br.J. Cancer. in press

2) Komiya E, Hatano R, Otsuka H, Itoh T, Yamazaki H, Yamada T, Dang NH, Tominaga M, Suga Y, Kimura U, Takamori K, Morimoto C, Ohnuma K.A possible role for CD26/DPPIV enzyme activity in the regulation of psoriatic pruritus.J Dermatol Sci. in press

3) Nomura S, Iwata S, Hatano R, Komiya E, Dang NH, Iwao N, Ohnuma K, MorimotoC. Inhibition of VEGF-dependent angiogenesis by the anti-CD82 monoclonal antibody 4F9 through regulation of lipid raft microdomains. Biochem Biophys Res Commun.2016;20:111-7

4) Hayashi M, Madokoro H, Yamada K, Nishida H, Morimoto C, Sakamoto M, Yamada T. A humanized anti-CD26 monoclonal antibody inhibits cell growth of malignant mesothelioma via retarded G2/M cell cycle transition. Cancer Cell Int.2016;30:16-35

5) Omata Y, Nakamura S ,Koyama T, Yasui T, Hirose J, Izawa N, Matsumoto T, Imai Y, Seo S, Kurokawa M, Tsutsumi S, Kadono Y, Morimoto C, Aburatani H, Miyamoto T, Tanaka S. Identification of Nedd9 as a TGF-ß-Smad2/3 Target Gene Involved in RANKL-induced Osteoclastogenesis by Comprehensive Analysis.PLos One. 2016 ;11:e0157992

6) Mizutani N, Abe M, Matsuoka S, Kajino K, Wakiya M, Ohtsuji N, Hatano R, Morimoto C, Hino O. Establishment of anti-mesothelioma monoclonal antibodies.　BMC Res Notes. 2016;9:324

7) Ikeda T, Fragiadaki M,Shi-wen Xu, Ponticos M,　Khan K,　Denton C, Garcia P,　Bou-Gharios G, Yamakawa　A, Morimoto C, Abraham D.Transforming growth factor-β-induced CUX1 isoforms are associated with fibrosis in systemic sclerosis lung fibroblasts. Biochemistry and Biophysics Reports 7. 2016: 246-252

8) Ohnuma K, Hatano R, Itoh T, Iwao N, Dang NH, Morimoto C. Role of IL-26+CD26+CD4 T Cells in Pulmonary chronic graft-versus-host disease and treatment with Caveolin-1- I g Fc conjugate. Crit　Rev　Immunol. 2016;36:239-267

9) Hayashi M, Madokoro H, Yamada K, Nishida H,　Morimoto C, Sakamoto M, Yamada T. A humanized anti-CD26 monoclonal antibody inhibits cell growth of

malignant mesothelioma via retarded G2/M cell cycle transition. Cancer Cell Int. 16:35, 2016. doi:10.1186/s12935-016-0310-9. PMID: 27134571

10) Inaishi J, Saisyo M, Sato S, Kou K, Murakami R, Watanabe Y, KitagoM, Kitagawa Y, Yamada T, Itoh H. Effects of obesity and diabetes on alpha and beta cell mass in surgically resected human pancreas. Journal of Clinical Endocrinology & Metabolism 101:2874-82, 2016. doi:10.1210/jc.2016-1374.

11) Nogami Y, Fujii-Nishimura Y, Banno K, Suzuki A, Hibi T, Murakami K, Yamada T, Sugiyama H, Morishima Y, Aoki D. Anisakiasis mimics cancer recurrence: Two cases of extragastrointestinal anisakiasis suspected to be recurrence of gynecological cancer on PET-CT and molecular biological investigation. BMC Med Imaging.16:31,2016. doi: 10.1186/s12880-016-0134-z. PMID: 27112922

12) Kato K, Gemba K, Fujimoto N, Aoe K, Takeshima Y, Inai K, and Kishimoto T. Computed Tomographic Features of Malignant Peritoneal Mesothelioma. Anticancer Research, 36: 1067-1072,2016.

13) Kato K, Gemba K, Fujimoto N, Aoe K, Takeshuma Y, Inai K & Kishimoto T. Fatal pleural mesothelioma in Japan(2003-2008):evaluation of computed tomography findings. Jpn J Radiol. 34:432-8,2016.

14) Hara N, Fujimoto N, Miyamoto Y, Yamagishi T, Asano M, Fuchimoto Y, Wada S, Ozaki S, Nishi H, Kishimoto T. Angiosarcoma of the thoracic wall responded well to nanoparticle albumin-bound paclitaxel: A case report. Drug Discov Ther. 10:114-6,2016.

15) Kato K, Gemba K, Fujimoto N, Aoe K, Takeshima Y, Inai K, Kishimoto T. Pleural irregularities and mediastinal pleural involvement in early stages of malignant pleural mesothelioma and benign asbestos pleural effusion. European Journal of Radiology. 85:1594-1600,2016.

16) Kushitani K, Amatya VJ, Okada Y, Katayama Y, Mawas AS, Miyata Y, Okada M, Inai K, Kishimoto T, Takeshima Y. Utility and pitfall of Immunohistochemistry in the Differential Diagnosis between Epithelioid Mesothelioma and Poorly Differentiated Lung Squamous Cell Carcinoma. Histopathology.doi: 10.1111/his.13073,2016.

17) Amatya VJ, Kushitani K, Mawas AS, Miyata Y, Okada M, Kishimoto T,

Inai K, Takeshima Y. MUC4, a novel immunohistochemical marker identified by gene expression profiling, differentiates pleural sarcomatoid mesothelioma from lung sarcomatoid carcinoma. Mod Pathol. 2017 Jan 27. doi: 10.1038/modpathol

18) Kubo T, Fujiwara K, Hotta K, Okada T, Kuyama S, Harita S, Ninomiya T, Kamei H, Hosokawa S, Bessho A, Maeda T, Kozuki T, Fujimoto N, Ninomiya K, Takemoto M, Kanazawa S, Takigawa N, Tabata M, Tanimoto M, Ueoka H, Kiura K. A phase II study of topotecan and cisplatin with sequential thoracic radiotherapy in elderly patients with small cell lung cancer; Okayama Lung Cancer Study Group 0102. Cancer Chemother Pharmacol. 2016 Oct;78(4):769-74. doi: 10.1007/s00280-016-3135-2.

19) 森本幾夫．臨床リウマチ医のための基礎講座　CD26分子に基づくトランスレーショナルリサーチ．臨床リウマチ．2016;28:91-4
20) 森本幾夫、大沼圭．CD26分子に基づく悪性中皮腫への新治療法開発．癌と化学療法 2016;43:855-62
21) 大沼圭、森本幾夫．標的別分子標的薬６）モノクローナル抗体、腎臓内科、2016;4:52-60
22) 岸本 卓巳、藤本 伸一、西 英行：胸膜中皮腫の病理と診断（治療）．希少がんの病理と診断 ,2016,43:513-5

2.著書

1) Ohnuma K, Hatano R, Yamazaki H, KanekoY, Dang NH, Morimoto C. CD-26 targeted Therapy :A New Horizon in Malignant Pleural Mesothelioma Management, Horizons in Cancer Research,2016, Nova Science Publishers,Inc.
2) 山田健人.抗体薬物複合体(ADC)の設計開発．第2章　核内移行するヒト化抗CD26モノクローナル抗体-TFⅡH阻害剤複合体．シーエムシー出版　監修：松村保広 2016年5月20日 ISBN978-4-7813-1159-3

3.学会発表

1) 森本幾夫,CD26の機能と治療応用.中皮腫シンポジウム,2016年10月29日,兵庫
2) 波多野良、大沼圭、石井智徳、岩田哲史、奥村康、関川巖、森本幾夫. CD26陽性T細胞サブセットに基づく全身性エリテマトーデスの病態解析. 第60回日本リウマチ学会、横浜(会場：パシフィコ横浜)、2016年 4月21-23日
3) 古宮　栄利子, 波多野 良, 大塚 春奈, 伊藤 匠, 山田 健人, 冨永　光俊, 高森　建二, 大沼 圭, 森本 幾夫: 乾癬においてCD26/DPPIVはsubstance Pの切断を促進してかゆみを調節する 第31回日本乾癬学会学術大会, ホテル東日本宇都宮, 2016年9月2-3日
4) Eriko Komiya, Ryo Hatano,

Haruna Otsuka, Takumi Itoh, Taketo Yamada, Mitsutoshi Tominag, Kenji Takamori, Kei Ohnuma, Chikao Morimoto: CD26/DPPIV-mediated regulation of pruritus in psoriasis. 研究皮膚科学会　第41回年次学術大会・総会, 仙台国際会議場, 2016年11月9-11日

5) 林 睦、間所裕子、山田幸司、西田浩子、坂元亨宇、森本幾夫、山田健人 Humanized anti-CD26 antibody conjugated with RNA polymerase II inhibitor Triptolide suppresses tumor　第105回日本病理学会総会（仙台）2016年5月12-14日

6) Murakami R, Yamada T, Saisho Y. Relationship between intra-pancreatic fat content and beta and alpha cell mass in humans with and without diabetes.The 52nd European Association for the Study of Diabetes(EASD) Annual Meeting, 12 - 16 September, 2016 Munich, Germany

7) Fujimoto N, Yamagishi T, Miyamoto Y, Asano M, Fuchimoto Y, Wada S, Ozaki S, Nishi H, Kishimoto T. Brain Metastases in Malignant Pleural Mesothelioma. The 13rd International Conference of the International Mesothelioma Interest Group. [May 1-4, 2016, Birmingham, England]

8) 藤本伸一、児島葉子、岸本卓己．労災疾病等医学研究・両立支援報告．悪性胸膜中皮腫の診断における胸水中のsecretory leukocyte pepitidase inhibitor (SLPI)の有用性について．第64回日本職業災害医学会．【平成28年10月22日、仙台】

9) Fujimoto N, Takada K, Miyamoto Y, Asano M, Fuchimoto Y, Wada S, Ozaki S, Kishimoto T. Diagnostic value of secretary leukocyte peptide inhibitor (SLPI) in pleural fluid in malignant pleural mesothelioma. 17th World Conference of Lung Cancer. Dec 4-7, 2016, Vienne, Austria.

I. 知的財産権の出願・登録状況（予定を含む）

1. 特許取得

なし

2. 実用新案登録

なし

3. その他

なし

Ⅱ．　分担研究報告

労災疾病臨床研究事業費補助金
分担研究報告書

ヒト化CD26抗体とYB1阻害アンチセンスとの併用療法の検討

研究代表者　森本　幾夫　順天堂大学大学院医学研究科
免疫病・がん先端治療学講座　客員教授

研究協力者　岡本　俊博　免疫病・がん先端治療学講座　研究補助員

研究協力者　波多野　良　免疫病・がん先端治療学講座　博士研究員

研究協力者　山崎　裕人　免疫病・がん先端治療学講座　協力研究員

研究協力者　中野　賢二　九州大学　先端融合医療ﾚﾄﾞｯｸｽﾅﾋﾞ研究拠点　教授

研究要旨

悪性胸膜中皮腫はアスベストばく露によって起こる胸膜中皮由来の難治性悪性腫瘍であり、現時点で満足できる治療法はなく、新たな治療法の確立が望まれる。われわれは、新規治療標的分子として悪性胸膜中皮腫細胞に発現するCD26に着目し、ヒト化CD26抗体を開発しフランスにて第I相臨床試験を行った。安全性が確認されるとともに治療薬としての有効性を示唆する結果も得られ、平成29年春から国内での第I/II相臨床試験を予定している。しかしながら、CD26抗体単剤投与では、Stabilized Diseaseが認められるも完全寛解までは得られず、悪性胸膜中皮腫患者に完全寛解と肺機能改善をもたらす安全かつ有効なCD26抗体との革新的な併用療法の開発が望まれる。Y-box binding protein (YB-1)はがんの浸潤・転移促進に関与することから、有用な治療標的として着目されている分子であり、近年、共同研究者の中野賢二博士により良質なYB-1 antisense oligonucleotide (YB-1 AON)が開発された。昨年度に、in vitro及びin vivoの結果からCD26抗体とYB-1 AONとの併用の有用性を示唆する成果が得られた。YB-1 AON処理によりYB1の発現が減少するとともにCD26の発現も低下することが示された。CD26ノックダウン及びCD26抗体処理中皮腫細胞株のDNAマイクロアレイデータから、様々な癌で予後因子として知られるcyclophilin Aを見出し、cyclophilin Aの発現がCD26抗体及びYB-1 AONそれぞれ単剤で抑制され、両者の併用によりさらに抑制されることを示した。今後cyclophilin Aに着目してCD26抗体とYB-1 AONの併用メカニズムの詳細を明らか

A.研究目的

悪性胸膜中皮腫はアスベストばく露によって起こる胸膜中皮由来の難治性悪性腫瘍である。アスベストばく露から発症までの潜伏期間は30-50年とされ、日本を含めアジアやヨーロッパなど世界規模で胸膜中皮腫患者数は今後ますます増加すると考えられている。悪性胸膜中皮腫に対しては手術療法、

化学療法、放射線療法などが行われるが、いずれも満足できる治療成績ではなく、化学療法の標準治療法とされているアリムタ・シスプラチンの併用投与でも生存期間中央値は約 1 年と非常に短い。このことから、新たな治療法の確立が切望されている。われわれは、新規治療標的分子として悪性胸膜中皮腫細胞に発現する CD26 に着目し、ヒト化 CD26 抗体を開発しフランスにて悪性胸膜中皮腫を中心とした CD26 陽性腫瘍に対する第 I 相臨床試験を行った。特記すべき副作用もなく安全性が確認されるとともに、抗がん剤抵抗性の悪性胸膜中皮腫患者 19 例中 10 例が Stabilized Disease (SD)となり治療薬としての有効性を示唆する結果も得られ、平成 29 年春から国内での第 I/II 相臨床試験を予定している。しかしながら、ヒト化 CD26 抗体単剤投与を行った上記の臨床試験では、SD が認められるも完全寛解までは得られず、副作用の少ない安全かつ有効な CD26 抗体との併用療法の開発が望まれる。

Y-box binding protein (YB-1)はコールドショック蛋白族メンバーに属し、RNA の転写・翻訳の制御に関係するタンパク質で、ヒト癌細胞の核内と細胞質に局在する。P-糖蛋白質(MDR1, ABCB1)などの ABC トランスポーターや DNA 修復関連酵素の発現を上昇させ、広く薬剤耐性の獲得について重要な鍵を握るとされている。またさまざまな癌種において、YB-1 の核内局在や発現レベルはがんにおける薬剤耐性や予後の有用な予測因子ともいわれている。更にがん細胞の上皮間葉転換(EMT)を誘発し、浸潤、転移の促進にも関与することから、がんの有用な治療標的として注目されている。近年、共同研究者の九州大学中野賢二博士により、生物活性や安定性に優れた良質な YB-1 antisence oligonucleotide(YB-1 AON)が開発され、膵がんに対して増殖抑制効果、浸潤・転移抑制効果を示すことが報告された(特願 2012-89772)。

そこで、悪性胸膜中皮腫患者に完全寛解、及び肺機能改善をもたらす革新的な CD26 抗体との併用療法の確立を目指し、悪性胸膜中皮腫細胞株の浸潤及び増殖に対するヒト化 CD26 抗体と YB-1 AON の併用効果を検討するとともに、CD26 抗体、YB-1 AON が CD26 と YB1 の発現に及ぼす影響、両者の併用の分子メカニズムについて検討した。

B. 研究方法

1) 細胞

本研究には、CD26 陽性ヒト悪性胸膜中皮腫細胞株 H226 及び JMN を用いた。

2) 抗体及び試薬

ヒト化 CD26 抗体 YS110 (Human IgG1 isotype)は Y's therapeutics により開発された。Goat anti-Human CD26 pAb (AF1180) は R&D Systems より購入した。Rabbit anti-Human YB1 mAb (clone ab74182)は abcam より購入した。YB1 antisense oligonucleotide (YB-1 AON)は九州大学 中野賢二博士によって開発されたものを用いた。cyclophilin A siRNA は Sigma より購入した。Control siRNA は Qiagen より購入した。YB-1 AON、control siRNA をどちらも終濃度 5, 10, 15, 20 nM、cyclophilin A は終濃度 20 nM で、Lipofectamine RNAiMAX Reagent (Thermo Fisher Scientific)を用いて transfection を行った。

3) In vitro 浸潤アッセイ及び増殖アッセイ

In vitro の浸潤測定には Boyden chamber アッセイを使用した。マトリゲルでコーティングされたインサートウェルを用い、control siRNA 及び YB-1 AON を transfection して 48 時間後に 3 x 10^4 個/ウェルで細胞を播種し、10% ウシ胎児血清(FCS)を誘引物質として用いた。一方、CD26 抗体は細胞の播種と同時に添加した。浸潤した細胞はディフ・クイック(シスメックス)を用いて染色し、24, 48, 72 時間後における細胞の浸潤を測定した。

In vitro 増殖アッセイには 96 well プレートを用い、control siRNA 及び YB-1 AON を transfection して 48 時間後に 2-2.5 x 10^4 個/ウェルで細胞を播種した。CD26 抗体は細胞の播種と同時に添加した。24, 48, 72 時間後に MTT アッセイを行い、細胞増殖を測定した。

4) Flow cytometry

細胞を trypsin 処理して回収した後、FACS buffer (1%FCS 含有 PBS)で懸濁した。細胞膜上の CD26 の発現は、PE-conjugated Mouse anti-Human CD26 mAb (clone M-A261, BD Biosciences)を用いて染色した。Flow cytometry の解析は FACSCalibur (BD Biosciences)を用いて行った。

5) 免疫沈降及び Western Blot

細胞溶解液で細胞を処理後 SDS で denature を行い western blot に用いるサンプルを準備した。免疫沈降では、細胞溶解液に mouse anti-CD26 抗体(1F7) 10 μg あるいは mouse anti-cyclophilin A mAb(clone 1F4-1BO, abcam) 10 μg を 4℃で 24 時間反応させ、protein G セファロースビーズで回収した。1 レーンあたり 5-10 μg のタンパクを SDS-PAGE に供し、ウェット式ブロッティングにて membrane に transfer した後、各種抗体を用いてウェスタンブロットを行った。検出には LAS 4000 (GE Healthcare)を用いた。

6) Real-Time RT-PCR

Total RNA は RNeasy Mini kit (Qiagen)を用いて抽出し、PrimeScript II first strand cDNA synthesis kit (TaKaRa Bio)により cDNA を作製した。Human HPRT1 を内因性コントロールとして 7500 Real-Time PCR System と SYBR Select Master Mix (Applied Biosystems)を用いて mRNA の定量を行った。

7) Polysome の分画

Polysome はショ糖密度勾配超遠心法により分画した。Control siRNA あるいは YB-1 AON (20 nM) を細胞に transfection し、48 時間後に溶解液を作成した。それぞれ 50, 40, 30, 20, 10% のショ糖を含む polysome extraction buffer を 2 ml ずつ重層したステップグラディエントを作製し、そこに細胞溶解液 1 ml を重層してから、超遠心機 (Hitachi Himac CP100α)を用いて 38000 rpm 2 時間の超遠心を行った。遠心後、上層より 1 ml ずつ溶液を回収し、フラクションに分けた。254 nm で吸光度を測定し、translation-inactive 及び -active のフラクションを確認した。各フラクション(0.5 ml)より phenol/choloroform/isoamyl alcohol を用いてタンパクを除去したのち、3 M sodium acetate (pH 5.2)で RNA を沈殿後、

70%エタノールで精製した。CD26 mRNA発現の測定には、Real-Time RT-PCRを用いた。

8) DNAマイクロアレイ解析

CD26ノックダウン細胞のDNAマイクロアレイ解析は、細胞にそれぞれcontrol siRNAまたは CD26 siRNAをtransfectionし、24時間後に抽出したTotal RNAを用いた。CD26抗体処理細胞のDNAマイクロアレイ解析は、細胞にヒト化CD26抗体（10 μg/ml）を添加し、24時間後に抽出したTotal RNAを用いた。変動遺伝子の解析は、東レの3D-Geneマイクロアレイ解析に委託した。

9) 統計処理

統計解析にはt検定を用い、併用効果の解析には two-way ANOVAを使用した。

(倫理面への配慮)

ヒト化CD26抗体及びYB1-ASOの抗腫瘍効果を評価するためのマウスを用いた動物実験は、順天堂大学医学部実験動物委員会の審査を受け承認されている(承認番号280025)。

C. 研究結果

1) *in vitro*でのYB-1 AON単剤による増殖及び浸潤抑制

まずYB-1 AON単剤での悪性中皮腫細胞株の増殖及び浸潤に対する効果を詳細に検討した。control siRNAあるいは YB-1 AONを5, 10, 15, 20 nMで細胞にtransfectionし、48時間後に細胞からタンパク質を抽出して、ウェスタンブロットを行った。YB-1 AON 5 nMでは、H226、JMNともにYB-1の発現抑制は弱かったが、15 nM 及び 20 nMでは80 %以上抑制した(図1)。

次に、同様の条件で増殖への影響を検討した。YB-1 AON transfection後48時間の細胞を96 well plateに播種し、それぞれ24, 48, 72時間後にMTTアッセイを行ったところ、H226では、YB-1 AON 15, 20 nMは48時間で、それぞれ 81%、92%増殖を抑制し、72時間ではそれぞれ83%、91%抑制した。JMNではYB-1 AON 15、20 nMは、48時間でそれぞれ 55%、58%増殖を抑制し、72時間ではそれぞれ69%、73%抑制した(図1)。

次に、浸潤への影響を検討した。YB-1 AON transfection 後 48 時間の細胞をBoyden chamber に播種し、24, 48, 72時間後にアッセイを行ったところ、H226、JMNともに YB-1 の発現低下に応じて浸潤が抑制された。H226ではYB-1 AON 15、20nMは48時間でそれぞれ47%、32%抑制し、72時間ではそれぞれ78%、66%抑制した。JMNではYB-1 AON 15、20nMは48時間でそれぞれ49%、51%抑制し、72時間ではそれぞれ64%、68%抑制した(図1)。

このことから、YB-1 AONは悪性中皮腫細胞株に対しても単剤で増殖及び浸潤を抑制することが示された。

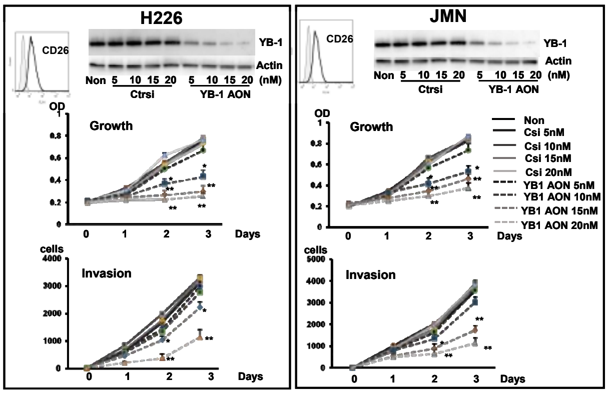

図1 YB-1 AONの濃度依存的に、YB-1タンパク発現および増殖と浸潤が抑制された

2) YB-1 AON 処理と CD26 抗体処理が CD26 と YB-1 の発現に与える影響の解析

YB-1 は様々な遺伝子の転写・翻訳の制御に関わるタンパク質である。そこで、ヒト化 CD26 抗体と YB-1 AON の併用を考えるうえで、YB-1 AON が CD26 発現に与える影響ならびに CD26 抗体が YB-1 の発現に与える影響の解析を行った。

H226 細胞に control siRNA 及び YB-1 AON を 5、10、15、20 nM で transfection して 48 時間後に細胞表面における CD26 発現を解析したところ、YB-1 発現の減少に応じて CD26 の細胞膜上の発現も減少していた(図 2)。同時に、細胞全体の CD26 のタンパク発現をウェスタンブロットで測定したところ、同様に YB-1 発現の減少に応じて CD26 の発現が減少していた(図 2)。一方、CD26 の mRNA 発現への影響に関しても、control siRNA 及び YB-1 AON を transfection して 24 時間後の CD26 mRNA 発現量を Real-Time RT-PCR で測定したが、YB-1 AON による CD26 の mRNA レベルでの大きな発現低下は認められなかった(図 2)。JMN においても同様に、YB-1 AON により細胞表面および細胞全体の CD26 タンパク発現が減少したが、mRNA レベルでの大きな発現低下は認められなかった(データ未掲載)。

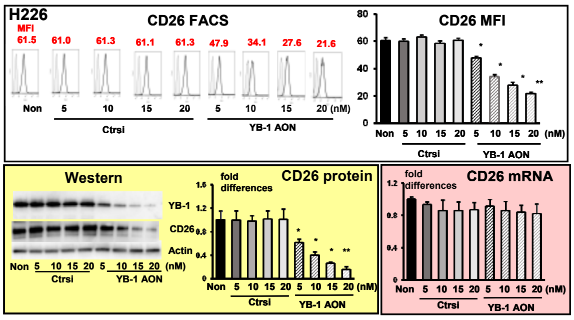

図2 YB-1 AONの濃度依存的に、CD26のタンパク発現が抑制された。一方で、CD26のmRNAレベルでの大きな発現低下は認められなかった。

そこで、ショ糖密度勾配法により H226 及び JMN から polysome を分画し、translation active な CD26 の mRNA 発現を測定した。その結果、H226、JMN ともに YB-1 AON 20 nM 処理で CD26 mRNA の Total 量に変化はなかったが、translation active な polysome 分画における CD26 の mRNA 量は減少していた(図 3：JMN の結果は未掲載)。これらの結果から、YB-1 AON は CD26 の mRNA からタンパクへの翻訳を抑制することで、CD26 のタンパク発現量を低下させることが示唆された。

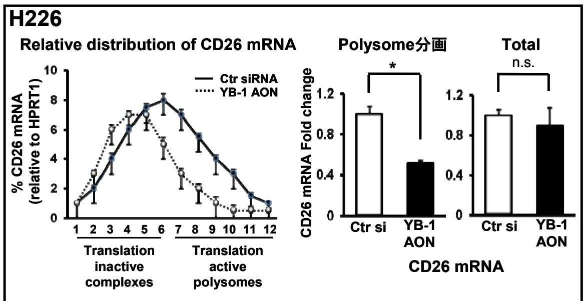

図3 YB-1 AON処理により、CD26 mRNAのTotal量では変化が見られなかったが、Polysome分画におけるTranslation activeなCD26 mRNA量は減少していた。

また、以上の実験と並行し、YB-1 AON の YB-1 発現に対するノックダウン効果と、CD26 の発現減少に対する time course study も行った。細胞に control siRNA あるいは YB-1 AON を 20 nM で transfection し、1、3、7、14 日後にサンプリングを行い、FACS と Western blot で解析した。H226 では、YB-1 AON により YB-1 の発現は 1 日目から減少したが、14 日目には回復していた。一方で CD26 発現は、細胞表面及び細胞全体において、ともに 3 日目から特に低下が見られたが、14 日目では回復傾向が見られた(図 4)。JMN でも同様の結果であった(データ未掲載)。

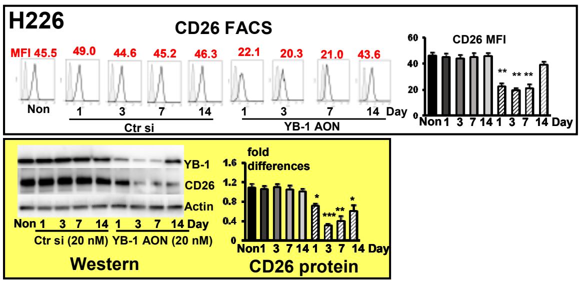

図4　YB-1 AON処理により、YB-1の発現はDay1から低下し、Day14では処理前と同等の発現レベルに戻っていた。CD26の発現はDay3から特に低下が見られ、Day14では回復傾向が見られた。

ヒト化 CD26 抗体と YB-1 AON との併用を考え、CD26 抗体処理が YB-1 の発現に影響するかに関しても検討した。H226 及び JMN に control IgG または CD26 抗体を 5, 10, 15, 20 μg/ml で添加した後、1、2、3 日目にサンプルを採取し、ウェスタンブロットを行った。その結果、CD26 抗体処理による YB-1 の発現への影響は認められなかった(図 5：JMN の結果は未掲載)。

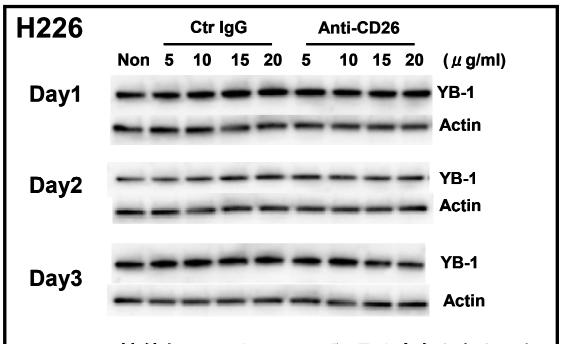

図5　CD26抗体処理ではYB-1の発現は変わらなかった。

3) ヒト化 CD26 抗体と YB-1 AON の併用効果の分子メカニズムに関する検討

昨年度に、H226 と JMN を用いて、ヒト化 CD26 抗体と YB-1 AON の併用により、細胞増殖ならびに浸潤の抑制効果がそれぞれ単剤よりも増強されることを報告した(昨年度報告書参照)。さらに、in vivo growth における CD26 抗体と YB-1 AON の併用効果についても検討を行い、SCID マウスに H226 あるいは JMN を皮下移植したのち、翌日より suboptimal dose (200 μg/mouse) の CD26 抗体を週 2 回腹腔内投与、YB-1 AON (200 μg/mouse)を週 1 回尾静脈投与した。移植 14 日後に腫瘍を摘出し、重量を測定したところ、移植実験においても CD26 抗体と YB-1 AON の併用により、腫瘍増殖抑制効果がそれぞれ単剤よりも増強された(昨年度報告書参照)。

これまでの結果から、悪性中皮腫細胞株では YB-1 AON により、細胞の増殖及び浸潤が抑制され、同時に CD26 のタンパク発現が低下することが示された。YB-1 AON 処理によって CD26 のタンパク発現が低下することに着目し、CD26 ノックダウン、または CD26 抗体処理をした H226 及び JMN の DNA マイクロアレイ解析を行い、CD26 抗体と YB-1 AON の併用効果の分子メカニズムの検討を行った。

CD26 のノックダウンによって遺伝子発現が 1/2 以下に低下する浸潤関連分子を抽出したところ、H226 では 22 個、JMN では 16 個の候補が見つかった。そのうち PPIA、HGF、SFRP1 は両株で共通して発現が低下した遺伝子であった。このうち、種々のがんで過剰発現するだけでなく、増殖や浸潤に関与し、さらには予後予測因子としても報告されている PPIA (cyclophilin A) に着目した。

ヒト化 CD26 抗体で処理した H226 及び JMN の DNA マイクロアレイでは、H226, JMN ともに 20%以上発現が低下した浸潤関連遺伝子として、RCC2、PA2G4、PPIA、CYTSA、RPS27A、UBB、TBRG4、PDPN などがあった。そのうち、PPIA の発現が最も強く抑制されていた(表 1)。

表1 ヒト化CD26抗体処理により20%以上発現が低下する浸潤関連遺伝子

分子	H226 (処理後発現 %)	JMN (処理後発現 %)
RCC2	79%	79%
PA2G4	78	80
PPIA (CypA)	64	63
CYTSA	77	67
RPS27A	66	62
UBB	71	71
TBRG4	77	78
PDPN	69	70

DNAマイクロアレイの解析結果からCD26の発現低下にともない減少する遺伝子としてcyclophilin Aを見出した。そこで次に、CD26とcyclophilin Aの細胞内でのassociationの可能性を検討した。細胞溶解液をCD26抗体(1F7)で免疫沈降し、cyclophilin A抗体でウェスタンブロットを行ったところ、H226、JMNともに18 kDaにバンドが見られた。この結果によりcyclophilin AはCD26抗体で共沈し、両者はassociateしている可能性が示唆された(図6)。

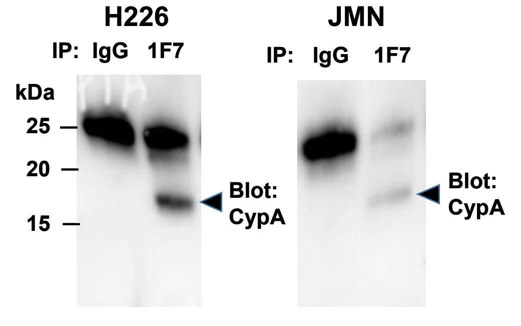
H226
JMN
IP: IgG 1F7
IP: IgG 1F7
kDa
25
20
15
Blot: CypA
Blot: CypA

図6 CypAはCD26抗体で共沈し、両者は細胞内でassociateしている可能性が示唆された。

次にCD26抗体とYB-1 AONのcyclophilin A発現に対する効果を検討した。H226およびJMNをYB-1 AON 20 nMでtransfectionし、48時間後に採取したサンプルでウェスタンブロットしたところ、CD26の発現が抑制されただけでなく、cyclophilin Aの発現も抑制されていた(図7)。ヒト化CD26抗体(10 µg/ml)を48時間処理した場合でも、H226、JMNともにcyclophilin Aの発現低下が見られた(図7)。YB-1 AON 20 nMでtransfectionして48時間後に96 well plateに細胞を播種し、同時にCD26抗体(10 µg/ml)を添加して48時間後に回収したサンプルでは、cyclophilin A発現は、YB-1 AON、CD26抗体それぞれ単独よりも、併用した場合の方がより強く抑制された(図7)。

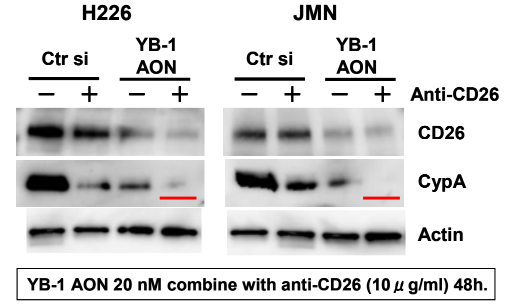
H226
JMN
Ctr si
YB-1 AON
Ctr si
YB-1 AON
− + − +
− + − +
Anti-CD26
CD26
CypA
Actin
YB-1 AON 20 nM combine with anti-CD26 (10μg/ml) 48h.

図7 CypAの発現はCD26抗体及びYB-1 AONそれぞれ単剤で抑制され、併用によりさらに強く抑制された。

最後に、悪性中皮腫細胞株においてもcyclophilin Aは、増殖及び浸潤を促進しているかどうかをcyclophilin A-siRNAを用いて検討した。細胞にsiRNAを20 nMでtransfectionし、48時間後に96 well plateまたはBoyden chamberに播種したのち、さらにその48時間後にMTTアッセイとinvasionアッセイを行った。その結果、H226、JMNにおいてcyclophilin A -siRNAは2種類とも、増殖及び浸潤を抑制した(図8)。この結果から、悪性中皮腫細胞でもcyclophilin Aは、増殖及び浸潤を促進していることが示唆された。

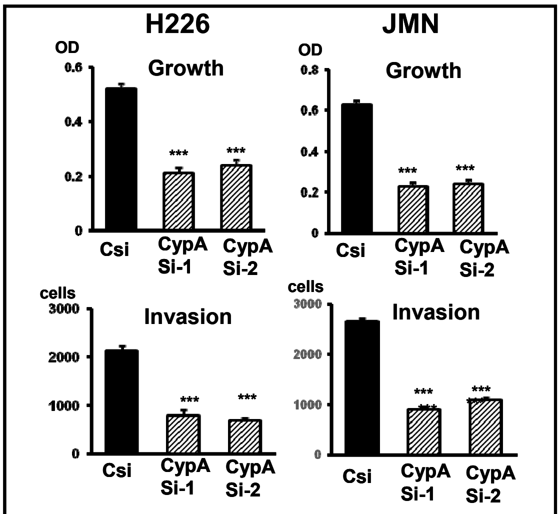

図8 CypAのノックダウンにより、in vitroで悪性中皮腫株の増殖および浸潤が抑制された。

D. 考察

悪性中皮腫に対するヒト化 CD26 抗体と YB-1 AON の併用療法を考案するために、CD26 発現に対する YB-1 AON の作用を検討したが、YB-1 のノックダウンにより濃度依存的に CD26 のタンパク発現が抑制され、それとともに強い増殖抑制効果、浸潤抑制効果が見られた。この結果から、YB-1 AON による増殖及び浸潤の抑制には、CD26 の発現抑制が関与している可能性が示唆された。

YB-1 は EMT 関連因子である snail1 や HIF1α の発現を translation レベルで制御していることが報告されている (Cancer Cell 15:402 2009; Cancer Cell 2:682 2015)。また YB-1 AON による CD26 発現の抑制においても、YB-1 AON は translation レベルで抑制していることが示唆された。一方で、細胞を CD26 抗体で処理しても、YB-1 の発現には影響しなかった。

YB-1 AON の time course study では、YB-1 AON は少なくとも transfection 後 7 日間は YB-1 に対するノックダウン効果があり、濃度依存的に CD26 の発現抑制が見られた。この結果より、生体に使用する場合は少なくとも週 1 回以上の頻度で、YB-1AON の投与が必要であると考えられた。

YB-1 AON と CD26 抗体は、それぞれ単独でも in vitro で中皮腫細胞の増殖と浸潤を抑制するが、両者を併用することで、それらの効果が増強された。さらに in vivo での移植実験においても、YB-1 AON の増殖抑制効果は、CD26 抗体の併用により増強された。その併用効果の分子メカニズムとして、YB-1 AON 処理によって CD26 のタンパク発現が低下したため、CD26 ノックダウン及び CD26 抗体処理後の DNA マイクロアレイ解析を行い、我々は候補分子の一つとして cyclophilin A に着目した。CD26 抗体または YB-1 AON の処理により、それぞれ単剤で cyclophilin A の発現が抑制されたが、両者を併用することにより強く抑制された。また cyclophilin A のノックダウン実験により、cyclophilin A は悪性中皮腫でも、増殖及び浸潤を促進している可能性が示唆された。したがって悪性中皮腫細胞においては、CD26 抗体と YB-1 AON の併用による増殖及び浸潤抑制作用の分子メカニズムの一つとして、cyclophilin A の関与が示唆された。

cyclophilin A は、癌細胞の増殖や浸潤を促進することが報告されている (Nat Med 21:572 2015; Nat Chem Biol 12:117 2016)。さらに、子宮内膜癌、食道扁平上皮癌、腎明細胞癌などにおいては、予後予測因子であることが報告されている (Mol Cell Proteomics 7:1810 2008; Genet Test Mol Biomarkers 19:182 2015; Cancer Biol Ther 11:535 2011)。今回、悪性中皮腫細胞株において YB-1 AON 及び CD26 抗体が、

cyclophilin A の発現を抑制することが示されたが、悪性中皮腫において cyclophilin A が予後予測因子であれば、CD26 抗体や YB-1 AON を悪性中皮腫の治療に用いる意義もさらに強くなると考えられる。そのため、悪性中皮腫病理組織での cyclophilin A の発現や、予後因子としての可能性の検討も今後は必要になると予想される。さらに、CD26 陽性細胞での cyclophilin A の役割や、YB-1 AON や CD26 抗体が cyclophilin A 発現を抑制するメカニズムについても、順次研究する予定である。

E. 結論

In vitro 及び in vivo study 解析において、YB-1 AON と CD26 抗体の併用の有用性が示唆された。YB-1 AON 及び CD26 抗体はそれぞれ単剤で cyclophilin A の発現を抑制するが、併用することでさらに強く発現を抑制することが示され、併用効果の分子メカニズムの一つである可能性が示唆された。今後より詳細に、cyclophilin A の発現制御メカニズムを研究していく予定である。

F. 次年度以降の計画

cyclophilin A の CD26 陽性細胞における役割、YB-1 AON 及び CD26 抗体による cyclophilin A の発現制御メカニズムを詳細に検討する。さらに、悪性中皮腫病理組織における cyclophilin A の発現と予後因子としての可能性を検討する。

G. 研究発表

1. 論文発表

1) Angevin E, Isambert N, Trillet-Lenoir V, You B, Alexandre J, Zalcman G, Vielh P, Farace F, Valleix F, Podoll T, Kuramochi Y, Miyashita I, Hosono O, Dang NH, Ohnuma K, Yamada T, Kaneko Y, Morimoto C. First-in-Human phase 1 of YS110, a monoclonal antibody directed against CD26 in advanced CD26-expressing cancers. Br.J. Cancer. in press

2) Komiya E, Hatano R, Otsuka H, Itoh T, Yamazaki H, Yamada T, Dang NH, Tominaga M, Suga Y, Kimura U, Takamori K, Morimoto C, Ohnuma K.A possible role for CD26/DPPIV enzyme activity in the regulation of psoriatic pruritus.J Dermatol Sci. in press

3) Nomura S, Iwata S, Hatano R, Komiya E, Dang NH, Iwao N, Ohnuma K, MorimotoC. Inhibition of VEGF-dependent angiogenesis by the anti-CD82 monoclonal antibody 4F9 through regulation of lipid raft microdomains. Biochem Biophys Res Commun.2016;20:111-7

4) Hayashi M, Madokoro H, Yamada K, Nishida H, Morimoto C, Sakamoto M, Yamada T. A humanized anti-CD26 monoclonal antibody inhibits cell growth of malignant mesothelioma via retarded G2/M cell cycle transition. Cancer Cell Int.2016;30:16-35

5) Omata Y, Nakamura S ,Koyama T, Yasui T, Hirose J, Izawa N, Matsumoto T, Imai Y, Seo S,

Kurokawa M, Tsutsumi S, Kadono Y, Morimoto C, Aburatani H, Miyamoto T, Tanaka S. Identification of Nedd9 as a TGF-ß-Smad2/3 Target Gene Involved in RANKL-induced Osteoclastogenesis by Comprehensive Analysis.PLos One. 2016 ;11:e0157992

6) Mizutani N, Abe M, Matsuoka S, Kajino K, Wakiya M, Ohtsuji N, Hatano R, Morimoto C, Hino O. Establishment of anti-mesothelioma monoclonal antibodies.　BMC Res Notes. 2016;9:324

7) Ikeda T, Fragiadaki M,Shi-wen Xu, Ponticos M,　Khan K,　Denton C, Garcia P,　Bou-Gharios G, Yamakawa　A, Morimoto C, Abraham D.Transforming growth factor-β-induced CUX1 isoforms are associated with fibrosis in systemic sclerosis lung fibroblasts. Biochemistry and Biophysics Reports 7. 2016: 246-252

8) Ohnuma K, Hatano R, Itoh T, Iwao N, Dang NH, Morimoto C. Role of IL-26+CD26+CD4 T Cells in Pulmonary chronic graft-versus-host disease and treatment with Caveolin-1-Ｉg Fc conjugate. Crit Rev　Immunol.　2016;36:239-267

9) 森本幾夫．臨床リウマチ医のための基礎講座　CD26分子に基づくトランスレーショナルリサーチ. 臨床リウマチ. 2016;28:91-4

10) 森本幾夫、大沼圭．CD26分子に基づく悪性中皮腫への新治療法開発．癌と化学療法 2016;43:855-62

11) 大沼圭、森本幾夫．標的別分子標的薬 ６）モノクローナル抗体、腎臓内科、2016;4:52-60

2. 著書

1) Ohnuma K, Hatano R, Yamazaki H, KanekoY, Dang NH, Morimoto C. CD-26 targeted Therapy :A New Horizon in Malignant Pleural Mesothelioma Management, Horizons in Cancer Research,2016, Nova Science Publishers,Inc.

3. 学会発表

1) 森本幾夫,CD26の機能と治療応用.中皮腫シンポジウム,2016年10月29日,兵庫

2) 波多野良、大沼圭、石井智徳、岩田哲史、奥村康、関川巖、森本幾夫. CD26陽性T細胞サブセットに基づく全身性エリテマトーデスの病態解析．第60回日本リウマチ学会、横浜(会場：パシフィコ横浜)、2016年 4月21-23日

3) 古宮　栄利子, 波多野 良, 大塚 春奈, 伊藤 匠, 山田 健人, 冨永　光俊, 高森　建二, 大沼 圭, 森本 幾夫: 乾癬においてCD26/DPPIVはsubstance Pの切断を促進してかゆみを調節する 第31回日本乾癬学会学術大会, ホテル東日本宇都宮, 2016年9月2-3日

4) Eriko Komiya, Ryo Hatano, Haruna Otsuka, Takumi Itoh, Taketo Yamada, Mitsutoshi Tominag, Kenji Takamori, Kei Ohnuma, Chikao Morimoto: CD26/DPPIV-mediated

regulation of pruritus in psoriasis.
研究皮膚科学会　第41回年次学術大会・総会, 仙台国際会議場, 2016年11月9-11日

H. 知的財産権の出願・登録状況（予定を含む）

1. 特許取得

   なし

2. 実用新案登録

   なし

3. その他

   なし

労災疾病臨床研究事業費補助金
分担研究報告書

中皮腫におけるCD26およびYB-1発現について

研究分担者　　山田　健人　埼玉医科大学 病理学・教授

研究要旨
悪性中皮腫の新規治療法として期待されるヒト化CD26抗体療法およびYB-1アンチセンス療法においては、腫瘍組織におけるCD26およびYB-1分子の発現の適確な評価が重要である。本研究では、すでに確立されたCD26発現評価方法とともに、新たにYB-1発現評価方法の確立を通じて、中皮腫検体における本分子群の免疫染色での発現評価法について検討した。その結果、73症例において、CD26およびYB-1は、それぞれ60、68症例で陽性であり、CD26陰性12症例中では4症例でYB-1陰性であった。また肉腫型中皮腫ではCD26発現頻度は低いが、YB-1は高率に発現していることを見出した。また、これらの染色標本をデジタル画像とし、半定量的に発現量の解析を行い、CD26の細胞内発現局在とその強度を半定量化しうることを見出すとともに、YB-1については細胞質に90%以上の発現が認められることを明らかにした。

A. 研究目的

仏にて施行されたヒト化CD26抗体療法の第1相臨床試験では、特記すべき有害事象なく、26症例中13症例で「安定」(Stabilized Disease;SD)への導入が可能であり、安全性のみならず、その腫瘍効果も期待される成果が得られた。本研究課題では、このCD26抗体療法とともに中皮腫細胞の増殖・細胞死を司る他の分子メカニズムを阻害することで、相加相乗効果を狙った新規治療法を目指している。その標的分子が、YB-1である。YB-1は、Ybox (CAAT/ATTG)と呼ばれる塩基配列を認識して標的遺伝子に結合する転写因子の一つであり、cold shock domain蛋白スーパーファミリーに属する。本分子は、細胞周期関連分子や癌抑制分子などの細胞増殖や腫瘍悪性化に関与する転写・翻訳を制御するとともに、DNA-RNAとの結合を介して翻訳にも関わる多機能分子である。このYB-1は、ヒトがんにおける発現解析から、肺癌や乳癌の抗がん剤感受性や予後と相関するとの報告がなされている。また研究協力者・中野賢二博士は、このYB-1に対するアンチセンス療法の開発にすでに成功している。

そこで本研究においては、まず悪性中皮腫症例におけるCD26とYB-1発現を詳細に明らかにし、CD26とともにYB-1が中皮腫における標的分子としてどのような発現パターンを示すのかを明らかにし、CD26抗体およびYB-1アンチセンスの併用療法にそなえた基礎的検討を行うものである。またCD26発現は現在用いられているアリムタ、シスプラチンなど化学療法剤の治療効果予

測バイオマーカーとしても有望な結果を得て報告(Clin Cancer Res 18:1447, 2012)してきたが、さらにCD26およびYB−1発現を細胞局在、陽性率、陽性強度など様々な要素で解析し、各種の臨床パラメーターとの相関を明らかにすることで、バイオマーカーとなりうるかどうかを検討することを目的とした。

B. 研究方法

YB-1の発現解析には、抗YB-1抗体（Rabbit monoclonal antibody(EP2708Y), ABCAM社ab76149）を用いた。本抗体は、ヒトYB-1のC末端領域を抗原として作成されたものであり、ヒトおよびげっ歯類のYB-1と反応する。YB−1陽性対照標本としては、ヒト癌細胞株（HeLa, SW480, A549, MCF7）を免疫不全マウス（NOD/SCID）皮下に移植して形成された腫瘍をホルマリン固定したものを用いた。またヒト組織としては、ホルマリン固定したパラフィン切片（CD26陽性である正常ヒト腎、肝、前立腺及び悪性中皮腫の組織および肺）を用いた。抗原賦活化として、オートクレーブ処置（120℃、20分、0.01M Citrate Buffer pH8.0）を行い、二次抗体は、Peroxidase付加抗ラビットIgG抗体(ImmPRESS社製)を用い、発色は、DAB液（Simple Stain DAB, Histofine）を用いた。

岡山労災病院および山口宇部医療センターにおける中皮腫73症例の腫瘍の病理組織（生検及び手術材料、10%ホルマリン固定、パラフィン切片）について、CD26の免疫染色を行った。抗原賦活化は、オートクレーブ処置（120℃、20分、0.01M Citrate Buffer pH8.0）を行った。抗CD26抗体は、仏の臨床試験で使用したR&D社製抗CD26ヤギ・ポリクロナール抗体（Lot.No. JOQ107061）を用いた。二次抗体は、Peroxidase付加抗ヤギIgG抗体(ImmPRESS社製)あるいはPeroxidase付加抗マウスIgG抗体(ImmPRESS社製)を用い、発色は、DAB液（Simple Stain DAB, Histofine）を用いた。いずれの染色においても、陽性対照には、正常ヒト腎、肝、前立腺及び悪性中皮腫を用い、陰性対照には、これらの正常組織切片内の各種組織（平滑筋、脂肪組織、結合組織など）とCD26陰性肺癌組織を用いた。

（倫理面への配慮）

患者検体などについては研究対象者に対する人権擁護上の配慮及び研究により研究対象者が受ける不利益、利益等の説明を患者及び遺族に対して行い、書面でのインフォームド・コンセントを得ている。また病理組織について免疫染色してCD26発現を解析する研究については、慶應義塾大学医学部および埼玉医科大学の倫理委員会の審査にて承認されている（承認番号20120100および794）。

C. 研究結果

中皮腫組織73例（上皮型55例、二相型9例、肉腫型9例）について、同様にYB-1の免疫染色を行った。その結果、中皮腫組織において、YB-1は腫瘍細胞の細胞質に瀰漫性に強陽性となり、その頻度は73例中68例が陽性であった（図1および表1）。また腫瘍組織における腫瘍血管の内皮細胞において、細胞質にYB-1発現を認めた。次にこれらの中皮腫組織におけるYB−1陽性所見が真にYB−1蛋白であるかどうかを確認する

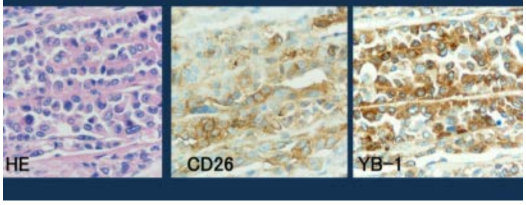

図1　中皮腫(二相型、上皮型成分)におけるCD26, YB−1発現

ために、一次抗体について YB−1 蛋白による吸収実験を行った。ラビット抗ヒト YB-1 モノクローナル抗体と YB-1 蛋白を 4℃で 3 時間反応させた後、同様に免疫染色を施行した。その結果、中皮腫組織および血管内皮細胞における YB−1 陽性像がほぼ完全に消失したことから、この YB-1 の免疫染色は特異的に切片上の YB-1 蛋白発現を認識していると考えられた。

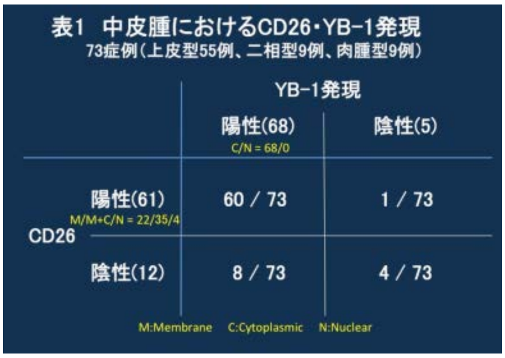

表1　中皮腫におけるCD26・YB−1発現
73症例（上皮型55例、二相型9例、肉腫型9例）

		YB−1発現	
		陽性(68) C/N = 68/0	陰性(5)
CD26	陽性(61) M/M+C/N = 22/35/4	60 / 73	1 / 73
	陰性(12)	8 / 73	4 / 73

M:Membrane　C:Cytoplasmic　N:Nuclear

次に上記の中皮腫 73 症例について、ヒツジ抗ヒト CD26 ポリクローナル抗体を用いて同一検体での CD26 染色を行った（図 1 および表 1）。その結果、CD26 陽性症例は 73 例中 60 例であり、CD26 陰性 12 症例中 4 症例は YB-1 も陰性であった。一方、CD26 陽性 60 例中、YB-1 陰性例は 1 例であった。

次に、これらの染色標本をデジタル画像とし、imageProPlus プログラムにて詳細に半定量的に発現解析を行った。その結果、CD26 の細胞内発現局在とその強度を半定量化しうることを見出すとともに、YB-1 は細胞質に 90%以上の発現が認められることを明らかにした。今後、このデータベースを元に臨床パラメーターとの相関について検討する予定である。

D. 考察

YB-1 は、転写・翻訳に関わる分子であるが、興味深いことに免疫染色での観察では、YB-1 タンパク質の主たる局在部位は細胞質であり、核の陽性像はほとんど得られていない。一方、CD26 は、細胞膜貫通型の細胞表面に局在する糖蛋白質であるが、細胞内での局在は、細胞膜のみならず細胞質でのライソゾームや核内と広範囲である。これらの二つの分子のがん細胞における局在は重要な意味を持つが、免疫染色での観察では、CD26 と YB-1 が中皮腫細胞の細胞質において、類似した瀰漫性の局在を示すことは、これらの分子の相互作用の可能性がある。本研究課題では、CD26 を標的とした抗体療法は、抗体による免疫学的細胞傷害や CD26 機能の抑制が主体であり、腫瘍細胞の細胞表面 CD26 は抗体により細胞質内に内在化される。一方、YB-1 を標的としたアンチセンス療法は、アンチセンスによる YB-1 蛋白発現抑制が主体である。このように併用療法においては、抗体により CD26 は細胞質内での増加とその核内移行が惹起され、一方、YB-1 蛋白はアンチセンスにより減少することが想像されるが、その場合に、中皮腫細胞における細胞増殖や細胞死の変化がどうなるか、さらなる検証が期待される。

また悪性中皮腫における CD26 および YB-1 発現について細胞局在、陽性率、陽性強度などの各種パラメーターで詳細に定量

評価することで、抗体療法の効果や予後などとの関連性あるいは臨床パラメーターを検証する基礎を構築していくことが重要と考える。

E. 結論

中皮腫検体における YB-1 の発現評価方法および半定量的解析法を確立した。その結果、85%の症例において CD26 と YB-1 の共発現が明らかとなり、細胞内局在においても細胞質内での共在が示された。

F. 最終年度の計画

前年度に引き続き、中皮腫組織（岡山労災病院 20 例、山口宇部医療センター13 例）について YB-1 と CD26 の発現を検討し、YB-1 と CD26 の発現レベルと臨床病理学的指標である、1）特異な浸潤増殖態度、2）遠隔転移、3）治療反応性、4）病期・生存期間、との関連を解析する。また森本博士らが見出しつつある CD26 シグナル系と YB-1 シグナル系の標的遺伝子やシグナルのクロストークする中でバイオマーカーとなりうる分子について免疫染色にて発現を検討して、中皮腫の臨床病理学的指標との関連を解析する予定である。

G. 研究発表

1. 論文発表

1) Angevin E, Isambert N, Trillet-Lenoir V, You B, Alexandre J, Zalcman G, Vielh P, Farace F, Valleix F, Podoll T, Kuramochi Y, Miyashita I, Hosono O, Dang NH, Ohnuma K, Yamada T, Kaneko Y, Morimoto C. First-in-Human phase 1 of YS110, a monoclonal antibody directed against CD26 in advanced CD26-expressing cancers. Br.J. Cancer. in press

2) Hayashi M, Madokoro H, Yamada K, Nishida H, Morimoto C, Sakamoto M, Yamada T. A humanized anti-CD26 monoclonal antibody inhibits cell growth of malignant mesothelioma via retarded G2/M cell cycle transition. Cancer Cell Int. 16:35, 2016.

3) Inaishi J, Saisyo M, Sato S, Kou K, Murakami R, Watanabe Y, KitagoM, Kitagawa Y, Yamada T, Itoh H. Effects of obesity and diabetes on alpha and beta cell mass in surgically resected human pancreas. Journal of Clinical Endocrinology & Metabolism 101(7):2874-82, 2016.

4) Nogami Y, Fujii-Nishimura Y, Banno K, Suzuki A, Hibi T, Murakami K, Yamada T, Sugiyama H, Morishima Y, Aoki D. Anisakiasis mimics cancer recurrence: Two cases of extragastrointestinal anisakiasis suspected to be recurrence of gynecological cancer on PET-CT and molecular biological investigation. BMC Med Imaging.16:31,2016.

2. 著書

1) 核内移行するヒト化抗 CD26 モノクローナル抗体-TFⅡH 阻害剤複合体山田健人　抗体薬物複合体(ADC)の設計開発　シーエムシー出版　監修： 松村保広　P94-103, 2016 年 5 月 20 日

3. 学会発表

1) 林 睦、間所裕子、山田幸司、西田浩子、坂元亨宇、森本幾夫、山田健人 Humanized anti-CD26 antibody conjugated with RNA polymerase II inhibitor Triptolide suppresses tumor 第 105 回日本病理学会総会（仙台）2016 年 5 月 12-14 日

2) Murakami R, Yamada T, Saisho Y. Relationship between intra-pancreatic fat content and beta and alpha cell mass in humans with and without diabetes.The 52nd European Association for the Study of Diabetes(EASD) Annual Meeting, 12 - 16 September, 2016 Munich, Germany

3) Komiya E, Hatano R, Otsuka H, Itoh T, Yamada T, Tominaga M, Takamori L, Okumura K, Morimoto C. CD26/DPPIV-mediated regulation of pruritus in psoriasis.The 41st Annual Meeting of the Japanese Society for Investigative Dermatology 12 – 11 September, 2016 Sendai, Japan

H. 知的財産権の出願・登録状況（予定を含む）

1. 特許取得

なし

2. 実用新案登録

なし

3. その他

なし

労災疾病臨床研究事業費補助金
分担研究報告書

ヒト化 CD26 抗体の免疫チェックポイント阻害薬としての新たな可能性：CD26 共刺激シグナルによる IL-10, BTLA, LAG3 の発現誘導

研究代表者　森本　幾夫　順天堂大学大学院医学研究科
免疫病・がん先端治療学講座　客員教授

研究分担者　山田　健人　埼玉医科大学医学部　病理学　教授

研究協力者　波多野　良　順天堂大学大学院医学研究科
免疫病・がん先端治療学講座　博士研究員

研究協力者　大沼　圭　順天堂大学大学院医学研究科
免疫病・がん先端治療学講座　准教授

研究要旨

悪性胸膜中皮腫はアスベストばく露によって起こる難治性悪性腫瘍であり、現時点で満足できる治療法はなく、新たな治療法の確立が望まれる。われわれは、新規治療標的分子として悪性胸膜中皮腫に発現する CD26 に着目し、ヒト化 CD26 抗体を開発しフランスにて第 I 相臨床試験を行った。安全性が確認されるとともに治療薬としての有効性を示唆する結果も得られ、平成 29 年春から国内での第 I/II 相臨床試験を予定している。有効かつ安全な CD26 抗体との併用療法の開発とともに、CD26 抗体の抗腫瘍作用メカニズムの更なる解明は極めて重要である。CD26 は T 細胞に活性化シグナルを伝達する共刺激分子としても機能するため、CD26 抗体は免疫系にも影響する可能性が考えられる。昨年度に、CD26 シグナルによって免疫チェックポイント分子 BTLA と LAG3 の高発現、抑制性サイトカイン IL-10 高産生が誘導されることを報告した。今年度は、がん細胞周囲に多く存在するプロスタグランジンやアデノシン等の免疫抑制性因子が様々な免疫チェックポイント分子の発現とともに CD26 の発現も増強させること、BTLA の顕著な発現増強は CD26 共刺激に特徴的であることを明らかにした。このことから、CD26 抗体は T 細胞への CD26 シグナルの伝達をブロックし、特に IL-10 産生と BTLA の発現誘導を阻害する免疫チェックポイント阻害薬としても作用する可能性が示唆される。

A. 研究目的

悪性胸膜中皮腫はアスベストばく露によって起こる胸膜中皮由来の難治性悪性腫瘍である。アスベストばく露から発症までの潜伏期間は 30-50 年とされ、日本を含めアジアやヨーロッパなど世界規模で胸膜中皮腫患者数は今後ますます増加すると考えられている。悪性胸膜中皮腫に対しては手術療法、

化学療法、放射線療法などが行われるが、いずれも満足できる治療成績ではなく、新たな治療法の確立が望まれる。われわれは、新規治療標的分子として悪性胸膜中皮腫細胞に発現するCD26に着目し、ヒト化CD26抗体を開発しフランスにて第I相臨床試験を行った。特記すべき副作用もなく安全性が確認されるとともに、抗がん剤抵抗性の悪性中皮腫患者19例中10例がStabilized Disease (SD)となり治療薬としての有効性を示唆する結果も得られた。平成29年春から国内での第I/II相臨床試験を予定しているが、有効かつ安全なCD26抗体との併用療法の開発とともに、CD26抗体の抗腫瘍作用メカニズムの更なる解明は極めて重要である。

我々はこれまでにヒト化CD26抗体の抗腫瘍作用メカニズムとして、抗体医薬特有の抗体依存性細胞傷害(ADCC)活性・補体依存性細胞傷害(CDC)活性に加え、CD26陽性腫瘍に抗体が結合することによる直接的な作用があることを明らかにしてきた。がん細胞の細胞膜上のCD26にヒト化CD26抗体が結合すると、cyclin dependent kinase inhibitorであるp21やp27の発現が上昇しcell cycle arrestを起こさせること(Clin Cancer Res. 2001, Immunology. 2002, Clin Cancer Res. 2007, Cancer Cell Int. 2016)、CD26抗体とCD26の複合体が細胞膜から細胞質、さらに核内へと移行し、RNA polymerase IIのサブユニットであるPOLR2A遺伝子の転写領域下流に結合することでPOLA2Aの転写を抑制し増殖抑制に働くことを明らかにした(PLoS One. 2013)。また、CD26はcollagenやfibronectinとの結合タンパクであるが、CD26抗体が結合することでそれらのタンパクへの接着が阻害され(Clin Cancer Res. 2007)、このことからCD26抗体がCD26陽性腫瘍の浸潤・転移の抑制にも働くことが示唆された。

CD26はヒトT細胞に活性化シグナルを伝達するT細胞共刺激分子であり、CD26抗体はCD26のリガンドであるcaveolin-1のCD26への結合をブロックする。また、CD26の機能の一つにdipeptidyl peptidase IV (DPPIV)酵素活性があり、N末から2番目にプロリンまたはアラニンを有するペプチドの2アミノ酸を切断する。生体内で様々な生理活性物質がその基質となることが知られているが、いくつかのケモカインもDPPIVによる切断を受けその細胞遊走活性が不活性化される。CD26抗体はDPPIV酵素活性自体に直接は影響しないが、フランスでの第I相臨床試験の結果からヒト化CD26抗体の投与により血中の可溶性CD26の量が顕著に低下し、DPPIV酵素活性も同様に低下することが示されている。DPPIV酵素活性の低下によりケモカインの切断と不活性化が抑えられ、免疫細胞が腫瘍組織に遊走しやすくなる可能性が考えられる(Nat Immunol. 2015)。これらの知見から、CD26抗体は免疫系にも影響する可能性が強く示唆される。

近年、がんの新たな治療法として免疫系に抑制シグナルを伝達するチェックポイント分子をブロックすることで腫瘍免疫を活性化させる免疫チェックポイント阻害薬が非常に注目されており、CTLA4抗体やPD1抗体は既に臨床現場で用いられ始めている。われわれは最近、ヒトCD4 T細胞に強いCD26共刺激シグナルが伝達すると免疫チェックポイント分子LAG3の発現と代表的な抑制性サイトカインIL-10の産生が強く

誘導されることを報告した(J Immunol. 2015)。また、昨年度にCD26共刺激はCD28共刺激と比較して、CD4 T細胞・CD8 T細胞のどちらに対しても免疫チェックポイント分子BTLAの発現を顕著に増強させることを報告した。そこで、CD26抗体が免疫チェックポイント阻害薬としても機能する可能性を考え、更なる解析を行った。

B. 研究方法

1) ヒトT細胞の調製

順天堂大学医学部研究等倫理委員会での承認を得て、インフォームド・コンセントを書面で得られた成人健常者の末梢血から、Ficoll密度分離法により末梢血単核球(PBMC)を調製した。PBMCからT細胞への精製にはMACS(磁気細胞分離)システム(Miltenyi Biotec)を用いた。ヒトCD4 T細胞、CD8 T細胞への精製には、それぞれhuman CD4$^+$ T cell isolation kit, human CD8$^+$ T cell isolation kit (Miltenyi Biotec)を使用し、それぞれCD3$^+$CD4$^+$ が97%以上、CD3$^+$CD8$^+$ CD56^{nega} が 95%以上であることをFACS Calibur (BD Biosciences)にて確認した。また、岡山労災病院で倫理委員会での承認を得て、インフォームド・コンセントを書面で得られた悪性中皮腫・良性石綿胸水の患者から末梢血と胸水の提供を受けた。末梢血からFicoll密度分離法によりPBMCを調製した。胸水を1800rpm, 7min, 4℃で遠心し、胸水細胞を得た。上記と同様にMACSシステムを用いて、PBMC及び胸水細胞からT細胞への精製を行った。

2) 抗体と試薬

ヒトT細胞の刺激にはanti-CD3 mAb (OKT3), anti-CD28 mAb (4B10)及びanti-CD26 mAb (1F7)を用いた。Flow cytometryには下記のヒト抗原特異抗体を用いた。FITC-labeled anti-CD28 mAb (clone CD28.2), PE-labeled anti-CD26 mAb (clone M-A261) 及び APC-labeled anti-CTLA4 mAb (clone BNI3)はBD Biosciencesから購入した。FITC-labeled anti-LAG3 mAb (clone 3DS223H)とPE/Cy7-labeled anti-TIGIT mAb (clone MBSA43)はeBioscienceから購入した。PerCP/Cy5.5-labeled anti-CD244 (2B4) mAb (clone C1.7), PerCP/Cy5.5-labeled anti-CD73 mAb (clone AD2), PE/Cy7-labeled anti-Tim3 mAb (clone F38-2E2), PE/Cy7-labeled anti-CD160 mAb (clone BY55), APC-labeled anti-PD1 mAb (clone EH12.2H7), APC-labeled anti-BTLA mAb (clone MIH26), APC-labeled anti-CD39 mAb (clone A1) 及び APC-labeled anti-DNAM1 (CD226) (clone 11A8)はBioLegendから購入した。組換えヒトTGF-β1及びヒトIL-10はBioLegendから購入した。Prostaglandin E$_2$ (PGE$_2$)及びL-KynurenineはWakoから購入した。AdenosineはSigmaから購入した。ヒトPD-L1の細胞外領域とヒトIgG$_1$のFc領域との融合タンパクPDL1-IgはR&D Systemsから購入した。

3) フローサイトメトリー

精製した末梢血CD4 T細胞、CD8 T細胞を、抗CD3抗体0.5 μg/mlと抗CD28抗体または抗CD26抗体10 μg/mlで固相化した96 well平底プレート(Costar)に1 x 10^5 cells/wellで播種し、組換えTGF-β1、IL-10、 PGE₂、L-Kynurenine、Adenosine、PDL1-Ig をそれぞれ終濃度 10 ng/ml、10 ng/ml、100 nM、100 μM、25 μM、10 μg/ml となるよう添加した。96 時間後に細胞を回収して、細胞膜上の免疫チェックポイント分子及び CD26 の発現を解析した。活性化刺激を入れる前の PBMC 及び胸水細胞から精製した直後の CD4 T 細胞、CD8 T 細胞に関しても同様の解析を行った。FACSCalibur (BD Biosciences)で測定を行い、得られたデータを FlowJo (Tree Star)で解析した。

4) 血清中 IL-10 濃度の定量

健常者 7 例ならびに、フランスでのヒト化 CD26 抗体の第 I 相臨床試験患者の中で SD が持続した症例 2 例、Progressive Disease (PD)症例 2 例の血清中 IL-10 濃度を測定した。IL-10 の定量には BD OptEIA Human IL-10 ELISA Kit (BD Biosciences)を用いた。450/570 nm の吸光値を microplate reader (Bio-Rad)で測定し、得られたデータを Microplate Manager 6 (Bio-Rad)で解析した。

(倫理面への配慮)

成人健常者ならびにフランスでの第 I 相臨床試験の末梢血、岡山労災病院の悪性中皮腫患者・良性石綿胸水患者の末梢血及び胸水を用いた研究については、順天堂大学医学部研究等倫理委員会の審査を受け承認されている(承認番号 2015008)。末梢血及び胸水の提供を受ける際には、研究対象者に対する人的擁護上の配慮及び研究により研究対象者が受ける不利益、利益等の説明を行い、書面でのインフォームド・コンセントを得ている。

C. 研究結果

1) 健常者末梢血 CD4 T 細胞、CD8 T 細胞における各種免疫チェックポイントの分子の発現

近年、免疫系に抑制シグナルを伝達するチェックポイント分子をブロックすることで腫瘍免疫を活性化させる免疫チェックポイント阻害薬が新たながん治療法として非常に注目されている。様々ながん種において様々な免疫チェックポイント分子の発現が報告されているが、いずれも CD8 T 細胞にスポットが当てられている。われわれは腫瘍微小環境において CD8 T 細胞の抑制だけでなく、CD4 T 細胞の抑制も免疫応答の不活性化を起こさせるうえで重要な現象と考え、昨年度に引き続き、CD8 T 細胞とともに CD4 T 細胞の解析も行っている。まず近年着目されている免疫チェックポイント分子に関して、それぞれのリガンドとの関係を図 1 にまとめた。

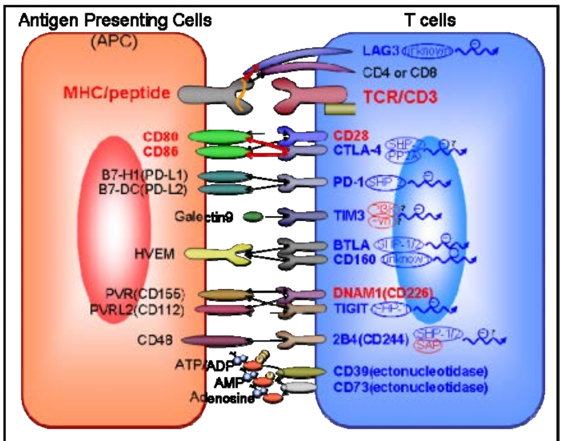
Antigen Presenting Cells
(APC)
T cells
LAG3
unknown
CD4 or CD8
MHC/peptide
TCR/CD3
CD80
CD86
CD28
CTLA-4
SHP-2
PP2A
B7-H1(PD-L1)
B7-DC(PD-L2)
PD-1
SHP-2
Galectin9
TIM3
PI3K
Fyn
HVEM
BTLA
SHP-1/2
CD160
unknown
PVR(CD155)
PVRL2(CD112)
DNAM1(CD226)
TIGIT
SHP-1
CD48
2B4(CD244)
SHP-1/2
SAP
ATP/ADP
AMP
Adenosine
CD39(ectonucleotidase)
CD73(ectonucleotidase)

図1 近年着目されているcoinhibitory(Immune checkpoint) molecule

メラノーマに対する治療薬として既に承認されている CTLA4 抗体、PD1 抗体に加え、LAG3 抗体も様々がん種に対する臨床試験が行われている。その他にも TIM3、BTLA、CD160、TIGIT なども最近の総説で有望な

免疫チェックポイント阻害薬の標的分子として取り上げられている。

まず、健常者の末梢血 CD4 T 細胞、CD8 T 細胞に発現している免疫チェックポイント分子の解析を行った。健常者 6 名の解析を行った結果、発現している割合に個人差はあるが、いずれの提供者でも PD1、TIGIT、2B4(CD244)、CD39、CD73 は CD4 T 細胞の 5%以上に発現していた。CD160 も 3%程度ながら発現が認められた。CTLA4、LAG3、TIM3、BTLA に関しては 3%未満の非常に少数の細胞集団にのみ発現していることが示された。CD8 T 細胞に関しても CD4 T 細胞と発現している割合に違いはあるが、発現している分子は共通しており、PD1、TIGIT、2B4(CD244)、CD39、CD73 が CD8 T 細胞の 5%以上に発現していた。特に 2B4 (CD244)と CD73 は、CD4 T 細胞と比較して CD8 T 細胞に高い割合で発現していることが示された。CD160 も 3-5%程度の発現が認められ、CTLA4、LAG3、TIM3、BTLA に関しては CD4 T 細胞と同様に極少数の細胞集団にのみ発現していることが示された(昨年度報告書参照)。

2) CD26 共刺激によって特徴的に発現が増強する免疫チェックポイント分子の解析

免疫応答を負に制御する免疫チェックポイント分子は、慢性的な免疫応答の持続を制御するために生体内に本来備わっている機構であり、抗原感作されて活性化した T 細胞に発現が誘導されることが多い。そこでまず、健常者の末梢血 CD4 T 細胞、CD8 T 細胞に in vitro で T cell receptor (TCR)刺激をした後の各種免疫チェックポイント分子の発現を解析した。健常者 6 名の解析を行った結果、活性化刺激によって誘導される割合に個人差はあるが、いずれの提供者でも CTLA4、PD1、LAG3、TIM3、BTLA では、代表的な T 細胞活性化刺激である CD28 共刺激、CD26 共刺激ともに刺激強度依存的なの発現上昇が認められた。中でも CD4 T 細胞の BTLA と LAG3、CD8 T 細胞の BTLA は CD28 共刺激と比較して CD26 共刺激によって顕著に発現が増強することが示された(昨年度報告書、図 3 参照)。TIGIT は TCR 刺激によって発現強度の上昇が見られるが、CD26 や CD28 の刺激強度依存的な発現上昇は認められなかった。CD39 と CD160 は共刺激によってわずかな発現上昇が認められた。一方、CD8 T 細胞に刺激前から高い割合で発現している 2B4(CD244)と CD73 に関しては、CD28 共刺激、CD26 共刺激によって発現が低下した。

がん細胞の周囲に浸潤した T 細胞では各種免疫チェックポイント分子の発現が上昇していることが報告されている。がん微小環境では、がん細胞の影響によって抑制性のフェノタイプを獲得した制御性 T 細胞や骨髄由来免疫抑制細胞、またがん細胞自身が産生する TGF-βや IL-10 といった代表的な免疫抑制性サイトカインに加え、シクロオキシゲナーゼ(COX)によって産生されるプロスタグランジン、インドールアミン-2,3-ジオキシゲナーゼ(IDO)によって産生されるキヌレニンとトリプトファンの枯渇、CD39/CD73 を介して ATP/ADP から産生されるアデノシン、PD-L1 の発現上昇にともなう PD-1 シグナルの増強など、様々な免疫抑制シグナルが増加していることが考えられる。そこで、それらがん細胞周囲に多く存在すると考えられる免疫抑制性因子が免疫

チェックポイント分子の発現に与える影響を解析した。健常者の末梢血 CD8 T 細胞をTCR 刺激がない状態でTGF-β、IL-10、PGE_2、L-Kynurenine、Adenosine、PDL1-Ig と培養した結果、各種免疫チェックポイント分子の発現に大きな変化は認められなかった(図 2)。一方、CD28 共刺激条件下では様々な因子で発現の変化が見られ、中でも特徴的な変化として、TGF-βによる PD1 の発現増強、PGE_2、L-Kynurenine、Adenosine による TIM3 の発現増強、PGE_2 による 2B4(CD244)と CD39 の発現増強が顕著であった(図 2)。それらの因子の CD26 の発現への影響も解析したところ、興味深いことに PGE_2、L-Kynurenine、Adenosine によって CD26 の発現も顕著に増強することが示唆された(図 2)。BTLA、CTLA4、LAG3、TIGIT、CD160、CD73 の発現に対しては大きな変化は認められなかった(データ未掲載)。CD26 共刺激条件下では、TGF-βによる PD1 の顕著な発現増強は CD28 共刺激と同様に認められたが、免疫抑制性因子による T 細胞の活性化自体の抑制作用が CD28 共刺激条件下よりも全般的に強く見られ、TIM3 や 2B4(CD244)、CD39、CD26 の発現増強に関しては今回の条件では認められなかった(図 2)。

これらの結果から、がん細胞周囲の環境では、PD1 や TIM3、2B4(CD244)、CD39 など様々な免疫チェックポイント分子の発現が増強し得ることが示唆された。また、それらの免疫抑制性因子は CD26 の発現増強にも作用することが示唆され、このことからがん細胞周囲では CD26 シグナルが増強している可能性が考えられる。今回検討した様々な免疫抑制性因子では BTLA の発現増強は見られなかったが、強い CD26 シグナルが伝達すると CD4 T 細胞、CD8 T 細胞ともに BTLA の発現が顕著に増強することを明らかにしており(図 2)、BTLA の発現誘導は CD26 共刺激に特異的なシグナルである可能性が考えられる。

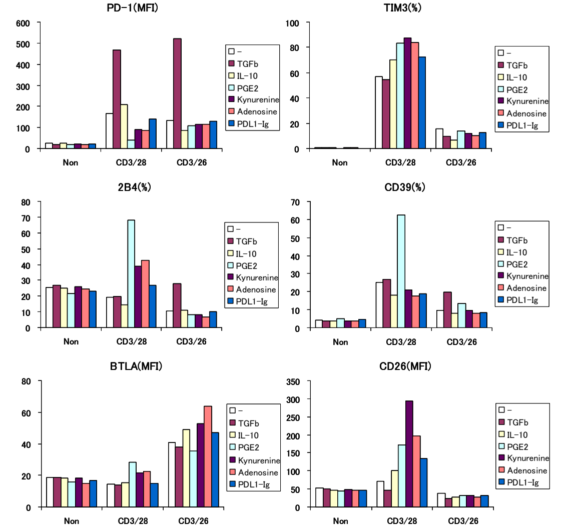

図2　がん細胞周囲に存在する免疫抑制性因子は様々な免疫チェックポイント分子に加え、CD26の発現も増強させることが示唆される

3) ヒト化 CD26 抗体の免疫チェックポイント阻害薬としての新たな可能性

これまでの健常者の末梢血 T 細胞を用いた検討により、われわれは強い CD26 共刺激シグナルが伝達することで誘導される特徴的な免疫チェックポイント分子ならびに抑制性サイトカインとして、CD4 T 細胞の BTLA、LAG3、IL-10、CD8 T 細胞の BTLA を明らかにした(図 3)。

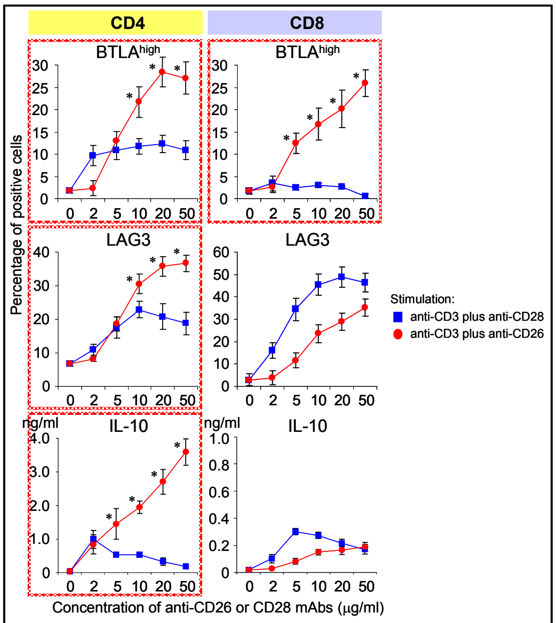

図3　CD26共刺激によるBTLA, LAG3, IL-10の発現誘導

CD26 の細胞内ドメインには ITIM や ITSM のような既存のシグナル伝達タンパク結合配列は存在しない。そのため、従来の免疫チェックポイント阻害薬は、PD1 に代表される T 細胞に直接抑制性シグナルを伝達する分子とリガンドとの結合をブロックすることで免疫応答を活性化させるが、ヒト化 CD26 抗体の場合は、CD26 とリガンド caveolin-1 との結合をブロックすることで、直接抑制性シグナルの伝達を阻害するのではなく、CD26 シグナルによる BTLA や LAG3、IL-10 の発現誘導を阻害し、それにより免疫応答を活性化させる、すなわち免疫チェックポイント阻害薬として機能する可能性が考えられる(図 4)。

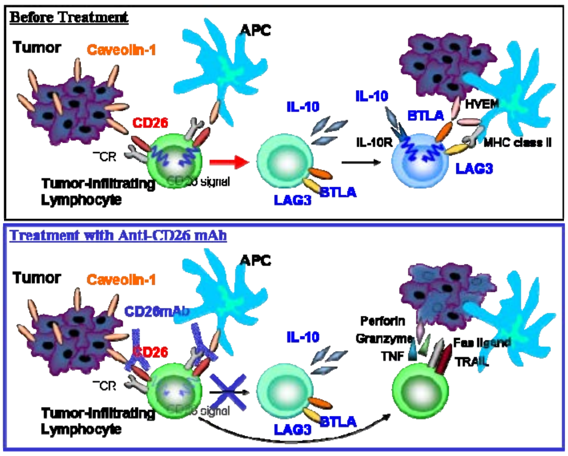
Before Treatment
Tumor
Caveolin-1
APC
CD26
TCR
Tumor-infiltrating Lymphocyte
CD26 signal
IL-10
IL-10R
BTLA
HVEM
MHC class II
LAG3
Treatment with Anti-CD26 mAb
CD26mAb
Perforin
Granzyme
TNF
Fas ligand
TRAIL

図4　ヒト化CD26抗体はCD26共刺激シグナルによる IL-10, BTLA, LAG3の発現誘導をブロックする可能性が考えられる

免疫チェックポイント阻害薬が、腫瘍免疫の活性化に働くことを直接証明するためには、NY-ESO-1 のようながん抗原が陽性の患者を選択し、腫瘍細胞塊に浸潤した T 細胞の中で、MHC テトラマーが結合するがん抗原特異的な T 細胞の機能解析がなされている。しかしながら、メラノーマのようによく研究されているがんと異なり、悪性中皮腫ではがん抗原が解明されていないうえに、腫瘍細胞塊の入手、また、研究に足る細胞数の確保など研究遂行が困難な要素が多い。

そこで、悪性中皮腫患者に対するヒト化 CD26 抗体の臨床試験検体を用いて、がん細胞に特異的な T 細胞に特化しての解析ではないが、抗体投与による血清中の IL-10 濃度の変動や、末梢血 T 細胞の BTLA や LAG3 の発現の変動を経時的に解析することを計画している。予備検討として、フランスでの第 I 相臨床試験において、ヒト化 CD26 抗体の治療効果が見られた SD 持続症例 2 例と、治療効果が認められなかった PD 症例 2 例の CD26 抗体 3 回目投与前 Day29 時点での血清中 IL-10 濃度ならびに健常者 7 名の血清中 IL-10 濃度を ELISA で測定した結果、健

常者ではいずれも検出限界 15.6 pg/ml 未満だったのに対し、悪性中皮腫(MPM)患者の PD 症例では 2 名とも血清中 IL-10 濃度が 50 pg/ml 以上の高値を示した(図 5)。一方で、SD 持続症例では 2 名とも健常者と同様に検出限界 15.6 pg/ml 未満の低値であった(図 5)。このことから、まだ少数例での検討ながら、悪性中皮腫患者では健常者と比較して血清中 IL-10 濃度が上昇しており、CD26 抗体による治療効果がよく見られる症例では IL-10 濃度が低下している可能性が考えられる。今後、国内での第 I/II 相臨床試験検体を用いて、より多くの検体数でかつ投与前からの経時的な変動を解析する予定である。

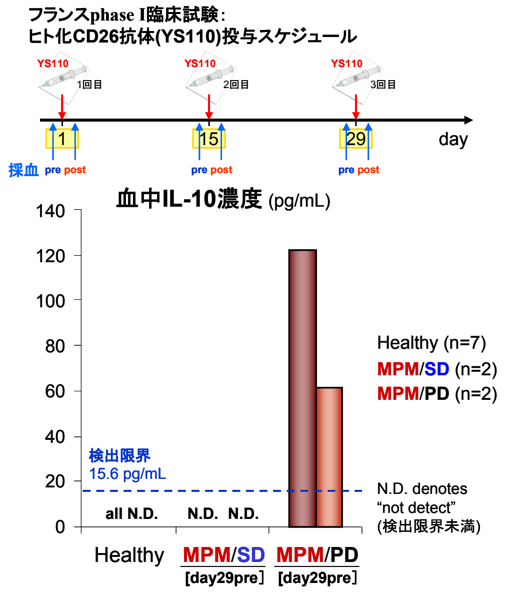

図5 ヒト化CD26抗体投与により悪性中皮腫患者の IL-10産生が抑制される可能性が示唆される

また、悪性中皮腫患者の腫瘍細胞塊と比較すると胸水の方が入手しやすく、また量も多く得やすい。そこで、末梢血よりも悪性中皮腫の影響をより受けていることが予想される胸水中 T 細胞の免疫チェックポイント分子の発現、エフェクター分子の発現、CD26 の発現に特に着目して解析を行っている。こちらもまだ、悪性中皮腫患者 2 例、良性石綿胸水患者 1 例の少数例での検討結果だが、悪性中皮腫患者の胸水中 CD4 T 細胞、CD8 T 細胞ともに健常者の末梢血 T 細胞、悪性中皮腫患者の末梢血 T 細胞、良性石綿胸水患者の末梢血 T 細胞、胸水中 T 細胞と比較して BTLA の発現が高いことが示唆された(図 6)。今後、より検体数を増やして胸水 T 細胞に特徴的な免疫チェックポイント分子の発現パターンや CD26 の発現、T 細胞のサブセット解析を進め、悪性中皮腫の影響を受けた T 細胞の特性を解明する予定である。

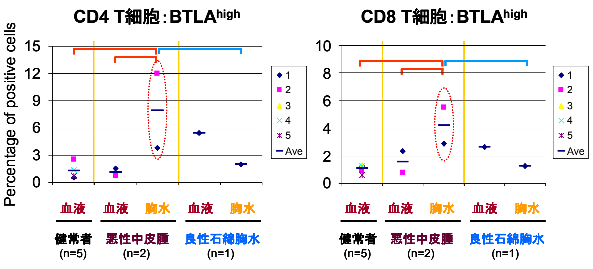

図6 悪性中皮腫患者の胸水中CD4 T細胞とCD8 T細胞は ともにBTLAの発現が上昇している可能性が示唆される

CD26 共刺激は CD4 T 細胞に対して BTLA と LAG3 の高発現、IL-10 の高産生を誘導し、CD8 T 細胞に対しても CD28 共刺激と比較して BTLA の発現を顕著に誘導することから、ヒト化 CD26 抗体がそれら抑制性分子の発現誘導を阻害する免疫チェックポイント阻害薬としても機能する可能性が考えられる。

D. 考察

ヒト化 CD26 抗体の抗腫瘍作用メカニズムの更なる解明を目的として、CD26 抗体の免疫系への影響、特に新たながん治療法として近年非常に注目されている免疫チェックポイント阻害薬としても機能する可能性について昨年度に引き続き検討している。

免疫チェックポイント分子の多くが、その細胞内ドメインにSHP-1/2をはじめとしたフォスファターゼが会合し、T細胞受容体からのシグナル伝達(キナーゼカスケード)を阻害することでT細胞の活性化を負に制御する。CD26の細胞内ドメインはわずか6アミノ酸で構成されており、フォスファターゼが会合することが知られているITIMやITSMと呼ばれる既存の配列は存在しない。このことから、CD26分子の細胞内ドメインを介して直接抑制性のシグナルが伝達する可能性は低いと考えられる。そのため、CD26分子を介して直接抑制性シグナルが伝達するのではなく、CD26シグナルによって抑制機能を有する免疫チェックポイント分子を誘導し、それらを介して免疫応答を負に制御する、すなわち免疫チェックポイント分子として機能する可能性を検討している。これまでの結果から、CD26共刺激はCD4 T細胞に対してBTLAとLAG3の高発現、IL-10の高産生を誘導し、CD8 T細胞に対してもCD28共刺激と比較してBTLAの発現を顕著に誘導することが示された。また、がん細胞周囲に多く存在すると考えられる免疫抑制性因子のうち、TGF-βはPD1の、PGE_2、L-Kynurenine、AdenosineはTIM3の、PGE_2は2B4 (CD244)とCD39の発現を顕著に増強させることが示された。興味深いことに、PGE_2、L-Kynurenine、AdenosineはCD26の発現も顕著に増強することが示唆され、がん細胞周囲に浸潤したT細胞はCD26の発現が増強している可能性が考えられる。

ヒト化CD26抗体が免疫チェックポイント阻害薬としても機能して、腫瘍免疫を増強させることを直接的に証明するためには、がん抗原特異的なT細胞のエフェクター機能の解析が望まれるが、メラノーマのようによく研究されているがんとは異なり、悪性中皮腫ではがん抗原が特定されていないうえ、腫瘍細胞塊の入手も難しいなど研究の遂行が難しい要素が多い。そこで、がん細胞に特異的なT細胞に特化しての解析ではないが、平成29年春から予定しているヒト化CD26抗体の国内第I/II相臨床試験で、ヒト化CD26抗体を投与した後の末梢血T細胞のエフェクター機能、IL-10産生能、チェックポイント分子の発現変化についても、特にBTLAとLAG3に着目して解析を行う予定である。また、悪性中皮腫患者における免疫チェックポイント分子の発現パターンを末梢血T細胞、胸水中T細胞、悪性中皮腫周囲に浸潤したT細胞を用いて解析する。

われわれは強いCD26共刺激シグナルによってCD4 T細胞のIL-10高産生が誘導されるメカニズムの一端として、CD26共刺激ではCD28共刺激よりもNFATシグナルが強く、またERK1/2シグナルが強度はCD28刺激よりも弱いながら長時間持続することを示した(J Immunol. 2015)。また、CD26共刺激により転写因子EGR2の発現が強く誘導され、IL-10産生やLAG3発現に関与していることが示唆された。今後、IL-10産生やLAG3発現の誘導に関わるシグナル伝達経路の更なる解明とともに、BTLAの発現を誘導するシグナル伝達経路、及び転写因子についての解析が必要となる。それらの抑制性因子の発現を特異的に制御するシグナル伝達経路を明らかにできれば、そのシグナルを阻害する低分子化合物を抗体に代わる免疫チェックポイント阻害薬として応用できる可能性も期待できる。

これらの研究により、悪性中皮腫の影響を受けたT細胞の特性を明らかにするとともに、CD26抗体が免疫チェックポント阻害薬としても機能しているかを明らかにする。また、血清中のIL-10濃度や末梢血T細胞のBTLA、LAG3の発現の経時的なモニタリングが、ヒト化CD26抗体の治療有効性を予測するバイオマーカーになりうる可能性も考えられるため、その点にも着目して解析を行う。

E. 結論

CD26共刺激は健常者の末梢血CD4 T細胞に対してBTLAとLAG3の高発現、IL-10の高産生を誘導し、CD8 T細胞に対してもCD28共刺激と比較してBTLAの発現を顕著に誘導する。がん細胞の周囲に多く存在すると考えられる免疫抑制性因子は様々な免疫チェックポイント分子の発現とともに、CD26の発現も増強させることが示唆された。特にBTLAの発現誘導に関しては、CD26共刺激に特徴的であることが示唆された。

F. 次年度以降の計画

悪性中皮腫自身やその周囲の細胞にBTLAやLAG3、そのリガンドであるHVEMやMHC class IIが発現しているか免疫組織染色で検討する。また、CD26共刺激に特徴的なBTLAの発現誘導に関わるシグナル伝達経路、及び転写因子についての解析が必要となる。さらに、本年度に引き続き、悪性中皮腫患者の末梢血T細胞、胸水T細胞、悪性中皮腫周囲に浸潤したT細胞を用いて、各種免疫チェックポイント分子の発現パターンやエフェクター分子、CD26の発現を解析するとともに、CD26抗体の国内第I/II相臨床試験検体を用いて、CD26抗体投与による血清中IL-10濃度、末梢血T細胞上のBTLA、LAG3の発現変動を経時的にモニタリングしていく予定である。

G. 研究発表

1. 論文発表

1) Angevin E, Isambert N, Trillet-Lenoir V, You B, Alexandre J, Zalcman G, Vielh P, Farace F, Valleix F, Podoll T, Kuramochi Y, Miyashita I, Hosono O, Dang NH, Ohnuma K, Yamada T, Kaneko Y, Morimoto C.
First-in-Human phase 1 of YS110, a monoclonal antibody directed against CD26 in advanced CD26-expressing cancers. Br.J. Cancer. in press
2) Komiya E, Hatano R, Otsuka H, Itoh T, Yamazaki H, Yamada T, Dang NH, Tominaga M, Suga Y, Kimura U, Takamori K, Morimoto C, Ohnuma K.A possible role for CD26/DPPIV enzyme activity in the regulation of psoriatic pruritus.J Dermatol Sci. in press
3) Nomura S, Iwata S, Hatano R, Komiya E, Dang NH, Iwao N, Ohnuma K, MorimotoC. Inhibition of VEGF-dependent angiogenesis by the anti-CD82 monoclonal antibody 4F9 through regulation of lipid raft microdomains. Biochem Biophys Res Commun.2016;20:111-7
4) Hayashi M, Madokoro H, Yamada K, Nishida H, Morimoto C, Sakamoto M,

Yamada T. A humanized anti-CD26 monoclonal antibody inhibits cell growth of malignant mesothelioma via retarded G2/M cell cycle transition. Cancer Cell Int.2016;30:16-35

5) Omata Y, Nakamura S ,Koyama T, Yasui T, Hirose J, Izawa N, Matsumoto T, Imai Y, Seo S, Kurokawa M, Tsutsumi S, Kadono Y, Morimoto C, Aburatani H, Miyamoto T, Tanaka S. Identification of Nedd9 as a TGF-β-Smad2/3 Target Gene Involved in RANKL-induced Osteoclastogenesis by Comprehensive Analysis.PLos One. 2016 ;11:e0157992

6) Mizutani N, Abe M, Matsuoka S, Kajino K, Wakiya M, Ohtsuji N, Hatano R, Morimoto C, Hino O. Establishment of anti-mesothelioma monoclonal antibodies. BMC Res Notes. 2016;9:324

7) Ikeda T, Fragiadaki M,Shi-wen Xu, Ponticos M, Khan K, Denton C, Garcia P, Bou-Gharios G, Yamakawa A, Morimoto C, Abraham D.Transforming growth factor-β-induced CUX1 isoforms are associated with fibrosis in systemic sclerosis lung fibroblasts. Biochemistry and Biophysics Reports 7. 2016: 246-252

8) Ohnuma K, Hatano R, Itoh T, Iwao N, Dang NH, Morimoto C. Role of IL-26+CD26+CD4 T Cells in Pulmonary chronic graft-versus-host disease and treatment with Caveolin-1-Ｉg Fc conjugate. Crit Rev Immunol. 2016;36:239-267

9) 森本幾夫. 臨床リウマチ医のための基礎講座 CD26 分子に基づくトランスレーショナルリサーチ. 臨床リウマチ. 2016;28:91-4

10) 森本幾夫、大沼圭. CD26 分子に基づく悪性中皮腫への新治療法開発. 癌と化学療法 2016;43:855-62

11) 大沼圭、森本幾夫. 標的別分子標的薬６）モノクローナル抗体、腎臓内科、2016;4:52-60

2. 著書

1) Ohnuma K, Hatano R, Yamazaki H, KanekoY, Dang NH, Morimoto C. CD-26 targeted Therapy :A New Horizon in Malignant Pleural Mesothelioma Management, Horizons in Cancer Research,2016, Nova Science Publishers,Inc.

3. 学会発表

1) 森本幾夫,CD26 の機能と治療応用.中皮腫シンポジウム,2016 年 10 月 29 日,兵庫

2) 波多野良、大沼圭、石井智徳、岩田哲史、奥村康、関川巌、森本幾夫. CD26 陽性 T 細胞サブセットに基づく全身性エリテマトーデスの病態解析. 第 60 回日本リウマチ学会、横浜(会場：パシフィコ横浜)、2016 年 4 月 21-23 日

3) 古宮 栄利子, 波多野 良, 大塚 春奈, 伊藤 匠, 山田 健人, 冨永 光俊, 高森

建二, 大沼 圭, 森本 幾夫: 乾癬において CD26/DPPIV は substance P の切断を促進してかゆみを調節する 第 31 回日本乾癬学会学術大会, ホテル東日本宇都宮, 2016 年 9 月 2-3 日

4) Eriko Komiya, Ryo Hatano, Haruna Otsuka, Takumi Itoh, Taketo Yamada, Mitsutoshi Tominag, Kenji Takamori, Kei Ohnuma, Chikao Morimoto: CD26/DPPIV-mediated regulation of pruritus in psoriasis. 研究皮膚科学会第 41 回年次学術大会・総会, 仙台国際会議場, 2016 年 11 月 9-11 日

H. 知的財産権の出願・登録状況（予定を含む）

1. 特許取得
   なし
2. 実用新案登録
   なし
3. その他
   なし

労災疾病臨床研究事業費補助金
分担研究報告書

中皮腫治療におけるCD26の役割：
可溶性CD26/DPPⅣは治療奏効性判定のバイオマーカーか

研究代表者　森本　幾夫　順天堂大学大学院医学研究科
免疫病・がん先端治療学講座　客員教授

研究協力者　大沼　　圭　順天堂大学大学院医学研究科
免疫病・がん先端治療学講座　准教授

研究協力者　金子　有太郎　Y's AC株式会社

研究要旨

悪性胸膜中皮腫はアスベストばく露によっておこる胸膜中皮由来の難治性悪性腫瘍であり、現時点で満足できる治療法はなく、新たな治療法の確立が望まれる。

我々は新規治療標的分子としてCD26分子に着目し、ヒト化CD26抗体を開発しフランスにてFirst in Man第1相臨床試験を化学療法抵抗性悪性中皮腫及びその他CD26陽性悪性腫瘍をターゲットに行ない、安全性が確認された。患者総計33例でヒト化CD26抗体投与1ヶ月後2週間後にmodified RECIST評価により13例がProgressive disease(PD)、13例がStabilized disease(SD)、7例が評価出来ずであった。

特に悪性中皮腫症例においては評価可能例の19例中10例がSDと評価され、5例が6ヶ月以上、1例が3ヶ月以上SDが継続し、有効性を示唆するデータが得られた。

ヒト化CD26抗体投与患者において血清中の可溶性CD26/DPPⅣ酵素値を測定したところ、ヒト化CD26抗体の投与量が増加するにつれて可溶性CD26/DPPⅣ値が低下する傾向にあった。PD、SD患者を識別できるバイオマーカーは存在しないかということでヒト化CD26抗体（YS110）投与後の患者血清中の可溶性CD26/DPPⅣ酵素値に注目して解析した。

その結果SD患者はPD患者と比べて可溶性CD26/DPPⅣ酵素値ともに特にDay29ヒト化CD26抗体投与前において有意に低値（可溶性CD26：$P=0.016$、DPPⅣ値：$P=0.0267$）（Wilcoxon sum test）であった。これらの結果から血清可溶性CD26/DPPⅣ酵素値はヒト化CD26抗体投与によるPD及びSDを予測するバイオマーカーとなる可能性が示唆された。

A. 研究目的

悪性胸膜中皮腫はアスベストばく露によって起こる胸膜中皮由来の難治性悪性腫瘍である。アスベストばく露から発症までの潜伏期間は 30-50 年とされ、日本を含めアジアやヨーロッパなど世界規模で胸膜中皮腫患者数は今後ますます増加すると考えられている。悪性胸膜中皮腫に対しては手術療法、化学療法、放射線療法などが行われるが、いずれも満足できる治療成績ではなく、新たな治療法の確立が望まれる。われわれは、新規治療標的分子として悪性胸膜中皮腫細胞に発現する CD26 に着目し、ヒト化 CD26 抗体を開発しフランスにて First in Man 第 I 相臨床試験を化学療法抵抗性悪性中皮腫及びその他 CD26 陽性悪性腫瘍をターゲットに施行した。特記すべき副作用もなく安全性も確認された。

総計 33 例で 22 例が悪性中皮腫、10 例が腎癌及び 1 例が尿路上皮癌で、1 ヶ月投与後 2 週間後に modified RECIST 評価により、13 例が Progressive disease(PD), 13 例が Stabilized disease(SD), 7 例が評価出来ずであった。

抗がん剤抵抗性の悪性中皮腫症例の評価可能例の 19 例中 10 例が SD と評価され、5 例が 6 ヶ月以上、1 例が 3 ヶ月以上 SD が継続し、有効性を示唆するデータが得られた。

可溶性 CD26 は DPPⅣ酵素活性を含み、血清及び胸水中に存在する。現在糖尿病治療薬として DPPⅣ酵素阻害薬が広く用いられているがヒト化 CD26 抗体投与では血清中の可溶性 CD26 値及び DPPⅣ酵素値が下がる可能性があり治療経過でモニターしていくことは抗体療法が安全に行われるために必須である。フランスの第 1 相臨床試験においてヒト化 CD26 抗体投与の全患者検体について血清中の可溶性 CD26／DPPⅣ酵素値を測定したところヒト化 CD26 抗体の投与量が増加するにつれて可溶性 CD26/DPPⅣ値が低下する傾向にあった。今まで我々は血清中の可溶性 CD26/DPPⅣ値は全身性エリテマトーデス（SLE）の活動性や HIV RNA ウィルス値と相関関係を示しバイオマーカーとなる可能性を報告した。（Kobayashi H, Morimoto C et al. 2002;29:1858, Hosono O, Morimoto C et al. Clin Immunol. 1999;91:283）

そこで PD、SD を識別できるバイオマーカーは存在しないかということでヒト化 CD26 抗体（YS110）投与後の患者血清中の可溶性 CD26 及び DPPⅣ酵素値に注目して解析した。

B. 研究方法

1)患者検体

フランスで実施されたヒト化 CD26 抗体投与の第 1 相臨床試験における対象症例において Day1 から Day29 までの可溶性 CD26/DPPⅣ値がすべて揃っている 23 症例について解析した。

2)可溶性 CD26/DPPⅣ酵素活性値の測定

可溶性 CD26/DPPⅣ値の測定は順天堂大学の森本研究室で行った。この測定において開発したサンドウィッチ ELISA 法は治療抗体のヒト化 CD26 抗体とはクロス反応は示さない(Ohnuma et al. Comparison of two commercial ELISAs against an in-house ELISA for measuring soluble CD26 in human serum. J Clin Lab Anal. 2015;29:106)

（倫理面への配慮）

本研究の、特に臨床研究においては、文書により被験患者本人の同意を得た上で行うものとする。本研究にまつわる個人情報は厳重な管理のもと守秘義務を遵守する。また解析検討結果を公表する際には個人名の漏えい防止を徹底し、プライバシーの保護に努める。さらに個人に帰属する結果を個人に求められた場合には、その個人本人のもののみ伝達する旨である。

なお、フランスで実施されたヒト化 CD26 抗体投与の第 1 相臨床試験における対象症例血清中の可溶性 CD26 及び DPPIV 酵素活性の測定及びコントロール症例の可溶性 CD26 及び DPPIV 酵素活性の測定については順天堂大学倫理審査委員会の審査にて承認されている（順天医倫第 2012076 及び 2012087）。

試料を匿名化することで個人のプライバシーが漏れることのないように配慮した。

C．研究結果

1）フランスの第 1 相臨床試験の患者検体について

フランスの臨床検体においてヒト化 CD26 抗体投与後の可溶性 CD26/DPPIV値が Day1 投与前、Day1 投与後、Day15 投与前、Day15 投与後、Day29 投与前、Day29 投与後とすべて揃っている 23 症例について、6ヶ月以上 Progression Free Survival(PFS)の患者 7 例、これを longSD とする。またそれ以下の PFS　5 例を shortSD とし、さらに PD11 例について検討した。表 1 にこれらの患者のヒト化 CD26 投与量、投与間隔(毎週または隔週)、PFS(days)及び CD26 の腫瘍組織の染色パーセントを示した。更にこれらの患者のヒト化 CD26 抗体量、Day1、Day15、Day29 におけるヒト化 CD26 抗体投与前、投与後における血清中の可溶性 CD26 値を表 2 に示した。（血清 DPPIV値についてはスペースのため省略するが可溶性 CD26 値と同様の動きを示した）。

表 1

SD 及び PD 患者のヒト化 CD26 抗体投与量、投与間隔、PFS について

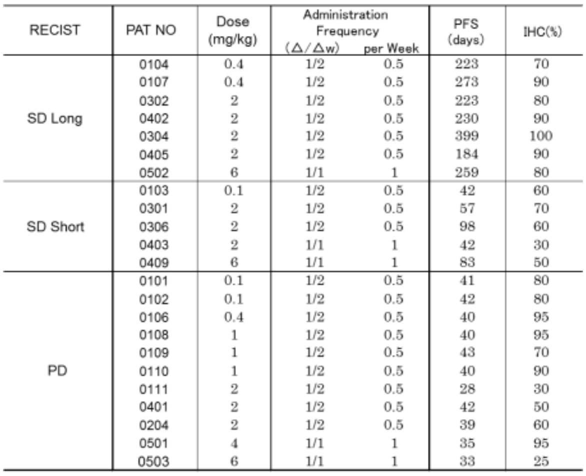

RECIST	PAT NO	Dose (mg/kg)	Administration Frequency (△/△w)	per Week	PFS (days)	IHC(%)
SD Long	0104	0.4	1/2	0.5	223	70
	0107	0.4	1/2	0.5	273	90
	0302	2	1/2	0.5	223	80
	0402	2	1/2	0.5	230	90
	0304	2	1/2	0.5	399	100
	0405	2	1/2	0.5	184	90
	0502	6	1/1	1	259	80
SD Short	0103	0.1	1/2	0.5	42	60
	0301	2	1/2	0.5	57	70
	0306	2	1/2	0.5	98	60
	0403	2	1/1	1	42	30
	0409	6	1/1	1	83	50
PD	0101	0.1	1/2	0.5	41	80
	0102	0.1	1/2	0.5	42	80
	0106	0.4	1/2	0.5	40	95
	0108	1	1/2	0.5	40	95
	0109	1	1/2	0.5	43	70
	0110	1	1/2	0.5	40	90
	0111	2	1/2	0.5	28	30
	0401	2	1/2	0.5	42	50
	0204	2	1/2	0.5	39	60
	0501	4	1/1	1	35	95
	0503	6	1/1	1	33	25

表 2

L-SD 及び PD 患者の血清中 sCD26（ng/ml）

RECIST	PAT NO	Dose (mg/kg)	Day 1		Day 15		Day 29	
			Pre	Post	Pre	Post	Pre	Post
SD Long	0104	0.4	1089.22	327.88	997.67	366.85	327.88	102.51
	0107	0.4	730.67	222.14	616.00	191.38	255.30	43.75
	0302	2	685.00	330.43	423.25	300.56	318.13	196.61
	0402	2	1281.88	499.32	557.84	329.45	482.85	233.43
	0304	2	1246.44	585.04	670.43	447.97	522.54	149.69
	0405	2	759.19	230.88	149.26	71.95	113.28	82.29
	0502	6	1027.35	578.24	285.60	287.10	302.85	261.87
SD Short	0103	0.1	1227.59	406.36	1185.47	377.82	963.48	303.28
	0301	2	396.80	186.45	258.26	203.89	136.75	83.00
	0306	2	1139.26	596.15	454.91	219.73	390.11	288.33
	0403	2	1348.38	758.28	250.70	275.65	227.26	234.84
	0409	6	712.12	349.81	121.88	110.19	140.64	144.18
PD	0101	0.1	1007.19	281.23	894.04	256.55	870.07	237.90
	0102	0.1	1313.63	436.45	1082.35	342.77	812.57	255.92
	0106	0.4	1529.37	494.81	1094.18	457.99	878.23	334.75
	0108	1	661.47	209.96	741.49	334.40	727.28	267.68
	0109	1	997.84	410.43	418.61	347.86	753.60	398.10
	0110	1	876.91	318.42	656.25	285.51	589.05	288.52
	0111	2	960.14	384.98	619.27	338.66	476.93	228.04
	0401	2	715.40	325.69	390.18	234.23	394.90	171.15
	0204	2	832.10	368.26	363.75	190.55	331.78	169.02
	0501	4	830.83	385.37	317.71	288.19	215.84	191.20
	0503	6	721.08	352.52	199.01	164.04	177.21	161.56

2）ヒト化 CD26 抗体投与前後の血清可溶性 CD26 値の動きについて

ヒト化 CD26 抗体投与前後の Day1、Day15、Day29 における longSD,　shortSD, PD 患者の可溶性 CD26 値の変化を検討した。図 1 に示すように Day1、Day15、Day29 においていずれも投与後可溶性 CD26 値は低下し、その後再び上昇し、再投与により再度可溶性 CD26 は低下した。PD 患者に注目すると SD 患者と比較すると特にヒト化 CD26 抗体投与前で可溶性 CD26 値の低下がそれほどでもないことが明らかとなった。またヒト化 CD26 抗体の Day1 投与前の可溶性 CD26 値のスコアを 100 としてヒト化 CD26 抗体投与後の前投与時の可溶性 CD26 値の推移を検討した。図 2 に示すように SD12 例、PD11 例に分けて可溶性 CD26 値について、特に投与前 Day29 では PD 患者は SD 患者と比して可溶性 CD26 値は有意に高いことが明らかとなった（Wilcoxon rank sum test P=0.016)。同様に Day1 抗体投与前の DPPⅣ酵素活性値のスコアーを 100 とした DPPⅣ値の推移を検討した。図 3 に示すように DPPⅣ酵素活性に関しても PD 及び SD 患者の間で有意差があることが明らかとなった（Wilcoxon rank sum test P=0.0267）。本研究から血清中の可溶性 CD26／DPPⅣ値はヒト化 CD26 抗体投与による PD 及び SD を識別するバイオマーカーとなる可能性が示唆された。

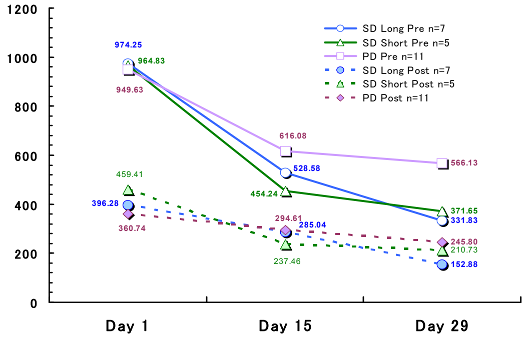

図 1

Long SD, short SD, PD 患者のヒト化 CD26 抗体投与前、投与後の血清可溶性 CD26 値の推移

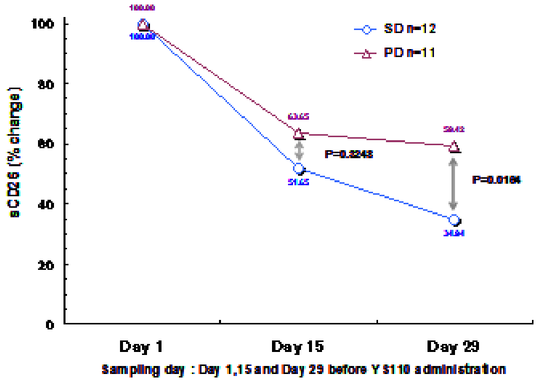

Association of the clinical response to YS110 with serum sCD26 levels at pre-dosing of YS110 on Day 1,Day 15 and Day 29
P value: Wilcoxon Rank sum Test

図 2

血清中可溶性 CD26 値(Day1 Pre のスコアを 100 とした Day15 Pre、Day29 Pre の推移)

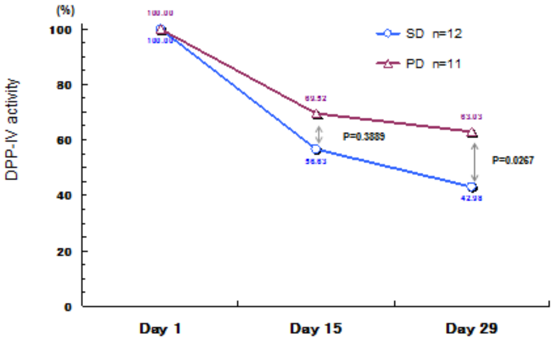

P:by Wilcoxon rank sum test

図 3

血清中 DPPIV 値(Day1 Pre のスコアを 100 とした Day15 Pre、Day29 Pre の推移)

D. 考察

フランスにてヒト化 CD26 抗体の First in Man 第 1 相臨床試験を化学療法抵抗性悪性中皮腫及びその他 CD26 陽性悪性腫瘍をターゲットに施行した。特記すべき副作用もなく安全性も確認された。統計 33 例で 1 ヶ月投与後 2 週間後に modified RECIST 評価により 13 例が Progressive disease(PD)、13 例が Stabilized disease(SD)、7 例が評価出来ずであった。

更に悪性中皮腫症例においては評価可能例の 19 例中 10 例が SD と評価され、5 例が 6 ヶ月以上、1 例が 3 ヶ月以上継続し、有効性を示唆するデータも得ることが出来た。

フランスの臨床試験において患者血清中の可溶性 CD26/DPPⅣ酵素値がヒト化 CD26 抗体投与で低下していく傾向にあり、今まで SLE や HIV においてこの値は活動性や HIV ウィルス価のバイオマーカーになる可能性を報告していることから、可溶性 CD26/DPPⅣ値に注目した。その結果血清中の可溶性 CD26/DPPⅣ値はヒト化 CD26 抗体投与による PD 及び SD を識別するバイオマーカーとなる可能性が示唆された。

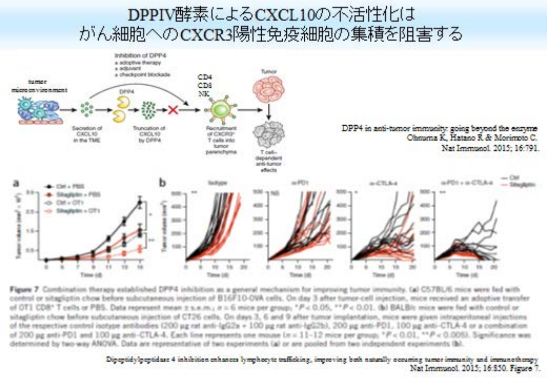
DPPIV酵素によるCXCL10の不活性化は
がん細胞へのCXCR3陽性免疫細胞の集積を阻害する

DPP4 in anti-tumor immunity: going beyond the enzyme
Ohnuma K, Hatano R & Morimoto C.
Nat Immunol. 2015; 16:791.

Figure 7 Combination therapy established DPP4 inhibition as a general mechanism for improving tumor immunity. (a) C57BL/6 mice were fed with control or sitagliptin chow before subcutaneous injection of B16F10-OVA cells. On day 3 after tumor-cell injection, mice received an adoptive transfer of OT1 CD8+ T cells or PBS. Data represent mean ± s.e.m.; n = 6 mice per group; *P < 0.05, **P < 0.01. (b) BALB/c mice were fed with control or sitagliptin chow before subcutaneous injection of CT26 cells. On days 3, 6 and 9 after tumor implantation, mice were given intraperitoneal injections of the respective control isotype antibodies (200 μg rat anti-IgG2a + 100 μg rat anti-IgG2b), 200 μg anti-PD1, 100 μg anti-CTLA-4 or a combination of 200 μg anti-PD1 and 100 μg anti-CTLA-4. Each line represents one mouse (n = 11–12 mice per group; *P < 0.01, **P < 0.005). Significance was determined by two-way ANOVA. Data are representative of two experiments (a) or are pooled from two independent experiments (b).

Dipeptidylpeptidase 4 inhibition enhances lymphocyte trafficking, improving both naturally occurring tumor immunity and immunotherapy
Nat Immunol. 2015; 16:850. Figure 7.

tumor microenvironment
Inhibition of DPP4
a adoptive therapy
a adjuvant
a checkpoint blockade
DPP4
CD4
CD8
NK
Tumor
Secretion of CXCL10 in the TME
Truncation of CXCL10 by DPP4
Recruitment of CXCR3+ T cells into tumor parenchyma
T cell-dependent anti-tumor effects
a
Ctrl + PBS
Sitagliptin + PBS
Ctrl + OT1
Sitagliptin + OT1
Time (d)
b
Isotype
α-PD1
α-CTLA-4
α-PD1 + α-CTLA-4
Ctrl
Sitagliptin
NS
Time (d)

図 4

DPPⅣ酵素による CXCL10 の不活性化はがん細胞への CXCR3 陽性免疫細胞の集積を阻害する

図 4 は我々が Nature Immunology に発表した DPPⅣ酵素と腫瘍免疫のスキームである。（Ohnuma K, Hatano R, and Morimoto C DPP Ⅳ in anti-Tumor immunity: going beyond the enzyme：Nature Immunology 16:791-792,2015）

担癌マウスに現在糖尿病治療薬として用いられているシタグリプチンをエサに混ぜて食べさすことにより DPPⅣ酵素の基質 CXCL10 の不活性化を抑制し、その結果 CXCR3 陽性 T 細胞が腫瘍組織にリクルートされ、腫瘍を破壊していくというものである。更に図 4 下段に示すように免疫チェックポイント阻害薬の CTLA-4 及び PD-1 抗体に DPPⅣ酵素阻害薬を上乗せして投与することにより、その群では他群と比較してほとんど腫瘍は縮小した。このように DPPⅣ酵素活性阻害は腫瘍免疫の促進に関与する可能性を示唆した。

フランスでの臨床検体の解析からヒト化 CD26 抗体投与 SD 患者において血清可溶性 CD26/DPP Ⅳ 酵素値が PD 患者より Day29pre 時で有意に低いことは DPPⅣ酵素活性阻害が腫瘍免疫促進に関与していることを支持する結果であった。また、PD-1/PD-L1 及び CTLA-4 抗体との併用療法なども今後検討すべき課題と思われ、ヒト化 CD26 抗体の作用機序について免疫チェックポイント阻害以外の作用機序についても今後検討すべきと思われる。

図 2、図 3 から特に PD の患者つまり Day29 でヒト化 CD26 抗体投与後 2 週間の RECIST 評価により抗体投与は PD の評価ならこの時点で終了するが、更にヒト化 CD26 抗体の投与を継続することで可溶性

CD26/DPPⅣ値が低下すればPDからSDに移行する可能性があるのかなど今後の検討課題と思われる。

ヒト化 CD26 抗体は本邦においても悪性中皮腫をターゲットにした第1相臨床試験は本年春からスタートするがその結果が期待される。

E. 結論

ヒト化 CD26 抗体の化学療法抵抗性悪性中皮腫及びその他 CD26 陽性悪性腫瘍をターゲットにしたフランスのFirst in Man第1相臨床試験において血清中の可溶性CD26/DPPⅣ酵素活性値がPD及びSDを識別できるバイオマーカーとなる可能性が示唆された。

F. 次年度以降の計画

フランスでの第1相臨床試験の解析からPD, SD の識別に血清可溶性 CD26/DPPⅣ値が有用な可能性が示唆されたことから血清DPPⅣが腫瘍免疫亢進に働いている可能性を探るためフランスの検体及び本年春からスタートする本邦第1相臨床試験患者血清中のDPPⅣ酵素の基質であるCXCL10などケモカインの切断様式につついて解析する。

G. 研究発表.

1. 論文発表

1) Angevin E, Isambert N, Trillet-Lenoir V, You B, Alexandre J, Zalcman G, Vielh P, Farace F, Valleix F, Podoll T, Kuramochi Y, Miyashita I, Hosono O, Dang NH, Ohnuma K, Yamada T, Kaneko Y, Morimoto C. First-in-Human phase 1 of YS110, a monoclonal antibody directed against CD26 in advanced CD26-expressing cancers. Br.J. Cancer. in in press

2) Komiya E, Hatano R, Otsuka H, Itoh T, Yamazaki H, Yamada T, Dang NH, Tominaga M, Suga Y, Kimura U, Takamori K, Morimoto C, Ohnuma K.A possible role for CD26/DPPIV enzyme activity in the regulation of psoriatic pruritus.J Dermatol Sci. in press

3) Nomura S, Iwata S, Hatano R, Komiya E, Dang NH, Iwao N, Ohnuma K, MorimotoC. Inhibition of VEGF-dependent angiogenesis by the anti-CD82 monoclonal antibody 4F9 through regulation of lipid raft microdomains. Biochem Biophys Res Commun.2016;20:111-7

4) Hayashi M, Madokoro H, Yamada K, Nishida H, Morimoto C, Sakamoto M, Yamada T. A humanized anti-CD26 monoclonal antibody inhibits cell growth of malignant mesothelioma via retarded G2/M cell cycle transition. Cancer Cell Int.2016;30:16-35

5) Omata Y, Nakamura S ,Koyama T, Yasui T, Hirose J, Izawa N, Matsumoto T, Imai Y, Seo S, Kurokawa M, Tsutsumi S, Kadono Y, Morimoto C, Aburatani H, Miyamoto T, Tanaka S. Identification of Nedd9 as a TGF-β-Smad2/3 Target Gene Involved in RANKL-induced Osteoclastogenesis by Comprehensive Analysis.PLos One. 2016 ;11:e0157992

6) Mizutani N, Abe M, Matsuoka S, Kajino K, Wakiya M, Ohtsuji N, Hatano R, Morimoto C, Hino O. Establishment of

anti-mesothelioma monoclonal antibodies. BMC Res Notes. 2016;9:324

7) Ikeda T, Fragiadaki M,Shi-wen Xu, Ponticos M,　Khan K,　Denton C, Garcia P,　Bou-Gharios G,　Yamakawa　A, Morimoto C,　Abraham D.Transforming growth factor-β-induced CUX1 isoforms are associated with fibrosis in systemic sclerosis lung fibroblasts. Biochemistry and Biophysics Reports 7. 2016: 246-252

8) Ohnuma K, Hatano R, Itoh T, Iwao N, Dang NH, Morimoto C. Role of IL-26+CD26+CD4 T Cells in Pulmonary chronic graft-versus-host disease and treatment with Caveolin-1-Ｉg Fc conjugate. Crit　Rev　Immunol. 2016;36:239-267

9) 森本幾夫. 臨床リウマチ医のための基礎講座 CD26分子に基づくトランスレーショナルリサーチ.　臨床リウマチ.　2016;28:91-4

10) 森本幾夫、大沼圭.　CD26分子に基づく悪性中皮腫への新治療法開発.　癌と化学療法 2016;43:855-62

11) 大沼圭、森本幾夫。標的別分子標的薬６）モノクローナル抗体、腎臓内科、2016;4:5260

2. 著書

1) Ohnuma K, Hatano R, Yamazaki H, KanekoY, Dang NH, Morimoto C. CD-26 targeted Therapy :A New Horizon in Malignant Pleural Mesothelioma Management, Horizons in Cancer Research,2016, Nova Science Publishers,Inc.

3. 学会発表

1) 森本幾夫,CD26の機能と治療応用.中皮腫シンポジウム,2016年10月29日,兵庫

2) 波多野良、大沼圭、石井智徳、岩田哲史、奥村康、関川巖、森本幾夫. CD26陽性T細胞サブセットに基づく全身性エリテマトーデスの病態解析. 第60回日本リウマチ学会、横浜(会場：パシフィコ横浜)、2016年 4月21-23日

3) 古宮　栄利子, 波多野 良, 大塚 春奈, 伊藤 匠, 山田 健人, 冨永　光俊, 高森建二, 大沼 圭, 森本 幾夫: 乾癬においてCD26/DPPIVはsubstance Pの切断を促進してかゆみを調節する 第31回日本乾癬学会学術大会, ホテル東日本宇都宮, 2016年9月2-3日

4) Eriko Komiya, Ryo Hatano, Haruna Otsuka, Takumi Itoh, Taketo Yamada, Mitsutoshi Tominag, Kenji Takamori, Kei Ohnuma, Chikao Morimoto: CD26/DPPIV-mediated regulation of pruritus in psoriasis. 研究皮膚科学会第41回年次学術大会・総会, 仙台国際会議場, 2016年11月9-11日

H. 知的財産権の出願・登録状況（予定を含む）

1. 特許取得

なし

2. 実用新案登録

なし

3. その他

なし

Ⅲ.　研究成果の刊行に関する一覧表

＜研究成果の刊行に関する一覧表＞

【書　籍】

著者氏名	論文タイトル名	書籍全体の編集者名	書　籍　名	出版社名	出版地	ページ	出版年
Ohnuma K, Hatano R, Yamazaki H, KanekoY, Dang NH, Morimoto C	CD-26 targeted Therapy : A New Horizon in Malignant Pleural Mesothelioma Management		Horizons in Cancer Research	Nova Science Publishers, Inc	USA		2016年
山田健人	核内移行するヒト化抗CD26モノクローナル抗体-TFⅡH阻害剤複合体	松村保広	抗体薬物複合体(ADC)の設計開発	シーエムシー出版	東京	94－103	2016年

【雑　誌】

発表者氏名	論文タイトル名	発表誌名	巻号	ページ	出版年
Angevin E, Isambert N, Trillet-Lenoir V, You B, Alexandre J, Zalcman G, Vielh P, Farace F, Valleix F, Podoll T, Kuramochi Y, Miyashita I, Hosono O, Dang NH, Ohnuma K, Yamada T, Kaneko Y, Morimoto C	First-in-Human phase 1 of YS110, a monoclonal antibody directed against CD26 in advanced CD26-expressing cancers.	Br.J. Cancer			In Press

発表者氏名	論文タイトル名	発表誌名	巻号	ページ	出版年
Komiya E, Hatano R, Otsuka H, Itoh T, Yamazaki H, Yamada T, Dang NH, Tominaga M, Suga Y, Kimura U, Takamori K, Morimoto C, Ohnuma K	A possible role for CD26/DPPIV enzyme activity in the regulation of psoriatic pruritus	J Dermatol Sci			In Press
Nomura S, Iwata S, Hatano R, Komiya E, Dang NH, Iwao N, Ohnuma K, Morimoto C	Inhibition of VEGF-dependent angiogenesis by the anti-CD82 monoclonal antibody 4F9 through regulation of lipid raft microdomains	Biochem Biophys Res Commun	20	111-7	2016
Hayashi M, Madokoro H, Yamada K, Nishida H, Morimoto C, Sakamoto M, Yamada T	A humanized anti-CD26 monoclonal antibody inhibits cell growth of malignant mesothelioma via retarded G2/M cell cycle transition	Cancer Cell Int	30	16-35	2016
Omata Y, Nakamura S ,Koyama T, Yasui T, Hirose J, Izawa N, Matsumoto T, Imai Y, Seo S, Kurokawa M, Tsutsumi S, Kadono Y, Morimoto C, Aburatani H, Miyamoto T, Tanaka S	Identification of Nedd9 as a TGF-ß-Smad2/3 Target Gene Involved in RANKL-induced Osteoclastogenesis by Comprehensive Analysis	PLos One	11	e0157992	2016

発表者氏名	論文タイトル名	発表誌名	巻号	ページ	出版年
Mizutani N, Abe M, Matsuoka S, Kajino K, Wakiya M, Ohtsuji N, Hatano R, Morimoto C, Hino O	Establishment of anti-mesothelioma monoclonal antibodies	BMC Res Notes	9	324	2016
Ikeda T, Fragiadaki M,Shi-wen Xu, Ponticos M,　Khan K, Denton C, Garcia P,　Bou-Gharios G, Yamakawa　A, Morimoto C, Abraham D.	Data on CUX1 isoforms in idiopathic pulmonary fibrosis lung and systemic sclerosis skin tissue sections	Biochemistry and Biophysics Reports	8	1377－80	2016
Ohnuma K, Hatano R, Itoh T, Iwao N, Dang NH, Morimoto C	Role of IL-26+CD26+CD4 T Cells in Pulmonary chronic graft-versus-host disease and treatment with Caveolin-1- I g Fc conjugate	Crit　Rev Immunol	36	163-237	2016
Hayashi M, Madokoro H, Yamada K, Nishida H,　Morimoto C, Sakamoto M, Yamada T	A humanized anti-CD26 monoclonal antibody inhibits cell growth of malignant mesothelioma via retarded G2/M cell cycle transition	Cancer Cell Int	16	35	2016
Inaishi J, Saisyo M, Sato S, Kou K, Murakami R, Watanabe Y, KitagoM, Kitagawa Y, Yamada T, Itoh H	Effects of obesity and diabetes on alpha and beta cell mass in surgically resected human pancreas	Journal of Clinical Endocrinology & Metabolism	101	2874-82	2016

発表者氏名	論文タイトル名	発表誌名	巻号	ページ	出版年
Nogami Y, Fujii-Nishimura Y, Banno K, Suzuki A, Hibi T, Murakami K, Yamada T, Sugiyama H, Morishima Y, Aoki D	Anisakiasis mimics cancer recurrence: Two cases of extragastrointestinal anisakiasis suspected to be recurrence of gynecological cancer on PET-CT and molecular biological investigation	BMC Med Imaging	16	31	2016
Kato K, Gemba K, Fujimoto N, Aoe K, Takeshima Y, Inai K, and Kishimoto T	Computed Tomographic Features of Malignant Peritoneal Mesothelioma	Anticancer Research	36	1067-72	2016
Kato K, Gemba K, Fujimoto N, Aoe K, Takeshuma Y, Inai K & Kishimoto T	Fatal pleural mesothelioma in Japan(2003-2008):evaluation of computed tomography findings	Jpn J Radiol	34	432-8	2016
Hara N, Fujimoto N, Miyamoto Y, Yamagishi T, Asano M, Fuchimoto Y, Wada S, Ozaki S, Nishi H, Kishimoto T	Angiosarcoma of the thoracic wall responded well to nanoparticle albumin-bound paclitaxel: A case report	Drug Discov Ther	10	114-6	2016
Kato K, Gemba K, Fujimoto N, Aoe K, Takeshima Y, Inai K, Kishimoto T	Pleural irregularities and mediastinal pleural involvement in early stages of malignant pleural mesothelioma and benign asbestos pleural effusion	European Journal of Radiology	85	1594-1600	2016
Kushitani K, Amatya VJ, Okada Y, Katayama Y, Mawas AS, Miyata Y, Okada M, Inai K, Kishimoto T, Takeshima Y	Utility and pitfall of Immunohistochemistry in the Differential Diagnosis between Epithelioid Mesothelioma and Poorly Differentiated Lung Squamous Cell Carcinoma				2016

発表者氏名	論文タイトル名	発表誌名	巻号	ページ	出版年
Amatya VJ, Kushitani K, Mawas AS, Miyata Y, Okada M, Kishimoto T, Inai K, Takeshima Y	MUC4, a novel immunohistochemical marker identified by gene expression profiling, differentiates pleural sarcomatoid mesothelioma from lung sarcomatoid carcinoma	Mod Pathol			2017
Kubo T, Fujiwara K, Hotta K, Okada T, Kuyama S, Harita S, Ninomiya T, Kamei H, Hosokawa S, Bessho A, Maeda T, Kozuki T, Fujimoto N, Ninomiya K, Takemoto M, Kanazawa S, Takigawa N, Tabata M, Tanimoto M, Ueoka H, Kiura	A phase II study of topotecan and cisplatin with sequential thoracic radiotherapy in elderly patients with small cell lung cancer; Okayama Lung Cancer Study Group 0102	Cancer Chemother Pharmacol	78	769-74	2016
森本幾夫	臨床リウマチ医のための基礎講座　CD26分子に基づくトランスレーショナルリサーチ	臨床リウマチ	28	91-4	2016
森本幾夫、大沼圭	CD26分子に基づく悪性中皮腫への新治療法開発	癌と化学療法	43	855-62	2016
岸本 卓巳、藤本 伸一、西 英行	胸膜中皮腫の病理と診断（治療）	希少がんの病理と診断	43	513-17	2016

Ⅳ.　研究成果の別刷

Chapter

1. CD26-TARGETED THERAPY: A NEW HORIZON IN MALIGNANT PLEURAL
2. MESOTHELIOMA MANAGEMENT

Kei Ohnuma[1, *], MD, PhD, Ryo Hatano[1], PhD,
Hiroto Yamazaki[1], MD, PhD,
Yutaro Kaneko [2], Nam H. Dang[3], MD, PhD,
and Chikao Morimoto[1], MD, PhD
[1]Department of Therapy Development and Innovation for Immune Disorders and Cancers,
Graduate School of Medicine,
Juntendo University, Tokyo, Japan
[2]Y's AC Co., Ltd., Tokyo, Japan
[3]Division of Hematology/Oncology, University of Florida,
Gainesville, FL, US

ABSTRACT

Malignant pleural mesothelioma (MPM) is a rare and aggressive neoplasm deriving from the pleural mesothelial lining. More than 80% of cases are related to previous professional asbestos exposure, with its worldwide incidence being expected to increase in the future. Despite the modest clinical benefit of a multimodality treatment approach including surgery, combination chemotherapy and radiation, prognosis remains grim with poor overall survival. For the vast majority of MPM patients ineligible for potentially curative surgery at diagnosis, systemic chemotherapy is the best option to improve survival. The only treatment with level-one level of evidence for improving clinical outcome is the regimen consisting of a platinum doublet with an antifolate. It is possible that standard cytotoxic therapies for MPM have reached a therapeutic plateau, and new approaches based on deregulated pathways and targeted therapies are required to improve survival of MPM patients. We have had a long-standing interest in the role of CD26 in

---

*

[*] Corresponding Author Email: kohnuma@juntendo.ac.jp.

cancer biology and its suitability as a novel therapeutic target in selected neoplasms. Our previous work demonstrated that CD26 is preferentially expressed in MPM cells but not in normal mesothelial cells, and suggested that CD26 expression level correlates with clinical outcomes. More recently, we showed that the CD26-positive population of $CD24^+CD9^+$ MPM cells exhibits cancer stem cell features. We also reported robust *in vivo* data on the anti-tumor activity of anti-CD26 monoclonal antibody in mouse xenograft models. We herein review significant novel findings and the early clinical development of a CD26-targeted therapy for MPM, advances that can lead to a more hopeful future for MPM patients.

Keywords: malignant pleural mesothelioma, CD26, DPPIV, YS110

INTRODUCTION

Malignant pleural mesothelioma (MPM) is a rare and aggressive neoplasm arising from the pleural mesothelial lining (Kondola et al., 2016), with more than 80% of cases being related to previous occupational asbestos exposure (Myers, 2012; Shersher and Liptay, 2013). Peak incidence of MPM has been reached in the United States, while its incidence is predicted to increase further in the next decades in developing countries where asbestos has not yet been prohibited (Myers, 2012; Shersher and Liptay, 2013). Worldwide, about 80% of mesothelioma deaths occur in ten countries, with Japan, United Sates and United Kingdom being in the top three (van Meerbeeck and Damhuis, 2011; Robinson, 2012). Despite the modest clinical benefit of a multimodality treatment approach including surgery, combination chemotherapy and radiation, prognosis remains grim with poor overall survival (Abdel-Rahman and Kelany, 2015; Maggioni et al., 2016). For the vast majority of MPM patients ineligible for potentially curative surgery at diagnosis, systemic chemotherapy is the best option to improve survival (Kondola et al., 2016). The only treatment with level-one level of evidence for improving clinical outcome is the regimen consisting of a platinum doublet with an antifolate (Haas and Sterman, 2013). With this combined chemotherapy, patients with good performance status have a median overall survival (OS) of approximately 1 year, and a median progression free survival (PFS) of less than 6 months (van Meerbeeck et al., 2005). There is no standard second line treatment with documented ability to prolong survival. Due to the lack of efficacy of conventional treatments, novel therapeutic strategies are urgently needed to improve outcomes of MPM (Astoul et al., 2012; Haas and Sterman, 2013; Kondola et al., 2016).

Successful treatment of MPM depends on an in-depth understanding of the biology of mesothelioma. Our group has had a long-standing interest in the role of CD26 in cancer biology and its suitability as a novel therapeutic target in selected neoplasms (Thompson et al., 2007; Havre et al., 2008; Ohnuma and Morimoto, 2013). CD26 is a 110-kDa, type II transmembrane glycoprotein with known dipeptidyl peptidase IV (DPPIV, EC 3.4.14.5) activity in its extracellular domain and is capable of cleaving N-terminal dipeptides with either L-proline or L-alanine at the penultimate position (Ohnuma et al., 2008a). CD26 activity is dependent on cell type and the microenvironment factors that can influence its multiple biological roles (Thompson et al., 2007; Ohnuma et al., 2011). Although CD26 expression is enhanced following activation of resting T cells, $CD4^{+}\,CD26^{high}$ T cells respond maximally to recall antigens such as tetanus toxoid (Morimoto et al., 1989; Dang et al., 1990c). Cross-linking of CD26 with CD3 by solid-phase immobilized monoclonal antibodies (mAbs) can induce T-cell costimulation and IL-2 production by $CD26^{+}$ T cells (Dang et al., 1990a; Morimoto and Schlossman, 1998). In addition, anti-CD26 antibody treatment of T cells enhances activation associated with tyrosine phosphorylation of signaling molecules such as CD3ζ and $p56^{lck}$, while its DPPIV enzyme activity is required for CD26-mediated T cell costimulation (Tanaka et al., 1993; Hegen et al., 1997; Ishii et al., 2001). CD26 therefore has an important role in T cell biology and overall immune function (Morimoto and Schlossman, 1998; Ohnuma et al., 2008a).

CD26 is also expressed on various tumors including MPM, renal cell carcinoma (RCC), colorectal cancer, hepatocellular carcinoma, lung cancer, prostate cancer, gastrointestinal stromal tumor, thyroid cancer, and hematologic malignancies such as T-anaplastic large cell lymphoma, T-lymphoblastic lymphoma and T-acute lymphoblastic leukemia (Thompson et al., 2007; Havre et al., 2008; Ohnuma and Morimoto, 2013). In addition to its expression in cancer cells, CD26 regulates topoisomerase IIα level in hematological malignancies, affecting sensitivity to doxorubicin and etoposide (Yamochi et al., 2005). Moreover, CD26 itself appears to be a novel therapeutic target, and anti-CD26 mAb treatment resulted in both *in vitro* and *in vivo* anti-tumor activity against selected tumor types including MPM (Ho et al., 2001; Inamoto et al., 2006; Inamoto et al., 2007). Our previous work demonstrated that CD26 is preferentially expressed in MPM cells but not in normal mesothelial cells, and suggested that CD26 expression level correlates with clinical outcomes, while being a potential therapeutic target in MPM (Amatya et al., 2011; Aoe et al., 2012). We herein review mainly our significant novel findings and the early clinical development of a CD26-targeted therapy for MPM.

MOLECULAR CHARACTERIZATION OF CD26

In 1979, a large molecular weight complex composed of adenosine deaminase (ADA) activity was found to be an ADA-binding protein (ADBP), also known as adenosine deaminase complexing protein-2 (ADCP2) (Daddona and Kelley, 1979). In 1992, this ADBP or ADCP2 is determined to be identical to CD26, a T-cell activation molecule and a 110-kD glycoprotein that is present also on epithelial cells of various tissues including the liver, kidney, and intestine (Hopsu-Havu and Glenner, 1966; Marguet et al., 1992; Tanaka et al., 1992). The human CD26 cDNA contains a 3,465 base pair (bp) open reading frame that encodes a 766 amino acid protein. The human CD26 amino acid sequence has 85% amino acid identity with the mouse and rat CD26, and 37% amino acid identity with *D. melanogaster* (Marguet et al., 1992; Tanaka et al., 1992). The 5’-flanking region does not contain a TATA box or CAAT box, commonly found in housekeeping genes (Bohm et al., 1995). CD26 does contain a 300 bp G-C rich region with potential binding sites for NF-κB, AP2, or Sp1 (Erickson et al., 2000b). CD26 expression is activated by interferons (IFNs) and retinoic acid in chronic lymphocytic leukemia via Stat1α and the GAS (IFN-γ activaton site) response element (TTCnnnGAA located at bp -35 to -27) in the CD26 promoter (Bauvois et al., 2000). A hepatocyte nuclear factor 1 binding site at position -150 to -131 of the CD26 gene regulates CD26 expression in human intestinal (Caco-2) and hepatic epithelial (HepG2) cell lines (Erickson et al., 1999; Erickson et al., 2000a).

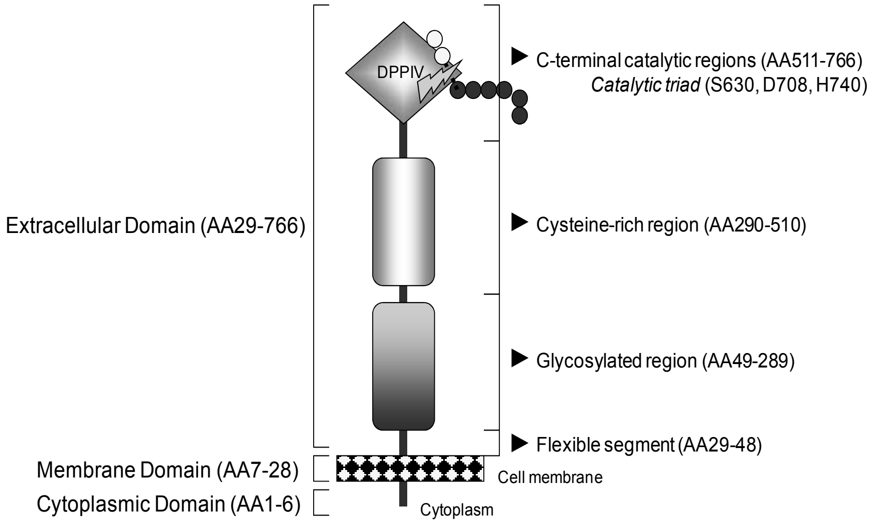
DPPIV
C-terminal catalytic regions (AA511-766)
Catalytic triad (S630, D708, H740)
Extracellular Domain (AA29-766)
Cysteine-rich region (AA290-510)
Glycosylated region (AA49-289)
Flexible segment (AA29-48)
Membrane Domain (AA7-28)
Cell membrane
Cytoplasmic Domain (AA1-6)
Cytoplasm

Figure 1. Schematic diagrams of the amino acids of human CD26.
Human CD26 cDNA is composed of 2,301 base pairs, translated to a 766 amino acid protein. DDPIV catalyzes the hydrolysis of N-terminal dipeptides from polypeptides with proline or alanine in the penultimate position. See text for further details.

CD26 is a multifunctional membrane-bound glycoprotein present as a homodimer on the surface of most cell types (Chien et al., 2004; Ohnuma et al., 2008a). Human CD26 is composed of 766 amino acids (Figure 1), including a short cytoplasmic domain of 6 amino acids, a transmembrane region of 24 amino acids, and an extracellular domain with dipeptidyl peptidase activity which selectively removes the N-terminal dipeptide from peptides with proline or alanine at the penultimate position (Heins et al., 1998; Ohnuma et al., 2008a). Analysis of single amino acid point mutations in the β-propeller motif identified Glu205 and Glu206 to be essential for DPPIV enzyme activity, and the central tunnel and α/β-hydrolase domains both participate in DPPIV inhibitor binding (David et al., 1993; Abbott et al., 2000; Rasmussen et al., 2003). CD26/DPPIV was initially considered to cleave peptides only after a proline or alanine residue, but its substrates are now known include hydroxyproline, serine, glycine, valine, threonine, and leucine (Yaron and Naider, 1993; Abbott et al., 2000; Bjelke et al., 2006). CD26 binds to caveolin-1 on antigen presenting cells (APC), and residues 201 to 211 of CD26 along with the serine catalytic site at residue 630, which constitute a pocket structure of CD26/DPPIV, contribute to its binding to the caveolin-1 scaffolding domain (Ohnuma et al., 2004). This region in CD26 contains a caveolin-binding domain (Φ*X*Φ*XXXX*Φ*XX*Φ; Φ and *X* depict aromatic residue and any amino acid, respectively), specifically WVYEEEVFSAY in CD26. These observations strongly support the notion that DPPIV enzyme activity is necessary for CD26-mediated T-cell costimulatory activation, as demonstrated in our previous work using CD26-targeted mAbs (Tanaka et al., 1993; Morimoto and Schlossman, 1998). Single amino acid point mutation analysis showed that His750 residue is responsible for dimerization (Chien et al., 2004), which is required for T cell costimulation signaling (Ohnuma et al., 2007).

A soluble form of the protein with conserved DPPIV enzyme activity (sCD26 or sDPPIV) is present in the serum and other body fluids, presumably as a result of shedding or secretion from different cell types (Nagatsu et al., 1968; Iwaki-Egawa et al., 1998; Cordero et al., 2009; Rohrborn et al., 2014). The soluble form lacks the transmembrane region and cytoplasmic residues, as it begins at the 39th amino acid residue (Iwaki-Egawa et al., 1998). This form also exists as a dimer and has been detected in seminal fluid as a larger oligomer (>900 kDa) (Iwaki-Egwa et al., 1998). DPPIV enzyme activity is involved in the activation/inactivation of a number of chemokines and cytokines to regulate immune and endocrinological functions as well as cancer cell biology. (De Meester et al., 2000; Thomspn et al., 2007; Havre et al., 2008; Ohnuma et al., 2008a; Ohnuma and Morimoto, 2013). The clinical significance of sCD26 or sDPPIV in MPM patients has been shown in our recent study, which included 80 MPM patients, 79 subjects with past asbestos exposure (SPE), and 134 patients with other benign pleural diseases (OPD) as a control group (Fujimoto et al., 2014). Serum sCD26 levels and sDPPIV enzyme activity in patients with MPM were significantly decreased compared with those in the SPE group. The level of serum sCD26 was significantly decreased in patients with advanced stages of MPM compared with those with earlier stages. The median OS of patients with MPM who had higher DPPIV enzyme activity was significantly longer than that of those with lower DPPIV enzyme activity. The sCD26 levels in the pleural fluid of MPM patients with an epithelioid subtype were significantly increased compared with the OPD cohort. Moreover, DPPIV enzyme activity in the pleural fluid of patients with MPM with an epithelioid subtype was significantly increased compared with that in the OPD cohort. Patients with MPM who had lower specific DPPIV activity, determined as the ratio of DPPIV activity to sCD26 protein quantification, exhibited significantly prolonged survival compared with those with higher specific DPPIV activity. Serum sCD26 and DPPIV enzyme activity appear to be useful biomarkers for differentiating patients with MPM from SPE. In addition, the sCD26 level and DPPIV enzyme activity in pleural fluid appear to be biomarkers in patients with the MPM epithelioid subtype. DPPIV activity in serum or pleural fluid may also be predictive markers for the prognosis of MPM patients (Fujimoto et al., 2014).

CD26 AND IMMUNE FUNCTION

In human peripheral blood, CD26 is found on $CD4^+$ T memory cells and $CD8^+$ effector/memory T cells (Morimoto et al., 1989; Dang et al., 1990c; Hatano et al., 2013). It has been reported that 0-5% of freshly isolated $CD20^+$ B cells do express the CD26 antigen (Buhling et al., 1995). Following stimulation with PMA (phorbol 12-Myristate 13-acetate) or *Streptococcus aureus* protein, the fraction of CD26-positive cells increased to 51% (Morimoto and Schlossman, 1998; Fujimaki et al., 2008). Meanwhile, CD26 is not expressed or is found only at low levels on monocytes of healthy adults (Stohlawetz et al., 1998; Ohnuma et al., 2001). Flow cytometric analysis of dendritic antigen-presenting cells (DC) generated from peripheral blood of normal donors in the presence of granulocyte/macrophage colony-stimulating factor and IL-4 revealed intermediate levels of CD26 expression during a 2-week culture period (Alijagic et al., 1995). Only a small fraction of peripheral NK cells was found to express CD26 (Buhling et al., 1994).

CD26 is a co-stimulatory molecule for T-cell signal transduction. While CD26 expression is enhanced following activation of resting T cells, $CD4^+CD26^{high}$ T cells respond maximally to recall antigens such as tetanus toxoid (Dang et al., 1990c; Morimoto and Schlossman, 1998). Moreover, we have previously reported that effector CD26-mediated costimulatory activity is exerted via its DPPIV enzymatic activity (Tanaka et al., 1993). In addition, $CD4^+$ T cells with *in vitro* transendothelial migratory capacity appear to express high CD26 (Masuyama et al., 1992), and patients with autoimmune diseases such as multiple sclerosis, Grave's disease, and rheumatoid arthritis have been found to have increased numbers of $CD4^+CD26^+$ T cells in inflamed tissues as well as in their peripheral blood, with enhancement of CD26 expression in these autoimmune diseases correlating with disease activity (Ohnuma et al., 2011). Moreover, $CD26^{high}CD8^+$ T cells in humans belong to early effector memory T cells, and $CD26^{high}CD8^+$ T cells exhibit increased expression of granzyme B, TNF-α, IFN-γ and Fas ligand, and exert cytotoxic effect with CD26-mediated costimulation (Hatano et al., 2013).

The cytoplasmic tail of CD26 is responsible for T-cell costimulation induced by anti-CD3 plus caveolin-1 (Ohnuma et al., 2007). Our work found that CARMA1 binds to the cytoplasmic tail of dimeric CD26, and that a PDZ domain in CARMA1 is necessary for binding to CD26 (Ohnuma et al., 2007). Following its phosphorylation, CARMA1 functions as a signaling intermediate downstream of PKCθ (protein kinase θ) and upstream of IKK (IκB kinase) in the TCR (T cell receptor) signaling transduction pathway, which leads eventually to NF-κB activation. Dimeric CD26, but not monomeric CD26, binds to CARMA1 (Ohnuma et al., 2007). The enzymatic pocket structure of the DPPIV catalytic site is necessary for binding of CD26 to caveolin-1, leading to the upregulation of CD86 expression on APC (Ohnuma et al., 2005). Dimerization of CD26 is therefore not only necessary for binding to caveolin-1, but also serves as a scaffolding structure for the cytoplasmic signaling molecule CARMA1. Overall, CD26 ligation by caveolin-1 on APC recruits CD26-interacting CARMA1 to lipid rafts, resulting in the formation of a CARMA1-Bcl10-MALT1-IKK complex, and this membrane-associated Bcl10 complex then activates IKK through ubiquitination of NEMO (NF-κB essential modulator) (Ohnuma et al., 2008b).

We recently reported that CD3/CD26 costimulation induces the development of a population of human type 1 regulatory T (T_{reg}) cells from $CD4^+$ T cells with high level of IL-10 production and lymphocyte-activation gene 3 (LAG3) expression (Hatano et al., 2015). Other investigators have also reported that the $CD26^+CD39^-$ T_{reg} subset among $CD4^+$ T_{reg} exhibits high level of IL-10 expression (Hua et al., 2015). These findings strongly suggest that a specific subset of $CD26^+$ T cells plays a role in immune checkpoint system, and that the CD26 molecule may be a novel target for a therapeutic approach involving immune checkpoint blockade.

EXPRESSION OF CD26 IN MPM

Our previous work analyzing extracellular matrix interactions and intracellular signaling events demonstrated that the malignant mesothelial cell line JMN expresses CD26 (Dang et al., 1990b). Our recent in-depth studies of CD26 expression in MPM revealed that CD26 is preferentially expressed in MPM cells but not in normal mesothelial cells (Amatya et al., 2011; Aoe et al., 2012). Tissue samples from eighty one epithelioid (49 differentiated and 32 less differentiated), 34 sarcomatoid, 19 biphasic mesothelioma patients and 8 mesothelioma cell lines were examined via immunohistochemistry for membranous and cytoplasmic expression. Cytoplasmic expression of CD26 was observed in all histological types of mesothelioma, being found in 65 of 81 (80%) of epithelioid mesotheliomas, and 17 of 18 (95%) of epithelioid component of biphasic mesothelioma. Meanwhile, membranous expression of CD26 was not found in sarcomatoid mesothelioma or sarcomatoid component of biphasic mesothelioma (Figure 2). Moreover, 7 out of 8 mesothelioma cell lines (MESO1, MESO4, HMMME, H226, H2452, H28, and H2052), including sarcomatoid types, exhibited CD26 expression, with the MSTO-211H (MSTO) mesothelioma cell line having no expression of CD26 (Amatya et al., 2011). These same 7 mesothelioma cell lines also demonstrated membranous expression of CD26 in cellblock preparation.

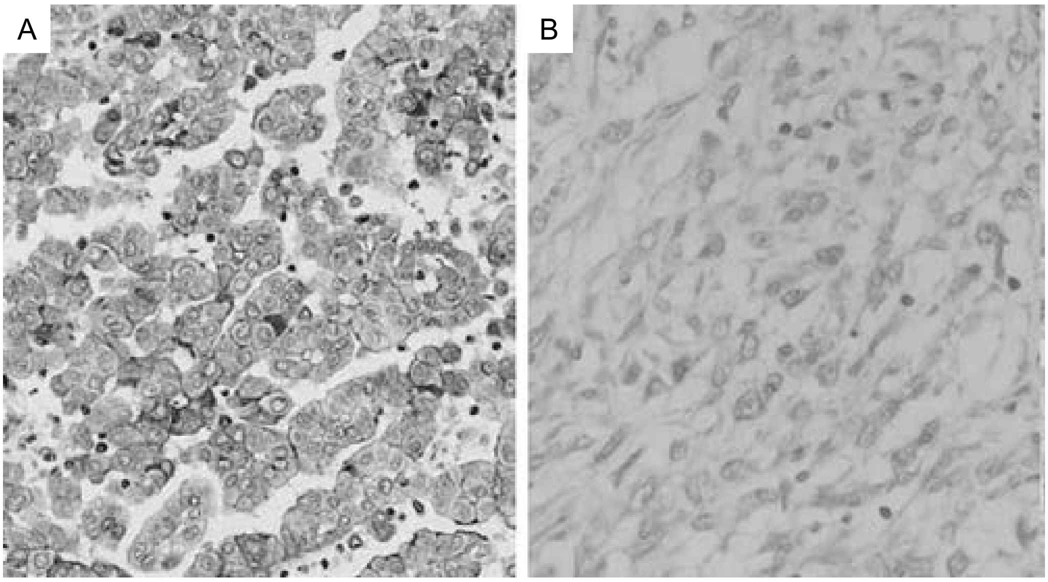

Figure 2. Immunohistochemical staining of MPM with anti-CD26.
Representative serial sections of resected specimens of MPM.
(A) Epithelioid mesothelioma for anti-CD26 immunohistochemistry, showing membranous expression of CD26.
(B) Sarcomatoid mesothelioma for anti-CD26 immunohistochemistry, showing only cytoplasmic expression with inconspicuous membranous expression of CD26.
This figure is reprinted with permission from K Aoe *et al.*, *Clin Cancer Res* 18:147-1456, 2012.

CLINICAL RELEVANCE OF CD26 EXPRESSION AND MPM

To explore the role of CD26 for MPM in the clinical setting as a prognostic and therapeutic biomarker, we evaluated 79 MPM cases for CD26 expression and clinical outcome (Aoe et al., 2012).

Fifty-eight patients with mesothelioma (73.4%) expressed CD26 on the mesothelioma cell membrane. The majority of patients with epithelioid and biphasic type of mesothelioma expressed CD26 on the mesothelioma cell membrane, whereas none of the patients with the sarcomatoid type did. It should be noted that diffuse staining for CD26 in the cytoplasm of the mesothelioma cells was observed in all patient samples, even in patients with the sarcomatoid type (Figure 2). We next evaluated the prognostic significance of CD26 membrane expression and other clinicopathological factors in those patients (Aoe et al., 2012). The median survival time (MST) for all mesothelioma patients in the current study was 13.9 months, with the 1-year survival rate being 58.9%. Older age, sarcomatoid histology, advanced stage, absence of extrapleural pneumonectomy (EPP), absence of chemotherapy, and best supportive care were factors associated with poor prognosis. However, no significant relationship between membranous CD26 expression in malignant mesothelioma and survival was observed (MST, 15.0 *vs*. 10.8 months, P=0.1384). Potential relationship between CD26 expression and chemotherapy response and survival was also analyzed. Of the 56 patients treated with chemotherapy, 15 patients had adjuvant chemotherapy, and one patient died prior to evaluation of response to chemotherapy. Therefore, we evaluated the relationship between membranous CD26 expression and response to chemotherapy for 40 patients. The response rate to chemotherapy was marginally associated with membranous CD26 expression (P=0.053). There was a trend toward an association between higher level of CD26 membrane expression and better response to chemotherapy. Univariate analysis of survival time for patients who received chemotherapy demonstrated that membranous CD26 expression was a significant factor associated with better survival (MST, 18.6 *vs*. 10.7 months, P=0.0083). In addition, other clinicopathological factors, including epithelioid histology type, lower stage, EPP or treatment with pemetrexed were also observed to be associated with overall survival. Multivariate analysis for response to chemotherapy showed that epithelioid histology (P=0.016) and EPP (P=0.005) had independent prognostic significance. Membranous CD26 expression showed a hazard ratio of 1.947, but without statistically significant value (P=0.067). Taken together, we concluded that the CD26 molecule is a reliable biomarker for predicting potential therapeutic outcome following chemotherapy (Aoe et al., 2012).

MPM CANCER CELL BIOLOGY OF CD26

Since CD26 membrane expression on mesothelioma cells appears to be a predictive marker of response to chemotherapy, we next attempted to characterize in details the CD26-positive cells of mesothelioma cell lines. For this purpose we sorted naturally occurring CD26-positive MESO1 mesothelioma cells and subdivided them into CD26-positive and CD26-negative cells. Such cells were subsequently cultured for the indicated days. $CD26^{high}$ cells always exhibited higher level of proliferative activity than CD26-negative cells. Similarly, $CD26^{high}$ cells from other naturally occurring CD26-positive mesothelioma cell lines such as H226 and H28 cell lines consistently had higher level of proliferation than CD26-negative cells from the same cell lines. Moreover, CD26-knockdown of MESO1, JMN and H28 cells resulted in reduced proliferation as compared to wild type CD26-positive MESO-1, JMN and H28 cells,_respectively. These results hence suggest that CD26-positive mesothelioma cells have generally robust growth activity (Aoe et al., 2012). Since highly proliferative cells are typically sensitive to chemotherapeutic agents, our present data support the notion that mesothelioma patients with tumors expressing high level of CD26 generally have chemosensitive disease, as discussed in the preceding section.

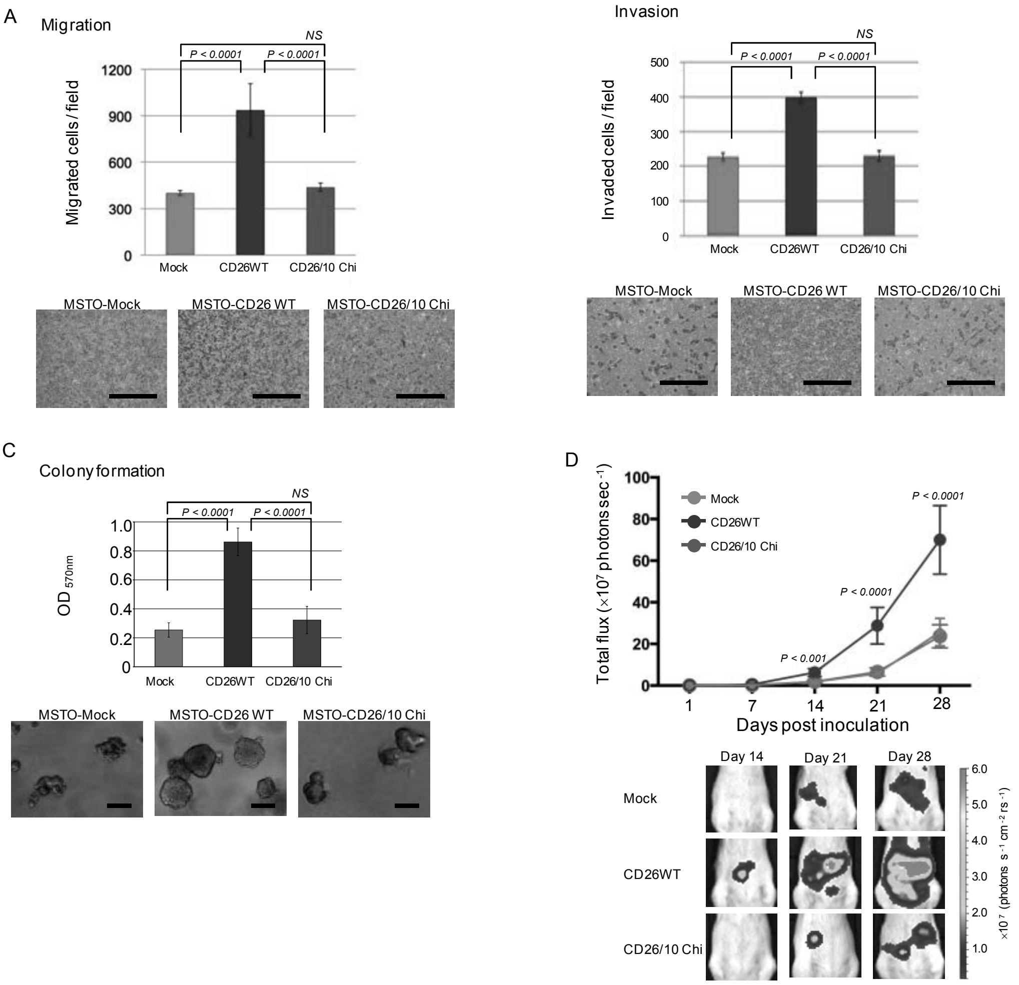

Figure 3. The cytoplasmic region of CD26 is required for cell migration, invasion and colony formation.
(A) Cells were seeded on top of a Boyden chamber. The number of cells that migrated through the uncoated filter in the lower chamber was counted. The mean number of cells per field was determined from 5 fields per filter (mean ± SEM; n=5 experiments with triplicates). A significant increase of MSTO-CD26WT is indicated as *P*<0.0001 (*v.s.* MSTO-Mock or MSTO-CD26/10Chi), as calculated by ANOVA with Tukey-Kramer *post-hoc* test. *NS* denotes 'not significant'. Representative microphotographs of cells migrating through the filter were shown in the lower panels (crystal violet staining). Scale bars indicate 200μm.
(B) Cells were seeded on top of Matrigel-coated chamber inserts. The number of cells that invaded through the Matrigel in the lower chamber was counted. The mean number of cells per field was determined from 5 fields per filter (mean ± SEM; n=5 experiments with triplicates). A significant increase of MSTO-CD26WT is indicated as *P*<0.0001 (*v.s.* MSTO-Mock or MSTO-CD26/10Chi), as calculated by ANOVA with Tukey-Kramer *post-hoc* test. *NS* denotes 'not significant'. Representative microphotographs of cells invading through the filter were shown in the lower panels (crystal violet staining). Scale bar indicates 200μm.
(C) Cells were plated in a cell suspension agar matrix between layers of base agar matrix. After 1 week, the agar matrix was solubilized, and cells were stained with MTT solution. Absorbance at 570nm was measured (mean ± SEM; n=5 experiments with triplicates). A significant increase of MSTO-CD26WT is indicated as *P*<0.0001 (*v.s.* MSTO-Mock or MSTO-CD26/10Chi), as calculated by ANOVA with Tukey-Kramer *post-hoc* test. *NS* denotes 'not significant'. Representative microphotographs of cells grown in soft agar just prior to solubilization to indicate cell size and morphology were shown in the lower panels (phase-contrast imaging). Original magnification, ×8. Scale bars indicate 50μm.
(D) SCID mice were injected i.p. with 1×10^5 luciferase-expressing MSTO-Mock, MSTO-CD26WT or MSTO-CD26/10Chi cells. Tumor growth was measured by *in vivo* bioluminescence photometry, with imaging data of

each cohort being indicated as total flux of photons per second (mean ± SEM; n=20). A significant increase of MSTO-CD26WT is indicated as $P<0.0001$ (*v.s.* MSTO-Mock or MSTO-CD26/10Chi), as calculated by ANOVA with Tukey-Kramer *post-hoc* test. Representative optical bioluminescence imaging of each cohort mice was shown with intensity of luminescence as heat maps in the lower panels.
This figure is reprinted with permission from J Yamamoto *et al*., *Br J Cancer* 110:2232-2245, 2014.

To extend our previous studies on the relationship between high proliferative activity and invasiveness and high expression level of CD26, we analyzed the signaling events downstream of CD26 in MPM. With the proximal signaling events associated with the cytoplasmic region of CD26 being previously shown in normal human T lymphocytes (Ohnuma et al., 2007), it is conceivable that similar CD26-mediated proximal events may play a role in MPM cell biology. To define the crucial role of the CD26 cytoplasmic region in regulating migratory, invasive or proliferative activity of MPM cells, we used a mutant construct of CD26 in which its cytoplasmic region was replaced with that of human CD10 (CD26-CD10 chimeric receptor), which was shown to abrogate CD26-mediated costimulation in T cells (Ohnuma et al., 2007). CD10, as is the case with CD26, is a type II transmembrane glycoprotein with a relatively short cytoplasmic tail containing signal sequence that has an expected membrane topology similar to CD26 (Ogata et al., 1989; Maguer-Satta et al., 2011). We transfected CD26-negative parental MSTO cells with full-length human CD26 (CD26WT) or CD26-CD10 chimeric receptor (CD26/10Chi) to establish MSTO-CD26WT or MSTO-CD26/10Chi, respectively (Yamamoto et al., 2014). A significant increase in migration was observed in MSTO-CD26WT as compared to MSTO-Mock (vector alone) or MSTO-CD26/10Chi (Figure 3A). Similarly, an increase in invasion was also observed in MSTO-CD26WT as compared to MSTO-Mock or MSTO-CD26/10Chi (Figure 3B). Moreover, a significant increase in colony formation was observed in MSTO-CD26WT as compared to MSTO-Mock or MSTO-CD26/10Chi (Figure 3C). To extend the above *in vitro* results to *in vivo* experimentation, we performed a cell growth assay using xenograft mice. A significant increase in *in vivo* tumor growth was observed with MSTO-CD26WT as compared to MSTO-Mock or MSTO-CD26/10Chi (Figure 3D). These results suggest that the cytoplasmic region of CD26 is important for CD26 function in such MPM biological processes as cell migration, invasion and anchorage-independent cell growth as well as *in vivo* tumor growth, and clinical benefit may be obtained by targeting the CD26 molecule in MPM therapy.

CD26 AND CANCER STEM CELLS IN MPM

The putative existence of cancer stem cell (CSC) is a widely accepted notion at the present time (Reya et al., 2001). CSC proliferates in an asymmetric cell division-like manner, exhibits various stem cell signatures, and is believed to be a potential reason for resistance to therapy. Recent studies have demonstrated the existence of CSCs not only in hematologic malignancies but also solid tumors (Frank et al., 2010; Wang and Dick, 2005). Our recent work identified SP (side-population), CD9, CD24, and CD26 as MPM CSC markers that correlated with primary stem cell signatures (Ghani et al., 2011). SP cells of H226 and H2452 cell lines, and CD24-positive cells of JMN and H226 cell lines proliferated in an asymmetric cell division-like manner. The expression of CD26 closely correlated with that of CD24 in sarcomatoid type cell lines. In addition, CD9 and CD24-positive cells displayed a higher potential to generate spheroid colony than negative cells in the stem cell medium. Moreover, these marker-positive cells had a clear tendency to generate larger tumors in mouse transplantation assay (Ghani et al., 2011). We further analyzed the CSC properties of CD24 and CD26-positve MPM cells (Yamazaki et al., 2012). We established RNA interference (RNAi) -knockdown MPM cells and found that these markers correlated significantly with chemoresistance, proliferation, and *in vitro* invasion potential. Interestingly, while MESO1 cells expressed both CD24 and CD26, the presence of each of these two markers was correlated with different CSC property. To distinguish intracellular signals downstream of these cell surface antigens, we performed DNA microarray analysis of $CD24^+$ and $CD24^-$ cells of JMN and H226, $CD24^+CD26^+$ and $CD24^-CD26^-$ cells of MESO1, and control-short hairpin RNA (shRNA) and CD24-shRNA cells of MESO1. We found that several genes related to cancer development and stem cell signatures were differentially regulated. Among the genes up-regulated in the positive cells, insulin-like growth factor binding protein 7 (IGFBP7) was commonly up-regulated in all experiments (fold change, JMN-$CD24^+$, 2.5×; H226-$CD24^+$, 3.3×; MESO1-$CD24^+CD26^+$, 27.3×; MESO1-control/CD24-shRNA, 1.9×). In $CD24^+CD26^+$/$CD24^-CD26^-$ cells and control/$CD24^-$ shRNA cells of MESO-1, IGFBP3 (another member of IGFBP, 7.9× and 5.8×, respectively), a cancer gene Wnt5A (5.2× and 6.3×, respectively), and hematopoietic/lymphoid stem cell antigen CD127 (interleukin 7 receptor, IL7R, 10.5× and 3.0×, respectively) were also significantly up-regulated. The microarray data of these genes were further confirmed by RT-PCR in the CD24/CD26-isolated MESO1 cells. Interestingly, expression of IGFBP3 and IGFBP7 was well-correlated with that of CD26, rather than CD24. Meanwhile, expression of Wnt5A and IL7R was correlated with not only CD24 but also CD26 expression, while their expression was completely absent in the $CD24^-CD26^-$ cells. These data suggest that CD24 and CD26 expression correlated with several cancer and stemness genes. In addition to gene expression profiles, our examination of downstream signaling events relating to IGFBP3 and IGFBP7 showed that phosphorylation of ERK (extracellular signal-regulated kinase) by EGF (epidermal growth factor) stimulation was significantly affected by the expression of CD26, but not CD24. Taken together, our data suggest that CD24 and CD26 differentially regulate the CSC potentials of MPM and could be promising targets for CSC-oriented therapy.

ASSOCIATION OF CD26 AND EXTRACELLULAR MATRIX IN MPM

To further explore the molecular mechanisms involved in the highly proliferative activity of CD26-positive MPM cells, we focused on the interaction between CD26 and CD9, and identified as novel markers for cancer stem cells in malignant mesothelioma (Ghani et al., 2011). We found that CD26 and CD9 co-modulated and coprecipitated with each other in the malignant mesothelioma cell lines MESO1 and MSTO (Okamoto et al., 2014). RNAi study revealed that depletion of CD26 led to increased CD9 expression, while depletion of CD9 resulted in increased CD26 expression. Consistent with these findings was the fact that gene transfer of CD26 into CD26-negative MSTO cells reduced CD9 expression. Cell invasion assay showed that overexpression of CD26 or gene depletion of CD9 led to enhanced invasiveness, while CD26 gene depletion resulted in reduced invasive potential. Furthermore, co-precipitation studies demonstrated an association between CD26 and α5β1 integrin, suggesting that this enhanced invasiveness may be partly mediated by α5β1 integrin. Finally, gene depletion of CD9 resulted in elevated protein levels and tyrosine phosphorylation of FAK (focal adhesion kinase) and Cas-L/NEDD9, which are downstream signaling molecules of β1 integrin, while depletion of CD26 led to a reduction in the levels of these molecules. Collectively, our findings suggest that CD26 potentiates tumor cell invasion through its interaction with α5β1 integrin, and CD9 negatively regulates tumor cell invasion by reducing the level of CD26-α5β1 integrin complex through an inverse correlation between CD9 and CD26 expression (Okamoto et al., 2014).

Along with our previous observation that depletion of CD26 by RNAi resulted in the loss of adhesive property, suggesting that CD26 is a binding protein to the extracellular matrix (ECM), the above observation regarding the CD26-α5β1 integrin complex suggests that CD26 regulates the interaction of MPM cells with the ECM via yet-to-be-determined integrin adhesion molecules. More recently, we found that expression of CD26 upregulates periostin secretion by MPM cells, leading to enhanced MPM cell migratory and invasive activity (Komiya et al., 2014). Periostin is a secreted cell adhesion protein of approximately 90kDa, which shares a homology with the insect cell adhesion molecule fasciclin I (FAS1) (Morra and Moch, 2011). Moreover, we showed that upregulation of periostin expression results from the nuclear translocation of the basic helix-loop-helix transcription factor Twist1, a process that is mediated by CD26-associated activation of Src phosphorylation. In the clinical setting, periostin upregulation has been reported for many cancer types including MPM, and may potentially be a tumor-enhancing factor (Morra and Moch, 2011). Previous work also suggested that periostin expression in MPM cells may be an independent prognostic factor for overall survival (Schramm et al., 2010). Periostin was shown to be not only a marker of epithelial-mesenchymal transition (EMT), but to be itself an inductor of this phenomenon (Yan and Shao, 2006). Our results hence suggest that CD26 expression is associated with EMT via its regulation of periostin.

We demonstrated that CD9 suppresses cell adhesion by inhibiting CD26-$\alpha 5\beta 1$ integrin complex through its negative regulation of CD26 (Okamoto et al., 2014). These observations show that CD26 regulates the interaction of MPM cells with the ECM via the integrin adhesion molecules. Meanwhile, as described above, we have shown that the cytoplasmic 6 amino acid residues of CD26 are required for regulating migratory, invasive or proliferative activity of MPM cells. To define the molecular details involved in the critical role of the CD26 cytoplasmic region, we used affinity purification and LC-MS/MS (liquid chromatography-tandem mass spectrometry) to identify the proteins that are associated with the CD26 cytoplasmic domain (Yamamoto et al., 2014). In these experiments, membrane fractions of MSTO-Mock, MSTO-CD26WT or MSTO-CD26/10Chi were harvested in native conditions and subjected to affinity purification using anti-CD26 mAb. We demonstrated that the cytoplasmic region of CD26 plays a crucial role in MPM tumor biology through its linkage to somatostain receptor 4 (SSTR4) and SHP-2 protein tyrosine kinase in cell membrane lipid rafts, leading to cytostatic effects in MPM cells without direct association of the ECM to CD26 (Yamamoto et al., 2014).

In view of the findings above, we propose that CD26 forms macromolecular complexes in the cell surface of MPM (Figure 4), and plays a pivotal role in the malignant activity of MPM by connecting periostin and ECM to intracellular signaling events. It is therefore conceivable that targeting CD26 may be a novel and effective therapeutic approach for MPM.

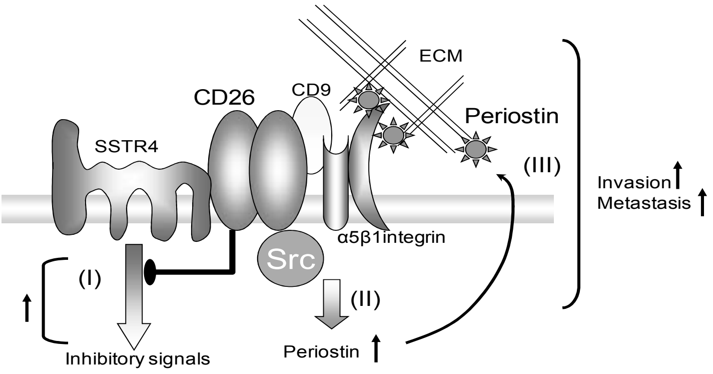

Figure 4. Macromolecular complex associated with cell surface CD26 in MPM.
(I) In CD26-negative MPM cells, SSTR4 mediated inhibitory signaling to suppress cell proliferation and motility. In contrast, by locking the signaling domain of SSTR4 with CD26 association, SSTR4-mediated anti-tumor effects were abrogated, leading to increased cell proliferation and motility in CD26-positive MPM cells.
(II) In addition, CD26 regulated extracellular matrix (ECM)-associated tumor cell behavior in association with integrins and periostin-ECM complex. CD9 suppressed cell invasion and migration by inhibiting the formation of CD26-$\alpha 5\beta 1$ integrin complex. Moreover, expression of CD26 upregulated periostin secretion by MPM cells,

leading to enhanced MPM cell migratory and invasive activity. Moreover, we showed that upregulation of periostin expression resulted from the nuclear translocation of the basic helix-loop-helix transcription factor Twist1, a process that was mediated by CD26-associated activation of Src phosphorylation.

(III) Periostin is a secreted cell adhesion protein. The N-terminal region regulates cellular functions by binding to integrins at the plasma membrane of the cells through cell adhesion domain. The C-terminal region of the protein regulates cell–matrix organization and interaction by binding such ECM proteins, leading to increased MPM cell motility. CD26 molecule in MPM plays a pivotal role in connecting ECM to intracellular signaling events associated with cell proliferation and motility.

PRECLINICAL PROOF-OF-CONCEPT (POC) STUDY OF ANTI-CD26 MAB THERAPY FOR MPM

As described in the preceding sections, CD26/DPPIV is expressed at a high level on the surface of malignant mesothelioma cells, but not on cells derived from normal mesothelial cells. These intriguing findings propelled our development of CD26-targeted therapy for MPM. For this purpose, we had developed a novel humanized anti-CD26 mAb, namely YS110. YS110 is a recombinant DNA-derived humanized mAb that selectively binds with high affinity to the extracellular domain of CD26. The antibody is an $IgG_1\kappa$ with a molecular weight of 144 kDa and was humanized via an *in silico* design based on the amino acid sequence of anti-human CD26 murine mAb (14D10), which inhibited tumor cell growth, migration and invasion, and enhanced survival of mouse xenograft models (Inamoto et al., 2006). YS110 is produced by fermentation in CHO mammalian cell suspension culture with the Glutamine Synthetase Expression System. *In vitro* pharmacologic evaluation of YS110 demonstrated its selective binding to human CD26 on a number of human cancer cell lines and tissues, with no apparent effect on immune activation and no inhibition of DPPIV activity, while exhibiting direct cytotoxic effect on certain human CD26-positive cancer cell lines. Moreover, our *in vitro* data indicated that YS110 induces cell lysis of MPM cells via antibody-dependent cell-mediated cytotoxicity (ADCC) in addition to its direct anti-tumor effect via cyclin-dependent kinase inhibitor (CDKI) $p27^{kip1}$ and $p21^{cip1}$ accumulation (Inamoto et al., 2007; Hayashi et al., 2016). *In vivo* experiments with mouse xenograft models involving human MPM cells demonstrated that YS110 treatment drastically inhibits tumor growth in tumor-bearing mice and reduces formation of metastases, resulting in enhanced survival (Inamoto et al., 2007; Okamoto et al., 2014; Yamamoto et al., 2014). Our data strongly suggest that YS110 may have potential clinical use as a novel cancer therapeutic agent for CD26-positive malignant mesothelioma.

FIRST-IN-HUMAN PHASE I CLINICAL TRIAL OF YS110 FOR MPM

In the POC studies using preclinical models, *in vivo* administration of 14D10 or YS110 resulted in inhibition of tumor cell growth, migration and invasion, and enhanced survival of mouse xenograft models inoculated with RCC or MPM (Inamoto et al., 2006; Inamoto et al., 2007; Okamoto et al., 2014; Yamamoto et al., 2014). In addition to our robust *in vitro* and *in vivo* data on antibody-mediated dose-dependent tumor growth inhibition, YS110 exhibited excellent safety and pharmacological profiles in non-human primate models using single and repeated increasing intravenous doses. Considering the lack of T cell proliferation and cytokine production *in vitro*, YS110 was therefore considered not to have an agonistic nor activating effect on human CD26-positive lymphocytes. Other key safety findings were obtained from studies involving cymologus monkeys which express YS110-reactive CD26 molecules, with similar tissue distribution profiles and expression levels to human

CD26. We therefore conducted the first-in-human (FIH) clinical trial of YS110 for patients with MPM and other CD26-positive solid tumors (Angevin et al., 2015).

Thirty-three heavily pre-treated patients with CD26-positive cancers including 22 malignant mesothelioma, 10 RCC and 1 urothelial carcinoma underwent YS110 administration. A total of 232 infusions (median 3 [range 1-30]) of YS110 were administered across 6 dose levels ranging from 0.1 to 6 mg/kg. Maximum tolerated dose (MTD) was not reached and 2 dose limiting toxicities (DLTs) (1 patient with grade 3 anaphylactic reaction at 1 mg/kg and 1 patient with grade 3 allergic reaction at 2 mg/kg) were reported with complete resolution following dose omission. Subsequent use of systemic steroid prophylaxis and exclusion of patients with significant allergy histories improved safety profile. No dose-dependent adverse events were observed. Blood exposure pharmacokinetics parameters (AUC and C_{max}) increased in proportion with the dose. Cytokines and immunophenotyping assays indicated CD26 target modulation with no occurrence of infectious nor autoimmune disease complications. These results demonstrated that YS110 is tolerable in human subjects.

A secondary objective of this FIH study was to evaluate the potential antitumor activity of YS110 according to RECIST 1.0 criteria (or modified RECIST criteria for mesothelioma). No objective response was achieved in any of the treated patients. However, stable disease as the best overall response was observed in 13 out of the 26 valuable patients on Day 43 of the first cycle (1 at 0.1 mg/kg, 2 at 0.4 mg/kg, 7 at 2.0 mg/kg, 1 at 4.0 mg/kg and 2 at 6.0 mg/kg). Prolonged stabilization was observed in 9 out of 13 stable disease patients who have received a total of 161 (6 to 30) infusions with a median PFS of 32 weeks (12 – 57 weeks). This FIH study conclusively demonstrated that YS110 exhibits a favorable safety profile and substantial clinical activity in heavily pretreated CD26-positive MPM patients who had previously progressed on conventional standard chemotherapies (Angevin et al., 2015).

DPPIV ENZYME ACTIVITY AND EFFICACY OF YS110 IN MPM

The FIH clinical study of YS110 revealed that an increase in YS110 infusion dose was associated with decreased serum sCD26 level, particularly in cohorts 4-6 (2.0 to 6.0mg/kg), with an approximately 80% decrease in sCD26 level (Angevin et al., 2015). Moreover, since sCD26 level reflects DPPIV enzyme activity in sera (Durinx et al., 2000), similar reduction in DPPIV enzyme activity was observed, again particularly in patients in cohorts 4-6. Although DPPIV inhibitors are clinically used as oral hypoglycemic agents (Drucker and Nauck, 2006), hypoglycemia was not observed during YS110 administration. Of note is the fact that greater than 80% inhibition of serum DPPIV activity was obtained 24 hours after oral administration of clinically available DPPIV inhibitors (drug information published by manufacturers of sitagliptin, vildagliptin, saxagliptin and *etc.*), a level of inhibition comparable to that seen in patients treated with YS110. Our current data would therefore indicate that YS110 therapy is tolerable in the clinical setting.

Recent work has demonstrated the functional role of DPPIV-mediated post-translational modification of chemokines in regulating tumor immunity through its interaction with its substrate CXCL10 (Barreira da Silva et al., 2015). Barreira de Silvia *et al.* use *in vivo* tumor-transplant models to show that DPPIV inhibition reduces tumor growth through the preservation of bioactive CXCL10 in the tumor microenvironment (TME). In the normal physiological state, CXCL10 is rapidly degraded by DPPIV, resulting in decreased recruitment and migration of $CXCR3^+$ T cells into the TME (Figure 5) (Ohnuma et al., 2015). CXCR3 has been shown to be a functional receptor for CXCL10 (Proost et al., 2001). In contrast, DPPIV inhibition enhances tumor rejection by preserving the full-length biologically active form of CXCL10, leading to increased trafficking of $CXCR3^+$ T cells into the TME (Figure 5) (Ohnuma et al., 2015). This anti-tumor response is potentiated in combination with other anti-tumor immunotherapeutic approaches including CpG adjuvant therapy, adoptive T cell transfer therapy and checkpoint blockade therapy (anti-CTLA-4 and anti-PD-1) (Barreira da Silva et al., 2015). In view of these recent findings, data from our current trial showing that serum DPPIV activity was decreased following treatment with YS110 in a dose-dependent manner would suggest that anti-tumor activity via DPPIV inhibition may constitute yet another mechanism of action for the anti-tumor activity of YS110.

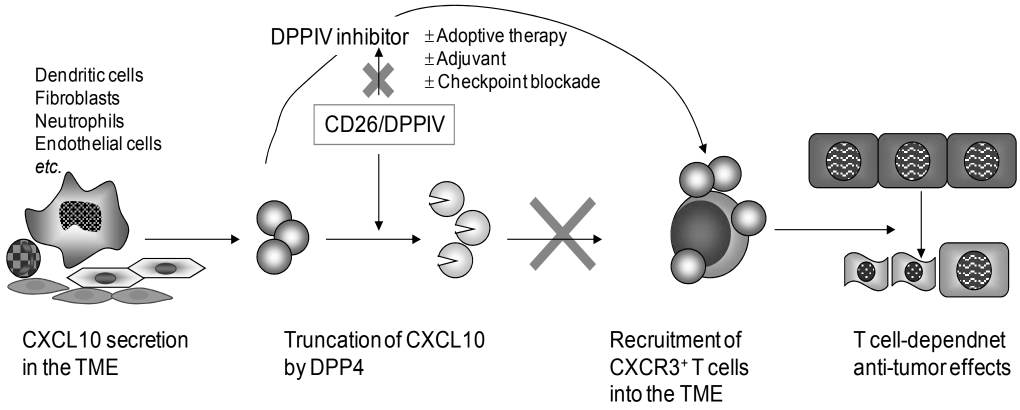
DPPIV inhibitor
±Adoptive therapy
±Adjuvant
±Checkpoint blockade
Dendritic cells
Fibroblasts
Neutrophils
Endothelial cells
etc.
CD26/DPPIV
CXCL10 secretion in the TME
Truncation of CXCL10 by DPP4
Recruitment of CXCR3⁺ T cells into the TME
T cell-dependnet anti-tumor effects

Figure 5. DPPIV inhibition suppresses truncation of its ligand CXCL10, leading to recruitment of CXCR3$^+$ T cells into tumor parenchyma.
In vivo tumor-transplant models showed that DPPIV inhibition reduced tumor growth through the preservation of bioactive CXCL10 in the tumor microenvironment (TME). In the normal physiological state, CXCL10 was rapidly degraded by CD26/DPPIV, resulting in decreased recruitment and migration of CXCR3$^+$ T cells into the tumor parenchyma. In contrast, DPPIV inhibition enhanced tumor rejection by preserving the full-length biologically active form of CXCL10, leading to increased trafficking of CXCR3$^+$ T cells into the tumor parenchyma. This anti-tumor response was potentiated in combination with other anti-tumor immunotherapeutic approaches including CpG adjuvant therapy, adoptive T cell transfer therapy and checkpoint blockade therapy such as anti-CTLA-4 and anti-PD-1.
This figure is reproduced with permission from K Ohnuma *et al.*, *Nat Immunol* 16:791-792, 2015.

MECHANISMS OF ACTION OF YS110 IN MPM

We previously showed that depletion of CD26 by RNAi results in the loss of adhesive property, suggesting that CD26 is a binding protein to the ECM (Inamoto et al., 2007). Moreover, our *in vitro* data indicate that YS110 induces cell lysis of MPM cells via ADCC in addition to its direct anti-tumor effect via CKDI p27^{kip1} accumulation (Inamoto et al., 2007). More recently, we evaluated the direct anti-tumor effect of YS110 against the MPM cell lines H2452 and JMN, and investigated its effects on cell cycle and on the cell cycle regulator molecules (Hayashi et al., 2016). YS110 suppressed the proliferation of H2452 cells by approximately 20% in 48 hours of incubation. Cell cycle analysis demonstrated that the percentage of cells in G2/M phase increased by 8.0% on average following YS110 treatment; in addition, level of the cell cycle regulator p21^{cip1} was increased and cyclin B1 was decreased after YS110 treatment. Inhibitory phosphorylation of both cdc2 (Tyr15) and cdc25C (Ser216) was elevated. Furthermore, activating phosphorylation of p38 MAPK (Thr180/Tyr182) and ERK1/2 (Thr202/Tyr204) was augmented following 24 hours of YS110 treatment. In addition, we investigated the synergistic effects of YS110 and the anti-tumor agent pemetrexed on selected MPM cell lines in both *in vitro* and *in vivo* studies. Pemetrexed rapidly induced CD26 expression on cell surface, and treatment with both YS110 and pemetrexed inhibited *in vivo* tumor growth accompanied by a synergistic reduction in the MIB-1 index.

We also demonstrated that treatment with YS110, which inhibited cancer cell growth, induced nuclear translocation of both cell-surface CD26 and YS110 (Yamada et al., 2009; Yamada et al., 2013). In response to YS110 treatment, CD26 was translocated into the nucleus via caveolin-dependent endocytosis, and interacted with a genomic flanking region of the *POLR2A* gene, a component of RNA polymerase II. This interaction consequently led to transcriptional repression of the *POLR2A* gene, resulting in retarded cancer cell proliferation. Furthermore, impaired nuclear transport of CD26 reversed the *POLR2A* repression induced by YS110 treatment. These findings reveal that nuclear CD26 functions in the regulation of gene expression and tumor growth, while yet another novel mechanism of action of anti-CD26 mAb therapy may involve the regulation of inducible traffic of surface CD26 molecules into the cell nucleus.

Taken together, we summarize the mechanisms of action of YS110 in MPM as follows; (i) a direct cytotoxic effect on certain human CD26-positive cancer cell lines (ADCC), (ii) a direct anti-tumor effect through the induction of cell cycle arrest by induction of p27^{kip1} and p21^{cip1} expression, (iii) following internalization of the CD26-YS110 complexes, an inhibition of invasion and migration of tumor cells by decreased binding to the collagen/fibronectin microenvironment matrix, and (iv) the nuclear translocation of CD26 molecules by internalization of the CD26-YS110 complexes to inhibit proliferation of MPM cells via suppression of *POLR2A* gene expression.

COMPANION DIAGNOSTICS FOR CD26-TARGETING THERAPY

The development of companion diagnostic agents to be used in conjunction with the appropriate therapeutic modalities is essential to maximize therapeutic effectiveness while minimizing associated toxicities. Detection of tumor CD26 expression is critical to determining potential eligibility for treatment with YS110, and it is also important to determine whether CD26 expression on tumors or lymphocytes is affected by anti-CD26 mAb therapy. Immunohistochemical staining of CD26 with the many anti-CD26 mAbs previously developed in our laboratory did not reveal an anti-CD26 mAb that can clearly detect the denatured CD26 molecule in formalin-fixed paraffin-embedded tissues (Dong et al., 1998; Hatano et al., 2014). Meanwhile, testing of several commercially available anti-CD26 mAbs designated as research reagents for immunohistochemical staining indicated that these mAbs could stain the denatured CD26 in formalin-fixed tissues, but not with sufficient clarity. On the other hand, our testing of commercially available anti-CD26 polyclonal antibodies (pAbs) showed that these pAbs exhibited reliable staining pattern and intensity (Amatya et al., 2011; Yamada et al., 2013). However, the disadvantage of pAbs is the potential lot-to-lot variability in staining pattern and intensity, which makes pAbs not the ideal reagents for diagnostic testing of patient specimens in the clinical setting, where consistency and uniformity are required. For this purpose, we recently developed novel anti-human CD26 mAbs that can be used as companion diagnostic reagents suitable for immunohistochemical staining of CD26 in formalin-fixed tissue sections with reliable clarity and intensity (Hatano et al., 2014). Since these mAbs display no cross-reactivity with the therapeutic humanized anti-CD26 mAb, they may be suitable for assays analyzing CD26 expression during or following treatment with the humanized anti-CD26 mAb YS110, with important implications in the clinical setting.

CONCLUSION

While the incidence of MPM continues to increase worldwide, standard chemotherapy does not lead to significant increase in survival. Our increased understanding of the biology and novel therapeutic targets of MPM will pave the way for better treatment options in the future.

Our FIH study showed that YS110 therapy is generally well-tolerated with preliminary evidence of activity in patients with advanced/refractory CD26-expresing cancers including MPM. Our findings also suggest that further clinical development of YS110 such as its use as part of combination therapies with other antineoplastic agents is warranted.

ACKNOWLEDGEMENTS

This study was supported in part by a grant of the Ministry of Education, Science, Sports and Culture, Japan (K.O. and C.M.), a grant of the Ministry of Health, Labour, and Welfare, Japan (C.M.) and a Grant-in-Aid (S1311011) from the Foundation of Strategic Research Projects in Private Universities from the Ministry of Education, Culture, Sports, Science, and Technology, Japan (K.O. and C.M.).

REFERENCES

Abbott, C.A., Yu, D.M., Woollatt, E., Sutherland, G.R., McCaughan, G.W., Gorrell, M.D. (2000). Cloning, expression and chromosomal localization of a novel human dipeptidyl peptidase (DPP) IV homolog, DPP8. *FEBS J.* 267, 6140-6150.

Abdel-Rahman, O., Kelany, M. (2015). Systemic therapy options for malignant pleural mesothelioma beyond first-line therapy: a systematic review. *Expert Rev. Respir. Med.* 9, 533-549.

Alijagic, S., Moller, P., Artuc, M., Jurgovsky, K., Czarnetzki, B.M., Schadendorf, D. (1995). Dendritic cells generated from peripheral blood transfected with human tyrosinase induce specific T cell activation. *Eur. J. Immunol.* 25, 3100-3107.

Amatya, V.J., Takeshima, Y., Kushitani, K., Yamada, T., Morimoto, C., Inai, K. (2011). Overexpression of CD26/DPPIV in mesothelioma tissue and mesothelioma cell lines. *Oncol. Rep.* 26, 1369-1375.

Angevin, E., Isambert, N., Trillet-Lenoir, V.T., You, B., Alexandre, J., Zalcman, G., Viehl, P., Farace, F., Valleix, F., Podoll, T., Kuramochi, K., Miyashita, I., Hosono, O., Dang, N.H., Ohnuma, K., Yamada, T., Kaneko, Y., Morimoto, C. (2015). First-in-human phase I administration of YS110, a monoclonal antibody directed against the CD26 immunostimulatory molecule in advanced cancer patients. *J. Clin. Oncol.* 33, supple; abstr 2519.

Aoe, K., Amatya, V.J., Fujimoto, N., Ohnuma, K., Hosono, O., Hiraki, A., Fujii, M., Yamada, T., Dang, N.H., Takeshima, Y., Inai, K., Kishimoto, T, Morimoto, C. (2012). CD26 overexpression is associated with prolonged survival and enhanced chemosensitivity in malignant pleural mesothelioma. *Clin. Cancer Res.* 18, 1447-1456.

Astoul, P., Roca, E., Galateau-Salle, F., Scherpereel, A. (2012). Malignant pleural mesothelioma: from the bench to the bedside. *Respiration* 83, 481-493.

Barreira da Silva, R., Laird, M.E., Yatim, N., Fiette, L., Ingersoll, M.A., Albert, M.L. (2015). Dipeptidylpeptidase 4 inhibition enhances lymphocyte trafficking, improving both naturally occurring tumor immunity and immunotherapy. *Nat. Immunol.* 16, 850-858.

Bauvois, B., Djavaheri-Mergny, M., Rouillard, D., Dumont, J., Wietzerbin, J. (2000). Regulation of CD26/DPPIV gene expression by interferons and retinoic acid in tumor B cells. *Oncogene* 19, 265-272.

Bjelke, J.R., Kanstrup, A.B., Rasmussen, H.B. (2006). Selectivity among dipeptidyl peptidases of the S9b family. *Cell. Mol. Biol.* 52, 3-7.

Bohm, S.K., Gum, J.R., Jr., Erickson, R.H., Hicks, J.W., Kim, Y.S. (1995). Human dipeptidyl peptidase IV gene promoter: tissue-specific regulation from a TATA-less GC-rich sequence characteristic of a housekeeping gene promoter. *Biochem. J.* 311, 835-843.

Buhling, F., Junker, U., Reinhold, D., Neubert, K., Jager, L., Ansorge, S. (1995). Functional role of CD26 on human B lymphocytes. *Immunol. Lett.* 45, 47-51.

Buhling, F., Kunz, D., Reinhold, D., Ulmer, A.J., Ernst, M., Flad, H.D., Ansorge, S. (1994). Expression and functional role of dipeptidyl peptidase IV (CD26) on human natural killer cells. *Nat. Immun*. 13, 270-279.

Chien, C.H., Huang, L.H., Chou, C.Y., Chen, Y.S., Han, Y.S., Chang, G.G., Liang, P.H., Chen, X. (2004). One site mutation disrupts dimer formation in human DPP-IV proteins. *J. Biol. Chem.* 279, 52338-52345.

Cordero, O.J., Salgado, F.J., Nogueira, M. (2009). On the origin of serum CD26 and its altered concentration in cancer patients. *Cancer Immunol. Immunother*. 58, 1723-1747.

Daddona, P.E., Kelley, W.N. (1979). Human adenosine deaminase. Stoichiometry of the adenosine deaminase-binding protein complex. *Biochim. Biophys. Acta*. 580, 302-311.

Dang, N.H., Torimoto, Y., Deusch, K., Schlossman, S.F., Morimoto, C. (1990a). Comitogenic effect of solid-phase immobilized anti-1F7 on human CD4 T cell activation via CD3 and CD2 pathways. *J. Immunol.* 144, 4092-4100.

Dang, N.H., Torimoto, Y., Schlossman, S.F., Morimoto, C. (1990b). Human CD4 helper T cell activation: functional involvement of two distinct collagen receptors, 1F7 and VLA integrin family. *J. Exp. Med.* 172, 649-652.

Dang, N.H., Torimoto, Y., Sugita, K., Daley, J.F., Schow, P., Prado, C., Schlossman, S.F., Morimoto, C. (1990c). Cell surface modulation of CD26 by anti-1F7 monoclonal antibody. Analysis of surface expression and human T cell activation. *J. Immunol.* 145, 3963-3971.

David, F., Bernard, A.M., Pierres, M., Marguet, D. (1993). Identification of serine 624, aspartic acid 702, and histidine 734 as the catalytic triad residues of mouse dipeptidyl-peptidase IV (CD26). A member of a novel family of nonclassical serine hydrolases. *J. Biol. Chem.* 268, 17247-17252.

De Meester, I., Durinx, C., Bal, G., Proost, P., Struyf, S., Goossens, F., Augustyns, K., Scharpe, S. (2000). Natural substrates of dipeptidyl peptidase IV. *Adv. Exp. Med. Biol.* 477, 67-87.

Dong, R.P., Tachibana, K., Hegen, M., Scharpe, S., Cho, D., Schlossman, S.F., Morimoto, C. (1998). Correlation of the epitopes defined by anti-CD26 mAbs and CD26 function. *Mol. Immunol.* 35, 13-21.

Drucker, D.J., Nauck, M.A. (2006). The incretin system: glucagon-like peptide-1 receptor agonists and dipeptidyl peptidase-4 inhibitors in type 2 diabetes. *Lancet* 368, 1696-1705.

Durinx, C., Lambeir, A.M., Bosmans, E., Falmagne, J.B., Berghmans, R., Haemers, A., Scharpe, S., De Meester, I. (2000). Molecular characterization of dipeptidyl peptidase activity in serum: soluble CD26/dipeptidyl peptidase IV is responsible for the release of X-Pro dipeptides. *FEBS J.* 267, 5608-5613.

Erickson, R.H., Gum, J.R., Lotterman, C.D., Hicks, J.W., Lai, R.S., Kim, Y.S. (1999). Regulation of the gene for human dipeptidyl peptidase IV by hepatocyte nuclear factor 1α. *Biochem. J.* 338, 91-97.

Erickson, R.H., Lai, R.S., Kim, Y.S. (2000a). Role of hepatocyte nuclear factor 1α and 1β in the transcriptional regulation of human dipeptidyl peptidase IV during differentiation of Caco-2 cells. *Biochem. Biophys. Res. Commun*. 270, 235-239.

Erickson, R.H., Lai, R.S., Lotterman, C.D., Kim, Y.S. (2000b). Identification of upstream stimulatory factor as an activator of the human dipeptidyl peptidase IV gene in Caco-2 cells. *Gene* 258, 77-84.

Frank, N.Y., Schatton, T., Frank, M.H. (2010). The therapeutic promise of the cancer stem cell concept. *J. Clin. Invest.* 120, 41-50.

Fujimaki, W., Takahashi, N., Ohnuma, K., Nagatsu, M., Kurosawa, H., Yoshida, S., Dang, N.H., Uchiyama, T., Morimoto, C. (2008). Comparative study of regulatory T cell function of human CD25CD4 T cells from thymocytes, cord blood, and adult peripheral blood. *Clin. Dev. Immunol.* 2008, 305859.

Fujimoto, N., Ohnuma, K., Aoe, K., Hosono, O., Yamada, T., Kishimoto, T., Morimoto, C. (2014). Clinical significance of soluble CD26 in malignant pleural mesothelioma. *PLoS ONE* 9, e115647.

Ghani, F.I., Yamazaki, H., Iwata, S., Okamoto, T., Aoe, K., Okabe, K., Mimura, Y., Fujimoto, N., Kishimoto, T., Yamada, T., Xu, C.W., Morimoto, C. (2011). Identification of cancer stem cell markers in human malignant mesothelioma cells. *Biochem. Biophys. Res. Commun.* 404, 735-742.

Haas, A.R., Sterman, D.H. (2013). Malignant pleural mesothelioma: update on treatment options with a focus on novel therapies. *Clin. Chest Med.* 34, 99-111.

Hatano, R., Ohnuma, K., Otsuka, H., Komiya, E., Taki, I., Iwata, S., Dang, N.H., Okumura, K., Morimoto, C. (2015). CD26-mediated induction of EGR2 and IL-10 as potential regulatory mechanism for CD26 costimulatory pathway. *J. Immunol.*194, 960-972.

Hatano, R., Ohnuma, K., Yamamoto, J., Dang, N.H., Morimoto, C. (2013). CD26-mediated co-stimulation in human CD8$^+$ T cells provokes effector function via pro-inflammatory cytokine production. *Immunology* 138, 165-172.

Hatano, R., Yamada, T., Matsuoka, S., Iwata, S., Yamazaki, H., Komiya, E., Okamoto, T., Dang, N.H., Ohnuma, K., Morimoto, C. (2014). Establishment of monoclonal anti-human CD26 antibodies suitable for immunostaining of formalin-fixed tissue. *Diagn. Pathol.* 9, 30.

Havre, P.A., Abe, M., Urasaki, Y., Ohnuma, K., Morimoto, C., Dang, N.H. (2008). The role of CD26/dipeptidyl peptidase IV in cancer. *Front. Biosci.* 13, 1634-1645.

Hayashi, M., Madokoro, H., Yamada, K., Nishida, H., Morimoto, C., Sakamoto, M., Yamada, T. (2016). A humanized anti-CD26 monoclonal antibody inhibits cell growth of malignant mesothelioma via retarded G2/M cell cycle transition. *Cancer Cell Int.* 16, 35.

Hegen, M., Kameoka, J., Dong, R.P., Schlossman, S.F., Morimoto, C. (1997). Cross-linking of CD26 by antibody induces tyrosine phosphorylation and activation of mitogen-activated protein kinase. *Immunology* 90, 257-264.

Heins, J., Welker, P., Schonlein, C., Born, I., Hartrodt, B., Neubert, K., Tsuru, D., Barth, A. (1988). Mechanism of proline-specific proteinases: (I) Substrate specificity of dipeptidyl peptidase IV from pig kidney and proline-specific endopeptidase from Flavobacterium meningosepticum. *Biochim. Biophys. Acta* 954, 161-169.

Ho, L., Aytac, U., Stephens, L.C., Ohnuma, K., Mills, G.B., McKee, K.S., Neumann, C., LaPushin, R., Cabanillas, F., Abbruzzese, J.L., Morimoto, C., Dang, N.H. (2001). *In vitro* and *in vivo* antitumor effect of the anti-CD26 monoclonal antibody 1F7 on human CD30+ anaplastic large cell T-cell lymphoma Karpas 299. *Clin. Cancer Res.* 7, 2031-2040.

Hopsu-Havu, V.K., Glenner, G.G. (1966). A new dipeptide naphthylamidase hydrolyzing glycyl-prolyl-β-naphthylamide. *Histochemie. Histochemistry* 7, 197-201.

Hua, J., Davis, S.P., Hill, J.A., Yamagata, T. (2015). Diverse gene expression in human regulatory T cell subsets uncovers connection between regulatory T cell genes and suppressive function. *J. Imunol.* 195, 3642-3653.

Inamoto, T., Yamada, T., Ohnuma, K., Kina, S., Takahashi, N., Yamochi, T., Inamoto, S., Katsuoka, Y., Hosono, O., Tanaka, H., Dang, N.H., Morimoto, C. (2007). Humanized anti-CD26 monoclonal antibody as a treatment for malignant mesothelioma tumors. *Clin. Cancer Res.*13, 4191-4200.

Inamoto, T., Yamochi, T., Ohnuma, K., Iwata, S., Kina, S., Inamoto, S., Tachibana, M., Katsuoka, Y., Dang, N.H., Morimoto, C. (2006). Anti-CD26 monoclonal antibody-mediated G1-S arrest of human renal clear cell carcinoma Caki-2 is associated with retinoblastoma substrate dephosphorylation, cyclin-dependent kinase 2 reduction, p27^{kip1} enhancement, and disruption of binding to the extracellular matrix. *Clin. Cancer Res.* 12, 3470-3477.

Ishii, T., Ohnuma, K., Murakami, A., Takasawa, N., Kobayashi, S., Dang, N.H., Schlossman, S.F., Morimoto, C. (2001). CD26-mediated signaling for T cell activation occurs in lipid rafts through its association with CD45RO. *Proc. Natl. Acad. Sci. USA*. 98, 12138-12143.

Iwaki-Egawa, S., Watanabe, Y., Kikuya, Y., Fujimoto, Y. (1998). Dipeptidyl peptidase IV from human serum: purification, characterization, and N-terminal amino acid sequence. J. *Biochem.* 124, 428-433.

Komiya, E., Ohnuma, K., Yamazaki, H., Hatano, R., Iwata, S., Okamoto, T., Dang, N.H., Yamada, T., Morimoto, C. (2014). CD26-mediated regulation of periostin expression contributes to migration and invasion of malignant pleural mesothelioma cells. *Biochem. Biophys. Res. Commun.* 447, 609-615.

Kondola, S., Manners, D., Nowak, A.K. (2016). Malignant pleural mesothelioma: an update on diagnosis and treatment options. *Ther. Adv. Respir. Dis*. 10, 275-288.

Maggioni, C., Barletta, G., Rijavec, E., Biello, F., Gualco, E., Grossi, F. (2016). Advances in treatment of mesothelioma. *Expert Opin. Pharmacother*. 17, 1197-1205.

Maguer-Satta, V., Besancon, R., Bachelard-Cascales, E. (2011). Concise review: neutral endopeptidase (CD10): a multifaceted environment actor in stem cells, physiological mechanisms, and cancer. *Stem Cells* 29, 389-396.

Marguet, D., Bernard, A.M., Vivier, I., Darmoul, D., Naquet, P., Pierres, M. (1992). cDNA cloning for mouse thymocyte-activating molecule. A multifunctional ecto-dipeptidyl peptidase IV (CD26) included in a subgroup of serine proteases. *J. Biol. Chem*. 267, 2200-2208.

Masuyama, J., Berman, J.S., Cruikshank, W.W., Morimoto, C., Center, D.M. (1992). Evidence for recent as well as long term activation of T cells migrating through endothelial cell monolayers *in vitro*. *J. Immunol.* 148, 1367-1374.

Morimoto, C., Schlossman, S.F. (1998). The structure and function of CD26 in the T-cell immune response. *Immunol. Rev.* 161, 55-70.

Morimoto, C., Torimoto, Y., Levinson, G., Rudd, C.E., Schrieber, M., Dang, N.H., Letvin, N.L., Schlossman, S.F. (1989). 1F7, a novel cell surface molecule, involved in helper function of CD4 cells. *J. Immunol.* 143, 3430-3439.

Morra, L., Moch, H. (2011). Periostin expression and epithelial-mesenchymal transition in cancer: a review and an update. *Virchows Arch*. 459, 465-475.

Myers, R. (2012). Asbestos-related pleural disease. *Curr. Opin. Pulm. Med.* 18, 377-381.

Nagatsu, I., Nagatsu, T., Yamamoto, T. (1968). Hydrolysis of amino acid beta-naphthylamides by aminopeptidases in human parotid salva and human serum. *Experientia* 24, 347-348.

Ogata, S., Misumi, Y., Ikehara, Y. (1989). Primary structure of rat liver dipeptidyl peptidase IV deduced from its cDNA and identification of the NH_2-terminal signal sequence as the membrane-anchoring domain. *J. Biol. Chem*. 264, 3596-3601.

Ohnuma, K., Dang, N.H., Morimoto, C. (2008a). Revisiting an old acquaintance: CD26 and its molecular mechanisms in T cell function. *Trends Immunol*. 29, 295-301.

Ohnuma, K., Hatano, R., Morimoto, C. (2015). DPP4 in anti-tumor immunity: going beyond the enzyme. *Nat. Immunol*. 16, 791-792.

Ohnuma, K., Hosono, O., Dang, N.H., Morimoto, C. (2011). Dipeptidyl peptidase in autoimmune pathophysiology. *Adv. Clin. Chem*. 53, 51-84.

Ohnuma, K., Morimoto, C. (2013). DPP4 (dipeptidyl-peptidase 4). *Atlas Genet. Cytogenet. Oncol. Haematol.* 17, 301-312.

Ohnuma, K., Munakata, Y., Ishii, T., Iwata, S., Kobayashi, S., Hosono, O., Kawasaki, H., Dang, N.H., Morimoto, C. (2001). Soluble CD26/dipeptidyl peptidase IV induces T cell proliferation through CD86 up-regulation on APCs. *J. Immunol.* 167, 6745-6755.

Ohnuma, K., Takahashi, N., Yamochi, T., Hosono, O., Dang, N.H., Morimoto, C. (2008b). Role of CD26/dipeptidyl peptidase IV in human T cell activation and function. *Front. Biosci.* 13, 2299-2310.

Ohnuma, K., Uchiyama, M., Yamochi, T., Nishibashi, K., Hosono, O., Takahashi, N., Kina, S., Tanaka, H., Lin, X., Dang, N.H., Morimoto, C. (2007). Caveolin-1 triggers T-cell activation via CD26 in association with CARMA1. *J. Biol. Chem.* 282, 10117-10131.

Ohnuma, K., Yamochi, T., Uchiyama, M., Nishibashi, K., Iwata, S., Hosono, O., Kawasaki, H., Tanaka, H., Dang, N.H., Morimoto, C. (2005). CD26 mediates dissociation of Tollip and IRAK-1 from caveolin-1 and induces upregulation of CD86 on antigen-presenting cells. *Mol. Cell. Biol.* 25, 7743-7757.

Ohnuma, K., Yamochi, T., Uchiyama, M., Nishibashi, K., Yoshikawa, N., Shimizu, N., Iwata, S., Tanaka, H., Dang, N.H., Morimoto, C. (2004). CD26 up-regulates expression of CD86 on antigen-presenting cells by means of caveolin-1. *Proc. Natl. Acad. Sci. USA*. 101, 14186-14191.

Okamoto, T., Iwata, S., Yamazaki, H., Hatano, R., Komiya, E., Dang, N.H., Ohnuma, K., Morimoto, C. (2014). CD9 Negatively Regulates CD26 expression and inhibits CD26-mediated enhancement of invasive potential of malignant mesothelioma cells. *PLoS ONE* 9, e86671.

Proost, P., Schutyser, E., Menten, P., Struyf, S., Wuyts, A., Opdenakker, G., Detheux, M., Parmentier, M., Durinx, C., Lambeir, A.M., Neyts, J., Liekens, S., Maudgal, P. C., Billiau, A., Van Damme, J. (2001). Amino-terminal truncation of CXCR3 agonists impairs receptor signaling and lymphocyte chemotaxis, while preserving antiangiogenic properties. *Blood* 98, 3554-3561.

Rasmussen, H.B., Branner, S., Wiberg, F.C., Wagtmann, N. (2003). Crystal structure of human dipeptidyl peptidase IV/CD26 in complex with a substrate analog. *Nat. Struct. Biol.* 10, 19-25.

Reya, T., Morrison, S.J., Clarke, M.F., Weissman, I.L. (2001). Stem cells, cancer, and cancer stem cells. *Nature* 414, 105-111.

Robinson, B.M. (2012). Malignant pleural mesothelioma: an epidemiological perspective. *Ann. Cardiothorac. Surg*. 1, 491-496.

Rohrborn, D., Eckel, J., Sell, H. (2014). Shedding of dipeptidyl peptidase 4 is mediated by metalloproteases and up-regulated by hypoxia in human adipocytes and smooth muscle cells. *FEBS Lett*. 588, 3870-3877.

Schramm, A., Opitz, I., Thies, S., Seifert, B., Moch, H., Weder, W., Soltermann, A. (2010). Prognostic significance of epithelial-mesenchymal transition in malignant pleural mesothelioma. *Eur. J. Cardiothorac. Surg*. 37, 566-572.

Shersher, D.D., Liptay, M.J. (2013). Multimodality treatment of pleural mesothelioma. *Surg. Oncol. Clin. N. Am.* 22, 345-355.

Stohlawetz, P., Hahn, P., Koller, M., Hauer, J., Resch, H., Smolen, J., Pietschmann, P. (1998). Immunophenotypic characteristics of monocytes in elderly subjects. *Scand. J. Imunol*. 48, 324-326.

Tanaka, T., Camerini, D., Seed, B., Torimoto, Y., Dang, N.H., Kameoka, J., Dahlberg, H.N., Schlossman, S.F., Morimoto, C. (1992). Cloning and functional expression of the T cell activation antigen CD26. *J. Immunol*. 149, 481-486.

Tanaka, T., Kameoka, J., Yaron, A., Schlossman, S.F., Morimoto, C. (1993). The costimulatory activity of the CD26 antigen requires dipeptidyl peptidase IV enzymatic activity. *Proc. Natl. Acad. Sci. USA*. 90, 4586-4590.

Thompson, M.A., Ohnuma, K., Abe, M., Morimoto, C., Dang, N.H. (2007). CD26/dipeptidyl peptidase IV as a novel therapeutic target for cancer and immune disorders. *Mini Rev. Med. Chem.* 7, 253-273.

van Meerbeeck, J.P., Damhuis, R. (2011). Facts, rumours and speculations about the mesothelioma epidemic. *Respirology* 16, 1018-1019.

van Meerbeeck, J.P., Gaafar, R., Manegold, C., Van Klaveren, R.J., Van Marck, E.A., Vincent, M., Legrand, C., Bottomley, A., Debruyne, C., Giaccone, G. (2005). Randomized phase III study of cisplatin with or without raltitrexed in patients with malignant pleural mesothelioma: an intergroup study of the European Organisation for Research and Treatment of Cancer Lung Cancer Group and the National Cancer Institute of Canada. *J. Clin. Oncol.* 23, 6881-6889.

Wang, J.C., Dick, J.E. (2005). Cancer stem cells: lessons from leukemia. *Trends Cell. Biol.* 15, 494-501.

Yamada, K., Hayashi, M., Du, W., Ohnuma, K., Sakamoto, M., Morimoto, C., Yamada, T. (2009). Localization of CD26/DPPIV in nucleus and its nuclear translocation enhanced by anti-CD26 monoclonal antibody with anti-tumor effect. *Cancer Cell Int.* 9, 17.

Yamada, K., Hayashi, M., Madokoro, H., Nishida, H., Du, W., Ohnuma, K., Sakamoto, M., Morimoto, C., Yamada, T. (2013). Nuclear localization of CD26 induced by a humanized monoclonal antibody inhibits tumor cell growth by modulating of POLR2A transcription. *PLoS ONE* 8, e62304.

Yamamoto, J., Ohnuma, K., Hatano, R., Okamoto, T., Komiya, E., Yamazaki, H., Iwata, S., Dang, N.H., Aoe, K., Kishimoto, T., Yamada, T., Morimoto, C. (2014). Regulation of somatostatin receptor 4-mediated cytostatic effects by CD26 in malignant pleural mesothelioma. *Br. J. Cancer* 110, 2232-2245.

Yamazaki, H., Naito, M., Ghani, F.I., Dang, N.H., Iwata, S., Morimoto, C. (2012). Characterization of cancer stem cell properties of CD24 and CD26-positive human malignant mesothelioma cells. *Biochem. Biophys. Res. Commun.* 419, 529-536.

Yamochi, T., Yamochi, T., Aytac, U., Sato, T., Sato, K., Ohnuma, K., McKee, K.S., Morimoto, C., Dang, N.H. (2005). Regulation of p38 phosphorylation and topoisomerase IIα expression in the B-cell lymphoma line Jiyoye by CD26/dipeptidyl peptidase IV is associated with enhanced *in vitro* and *in vivo* sensitivity to doxorubicin. *Cancer Res.* 65, 1973-1983.

Yan, W., Shao, R. (2006). Transduction of a mesenchyme-specific gene periostin into 293T cells induces cell invasive activity through epithelial-mesenchymal transformation. *J. Biol. Chem.* 281, 19700-19708.

Yaron, A., Naider, F. (1993). Proline-dependent structural and biological properties of peptides and proteins. *Crit. Rev. Biochem. Mol. Biol.* 28, 31-81.

RR

第2章　核内移行するヒト化抗CD26モノクローナル抗体-TFⅡH阻害剤複合体

山田健人*

1　はじめに

CD26は，細胞膜表面に局在するTリンパ球共刺激分子であり，ヘルパーT細胞のマーカーとして見出された。このCD26は，C末端にセリンプロテアーゼの一つであるDipeptidyl Peptidase-4（DPP-Ⅳ）を持つとともに，別の領域では，細胞外基質であるファイブロネクチンやコラーゲン，あるいはアデノシンデアミナーゼと結合し，さまざまな細胞内情報伝達を調節する働きも有していると考えられている1)。正常組織・細胞においては，Tリンパ球以外に，腎近位尿細管上皮，肝毛細胆管，破骨細胞，血管内皮細胞などに発現している。このCD26は，一部の悪性リンパ腫・白血病や腎癌，大腸癌，甲状腺癌に発現していることが知られていたが，最近，悪性中皮腫において85％以上の症例において発現していることが明らかとなった2〜5)。また中皮腫や大腸癌においては，CD26ががん幹細胞のマーカーであることが報告され6,7)，さらにCD26が広範ながんに発現しており，がん細胞の増殖や浸潤，転移にも関与することが明らかとなりつつある1,8)。

2　抗CD26モノクローナル抗体とそのヒト化

このようにがん細胞の細胞表面に発現するCD26を分子標的療法の標的分子として捉える抗体療法の開発が試みられた。順天堂大学・森本幾夫博士らが開発したマウス抗ヒトCD26モノクローナル抗体の幾つかのクローンは，ヒトがん細胞株に対して抗腫瘍作用を有すことが判明した1)。そこで，ワイズ・セラピューティックス社は，これらの抗体の中から，抗腫瘍効果が強いクローン14D10を選択し，そのcDNAを元にしてAbmaxis *in-silico* Immunization（AISIM）法により，*in silico*でアミノ酸をヒト型に置換することで，親和性を維持したヒト化モノクローナル抗体YS110を開発した。このYS110抗体（ヒトIgG1サブタイプ）は，元となったクローン14D10抗体よりも，ヒトCD26分子に対する親和性が高く，またCD26の細胞外基質への接着阻害能やCD26陽性がん細胞に対する増殖抑制能が亢進していた3)。またYS110は，マウスやラットなどのげっ歯類CD26には反応しないが，毒性試験に用いるサルとは交叉反応が認められた。またYS110はCHO細胞により分泌され，精製されるが，安定した高い生産性を示した。

---

* Taketo Yamada　埼玉医科大学　医学部　病理学　教授

3　ヒト化抗CD26モノクローナル抗体YS110の抗腫瘍効果と分子機構（図1）

通常，抗体療法では，抗体が細胞表面で標的分子と結合した後，抗体のFc領域を介した細胞傷害作用が惹起されることで細胞傷害が誘導される。この抗体依存性細胞介在性細胞傷害（antibody-dependent cellular cytotoxicity：ADCC）に加えて，補体依存性細胞障害活性（complement-dependent cytotoxicity：CDC）などの免疫学的機序により，がん細胞が攻撃される。YS110においても，このADCCおよびCDCによる抗がん作用が認められた[3]。

一方，培養ヒトがん細胞へのYS110添加あるいはADCCやCDCが機能しない免疫不全マウス担がんモデルへのYS110の投与においても，ヒトがん細胞の抗がん作用が判明し，YS110が

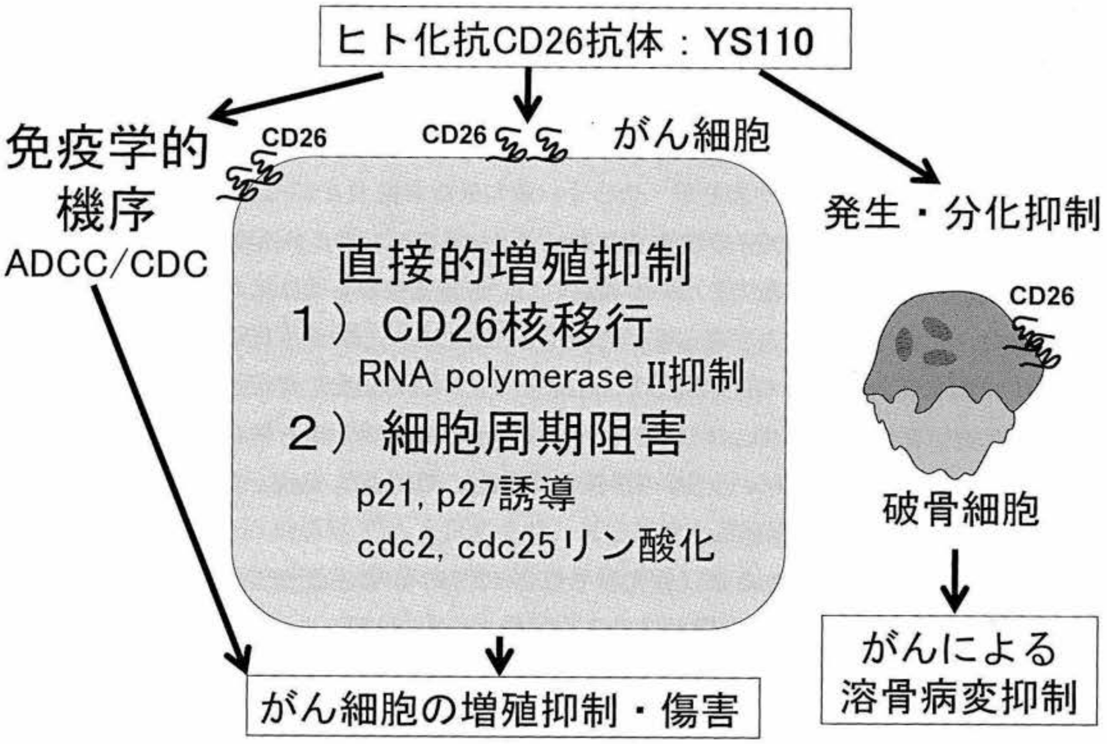
ヒト化抗CD26抗体：YS110
免疫学的機序
ADCC/CDC
CD26
CD26
がん細胞
直接的増殖抑制
1）CD26核移行
RNA polymerase Ⅱ抑制
2）細胞周期阻害
p21, p27誘導
cdc2, cdc25リン酸化
発生・分化抑制
CD26
破骨細胞
がんによる溶骨病変抑制
がん細胞の増殖抑制・傷害

図1　ヒト化抗CD26モノクローナル抗体YS110のがん細胞への多彩な作用機序

YS110は，IgG1サブタイプに属し，抗体依存性細胞介在性細胞傷害（antibody-dependent cellular cytotoxicity：ADCC）や補体依存性細胞障害活性（complement-dependent cytotoxicity：CDC）による免疫学的機序によるがん細胞傷害能を持つ。一方，がん細胞の細胞膜表面に存在するCD26に結合することにより，がん細胞に対して直接的細胞増殖抑制能を有する。その機序は，一つは，YS110と結合したCD26がカベオリン依存性に細胞質に内在化し，さらに核内に移行することで，RNA polymerase Ⅱのサブユニット POLR2Aの転写を抑制することによる。またYS110が細胞膜CD26に結合することにより，細胞周期関連分子の発現誘導やリン酸化促進を介して，細胞増殖を抑制する。一方，YS110は破骨細胞の分化抑制を誘導し，破骨細胞の活性を低下させるため，がんの骨転移における溶骨性病変を抑制する効果を持つ。このようにYS110は，一つの抗体であるが多種にわたる分子機構を介して，がん細胞の増殖浸潤や骨病変の抑制に効果的に寄与しうるユニークな抗体療法となることが期待されている。

直接的にがん細胞に働き，抗腫瘍効果を発揮しうると推測された[3]。その直接的抗がん作用の分子機構の一つは，YS110が細胞膜CD26に結合することにより，細胞周期関連分子p21，p27の発現誘導やcdc2, cdc25のリン酸化促進を介して，細胞増殖を抑制することであった[1, 3]。

いま一つの分子機構が，YS110によるCD26の核移行誘導であった。がん細胞をYS110で処理すると，YS110と結合したCD26がカベオリン依存性に細胞質に内在化し，さらにCD26-YS110複合体が，核内に移行することでRNA polymerase Ⅱのサブユニット POLR2Aの転写を抑制することが判明した[9, 10]。このCD26とYS110の核移行は，CD26を発現する正常細胞（Tリンパ球，血管内皮細胞）では観察されず，がん細胞特異的な現象であった。抗体はもちろんのことであるがCD26にも核移行シグナルはなく，なんらかの核輸送分子と相互作用をすることで核へ移行するものと推測された。このCD26-YS110複合体の核移行は，がん細胞のYS110処理後，30分より観察され，2時間をピークとして4時間後まで観察され，Nystatin処理あるいはカベオリンsiRNA処理により核移行は阻害されたが，Monodansylcadaverineでは阻害されなかったことから，クラスリン依存性ではなくカベオリン依存性のエンドサイトーシスによるものであることが明らかとなった。さらに免疫不全マウスに移植したヒトがん細胞が腫瘍を形成した後，YS110を投与すると*in vivo*においてもCD26およびYS110ががん細胞の核内において観察された[10]。

そこで，核内におけるCD26の機能を探索するためにクロマチン免疫沈降法により，核内CD26が結合しているDNA配列について検討した。核抽出液からCD26を免疫沈降して得られたDNA断片をクローニングして塩基配列を決定したところ，一つが，RNA polymerase Ⅱのサブユニット POLR2A遺伝子の近傍領域であった。そこでPOLR2A遺伝子の調節領域を含むレポーター遺伝子を作製し，CD26の結合性や転写における抑制効果を検討したところ，YS110処理により抗体の量依存性かつCD26の核移行依存性にPOLR2A発現が抑制され，細胞増殖抑制が誘導されることが判明した[10]。

一方，興味深いことにYS110は，骨代謝や骨リモデリングに重要な機能を有する破骨細胞の分化を抑制し，破骨細胞の活性を低下させることで，がんの骨転移における溶骨性病変を抑制する効果を持つことが明らかとなった[11]。

このようにYS110という一つの抗体が，多岐にわたる分子機構を介して，がん細胞の増殖浸潤や骨病変の抑制に効果的に寄与しうることが期待されている（図1）。

このYS110は，サルを用いた安全性試験やGMP準拠の抗体作製を経て，欧州連合における臨床治験申請を行い，2009年からフランスGustave Roussy Instituteを中心として，第Ⅰ相臨床試験が実施され，2015年10月に終了した。その結果，重篤な有害事象は観察されず，中皮腫症例においては，19例中10例がmodified RECIST評価でStable Disease（SD）と判定され，5例が6ヶ月以上SDを継続，1例が3ヶ月以上SDを継続し，YS110単独での治療の有効性を示唆する結果が得られた[12]。

4　YS110へのTFⅡH阻害剤結合による新規ADC（Y-TR1）の開発

CD26陽性のがん細胞をYS110で処理すると，YS110と結合したCD26がカベオリン依存性に細胞質，さらに核内に移行してRNA polymerase Ⅱのサブユニット POLR2Aの転写を抑制することで細胞増殖抑制を惹起することから，YS110へRNA polymerase Ⅱの機能阻害分子を結合させることで，核内で効率良く抗がん作用を発揮しうるADCの開発を試みた。RNA polymerase Ⅱは，タンパク質をコードするほとんどの遺伝子の転写に必須なきわめて重要な酵素であり，その機能阻害剤としては，アマニチンなどの分子が知られているが，いずれも毒性が強く抗がん剤として患者さんへ全身投与するのは難しいとされてきた。またYS110がRNA polymerase Ⅱのサブユニットである POLR2A遺伝子の転写を抑制することから，RNA polymerase Ⅱ自体の阻害剤ではなく，RNA polymerase Ⅱとともに転写に必須とされる基本転写因子群TFⅡHを標的とした阻害剤をYS110へ結合する薬剤として選択した。その中でTriptolideは，RNA polymerase Ⅱによる転写イニシエーションに関わる因子TFⅡHのサブユニットXBP/ERCC3に結合すことで，DNA依存性ATPase活性を阻害し，結果としてほとんどの遺伝子のRNA polymerase Ⅱによる転写を抑制する分子（$C_{20}H_{24}O_6$，分子量360.4）である[13]。またTriptolideはTFⅡH阻害効果は強いものの，難容性であり，薬剤としての使用は難しいと考えられていた。そこで，このTriptolideをYS110に結合させることで，がん細胞特異的に核内に取り込まれることを目論んで，全身での毒性を低く抑えた新規ADCの作製を行った。

このTriptolideにSH基を導入して，S-S結合により化学的に安定な二量体とした。このS-S結合はTCEP還元ゲルを用いて還元され単量体（TR1と命名）としたものをYS110との結合に用いた。YS110にheterobifunctionalリンカーSuccinimidyl 4-[*N*-Maleimidomethyl] Cyclohexane-1-Carboxylate（SMCC）を結合させ，非結合のSMCCをHiTrap脱塩カラムで除去した後，Triptolide誘導体TR1と反応させ，反応産物から非結合TR1を除去してから，抗体を精製し，YS110-Triptolide誘導体TR1結合分子（Y-TR1と命名）とした（図2）。Y-TR1は，まず抗体としてのヒトCD26分子との親和性や結合力価を検討し，その親和性や結合力価にはほとんど低下がないことを確認した。次にY-TR1において，抗体YS110一分子あたりどのくらいのTR1分子が結合しているかを評価した。質量分析器MALDI-TOF massを用いてYS110とY-TR1の質量を測定し，その差をTR1分子量で割ることで，YS110一分子あたり6～7個のTR1分子が結合していることが判明した（図3）。

5　Y-TR1の抗がん作用

この新規ADCであるY-TR1のCD26陽性ヒトがん細胞に対する抗がん作用を検討した。培養細胞としては，CD26陰性中皮腫細胞MSTO-211HにCD26発現ベクターを導入した安定発現細胞株（MSTO-CD26クローン12）と対照としてネオマイシン耐性遺伝子のみを導入した安

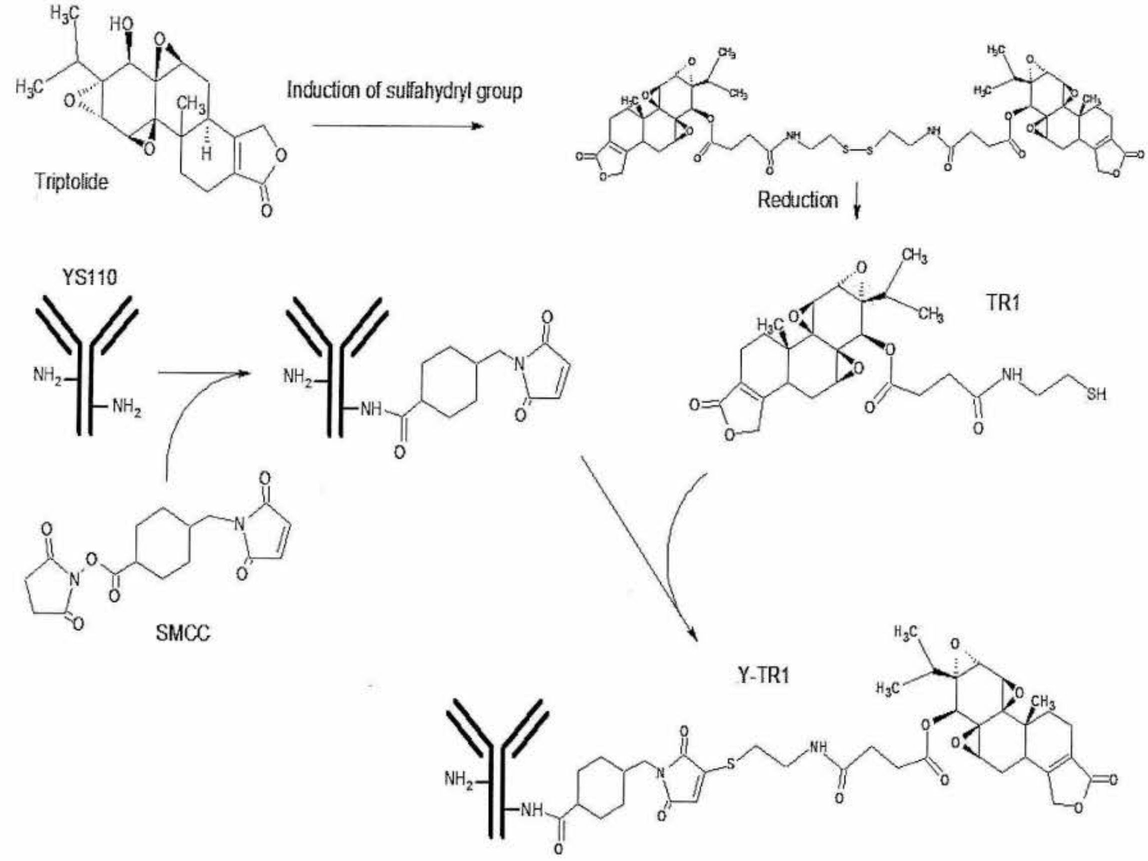

図2　ヒト化抗CD26モノクローナル抗体YS110へのTriptolide誘導体TR1の結合方法
TriptolideにSH基を導入して，S-S結合により化学的に安定な二量体とした。S-S結合はTCEP還元ゲルを用いて還元され単量体のTR1としたものをYS110との結合に用いた。YS110にheterobifunctionalリンカーSMCCを結合させ，さらにTR1と反応させ，反応産物から非結合TR1を除去し，抗体を精製し，Y-TR1とした。

定発現細胞株（MSTO-wt），CD26陽性中皮腫細胞JMN，ヒトT細胞白血病由来のCD26陰性Jurkat細胞株にヒトCD26発現ベクターを遺伝子導入したCD26安定発現細胞株（Jurkat-CD26）と対照としてネオマイシン耐性遺伝子のみを導入した安定発現細胞株（Jurkat-wt）を使用した（順天堂大学・森本幾夫博士より供与）。*In vitro*での抗がん作用は，培養液にTriptolide, TR1, YS110およびY-TR1を添加し，48時間後にWST-1アッセイで評価した（図4および表1）。その結果，CD26陽性JMN細胞では，Triptolideはきわめて強い増殖抑制効果を示し（half maximal（50%）inhibitory concentration（IC50）：15 nM），Triptolide誘導体であるTR1は，IC50でおよそ1/12に低下していた（IC50：180 nM）。またMSTO細胞でもTriptolideではIC50が10 nM，TR1ではIC50が250 nMと低下していた。この活性の低下は，TriptolideへのSH基の導入によるものと推測された。一方，YS110にTR1を結合させたY-TR1は，JMN細胞において，YS110では100 μg/mLでプラトーとなり，その時の増殖抑制率は20%であったが（IC50測定不能），Y-TR1では，50 μg/mLでプラトーとなり，その時

表1　培養がん細胞株への Triptolide, TR1 および Y-TR1 の増殖抑制効果

細胞株	由来	CD26 発現	IC50 of Triptolide (nM)	IC50 of TR1 (nM)	IC50 of Y-TR1 (μg/mL)
MSTO-wt	中皮腫	−	10	250	35
MSTO-CD26 clone12	中皮腫	+	10	250	10
JMN	中皮腫	+	15	180	25
Jurkat-wt	白血病	−	10	ND	100
Jurkat-CD26	白血病	+	6	ND	30

IC50：half maximal（50%）inhibitory concentration

ヒト悪性中皮腫由来 MSTO-211H 細胞は，CD26 発現のない細胞株である。この細胞株にヒト CD26 発現ベクターを遺伝子導入し，CD26 安定発現細胞株 MSTO-CD26 clone 12 を作製して使用した。対照として，MSTO-211H 細胞にネオマイシン耐性遺伝子のみが導入された MSTO-wt 細胞株を使用した。ヒト悪性中皮腫由来 JMN 細胞株は CD26 の高発現を有する細胞である。またヒト T 細胞白血病由来の Jurkat 細胞株は CD26 発現のない細胞株である。この細胞株にヒト CD26 発現ベクターを遺伝子導入し，CD26 安定発現細胞株 Jurkat-CD26 と対照としてネオマイシン耐性遺伝子のみが導入された細胞株（Jurkat-wt）を作製して使用した。

その結果，Triptolide に比べて TR1 の IC50 は，1/12-25 へ低下していた。また Y-TR1 による細胞増殖抑制能について検討したところ，CD26 発現細胞は CD26 の発現がない細胞と比較して，IC50 は 1/3.3-3.5 と低下していた。

の増殖抑制率は 85％を示した（IC50：25 μg/mL）（図 4）。また Y-TR1 の効果において，CD26 発現 MSTO-CD26 細胞と Jurkat-CD26 細胞では，CD26 を発現しない MSTO-wt 細胞と Jurkat-wt 細胞と比べて，IC50 は 1/3.3-3.5 と低下していた（表 1）。これらの結果は，TR1 は Triptolide に比べて抗がん活性が低下しているものの，YS110 との結合により Y-TR1 は YS110 よりも強い抗がん効果を発揮することが明らかとなった。

次に *in vivo* における Y-TR1 の抗がん効果を検討した。ヒト悪性中皮腫細胞株 JMN を免疫不全マウス NOD/SCID に皮下移植したモデルを用いて，マウス抗ヒト CD26 モノクローナル抗体 14D10，YS110，Y-TR1 の造腫瘍性への影響を解析した。JMN 細胞移植後，3 日目より，上記の抗体を 8 mg/kg 体重で週 3 回腹腔内投与し，3 週後に腫瘍を摘出して，腫瘍の重量を計測した。その結果，対照群（ヒト IgG1 投与）と比較して，YS110 投与群では 30％程度の抑制効果を示したが，Y-TR1 投与群では，75％までの高い抑制効果を示した（図 5）。

6　考察

CD26 は，正常では T リンパ球をはじめとした様々な細胞に発現しており，細胞の接着や増殖などにおいて多彩な機能を有している分子である。また CD26 は，C 末端にセリンプロテアーゼの一つである Dipeptidyl Peptidase-4（DPP-Ⅳ）を持つが，この阻害剤は糖尿病の治療薬として世界中で広く使用されている。一方，がん細胞において，CD26 は広汎ながん腫において高発現がある。ヒト化抗 CD26 モノクローナル抗体 YS110 は，このがん細胞表面の CD26 に結合

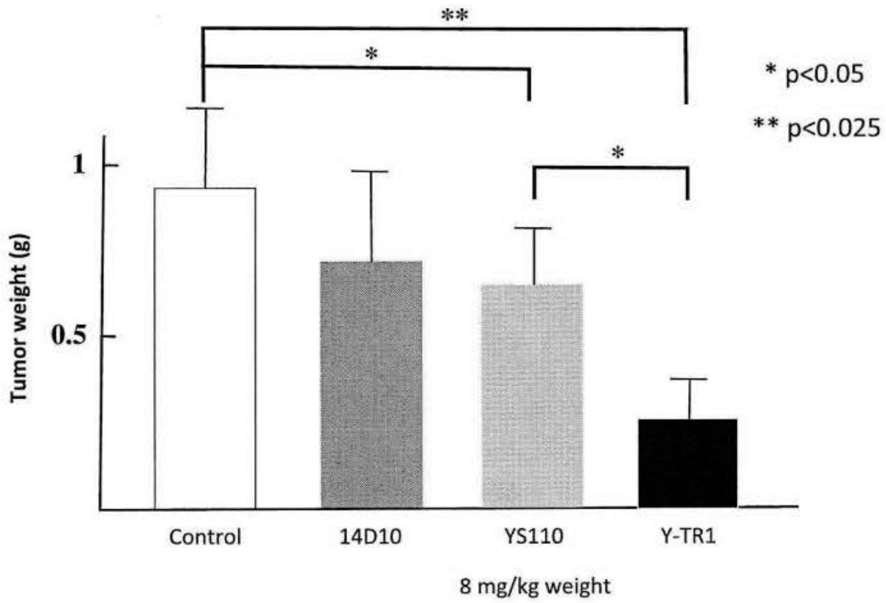

図5　Y-TR1のヒト中皮腫細胞株に対する*in vivo*での増殖抑制効果

ヒト悪性中皮腫細胞株JMNを免疫不全マウスNOD/SCIDに皮下移植したモデルを用いて，マウス抗ヒトCD26モノクローナル抗体14D10，YS110，Y-TR1の造腫瘍性への影響を解析した。JMN細胞移植後，3日目より，上記の抗体を8 mg/kg体重で週3回腹腔内投与し，3週後に腫瘍を摘出して，腫瘍の重量を計測した。対照群（ヒトIgG1投与）と比較して，YS110投与群では30％程度の抑制効果を示したが，Y-TR1投与群では，75％までの抑制効果を示した。

するとCD26とともにエンドサイトーシスにより細胞質内に取り込まれ，さらに核へ移行する。このYS110によるCD26の核移行が，正常Tリンパ球や血管内皮細胞では見られないことから，がん細胞特異的な現象と考えられる。このがん細胞特異性から，YS110が，がん細胞の核への物質輸送に有用と考え，本稿では，核内へ移行したCD26が，RNA polymerase Ⅱのサブユニット POLR2A遺伝子の転写を抑制することで細胞増殖抑制を惹起することに着目して，YS110へRNA polymerase Ⅱの基本転写因子群であるTFⅡH阻害剤を結合させたADCの開発について述べた。このYS110は，さらに毒性が強く全身投与できない様々な抗がん分子や分子標的薬を結合させることで，広大な可能性を有していると考えている。

RNA polymerase Ⅱは，タンパク質をコードする遺伝子のほとんどの転写に必須な酵素であり，細胞の生存・維持・増殖に不可欠な分子である。そのため，以前よりその阻害剤やRNAiが抗がん分子としての可能性が考慮されていた14)。最近，Liuらは，大腸癌において，p53遺伝子の近傍にRNA polymerase ⅡのサブユニットPOLR2A遺伝子があることで，p53遺伝子の欠失とともにPOLR2A遺伝子も欠失している症例が多いことを見出し，これらのPOLR2A遺伝子のヘテロ欠失がある大腸癌細胞では，毒性が強いRNA polymerase Ⅱ阻害剤アマニチンが，より低濃度で抗がん作用を示すことを報告した15)。このことからp53遺伝子の欠失があるがん症例においては，ドラッグデリバリーの方法を駆使すれば，RNA polymerase Ⅱ阻害剤が抗がん剤として使用できる可能性を示唆しており，実際に，Liuらはアマニチンを結合させた抗

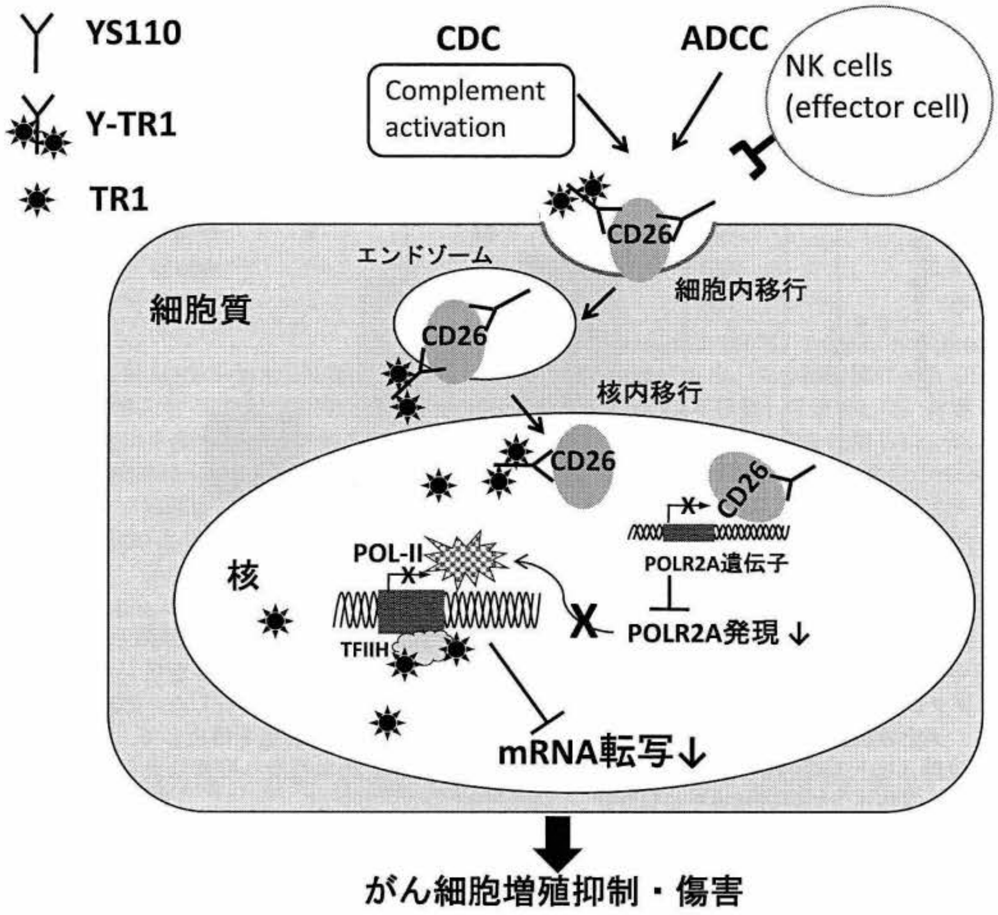
YS110
Y-TR1
TR1
CDC
Complement activation
ADCC
NK cells (effector cell)
CD26
エンドゾーム
細胞内移行
細胞質
CD26
核内移行
CD26
CD26
POLR2A遺伝子
POL-II
核
TFIIH
POLR2A発現↓
mRNA転写↓
がん細胞増殖抑制・傷害

図6　ヒト化抗CD26モノクローナル抗体YS110へのTFⅡH阻害剤結合による新規ADCの抗がん機序
YS110はがん細胞表面CD26と結合し，その後，カベオリン依存性に細胞質に移動し，さらに核内に移行することで，RNA polymerase Ⅱのサブユニット POLR2Aの転写を抑制する。このYS110にTFⅡH阻害剤Triptolide誘導体TR1を結合させたADCは，がん細胞の細胞質・核へTR1を運搬し，核内でTFⅡHを阻害することによりRNA polymerase Ⅱの機能障害を惹起し，多くの遺伝子のmRNA転写を阻害することにより，がん細胞の増殖抑制および細胞傷害を誘導する。

epithelial cell adhesion molecule抗体が，p53遺伝子の欠失がある大腸癌細胞を移植したマウスモデルで腫瘍を縮小させることに成功している[15)]。この点において，本稿で紹介したYS110は，YS110によるPOLR2A転写抑制による発現低下を誘導することから，p53遺伝子欠失に伴ったPOLR2A遺伝子欠失がない症例においても有効であり，さらにY-TR1という新規ADCが，一つの薬剤でPOLR2A発現低下とTHⅡF阻害の両面からRNA polymerase Ⅱの機能阻害を行うことで，より効果が高く，耐性ができにくい分子標的療法となりうると期待される。

文　　献

1）P. A. Havre *et al.*, *Front. Biosci.*, **13**, 1634（2008）
2）T. Yamada, *Keio J. Med.*, **60**, 37（2011）
3）T. Inamoto *et al.*, *Clin. Cancer Res.*, **13**, 4191（2007）
4）K. Aoe *et al.*, *Clin. Cancer Res.*, **18**, 1447（2012）
5）T. Inamoto *et al.*, *Clin. Cancer Res.*, **12**, 3470（2006）
6）R. Pang *et al.*, *Cell Stem Cell*, **6**, 603（2010）
7）F. I. Ghani *et al.*, *Biochem. Biophys. Res. Commun.*, **404**, 735（2011）
8）V. J. Amatya *et al.*, *Oncol. Rep.*, **26**, 1369（2011）
9）K. Yamada *et al.*, *Cancer Cell Int.*, **9**, 17（2009）
10）K. Yamada *et al.*, *PLoS One*, **8**, e62304（2013）
11）H. Nishida *et al.*, *J. Bone Miner. Res.*, **29**, 2439（2014）
12）E. Angevin *et al.*, 2015 American Society of Clinical Oncology（ASCO）Annual Meeting, Chicago, USA（2015）
13）D. V. Titov *et al.*, *Nat. Chem. Biol.*, **7**, 182（2011）
14）O. R. Mook *et al.*, *Cancer Gene Ther.*, **16**, 532（2009）
15）Y. Liu *et al.*, *Nature*, **520**, 697（2015）

First-in-Human phase 1 of YS110, a monoclonal antibody directed against CD26 in advanced CD26-expressing cancers.

***Eric Angevin*[1], *Nicolas Isambert*[2], *Véronique Trillet-Lenoir*[3], *Benoit You*[3], *Jérôme Alexandre*[4], *Gérard Zalcman*[5], *Philippe Vielh*[6], *Françoise Farace*[6], *Fanny Valleix*[7], *Thomas Podoll*[8], *Yu Kuramochi*[9], *Itaru Miyashita*[9], *Osamu Hosono*[10], *Nam H Dang*[11], *Kei Ohnuma*[12], *Taketo Yamada*[13], *Yutaro Kaneko*[14]; *Chikao Morimoto*[12]**

[1] Gustave Roussy, DITEP – Drug Development Department, Villejuif, France

[2] Centre Georges-François Leclerc, Unité de Phases Précoces, Dijon, France

[3] Institut de Cancérologie des Hospices Civils de Lyon, CITOHL, Lyon, France

[4] Hôpital Cochin, Paris, France

[5] Centre Hospitalier Universitaire (CHU) de Caen, Centre de Recherche Clinique/Essais de phases précoces, France

[6] Gustave Roussy, Translational Research Laboratory, Villejuif, France

[7] FV Clinical subcontractor for SynteractHCR SAS, Levallois-Perret, France

[8] Y's therapeutics Inc., USA, Redwood City, USA

[9] Kissei Pharmaceutical Co., Ltd., Tokyo, Japan

[10] Department of Rheumatology and Allergy, IMSUT Hospital, The Institute of Medical Science, The University of Tokyo, Tokyo, Japan

[11] Division of Hematology/Oncology, University of Florida, USA

[12] Department of Therapy Development and Innovation for Immune Disorders and Cancers, Graduate School of Medicine, Juntendo University, Tokyo, Japan

[13] Keio University, School of Medicine Tokyo and Saitama Medical University, Japan

[14] Y's AC Co., Ltd., Tokyo, Japan

Corresponding author:

Eric Angevin, MD, PhD

Drug Development Department (DITEP)

Gustave Roussy

114 rue Edouard Vaillant

94805 Villejuif, France

Tel: +33 (0)1.42.11.50.35

Fax: +33 (0)1.42.11.65.30

E-mail: eric.angevin@gustaveroussy.fr

This study has been previously selected for presentation at the ASCO2015 meeting
Running title: Phase 1 study of YS110 in solid tumors
Total number of figures and tables: 6

Funding: This study was supported by Y's AC, Kissei Pharmaceutical Co., Ltd., Tokyo, Japan and Japan Agency for Medical Research and Development (AMED)

EUDRACT Study n° 2008-004407-56

Conflicts of interest: Yutaro Kaneko is an employer of Y's AC Co., LTD., Japan, Thomas Podoll is an employer of Y's Therapeutics Inc., USA. and Yu Kuramochi and Itaru Miyashita are employees of Kissei Pharmaceutical Co., Ltd., Tokyo, Japan. Chikao Morimoto, Kei Ohnuma, and Nam H Dang are stock holders of Y's AC Co., Ltd. The remaining authors have no relevant relationships to disclose.

Word count: 4954/5000 (excluding references and tables)

Key words: CD26, phase I, mesothelioma, immune checkpoint

ABSTRACT (204 words)

Background: YS110 is a humanized IgG1 monoclonal antibody with high affinity to the CD26 antigen. YS110 demonstrated preclinical anti-tumor effects without significant side effects. Methods: This FIH study was designed to determine the Maximal Tolerated Dose (MTD) and Recommended Phase 2 Dose (RP2D), to assess the tolerance, pharmacokinetics (PK) and pharmacodynamics (PD) profiles of YS110 and preliminary efficacy. YS110 were initially administered intravenously once every 2 weeks (Q2W) for 3 doses and then, based on PK data, once every week (Q1W) for 5 doses in patients with CD26-expressing solid tumors.

Results: Thirty-three patients (22 mesothelioma) received a median of 3 [range 1-30] YS110 infusions across 6 dose levels (0.1 to 6 mg/kg). MTD was not reached and 2 DLTs (infusion hypersensitivity reactions) led to the institution of a systemic premedication. Low grade asthenia (30.3%), hypersensitivity (27.3%), nausea (15.2%), flushing (15.2%), chills (12.1%) and pyrexia (12.1%) were reported as ADRs. PK parameters (AUC and Cmax) increased in proportion with the dose. sCD26/DPPIV assays indicated CD26 modulation. Prolonged stable diseases were observed in 13 out of 26 evaluable patients.

Conclusion: YS110 is well tolerated up to 6 mg/kg Q1W, which has been defined as the RP2D, with encouraging prolonged disease stabilizations observed in a number of patients with advanced/refractory mesothelioma.

INTRODUCTION

CD26 is a 110-kDa, type II transmembrane glycoprotein with known dipeptidyl peptidase IV (DPPIV, EC 3.4.14.5) activity in its extracellular domain and is capable of cleaving N-terminal dipeptides with either L-proline or L-alanine at the penultimate position (Torimoto et al, 1992; Ohnuma et al, 2008). CD26 activity is dependent on cell type and the microenvironment factors that can influence its multiple biological roles (Havre et al, 2008; Ohnuma et al, 2011). Robust evidence from our accumulating data indicates that CD26 has an important role in T cell biology and overall immune function (Morimoto et al, 1989; Morimoto et al, 1998, Dang et al, 1990a; Dang et al, 1990b, Tanaka et al, 1993, Hegen et al, 1997,Ohnuma et al, 2008; Morimoto et al, 1998).

CD26 is also expressed on various tumors such as malignant pleural mesothelioma (MPM), renal cell carcinoma (RCC), colorectal cancer (CRC), hepatocellular carcinoma, lung cancer, prostate cancer, gastrointestinal stromal tumor, thyroid cancer, and hematologic malignancies such as T-anaplastic large cell lymphoma, T-lymphoblastic lymphoma and T-acute lymphoblastic leukemia (Havre et al, 2008).

Our previous work demonstrated that CD26 is preferentially expressed in MPM cells but not in normal mesothelial cells (Amatya et al, 2011), and suggested that membranous expression of CD26 is of potential importance in the treatment of MPM patients (Aoe et al, 2012). More recently, we demonstrated that the CD26-positive population of CD24+CD9+ MPM cells exhibits the cancer stem cell features (Ghani et al, 2011; Yamazaki et al, 2012). We also reported robust in vivo data on the anti-tumor activity of anti-CD26 mAb in mouse xenograft models (Ho et al, 2011 ; Inamoto et al, 2006 ; Inamoto, et al, 2007 ; Okamoto et al, 2014 ; Yamamoto et al, 2014).

YS110 is a recombinant DNA-derived humanized monoclonal antibody that selectively binds

with high affinity to the extracellular domain of CD26. The antibody is an IgG1 kappa with a molecular weight of 144 kDa and was humanized via an in silico design based on the amino acid sequence of anti-human CD26 murine mAb (14D10), which inhibited tumor cell growth, migration and invasion, and enhanced survival of mouse xenograft models (Inamoto et al, 2006). The gene of YS110 is deposited to ATCC in designated with accession No.PTA-7695. The gene is preserved in DH5α Escherichia coli with plasmid having insert of heavy and light chain of a humanized monoclonal antibody against human CD 26 cDNA. The strain designation is S604069.YST-pABMC 148(x411).YS110 is produced by fermentation in mammalian cell (Chinese Hamster Ovary) suspension culture with the Glutamine Synthetase Expression System. In vitro pharmacologic evaluation of YS110 demonstrated its selective binding to human CD26 on a number of human cancer cell lines and tissues and no evidence for immune activation and no effect on DPPIV activity, while exhibiting direct cytotoxic effect on certain human CD26-positive cancer cell lines (Inamoto et al, 2006). In addition to antibody-dependent cellular cytotoxicity (ADCC) and complement-dependent cytotoxicity (CDC) (Inamoto et al, 2006), YS110 induces tumor cell lysis in vitro via alternative original mechanisms: (i) a direct anti-tumor effect through the induction of cell cycle arrest by induction of p27kip1 expression (Inamoto et al, 2006 ; Inamoto, et al, 2007), (ii) following internalization of the CD26-YS110 complexes, an inhibition of invasion and migration of tumors cells by decreased binding to the collagen/fibronectin microenvironment matrix (Inamoto et al, 2006 ; Inamoto, et al, 2007), and (iii) the nuclear translocation of CD26 molecules by internalization of the CD26-YS110 complexes to inhibit proliferation of MPM cells via suppression of POLR2A gene expression (Yamada et al, 2013). In further studies using preclinical models, in vivo administration of YS110 resulted in inhibition of tumor cell growth, migration and invasion, and enhanced survival of mouse xenograft models inoculated with RCC or MPM (Inamoto, et al, 2007 ; Okamoto et al, 2014 ; Yamamoto et al, 2014).

In addition to our robust in vitro and in vivo data on antibody-mediated dose-dependent tumor growth inhibition, YS110 exhibited excellent safety and pharmacological profiles in non-human primate models using single and repeated increasing intravenous doses. Considering the lack of T-cell proliferation and cytokine production in vitro, YS110 was therefore considered not to have an agonistic nor activating effect on human CD26-positive lymphocytes.

This first-in-human phase 1 clinical trial aims to evaluate the safety, pharmacokinetic/pharmacodynamic profiles, and preliminary anti-tumor effects of YS110 in patients with CD26-expressing solid tumors and, particularly, refractory malignant mesothelioma, a tumor type in which successful therapeutic advances are expected to be warranted for a long time.

MATERIALS AND METHODS

Patients

Eligible patients were 18 to 80 years old with locally advanced, inoperable or refractory solid tumors that were histologically documented to express the CD26 molecule. Cancer histologies included mesothelioma (pleural or peritoneal) or other solid tumors such as non-small cell lung carcinoma, renal cell carcinoma, or hepatocellular carcinoma. All patients were in relapse following or were refractory to prior standard therapies (regardless of the number of prior treatment lines), with a progressive evaluable/measurable disease. Other key inclusion criteria included Eastern Cooperative Oncology Group (ECOG) performance status score ≤2, adequate bone marrow, liver, and renal function; at least 4 weeks from prior surgery, chemotherapy, external radiotherapy or immunotherapy (at least 6 weeks from prior nitrosoureas). All patients provided written informed consent. This study was conducted according to the Declaration of Helsinki and was approved by an ethics committee and the French National Drug Agency.

CD26 immunohistochemistry screening

Analysis of CD26 tumor expression for pre-screening was performed centrally at Gustave Roussy by conventional immunohistochemistry performed on formalin-fixed paraffin embedded (FFPE) archival tumor samples using a anti-human CD26 goat polyclonal antibody (AF1180, R&D Systems, Minneapolis, USA) as previously described (Aoe et al, 2012). Briefly, all patients were prescreened for confirmed CD26-positive expression, defined as ≥ 20% of the tumor cells (1+, 2+ or 3+ intensity) and verified independently by two pathologists (P. Vielh and T. Yamada). (Figure 1)

Study design

This First-In-Human study was designed as a classical 3+3 dose-escalating phase 1 trial of the single agent YS110 (Supplementary Table 1). The primary objective was to determine the maximum tolerated dose (MTD) based on the occurrence of dose limiting toxicity (DLT) and a recommended phase 2 dose (RP2D). Initially, cohorts 1 to 4 each planned to enroll 3, and up to 6, patients sequentially to evaluate escalating YS110 doses at 0.1 mg/kg, 0.4 mg/kg, 1 mg/kg and 2 mg/kg for a total of three infusions of YS110 on Days 1, 15 and 29 (one treatment cycle, Q2W). Based on preliminary PK data, the protocol was then subsequently amended to allow patients to receive a total of five infusions of YS110 on Days 1, 8, 15, 22 and 29 (one treatment cycle, Q1W) at 2 mg/kg, 4 mg/kg, and 6 mg/kg. Each cohort included a 24-hour monitoring period following each infusion during the first cycle for evaluation of safety, dose-limiting toxicities (DLTs) and pharmacokinetics. Patients who completed one cycle and demonstrated a clinical response or stable disease could receive the second cycle of YS110 treatment cycles at the same dose and dosing frequency, until disease progression or a significant observed serious adverse event (SAE). If the patient continued the treatment, the second cycle was to begin initially four weeks (later amended to two weeks) after the last infusion of the first cycle (initially Day 57; after amendment, Day 43). For the subsequent cycles, the latency period between the last administration of a cycle and the beginning of the next cycle was two weeks. Secondary objectives of the study were to assess the safety and tolerability profile, pharmacokinetics, pharmacodynamics, preliminary antitumor activity, and to collect survival data.

Safety

All adverse events and SAEs occurring from the informed consent signature up to 30 days after the last dose were reported according to the National Cancer Institute Common Terminology Criteria for Adverse Events (CTCAE v3.0). An adverse drug reaction (ADR) was defined as an AE documented as possibly, probably or definitely related to the study drug or with unknown relationship to the study drug. A treatment-emergent adverse event (TEAE) was defined as an AE with onset on or after the first infusion. The DLT period was 2 weeks after the first YS110 infusion, whatever the dose schedule. DLTs were defined as any grade ≥3 non hematological toxicity or a hematological toxicity of grade ≥4. This definition was later amended to exclude reversible grade 3 infusion reactions defined as allergic reaction/hypersensitivity, fever, pain, bronchospasm, wheezing or hypoxia, occurring during the first dose infusion and resolving with a reduced infusion rate, a stop of the infusion, supportive care and/or the administration of corticosteroids (Supplementary Table S2). In case of treatment discontinuation due to reversible Grade 3 infusion reactions, the patient was to be replaced with a new patient of the same cohort.

Efficacy

Preliminary clinical efficacy was evaluated by radiologic and tumor marker assessments performed at screening at Day 43 of each treatment cycle, and at end of treatment until progressive disease or withdrawal of consent. Tumor response was evaluated based on RECIST 1.0 criteria and defined as partial response (PR) or progressive disease (PD) or stable disease (SD). PR was defined as ≥30% decrease in the sum of the longest diameter (LD) of target lesions, PD was defined as ≥20% increase in the sum of the LD of target lesions and stable disease was defined as neither sufficient shrinkage to qualify for PR nor sufficient increase to qualify for PD. Patients with mesothelioma were assessed according to modified RECIST criteria.

Pharmacokinetics

Serial blood samples were obtained at pre and post YS110 administration at Day 1, Day 8, Day 15 and Day 29 at specified time points throughout the study. Serum levels of YS110 were analyzed by ELISA by Alta Intertek, USA. The method of blood sample collection is described in Supplementary information.

Pharmacodynamics

All treated patients with appropriate post baseline samples were evaluable for pharmacodynamics analyses on blood samples collected at days 0 (baseline), 1 (post-infusion), 2, 15 (pre- & post-infusion), 29 (pre- & post-infusion) for immunomonitoring and soluble CD26 (sCD26) / DPPIV (sDPPIV) activity assessments.

Immunomonitoring: Immunomonitoring was performed centrally in the translational research laboratory at Institut Gustave Roussy, France (F Farace). Immunophenotyping was performed for the monitoring of peripheral blood lymphocyte (PBL) CD26+ T (i.e. CD3+CD4+, CD3+CD8+) and NK (i.e. CD3-CD16+/-CD56+) subpopulations by flow cytometry using fluorochrome-conjugated commercially-available specific mAbs with relevant isotypic controls (all provided from Pharmingen, New Jersey, USA). To ensure the specificity of the CD26 staining in blood samples collected under YS110 treatment, competition and cross-blocking experiments using the two different CD26 mAb clones 5K78 (Santa Cruz Biotechnologies, Inc., Dallas, USA) and M-A261 (BD Pharmingen, San Jose, USA) were also performed.

Dosages of serum cytokines (i.e. interleukin 6 [IL-6], tumor necrosis factor α [TNF-α] and interleukin 2 [IL-2]) were investigated by standard commercially-available ELISA assays (R&D Systems, Minneapolis, USA).

Soluble CD26 (sCD26) and DPPIV activity assessments: Assays for soluble CD26 and DPP4 were developed in the Morimoto's laboratory (Juntendo university, Japan) using anti-human CD26 murine mAbs that exhibit no cross-reactivity with the therapeutic humanized anti-CD26 mAb YS110 as described previously (Dong et al, 1998 ; Ohnuma et al, 2015a). The sampling times for sCD26 were identical to that for immunomonitoring.

Statistical analyses

Descriptive statistics were used to summarize the data. The patient sampling size was a function of the 3+3 dose escalation schedule. The realized sample size was dependent on the number and pattern of observed DLTs. The maximum sample size was a consequence of the design's sampling requirements and the number of dose levels. In this trial with six dose levels, the maximum number of patients being exposed in each dose level was determined according to the DTL occurrence rate and confirmation of safety.

RESULTS

Screening for CD26 expression

A total of 136 patients signed an informed consent form and were screened for CD26 expression on a FFPE archival tumor tissue sample. Mesothelioma which was previously reported as one of the CD26-expressing tumor types was a main target indication with 60 patients screened (n=60, 53% were CD26+ cases). Examples of CD26 immunohistochemistry and scoring are presented in Figure 1. Other tumor types screened included renal cell carcinoma (n=18, 71% CD26+ cases), hepatocellular carcinoma (n=7, 22% CD26+ cases) and various other tumor types (n=31, 13% CD26+ cases). Overall, 56 (41%) patients were considered as CD26+ with the mean percentage of CD26 expression on tumor cells of 69% [range 20% - 100%] in the tested samples.

Patient characteristics

Thirty-four CD26+ patients (19 males and 15 females) were enrolled in the study and treated at 5 investigational sites in France, with 33 patients being evaluable (19 males and 14 females). The most common tumor types were mesothelioma (n=23, 69.7%), renal cell carcinoma (n=9, 27.3%) and one patient had an urothelial carcinoma (n=1; 3.0%). All mesothelioma patients were diagnosed with the epithelioid histology and were all in advanced inoperable disease or refractory to previous line of treatment. Other tumor type were in stage III/IV Twenty-two patients were treated according to the Q2W schedule at 0.1 (n=3), 0.4 (n=3), 1 (n=6) and 2 mg/kg (n=10) and 11 according to the Q1W schedule at 2 (n=4), 4 (n=3) and 6 (n=4) mg/kg (Table 1). The median percentage of CD26+ tumor cells in archival samples from the patients treated was 63 % [range 25% – 100%].

Safety

Eighteen patients received at least one cycle of YS110 with 3 infusions per cycle and 7 patients completed at least one cycle with 5 infusions per cycle. Nine patients did not complete the first cycle.

During the DLT observation period (i.e. 15 days following the first infusion), 2 DLTs were reported as serious unexpected adverse events (SUSARs) consisting of grade 3 infusion reactions (one patient at the Q2W 1 mg/kg dose level and another patient at the Q2W 2 mg/kg dose level) that completely resolved with supportive treatment, but led to permanent discontinuation of treatment. Since both patients had a history of allergies, consequently, the protocol was subsequently amended to add clinically relevant allergies as a new excluding criterion, as well as the administration of a systematic steroid prophylaxis prior to each infusion to better control potential infusion reactions (chills, fever, flushing, hypotension and respiratory disorders). With these modifications, dose escalation was possible up to 6 mg/kg in 4 patients without DLTs. Per protocol, dose escalation was stopped at the highest level of 6 mg/kg without the MTD being achieved.

All patients had one or more AEs and 113 Adverse Drug Reactions (ADRs) considered to be possibly related to YS110 were reported by 30 (90.9%) patients. The most frequently reported Adverse Events (AEs) regardless of potential relationship to YS110 were asthenia (54.5%) and aggravation of prior conditions (30.3%). AEs (related or not to treatment) occurring in more than 10% of the patients are reported in Table 2 according to System Organ Class (SOC) and Preferred Term (PT). The majority of AEs were of mild (grade 1) or moderate (grade 2) severity. The most commonly reported grade ≥3 AEs were dyspnea (21.2%), hypersensitivity (15.2%), aggravation of prior conditions (15.2%) general physical health deterioration (12.1%), and hyperglycemia (12.1%). Eight patients (24.2%) discontinued YS110 due to adverse events; most adverse events leading to discontinuation were considered unrelated to YS110, except for the 2 patients with infusion reactions considered as DLTs. Twenty-seven SAEs were reported in this study in 18 patients. Except for the 2 DLTs, all other SAEs, most commonly general physical health deterioration, were considered to be unrelated to YS110 but rather related to consequences of disease progression as assessed by the investigator, including the 6 patient deaths during the study. No dose-dependent AEs were observed. Low grade asthenia (30.3%), hypersensitivity (27.3%), nausea (15.2%), flushing (15.2%), chills (12.1%), and pyrexia (12.1%) were reported as ADRs.

No clinically significant abnormalities were observed in hematology and clinical chemistry laboratory parameters, as well as in ECG findings.

The main limiting toxicities in the study were infusion reactions, two being considered as DLTs leading to permanent discontinuation of treatment. Six severe hypersensitivity reactions were reported in five patients receiving a dose of 2.0 mg/kg and a severe anaphylactic reaction was reported in one patient receiving a dose of 1.0 mg/kg. These ADRs, occurring mainly at the first infusion, were reversible and manageable with curative corticosteroids and antihistaminic drugs and further prevented by a systemic corticosteroids premedication. Overall, these ADRs that did not appear to be related either to the dose level of YS110 nor the Q2W or Q1W schedule.

Pharmacokinetics

Following single and repeat intravenous infusions of YS110, there was a trend toward decreasing clearance (CL), increasing half-life time ($T_{1/2}$) and increasing exposure (Cmax, $AUC_{0\text{-}168}$, $AUC_{0\text{-}\infty}$) with increasing doses, suggesting that CL was saturating across the dose range studied. Mean volume of distribution (Vz, Vss) was similar or slightly higher than human serum volume, indicative of YS110 being primarily found in serum and consistent with prior observations for monoclonal antibodies. In general, exposure increased as the dose increased. While increases in C_{max} appeared to be dose proportional, increases in $AUC_{0\text{-}168}$ and $AUC_{0\text{-}\infty}$ were greater than dose proportional, and this was consistent with the trend of decreasing CL with increasing doses (Table 3). In addition, YS110 PK parameters changed with repeat dosing. For doses ranging from 1 to 6 mg/kg, mean CL was approximately 1.1 to 1.6 fold higher on Day 1 (vs. Day 29) while mean $T_{1/2}$ increased approximately 1.2 to 2.3 fold and exposure ($AUC_{0\text{-}168}$) increased approximately 1.3 to 1.8 fold on Day 29 vs. Day 1 (Table 3).

For the initial dose levels (0.1, 0.4, 1 and 2 mg/kg), YS110 was administered on a Q2W schedule on days 1, 15 and 29. As expected, the maximum concentrations of YS110 (C_{max}) on days 1 and 29 were proportional to the dose levels. However, calculated half-lives (1 to 2 days) were shorter than expected for a humanized antibody and serum concentrations were at or below detectable levels (0.4 µg/mL) by 1 week post infusion. To maintain measurable YS110 trough concentrations between doses, dosing was increased to 5 doses on a Q1W schedule on days 1, 8, 15, 22 and 29 for dose levels 2, 4 and 6 mg/kg. C_{max} values on day 1 were roughly proportional to dose level. Mean half-lives increased with increasing dose levels, rising significantly from day 1 to day 15 to day 29 in the 2, 4 and 6 mg/kg cohorts (~1 day, ~2 days and ~3 days respectively), and resulting in drug accumulation between doses (Table 3). Impact from exposure to YS110 on anti-drug antibody (ADA) response appeared to be most pronounced in the 0.4 mg/kg dose cohort. The two subjects who were ADA positive on Day 29 of Cycle 1 had notably reduced exposure relative to the one ADA negative subject. There were no ADAs detected in the higher dose groups.

Efficacy

A secondary objective of the study was to evaluate for the potential antitumor activity of YS110 according to RECIST 1.0 criteria (or modified RECIST criteria for mesothelioma). No objective response was observed in the treated patients. However, stable disease per RECIST criteria as the best response was observed in 13 out of the 26 evaluable patients following the first cycle of treatment, as shown in the accompanying Waterfall Plot Chart (supplementary Figure S2). Overall median PFS was 43 days (Table 4) as determined by a Kaplan-Meier Plot (Supplementary Figure S3). However, PFS of 184-399 days was observed in 7 patients (5 cases of mesothelioma and 2 cases of renal cell carcinoma) out of 26 cases (mesothelioma:19 cases, renal cell carcinoma:6 cases and urinary tract carcinoma: 1 case). Table 4 summarizes the median number of infusions administered and median PFS according to the different dose levels and schedule.

Pharmacodynamics

Immunomonitoring

The CD26 immunophenotyping on peripheral T and NK lymphocyte subpopulations under YS110 treatment was validated by testing 2 different anti-CD26 mAb clones. Indeed, in the first twelve patients tested using the M-A261 mAb (BD Pharmingen), we observed a dramatic decrease of CD26+ cells consequently to YS110 administration, suggesting the lack of detection of the CD26 epitope due to YS110 binding. These results (not schown), led us to test in parallel another clone 5K78 (Santa Cruz Biotech.) showing that CD26+ cells were still detectable under YS110 treatment. The validation of this anti-CD26 mAb was ensured by competition and cross-blocking experiments using increasing dilutions of YS110 in the CD26 immunophenotyping assay demonstrating no modulation of CD26+ subpopulations using the 5K78 clone in contrast to the first clone tested.

At baseline in our series of patients, the mean ± sd (n=33) absolute values (x106/ml) of lymphocytes populations were 0.94(65.7%)±0.64 for CD3+CD4+, 0.33(34.5%)±0.26 for CD3+CD8+ T cells and 0.17(8.2%)±0.17 for CD3-CD16+/-CD56+ NK cells. The mean percentage of CD26+ subpopulations in the T-CD4, T-CD8 and NK cells were 24.7%, 8.2% and 5.2% respectively with a significant inter-patient variability. After YS110 infusions, the levels of the various PBL subpopulations decreased at day 1 and 2 (i.e. 24 to 48 hrs following YS110 infusions), with a subsequent recovery at day 15 and 29 pre-infusion samples in most patients (Supplementary Table S3). This decline in different PBL subpopulations was more frequently observed in patients that received higher doses (2, 4 and 6 mg/kg) of YS110. However, this trend was not statistically significant considering the inter-individual variations across the different dose levels.

Serum Cytokines: At baseline and during YS110, no serum IL-2 production was detectable in any of the patients. Significant rise of the pro-inflammatory cytokines IL-6 and TNF-α detected at day 1 and 2 following the first infusion of YS110 at 0.4, 1 and 2 mg/kg at various levels, including the first patient with a grade 3 infusion reactions DLT (at the Q1W 1 mg/kg dose level). Different kinetics of serum IL-6 and TNF-α receiving 2 mg/kg of YS110, while low or undetectable levels were observed in patients receiving 4.0 and 6.0 mg/kg of YS110, likely due to the administration of systemic steroid prophylaxis.

sCD26 and DPPIV activity in sera

To determine serum levels of sCD26 protein and DPPIV enzyme activity in each cohort before and after administration of YS110, we developed an in-house ELISA assay for sCD26 and DPPIV using anti-human CD26 murine mAbs exhibiting no cross-reactivity with the therapeutic humanized anti-CD26 mAb YS110 (Dong et al, 1998 ; Ohnuma et al, 2015a). As shown in Fig 2A, an increase in YS110 infusion dose was associated with decreased serum sCD26 level, particularly in the cohorts of patients treated at 2, 4 and 6 mg/kg, with an approximately 80% decrease in sCD26 level. Moreover, since CD26 level reflects DPPIV enzyme activity in the serum, a similar reduction in DPPIV enzyme activity was observed (Fig 2B).

DISCUSSION

YS110 is the first, and currently the only CD26-directed mAb in clinical trial. This FIH study demonstrates that YS110 therapy exhibits a favorable safety profile and results in encouraging disease stabilization in heavily pretreated CD26-positive MPM or RCC patients who had previously progressed on conventional standard therapies.

The spectrum of AEs, the most common of which were low grade asthenia, hypersensitivity, chills, pyrexia, nausea, vomiting and headache, was similar to that previously described with humanized mAbs treatment (Scott et al, 2012). Two DLTs were reported as SUSARs consisting in grade 3 infusion reactions that resolved with supportive treatment. Since both patients had a history of allergies, the protocol was subsequently amended to include clinically relevant allergies as a new excluding criterion, and the administration of systemic steroid prophylaxis has been implemented prior to each infusion at all cycles to better control such infusion reactions. In this study, high rate of hyperglycemia was observed in patients in the top dose cohorts, consistent with the well-known effect of corticosteroid on glucose levels. However, hyperglycemia resolved soon after cessation of steroid administration while YS110 was detected in sera, with decreased serum DPPIV activity. Taken together, it is probable that premedicated corticosteroid, but not YS110, induces the hyperglycemia observed in the patient cohorts receiving higher drug doses. With these new modifications, dose escalation up to 6 mg/kg was possible as in 4 patients in this cohort were treated without DLTs. Per protocol, 6 mg/kg was the highest dose level tested although the MTD was not achieved. The dose level of 6.0 mg/kg of YS110 was decided by study investigators to be the RP2D.

Total lymphocyte counts, as well as levels of CD26+ lymphocytes, fell at Day 2 below the baseline levels. However, total lymphocyte counts recovered to reach baseline level at Day 8 and thereafter. These data indicate that YS110 administration resulted in a decrease in levels of peripheral lymphocytes including the CD26-positive lymphocyte subset soon after drug administration, and it is probable that YS110-mediated suppression of peripheral lymphocyte levels, including the CD26-positive subset, resolved by as early as Day 8. Moreover, we observed a decrease in the level of the CD26-positive subset of peripheral lymphocytes following administration of YS110 alone without steroid prophylaxis in the 0.1 mg/kg – 2.0 mg/kg cohorts, as shown in Supplementary Table S3. Therefore, it is conceivable that YS110, but not premedication steroid, was responsible for the temporary effect on CD26-positive lymphocyte counts.

CD26 is also present in serum and other body fluids in a truncated form as sCD26/DPPIV, and our data also indicated that DPPIV enzyme activity decreased with increasing doses of YS110 (Fig 2B). Although DPPIV inhibitors are clinically used as oral hypoglycemic agents (Barreira et al, 2015), hypoglycemia was not observed during YS110 administration. Of note is the fact that greater than 80% inhibition of serum DPPIV activity was obtained 24 hours after oral administration of clinically available DPPIV inhibitors (Drug information published by each pharmaceutical company of sitagliptin, vildagliptin, saxagliptin and etc.), a level of inhibition comparable to that seen in patients treated with YS110. Our current data would therefore indicate that YS110 therapy is tolerable in the clinical setting.

The only treatment with level-one level of evidence for improving clinical outcome is the regimen consisting of a platinum doublet with an antifolate (van Meerbeeck et al, 2005). With this combined chemotherapy, patients with good performance status have a median overall survival of approximately 1 year, and a median PFS of less than 6 months. There is currently no standard second line treatment with demonstrated ability to prolong survival. Importantly, patients who failed this first line therapy have an extremely short survival (3.4 months), and are exposed to potentially life-threatening toxicities unnecessarily (Blayney et al, 2012). Due to the lack of efficacy of conventional therapeutic approaches, it is potentially significant that treatment with YS110 results in encouraging disease stabilization with a median PFS of 32 weeks (26 – 57 weeks) in 7 heavily pretreated CD26-positive patients who previously progressed on conventional therapies (Supplementary Figures S2 and S3).

Recent work has demonstrated the functional role of DPPIV-mediated post-translational modification of chemokines in regulating tumor immunity through its interaction with its substrate CXCL10 (Ohnuma et al, 2015b). Preservation of the full length, bioactive CXCL10 by DPPIV inhibition using the DPPIV inhibitor sitagliptin resulted in increased level of CXCR3+ effector T cells in the tumor microenvironment and subsequent tumor growth reduction (Ohnuma et al, 2015b). In view of these recent findings, data from our current trial showing that serum DPPIV activity was decreased following treatment with YS110 in a dose-dependent manner (Fig 2B). It would suggest that anti-tumor activity via DPPIV inhibition may constitute yet another mechanism of action for the anti-tumor activity of YS110, in addition to the mechanisms of action discussed above (Hatano et al, 2015).

We recently reported that CD3/CD26 costimulation induced the development of a human type 1 T reg cells from CD4+ T cells with high level of IL-10 production and lymphocyte-activation gene 3 (LAG3) expression (Nguyen et al, 2015). Preclinical models showed that antibody-mediated blocking of LAG3 as potential anti-cancer therapy led to enhanced activation of antigen-specific T cells at the tumor sites and disruption of tumor growth (Nishikawa et al, 2015). Moreover, anti-LAG3/anti-PD-1 antibody treatment cured most mice of established tumors that were largely resistant to single antibody treatment (Nishikawa et al, 2015).Taken together, it is conceivable that CD26 itself may be a functional inhibitory molecule of an immune checkpoint system in certain disease conditions, similar to LAG3 or PD-1. In this scenario, CD26 blockade by YS110 may potentially function as an immune checkpoint blockade therapy, which can mediate anti-tumor activity in CD26-negative as well as CD26-positive cancers.

Microarray analyses of MPM cell lines treated with YS110 indicated that anti-CD26 mAb therapy resulted in the down regulation of cytochrome c oxidase polypeptide I & II, and metallothione molecules that confer resistance to apoptosis or chemotherapeutic agents (Aoe et al, 2012). In addition, suppression of drug-resistant related transporters, DNA repair enzyme, and oncogenic protein expression was observed (Aoe et al, 2012). These preclinical results suggest that YS110 can function synergistically with other antineoplastic agents such as selected chemotherapeutic drugs to inhibit tumor growth.

Tumor surface expression of CD26/DPP4 may also have direct biological effects on the malignant behavior of tumors. In several human malignancies including colorectal CRC, chronic myeloid leukemia, gastric adenocarcinoma and MPM, CD26/DPP4 expression is reported to be a marker of cancer stem cells (Ghani et al, 2011 ; Yamazaki et al, 2012 ; Davies et al, 2015 ; Herrmann et al, 2014 ; Pang et al, 2010 ; Hatano et al, 2014). Given the potential role of CD26 surface expression in cancer biology, YS110 therapy may also influence tumor growth through its potential effect on the cancer stem cells of selected tumors.

In conclusion, our FIH study showed that YS110 therapy is generally well-tolerated up to 6 mg/kg Q1W, which has been defined as the RP2D and results in encouraging disease stabilization in a number of patients with advanced/refractory CD26-expressing cancers. Our findings also suggest that further clinical development of YS110 such as its use as part of combination therapies with other antineoplastic agents is warranted.

References

Amatya VJ, Takeshima Y, Kushitani K, Yamada T, Morimoto C, Inai K (2011) Overexpression of CD26/DPPIV in mesothelioma tissue and mesothelioma cell lines. Oncol Rep 26: 1369-1375, doi: 10.3892/or.2011.1449

Aoe K, Amatya VJ, Fujimoto N, Ohnuma K, Hosono, O. Hiraki A, Fujii M, Yamada T, Dang NH, Takeshima Y, Inai K, Kishimoto T, Morimoto C. (2012) CD26 overexpression is associated with prolonged survival and enhanced chemosensitivity in malignant pleural mesothelioma. Clin Cancer Res 18: 1447-1456, doi: 10.1158/1078-0432.CCR-11-1990

Barreira da Silva R, Laird ME, Yatim N, Fiette L, Ingersoll MA, Albert ML (2015) Dipeptidylpeptidase 4 inhibition enhances lymphocyte trafficking, improving both naturally occurring tumor immunity and immunotherapy. Nature immunology 16: 850-858, doi: 10.1038/ni.3201

Blayney JK, Ceresoli GL, Castagneto B, O'Brien ME, Hasan B, Sylvester R, Rudd R, Steele J, Busacca S, Porta C, Mutti L, O'Byrne KJ, Scullin P, Gaafar R, Baas P, Van Meerbeeck J, Fennell DA. (2012) Response to chemotherapy is predictive in relation to longer overall survival in an individual patient combined-analysis with pleural mesothelioma. Eur J Cancer 48:2983-29892, doi: 10.1016/j.ejca.2012.05.018

Dang NH, Torimoto Y, Sugita K, Daley JF, Schow P, Prado C, Schlossman SF, Morimoto C. (1990) Cell surface modulation of CD26 by anti-1F7 monoclonal antibody. Analysis of surface

expression and human T cell activation. J Immunol 145: 3963-3971,

Dang NH, Torimoto Y, Deusch K, Schlossman SF, Morimoto C (1990) Comitogenic effect of solid-phase immobilized anti-1F7 on human CD4 T cell activation via CD3 and CD2 pathways. J Immunol 144: 4092-4100,

Davies S, Beckenkamp A, Buffon A (2015) CD26 a cancer stem cell marker and therapeutic target. Biomed Pharmacother 71: 135-138, doi: 10.1016/j.biopha.2015.02.031

Dong RP, Tachibana K, Hegen M, Scharpe S, Cho D, Schlossman SF, Morimoto C. (1998) Correlation of the epitopes defined by anti-CD26 mAbs and CD26 function. Molecular immunology 35: 13-21,

Ghani FI, Yamazaki H, Iwata S, Okamoto T, Aoe K, Okabe K, Mimura Y, Fujimoto N, Kishimoto T, Yamada T, Xu CW, Morimoto C. (2011) Identification of cancer stem cell markers in human malignant mesothelioma cells. Biochem Biophys Res Commun 404: 735-742, doi: 10.1016/j.bbrc.2010.12.054

Hatano R, Yamada T, Matsuoka S, Iwata S, Yamazaki H, Komiya E, Okamoto T, Dang NH, Ohnuma K, Morimoto C. (2014) Establishment of monoclonal anti-human CD26 antibodies suitable for immunostaining of formalin-fixed tissue. Diagn Pathol 9: 30, doi: 10.1186/1746-1596-9-30

Hatano R, Ohnuma K, Otsuka H, Komiya E, Taki I, Iwata S, Dang NH, Okumura K, Morimoto C. (2015) CD26-mediated induction of EGR2 and IL-10 as potential regulatory mechanism for CD26 costimulatory pathway. J Immunol 194: 960-972, doi: 10.4049/jimmunol.1402143

Havre PA, Abe M, Urasaki Y, Ohnuma K, Morimoto C, Dang NH (2008) The role of CD26/dipeptidyl peptidase IV in cancer. Frontiers in bioscience 13: 1634-1645,

Hegen M, Kameoka J, Dong RP, Schlossman SF, Morimoto C (1997) Cross-linking of CD26 by antibody induces tyrosine phosphorylation and activation of mitogen-activated protein kinase. Immunology 90: 257-264,

Herrmann H, Sadovnik I, Cerny-Reiterer S, Rulicke T, Stefanzl G, Willmann M, Hoermann G, Bilban M, Blatt K, Herndlhofer S, Mayerhofer M, Streubel B, Sperr WR, Holyoake TL, Mannhalter C, Valent P. (2014) Dipeptidylpeptidase IV (CD26) defines leukemic stem cells (LSC) in chronic myeloid leukemia. Blood 123: 3951-3962, doi: 10.1182/blood-2013-10-536078

Ho L, Aytac U, Stephens LC, Ohnuma K, Mills GB, McKee KS, Neumann C, LaPushin R, Cabanillas F, Abbruzzese JL, Morimoto C, Dang NH. (2001) In vitro and in vivo antitumor effect of the anti-CD26 monoclonal antibody 1F7 on human CD30+ anaplastic large cell T-cell lymphoma Karpas 299. Clin Cancer Res 7: 2031-2040,

Inamoto T, Yamochi T, Ohnuma K, Iwata S, Kina S, Inamoto S, Tachibana M, Katsuoka Y, Dang NH, Morimoto C. (2006) Anti-CD26 monoclonal antibody-mediated G1-S arrest of human renal clear cell carcinoma Caki-2 is associated with retinoblastoma substrate dephosphorylation, cyclin-dependent kinase 2 reduction, p27kip1 enhancement, and disruption of binding to the extracellular matrix. Clin Cancer Res 12: 3470-3477, doi: 10.1158/1078-0432.CCR-06-0361

Inamoto T, Yamada T, Ohnuma K, Kina S, Takahashi N, Yamochi T, Inamoto S, Katsuoka Y, Hosono O, Tanaka H, Dang NH, Morimoto C. (2007) Humanized anti-CD26 monoclonal antibody as a treatment for malignant mesothelioma tumors. Clin Cancer Res 13: 4191-4200, doi: 10.1158/1078-0432.CCR-07-0110

Morimoto C, Torimoto Y, Levinson G, Rudd CE, Schrieber M, Dang NH, Letvin NL, Schlossman SF. (1989) 1F7, a novel cell surface molecule, involved in helper function of CD4 cells. J Immunol 143: 3430-3439,

Morimoto C, Schlossman SF (1998) The structure and function of CD26 in the T-cell immune response. Immunol Rev 161: 55-70,

Nguyen LT, Ohashi PS (2015) Clinical blockade of PD1 and LAG3--potential mechanisms of action. Nat Rev Immunol 15: 45-56, doi: 10.1038/nri3790

Nishikawa S, Konno M, Hamabe A, Hasegawa S, Kano Y, Fukusumi T, Satoh T, Takiguchi S, Mori M, Doki Y, Ishii H. (2015) Surgically resected human tumors reveal the biological significance of the gastric cancer stem cell markers CD44 and CD26. Oncol Lett. 9: 2361-2367, doi: 10.3892/ol.2015.3063

Ohnuma K, Dang NH, Morimoto C (2008) Revisiting an old acquaintance: CD26 and its molecular mechanisms in T cell function. Trends Immunol 29: 295-301, doi: 10.1016/j.it.2008.02.010

Ohnuma K, Hosono O, Dang NH, Morimoto C (2011) Dipeptidyl peptidase in autoimmune pathophysiology. Advances in clinical chemistry 53: 51-84,

Ohnuma K, Saito T, Hatano R, Hosono O, Iwata S, Dang NH, Ninomiya H, Morimoto C. (2015) Comparison of two commercial ELISAs against an in-house ELISA for measuring soluble CD26 in human serum. J Clin Lab Anal 29: 106-111, doi: 10.1002/jcla.21736

Ohnuma K, Hatano R, Morimoto C (2015) DPP4 in anti-tumor immunity: going beyond the enzyme. Nat Immunol 16: 791-792, doi: 10.1038/ni.3210

Okamoto T, Iwata S, Yamazaki H, Hatano R, Komiya E, Dang NH, Ohnuma K, Morimoto C. (2014) CD9 Negatively Regulates CD26 Expression and Inhibits CD26-Mediated Enhancement of Invasive Potential of Malignant Mesothelioma Cells. PLoS ONE 9: e86671, doi: 10.1371/journal.pone.0086671

Pang R, Law WL, Chu AC, Poon JT, Lam CS, Chow AK, Ng L, Cheung LW, Lan XR, Lan HY, Tan VP, Yau TC, Poon RT, Wong BC. (2010) A subpopulation of CD26+ cancer stem cells with metastatic capacity in human colorectal cancer. Cell Stem Cell 6: 603-615, doi: 10.1016/j.stem.2010.04.001

Scott AM, Wolchok JD, Old LJ (2012) Antibody therapy of cancer. Nat Rev Cancer 12: 278-287, doi:

10.1038/nrc3236

Tanaka T, Kameoka J, Yaron A, Schlossman SF, Morimoto C (1993) The costimulatory activity of the CD26 antigen requires dipeptidyl peptidase IV enzymatic activity. Proc Natl Acad Sci U S A 90: 4586-4590

Torimoto Y, Dang NH, Tanaka T, Prado C, Schlossman SF, Morimoto C (1992) Biochemical characterization of CD26 (dipeptidyl peptidase IV): functional comparison of distinct epitopes recognized by various anti-CD26 monoclonal antibodies. Molecular immunology 29: 183-92.

van Meerbeeck JP, Gaafar R, Manegold C, van Klaveren RJ, van Marck EA, Vincent M, Legrand C, Bottomley A, Debruyne C, Giaccone G. (2005) Randomized phase III study of cisplatin with or without raltitrexed in patients with malignant pleural mesothelioma: an intergroup study of the European Organisation for Research and Treatment of Cancer Lung Cancer Group and the National Cancer Institute of Canada. J Clin Oncol 23:6881-6889, doi: 10.1200/JCO.20005.14.589

Yamada K, Hayashi M, Madokoro H, Nishida H, Du W, Ohnuma K, Sakamoto M, Morimoto C, Yamada T. (2013) Nuclear localization of CD26 induced by a humanized monoclonal antibody inhibits tumor cell growth by modulating of POLR2A transcription. PLoS One 8: e62304, doi: 10.1371/journal.pone.0062304

Yamamoto J, Ohnuma K, Hatano R, Okamoto T, Komiya E, Yamazaki H, Iwata S, Dang NH, Aoe K, Kishimoto T, Yamada T, Morimoto C. (2014) Regulation of somatostatin receptor 4-mediated cytostatic effects by CD26 in malignant pleural mesothelioma. Br J Cancer 110: 2232-2245, doi: 10.1038/bjc.2014.151

Yamazaki H, Naito M, Ghani FI, Dang NH, Iwata S, Morimoto C (2012) Characterization of cancer stem cell properties of CD24 and CD26-positive human malignant mesothelioma cells. Biochem Biophys Res Commun 419: 529-536, doi: 10.1016/j.bbrc.2012.02.054

Table 1. Baseline demographics and disease characteristics

Number of patients (n = 33)		**Schedule & Dose levels (mg/kg)**						
Age, median (min-max) (yrs)	63 (41-76)							
ECOG PS 0 / 1 / 2 (%)	29 / 58 / 13							
Primary tumor type, n (%)		**Q2W**				**Q1W**		
		0.1	**0.4**	**1**	**2**	**2**	**4**	**6**
Mesothelioma (Meso)	22 (67)	3	2	2	6	3	2	4
Renal cell carcinoma (RCC)	10 (30)	-	1	4	4	-	1	-
Urothelial carcinoma (UTC)	1 (3)	-	-	-	-	1	-	-
Median number of prior therapies (min-max)	3 (1-11)							

Table 2. Adverse events (all grades) reported by ≥10% of patients overall in any cohort

Preferred Term (CTCAE v3) number of patients (%)	Dose levels (mg/kg)							
	0.1 (n=3)	0.4 (n=3)	1.0 (n=6)	2.0 (n=14)	4.0 (n=3)	6.0 (n=4)	All AEs / Grade 3-4 (n=33)	All ADRs^2 / Grade3-4 (n=33)
Asthenia	3 100.0)	2 (66.7)	0 (0.0)	8 (57.1)	2 (66.7)	3 (75.0)	18 (54.5)	10 (30.3)
Condition aggravated	1 (33.3)	0 (0.0)	1 (16.7)	4 (28.6)	1 (33.3)	3 (75.0)	10(30.3) 5 (15.2)	
Pyrexia[1]	2 (66.7)	1 (33.3)	1 (16.7)	3 (21.4)	0 (0.0)	1 (25.0)	8 (24.2)	4 (12.1)
Chest pain	1 (33.3)	1 (33.3)	1 (16.7)	2 (14.3)	0 (0.0)	0 (0.0)	5 (15.2)	
Chills[1]	2 (66.7)	1 (33.3)	1 (16.7)	0 (0.0)	0 (0.0)	0 (0.0)	4 (12.1)	4 (12.1)
General health deterioration	0 (0.0)	0 (0.0)	0 (0.0)	2 (14.3)	1 (33.3)	1 (25.0)	4 (12.1) 4 (12.1)	
Constipation	2 (66.7)	0 (0.0)	1 (16.7)	5 (35.7)	0 (0.0)	1 (25.0)	9 (27.3)	
Nausea	0 (0.0)	1 (33.3)	1 (16.7)	3 (21.4)	2 (66.7)	1 (25.0)	8 (24.2)	5 (15.2)
Vomiting	1 (33.3)	1 (33.3)	2 (33.3)	2 (14.3)	1 (33.3)	0 (0.0)	7 (21.2)	
Diarrhoea	0 (0.0)	2 (66.7)	1 (16.7)	1 (7.1)	0 (0.0)	1 (25.0)	5 (15.2)	
Dyspnea	2 (66.7)	1 (33.3)	3 (50.0)	5 (35.7)	0 (0.0)	3 (75.0)	14 (42.4) 7 (21.2)	
Hyperglycaemia	0 (0.0)	0 (0.0)	1 (16.7)	3 (21.4)	2 (66.7)	2 (50.0)	8 (24.2) 4 (12.1)	
Decreased appetite	0 (0.0)	1 (33.3)	1 (16.7)	3 (21.4)	1 (33.3)	1 (25.0)	7 (21.2)	
Headache	1 (33.3)	2 (66.7)	0 (0.0)	3 (21.4)	1 (33.3)	0 (0.0)	7 (21.2)	
Flushing[1]	0 (0.0)	0 (0.0)	0 (0.0)	1 (7.1)	2 (66.7)	3 (75.0)	6 (18.2)	5 (15.2)
Hypersensitivity[1]	0 (0.0)	0 (0.0)	1 (16.7)	8 (57.1)	0 (0.0)	0 (0.0)	9 (27.3) 5 (15.2)	9 (27.3) 5 (15.2)
Weight decreased	0 (0.0)	1 (33.3)	0 (0.0)	5 (35.7)	0 (0.0)	0 (0.0)	6 (18.2)	

N = number of patients

A subject with more than one finding in a specific category was only counted once; percentages are based on the total number of subjects in each treatment group. The table is sorted by descending subject count.Infusion reactions related to

Table 3. Cycle 1 pharmacokinetics parameters (mean±sd) for YS110 administration

Dose (mg/kg)	Dose Schedule	Day	$T_{1/2}$ (hr)	C_{max} (μg/mL)	AUC_{0-168} (hr*μg/mL)	$AUC_{0-\infty}$ (hr*μg/mL)	CL (mL/hr/kg)
0.4	Q2W	1	ND	ND	ND	ND	ND
		29	14.8±ND	5.85±ND	143±ND	145±ND	2.79±ND
1	Q2W	1	26.4±ND	22.7±5.68	768±73.3	692±ND	1.44±ND
		29	ND	43.5±29.3	979±NR	ND	1.05±NR
2	Q2W	1	36.4±12.2	39.0±9.94	1710±360	1810±472	1.16±0.245
		29	43.1±12.6	40.1±10.4	2080±943	2280±1110	1.03±0.435
2	Q1W	1	24.5±4.59	30.8±4.20	1180±243	1200±251	1.72±0.334
		15	31.5±NR	67.3±NR	2150±NR	2230±NR	1.22±NR
		29	29.8±NR	27.5±20.1	1650±NR	1720±NR	1.33±NR
4	Q1W	1	46.6±1.69	72.5±27.1	4340±1030	4740±1140	0.876±0.206
		15	70.4±NR	82.4±NR	6000±NR	7450±NR	0.678±NR
		29	76.2±ND	98.4±ND	7320±ND	9340±ND	0.547±ND
6	Q1W	1	67.8±13.8	150±22.9	10300±1800	12800±3250	0.490±0.116
		15	93.7±27.4	182±17.2	15700±3470	22800±8250	0.393±0.0793
		29	154±NR	205±23.6	18400±4320	39700±NR	0.340±0.0814

ND: not determined; NR: not reported;

Table 4. Time on YS110 treatment and median PFS of treated patients

Cohorts	Dose levels (mg/kg)	Cancer types (n)	Median Infusions N (min-max)	Median PFS days (min-max)
Q2W	**0.1**	**Meso (3)**	3 (3)	42 (41-)
Q2W	**0.4**	**Meso (2) RCC (1)**	18 (3-20)	223 (40-273)
Q2W	**1.0**	**Meso (2) RCC (4)**	3 (1-3)	40 (28-59)
Q2W	**2.0**	**Meso (6) RCC (4)**	3 (1-27)	57 (13-399)
Q1W	**2.0**	**Meso (3) UTC (1)**	5 (1-20)	47 (5-184)
Q1W	**4.0**	**Meso (3)**	4 (3-5)	32 (22-59)
Q1W	**6.0**	**Meso (4)**	17.5 (1-30)	58 (15-258)
All	**All**	**All**	**4 (1-30)**	**43 (5-399)**

PFS; progression free survival duration, Meso; malignant mesothelioma, RCC; renal cell carcinoma, UTC; urothelial carcinoma

Titles and legends to figures

Figure 1: Evaluation of CD26 staining by immunohistochemistry in cases of mesothelioma

Figure 2. Soluble CD26 (Fig.2A) and DPPIV activity (Fig. 2B) mean±sd profiles during cycle 1 at the different dose levels.

Fig 1

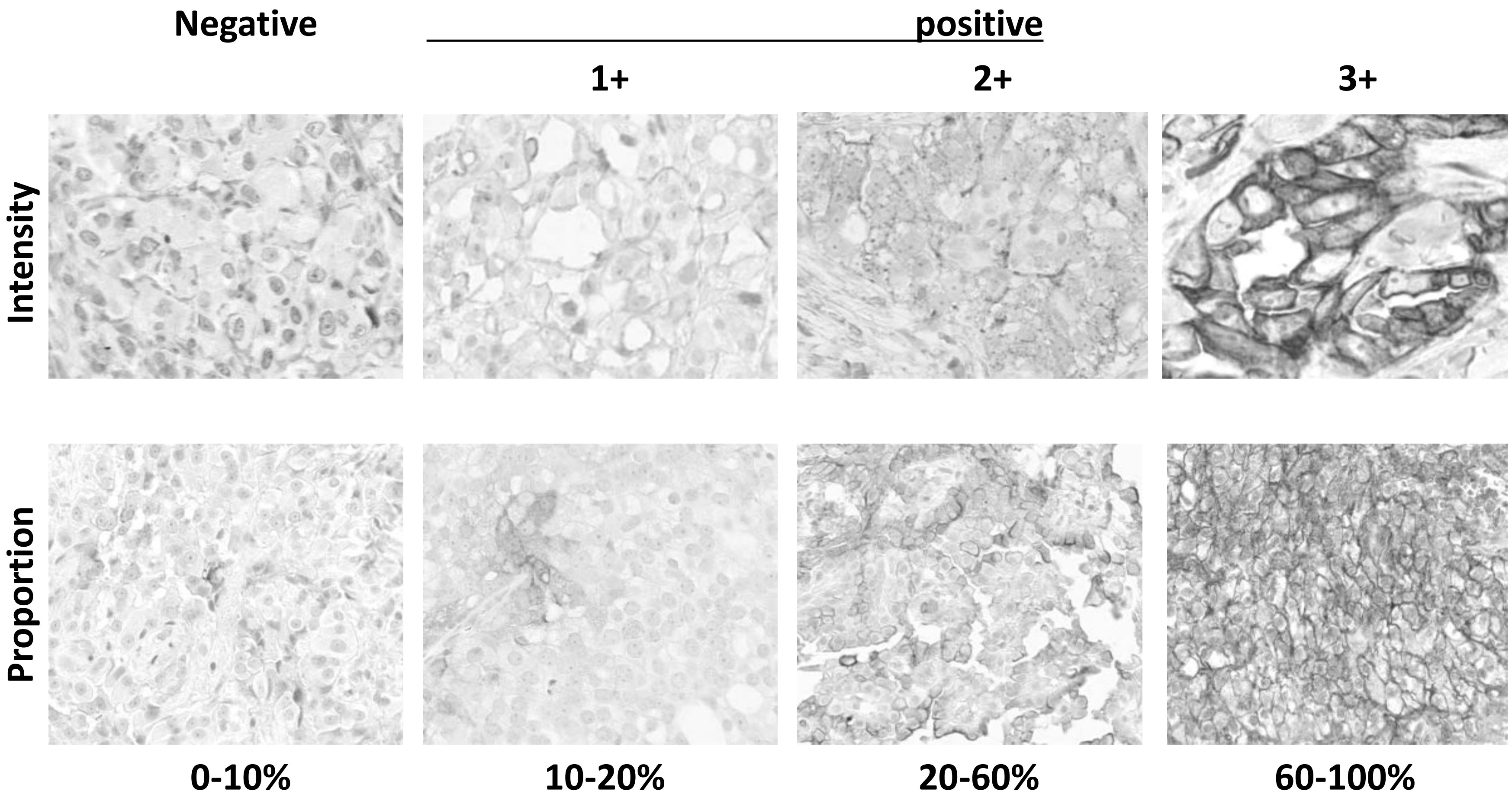
Negative
positive
1+
2+
3+
Intensity
Proportion
0-10%
10-20%
20-60%
60-100%

Fig 2

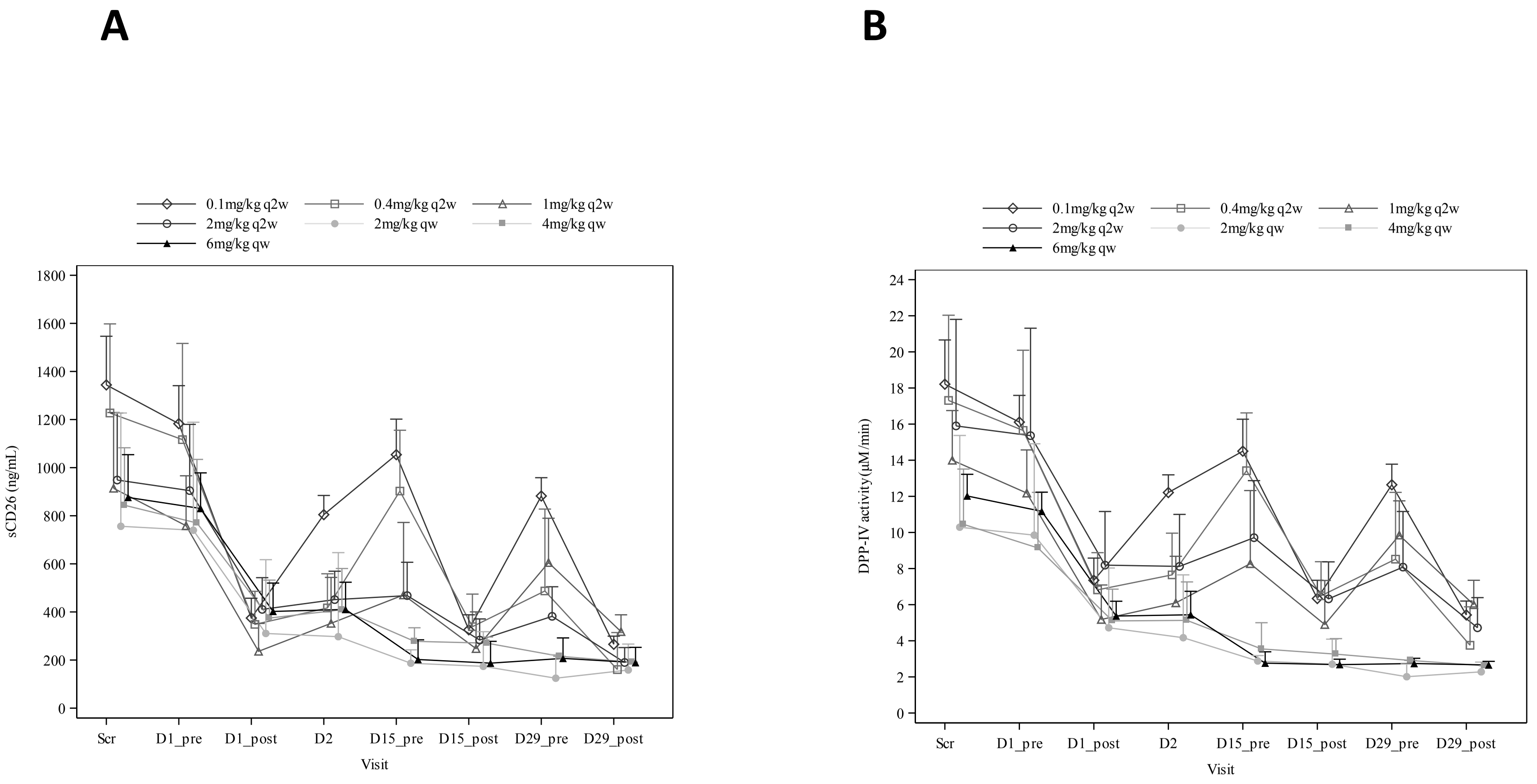
A
0.1mg/kg q2w
0.4mg/kg q2w
1mg/kg q2w
2mg/kg q2w
2mg/kg qw
4mg/kg qw
6mg/kg qw
sCD26 (ng/mL)
1800
1600
1400
1200
1000
800
600
400
200
0
Scr
D1_pre
D1_post
D2
D15_pre
D15_post
D29_pre
D29_post
Visit
B
0.1mg/kg q2w
0.4mg/kg q2w
1mg/kg q2w
2mg/kg q2w
2mg/kg qw
4mg/kg qw
6mg/kg qw
DPP-IV activity (μM/min)
24
22
20
18
16
14
12
10
8
6
4
2
0
Scr
D1_pre
D1_post
D2
D15_pre
D15_post
D29_pre
D29_post
Visit

A possible role for CD26/DPPIV enzyme activity in the regulation of psoriatic pruritus

Eriko Komiya PhD[a,b], Ryo Hatano PhD[a], Haruna Otsuka[a], Takumi Itoh[a,c],
Hiroto Yamazaki MD, PhD[a],Taketo Yamada MD, PhD[d,e], Nam H. Dang MD, PhD[f], Mitsutoshi Tominaga PhD[b], Yasushi Suga MD, PhD[g], Utako Kimura MD, PhD[g],
Kenji Takamori MD, PhD[b,g], Chikao Morimoto MD, PhD[a], Kei Ohnuma MD, PhD[a*]

[a] Department of Therapy Development and Innovation for Immune Disorders and Cancers, Graduate School of Medicine, Juntendo University, 2-1-1 Hongo, Bunkyo-ku, Tokyo 113-8421, Japan.
[b] Institute for Environmental and Gender Specific Medicine, Juntendo University Graduate School of Medicine, 2-1-1 Tomioka, Urayasu, Chiba 279-0021, Japan
[c] Graduate School of Health and Sports Science, Juntendo University, 1-1, Hiragagakuendai, Inzai, Chiba 270-1695, Japan
[d] Department of Pathology, Keio University school of Medicine, 35 Shinanomachi, Shinjuku-ku, Tokyo 160-8582, Japan.
[e] Department of Pathology Saitama Medical University, 38 Morohongo, Moroyama-cho, Iruma-gun, Saitama 350-0459, Japan.
[f] Division of Hematology/Oncology, University of Florida,
1600 SW Archer Road- Box 100278, Room MSB M410A, Gainesville, FL 32610, U.S.A.
[g] Department of Dermatology, Juntendo University Urayasu Hospital, 2-1-1 Tomioka, Urayasu, Chiba 279-0021, Japan.

∗ Corresponding author: Dr. K. Ohnuma, Department of Therapy Development and Innovation for Immune Disorders and Cancers, Graduate School of Medicine, Juntendo University, 2-1-1 Hongo, Bunkyo-ku, Tokyo 113-8421, Japan; TEL +81-3-3868-2310 FAX +81-3-3868-2310
E-mail: kohnuma@juntendo.ac.jp

Funding sources of this work

This work was supported by a Grant-in-Aid (S1311011) from the Foundation of Strategic Research Projects in Private Universities from the Ministry of Education, Culture, Sports, Science, and Technology, Japan; JSPS KAKENHI Grant Number 15H04879; JSPS KAKENHI Grant Number 15K15324; JSPS KAKENHI Grant Number 16H05345; JSPS KAKENHI Grant Number 26830114; a grant of the Ministry of Health, Labour, and Welfare, Japan (Grant Number 150401-01).

Conflicts-of-interest disclosure

The authors have no conflict of interest to declare.

This manuscript contains 6180 words in the text including the references (without figure legends), 54 references, 5 figures and 1 table.

ABSTRACT

Background: Psoriasis (PSO) is one of the most common chronic inflammatory skin diseases, and pruritus affects approximately 60-90% of patients with PSO. However, the pathogenesis of pruritus in PSO remains unclear. Dipeptidyl peptidase IV (DPPIV) enzyme activity is involved in the regulation of peptide hormones, chemokines and neurotransmitters.
Objectives: Our aim is to evaluate for a potential association between DPPIV and an increased risk of pruritus, and to identify possible underlying treatment targets in affected patients.
Methods: utilizing clinical serum samples of PSO patients and *in vivo* experimental pruritus models, we evaluated for a potential association between DPPIV and an increased risk for pruritus, and attempted to identify possible underlying treatment targets in pruritus of PSO.
Results: We first showed that levels of DPPIV enzyme activity in sera of patients with PSO were significantly increased compared to those of healthy controls. We next evaluated levels of substance-P (SP), which is a neurotransmitter for pruritus and a substrate for DPPIV enzyme. Truncated form SP cleaved by DPPIV was significantly increased in sera of PSO. In an *in vivo* pruritus model induced by SP, scratching was decreased by treatment with a DPPIV inhibitor. Moreover, DPPIV-knockout mice showed attenuation of scratching induced by SP. Finally, scratching was decreased following the administration of a DPPIV inhibitor in an imiquimod-induced PSO model. On the other hand, scratching induced by imiquimod was increased in DPPIV overexpressing-mice.
Conclusions: These results suggest that inhibition of DPPIV enzyme activity regulates pruritus in PSO.

Key words: CD26/DPPIV; substance P; pruritus; psoriasis.

Abbreviations: CD26KO, CD26/DPPIV knockout; DPPIV, dipeptidyl peptidase IV; DPPIV-Tg, CD26/DPPIV transgenic; IMQ, Imiquimod; NK-1R, nuerokinin-1 receptor; PSO, psoriasis; rsCD26(DPPIV+), recombinant soluble CD26 protein containing DPPIV enzyme activity; rsCD26(DPPIV-), recombinant soluble CD26 with deficient DPPIV enzyme activity; sCD26, soluble CD26; sDPPIV, soluble DPPIV enzyme activity; SP, substance P

1. INTRODUCTION

Psoriasis (PSO) is one of the most common inflammatory skin diseases, and is found in approximately 1-3% of the world general population [1]. For a long time, PSO had been considered as a non-pruritic dermatitis. However, more recently, a number of studies have demonstrated that approximately 60-90% of patients with PSO suffer from pruritus [1-6]. Although psoriatic patients consider pruritus as the most bothersome subjective sensation [5, 7], effective therapy for pruritus in PSO has not been established.

CD26 is a 110 kDa surface glycoprotein with dipeptidyl peptidase IV (DPPIV, EC 3.4.14.5) activity as a serine protease that cleaves dipeptides from the N-terminus of peptides at the penultimate position [8-10]. CD26 is also associated with T cell signal transduction processes as a costimulatory molecule, as well as being a marker of T cell activation [11, 12]. We have previously reported that CD26-mediated costimulatory activity is exerted via its DPPIV enzyme activity [13]. More recently, we have shown that serum soluble CD26 (sCD26) and DPPIV enzyme activity (sDPPIV) are inversely correlated with disease activity in patients with systemic lupus erythematosus [14]. In addition, sCD26 and sDPPIV are involved in the pathogenesis of various cancers including colorectal cancer, hepatocellular carcinoma, prostate cancer and malignant mesothelioma [15-19]. Other investigators have reported that CD26/DPPIV was upregulated in psoriatic skin and that DPPIV inhibitor ameliorated psoriasis [20-23], although the biological role of CD26/DPPIV in PSO has not yet been elucidated. Meanwhile, DPPIV enzyme activity has been widely studied in metabolic and endocrine disorders, and DPPIV inhibitors have been developed as a new class of anti-diabetic drugs which act by inhibiting DPPIV, the enzyme that inactivates incretin hormone [24-26]. The potentially important role played by CD26/DPPIV in the clinical setting has led to rising interest in serum sCD26 level and sDPPIV enzyme activity in various human conditions over the past decade.

Substance P (SP) is a neuropeptide involved in afferent neuronal signal transduction [27, 28]. Activation of sensory neurons in the skin causes the release of SP [29, 30]. Once released, SP binds to neurokinin receptors including neurokinin-1 receptor (NK-1R) found on keratinocytes and cutaneous nerve endings, resulting in the release of additional itch mediators [29, 31]. Substance P therefore appears to act to induce itch. It has been reported that the number of SP-containing nerves in the perivascular areas of pruritic psoriatic skin was increased and that expression of SP receptor in epidermis from pruritic psoriatic subjects was upregulated [3, 32]. On the other hand, SP consists of 11 amino acids residues and contains the DPPIV-target sequence at its N-terminal position [33]. Previous report utilizing DPPIV deficient rat showed that circulating SP was metabolized by DPPIV enzyme [34]. However, it is not clear whether degradation of SP by DPPIV enzyme affects pruritus in patients with PSO.

In the present study, utilizing clinical serum samples of PSO patients and *in vivo* experimental pruritus models, we evaluated for a potential association between DPPIV and an increased risk for SP-induced pruritus, and attempted to identify possible underlying treatment targets in pruritus of PSO. We showed that levels of DPPIV enzyme activity in sera of patients with PSO were significantly increased compared to those of healthy controls. Moreover, truncated form SP cleaved by DPPIV was significantly increased in sera of PSO. In an *in vivo* pruritus model induced by full-length SP, scratching was decreased by treatment with a DPPIV inhibitor. Moreover, scratching was increased following injection of truncated form SP. Furthermore, DPPIV-knockout mice showed attenuation of scratching induced by SP. Finally, scratching was decreased following the administration of a DPPIV inhibitor in an imiquimod (IMQ)-induced PSO model. On the other hand, scratching induced by IMQ was increased in DPPIV overexpressing transgenic (DPPIV-Tg) mice. These results suggest that inhibition of DPPIV enzyme activity regulates pruritus in PSO.

2. MATERIALS AND METHODS

2.1. Patients and serum collections and storage

The base cohort consisted of all PSO patients regularly seen and treated at the Juntendo Urayasu Hospital between May 2013 and October 2014. Peripheral blood samples were collected from 48 PSO patients and 18 healthy adult volunteers, using BD Vacutainer blood collection tube SSTII (BD, Franklin Lakes, NJ). Serum was obtained from 5 mL whole blood by centrifugation at 1500×*g* at 4°C for 10 min, and stored at -80°C in 500 μL aliquots. Human study protocols were approved by the Ethics Committees at the Juntendo Urayasu Hospital (Authorization Number 2013074). Informed consent was obtained from all patients. All studies on human subjects were conducted according to the principles set out in the Declaration of Helsinki.

2.2 Reagents and recombinant proteins

Recombinant full-length SP(1-11) and the DPPIV inhibitor sitagliptin were purchased from Peptide Institute (Osaka, Japan) and Sigma-Aldrich (St Louis, MO), respectively. Truncated SP(5-11) pyroglutamyl peptide was purchased from Eurofins Genomics (Ebersberg, Germany). Imiquimod (IMQ) (5% Beselna Cream) and control Absorptive cream were purchased from Mochida Pharmaceutical (Tokyo, Japan) and Nikko (Gifu, Japan), respectively. Recombinant sCD26 (rsCD26(DPPIV+)) was produced according to the method described previously [13].

2.3. Animals

C57BL/6 mice were purchased from CLEA Japan (Tokyo, Japan). CD26KO (CD26$^{-/-}$) mice developed from C57BL/6 mice were kindly gifted from the laboratory of Dr. Takeshi Watanabe at Kyusyu University (Fukuoka, Japan) [35]. DPPIV-Tg mice developed from C57BL/6 mice were kindly provided from the laboratory of Dr. Chien-Te K. Tseng at University of Texas Medical Branch (Texas) [36]. These mice were bred in-house and used at 8 to 11 weeks of age. They were kept under controlled temperature (23-25℃) and light (on time 8:00 A.M. to 8:00 P.M.) conditions. Food and water were freely available. All experiments on animals were approved by animal ethics committee in Juntendo University (Authorization Numbers 270242 and 280038).

2.4. sCD26 concentration and DPPIV enzyme activity assay procedure

For measurement of sCD26 concentration and DPPIV enzyme activity in human samples, serum samples were removed from the -80°C freezer and quickly thawed in a water bath at 37°C. All samples were centrifuged 3000×*g* for 5 min to discard debris, and were then assayed in duplicate. An in-house sandwich ELISA for sCD26 and sDPPIV enzyme was established in our laboratory [14, 37]. For evaluation of SP concentrations in human samples, the serum levels of SP and its fragments were evaluated utilizing two distinct ELISA kits, one detects SP(1-11), (2-11) and (3-11) (Substance P ELISA kit, Abcam, Cambridge, MA), and the other, SP(4-11) and (5-11) as well as SP(1-11), (2-11) and (3-11) (Substance P (Human, Rat, Mouse)-EIA kit, Phoenix Pharmaceuticals, Burlingame, CA). For DPPIV enzyme activity in murine samples, peripheral blood was harvested from tail vein at the indicated periods. After the blood samples were centrifuged to isolate sera, levels of DPPIV activity were measured utilizing DPPIV-Glo Protease Assay (Promega, Fitchburg, WI). For blood glucose analysis in murine sera, mice were put into an acrylic cage for 1 hour for acclimation and for food deprivation, followed by i.p. injection of 30 mM of sitagliptin or saline. Peripheral blood samples were harvested from tail vein, and the blood glucose concentrations were measured utilizing animal glucometer LAB Gluco (ForaCare Inc. CA) at the indicated periods.

2.5. In vitro digestion assay for SP and amino acid sequence analysis

Recombinant full-length SP(1-11) was incubated with rsCD26(DPPIV+) or rsCD26(DPPIV-) at a molecular ratio of 100:1. For DPPIV inhibition experiments, 5 nmol of sitagliptin was added to the recombinant full-length SP(1-11) and rsCD26(DPPIV+) at a molecular ratio of 100:1. After incubation at 37℃ for 4 hours, aliquots were transferred to PVDF membrane and subjected to N-terminal amino acid sequencing as determined by the Edman method (Toray Research Center Inc., Tokyo, Japan).

2.6. Itch murine models

For SP-induced itch murine model, mice hairs were clipped over the rostral part of the back one day before experiment. Under isoflurane anesthesia, mice received i.d. injection of full-length SP(1-11), truncated SP(5-11) or control solvent at the indicated doses, and then subjected to scratching behavior evaluation. For IMQ-induced psoriatic itch murine model, mice received a daily dose of 30 mg of IMQ or control vehicle cream on the shaved back for 5 days. On the 6th day, mice were subjected to scratching behavior evaluation as described below. On the 7th day, after macrophotographs of mice were taken, mice were sacrificed, and the skin specimens were harvested for histopathology examination.

2.7. Measurement of scratching behavior and locomotor activity

Before behavioral recording, the mice (4 animals per observation) were put into an acrylic cage (19.5×24×35 cm) for at least one hour for acclimation. Subsequently, the frequency of scratch behavior of the rostral back was analyzed by the SCLABA-Real system (NOVERTEC, Kobe, Japan) for the indicated time intervals, with observers being kept out of the experimental room. For evaluation of locomotor activities, mice were put into an acryl cage by the same method as in the scratching behavior evaluation, and were evaluated with the use of the SCLABA-Real tracking software. Locomotor activities were measured and expressed as the total horizontal moving distance of mice during itch behavioral experiments.

2.8. Tissue histopathology

Skin from the upper back of treated mice were fixed in 10% formalin, embedded in paraffin, sectioned, mounted on slides, and stained with hematoxylin and eosin (H&E) to determine pathology. Images were captured with an Olympus digital camera DP21 attached to an Olympus BX43 microscope using CellSens software (OLYMPUS, Tokyo, Japan). Slides were evaluated by a pathologist blinded to experimental groups.

2.9. Statistics

All experiments were performed in triplicates and repeated at least 3 times. Data were expressed as mean values±SEM (standard error of the mean), and were analyzed by two-tailed Student's *t* test for two group comparison or by ANOVA test for multiple comparison testing followed by the Tukey-Kramer *post-hoc* test. *P* values ≤ 0.05 were considered statistically significant. Calculations were performed and graphed using GraphPad Prism 6 (GraphPad Software Inc., La Jolla, CA).

3. RESULTS

3.1. Serum levels of sCD26 and sDPPIV enzyme are increased in patients with PSO

To determine whether sCD26 and sDPPIV enzyme play a role in PSO, we first evaluated levels of sCD26 and sDPPIV enzyme activity in sera of patients with PSO. For this purpose, peripheral blood samples were collected from healthy adult volunteers and PSO patients (regularly seen and treated at the Juntendo Urayasu Hospital). Of the 48 patients, mean (years ± S.D.) age was 49.9 (±16.9), male/female was 41/7. No patients with diabetes mellitus, hepatic or renal dysfunction were included in PSO cohort to exclude the possible influence of these conditions on serum levels of DPPIV enzyme activity [12, 24]. Of the 18 healthy adult volunteers, mean (years ± S.D.) age was 45.1 (±10.3), male/female was 15/3. All healthy adult volunteers had no history of cancers and chronic diseases including diabetes mellitus, hepatic diseases, allergic diseases, HIV infection, PSO and atopic dermatitis. There was no significant difference in body mass index between PSO and control cohorts (26.9±2.0 kg/m^2 *v.s.* 24.6±1.5 kg/m^2, *p*=0.287 by two-tailed Student's *t* test). Other demographic characteristics of the patients are summarized in Table 1.

As shown in Figure 1A, serum sCD26 concentration of PSO patients was significantly higher than that of healthy adults (1.02±0.28 μg/ml v.s. 0.64±0.16 μg/ml). Moreover, it has been reported that DPPIV enzymatic activity was correlated with the concentration of sCD26 in normal human sera [37, 38]. We therefore evaluated for potential correlation between DPPIV enzymatic activity and sCD26 level in the serum samples described above. For this purpose, we performed our in-house capture assay method using anti-human CD26 mAb as a capture antibody for detecting DPPIV enzyme activity specific to sCD26 [37]. Since commercially available DPPIV enzyme assay kits measure DPPIV activity in whole serum, but not in captured sCD26 molecules from the samples, it is possible that DPPIV-like peptidase activity other than that possessed by the captured sCD26 molecules was measured, leading to an overestimate of the DPPIV activity in the samples [39]. As shown in Figure 1B, serum levels of sDPPIV enzyme activity were also significantly higher in patients with PSO compared with healthy adult controls (17.38±4.18 μM/min *v.s.* 10.17±2.47 μM/min). These data suggest that DPPIV enzyme activity is increased in sera of patients with PSO, which is linked to a concomitant increase in sCD26 in the same patient population. These observations also suggest that DPPIV enzyme plays a role in the pathogenesis of PSO.

3.2. Truncated form of SP cleaved by DPPIV enzyme is increased in sera of PSO patients

It is well-known that many patients with PSO have pruritus that is generally refractory to therapy. Among various mediators of pruritus investigated in inflammatory skin diseases, SP is one of key molecules in an itch sensory nerve. While SP consists of 11 amino acids residues with dual DPPIV cleavage sites at its N-terminal position (Figure 2A), it is unclear whether truncation of SP by DPPIV enzyme plays a role in pruritus in inflammatory skin lesions. To determine whether DPPIV enzyme cleaves full-length SP(1-11), we performed *in vitro* digestion experiments utilizing recombinant sCD26 (rsCD26) protein. For this purpose, recombinant full-length SP(1-11) was incubated with rsCD26 protein containing DPPIV enzyme activity (rsCD26(DPPIV+)), and an amino acid sequence analysis was performed to determine the amino acid sequence of incubated SP. Our findings indicated that rsCD26(DPPIV+) digested recombinant full-length SP(1-11), resulting in a truncated form of SP(5-11) (Figure 2B-(a)), while mutant rsCD26 with deficient DPPIV enzyme activity (rsCD26(DPPIV-)) exhibited no digestive activity on SP(1-11) (Figure 2B-(b)). On the other hand, digestion of recombinant full-length SP(1-11) by rsCD26(DPPIV+) was inhibited by the presence of the DPPIV enzyme inhibitor sitagliptin (Figure 2B-(c)). These data indicate that native sCD26 containing DPPIV enzyme activity in sera degrades full-length SP(1-11), leading to the formation of SP(5-11).

To expand on these *in vitro* findings, we next analyzed the serum concentrations of full-length and truncated SP in patients with PSO. For this purpose, we utilized two different ELISA kits, one detects SP(1-11), (2-11) and (3-11), and the other, SP(4-11) and (5-11) as well as SP(1-11), (2-11) and (3-11). As shown in Figure 2C, levels of SP(1-11), (2-11) and (3-11) in sera of PSO were similar to those in healthy controls (0.23±0.11 ng/ml *v.s.* 0.22±0.11 μg/ml). On the other hand, serum levels of SP (4-11) and (5-11) were significantly increased in patients with PSO compared with healthy controls

(0.95±0.25 ng/ml *v.s.* 0.28±0.13 μg/ml) (Figure 2D). Taken together with the above data, our observations suggest that levels of SP degraded by DPPIV were increased in sera of patients with PSO, and that the increase in DPPIV activity appears to play an important role in PSO by truncation of SP.

3.3. DPPIV inhibitor suppresses SP-induced pruritus

We next utilized *in vivo* models to determine whether DPPIV activity regulates pruritus induced by SP. For this purpose, we established an itchy mouse model by intradermal injection (i.d.) of full-length SP(1-11) and quantified scratching behavior in mice to determine an itchy symptom. As shown in Figure 3A, mice treated with SP i.d. demonstrated increased scratching behavior in a dose-dependent manner of SP. Utilizing this itch model, we evaluated the effect of the DPPIV inhibitor sitagliptin on pruritus. Since we could not formally exclude the possibility that the DPPIV inhibitor induced hypoglycemia and decreased activity in treated mice, resulting in reduced scratching behavior, we measured the blood glucose levels in mice receiving sitagliptin. As shown in Figure 3B, suppression of DPPIV enzyme activity in mice sera was clearly observed from 5 to 30 minutes after intraperitoneal injection (i.p.) of sitagliptin at doses of 30 mM. Meanwhile, blood glucose levels in mice treated with 30 mM of sitagliptin were similar to those in mice treated with control saline (Figure 3C). These data suggest that *in vivo* DPPIV inhibition is observed in mice treated by i.p. sitagliptin, while mice receiving this regimen of sitagliptin did not develop hypoglycemia which might have an effect on locomotor activity. We therefore administered 30 mM of i.p. sitagliptin to SP-induced itchy model mice, and measured the frequency of scratching behavior for 1 hour. Under these experimental conditions, scratching behavior in SP(1-11) i.d. mice was significantly decreased in mice treated with sitagliptin (115.9±49.1 *v.s.* 13.56±9.4 times/hour) (Figure 3D). On the other hand, sitagliptin had no effect on the scratching behavior of mice treated with i.d. of control solvent (3.3±3.5 *v.s.* 9.3±9.5 times/hour) (*N.S.* in Figure 3D). Meanwhile, there were no significant differences in movement length among all cohorts, indicating that the decreased scratching behavior did not result from decreased mouse activity (Figure 3E). To further confirm that suppression of DPPIV enzyme activity decreased SP-induced pruritus, we used CD26/DPPIV knockout (CD26KO) mice to evaluate scratching behavior induced by SP(1-11). As shown in Figure 3F, SP-induced scratching behavior was significantly attenuated in CD26KO mice compared with that observed in C57BL/6 wild type mice (36.5±28.3 *v.s.* 97.0±50.9 times/hour). Meanwhile, there were no significant differences in movement length between CD26KO and wild type mice, indicating that the decreased scratching behavior did not result from decreased mouse activity (Figure 3G). To show effects of truncated form of SP(5-11) on pruritus, an itch mouse model experiment was conducted utilizing i.d. injection of recombinant SP(5-11) peptide. As shown in Figure 3H, mice treated with SP(5-11) i.d. demonstrated significant increase in scratching behavior (158.5±29.3 times/hour), compared with mice receiving control solvent (12.7±9.5 times/hour) or mice receiving full-length SP(1-11) (104.5±30.7 times/hour). Meanwhile, there were no significant differences in movement length among SP(1-11), SP(5-11)-treated and control mice, indicating that the increased scratching behavior did not result from increased mouse activity (Figure 3I). Taken together, our data suggest that SP-induced itch sensation is attenuated by inhibition of the DPPIV activity.

3.4. DPPIV inhibitor suppresses IMQ-induced psoriatic itch

To further determine that DPPIV inhibition affects pruritus, we evaluated scratching behavior utilizing an IMQ-induced psoriatic itch model [40, 41]. For this purpose, mice were treated with IMQ cream or control absorptive cream at a daily dose of 30 mg on the rostral part of the back for 5 consecutive days. As shown in Figure 4A, mice treated with control absorptive cream showed no sign of psoriatic features (panel a), while IMQ-treated mice exhibited psoriasis-like skin including erythema, scaling and thickness (panel b). Histopathology of skin specimens obtained from IMQ-treated mice showed hyperkeratosis, acanthosis and infiltration of inflammatory cells which were compatible to those found in psoriatic skin (panel e of Figure 4A). On the other hand, histopathology of skin specimens from control cream-treated mice showed none of these pathologic findings (panel d of Figure 4A). We next analyzed the serum concentrations of full-length and truncated SP in IMQ-treaed mice. As shown in Figure 4B, levels of SP(1-11), (2-11) and (3-11) in sera of IMQ-treated mice were similar to those in control cream-treated mice (0.32±0.06 ng/ml *v.s.* 0.39±0.01 μg/ml). On the other hand, serum levels of SP (4-11) and (5-11) were significantly increased in IMQ-treated mice compared with control cream-treated mice (0.63±0.09 ng/ml *v.s.* 0.32±0.08 μg/ml) (Figure 4C). Moreover, scratching behavior was significantly increased in IMQ-treated mice than control cream-treated mice (118.7±47.2 *v.s.* 26.7±20.9 times/hour) (Figure 4D). These data indicate that IMQ induces psoriatic itchy skin lesions in mice associated with an increase in the truncation of SP. Utilizing this psoriatic itch model, we analyzed the frequencies of itch scratching behaviors with DPPIV inhibitor administration. As shown in Figure 4D, IMQ-treated mice receiving sitagliptin showed significant decrease of scratching behavior compared with IMQ-treated mice receiving control solvent (31.0±16.0 *v.s.* 118.7±47.2 times/hour). Meanwhile, there was no change in scratching behavior between control cream-treated mice receiving sitaglitpin or control saline (30.8±17.8 *v.s.* 26.7±20.9 times/hour), with baseline levels of scratching behavior in both cohorts. Moreover, there were no significant differences in movement length among all cohorts, indicating that the decreased scratching behavior did not result from decreased mouse activity (Figure 4E). In addition, there was no additional phenotypic and histologic change induced by the administration of sitagliptin (panels c and f of Figure 4A), similar to those seen in IMQ-treated mice (panels b and e of Figure 4A). Taken together, our data suggest that treatment with the DPPIV inhibitor sitagliptin attenuates psoriatic itch sensation via a decrease in the truncated form of SP.

3.5. Overexpression of CD26/DPPIV exaggerates IMQ-induced psoriatic itch

Finally, to further determine that DPPIV enzyme activity is associated with pruritus, we used DPPIV-Tg mice to analyze scratching behavior. As shown in Figure 5A, DPPIV-Tg mice exhibited significant increase in DPPIV enzyme activity in sera compared with parental WT mice (177.5±34.4 *v.s.* 14.9±2.6 μM/min). Scratching behavior induced by IMQ cream was significantly increased in DPPIV-Tg mice than in WT mice (188.6±66.2 *v.s.* 107.6±45.9 times/hour) (Figure 5B). Meanwhile, there was no change in scratching behavior between WT and DPPIV-Tg mice treated with control cream (44.9±19.6 *v.s.* 40.5±15.5 times/hour), with baseline levels of scratching behavior in both cohorts (Figure 5B). Moreover, there were no significant differences in movement length between IMQ-treated WT and DPPIV-Tg mice, indicating that the observed increase in scratching behavior did not result from increased mouse activity (Figure 5C). Taken together with the above data, our findings strongly suggest that increased DPPIV enzyme activity exaggerates psoriatic pruritus and that DPPIV may be a novel target for treatment of itch sensation in psoriasis.

4. DISCUSSION

In the present study, we demonstrated that serum levels of DPPIV enzyme activity was significantly increased in patients with PSO, concomitant with elevation of truncated form of SP. Moreover, overexpression of DPPIV enzyme activity exaggerated itch scratching behavior in psoriatic pruritus murine model induced by IMQ cream. Furthermore, treatment with the DPPIV inhibitor sitagliptin improved itch scratching behavior in murine pruritus models induced by SP administration or IMQ cream.

Pruritus is an important symptom of PSO. Despite the fact that several studies have been undertaken to investigate the pathogenesis of pruritus in psoriasis, many aspects of this clinical manifestation have not yet been thoroughly examined [1, 32]. Therefore, the pathogenesis of this symptom is far from being well-understood and, as a consequence, effective therapy for pruritus in psoriatic patients still remains a significant challenge in the clinical setting [42]. It has been shown previously that keratinocytes expressed high levels of DPPIV and that DPPIV inhibition suppressed keratinocyte proliferation *in vitro*, and partially restored keratinocyte differentiation *in vivo* [43]. It has also been reported that DPPIV activity on keratinocytes was upregulated in PSO [22, 44], suggesting a potential role for DPPIV enzyme activity in the pathogenesis of PSO. While other investigators have reported a significant improvement in disease severity in patients with PSO treated with sitagliptin [21, 45], the precise mechanisms involved in the effect of DPPIV inhibition on PSO have not been elucidated.

DPPIV is expressed as CD26 on T cells and DPPIV-mediated T cell activation has been demonstrated [46]. Recent report showed that the T-cell bound expression of CD26/DPPIV in psoriatic skin was explicitly present, albeit in small quantities [44]. One hypothesis regarding the potential effect of DPPIV in PSO is that T cell activation mediated by DPPIV is associated with the pathogenesis of PSO [47]. Cytokines and chemokines represent the third key player in the psoriatic chronic immune response [48], and are mediators responsible for the activation and recruitment of infiltrating leucocytes, therefore playing a crucial role in the development and persistence of psoriatic skin lesions [49]. DPPIV likely has a pivotal role in the processing of these molecules [46]. The extracellular protease domain of DPPIV (both on keratinocytes and T cells) can cleave dipeptides from the amino terminus of proteins, such as cytokines and chemokines, which are abundantly present in a chronic immune response in PSO, resulting in alterations in receptor specificity and a subsequent reduction in biological activity. Taken together, it is conceivable that in PSO, a disease involving critical interplays among activated T cells, keratinocytes and cytokines, DPPIV can influence disease behavior by regulating all three components.

SP is a sensory undecapeptide of the tachykinin family distributed widely in the central and peripheral nervous systems, mediating the sensation of itch via small-diameter C fibers in the skin [50, 51]. Previous studies have reported that serum levels of SP were decreased in patients with PSO [52, 53, 54]. Meanwhile, since SP is cleaved by DPPIV enzyme and DPPIV enzyme activity is increased in PSO as shown in Figures 1 and 2, it is important for a detailed understanding of the role of SP in PSO to precisely measure the truncated form of SP separately from full-length SP. In our present study, we evaluated full-length SP(1-11) and truncated forms of SP and demonstrated that there was no change in the serum levels of full-length SP(1-11), SP(2-11) and SP(3-11) between PSO and healthy adult controls. However, we found that DPPIV enzyme activity and truncated form of SP were significantly increased in PSO, and that truncated form of SP(5-11) resulting from DPPIV enzyme activity is associated with an increase in itch sensation. In IMQ-induced PSO model, truncated form of SP was significantly increased in sera compared with control mice, and scratching behavior was decreased by administration of sitagliptin. On the other hand, there were no differences in serum levels of DPPIV enzyme activity between IMQ and control cream-treated mice (data not shown). It is conceivable that the persistent existence of psoriatic skin lesions may be required for the increased serum levels of DPPIV enzyme activity seen in PSO patients, and that SP truncation may result from the increased levels of DPPIV enzyme activity in skin lesions rather than in the circulation [22,24]. Regarding the specific receptors mediating the itch sensation of truncated SP, while SP-mediated itch has been reported to be mediated via full-length SP bound to NK-1R [29, 31], future studies will be performed to determine whether truncated form of SP acts on NK-1R as an agonistic mediator or targets other pruritic receptors.

Our current study has conclusively demonstrated that increase in DPPIV enzyme activity exacerbates pruritus in

PSO, and that inhibition of DPPIV enzyme reduces severity of itch scratching behavior. Moreover, our results suggest that DPPIV inhibitors are useful as therapeutic agents for pruritus including PSO. Additional studies will be conducted in the near future to better characterize and understand PSO-associated pruritus, which may lead to the development of novel effective antipruritic treatment modalities targeting the CD26/DPPIV molecule.

ACKNOWLEDGEMENTS

The authors thank Dr. Airi Jo-Watanabe (Department of Biochemistry, Juntendo University School of Medicine), Dr. Hyeon-cheol Lee (Department of Biochemistry, Juntendo University School of Medicine), Mr. Nobuaki Takahashi (Institute for Environmental and Gender Specific Medicine, Juntendo University Graduate School of medicine), Mrs. Hiroko Madokoro (Department of Pathology, Keio University School of Medicine) and Mrs. Yuka Narita (Department of Therapy Development and Innovation for Immune Disorders and Cancers, Juntendo University Graduate School of Medicine) for excellent technical assistances and thorough discussion.

FUNDING SOURCES

This work was supported by a Grant-in-Aid (S1311011) from the Foundation of Strategic Research Projects in Private Universities from the Ministry of Education, Culture, Sports, Science, and Technology, Japan; JSPS KAKENHI Grant Number 15H04879; JSPS KAKENHI Grant Number 15K15324; JSPS KAKENHI Grant Number 16H05345; JSPS KAKENHI Grant Number 26830114; a grant of the Ministry of Health, Labour, and Welfare, Japan (Grant Number 150401-01).

CONFLICTS-OF-INTEREST DISCLOSURE

The authors have no conflict of interest to declare.

REFERENCES

[1] J.C. Szepietowski, A. Reich, Pruritus in psoriasis: An update, Eur J Pain 20(1) (2016) 41-6.

[2] B. Amatya, G. Wennersten, K. Nordlind, Patients' perspective of pruritus in chronic plaque psoriasis: a questionnaire-based study, J Eur Acad Dermatol Venereol 22(7) (2008) 822-6.

[3] S.E. Chang, S.S. Han, H.J. Jung, J.H. Choi, Neuropeptides and their receptors in psoriatic skin in relation to pruritus, Br J Dermatol 156(6) (2007) 1272-7.

[4] G. Stinco, G. Trevisan, F. Piccirillo, S. Pezzetta, E. Errichetti, N. di Meo, F. Valent, P. Patrone, Pruritus in chronic plaque psoriasis: a questionnaire-based study of 230 Italian patients, Acta Dermatovenerol Croat 22(2) (2014) 122-8.

[5] J.C. Szepietowski, A. Reich, B. Wisnicka, Pruritus and psoriasis, Br J Dermatol 151(6) (2004) 1284.

[6] G. Yosipovitch, A. Goon, J. Wee, Y.H. Chan, C.L. Goh, The prevalence and clinical characteristics of pruritus among patients with extensive psoriasis, Br J Dermatol 143(5) (2000) 969-73.

[7] A. Reich, K. Welz-Kubiak, L. Rams, Apprehension of the disease by patients suffering from psoriasis, Postepy Dermatol Alergol 31(5) (2014) 289-93.

[8] D.A. Fox, R.E. Hussey, K.A. Fitzgerald, O. Acuto, C. Poole, L. Palley, J.F. Daley, S.F. Schlossman, E.L. Reinherz, Ta1, a novel 105 KD human T cell activation antigen defined by a monoclonal antibody, J Immunol 133(3) (1984) 1250-6.

[9] D.M. Nanus, D. Engelstein, G.A. Gastl, L. Gluck, M.J. Vidal, M. Morrison, C.L. Finstad, N.H. Bander, A.P. Albino, Molecular cloning of the human kidney differentiation antigen gp160: human aminopeptidase A, Proc Natl Acad Sci U S A 90(15) (1993) 7069-73.

[10] T. Tanaka, D. Camerini, B. Seed, Y. Torimoto, N.H. Dang, J. Kameoka, H.N. Dahlberg, S.F. Schlossman, C. Morimoto, Cloning and functional expression of the T cell activation antigen CD26, J Immunol 149(2) (1992) 481-6.

[11] C. Morimoto, S.F. Schlossman, The structure and function of CD26 in the T-cell immune response, Immunol Rev 161 (1998) 55-70.

[12] K. Ohnuma, N.H. Dang, C. Morimoto, Revisiting an old acquaintance: CD26 and its molecular mechanisms in T cell function, Trends Immunol 29(6) (2008) 295-301.

[13] T. Tanaka, J. Kameoka, A. Yaron, S.F. Schlossman, C. Morimoto, The costimulatory activity of the CD26 antigen requires dipeptidyl peptidase IV enzymatic activity, Proc Natl Acad Sci U S A 90(10) (1993) 4586-90.

[14] H. Kobayashi, O. Hosono, T. Mimori, H. Kawasaki, N.H. Dang, H. Tanaka, C. Morimoto, Reduction of serum soluble CD26/dipeptidyl peptidase IV enzyme activity and its correlation with disease activity in systemic lupus erythematosus, J Rheumatol 29(9) (2002) 1858-66.

[15] T. Inamoto, T. Yamada, K. Ohnuma, S. Kina, N. Takahashi, T. Yamochi, S. Inamoto, Y. Katsuoka, O. Hosono, H. Tanaka, N.H. Dang, C. Morimoto, Humanized anti-CD26 monoclonal antibody as a treatment for malignant mesothelioma tumors, Clin Cancer Res 13(14) (2007) 4191-200.

[16] E. Komiya, K. Ohnuma, H. Yamazaki, R. Hatano, S. Iwata, T. Okamoto, N.H. Dang, T. Yamada, C. Morimoto, CD26-mediated regulation of periostin expression contributes to migration and invasion of malignant pleural mesothelioma cells, Biochem Biophys Res Commun 447(4) (2014) 609-15.

[17] R. Pang, W.L. Law, A.C. Chu, J.T. Poon, C.S. Lam, A.K. Chow, L. Ng, L.W. Cheung, X.R. Lan, H.Y. Lan, V.P. Tan, T.C. Yau, R.T. Poon, B.C. Wong, A subpopulation of CD26+ cancer stem cells with metastatic capacity in human colorectal cancer, Cell Stem Cell 6(6) (2010) 603-15.
[18] B.A. Stecca, B. Nardo, P. Chieco, A. Mazziotti, L. Bolondi, A. Cavallari, Aberrant dipeptidyl peptidase IV (DPP IV/CD26) expression in human hepatocellular carcinoma, J Hepatol 27(2) (1997) 337-45.
[19] Y.X. Sun, E.A. Pedersen, Y. Shiozawa, A.M. Havens, Y. Jung, J. Wang, K.J. Pienta, R.S. Taichman, CD26/dipeptidyl peptidase IV regulates prostate cancer metastasis by degrading SDF-1/CXCL12, Clin Exp Metastasis 25(7) (2008) 765-76.
[20] H. Nagai, S. Fujiwara, Y. Takahashi, C. Nishigori, Ameliorating effect of the novel dipeptidyl peptidase-4 inhibitor teneligliptin on psoriasis: A report of two cases, J Dermatol 42(11) (2015) 1094-7.
[21] T. Nishioka, M. Shinohara, N. Tanimoto, C. Kumagai, K. Hashimoto, Sitagliptin, a dipeptidyl peptidase-IV inhibitor, improves psoriasis, Dermatology 224(1) (2012) 20-1.
[22] M. Novelli, P. Savoia, M.T. Fierro, A. Verrone, P. Quaglino, M.G. Bernengo, Keratinocytes express dipeptidyl-peptidase IV (CD26) in benign and malignant skin diseases, Br J Dermatol 134(6) (1996) 1052-6.
[23] R.G. van Lingen, M.K. Poll, M.M. Seyger, E.M. de Jong, P.C. van de Kerkhof, P.E. van Erp, Distribution of dipeptidyl-peptidase IV on keratinocytes in the margin zone of a psoriatic lesion: a comparison with hyperproliferation and aberrant differentiation markers, Arch Dermatol Res 300(10) (2008) 561-7.
[24] D.J. Drucker, Enhancing incretin action for the treatment of type 2 diabetes, Diabetes Care 26(10) (2003) 2929-40.
[25] G.A. Herman, A. Bergman, C. Stevens, P. Kotey, B. Yi, P. Zhao, B. Dietrich, G. Golor, A. Schrodter, B. Keymeulen, K.C. Lasseter, M.S. Kipnes, K. Snyder, D. Hilliard, M. Tanen, C. Cilissen, M. De Smet, I. de Lepeleire, K. Van Dyck, A.Q. Wang, W. Zeng, M.J. Davies, W. Tanaka, J.J. Holst, C.F. Deacon, K.M. Gottesdiener, J.A. Wagner, Effect of single oral doses of sitagliptin, a dipeptidyl peptidase-4 inhibitor, on incretin and plasma glucose levels after an oral glucose tolerance test in patients with type 2 diabetes, J Clin Endocrinol Metab 91(11) (2006) 4612-9.
[26] D. Kim, L. Wang, M. Beconi, G.J. Eiermann, M.H. Fisher, H. He, G.J. Hickey, J.E. Kowalchick, B. Leiting, K. Lyons, F. Marsilio, M.E. McCann, R.A. Patel, A. Petrov, G. Scapin, S.B. Patel, R.S. Roy, J.K. Wu, M.J. Wyvratt, B.B. Zhang, L. Zhu, N.A. Thornberry, A.E. Weber, (2R)-4-oxo-4-[3-(trifluoromethyl)-5,6-dihydro[1,2,4]triazolo[4, 3-a]pyrazin-7(8H)-yl]-1-(2,4,5-trifluorophenyl)butan-2-amine: a potent, orally active dipeptidyl peptidase IV inhibitor for the treatment of type 2 diabetes, J Med Chem 48(1) (2005) 141-51.
[27] C. De Felipe, J.F. Herrero, J.A. O'Brien, J.A. Palmer, C.A. Doyle, A.J. Smith, J.M. Laird, C. Belmonte, F. Cervero, S.P. Hunt, Altered nociception, analgesia and aggression in mice lacking the receptor for substance P, Nature 392(6674) (1998) 394-7.
[28] B. Pernow, Substance P, Pharmacol Rev 35(2) (1983) 85-141.
[29] M.K. Church, Y. Okayama, S. el-Lati, Mediator secretion from human skin mast cells provoked by immunological and non-immunological stimulation, Skin Pharmacol 4 Suppl 1 (1991) 15-24.
[30] A.E. Kremer, J. Feramisco, P.W. Reeh, U. Beuers, R.P. Oude Elferink, Receptors, cells and circuits involved in pruritus of systemic disorders, Biochim Biophys Acta 1842(7) (2014) 869-92.
[31] M. Schmelz, R. Schmidt, A. Bickel, H.O. Handwerker, H.E. Torebjork, Specific C-receptors for itch in human skin, J Neurosci 17(20) (1997) 8003-8.
[32] M. Nakamura, M. Toyoda, M. Morohashi, Pruritogenic mediators in psoriasis vulgaris: comparative evaluation of itch-associated cutaneous factors, Br J Dermatol 149(4) (2003) 718-30.
[33] E. Heymann, R. Mentlein, Liver dipeptidyl aminopeptidase IV hydrolyzes substance P, FEBS Lett 91(2) (1978) 360-4.
[34] T. Karl, T. Hoffmann, R. Pabst, S. von Horsten, Extreme reduction of dipeptidyl peptidase IV activity in F344 rat substrains is associated with various behavioral differences, Physiol Behav 80(1) (2003) 123-34.
[35] D. Marguet, L. Baggio, T. Kobayashi, A.M. Bernard, M. Pierres, P.F. Nielsen, U. Ribel, T. Watanabe, D.J. Drucker, N. Wagtmann, Enhanced insulin secretion and improved glucose tolerance in mice lacking CD26, Proc Natl Acad Sci U S A 97(12) (2000) 6874-9.
[36] A.S. Agrawal, T. Garron, X. Tao, B.H. Peng, M. Wakamiya, T.S. Chan, R.B. Couch, C.T. Tseng, Generation of a transgenic mouse model of Middle East respiratory syndrome coronavirus infection and disease, J Virol 89(7) (2015) 3659-70.
[37] K. Ohnuma, T. Saito, R. Hatano, O. Hosono, S. Iwata, N.H. Dang, H. Ninomiya, C. Morimoto, Comparison of two commercial ELISAs against an in-house ELISA for measuring soluble CD26 in human serum, J Clin Lab Anal 29(2) (2015) 106-11.
[38] T. Andrieu, V. Thibault, I. Malet, J. Laporte, B. Bauvois, H. Agut, A. Cahour, Similar increased serum dipeptidyl peptidase IV activity in chronic hepatitis C and other viral infections, J Clin Virol 27(1) (2003) 59-68.
[39] A. Sedo, R. Malik, Dipeptidyl peptidase IV-like molecules: homologous proteins or homologous activities?, Biochim Biophys Acta 1550 (2001) 107 - 116.
[40] L. van der Fits, S. Mourits, J.S. Voerman, M. Kant, L. Boon, J.D. Laman, F. Cornelissen, A.M. Mus, E. Florencia, E.P. Prens, E. Lubberts, Imiquimod-induced psoriasis-like skin inflammation in mice is mediated via the IL-23/IL-17 axis, J Immunol 182(9) (2009) 5836-45.
[41] K. Sakai, K.M. Sanders, M.R. Youssef, K.M. Yanushefski, L. Jensen, G. Yosipovitch, T. Akiyama, Mouse model of imiquimod-induced psoriatic itch, Pain (2016).
[42] A.S. Raut, R.H. Prabhu, V.B. Patravale, Psoriasis clinical implications and treatment: a review, Crit Rev Ther Drug

Carrier Syst 30(3) (2013) 183-216.

[43] A. Thielitz, D. Reinhold, R. Vetter, U. Bank, M. Helmuth, R. Hartig, S. Wrenger, I. Wiswedel, U. Lendeckel, T. Kahne, K. Neubert, J. Faust, C.C. Zouboulis, S. Ansorge, H. Gollnick, Inhibitors of dipeptidyl peptidase IV and aminopeptidase N target major pathogenetic steps in acne initiation, J Invest Dermatol 127(5) (2007) 1042-51.

[44] R.G. van Lingen, P.C. van de Kerkhof, M.M. Seyger, E.M. de Jong, D.W. van Rens, M.K. Poll, P.L. Zeeuwen, P.E. van Erp, CD26/dipeptidyl-peptidase IV in psoriatic skin: upregulation and topographical changes, Br J Dermatol 158(6) (2008) 1264-72.

[45] M. Lynch, A.M. Tobin, T. Ahern, D. O'Shea, B. Kirby, Sitagliptin for severe psoriasis, Clin Exp Dermatol 39(7) (2014) 841-2.

[46] K. Ohnuma, O. Hosono, N.H. Dang, C. Morimoto, Dipeptidyl peptidase in autoimmune pathophysiology, Adv Clin Chem 53 (2011) 51-84.

[47] M. Diani, G. Altomare, E. Reali, T cell responses in psoriasis and psoriatic arthritis, Autoimmun Rev 14(4) (2015) 286-92.

[48] J. Baliwag, D.H. Barnes, A. Johnston, Cytokines in psoriasis, Cytokine 73(2) (2015) 342-50.

[49] M.P. Schon, W.H. Boehncke, Psoriasis, N Engl J Med 352(18) (2005) 1899-912.

[50] F.O. Nestle, P. Di Meglio, J.Z. Qin, B.J. Nickoloff, Skin immune sentinels in health and disease, Nat Rev Immunol 9(10) (2009) 679-91.

[51] T. Akiyama, E. Carstens, Neural processing of itch, Neuroscience 250 (2013) 697-714.

[52] C. Remrod, S. Lonne-Rahm, K. Nordlind, Study of substance P and its receptor neurokinin-1 in psoriasis and their relation to chronic stress and pruritus, Arch Dermatol Res 299(2) (2007) 85-91.

[53] B. Amatya, K. Nordlind, C.F. Wahlgren, Responses to intradermal injections of substance P in psoriasis patients with pruritus, Skin Pharmacol Physiol 23(3) (2010) 133-8.

[54] T. Miyagaki, M. Sugaya, H. Suga, S. Morimura, M. Kamata, H. Ohmatsu, H. Fujita, Y. Asano, Y. Tada, T. Kadono, S. Sato, Serum soluble CD26 levels: diagnostic efficiency for atopic dermatitis, cutaneous T-cell lymphoma and psoriasis in combination with serum thymus and activation-regulated chemokine levels, J Eur Acad Dermatol Venereol 27(1) (2013) 19-24.

LEGENDS TO FIGURES

Figure 1. Serum levels of sCD26 and DPPIV enzyme activity in patients with PSO.

(A) Levels of sCD26 were measured in sera of PSO patients (n=48) or healthy adult volunteers (n=18). Levels of sCD26 in PSO patients were significantly increased as compared to healthy controls (1.02±0.28 *v.s.* 0.64±0.16 μg/ml; $P<0.0001$ by two-tailed Student's *t* test). Each dot indicates individual value. The horizontal lines in the middle of scattergrams indicate each mean value. sCD26 concentration was measured using our in-house capture method as described in Materials and Methods.

(B) Levels of sDPPIV enzyme activity were measured in sera of PSO patients (n=48) or healthy adult volunteers (n=18). Levels of sDPPIV enzyme activity in PSO patients were significantly increased as compared to healthy controls (17.38±4.18 *v.s.* 10.17±2.47 μM/min; $P<0.0001$ by two-tailed Student's *t* test). Each dot indicates individual value. The horizontal lines in the middle of scattergrams indicate each mean value. DPPIV enzyme activity was measured using our in-house capture method as described in Materials and Methods.

Figure 2. *In vitro* digestion assay of substance P (SP) and serum levels of full length and truncated SP in patients with PSO.

(A) Schematic diagram of amino acid sequence of full-length SP(1-11). Arrows indicate two DPPIV cleavage sites.

(B) The recombinant full-length SP(1-11) was incubated with rsCD26(DPPIV+) (*panel a*) or rsCD26(DPPIV-) (*panel b*). For DPPIV inhibition experiment, sitagliptin was added to recombinant full-length SP(1-11) and rsCD26(DPPIV+) (*panel c*). After incubation at 37℃ for 4 hours, aliquots were transferred to PVDF membrane and subjected to N-terminal amino acid sequencing as determined by the Edman method. The results of amino acid sequencing were shown in each right panel.

(C) The levels of SP(1-11), (2-11), and (3-11) were measured in sera of PSO patients (n=48) or healthy adult volunteers (n=18). There was no significant difference in the serum levels of SP(1-11), (2-11), and (3-11) between PSO patients and healthy controls (0.23±0.11 *v.s.* 0.22±0.11 ng/ml; $p=0.95$ by two-tailed Student's *t* test). Each dot indicates individual value. The horizontal lines in the middle of scattergrams indicate each mean value.

(D) The levels of SP(4-11) and (5-11), including SP(1-11), (2-11) and (3-11) concentrations, were measured in sera of PSO patients (n=48) or healthy adult volunteers (n=18). The serum levels of SP(4-11) and (5-11) including SP(1-11), (2-11) and (3-11) in PSO were significantly increased as compared to healthy controls (0.95±0.25 v.s. 0.28±0.13 ng/ml; $P<0.0001$ by two-tailed Student's *t* test). Each dot indicates individual value. The horizontal lines in the middle of scattergrams indicate each mean value.

Figure 3. Treatment with DPPIV inhibitor attenuates SP-induced Pruritus.

(A) Recombinant full-length SP(1-11) was injected at doses of 0 (saline), 100 or 200 nmol per site by i.d. into the rostral back of mice. The frequency of scratching behavior was counted for 1 hour as described in Materials and Methods. Mice receiving saline exhibited scratching behavior of 21.5±12.3 times/hour (n=6). On the other hand, mice receiving 100 or 200 nmol of SP exhibited scratching behavior of 68.3±17.9 or 106.3±18.6 times/hour, respectively (each, n=6), showing significant increase of scratching behavior in a dose-dependent manner of SP. Each dot indicates an individual value and the horizontal bar represents average value.

(B) Representative plot of mean values of serum DPPIV enzyme activity in mice receiving the DPPIV inhibitor sitagliptin is shown. Sitagliptin was injected at doses of 0.03, 0.5 or 30 mM by i.p. Peripheral blood was harvested at 0, 5, 15, 30 and 60 minutes after injection, and levels of DPPIV enzyme activity were determined as described in Materials and Methods. Serum levels of DPPIV activity were decreased in a dose-dependent manner of sitagliptin. At 30 mM of sitagliptin, DPPIV enzyme activity in mice clearly decreased to less than 20 % of the value prior to administration, and lasted for at least 30 minutes. Similar results were observed in independent experiments (n=6).

(C) Blood glucose levels in mice receiving the DPPIV inhibitor sitagliptin is shown (n=6). The blood glucose levels were measured at 0 (before 1 hour food deprivation), 60 (before 30 mM sitagliptin i.p. injection), 70, 90, 120 and 210 minutes. Hypoglycemia was not observed in mice treated with sitaglitpin in these experimental conditions.

(D) Mice were treated with recombinant full-length SP(1-11) (200 nmol per site) or physiological saline by i.d. and with sitagliptin (30 mM) or saline water by i.p (each, n=10). The frequency of scratching behavior of the rostral back was counted for 1 hour by the method as described in Materials and Methods. Scratching behavior was significantly increased in mice treated with 200 nmol of SP compared with control mice (115.9±49.1 *v.s.* 9.3±9.5 times/hour, $p<0.0001$ by ANOVA). DPPIV inhibition attenuated SP-induced itch scratching behavior (13.6±9.4 times/hour, $p<0.0001$ *v.s.* saline cohorts by ANOVA), while DPPIV inhibition alone showed no significant changes in scratching behavior (3.3±3.5 times/hour, *N.S.* denotes not significant). Each dot indicates an individual value and the horizontal bar represents average value.

(E) Locomotor activities of mice were measured as total horizontal moving distance during itch behavioral experiment as conducted in (D). There was no significant difference among control mice, mice receiving saline i.d. and sitagliptin i.p., mice receiving SP i.d. and saline i.p., and mice receiving SP i.d. and sitagliptin i.p. (Each, n=10; 16.9±14.1 *v.s.* 13.4±12.1 *v.s.* 15.1±16.2 *v.s.* 4.8±4.7 cm/hour, respectively). Each dot indicates an individual value and the horizontal bar represents average value. *N.S.* denotes 'not significant' by ANOVA.

(F) Wild type C57BL/6 (WT) and CD26 knockout (CD26KO) mice were treated with recombinant full-length SP(1-11) (200 nmol/site) by i.d. The frequency of scratching behavior was counted for 1 hour as described in Materials and Methods. The frequency of CD26KO mice scratching behavior was significantly decreased as compared to wild type mice (each, n=8, 97.0±50.9 *v.s.* 36.5±23.3 times/hour, $p<0.0001$ by two-tailed Student's *t* test). Each dot indicates an individual value and the horizontal bar represents average value.

(G) Conducted simultaneously with itch behavior experiment as shown in (F), locomotor activities of CD26KO mice were measured as described in Materials and Methods. There was no significant difference in locomotor activity between WT and CD26KO (5.9±4.1 *v.s.* 7.5±2.5 cm/hour, $p=0.535$ by two-tailed Student's *t* test). Each dot indicates an individual value and the horizontal bar represents average value.

(H) Mice were treated with recombinant full-length SP(1-11), truncated SP(5-11) (200 nmol per site) or control solvent (10%DMSO and 0.00625M acetate in physiological saline) by i.d. (each, n=6). The frequency of scratching behavior was evaluated by the same method as described in (D). Scratching behavior was significantly increased in mice treated with SP(1-11) (104.5±30.7 times/hour) or SP(5-11) (158.5±29.3 times/hour) than control mice (12.7±9.5 time/hour) (each $p<0.01$ by ANOVA). Moreover, scratching behavior was significantly increased in mice treated with SP(5-11) compared with mice receiving SP(1-11) ($p<0.01$ by ANOVA). Each dot indicates an individual value and the horizontal bar represents average value.

(I) Locomotor activities of mice were measured as total horizontal moving distance during itch behavioral experiment as conducted in (H). There was no significant difference among mice receiving control solvent, full-length SP(1-11) or truncated SP(5-11) i.d. (38.3±18.0 *v.s.* 30.2±12.5 *v.s.* 28.6±12.0 cm/hour). Each dot indicates an individual value and the horizontal bar represents average value. *N.S.* denotes 'not significant' by ANOVA.

Figure 4. DPPIV inhibitor attenuates Imiquimod-induced PSO derived itch.

C57BL/6 mice were treated with IMQ cream or control vehicle cream at a daily dose of 30 mg on the rostral part of back for 5 days. On the 6th day, mice were treated with i.p. of sitagliptin (30 mM) or physiological saline, and then subjected to scratching behavior and locomotor activity analyses.

(A) Representative macroscopic photographs of back skins of control cream-treated mice (*panel a*), IMQ cream-treated mice (*panel b*) or IMQ cream-treated mice receiving the DPPIV inhibitor sitagliptin (*panel c*) are shown. H&E staining histology of skin specimens obtained from each mouse is shown in *panels d, e or f,* respectively. Similar results were observed in independent experiments (n=6). Original magnification ×100. Scale bars, 100 μm.

(B) The levels of SP(1-11), (2-11), and (3-11) were measured in sera of IMQ or control cream-treated mice on the 6th day after treatment (each, n=3), utilizing the same ELISA kit as conducted in Figure 2C. There was no significant difference in the serum levels of SP(1-11), (2-11), and (3-11) between IMQ and control cream-treated mice (0.32±0.06 *v.s.* 0.39±0.01 ng/ml; $p=0.11$ by two-tailed Student's *t* test). Each dot indicates individual value. The horizontal lines in the middle of scattergrams indicate each mean value. *N.S.* denotes 'not significant'.

(C) The levels of SP(4-11) and (5-11), including SP(1-11), (2-11) and (3-11) concentrations, were measured in sera of IMQ or control cream-treated mice on the 6th day after treatment (each, n=3), utilizing the same ELISA kit as conducted in Figure 2D. The serum levels of SP(4-11) and (5-11) including SP(1-11), (2-11) and (3-11) in IMQ-treated mice were significantly increased as compared with control cream-treated mice (0.63±0.09 *v.s.* 0.32±0.08 ng/ml; $P<0.05$ by two-tailed Student's *t* test). Each dot indicates individual value. The horizontal lines in the middle of scattergrams indicate each mean value.

(D) The frequency of scratching behavior was counted for 2 hours after injection of sitagliptin or saline. Mice receiving sitagliptin showed significantly decreased IMQ-induced itch scratching behavior compared with IMQ-treated mice receiving saline (each, n=6; 31.0±16.0 *v.s.*118.7±47.2 times/hour, $p<0.0001$ by ANOVA). Meanwhile, treatment with the DPPIV inhibitor alone resulted in no significant change in the frequency of scratching behavior in control cream-treated mice (each, n=6; 30.8±17.8 *v.s.* 26.7±20.9, $p=0.989$ by ANOVA). Each dot indicates an individual value and the horizontal bar represents average value. *N.S.* denotes 'not significant'.

(E) Locomotor activities of mice were measured as total horizontal moving distance during itch behavioral experiment as conducted in (D). There was no significant difference among control cream-treated mice receiving saline or sitagliptin, and IMQ-treated mice receiving saline or sitagliptin i.p. (Each, n=6; 58.4±47.3 *v.s.* 51.4±23.1 *v.s.* 52.2±51.7 *v.s.* 38.7±32.9 cm/hour, respectively). Each dot indicates an individual value and the horizontal bar represents average value. *N.S.* denotes 'not significant' by ANOVA.

Figure 5. Overexpression of DPPIV aggravates IMQ-induced psoriatic itch.

(A) DPPIV enzyme activities in sera of Wild type C57BL/6 (WT) or DPPIV-Tg mice were determined as described in Materials and Methods. DPPIV-Tg mice exhibited a significant increase in DPPIV enzyme activity in sera compared with parental WT mice (each, n=6; 177.5±34.4 *v.s.* 14.9±2.6 μM, $p<0.0001$ by Student's *t* test). Each dot indicates an individual value and the horizontal bar represents average value.

(B) WT and DPPIV-Tg mice were treated with IMQ cream or control vehicle cream at a daily dose of 30 mg on the rostral part of the back for 5 days (each, n=8). Control cream-treated WT and DPPIV-Tg mice showed no significant difference in scratching behavior (44.9±19.6 *v.s.* 40.5±15.5 times/hour, p=0.993 by ANOVA), while IMQ-treated WT or DPPIV-Tg mice exhibited increased scratching behavior, compared with each control cream-treated mice (44.9±19.6 *v.s.* 107.6±46.9 or 40.5±15.5 *v.s.* 188.6±66.2 times/hour, respectively; each $p<0.0001$ by ANOVA). Scratching behavior induced by IMQ-treated DPPIV-Tg mice was significantly increased compared with IMQ-treated WT mice (188.6±66.2 *v.s.* 107.6±46.9 times/hour, $p<0.001$ by ANOVA). Each dot indicates an individual value and the horizontal bar represents average value. *N.S.* denotes 'not significant'.

(C) Locomotor activities of mice were measured as total horizontal moving distance during itch behavioral experiment as conducted in (B). There was no significant difference between WT and DPPIV-Tg mice treated with IMQ cream (Each, n=8; 15.8±12.6 *v.s.* 24.6±15.1 cm/hour, respectively; p=0.228 by Student's *t* test). Each dot indicates an individual value and the horizontal bar represents average value.

Table 1. Demographic Characteristics of Cohorts

Variable	Patients with PSO (n=48)	Healthy Control (n=18)
Age, years, mean±SD (range)	49.9±14.9 (19-88)	45.1±10.3 (25-65)
Male/Female, n (ratio)	41/7 (5.9)	15/3 (5.0)
BMI, kg/m^2, mean±SD (range)	26.9±2.0 (19.3-42.3)	24.6±1.5 (18.4-32.0)
PASI score, points, mean±SD (range)	12.2±12.0 (0.0-60.0)	N/A
Itch VAS, mm, mean±SD (range)	29.4±31.0 (0-100)	N/A
Use of Biologics [1], n (%)	13 (27.1%)	N/A
Use of Immunosuppressant [2], n (%)	2 (4.0%)	N/A

BMI, body mass index; n, number; N/A, not applicable; SD, standard deviation; PASI, psoriasis area and severity index at blood collection; PSO psoriasis; VAS, visual analogue scale at blood collection.

[1] Biologics includes anti-TNFα, anti-IL-12/23p40 and anti-IL-17A monoclonal antibody therapy.

[2] Immunosuppressant includes oral prednisolone and methotrexate.

Figure 1.

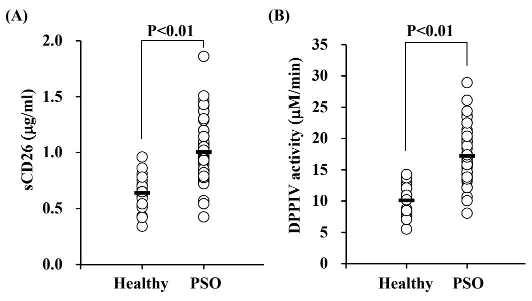

Figure 2.

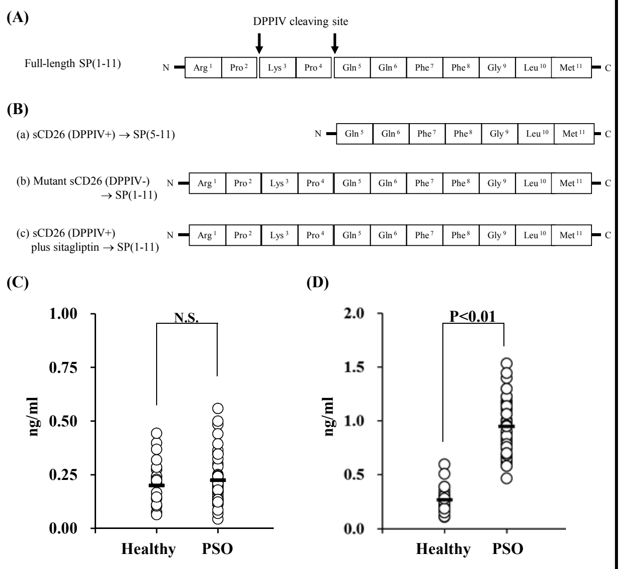

Figure 3.

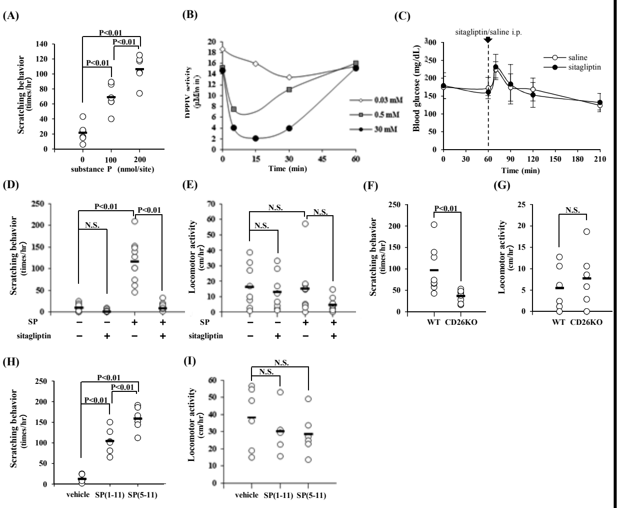

Figure 4.

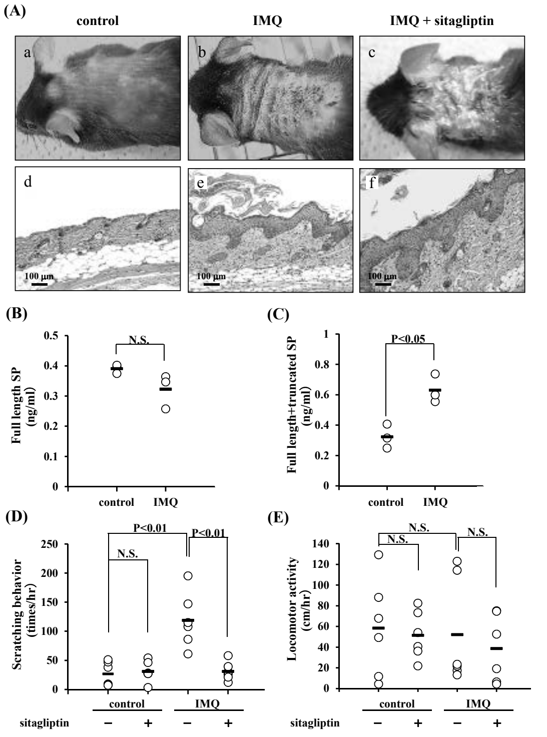
(A)
control
IMQ
IMQ + sitagliptin
a
b
c
d
e
f
100 μm
100 μm
100 μm
(B)
N.S.
Full length SP (ng/ml)
control
IMQ
(C)
P<0.05
Full length+truncated SP (ng/ml)
control
IMQ
(D)
P<0.01
P<0.01
N.S.
Scratching behavior (times/hr)
control
IMQ
sitagliptin
(E)
N.S.
N.S.
N.S.
Locomotor activity (cm/hr)
control
IMQ
sitagliptin

Figure 5.

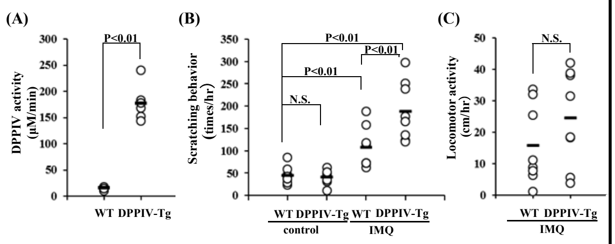
(A)
P<0.01
DPPIV activity (μM/min)
300
250
200
150
100
50
0
WT
DPPIV-Tg
(B)
P<0.01
P<0.01
P<0.01
N.S.
Scratching behavior (times/hr)
350
300
250
200
150
100
50
0
WT
DPPIV-Tg
control
WT
DPPIV-Tg
IMQ
(C)
N.S.
Locomotor activity (cm/hr)
50
40
30
20
10
0
WT
DPPIV-Tg
IMQ

Biochemical and Biophysical Research Communications 474 (2016) 111–117

Contents lists available at ScienceDirect

Biochemical and Biophysical Research Communications

journal homepage: www.elsevier.com/locate/ybbrc

Inhibition of VEGF-dependent angiogenesis by the anti-CD82 monoclonal antibody 4F9 through regulation of lipid raft microdomains

Sayaka Nomura [a], Satoshi Iwata [a, 1], Ryo Hatano [a, 1], Eriko Komiya [b], Nam H. Dang [c], Noriaki Iwao [d], Kei Ohnuma [e, *, 1], Chikao Morimoto [a, e, 1]

[a] *Division of Clinical Immunology, Advanced Clinical Research Center, The Institute of Medical Science, The University of Tokyo, 4-6-1 Shirokanedai, Minato-ku, Tokyo, 108-8639, Japan*
[b] *Department of Therapy Development and Innovation for Immune Disorders and Cancers, Graduate School of Medicine, Juntendo University, 2-1-1, Hongo, Bunkyo-ku, Tokyo, 113-8421, Japan*
[c] *Division of Hematology/Oncology, University of Florida, 1600 SW Archer Road- Box 100278, Room MSB M410A, Gainesville, FL, 32610, USA*
[d] *Department of Hematology, School of Medicine, Juntendo University, 2-1-1, Hongo, Bunkyo-ku, Tokyo, 113-8421, Japan*
[e] *Department of Rheumatology and Allergy, IMSUT Hospital, The Institute of Medical Science, The University of Tokyo, 4-6-1 Shirokanedai, Minato-ku, Tokyo, 108-8639, Japan*

ARTICLE INFO

Article history:
Received 5 April 2016
Accepted 18 April 2016
Available online 19 April 2016

Keywords:
CD82
4F9
VEGF
VGFR2
Angiogenesis

ABSTRACT

CD82 (also known as KAI1) belongs to the tetraspanin superfamily of type III transmembrane proteins, and is involved in regulating cell adhesion, migration and proliferation. In contrast to these well-established roles of CD82 in tumor biology, its function in endothelial cell (EC) activity and tumor angiogenesis is yet to be determined. In this study, we show that suppression of CD82 negatively regulates vascular endothelial growth factor (VEGF)-induced angiogenesis. Moreover, we demonstrate that the anti-CD82 mAb 4F9 effectively inhibits phosphorylation of VEGF receptor 2 (VEGFR2), which is the principal mediator of the VEGF-induced angiogenic signaling process in tumor angiogenesis, by regulating the organization of the lipid raft microdomain signaling platform in human EC. Our present work therefore suggests that CD82 on EC is a potential target for anti-angiogenic therapy in VEGFR2-dependent tumor angiogenesis.

© 2016 Elsevier Inc. All rights reserved.

1. Introduction

CD82 (also known as KAI1) belongs to the tetraspanin superfamily of type III transmembrane proteins, and is involved in the regulation of cell adhesion, migration and proliferation through the activation of downstream signaling processes [1]. We previously showed that CD82 was preferentially expressed on $CD4^{+}CD45RO^{+}$ memory T cells and that treatment with the anti-CD82 monoclonal antibody (mAb) 4F9 co-immobilized with a submitogenic dose of anti-CD3 mAb led to marked T cell proliferation [2]. Moreover, we dissected key aspects of the CD82-and β1 integrin-mediated signaling pathways through studies with Jurkat T cells with marginal expression of Cas-L/NEDD9 as well as those involving CD82-mediated tyrosine phosphorylation of Cas-L in peripheral T cells and H9 cells [3]. Meanwhile, CD82 expression on cancer cells suppresses tumor progression [1]. CD82 was originally identified as a suppressor of metastasis in a genetic screening assay for rat AT6.1 prostate cancer cells [4]. Subsequent studies showed that CD82 functions as a wide-spectrum suppressor of invasion and metastasis during cancer progression in many solid tumors [1,5]. Mechanistically, CD82 inhibits receptor tyrosine kinases (RTKs) (*e.g.*, epidermal growth factor receptor and hepatocyte growth factor

---

Abbreviations: BSA, bovine serum albumin; EC, endothelial cell; HUVEC, human umbilical vein endothelial cell; IL-6, interleukin-6; IL-6R, interleukin-6 receptor; mAb, monoclonal antibody; RTK, receptor tyrosine kinase; shCD82, shRNA against CD82; shRNA, short hairpin RNA; VEGF, vascular endothelial growth factor; VEGFR, vascular endothelial growth factor receptor; [^{3}H]-TdR, tritiated thymidine.

* Corresponding author. Department of Therapy Development and Innovation for Immune Disorders and Cancers, Graduate School of Medicine, Juntendo University, 2-1-1, Hongo, Bunkyo-ku, Tokyo, 113-8421, Japan.
E-mail address: kohnuma@juntendo.ac.jp (K. Ohnuma).

[1] Department of Therapy Development and Innovation for Immune Disorders and Cancers, Graduate School of Medicine, Juntendo University, 2-1-1, Hongo, Bunkyo-ku, Tokyo 113-8421, Japan

http://dx.doi.org/10.1016/j.bbrc.2016.04.081
0006-291X/© 2016 Elsevier Inc. All rights reserved.

receptor) and integrin signaling by promoting their internalization [6,7]. Recent studies demonstrated that CD82 expressed on melanoma cells suppresses environmental angiogenesis by inhibiting the production of interleukin-6 (IL-6) and vascular endothelial growth factor (VEGF) in melanoma cells [8].

Cancer angiogenesis is another fundamental process involved in tumor growth as it ensures adequate supply of oxygen and nutrients to promote cell growth and motility through the development of new blood vessels, potentially causing cancer progression and metastasis [9]. Angiogenesis involves coordinated endothelial cell (EC) proliferation, migration, branching and tube formation [10]. The VEGF family is a group of key proteins involved in the angiogenic pathway and is highly expressed in many tumor types [11]. Following increased production of VEGF induced by hypoxia, inflammatory cytokines, activation of oncogenes or silencing of oncosuppressor genes, the VEGF receptors (VEGFRs), which are expressed in tumor environmental vascular ECs, are activated to mediate cancer angiogenesis, promoting tumor growth and metastasis [12–14]. Therefore, suppression of cancer angiogenesis pathway by such agents as the anti-VEGF mAb bevacizumab, anti-VEGFR2 mAb ramucirumab, or the RTK inhibitors sorafenib and sunitinib represents novel treatment approaches for anticancer therapy [9,12,15].

Although CD82 is also expressed on EC as well as many neoplasms [1], a role for CD82 in EC activity and angiogenesis has not yet been clearly established. Recent study using *Cd82*-null mice showed that perturbation of CD82-ganglioside-CD44 signaling attenuates pathological angiogenesis by inhibiting EC movement [16], while *Cd82*-null mice display normal vessel development without obvious vascular defects [17]. Although VEGF-dependent EC activity plays an essential role in angiogenesis [18], a functional role for CD82 in association with VEGF/VEGFRs in EC activity has not yet been elucidated.

In this study, we show that suppression of CD82 negatively regulates VEGF-induced angiogenesis. Moreover, we demonstrate that the anti-CD82 mAb 4F9 effectively inhibits phosphorylation of VEGFR2, which is the principal mediator of the VEGF-induced angiogenic signaling process, by regulating the organization of the signaling platform, *i.e.*, lipid raft microdomains, in human EC. As a result, our present study suggests that CD82 on EC is a potential target for anti-angiogenic therapy in tumor angiogenesis.

2. Materials and methods

2.1. Antibodies, reagents and cells

Anti-human CD82 mAb 4F9 (mouse IgG1) was established in our laboratory as reported elsewhere [2]. Anti-VEGFR2 rabbit mAb (55B11), anti-phospho-VEGFR2 rabbit mAb (19A10) and anti-CD31 mouse mAb (89C2) were purchased from Cell Signaling Technology (USA). Suramin and recombinant human VEGF were purchased from Sigma–Aldrich (USA) and R&D Systems (USA), respectively. Human umbilical vein endothelial cells (HUVECs) were purchased from KURABO (Japan) and cultured according to the manufacturer's instruction. 293 FT cells for production of lentivirus particles were obtained from the ATCC (USA).

2.2. Generation of CD82-knockdown HUVECs using short hairpin (sh) RNA

Four clones of lentiviral shRNA against human CD82 (shCD82-RNA) and one control shRNA were purchased from Sigma–Aldrich (MISSION™ TRC shRNA Target Set), and each sequence of shCD82-RNA is shown in Supplemental Table. Each vector contained GFP tag as a selection marker. Lentivirus particles of shRNA were produced by 293 FT cells utilizing ViraPower™ Lentiviral Packaging Mix (Invitrogen, USA). After transfection of each shRNA lentivirus particle, GFP-positive HUVECs were purified using BD FACSAria cell sorter (BD Biosciences, USA), and expression of CD82 was confirmed by flow cytometry by the same method as described previously [3].

2.3. Cell migration and proliferation assays

HUVEC migration was assessed using 96-well microchamber plates (BD BioCoat Angiogenesis System, BD Biosciences). Cells were starved for 20 h in HuMedia-EB2 (KURABO) containing 0.1% bovine serum albumin (BSA). Cells were then harvested, resuspended in HuMedia-EB2 containing 0.1% BSA with indicated concentrations of anti-CD82 mAb 4F9 or suramin, and placed in the upper chamber of fibronectin-coated FluoroBlock Cell Culture Inserts (BD Biosciences) at a cell density of 5×10^4 cells per well. Cell migration was initiated by placing medium containing 10 ng/ml VEGF and 0.1% fetal bovine serum to the bottom chamber. After 18 h of incubation, cells were stained with 4 ng/ml calcein AM. Fluorescence in the cells that had migrated through the pores of the fluorescence blocking membrane was directly measured through the bottom of the chambers in a fluorescence plate reader at excitation/emission wavelengths of 485/530 nm (SpectraMax Gemini EM, Molecular Devices, USA) and analyzed using SoftMax Pro 5.2 software (Molecular Devices).

Cell proliferation was measured using [^{3}H]-thymidine ([^{3}H]-TdR) incorporation assay. HUVECs were seeded in HuMedia-EG2 (KURABO) containing indicated concentrations of mAbs or VEGF in collagen-coated 96-well plates (BD Biosciences) at a density of 2.5×10^4 cells per well. [^{3}H]-TdR (1 μCi/mL) was added and the cells were cultured for a further 18 h. Cells were then harvested and their radioactivity level was measured with a Liquid Scintillation Counter (Wallac 1205 Beta Plate; Perkin–Elmer Life Sciences, USA).

2.4. 2-D angiogenesis assay

After treatment with indicated concentrations of mAbs, VEGF or suramin, HUVECs were cultured utilizing the Angiogenesis Kit with the manufacturer's instruction (KURABO). The media containing each concentration of mAbs, VEGF or suramin were changed at 4, 7, 9 days, and cells were immunostained with anti-CD31 mAb at 11 days. Tube formation of HUVECSs was examined by photography under a microscope (Nikon DIAPHOT 300, Nikon, Japan) and quantified in 5 random fields utilizing Angiogenesis Image Analyzer v.2.0.0 (KURABO).

2.5. Measurement of phosphorylation of VEGFR2

HUVECSs were cultured in HuMedia-EG2 with 4F9 or control mouse IgG (each 10 μg/ml) for 12 h, followed by addition of VEGF (10 ng/ml). Cells were harvested at the indicated incubation period with VEGF, and lysates were then subjected to Western blot analysis according to the method described previously [19].

2.6. Lipid raft fractionation

HUVECs were cultured in HuMedia-EG2 with 4F9 or control mouse IgG (each 10 μg/ml) for 12 h, followed by a 5 min incubation period with VEGF (10 ng/ml). Cells were then harvested, and cell lysates were prepared for fractionation by sucrose density gradient ultracentrifugation by the same method as described previously [19].

2.7. Statistical analysis

Data were analyzed by two-tailed Student's *t* test for two group comparison or by ANOVA test for multiple comparison testing followed by the Tukey–Kramer *post-hoc* test. The level of significance was $p < 0.05$. The calculations were conducted using Prism6.0 software (GraphPad Software, USA).

3. Results

3.1. Knockdown of CD82 decreases EC migration, proliferation and angiogenesis

To determine the role of CD82 in vascular morphogenesis, we first examined cellular activity using a gene ablation approach. For this purpose, we used HUVECs in this study to address the functional role of human CD82 as an angiogenesis model. We first confirmed expression of CD82 in HUVECs by flow cytometry. As shown in Supplemental Fig. S1, cell surface expression of CD82 in HUVECs was clearly observed using the anti-CD82 mAb 4F9. Using 4 different shRNAs against CD82, we then established 4 clones of CD82-knockdown HUVECs with a lentivirus transfection system (shCD82-283, 300, 643 and 949). As shown in Supplemental Fig. S2, expression of cell surface CD82 was significantly decreased in each CD82-knockdown HUVECs than that in control shRNA-transfected HUVECs. Utilizing these shRNA HUVECs, we performed 2-D angiogenesis assay of fibroblast-coculture system. As shown in Fig. 1A, each CD82-knockdown HUVEC exhibited a significant decrease in the level of angiogenesis compared to control shRNA HUVEC. We next examined cell migration and proliferation. As shown in Fig. 1B, with increased doses of VEGF, control shRNA HUVECs displayed enhanced migratory activity. In contrast, CD82-knockdown HUVEC (shCD82-300 clone) exhibited a significant decrease in migratory activity while being cultured with VEGF (** in Fig. 1B). Moreover, cell proliferation decreased significantly in CD82-knockdown HUVEC (shCD82-300 clone) than control shRNA HUVECs (** in Fig. 1C). Other shCD82-HUVEC clones including shCD82-283, 643 and 949 exhibited decreased levels of migration and proliferation similar to those of shCD82-300 HUVEC (data not shown). These results suggest that the CD82 molecule plays a role in EC motility and angiogenesis.

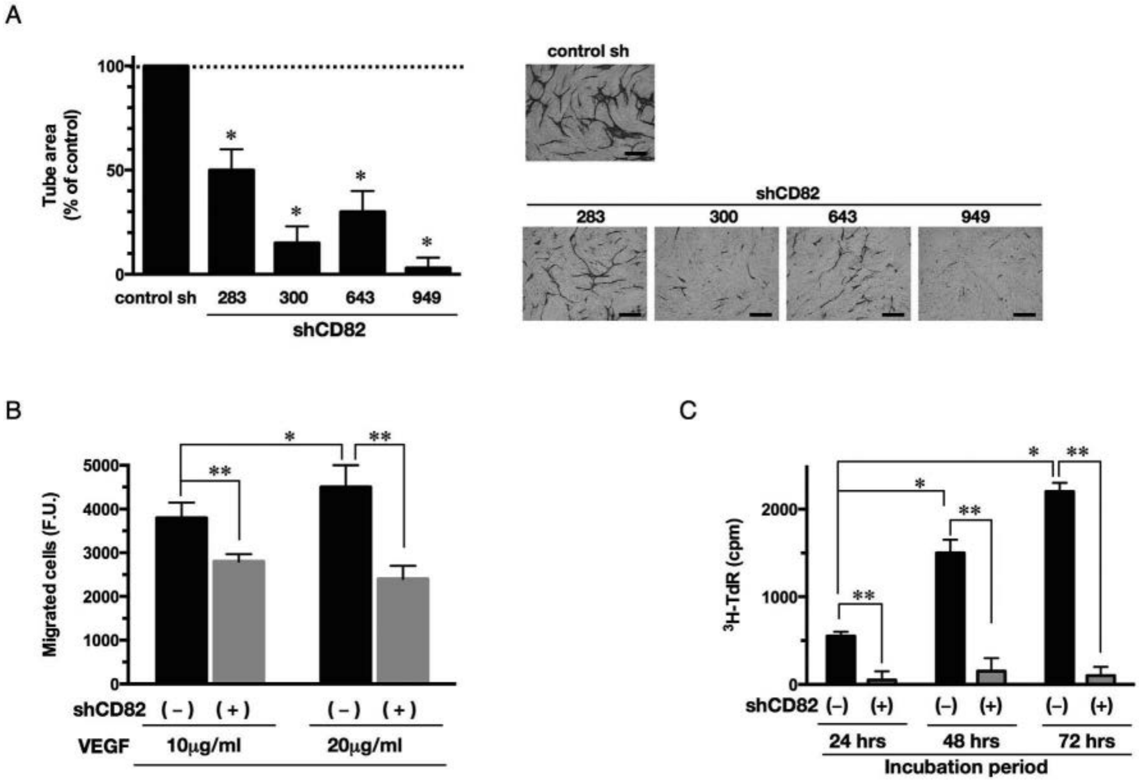

Fig. 1. Silencing of CD82 expression inhibited HUVEC tube formation, migration and proliferation. Four clones of CD82-knockdown HUVEC (shCD82-283, 300, 643 and 949) and one clone of control shRNA HUVEC were established by lentivirus-based shRNA transfection system. **(A)** Each shRNA HUVEC was cultured in wells seeded with normal human dermal fibroblasts, and was incubated in HuMedia-EG2 containing 10 ng/ml of VEGF. Angiogenesis was quantified by measuring CD31-stained area in 5 random fields utilizing Angiogenesis Image Analyzer. *Left panel* shows the results presented as the percentage of the mean values obtained in the percentage of tube area in control shRNA HUVECs. The mean values of percentage of tube area ± S.E. are shown (n = 5 experiments with triplicates), and the horizontal dotted line indicates a 100% level of control shRNA HUVECs. A significant decrease in angiogenesis of each CD82-knockdown HUVEC is indicated (*$P < 0.001$ *vs.* control shRNA). Representative microphotographs of tube formation of each shRNA HUVEC were shown in the *right five panels* (brown cells are anti-CD31 immunohistochemistry). Scale bars indicate 25 μm **(B)** CD82-knockdown HUVECs (shCD82-300) (shCD82 (+)) or control shRNA transfected HUVECs (shCD82 (−)) were seeded on the upper chamber of fibronectin-coated culture inserts with the lower chamber containing VEGF (10 or 20 ng/ml). The number of cells that migrated through the inserts in the lower chamber was measured as Calcein AM positive cells and the mean values ± S.E. of fluorescence units (F.U.) are shown (n = 5 experiments with triplicates). A significant increase in migration of control shRNA HUVECs was observed in a dose-dependent manner of VEGF (*$P < 0.05$). In contrast, a significant decrease in migration of shCD82 HUVECs was indicated in 10 and 20 ng/ml of VEGF (**$P < 0.001$ *vs.* control shRNA). **(C)** CD82-knockdown HUVECs (shCD82-300) (shCD82 (+)) or control shRNA transfected HUVECs (shCD82 (−)) were incubated with 10 ng/ml of VEGF. Proliferation of HUVECs was monitored by measuring [^{3}H]-thymidine (TdR) incorporation at 24, 48 or 72 h of culture. The mean values of [^{3}H]-TdR incorporation ± S.E. are shown (n = 5 experiments with triplicates). A significant increase in proliferation of control shRNA HUVECs was observed in a time course of culture (*$P < 0.05$). In contrast, a significant decrease in proliferation was indicated in shCD82 HUVECs (**$P < 0.001$ *vs.* control shRNA). (For interpretation of the references to colour in this figure legend, the reader is referred to the web version of this article.)

3.2. Anti-CD82 mAb 4F9 inhibits EC migration, proliferation and angiogenesis

We previously established the anti-CD82 mAb 4F9, which exerted a comitogenic effect on T cell costimulatory signaling pathway and caused cell spreading in H9 cells [2,3]. While these data indicate that 4F9 has a functional effect on CD82-expressing cells, we next hypothesized that EC activity is also regulated by treatment with 4F9. To assess the role of 4F9 in EC activity and angiogenesis, we therefore performed angiogenesis, migration or proliferation assays following 4F9 treatment. As shown in Fig. 2A, 4F9 treatment significantly decreased angiogenesis in a dose-dependent manner. In addition, this inhibitory effect of 4F9 on angiogenesis was comparable to that of suramin treatment, which is a potent inhibitor of VEGF (*** in Fig. 2A). Furthermore, we assessed cell migration and proliferation of HUVECs following 4F9 treatment. As shown in Fig. 2B, cell migration was reduced by treatment with 4F9 in a dose-dependent manner, an inhibitory effect that was comparable to that of suramin (** in Fig. 2B). Moreover, while no change in proliferative activity was observed after 24 h of 4F9 treatment, cell proliferation decreased significantly following a 48 h incubation period with 4F9 in a dose-dependent manner (Fig. 2C). In addition, 4F9 treatment exhibited a significant decrease in angiogenesis, migratory and proliferative activity while being cultured with high doses of exogeous VEGF up to 100 ng/ml (data not shown). These data strongly suggest that ligation of CD82 by the anti-CD82 mAb 4F9 leads to suppression of VEGF-dependent angiogenesis.

3.3. Anti-CD82 mAb 4F9 inhibits phosphorylation of VEGFR2 via control of CD82 distribution in lipid rafts

The VEGF family members bind three different RTK receptors: VEGFR1 (Flt-1), VEGFR2 (Flt-1-KDR) and VEGFR3 [12]. Among them, VEGFR2 is the principal mediator of VEGF-induced angiogenesis signaling in EC [12,20]. We next examined the effect of 4F9 treatment on VEGFR2 phosphorylation in HUVECs. As shown in Fig. 3A, 4F9 treatment in HUVECs significantly decreased phosphorylation of VEGFR2 by exogenous VEGF treatment, compared to that of control IgG. These data suggest that 4F9 inhibitory effect on EC activity is mediated at least partly via decreased VEGFR2 phosphorylation.

Previous work has shown that CD82 and VEGFR2 are components of lipid rafts and that CD82 is internalized through lipid rafts [16,21]. We therefore hypothesized that 4F9 treatment affects VEGFR2 phosphorylation by regulating CD82 in lipid rafts. To determine whether distribution of CD82 molecules in lipid rafts is altered by 4F9 treatment, we next analyzed the distribution pattern of CD82 in light density fractions by discontinuous sucrose gradient centrifugation. As shown in Fig. 3B, a slight proportion of CD82 is

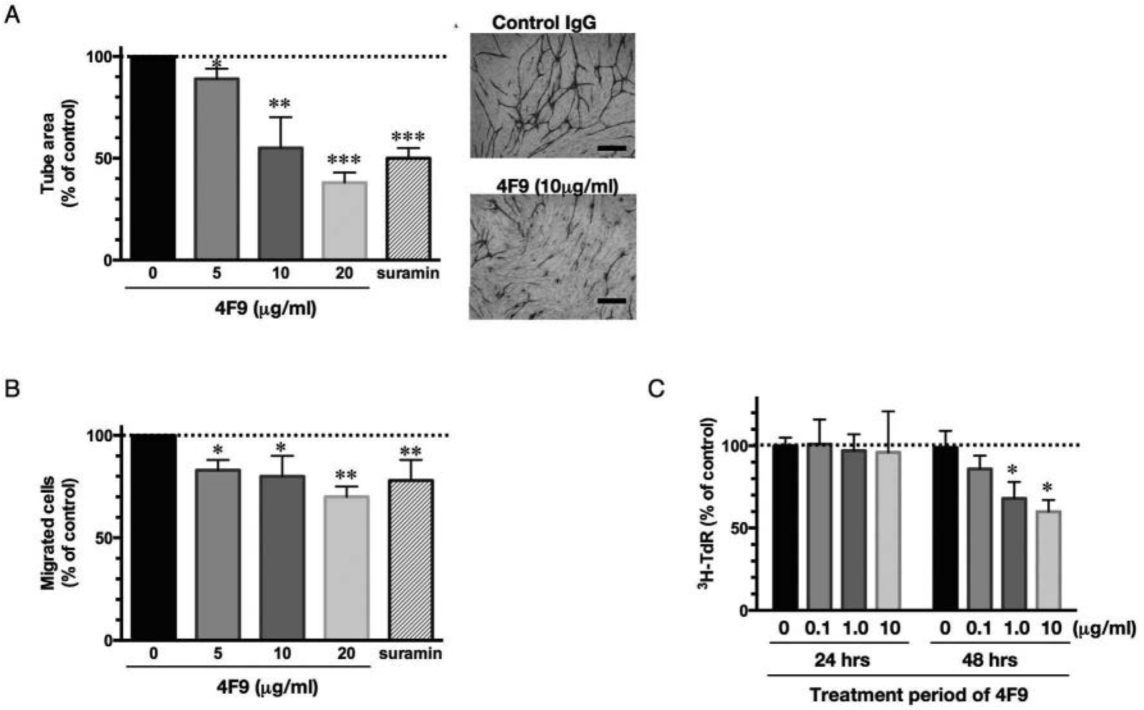

Fig. 2. Anti-CD82 mAb 4F9 inhibited HUVEC angiogenesis, migration and proliferation. **(A)** HUVECs were incubated with control mouse IgG (20 μg/ml, as indicated at 0 μg/ml of 4F9), 4F9 (5, 10, and 20 μg/ml) or suramin (50 μM), stained and measured for angiogenesis by the same method as in Fig. 1A. *Left panel* shows the results expressed as the percentage of the mean values obtained in the percentage of tube area in control IgG treated HUVECs. The mean values of percentage of tube area ± S.E. (n = 5 experiments with triplicates), and the horizontal dotted line indicates a 100% level of control IgG treatment. A significant decrease in angiogenesis was indicated in a dose-dependent manner for 4F9 as well as for suramin (*$P < 0.05$, **$P < 0.01$ or ***$P < 0.0001$ *vs*. control IgG). Representative microphotographs of tube formation of control IgG or 4F9-treated HUVECs were shown in the *right two panels* (brown cells are anti-CD31 immunohistochemistry). Scale bars indicate 25 μm. **(B)** Following treatment with control mouse IgG (20 μg/ml, as indicated at 0 μg/ml of 4F9), 4F9 (5, 10, and 20 μg/ml) or suramin (50 μM), HUVECs were seeded on the upper chamber of fibronectin-coated inserts with the lower chamber containing VEGF (10 ng/ml). The migrated cells were measured by the same method as in Fig. 1B. The results are expressed as the percentage of the mean values obtained in the fluorescence levels of control IgG treated HUVECs (±S.E. of five independently performed experiments with triplicates). The horizontal dotted line indicates a 100% level of control IgG treatment. A significant decrease in cell migration was indicated in a dose-dependent manner for 4F9 as well as for suramin (*$P < 0.05$ or **$P < 0.001$ *vs*. control IgG). **(C)** Following treatment with control mouse IgG (10 μg/ml, as indicated at 0 μg/ml of 4F9), 4F9 (0.1, 1.0, and 10 μg/ml), HUVECs were incubated with 10 ng/ml of VEGF. Proliferation of HUVECs was monitored by measuring [^{3}H]-TdR incorporation at 24 or 48 h of culture. The mean values of [^{3}H]-TdR incorporation ± S.E. are shown (n = 5 experiments with triplicates), and the horizontal dotted line indicates a 100% level of control IgG treatment. A significant decrease in proliferation after 48 h of culture was observed in a dose-dependent manner for 4F9. (*$P < 0.001$ as calculated by Student's *t* test). (For interpretation of the references to colour in this figure legend, the reader is referred to the web version of this article.)

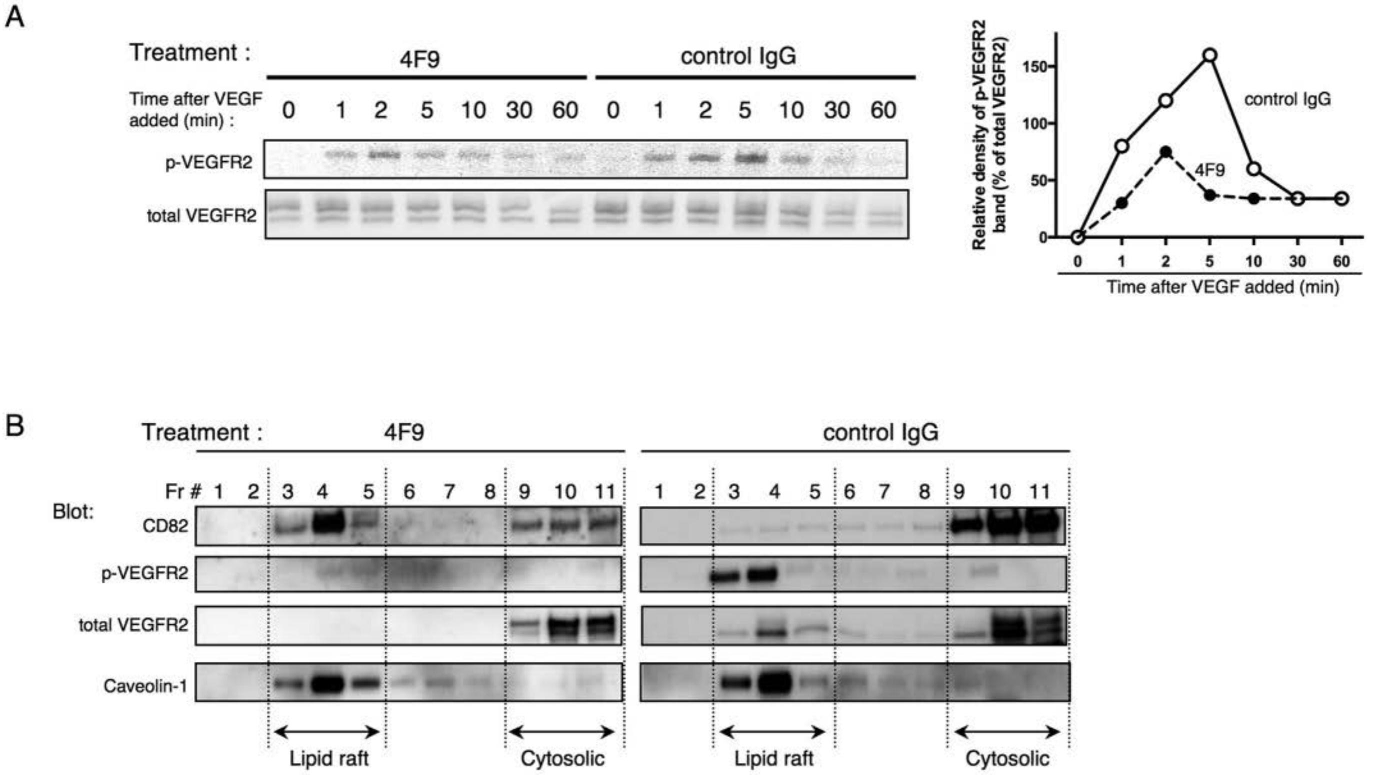

Fig. 3. Anti-CD82 mAb 4F9 inhibited phosphorylation of VEGFR2 via control of CD82 distribution in lipid rafts. **(A)** Following treatment with 4F9 or control mouse IgG (each 10 μg/ml) for 12 h, HUVECs were incubated with 10 ng/ml of VEGF for the indicated time periods. Cells were harvested, and cell lysates were subjected to Western blot analysis for phosphorylated (upper of left panel) or total VEGFR2 (lower of left panel). Phosphorylated VEGFR2 (p-VEGFR2) proteins in each time point were quantified by measuring p-VEGFR2 band density and are presented as the percentage of each corresponding band density of total VEGFR2 (right panel). In control IgG treated HUVECs, levels of phosphorylation of VEGFR2 increased from 1 to 10 min after VEGF addition (solid line). On the other hand, 4F9 treatment significantly decreased phosphorylation levels of VEGFR2 (dashed line). Similar results were obtained in three independent experiments. **(B)** HUVECs were treated with 4F9 or control mouse IgG (each 10 μg/ml) for 12 h, followed by incubation with 10 ng/ml of VEGF for 5 min. Light density lipid raft or heavy density cytosolic fractions were prepared by sucrose gradient ultracentrifugation. The distribution of CD82, p-VEGFR2, total VEGFR2 and caveolin-1 was determined by immunoblotting with specific antibodies. Caveolin-1 was a representative of lipid raft proteins and was used as a quantity control indicating equal amounts in the experiments (bottom panels). Fraction number (Fr#) 3–5 or 9–11 contains lipid raft or cytosolic fractions, respectively. After 4F9 treatment, CD82 molecule was recruited in the lipid raft fractions (upper panels), and VEGFR2 (both phosphorylated and total VEGFR2) were segregated from lipid raft to cytosolic fractions (middle two panels). Similar results were obtained in three independent experiments.

present in lipid raft fractions, while being mainly presented in the cytosolic fraction, in HUVECs treated with control IgG (upper right panel). On the other hand, 4F9 treatment markedly increased CD82 distribution in lipid raft fractions (left upper panel of Fig. 3B). These data suggest that engagement of CD82 by 4F9 alters its distribution level in lipid rafts. We next analyzed phosphorylation of VEGFR2 and its distribution in lipid rafts following 4F9 treatment. Upon treatment with control IgG, VEGF-induced phosphorylation of VEGFR2 was observed in lipid raft fractions, while phosphorylation level of VEGFR2 decreased following 4F9 treatment (second upper panels in Fig. 3B). Moreover, 4F9 treatment abrogated recruitment of VEGFR2 in lipid rafts (second lower panels of Fig. 3B), while distribution of the other lipid raft molecule caveolin-1 was not affected by 4F9 treatment (bottom panels of Fig. 3B). These data indicate that ligation of CD82 by 4F9 abrogates recruitment of VEGFR2 in lipid rafts and decreases VEGF-mediated phosphorylation of VEGFR2. Taken together with the data above, our findings strongly suggest that that 4F9 treatment inhibits VEGF-dependent angiogenesis through control of distribution of CD82 and VEGFR2 in lipid rafts.

4. Discussion

In this study, we showed that knockdown of CD82 expression decreased migration, proliferation and angiogenesis in HUVECs. Moreover, treatment with the anti-CD82 mAb 4F9 inhibited VEGF-dependent EC migration, proliferation and angiogenesis. Finally, we demonstrated that inhibition of HUVECs activity by 4F9 was achieved via CD82-dependent regulation of VEGFR2 recruitment in lipid rafts.

In contrast to the well-known characteristics of CD82 in tumor cell biology [1], its role in regulating vascular function is heretofore unclear. Recent study using *Cd82*-null mice showed that perturbation of CD82-ganglioside-CD44 signaling attenuates pathological angiogenesis by inhibiting EC movement [16], while *Cd82*-null mice display normal vessel development without obvious vascular defects [17]. In human vascular biology, VEGF is one of key proteins involved in the cancer angiogenesis pathway [9,13]. Sustained VEGF expression from cancer cells leads to the development and maintenance of a vascular network that promotes tumor growth and metastasis [13]. Binding of VEGF to VEGFR2 on ECs induces a downstream signaling process critical to EC motility, proliferation and survival [18]. Although VEGF-dependent EC activity plays an essential role in angiogenesis [18], a functional role for CD82 in association with VEGF/VEGFRs in EC activity has not yet been clearly established. Our data are novel and significant in that they demonstrate the association between CD82 and the regulation of VEGF-dependent EC functions, with knockdown of CD82 in HUVECs resulting in decrease of VEGF-dependent EC migration, proliferation and angiogenesis.

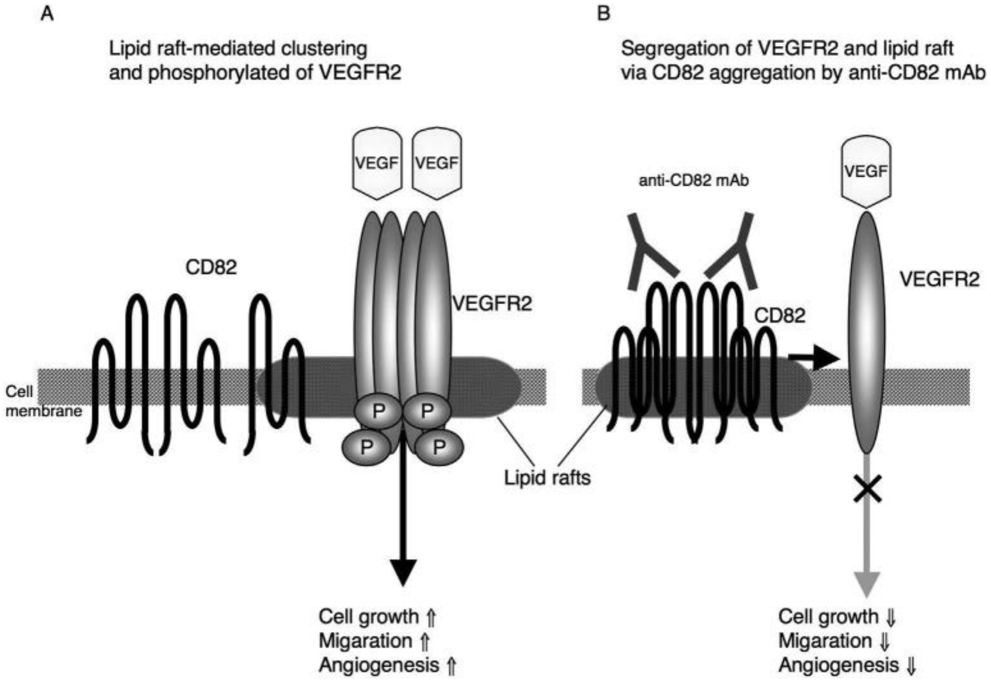

Fig. 4. Model for the regulation of VEGFR2 phosphorylation in lipid rafts via ligation of CD82 molecules by 4F9.

Targeting cancer angiogenesis has been a recent focus as anticancer therapy [9]. Studies on the role of VEGF in tumor progression have mostly been directed to the cancer angiogenesis effect exerted by VEGF and VEGFR on tumor environmental vascular network [9,22]. In the present study, we clearly demonstrated that the anti-CD82 mAb 4F9 inhibits EC migration, proliferation and angiogenesis. Since endothelial CD82 regulates VEGF-dependent tumor angiogenesis, 4F9 can be a novel drug candidate for anticancer therapy.

Binding of VEGF to VEGFR2 induces VEGFR2 dimerization and subsequent autophosphorylation of the intracellular tyrosine kinase domains, resulting in EC proliferation, movement and angiogenesis [12,20,23]. Our biochemical analysis demonstrates that 4F9 treatment affects the distribution of CD82 and VEGFR2 in lipid rafts, associated with decreased VEGFR2 phosphorylation and inhibition of EC migration, proliferation and angiogenesis. On the basis of our current results, we propose a model to describe the molecular mechanisms involved in 4F9 regulation of CD82 role in VEGF-dependent EC activity (Fig. 4); in physiological condition, CD82 molecules are mostly present outside of lipid rafts, which mediate clustering and phosphorylation of VEGFR2 upon VEGF binding (Fig. 4A). After ligation of CD82 molecules by 4F9, CD82 aggregates in lipid rafts with segregation of VEGFR2 out of lipid rafts, leading to attenuation of VEGF-dependent signaling (Fig. 4B). CD82 therefore plays an important role in VEGF-dependent EC activity as a membrane domain organizer.

Along with VEGF, IL-6 also plays a role of EC activity in melanoma angiogenesis [8]. It has been reported that the gp130 molecule involved in the IL-6 receptor (IL-6R) complex partially exists in lipid rafts and serves to activate signaling complex through lipid raft aggregation [24]. It is possible that CD82 regulates IL-6/IL-6R pathway-related EC activity via organization of membrane microdomains, a topic which will be examined in future studies.

In summary, the anti-CD82 mAb 4F9 effectively inhibits phosphorylation of VEGFR2 through the organization of lipid raft microdomains in human EC. Our present study hence suggests that CD82 on EC is potentially a suitable target for anti-angiogenic therapy in tumor angiogenesis.

The authors declare no competing financial interests

S.N. and S.I. contributed to the conception and design of the study, or acquisition of data, R.H., E.K. and N.I. contributed to analysis and interpretation of data, K.O. and C.M. designed the research, interpreted the data and wrote the paper, N.H.D. interpreted the data, assisted with the paper, and proofread the manuscript. All authors showed final approval of the version to be submitted.

Acknowledgements

This study was supported in part by a grant of the Ministry of Education, Science, Sports and Culture, Japan (K.O. and C.M.) (15H04879 and 15K15324), a grant of the Ministry of Health, Labour and Welfare, Japan (C.M.) and a Grant-in-Aid (S1311011) from the Foundation of Strategic Research Projects in Private Universities from the Ministry of Education, Culture, Sports, Science, and Technology, Japan (C.M.).

Appendix A. Supplementary data

Supplementary data related to this article can be found at http://dx.doi.org/10.1016/j.bbrc.2016.04.081.

Transparency document

Transparency document related to this article can be found online at http://dx.doi.org/10.1016/j.bbrc.2016.04.081.

References

[1] M. Zoller, Tetraspanins: push and pull in suppressing and promoting metastasis, Nat. Rev. Cancer 9 (2009) 40–55.
[2] Y. Nojima, T. Hirose, K. Tachibana, et al., The 4F9 antigen is a member of the

tetra spans transmembrane protein family and functions as an accessory molecule in T cell activation and adhesion, Cell Immunol. 152 (1993) 249–260.

[3] S. Iwata, H. Kobayashi, R. Miyake-Nishijima, et al., Distinctive signaling pathways through CD82 and β1 integrins in human T cells, Eur. J. Immunol. 32 (2002) 1328–1337.

[4] J.T. Dong, P.W. Lamb, C.W. Rinker-Schaeffer, et al., KAI1, a metastasis suppressor gene for prostate cancer on human chromosome 11p11.2, Science 268 (1995) 884–886.

[5] F.A. Malik, A.J. Sanders, W.G. Jiang, KAI-1/CD82, the molecule and clinical implication in cancer and cancer metastasis, Histol. Histopathol. 24 (2009) 519–530.

[6] E. Odintsova, T. Sugiura, F. Berditchevski, Attenuation of EGF receptor signaling by a metastasis suppressor, the tetraspanin CD82/KAI-1, Curr. Biol. 10 (2000) 1009–1012.

[7] S.C. Sridhar, C.K. Miranti, Tetraspanin KAI1/CD82 suppresses invasion by inhibiting integrin-dependent crosstalk with c-Met receptor and Src kinases, Oncogene 25 (2006) 2367–2378.

[8] Y. Tang, M. Bhandaru, Y. Cheng, et al., The role of the metastasis suppressor gene KAI1 in melanoma angiogenesis, Pigment. Cell Melanoma Res. 28 (2015) 696–706.

[9] H.L. Goel, A.M. Mercurio, VEGF targets the tumour cell, Nat. Rev. Cancer 13 (2013) 871–882.

[10] W. Risau, Mechanisms of angiogenesis, Nature 386 (1997) 671–674.

[11] L. Coultas, K. Chawengsaksophak, J. Rossant, Endothelial cells and VEGF in vascular development, Nature 438 (2005) 937–945.

[12] N. Ferrara, H.-P. Gerber, J. LeCouter, The biology of VEGF and its receptors, Nat. Med. 9 (2003) 669–676.

[13] P. Carmeliet, R.K. Jain, Angiogenesis in cancer and other diseases, Nature 407 (2000) 249–257.

[14] K. Nagao, K. Oka, HIF-2 directly activates CD82 gene expression in endothelial cells, Biochem. Biophys. Res. Commun. 407 (2011) 260–265.

[15] H. Hurwitz, L. Fehrenbacher, W. Novotny, et al., Bevacizumab plus irinotecan, fluorouracil, and leucovorin for metastatic colorectal cancer, N. Engl. J. Med. 350 (2004) 2335–2342.

[16] Q. Wei, F. Zhang, M.M. Richardson, et al., CD82 restrains pathological angiogenesis by altering lipid raft clustering and CD44 trafficking in endothelial cells, Circulation 130 (2014) 1493–1504.

[17] J.I. Risinger, M. Custer, L. Feigenbaum, et al., Normal viability of Kai1/Cd82 deficient mice, Mol. Carcinog. 53 (2013) 610–624.

[18] N. Ferrara, T. Davis-Smyth, The biology of vascular endothelial growth factor, Endocr. Rev. 18 (1997) 4–25.

[19] T. Ishii, K. Ohnuma, A. Murakami, et al., CD26-mediated signaling for T cell activation occurs in lipid rafts through its association with CD45RO, Proc. Natl. Acad. Sci. U. S. A. 98 (2001) 12138–12143.

[20] C. Fontanella, E. Ongaro, S. Bolzonello, et al., Clinical advances in the development of novel VEGFR2 inhibitors, Ann. Transl. Med. 2 (2014) 123.

[21] L. Labrecque, I. Royal, D.S. Surprenant, et al., Regulation of vascular endothelial growth factor receptor-2 activity by caveolin-1 and plasma membrane cholesterol, Mol. Biol. Cell 14 (2003) 334–347.

[22] J. Folkman, Tumor angiogenesis: therapeutic implications, N. Engl. J. Med. 285 (1971) 1182–1186.

[23] A. Kiba, H. Sagara, T. Hara, et al., VEGFR-2-specific ligand VEGF-E induces non-edematous hyper-vascularization in mice, Biochem. Biophys. Res. Commun. 301 (2003) 371–377.

[24] P.B. Sehgal, G.G. Guo, M. Shah, et al., Cytokine signaling: STATS in plasma membrane rafts, J. Biol. Chem. 277 (2002) 12067–12074.

Hayashi *et al. Cancer Cell Int (2016) 16:35*
DOI 10.1186/s12935-016-0310-9

Cancer Cell International

PRIMARY RESEARCH

Open Access

A humanized anti-CD26 monoclonal antibody inhibits cell growth of malignant mesothelioma via retarded G2/M cell cycle transition

Mutsumi Hayashi[1,2], Hiroko Madokoro[1], Koji Yamada[3], Hiroko Nishida[1], Chikao Morimoto[4], Michiie Sakamoto[1] and Taketo Yamada[1,5*]

Abstract

Background: Malignant Mesothelioma (MM) is a highly aggressive tumor with poor prognosis. Multimodal treatments and novel molecular targeted therapies against MM are in high demand in order treat this disease effectively. We have developed a humanized monoclonal antibody YS110 against CD26 expressed in 85 % of MM cases. CD26 is thought to be involved in tumor growth and invasion by interacting with collagen and fibronectin, or affecting signal transduction processes.

Methods: We evaluated the direct anti-tumor effect of YS110 against MM cell lines, NCI-H2452 and JMN, and investigated its effects on cell cycle and on the cell cycle regulator molecules. In addition, we investigated synergistic effects of YS110 and anti-tumor agent pemetrexed (PMX) against MM cell line both in vitro and in vivo.

Results: YS110 suppressed the proliferation of NCI-H2452 cells by approximately 20 % in 48 h. Based on cell cycle analysis, percentage of cells in G2/M phase increased 8.0 % on the average after YS110 treatment; in addition, cell cycle regulator p21 cip/waf1 was increased and cyclin B1 was decreased after YS110 treatment. Inhibitory phosphorylation of both cdc2 (Tyr15) and cdc25C (Ser216) were elevated. Furthermore, activating phosphorylation of p38 MAPK (Thr180/Tyr182) and ERK1/2 (Thr202/Tyr204) were augmented at 24 h after YS110 treatment. PMX rapidly induced CD26 expression on cell surface and the treatment with both YS110 and PMX inhibited in vivo tumor growth accompanied by a synergistic reduction in the MIB-1 index.

Conclusion: This is a first report of a novel anti-proliferative mechanism of the humanized anti-CD26 monoclonal antibody YS110, which resulted in G2/M cell cycle delay through regulation of quantity and activity of various cell cycle regulating molecules.

Keywords: Mesothelioma, CD26, Monoclonal antibody, G2/M transition, Pemetrexed

Background

Malignant mesothelioma (MM) is an aggressive cancer of the pleura, peritoneal cavity, pericardium, and scrotum and has a poor prognosis. MM is associated with occupational exposure to asbestos and, despite legislation introduced by many industrialized countries, the incidence is not expected to peak until 2020 due to the long latency between initial exposure and disease expression [1]. As single modality approach to treatment has failed to extend survival, multimodal treatment and novel molecular targeted therapies are highly sought after. Although extrapleural pneumonectomy (EPP) is a preferred treatment option, median survival among patients receiving EPP alone is less than 10 months [2]. EPP followed by high-dose radiation therapy (RT) has

---

*Correspondence: taketo@saitama-med.ac.jp
[5] Department of Pathology, Saitama Medical University, 38 Morohongo, Saitama, Moroyama-machi 350-0495, Japan
Full list of author information is available at the end of the article

© 2016 Hayashi et al. This article is distributed under the terms of the Creative Commons Attribution 4.0 International License (http://creativecommons.org/licenses/by/4.0/), which permits unrestricted use, distribution, and reproduction in any medium, provided you give appropriate credit to the original author(s) and the source, provide a link to the Creative Commons license, and indicate if changes were made. The Creative Commons Public Domain Dedication waiver (http://creativecommons.org/publicdomain/zero/1.0/) applies to the data made available in this article, unless otherwise stated.

been shown to prolong median survival to 33.8 months in patients with Stage 1 and Stage 2 MM but survival remained 10 months in patients with Stage 3 and Stage 4 MM [2]. A Phase 3 trial showed that combination of pemetrexed and cisplatin improved survival over cisplatin alone for inoperable patients [3]. According to recent multicenter trials of trimodality treatment that consisted of neoadjuvant chemotherapy (cisplatin and pemetrexed), EPP, and adjuvant RT led in the USA [2] and Europe [4], median survival of patients who completed the therapy was 29.1 months compared to 18.4 months in controls. Since the trimodality approach seems to be limited and because not all patient can tolerate aggressive therapies, novel molecular targeted therapies are highly desirable. To date, a number of molecular targeted agents have been evaluated in MM. While tyrosine kinase inhibitors against epidermal growth factor receptor (EGFR) and platelet-derived growth factor receptor (PDGFR) did not show clinically significant effects, histone deacetylase inhibitor (HDACI) and anti-angiogenic agents showed some clinical benefits and are undergoing Phase 3 trials [5]; however, none of these agents have been incorporated into clinical practice and efforts must continue in the area of both clinical research and search for novel target molecules.

CD26 is an 110 kD glycoprotein anchored in the cellular membrane with dipeptidyl peptidase IV activity. CD26 is also known as a co-stimulatory molecule of the T lymphocyte. CD26 binds to caveolin-1 on antigen-presenting cells and the interaction triggers signal transduction process leading to T cell proliferation and cytokine production [6]. Several recent studies have shown that CD26 is highly expressed in several malignancies, including MM, lung adenocarcinoma, hepatocellular carcinoma, prostate cancer, and thyroid cancer [7]. CD26 expression evaluated by immunohistochemistry was positive in 85 % of tested MM cases [8, 9]. Moreover, CD26 is thought to be involved in tumor growth and invasion through its interaction with collagen and fibronectin or by regulating activity of chemotactic peptides through its DPPIV activity. Furthermore, CD26 has been reported to be involved in signal transduction processes, including the p38 MAPK pathway. Though the mechanisms of action of CD26 have not been clarified, its enzymatic activity does not appear essential for its role in signal transduction process [10]. Considering its high rate of overexpression in MM and suspected function in tumor progression, we have developed a humanized an anti-CD26 antibody, designated YS110, as a targeted therapy against CD26-positive malignancies, including MM. We have previously reported the anti-tumor effects of YS110 against MM cells [11]. In addition to the anti-tumor effect via antibody-dependent-cell-mediated-cytotoxicity, YS110 showed direct anti-tumor effect via $p27^{kip1}$ accumulation [11]; however, the molecular mechanism of direct anti-tumor effect of YS110 against MM cell lines remains unknown.

The molecular mechanisms underlying the direct anti-tumor effect of several monoclonal antibodies have been investigated; for example, the anti-HER-2 antibody (Trastuzumab) and anti-EGFR antibody (Cetuximab) result in G1/S cell cycle arrest by upregulating the CDK inhibitor $p27^{kip1}$ via multiple signaling pathways [12, 13]. The anti-CD20 antibody (rituximab) can induce cell death of malignant B cell lymphoma cells in vitro via inhibition of the p38 MAPK, ERK1/2, and AKT anti-apoptotic survival pathways [14]. Most therapeutic antibodies against cancers that affect the cell cycle, including antibodies mentioned above, result in G1/S arrest. So far, only one anti-cancer antibody, the anti-human type 1 insulin-like growth factor receptor (IGF-IR) antibody A12 against androgen-independent prostate cancer cell line LuCaP 35 V, has been reported to cause G2/M cell cycle delay although its molecular mechanism is not yet understood [15].

In this study, we focused on evaluating the direct in vitro effect of the humanized anti-CD26 monoclonal antibody YS110 against the MM cell line NCI-H2452 and investigated its effect on the cell cycle and on cell cycle-regulating molecules. YS110 inhibited growth of YS110 with G2/M cell cycle arrest and altered the expression or phosphorylation state of cell cycle molecules. Furthermore, pemetrexed (PMX), a standard reagent against mesothelioma, rapidly induced CD26 expression on the cell surface and treatment with both YS110 and PMX inhibited in vivo tumor growth in a synergistic manner. This is the first report describing a novel anti-proliferative mechanism of the humanized anit-CD26 monoclonal antibody YS110, which resulted in G2/M cell cycle delay, through regulation of quantity and activity of various cell cycle-regulating molecules.

Results

YS110 inhibits mesothelioma cell proliferation

YS110 inhibits proliferation of the mesothelioma cell line NCI-H2452 in a concentration-dependent manner (Fig. 1). Maximum of growth inhibition was 18.3 % at 250 μg/mL of YS110. Based on this result, we used YS110 at 2 μg/mL, which showed 11.2 % of growth inhibition, in the following experiments.

YS110 induced G2/M cell cycle delay in mesothelioma cells

To investigate the mechanism responsible for the growth inhibition caused by YS110, cell-cycle distribution was determined by flow cytometry analysis. At 24 h after YS110 treatment, the percentage of cells in

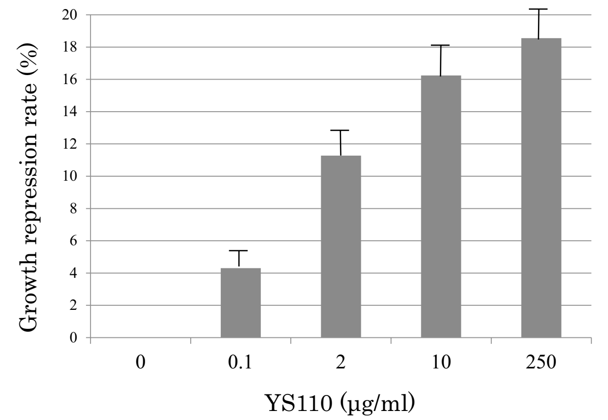

Fig. 1 YS110 inhibits NCI-H2452 cell proliferation. WST-1 assay revealed inhibition of NCI-H2452 cell proliferation with YS110 treatment in a concentration-dependent manner up to 18.6 %. The experiment was performed using 96 multi-well plates

the G2/M phase increased compared to the control. The representative experiment is shown (Fig. 2a). On the average of ten experiments, the percentage of G2/M phase cells were significantly increased after YS110 treatment ($p < 0.05$) (Fig. 2b). This cell cycle delay may be compatible with repression of cell proliferation. Furthermore, in another CD26 positive MM cell line NCI-H28, the percentage of cells in G2/M phase increased by 5 % on the average after YS110 treatment though its significance could not be proved statistically (data not shown).

YS110 alters cell cycle regulators

We investigated the alterations caused by YS110 treatment in the quantity and activation state of cell cycle regulators responsible for G2/M transition. At 24 h after YS110 treatment, the cell cycle regulator p21 increased while the positive regulatory subunit cyclin B1 decreased. Inhibitory phosphorylation of cdc2 on Tyr15 and inhibitory phosphorylation of cdc25C on Ser216, an upstream inhibitory regulator of cdc2, was elevated (Fig. 3a). Cdc25C phosphorylated on Ser216 is known to be sequestrated into cytoplasm and refrained from contact with cdc2 [16]. After YS110 treatment for 24 h, cytoplasmic whole cdc25C was elevated while nuclear whole cdc25C was decreased, as confirmed by densitometry analysis (Fig. 3b). At 6 h and 12 h after YS110 treatment, the amount of phosphorylated cdc2 and phosphorylated cdc25C were varied among experiments despite consistent increase at 24 h. No significant change in cdc25A and cdc25B was observed (data not shown).

YS110 elevates activating phosphorylation of p38 MAPK and ERK1/2

In order to determine the upstream regulator of cdc25C phosphorylation caused by YS110 treatment, expression and activation status of several molecules known to regulate cell cycle through cdc25C phosphorylation were examined. Activating phosphorylation of p38 MAPK (Thr180/Tyr182) and ERK1/2 (Thr202/Tyr204) were elevated 24 h after YS110 treatment (Fig. 4a). No significant change in chk1, chk2, or c-TAK1 was observed (data not shown). While the p38 inhibitor SB203580 failed to block G2/M arrest caused by YS110 (data not shown), the MEK1/2 inhibitor U0126 blocked G2/M arrest caused by YS110 according to cell cycle analysis using flowcytometry (Fig. 4b).

Pemetrexed (PMX) increased CD26 expression in mesothelioma cells in vitro

CD26 expression on the cell surface of JMN cells increased 15 % from 6 to 6.5 % 24 h after treatment with 10 µM of PMX based on flowcytometry analysis (Fig. 5a). In order to confirm the augmented expression of CD26 in JMN cells, Western blot analysis was performed. CD26 protein expression was rapidly induced in whole cell lysates by treatment with 10 µM of PMX at 1 h after PMX treatment; most augmentation of CD26 expression at 6 h and then this augmented expression continued to 24 h after PMX treatment (Fig. 5b). In order to examine the altered expression of CD26 in NCI-H2452 cells, Western blot analysis was performed. CD26 protein expression in NCI-H2452 cells was also rapidly induced in whole cell lysates by treatment with 10 µM of PMX at 1 h after PMX treatment; most augmentation of CD26 expression at 6 h and then this augmented expression continued to 24 h after PMX treatment (Fig. 5b).

Effective inhibition of in vivo *mesothelioma cell growth by combined treatment with both YS110 and PMX*

Combination effects of YS110 and PMX were examined using xenograft models with JMN cells transplanted into NOG mice subcutaneously. Mice were then monitored for the development and progression of tumors and the tumor size was determined by caliper measurement. Tumor size in mice treated with both YS110 and PMX was smaller than mice treated with only YS110 or PMX (data not shown). The weight of tumors with YS110 treatment was insignificantly reduced (Fig. 6A). PMX treatment induced a significant reduction in tumor weight ($p < 0.05$); the combination of YS110 and PMX treatment synergistically reduced tumor weight compared with YS110 single treatment and PMX single treatment ($p < 0.05$).

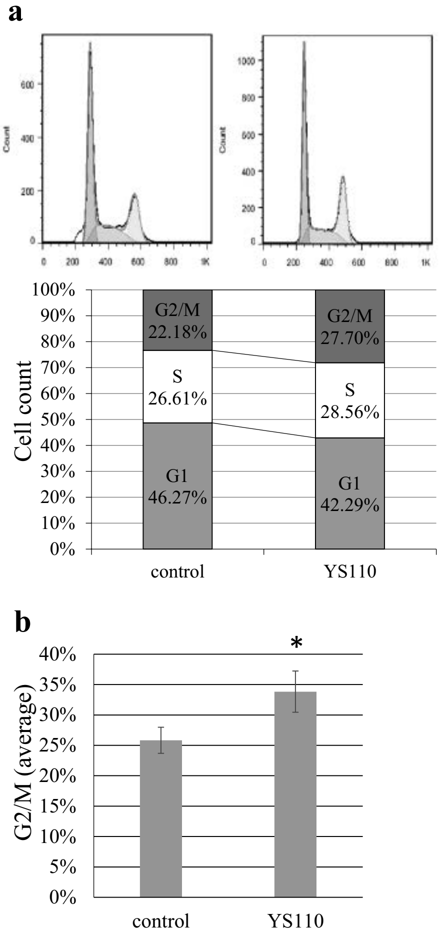

Fig. 2 YS110 induces G2/M cell cycle delay in NCI-H2452 cells. **a** Flowcytometry analysis using propidium iodide staining revealed that the percentage of G2/M phase cells increased while the percentage of G1 phase cells was reduced in NCI-H2452 cells treated 24 h with 2 μg/mL of YS110. A representative experiment is shown. **b** The average percentage of G2/M phase cells in NCI-H2452 cells treated 24 h with 2 μg/mL of YS110 was significantly increased (*$p < 0.05$)

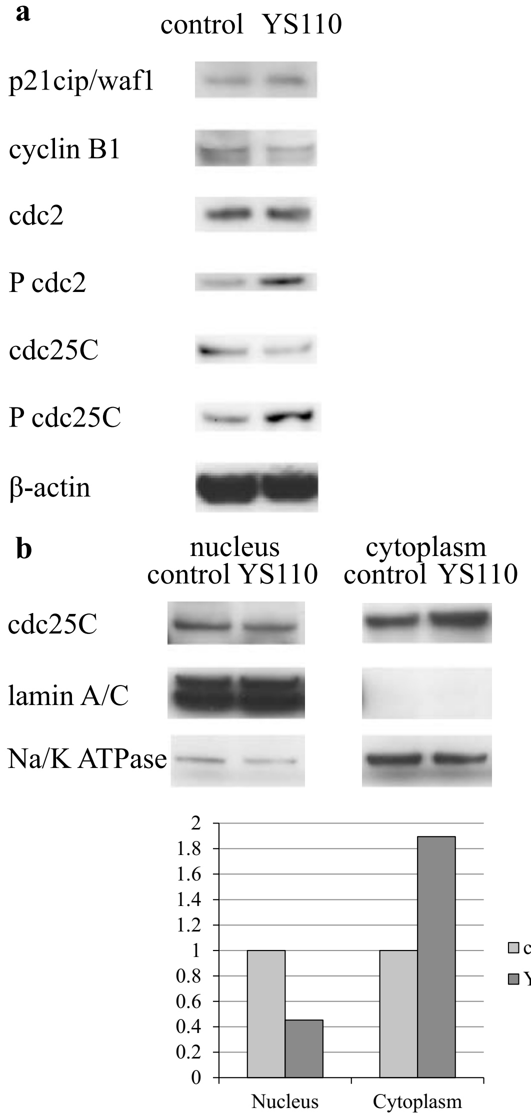

Fig. 3 YS110 alters expressions and phosphorylation of cell cycle regulators. **a** At 24 h after treatment with 2 μg/mL of YS110, p21 protein expression increased while cyclinB1 protein expression decreased. Inhibitory phosphorylation of cdc2 Tyr15 and cdc25C Ser216 were elevated while there was no significant change in whole cdc2 and cdc25C protein. β-actin was used as an internal control. **b** Alteration in subcellular distribution of whole cdc25C by YS110 treatment is shown. At 24 h after treatment with 2 μg/mL of YS110, nuclear cdc25C protein decreased while cytoplasmic cdc25C protein increased. LaminA/C was used as a nuclear marker and Na–K ATPase was used as a cytoplasmic marker. The *bar graph* demonstrates the densitometric analysis of a Western blot of whole cdc25C. Results are normalized by the densitometry of control cells. All experiments were performed in triplicate and a representative experiment is shown

Combination effects of tumor growth in vivo were examined by measuring the MIB-1 index histologically. The MIB-1 index was significantly decreased in tumors after YS110 or PMX single treatment compared with controls ($p < 0.05$; Fig. 6B, C). Combinatory treatment with YS110 and PMX significantly reduced the MIB-1 index compared to single treatment ($p < 0.05$; Fig. 6B, C).

Histology of the tumor derived from JMN cells in the xenograft model is shown in Fig. 6C. Sarcomatous mesothelioma is shown in HE staining (Fig. 6C-a) and stained with anti-CD26 polyclonal antibody (R&D) (Fig. 6C-b). The MIB-1 index was measured by immunohistochemistry using the anti-Ki-67 (MIB-1) monoclonal antibody. Staining of Ki-67 antigens in nucleus was shown in tumors treated with control IgG (Fig. 6C-c), YS110 (Fig. 6C-d), and both YS110 and PMX (Fig. 6C-e). The number of Ki-67 positive nuclei was decreased after combined treatment of YS110 and PMX and the necrotic area is indicated by an asterisk (Fig. 6C-e).

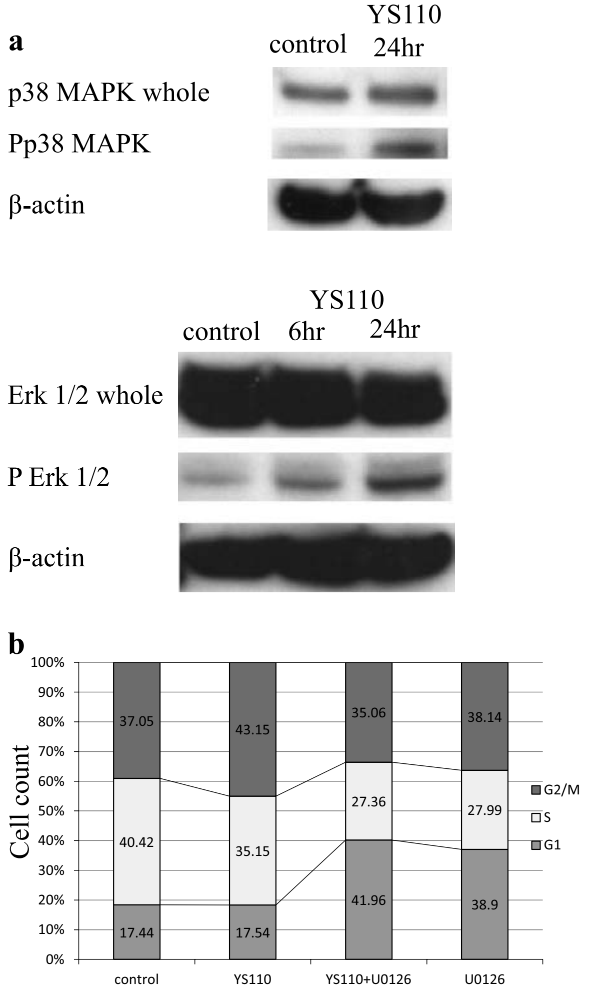

Fig. 4 YS110 augments phosphorylation of p38MAPK and ERK1/2. **a** Activating phosohorylation of p38 (Thr180/Tyr182) and ERK1/2 (Thr202/Tyr204) were elevated by 24 h after treatment with YS110 while no substantial changes of whole p38 and ERK1/2 protein were observed. β-actin was used as an internal control. **b** G2/M arrest caused by YS110 treatment was reversed by ERK1/2 activation inhibitor U0126 (10 μM). A proportion (43.15 %) of G2/M was elevated in cells with YS110 treatment compared with in cells without YS110 (control, 37.05 %) and the proportion of G2/M decreased in cells with both YS110 and U0126 treatment (35.06 %). All experiments were performed in triplicate and a representative experiment is shown

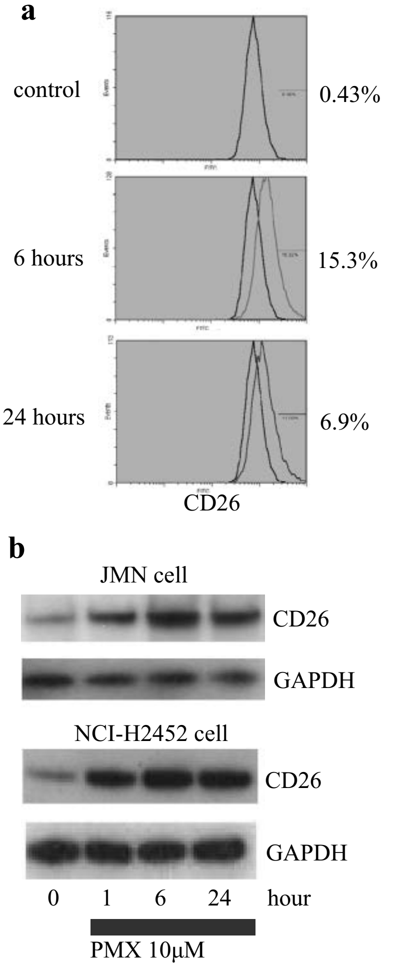

Fig. 5 Pemetrexed (PMX) increased CD26 expression in vitro. **a** Based on flowcytometry analysis, cell surface CD26 expression on JMN cells increased 6-24 h after treatment with 10 μM of PMX. **b** Based on Western blot analysis, the expression of CD26 protein was rapidly induced in whole cell lysates by treatment with 10 μM of PMX at 1–24 h. GAPDH was used as an internal control. All experiments were performed in triplicate and a representative experiment is shown

Discussion

Novel molecular targeted therapies are in high demand since the aggressive trimodality approach against MM has been proved to be limited. We developed a humanized monoclonal antibody against CD26, designated as YS110, a molecular targeted therapy against MM [11]. We expected YS110 to cause ADCC to eliminate CD26 positive MM cells. In addition to the ADCC effect, YS110 demonstrated direct anti-proliferative effects in vitro against CD26-positive MM cell lines. We proposed that investigation into the molecular mechanisms of the direct anti-proliferative effect against MM cells would be beneficial for both understanding anti-tumor effect of YS110, as well as uncover the underlying mechanism its proliferation and progression. Although the direct anti-proliferative effect of YS110 is limited to a repression rate of approximately 20 % in vitro, the molecular mechanism was associated with the proliferative signal transduction system and cell cycle. Cell cycle analysis revealed that YS110 caused significant delay of the G2/M transition. To our knowledge, only one anti-cancer MoAb, anti-IGF-IR antibody A12 against the androgen-independent prostate

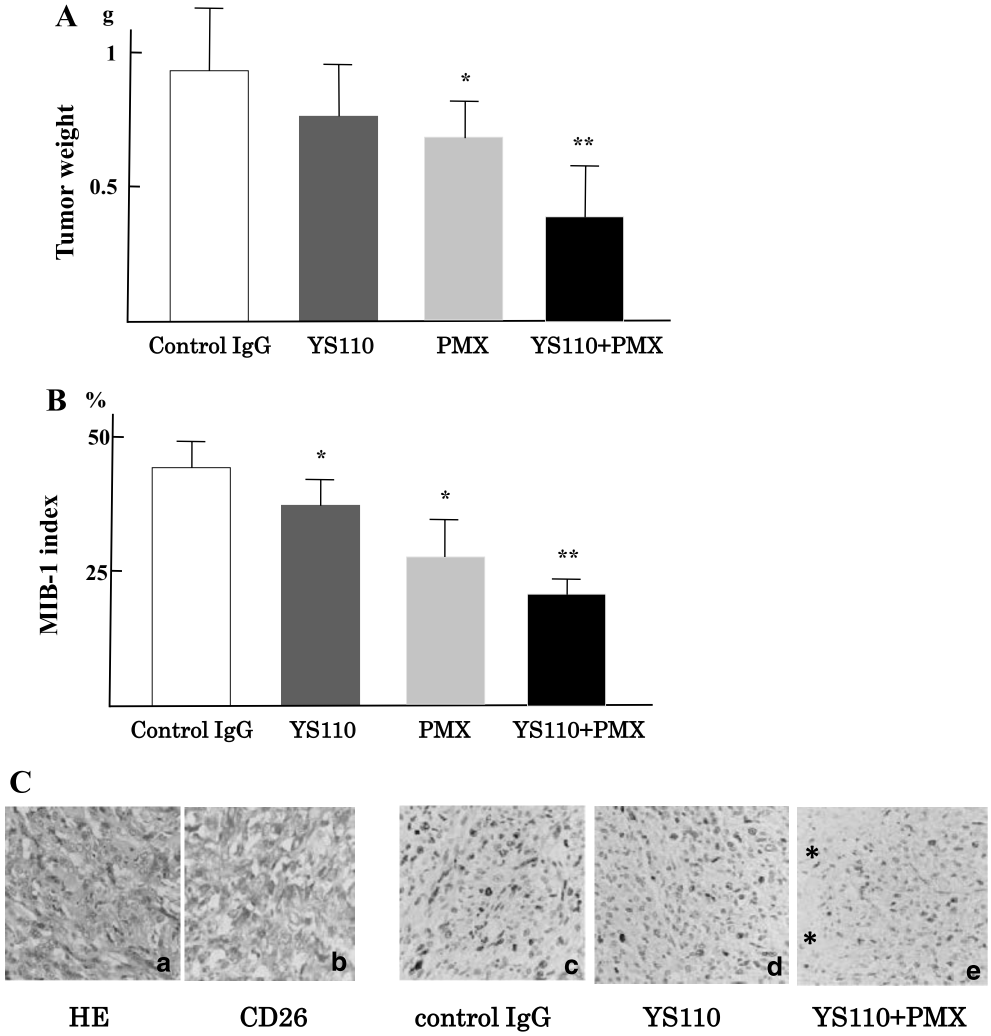

Fig. 6 Effective inhibition of mesothelioma cell growth in vivo. **A** Combination effects of YS110 and PMX were examined using xenograft models with JMN cells transplantation subcutaneously. The weight of tumors treated with YS110 was insignificantly reduced but PMX treatment induced a significantly reduced tumor weight (*$p < 0.05$). A combination of YS110 and PMX treatment reduced tumor weight compared with the weight of tumors with YS110 single treatment and PMX single treatment synergistically (**$p < 0.05$). **B** Combination effects of tumor growth in vivo were examined using a measurement of MIB-1 index histologically. MIB-1 index was significantly reduced with YS110 or PMX single treatment compared with control IgG treatment (*$p < 0.05$). The MIB-1 index after combinatory treatment with YS110 and PMX was significantly reduced compared with YS110 or PMX single treatment (**$p < 0.05$). **C** Sarcomatous mesothelioma is shown in HE staining (*a*) and stained with anti-CD26 polyclonal antibody (R&D) (*b*) MIB-1 index was measured by immunohistochemistry using the anti-Ki-67 monoclonal antibody (DAKO, clone MIB-1). Staining of Ki-67 antigens in nucleus is seen in tumors treated with control IgG (*c*), YS110 (*d*), and both YS110 and PMX (*e*). The number of Ki-67 positive nucleus was reduced after combinatory treatment of YS110 and PMX and the necrotic area is indicated by an *asterisk* (*e*)

cancer cell line LaCaP 35 V, has been reported to result in G2/M delay although its molecular mechanism is not yet understood [15]. Therefore, we are the first to report results on the molecular mechanisms underlying G2/M delay from a cancer targeted-antibody. In order to elucidate the mechanism of G2/M delay mediated by YS110, we analyzed the quantities and phosphorylation status of G2/M regulators using Western blot analysis. At 24 h after treatment with YS110, inhibitory phosphorylation of cdc2 and its upstream regulator cdc25C were elevated. Phosphorylation of Cdc25C on Ser216 is sequestrated into the cytoplasm and therefore restrained from contact with nuclear cdc2. Increased levels of cytoplasmic whole cdc25 protein and decreased levels of nuclear whole cdc25C protein at 24 h occurred after YS110 treatment, confirming sequestration. Western blot analysis also revealed an increased amount of cell cycle inhibitor p21 and decreased amount of cyclinB1 promotes

G2/M progression at 24 h after YS110 treatment. These alterations may be compatible with the retarded G2/M transition.

To determine the upstream regulator of the altered cdc25C phosphorylation state caused by YS110, we investigated several molecules known to regulate cdc25C. 24 h after YS110 treatment, activated phosphorylation levels of p38 MAPK (Thr180/Thy182) and ERK 1/2 (Thr202/Tyr204) were elevated. Inhibitor assays indicated that YS110 treatment activated the ERK signal pathway, but not the p38MAPK pathway, which induced G2/M delay.

MAPK activation results in many different biological responses, including proliferation, differentiation, and cell death. Although ERK1/2 activation is associated with cell survival and proliferation, a number of studies have shown that activation of ERK1/2 can mediate cell cycle arrest and cell death depending on the stimuli and cell types involved [17]. A number of anti-cancer reagents and an anti-cancer antibodies have been reported to induce G2/M cell cycle arrest and/or apoptosis mediated by ERK1/2 activation [18, 19]. These reagents, like YS110, cause G2/M cell cycle delay by inhibiting phosphorylation of cdc2 and cdc25C and by activating phosphorylation of ERK1/2. The G2/M delay caused by these drugs is antagonized by MEK inhibitors. Among monoclonal antibodies that have been investigated for their anti-cancer characteristics, the anti-CD40 antibody has been reported to cause apoptosis of diffuse large B-cell lymphoma cell lines with ERK1/2 activation through CD40 signaling [20]. In these reported cases, as well as our findings of YS110-CD26 interaction, the mechanisms underlying G2/M delay or apoptosis through ERK1/2 activation is still unknown. As for G1/S cell cycle regulation, a report has indicated that HER2 signaling related to trastuzumab treatment had effects on CDC25A protein stability [21]. The involvement of cell cycle regulators on the effect of anti-tumor antibodies should be further investigated.

Previously, we reported that YS110 induces intranuclear transportation of CD26. When bound to YS110, CD26 is translocated to the nucleus via caveolin-dependent endocytosis. This translocation suppresses transcription of the POLR2A gene, which encodes a large subunit of RNA polymerase, in MM cell lines [22, 23]. The relationship between POLR2A suppression and G2/M cell cycle delay also requires further investigation.

The NCI-H2452 cell line is derived from the epithelioid type of MM and its growth rate is lower than the sarcomatoid type of MM, the JMN cell line [24]. Profiles of cell cycling for synchronization assay in S-phase by thymidine block are available for NCI-H2452 cells but not for JMN cells. NCI-H2452 cells have no tumorigenicity in immunodeficient mice but JMN cells form subcutaneous tumors or diffuse and spread into the thorax [11, 22, and 23]; therefore, after YS110 treatment, we examined the in vitro cell cycle using NCI-H2452 cells and in the in vivo xenograft model using JMN cells.

Pemetrexed (PMX) induced augmented CD26 expression in both NCI-H2452 cells and JMN cells rapidly (Fig. 5b); this induction of cell surface CD26 on MM cells may be useful for anti-CD26 MoAb therapy against MM. The combination of YS110 and PMX therapy against xenografted MM tumors was applied using JMN cell transplanted immunodeficient mice. As a result, anti-tumor effects were significantly shown in xenografted tumors with YS110 and PMX combined treatment compared to tumors with single treatment of YS110 or PMX, which was accompanied by a significantly reduced MIB-1 index. The combined treatment with YS110 and PMX showed a tendency to retard both G1/S and G2/M transition; however, significant differences of G1/S or G2/M proportion were not seen between YS110 plus PMX treatment and YS110 or PMX single treatment (data not shown).

There have been many anti-cancer monoclonal antibodies (MoAbs) developed and their anti-cancer mechanisms are highly variable. Investigations into each molecular mechanism of an anti-cancer MoAb are significant because it is valuable for the optimization of antibody therapies against cancer and contributes to elucidating the mechanisms of oncogenesis and cancer proliferation. This is the first report of a novel anti-proliferative mechanism of a humanized anti-CD26 monoclonal antibody YS110 causing G2/M cell cycle delay through ERK1/2 phosphorylation and identifying PMX as a CD26 inducer.

Conclusions

Humanized anti-CD26 monoclonal antibody YS110 suppressed proliferation of CD26 positive MM cell lines through a novel mechanism causing G2/M cell cycle delay through ERK1/2 phosphorylation. Anti-tumor agent PMX was identified as a CD26 inducer.

Methods

Reagents and antibodies

The humanized anti-CD26 antibody YS110 was constructed from the anti-CD26 mouse monoclonal antibody 14D10 coding sequence as previously described [11] and normal human IgG1 (Southern Biotech, Birmingham, AL) was used as a control. Rabbit monoclonal antibody to cyclinB1, p21cip/waf1, cdc2, phospho-cdc2 (Tyr15), cdc25c, phospho-cdc25c (Ser216), Erk1/2, phospho-Erk1/2(Thr202/Tyr204), p38MAPK, and phosphor-p38MAPK (Thr180/Tyr182) were from Cell Signaling Technology Inc. (Danvers, MA) and the mouse monoclonal antibody against β-actin or Glyceraldehyde

3-phosphate dehydrogenase (GAPDH) was from DAKO (Glostrup, Denmark). The goat anti-CD26 polyclonal antibody and MEK 1/2 inhibitor U0126 was from Cell Signaling Technology Inc. (Danvers, MA).

Cell culture

NCI-H2452, NCI-H28 and JMN, CD26-positive cell lines established from malignant mesothelioma, were kind gifts from Dr. Chikao Morimoto (Departement of Therapy Development and Innovation for Immune Disorders and Cancers, Juntendo University). Both cell lines were grown in RPMI medium (Sigma-Aldrich, Tokyo, Japan) supplemented with 10 % heat-inactivated fetal bovine serum (FBS), ABPC (100 unit/mL), Streptomycin (100 μg/mL), and 5 % CO_2 at 37 °C.

Cell proliferation assay

The effect of YS110 on the proliferation of NCI-H2452 cells was measured using a colorimetric cell proliferation kit WST-1 (Roche Diagnostics, Tokyo, Japan) based on the colorimetric detection of a formazan salt. In brief, 5×10^3 NCI-H2452 cells were seeded in RPMI1640 medium supplemented with 10 % heat inactivated FBS on 96-well plate with or without 2 μg/mL YS110. After 48 h of incubation at 37 °C in 5 % CO_2, a reading at 450 nm was carried out according to the manufacturer's instructions. Background absorbance of each sample at 630 nm was subtracted from the readings at 450 nm. The experiment was performed in triplicate and a representative experiment is shown.

Cell cycle assay and flowcytometry

For the cell cycle study, NCI-H2452 and NCI-H28 cells were synchronized in the S-phase by a repeated thymidine block. In brief, 5×10^5 cells seeded in RPMI1640 medium supplemented with 10 % heat inactivated fetal bovine serum on 10 cm culture dishes were treated with 0.56 mM thymidine for 18 h, released for 10 h by three washes, and then treated again with 0.56 mM thymidine for 15 h. Synchronized cells were then returned to thymidine free medium with or without 2 μg/mL YS110 and incubated for 24 h. Cell cycle profiles were performed by flowcytometry using a procedure for propidium iodide staining of nuclei. Acquisition was performed using an EPICS XL/XL-MCL version 3.0 (Beckman Coulter, Brea, CA, USA) and data were analyzed using Flowjo software (TreeStar, Ashland, OR, USA). The experiment was performed in triplicate and a representative experiment is shown.

Western blotting

For total cell lysate preparation, NCI-H2452 cells or JMN cells cultured with or without 2 μg/mL YS110 for 24 h were lysed at 4 °C by lysis buffer with phosphatase inhibitors (50 mM Tris–HCl, 150 mM NaCl, 1 % NP-40, 0.25 % deoxycholate, 500 μM NaVO3, 50 mM NaF). For the preparation of nuclear and cytoplasmic extracts, NCI-H2452 cells were processed using NE-PER Nuclear and Cytoplasmic Extraction Reagents (Thermo scientific, Waltham, LA) according to the manufacturer's instruction. For Western blot analyses, 30 μg of each cell lysate was separated on an SDS–polyacrylamide gel and transferred to a PVDF membrane Hybond-P (GE Healthcare, Little Chalfont, UK). The membranes were blocked in blocking buffer [5 % dry milk and 0.2 % Tween 20 in Tris buffered saline (TBS)] for 2 h at room temperature, and incubated with the primary antibodies in antibody dilution buffer (5 % bovine serum albumin, 0.2 % Tween 20 in TBS) overnight at 4 °C. Dilutions of primary antibodies were 1:200, except anti p21cip/waf1 antibody, which was diluted at 1:100. After three washes, the blots were incubated with secondary antibodies (goat anti-rabbit polyclonal antibody and rabbit anti-mouse polyclonal antibody) diluted 1:1000 with dilution buffer for 1 h at room temperature and developed using the ECL Western Blotting Detection Reagents (GE Healthcare, Little Chalfont, UK). Quantification of relative band densities was performed using standard densitometry scanning techniques using ImageQuant 350 and ImageQuant TL software (GE Healthcare, Little Chalfont, UK). All the experiments performed in triplicate and a representative experiment is shown.

Xenograft model using human mesothelioma cell lines

NOD/Shi-scid, IL-2 receptor gamma null (NOG) mice were obtained from the Central Institute for Experimental Animals. JMN cells (1×10^6) were implanted subcutaneously in the back flank of NOG mice. Mice were injected intratumorally with control human IgG_1 ($n = 3$) or YS110 ($n = 3$) at doses of 5 mg/kg body weight. JMN cells expressing CD26 were inoculated into the thoracic cavities of NOG mice. Thereafter, mice were intraperitoneally injected with control human IgG_1 ($n = 3$) or YS110 (5 μg per injection; $n = 3$), and/or pemetrexed (PMX, purchased from Eli Lilly; 100 mg/kg body weight) commencing on the day of cancer cell injection. Each antibody was administered three times per week. Mice were then monitored for the development and progression of tumors. Tumor weight was measured by scale. All experiments were approved by the Animal Care and Use Committee of Keio University and were performed in accordance with the institute guidelines.

Histology and immunohistochemistry

Tumor tissues were fixed in 10 % neutral buffered formalin, embedded in paraffin, and sectioned at a thickness of 5 μm. Sections were paraffin depleted and rehydrated in a graded series of ethanol solutions. For histology, sections were stained with hematoxylin and eosin. For immunohistochemistry, sections were washed with PBS, subjected to antigen retrieval by heating at 100 °C in 0.01 M sodium citrate (pH 6.0) for 10 min, then treated with 3 % H_2O_2, before incubation with the following primary antibodies: goat anti-CD26 pAb (AF1180, R&D Systems, Minneapolis, MN) (1:100) and mouse anti-Ki-67 mAb (MIB-1, DAKO Japan) (1:100). Immune complexes were detected by using an ImmPRESS REAGENT KIT (Vector Laboratories, Burlingame, CA) with 3, 3′-diaminobenzidine, and sections were counterstained with hematoxylin

Statistical analyses

Statistical analyses were assessed using SPSS version 17.0 (SPSS Inc., Chicago, IL). The *p* value, from which statistical significance was assumed, was set to $p < 0.05$.

Abbreviations

MM: malignant mesothelioma; PMX: pemetrexed; NOG mouse: NOD/Shi-scid, IL-2 receptor gamma null mouse.

Authors' contributions

MH and TY designed and performed the research; HN and CM provided reagents and cells and examined protein expressions; HM, MS and TY analyzed the data; MH and TY wrote the manuscript. All authors read and approved the final manuscript.

Author details

[1] Department of Pathology, Keio University School of Medicine, 35 Shinanomachi, Tokyo, Shinjuku-ku 160-8582, Japan. [2] Department of Pediatrics, Keio University School of Medicine, 35 Shinanomachi, Tokyo, Shinjuku-ku 160-8582, Japan. [3] Laboratory of Nuclear Transport Dynamics, National Insititute of Biomedical Innovation, 7-6-8 Saito-Asagi, Ibaraki City, Osaka Prefecture 567-0085, Japan. [4] Department of Therapy Development and Innovation for Immune Disorders and Cancers, Juntendo University, 2-1-2 Hongo, Tokyo, Bunkyo-ku 113-8421, Japan. [5] Department of Pathology, Saitama Medical University, 38 Morohongo, Saitama, Moroyama-machi 350-0495, Japan.

Acknowledgements

We thank H. Suzuki for technical assistance and A. Sato and K. Tsutsumi for animal care and support of tumorigenicity assay.

Competing interests

YS110 was provided by Y's therapeutics. TY and CM are possessing non-listed stock of Y's therapeutics. MH and HN are paid by the consignment study cost of Y's therapeutics. TY and CM are advisers for Kissei Pharmaceutical Co., Ltd, which carried out the Phase I clinical trial for YS110 against CD26 positive cancers. HM, KY, and MS have no competing interests.

Ethical approval

All animal experiments were approved by the Animal Care and Use Committee of Keio University and were performed in accordance with the institute guidelines.

Funding

This study was supported by the Program for Promotion of Fundamental Studies in Health Sciences of the National Institute of Biomedical Innovation (07–17 to TY and CM), a Grant-in-Aid for Scientific Research (B) (23390086 and 16H04714 to TY and 22790355 to MH) and Global COE Program "Education and Research Center for Stem Cell Medicine" (to KY) from the Ministry of Education, Culture, Sports, Science and Technology of Japan, and a Grant-in-Aid for Drug Design Biomarker Research (H24-B10-003 to TY and CM) from the Ministry of Health, Labor and Welfare and a Grant-in-Aid for Industrial Accident Clinical Research (H27-150401-01 to TY and CM) from the Ministry of Health, Labor and Welfare.

Received: 23 December 2015 Accepted: 24 April 2016
Published online: 30 April 2016

References

1. Sugarbaker DJ. Multimodality management of malignant pleural mesothelioma: introduction. Semin Thorac Cardiovasc Surg. 2009;21:95–6.
2. Krug LM, Pass HI, Rusch VW, Kindler HL, Sugarbaker DJ, Rosenzweig KE, Flores R, Friedberg JS, Pisters K, Monberg M, Obasaju CK, Vogelzang NJ. Multicenter phase II trial of neoadjuvant pemetrexed plus cisplatin followed by extrapleural pneumonectomy and radiation for malignant pleural mesothelioma. J Clin Oncol. 2009;27:3007–13.
3. Vogelzang NJ, Rusthoven JJ, Symanowski J, Denham C, Kaukel E, Ruffie P, Gatzemeier U, Boyer M, Emri S, Manegold C, Niyikiza C, Paoletti P. Phase III study of pemetrexed in combination with cisplatin versus cisplatin alone in patients with malignant pleural mesothelioma. J Clin Oncol. 2003;21:2636–44.
4. Van Schil PE, Baas P, Gaafar R, Maat AP, Van de Pol M, Hasan B, Klomp HM, Abdelrahman AM, Welch J, van Meerbeeck JP. Trimodality therapy for malignant pleural mesothelioma: results from an EORTC phase II multicentre trial. Eur Respir J. 2010;36:1362–9.
5. Greillier L, Marco S, Barlesi F. Targeted therapies in malignant pleural mesothelioma: a review of clinical studies. Anticancer Drugs. 2011;22:199–205.
6. Ohnuma K, Uchiyama M, Yamochi T, Nishibashi K, Hosono O, Takahashi N, Kina S, Tanaka H, Lin X, Dang NH, Morimoto C. Caveolin-1 triggers T-cell activation via CD26 in association with CARMA1. J Biol Chem. 2007;282:10117–31.
7. Bauvois B. Transmembrane proteases in cell growth and invasion: new contributors to angiogenesis? Oncogene. 2004;23:317–29.
8. Aoe K, Amatya VJ, Fujimoto N, Ohnuma K, Hosono O, Hiraki A, Fujii M, Yamada T, Dang NH, Takeshima Y, Inai K, Kishimoto T, Morimoto C. CD26 overexpression is associated with prolonged survival and enhanced chemosensitivity in malignant pleural mesothelioma. Clin Cancer Res. 2012;18:1447–56.
9. Amatya VJ, Takeshima Y, Kushitani K, Yamada T, Morimoto C, Inai K. Overexpression of CD26/DPPIV in mesothelioma tissue and mesothelioma cell lines. Oncol Rep. 2011;26:1369–75.
10. Antczak C, De Meester I, Bauvois B. Ectopeptidases in pathophysiology. Bio Essays. 2001;23:251–60.
11. Inamoto T, Yamada T, Ohnuma K, Kina S, Takahashi N, Yamochi T, Inamoto S, Katsuoka Y, Hosono O, Tanaka H, Dang NH, Morimoto C. Humanized anti-CD26 monoclonal antibody as a treatment for malignant mesothelioma tumors. Clin Cancer Res. 2007;13:4191–200.
12. Le X-F, Pruefer F, Bast RC. HER2-targeting antibodies modulate the cyclin-dependent kinase inhibitor p27Kip1 via multiple signaling pathways. Cell Cycle. 2005;4:87–95.
13. Vincenzi B, Schiavon G, Silletta M, Santini D, Tonini G. The biological properties of cetuximab. Crit Rev Oncol Hematol. 2008;68:93–106.
14. Weiner GJ. Rituximab: mechanism of action. Semin Hematol. 2010;47:115–23.
15. Wu JD, Odman A, Higgins LM, Haugk K, Vessella R, Ludwig DL, Plymate SR. In vivo effects of the human type I insulin-like growth factor receptor antibody A12 on androgen-dependent and androgen-independent xenograft human prostate tumors. Clin Cancer Res. 2005;11:3065–74.
16. Takizawa CG, Morgan DO. Control of mitosis by changes in the subcellular location of cyclin-B1-Cdk1 and Cdc25C. Curr Opin Cell Biol. 2000;12:658–65.
17. Mebratu Y, Tesfaigzi Y. How ERK1/2 activation controls cell proliferation and cell death: is subcellular localization the answer? Cell Cycle. 2009;8:1168–75.
18. Zhang Z, Miao L, Lv C, Sun H, Wei S, Wang B, Huang C, Jiao B. Wentilactone B induces G2/M phase arrest and apoptosis via the Ras/Raf/MAPK signaling pathway in human hepatoma SMMC-7721 cells. Cell Death Dis. 2013;4:e657.

19. Chuang M-J, Wu S-T, Tang S-H, Lai X-M, Lai H-C, Hsu K-H, Sun K-H, Sun G-H, Chang S-Y, Yu D-S, Hsiao P-W, Huang S-M, Cha T-L. The HDAC inhibitor LBH589 induces ERK-dependent prometaphase arrest in prostate cancer via HDAC6 inactivation and down-regulation. PLoS One. 2013;8:e73401.
20. Hollmann CA, Owens T, Nalbantoglu J, Hudson TJ, Sladek R. Constitutive activation of extracellular signal-regulated kinase predisposes diffuse large B-cell lymphoma cell lines to CD40-mediated cell death. Cancer Res. 2006;66:3550–7.
21. Brunetto E, Ferrara AM, Rampoldi F, Talarico A, Cin ED, Grassini G, Spagnuolo L, Sassi I, Ferro A, Cuorvo LV, Barbareschi M, Piccinin S, Maestro R, Pecciarini L, Doglioni C, Cangi MG. CDC25A protein stability represents a previously unrecognized target of HER2 signaling in human breast cancer: implication for a potential clinical relevance in trastuzumab treatment. Neoplasia. 2013;15:579–90.
22. Yamada K, Hayashi M, Du W, Ohnuma K, Sakamoto M, Morimoto C, Yamada T. Localization of CD26/DPPIV in nucleus and its nuclear translocation enhanced by anti-CD26 monoclonal antibody with anti-tumor effect. Cancer Cell Int. 2009;9:17.
23. Yamada K, Hayashi M, Madokoro H, Nishida H, Du W, Ohnuma K, Sakamoto M, Morimoto C, Yamada T. Nuclear localization of CD26 induced by a humanized monoclonal antibody inhibits tumor cell growth by modulating of POLR2A transcription. PLoS ONE. 2013;8:e62304.
24. Penno MB, Askin FB, Ma H, Carbone M, Vargas MP, Pass HI. High CD44 expression on human mesotheliomas mediates association with hyaluronan. Cancer J Sci Am. 1995;1:196–203.

Submit your next manuscript to BioMed Central and we will help you at every step:

- We accept pre-submission inquiries
- Our selector tool helps you to find the most relevant journal
- We provide round the clock customer support
- Convenient online submission
- Thorough peer review
- Inclusion in PubMed and all major indexing services
- Maximum visibility for your research

Submit your manuscript at
www.biomedcentral.com/submit

BioMed Central

RESEARCH ARTICLE

Identification of Nedd9 as a TGF-β-Smad2/3 Target Gene Involved in RANKL-Induced Osteoclastogenesis by Comprehensive Analysis

Yasunori Omata[1☯], Shinya Nakamura[1☯], Takuma Koyama[1☯], Tetsuro Yasui[1], Jun Hirose[1], Naohiro Izawa[1], Takumi Matsumoto[1], Yuuki Imai[2], Sachiko Seo[3], Mineo Kurokawa[3], Shuichi Tsutsumi[4], Yuho Kadono[1], Chikao Morimoto[5], Hiroyuki Aburatani[4], Takeshi Miyamoto[1,6], Sakae Tanaka[1]*

1 Department of Orthopaedic Surgery, Faculty of Medicine, The University of Tokyo, Bunkyo-ku, Tokyo, Japan, **2** Division of Integrative Pathophysiology, Proteo-Science Center, Graduate School of Medicine, Ehime University, Ehime 791–0295, Japan, **3** Department of Hematology and Oncology, Graduate School of Medicine, University of Tokyo, Tokyo, Japan, **4** Genome Science Division, Research Center for Advanced Science and Technology (RCAST), The University of Tokyo, Tokyo, Japan, **5** Department of Therapy Development and Innovation for Immune Disorders and Cancers, Juntendo University, Tokyo, Japan, **6** Department of Orthopedic Surgery, Keio University, Tokyo, Japan

☯ These authors contributed equally to this work.
* TANAKAS-ORT@h.u-tokyo.ac.jp

Abstract

TGF-ß is a multifunctional cytokine that is involved in cell proliferation, differentiation and function. We previously reported an essential role of the TGF-ß -Smad2/3 pathways in RANKL-induced osteoclastogenesis. Using chromatin immunoprecipitation followed by sequencing, we comprehensively identified Smad2/3 target genes in bone marrow macrophages. These genes were enriched in the gene population upregulated by TGF-ß and downregulated by RANKL. Recent studies have revealed that histone modifications, such as trimethylation of histone H3 lysine 4 (H3K4me3) and lysine 27 (H3K27me3), critically regulate key developmental steps. We identified *Nedd9* as a Smad2/3 target gene whose histone modification pattern was converted from H3K4me3(+)/H3K4me27(+) to H3K4me3(+)/H3K4me27(-) by TGF-ß. *Nedd9* expression was increased by TGF-ß and suppressed by RANKL. Overexpression of *Nedd9* partially rescued an inhibitory effect of a TGF-ß inhibitor, while gene silencing of *Nedd9* suppressed RANKL-induced osteoclastogenesis. RANKL-induced osteoclastogenesis were reduced and stimulatory effects of TGF-ß on RANKL-induced osteoclastogenesis were partially abrogated in cells from *Nedd9*-deficient mice although knockout mice did not show abnormal skeletal phenotypes. These results suggest that *Nedd9* is a Smad2/3 target gene implicated in RANKL-induced osteoclastogenesis.

CrossMark
click for updates

OPEN ACCESS

Citation: Omata Y, Nakamura S, Koyama T, Yasui T, Hirose J, Izawa N, et al. (2016) Identification of Nedd9 as a TGF-β-Smad2/3 Target Gene Involved in RANKL-Induced Osteoclastogenesis by Comprehensive Analysis. PLoS ONE 11(6): e0157992. doi:10.1371/journal.pone.0157992

Editor: Dominique Heymann, Faculté de médecine de Nantes, FRANCE

Received: November 23, 2015

Accepted: June 8, 2016

Published: June 23, 2016

Copyright: © 2016 Omata et al. This is an open access article distributed under the terms of the Creative Commons Attribution License, which permits unrestricted use, distribution, and reproduction in any medium, provided the original author and source are credited.

Data Availability Statement: All relevant data are within the paper.

Funding: This work was supported by a Grant-in-aid for Scientific Research from the Japanese Ministry of Education, Culture, Sports, Science and Technology (#26253075). The URL is as follows; https://www.jsps.go.jp/j-grantsinai/index.html. The funders had no role in study design, data collection and analysis, decision to publish, or preparation of the manuscript.

Competing Interests: The authors have declared that no competing interests exist.

Introduction

Skeletal homeostasis is strictly controlled by osteoclasts, which mediate bone resorption, and osteoblasts, which regulate bone formation. Osteoclasts are multinucleated cells derived from monocyte-macrophage lineage hematopoietic progenitor cells and specifically differentiated for bone resorption [1]. The differentiation of osteoclasts is regulated by two cytokines: receptor activator of nuclear factor kappa B ligand (RANKL) and macrophage colony-stimulating factor (M-CSF). In addition to these two essential cytokines, we recently reported a critical role for TGF-ß in osteoclastogenesis [2] [3]. TGF-ß is abundantly stored in bone matrix and has profound biological functions such as angiogenesis, cellular differentiation, apoptosis and bone homeostasis [4] [5]. The binding of TGF-ß to its type II receptors recruits and phosphorylates type I receptors, which in turn activate downstream signaling including Smad and non-Smad pathways [6]. Phosphorylated Smad2/3 forms a complex with Smad4, and the molecular complex translocates into the nucleus and regulates specific gene expression [7] [8] [9].

We previously reported that TGF-ß is required for osteoclast differentiation in response to RANKL and M-CSF by regulating the interaction of Smad2/3 with TRAF (tumor necrosis factor receptor-associated factor) 6, an adaptor molecule associated with RANK [2]. In addition, we identified Smad2/3-binding sites in open chromatin regions during osteoclastogenesis and found that Smad2/3 binding is necessary for the nuclear translocation of c-Fos, an essential transcription factor for osteoclastogenesis [3]. Moreover, it was reported that combined treatment of TGF-ß and TNF-α promotes maximal osteoclast formation compared to treatment with other cytokine combinations in the presence of RANKL based on a multiparameter cytokine assay [10]. However, direct target genes that regulate osteoclast differentiation downstream of TGF-ß-Smad2/3 pathways still remain elusive.

Multiple epigenetic modifications, such as DNA methylation and, histone acetylation and methylation, are involved in organization of chromatin structures at various levels and regulation of gene expression. The methylated sites in H3 or H4 are mainly located in the histone tail (H3K4, H3K9, H3K36 and H4K20) and the center of the nucleosome (H3K79) [11]. Among the five histones, which are designated as H1, H2A, H2B, H3 and H4 [12], Stahl et al. reported that the methylation of histone H3 at lysine 4 is highly conserved and correlated with transcriptionally active nuclei in *Tetrahymena* [13]. Bernstein et al. revealed that histone modifications such as trimethylation of histone H3 lysine 4 (H3K4me3) and lysine 27 (H3K27me3) play a critical role in gene expression, and in embryonic stem cells, key developmental genes tend to change histone modification patterns from the H3K4me3/H3K27me3 bivalent pattern to the H3K4me3 monovalent pattern [14]. Similar modifications of histone methylation have been observed in many other types of cells, and we previously reported that RANKL induced bivalent to monovalent changes in the *nuclear factor of activated T-cells cytoplasmic 1* (*NFATc1*) gene during osteoclastogenesis [15]. Through chromatin immunoprecipitation with sequencing (ChIP-seq) analysis using anti-Smad2/3, anti-H3K4me3 and anti-H3K27me3 antibodies [16], here we investigated Smad2/3-regulating genes that are critically involved in the differentiation of osteoclasts and identified Nedd9 as a putative regulator of osteoclastogenesis downstream of TGF-ß-Smad2/3 pathways.

Results

Identification of genes regulated by the TGF-β-Smad2/3 axis

To identify genes regulated by the TGF-ß-Smad2/3 axis, we performed ChIP-seq analysis using anti-Smad2/3 antibody in M-CSF-dependent bone marrow macrophages (BMMs) treated with 2 ng/ml TGF-ß for 1.5 h. Total read number was 15,108,905, and 10,837,516 reads (71.7%)

were mapped to the mouse genome. A total of 2,786 Smad2/3-binding regions (SBRs) were identified (peak signal ratio ≥ 8). Genes with peak positions of SBRs between 10 kb upstream from transcription start sites (TSSs) and first intron were defined as Smad2/3 target genes, and 903 genes were selected as Smad2/3 target genes.

As shown in Fig 1A, we confirmed that Smad2/3 bound to the promoter regions of known TGF-ß-regulating genes such as *Cdkn1a*, *Smad7* and *Serpine1*. We selected Smad2/3-binding regions in 8 of these genes (*Serpine1*, *Cdkn1a*, *Smad7*, *Smad6*, *Ski*, *Tmepai*, *Nedd9 and Pdgfb*) and confirmed a TGF-ß-dependent increase in Smad2/3 binding by ChIP-realtime PCR (Fig 1B). SBRs were widely distributed from distant upstream regions to intronic regions, with prominent enrichment close to the TSSs of RefSeq genes (Fig 1C).

Histone modification by TGF-β

To analyze TGF-ß-induced histone modification, BMMs treated with 1 ng/ml TGF-ß [designated as TGF-ß(+) BMMs] or 5 μM SB431542 [TGF-ß(-) BMMs] were subjected to ChIP-seq analysis using anti-H3K4me3 or anti-H3K27me3 antibody. SB431542 is a potent and specific kinase inhibitor of TGF-ß type I receptor that strongly suppresses RANKL-induced osteoclastogenesis [2]. Genes with H3K4me3 peaks within +/- 1kb from the TSSs were defined as K4(+) genes (peak signal ratio ≥ 8), and genes with H3K27me3 peaks within +/- 1kb from the TSSs were defined as K27(+) genes (peak signal ratio ≥ 5). A total of 9,962 and 9,505 K4(+) genes and 2,600 and 2,827 K27(+) genes were identified in TGF-ß(-) and TGF-ß(+) BMMs, respectively. Smad2/3 target genes were significantly enriched in genes with K4(+)K27(+) marks in TGF-ß(-) BMMs and K4(+)K27(-) marks in TGF-ß(+) (7.8 fold enrichment; $P < 10^{-5}$ by chi square test) (Fig 2A). The average signal intensity of H3K4me3 around TSS was higher in TGF-ß(+) BMMs than in TGF-ß(-) BMMs while that of H3K27me3 was lower (Fig 2B). Indeed, mRNA expression of Smad target genes with K4(+)K27(+) marks in TGF-ß(-) BMMs and K4(+)K27(-) marks in TGF-ß(+) BMM were up-regulated after TGF-ß stimulation (Fig 2C).

TGF-β positively and RANKL negatively regulates Smad2/3 target genes

Using 14,177 probes (8,839 genes) with expression values of more than 70 by MOE430 GeneChips at least one time point, we found that Smad2/3 target genes were significantly enriched in the genes whose expression was more than 2-fold upregulated, but not in those whose expression was less than 0.5-fold downregulated, by TGF-ß (Fig 3, upper and lower panels; $P < 10^{-5}$ by chi square test). Enrichment scores calculated by Gene Set Enrichment Analysis (GSEA) [17] exhibited statistically significant enrichment ($P < 10^{-6}$) (Fig 3, lower panel).

We then analyzed the change of the expression of Smad2/3 target genes by RANKL stimulation. We used 16,631 probes (10,004 genes) with expression values of more than 70 at least one time point for further analysis. Interestingly, Smad2/3 target genes were significantly enriched in the genes whose expression was less than 0.5-fold downregulated, but not in those whose expression was more than 2-fold upregulated, after 24, 48 and 72 h of RANKL stimulation (Fig 4, upper and lower panels; $P < 10^{-5}$ by chi square test). In addition, genes whose histone modification was changed from K4(+)K27(+) to K4(+)K27(-) patterns by TGF-ß treatment were enriched in downregulated genes by RANKL (Fig 4, upper panel). The statistical significance of the enrichment was analyzed by calculating GSEA enrichment scores ($P < 10^{-6}$) (Fig 4, lower panel).

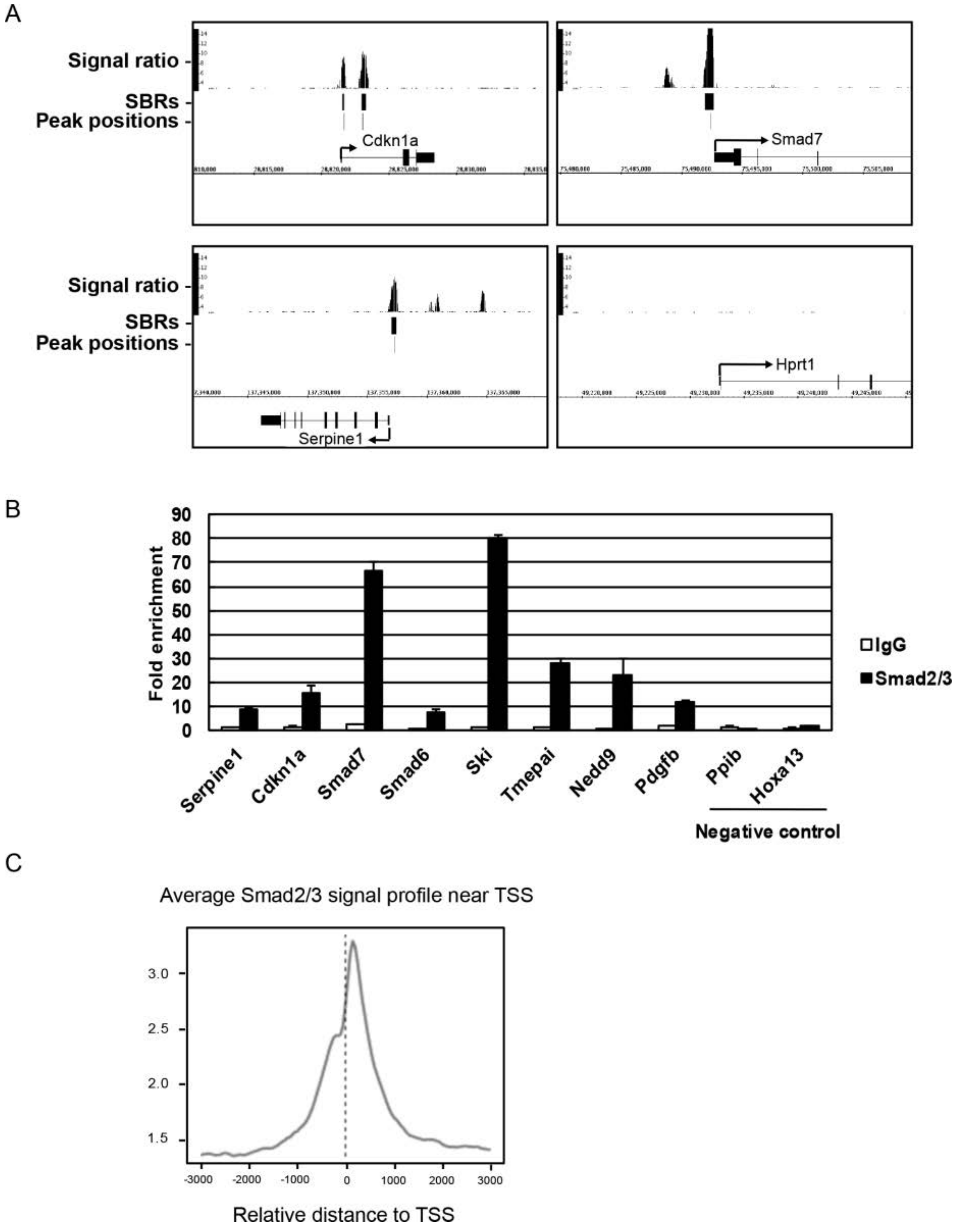

Fig 1. Identification of Smad2/3 binding sites. (A) BMMs were treated with 2 ng/ml TGF-ß for 1.5 h and cells were subjected to ChIP-seq analysis using anti-Smad2/3 antibody. Three known TGF-ß target genes (*Cdkn1a*, *Serpine1*, *and Smad7*) and a negative control gene (*Hprt1*) were analyzed as representative examples. Smad2/3-binding regions (SBRs; peak signal ratio ≥8) and the peak position

of each SBR are shown by black bars. (B) Eight positive regions and two negative regions for Smad2/3 binding were selected from ChIP-seq data and validated by realtime PCR. ChIP using mouse IgG was used as control. Values are presented as n-fold enrichment over Hprt1. (C) Average Smad2/3 signal profile around transcriptional start site (TSS) in ChIP-seq analysis. Smad2/3 binding was enriched around TSS.

doi:10.1371/journal.pone.0157992.g001

Identification of Nedd9 as a possible Smad2/3 target in BMMs

We identified 14 Smad2/3 target genes in which histone modification patterns changed from K4(+)K27(+) to K4(+)K27(-) by TGF-ß treatment (Fig 5A). Nedd9, also called Cas-L or HEF-1 (human enhancer of filamentation 1), is a member of the CAS (crk-associated substrate) family proteins [18] [19] [20]. Nedd9 is a scaffold protein localized in focal adhesion that is involved in the development and progression of cancer cells [21] [22] [23]. As shown in Fig 3A, Smad2/3 binding was enriched around the TSS of *Nedd9* gene. Histone modification status changed from K4(+)K27(+) to K4(+)K27(-) patterns by TGF-ß stimulation in BMMs and then returned to K4(+)K27(+) patterns in response to RANKL stimulation. In fact, *Nedd9* gene expression was upregulated by TGF-ß in BMMs and downregulated by RANKL stimulation (Fig 5B).

We then analyzed a potential function for Nedd9 in osteoclastogenesis. Retroviral overexpression of *Nedd9* significantly increased the expression of *Cathepsin K*, a marker gene of osteoclasts (Fig 6A). In addition, *Nedd9* overexpression partially rescued the inhibitory effect of SB431542 on RANKL-induced osteoclastogenesis ($P < 0.05$; Fig 6B–6D). Conversely, *Nedd9* knockdown by retrovirus carrying *shNedd9* markedly suppressed RANKL-induced osteoclastogenesis (Fig 7A–7C). All of these findings strongly suggest a critical function for Nedd9 in RANKL-induced osteoclastogenesis.

Finally, we assessed the function of Nedd9 in osteoclastogenesis using *Nedd9*-/- mice. BMMs from *Nedd9*-/- mice exhibited reduced osteoclastogenesis similar to *shNedd9*-treated cells (Fig 8A and 8B). Stimulatory effects of TGF-ß on RANKL-induced osteoclastogenesis observed in wild-type BMMs was reduced in *Nedd9*-deficient BMMs (Fig 8B). Expression of Cathepsin K, as determined by Western blotting, was downregulated in *Nedd9*-deficient osteoclasts as compared to wild-type osteoclasts (Fig 8C). However, no significant difference in the skeletal phenotypes, as assessed by soft X ray in the lower extremities, micro CT in lumbar vertebral bodies, and dual energy X ray absorptiometry was observed between *Nedd9*-knockout and wild-type mice (Fig 9A–9C).

Discussion

We previously reported that TGF-ß is indispensable for RANKL and M-CSF-induced osteoclastogenesis. However, the effector genes acting downstream of TGF-ß-Smad2/3 pathways remain elusive. In the present study, we comprehensively analyzed Smad2/3-binding regions and identified Smad2/3 target genes in BMMs by ChIP-seq analysis. Smad2/3 target genes were enriched in TGF-ß upregulated genes as expected. Interestingly, these genes were enriched in the gene population whose expression was downregulated by RANKL treatment, indicating the possibility that the role of TGF-ß is to prepare an appropriate condition for BMMs to differentiate into mature osteoclasts upon RANKL stimulation.

Histone modifications play important roles in cell differentiation. H3K4me3 is enriched in the active and poised promoter regions [24, 25], while H3K27me3 is involved in polycomb-mediated gene repression [26]. Recent studies have revealed that key developmental genes tend to change histone modification patterns from the H3K4me3/H3K27me3 bivalent pattern to the H3K4me3 monovalent pattern in various types of cells. In an attempt to narrow down the candidates of Smad2/3 target genes involving in osteoclast differentiation, we identified *Nedd9* as a Smad2/3 target gene whose histone modification pattern changed from K4(+)K27(+) to

A

TGF-β(-)		TGF-β(+)		Genes		SBRs		b/a	Enrichment	
K4	K27	K4	K27	a	% total genes	b	% total SBRs	%		## p<0.0001
any	any	any	any	21,194	100	903	100	4.3		
+	+	+	+	541	2.6	17	1.9	3.1	0.7	
+	+	+	-	21	0.1	7	0.8	33.3	7.8	##
+	+	-	+	56	0.3	0	0.0	0.0	0.0	
+	+	-	-	0	0.0	0	0.0	N/A	N/A	
+	-	+	+	27	0.1	4	0.4	14.8	3.5	
+	-	+	-	8013	37.8	550	60.9	6.9	1.6	##
+	-	-	+	0	0.0	0	0.0	N/A	N/A	
+	-	-	-	22	0.1	1	0.1	4.5	1.1	
-	+	+	+	2	0.0	0	0.0	0.0	0.0	
-	+	+	-	4	0.0	1	0.1	25.0	5.9	
-	+	-	+	964	4.5	16	1.8	1.7	0.4	##
-	+	-	-	14	0.1	2	0.2	14.3	3.4	
-	-	+	+	0	0.0	0	0.0	N/A	N/A	
-	-	+	-	15	0.1	2	0.2	13.3	3.1	
-	-	-	+	7	0.0	0	0.0	0.0	0.0	
-	-	-	-	4212	19.9	82	9.1	1.9	0.5	##

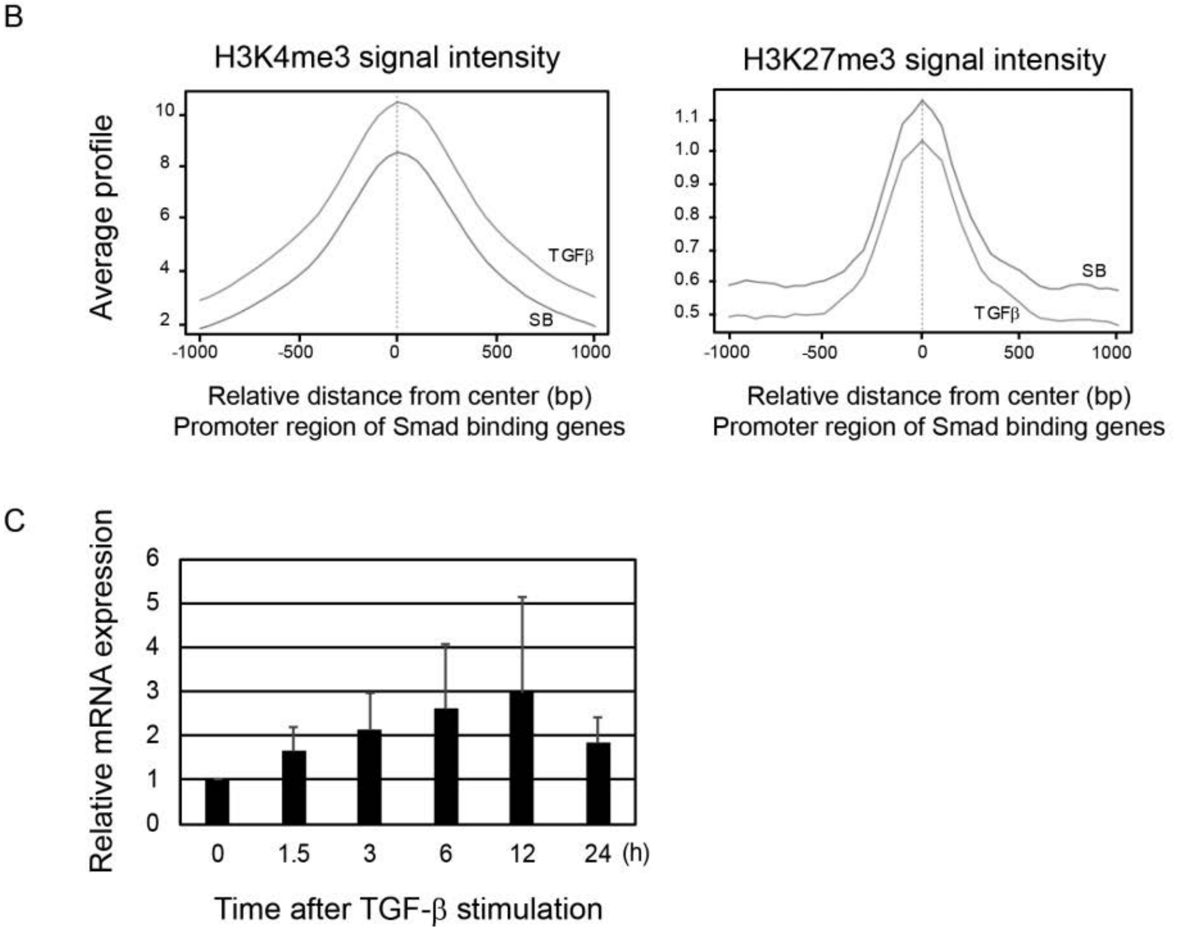

Fig 2. (A) Genes with H3K4me3 peaks within +/- 1 kb from TSS were defined as K4(+) genes, and genes with H3K27me3 peaks within +/- 1 kb from TSS were defined as K27(+) genes. Genes with each combination of K4 and K27 status were identified and enrichment of Smad2/3 target genes was calculated. Highest enrichment was observed in genes with K4(+)K27(+) marks in TGF-ß(-) BMMs and K4(+)K27(-) marks in TGF-ß (+) BMM. (B) The intensity of histone marks around TSS of Smad2/3 target genes. The signal intensity of H3K4me3 in BMMs treated with TGF-ß was higher than those treated with SB431542, while the signal intensity of H3K4me27 was lower in TGF-ß(+) BMMs than that in TGF-ß(-) BMMs. (C) mRNA expression of Smad target genes with K4(+)K27(+) marks in TGF-ß(-) BMMs and K4(+)K27(-) marks in TGF-ß(+) BMM.

doi:10.1371/journal.pone.0157992.g002

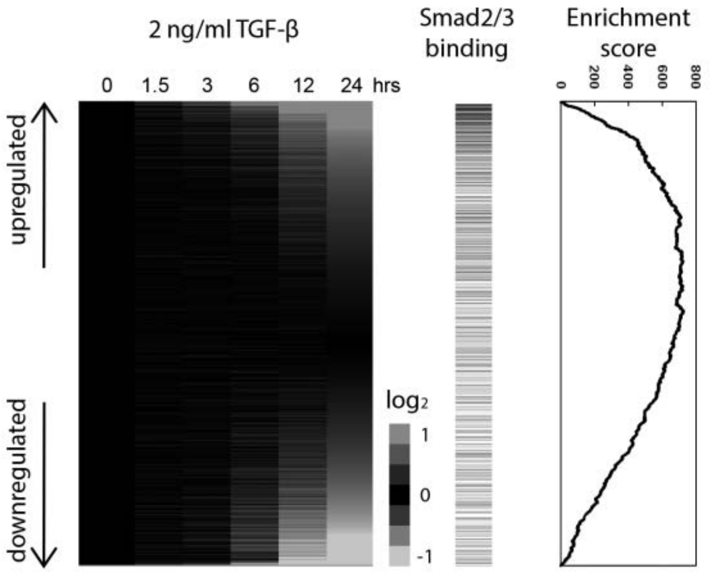

*p<10^{-5}

		All genes		Smad2/3 target genes		#b/#a
		Genes (#a)	% total genes	Genes (#b)	% total genes	%
Total		8839	100.0	592	100.0	6.7
≥ 2-fold increase	1.5 hrs	80	0.9	34	5.7	42.5*
	6 hrs	279	3.2	64	10.8	22.9*
	24 hrs	616	7.0	83	14.0	13.5*
≤ 0.5-fold decrease	1.5 hrs	47	0.5	4	0.7	8.5
	6 hrs	206	2.3	13	2.2	6.3
	24 hrs	684	7.7	29	4.9	4.2

Fig 3. Identification of downstream effectors of TGF-ß in osteoclastogenesis. Upper: The expression scores after TGF-ß stimulation of BMMs relative to time 0 are illustrated by a heat map with red or green color representing increased or decreased gene expression, respectively. The probes were sorted by the ratio at 24 h (ranked gene list). Horizontal bars indicate Smad2/3 target genes. GSEA enrichment scores are graphically shown in the right panel [17]. Smad2/3 target genes were significantly enriched in genes upregulated by TGF-ß. Lower: The expression scores after RANKL stimulation of BMMs relative to time 0 are illustrated by a heat map. Genes whose expression was upregulated more than 2-fold or downregulated less than 0.5-fold relative to RANKL treatment were counted. Enrichment of Smad2/3 target genes in up- or downregulated genes was evaluated by chi-square test ($P < 10^{-5}$).

doi:10.1371/journal.pone.0157992.g003

K4(+)K27(-) patterns in response to TGF-ß. Nedd9, also known as CasL and HEF1, was originally identified as a 105 kDa protein that is tyrosine phosphorylated by the ligation of ß1 integrins in peripheral T cells [18]. Nedd9 is induced by TGF-ß and directly interacts with Smads in various types of cells [27] [28]. We found that Smad2/3 binds to the promoter region of *Nedd9* gene and TGF-ß upregulates *Nedd9* expression in BMMs. Overexpression of *Nedd9* promoted and knockdown or knockout of *Nedd9* suppressed osteoclastogenesis, indicating a role of Nedd9 downstream of RANKL-RANK pathways. Previous studies reported that Nedd9 is

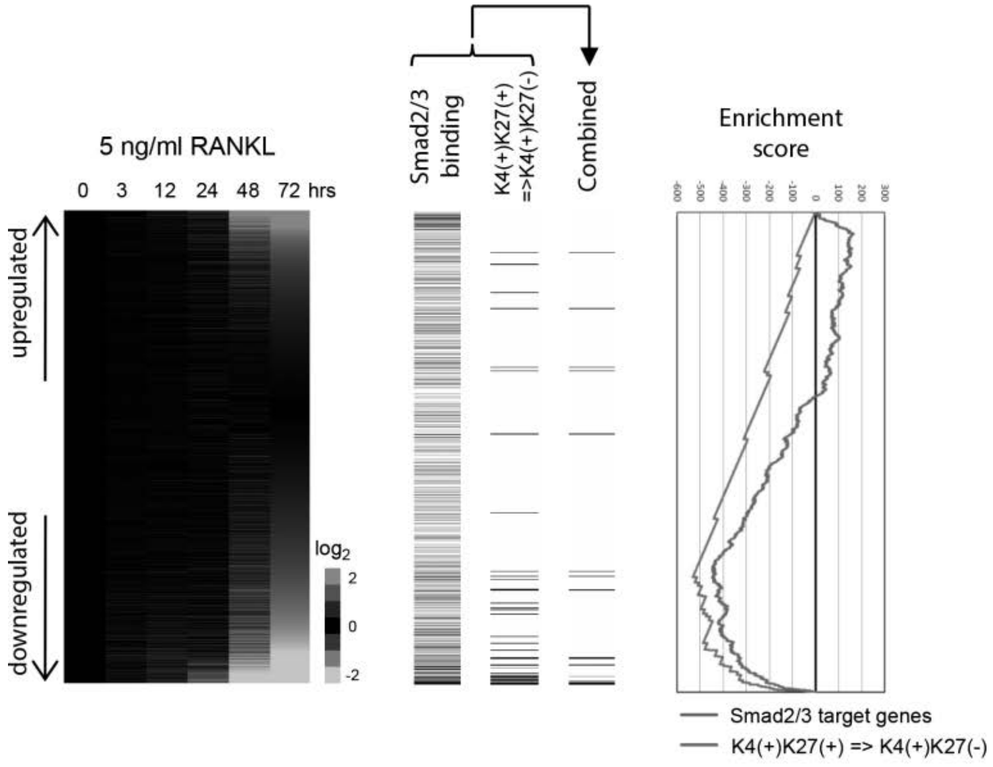

*$p<10^{-5}$

		All genes		Smad2/3 target genes		#b/#a
		Genes (#a)	% total genes	Genes (#b)	% total genes	%
Total		10,004	100.0	636	100.0	6.4
≥ 2-fold increase	3 hrs	145	1.4	19	3.0	13.1
	12 hrs	231	2.3	20	3.1	8.7
	24 hrs	1,450	14.5	67	10.5	4.6
	48 hrs	1,375	13.7	80	12.6	5.8
	72 hrs	1,291	12.9	103	16.2	8.0
≤ 0.5-fold decrease	3 hrs	282	2.8	15	2.4	5.3
	12 hrs	455	4.5	24	3.8	5.3
	24 hrs	1,286	12.9	139	21.9	10.8*
	48 hrs	1,963	19.6	238	37.4	12.1*
	72 hrs	2,279	22.8	211	33.2	9.3*

Fig 4. Upper: TGF-ß(+) BMMs were treated with 5 nM GST-RANKL for 0, 3, 12, 24, 48, and 72 h. Relative expression levels of Smad2/3 target genes as compared with those in time 0 are illustrated by a heat map. The probes were sorted by the value at 72 h after RANKL treatment. Horizontal bars indicate Smad2/3 target genes and genes with K4(+)K27(+) marks in TGF-ß(-) BMMs and K4(+)K27(-) marks in TGF-ß(+) BMMs. GSEA enrichment scores are graphically shown in the right panel. Lower: Enrichment of Smad2/3 target genes in the gene population whose relative expression levels were upregulated more than 2-fold or downregulated less than 0.5-fold by RANKL. Smad2/3 target genes were significantly enriched in downregulated genes by RANKL.

doi:10.1371/journal.pone.0157992.g004

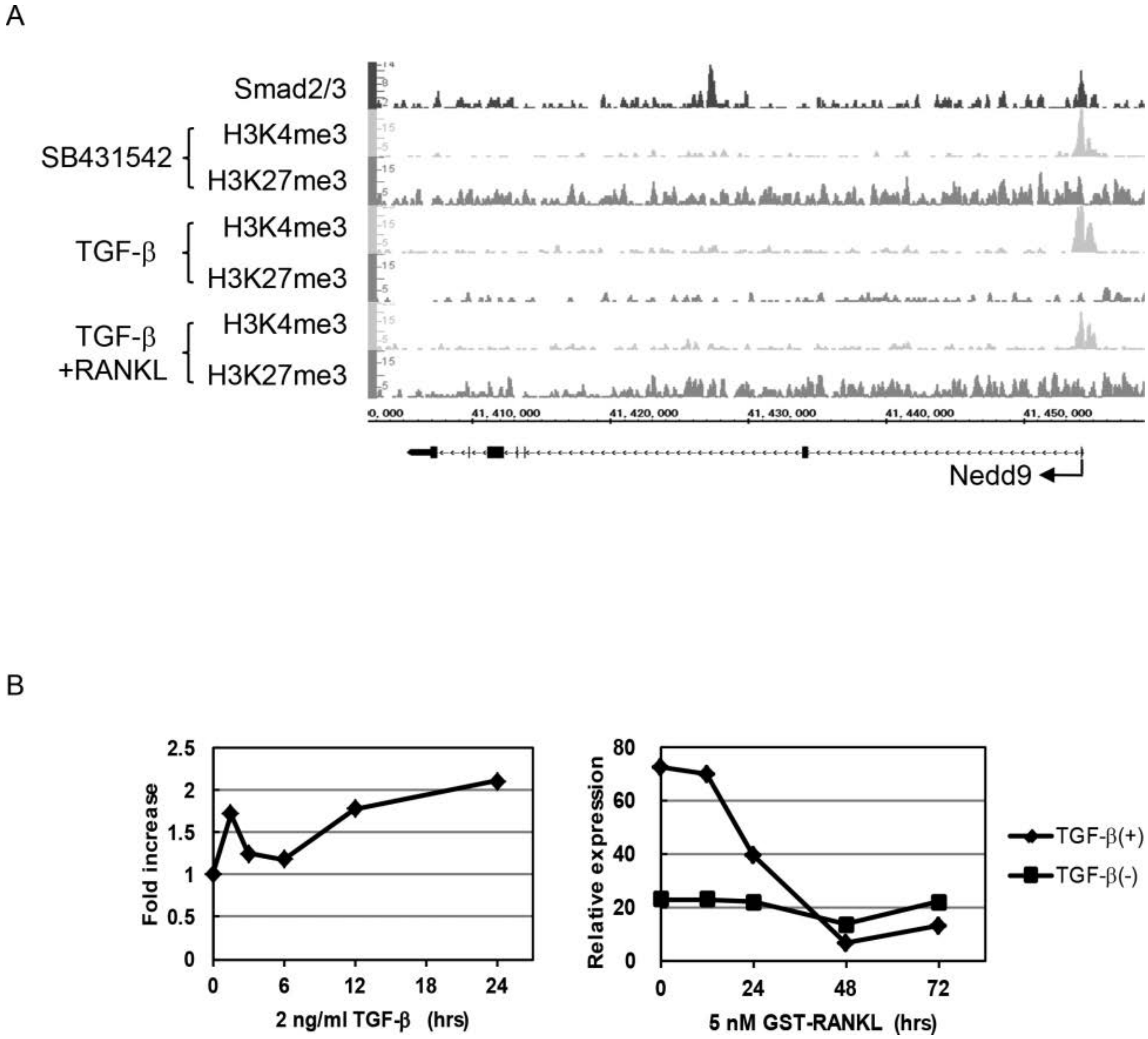

Fig 5. Epigenetic regulation of Nedd9 gene during osteoclastogenesis. (A) Smad2/3 binding and histone modification changes of *Nedd9* gene during osteoclastogenesis. Histone modification patterns in BMMs changed from K4(+)K27(+) to K4(+)K27(-) patterns by TGF-ß and returned to K4(+)K27(+) patterns after RANKL treatment. (B) *Nedd9* mRNA expression after TGF-ß or RANKL stimulation. The expression increased by TGF-ß stimulation and was reduced after RANKL treatment. The expression remained at low levels in the presence of SB431542.

doi:10.1371/journal.pone.0157992.g005

involved in tumor differentiation, migration and metastasis [29], and therefore, it is also possible that Nedd9 supports osteoclast motility as well.

A previous study reported the association between Nedd9 and Smad6 or Smad7 [30], and our ChIP-seq analysis showed that Smad2/3 bound to the promoter region of *Smad6* and *Smad7*. Although we did not address the association between inhibitory Smads and Nedd9 in BMMs, it is possible that Nedd9 regulates TGF-ß signaling in a negative feedback manner by interacting with inhibitory Smads.

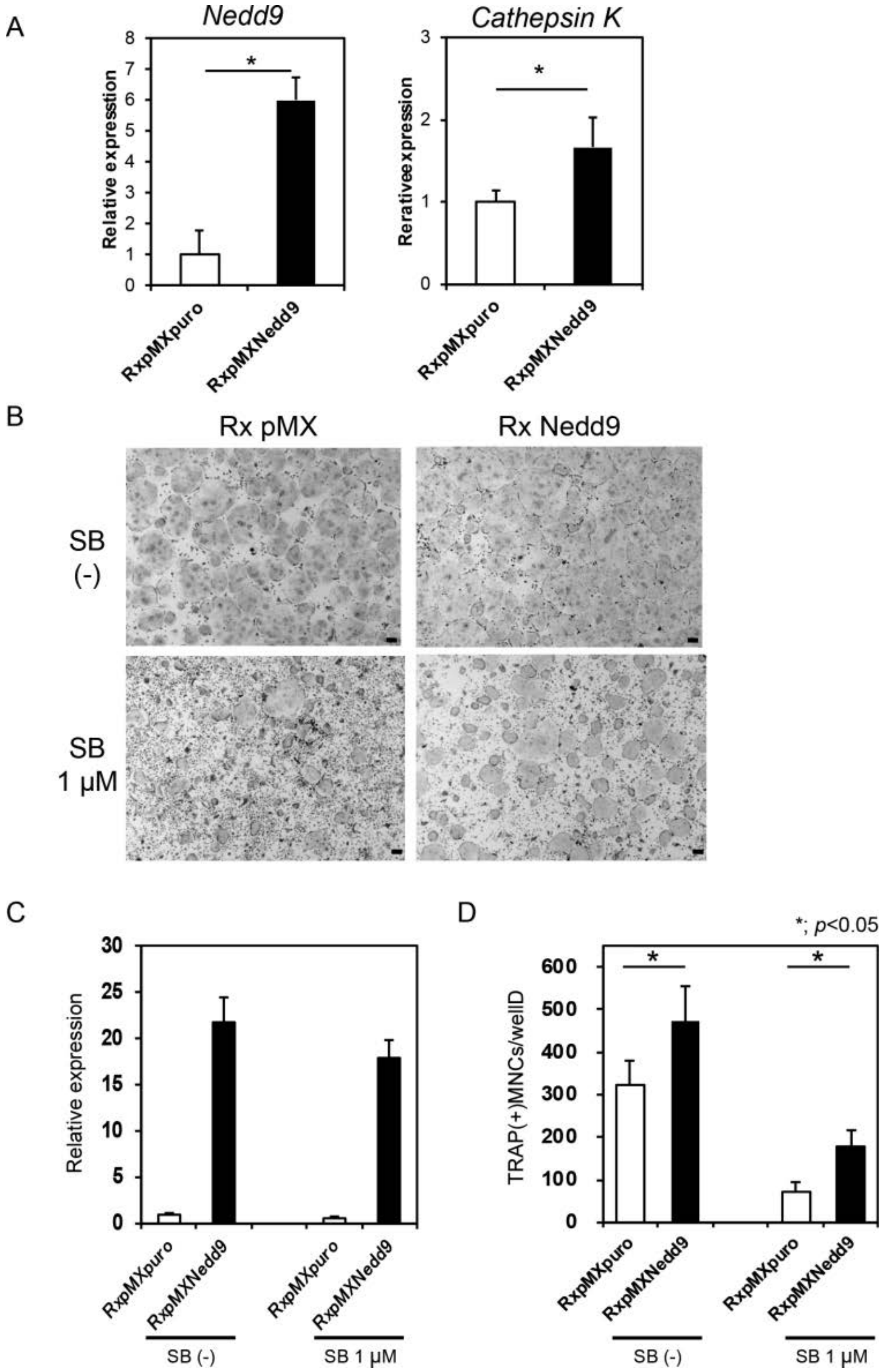

Fig 6. Nedd9 is critical for osteoclast differentiation. (A) Realtime PCR analysis of effects of retroviral overexpression of *Nedd9* gene on RANKL-induced osteoclastogenesis, as indicated by expression of *Nedd9* and *Cathepsin K* mRNAs. (B) Effects of SB431542 (SB) treatment on osteoclastogenesis, as evaluated by TRAP staining, in *Nedd9*-overexpressing cells treated with RANKL. Overexpression of *Nedd9* increased

RANKL-induced osteoclastogenesis. SB431542 suppressed osteoclastogenesis, which was partly recovered by *Nedd9* overexpression. Cultures were stained by TRAP. Bars = 100 μm. (C) The expression of *Nedd9* gene as determined by realtime PCR. (D) The number of TRAP positive osteoclasts was significantly increased by *Nedd9* overexpression, and the suppression of osteoclastogenesis by SB431542 was partly suppressed by *Nedd9* overexpression. *$P < 0.05$.

doi:10.1371/journal.pone.0157992.g006

The role of Nedd9 in skeletal homeostasis *in vivo* is not clear. Seo et al. generated *Nedd9*-deficient mice and reported that lymphocyte trafficking was altered [22]. In addition, Katayose et al. recently reported that *Nedd9*-/- mice exhibited decreased onset of collagen-induced arthritis compared with wild-type mice and that joint destruction was reduced in the knockout mice [31]. We found that RANKL-induced osteoclastogenesis was impaired in BMMs from *Nedd9*-/- mice, and the stimulatory effect of TGF-ß on RANKL-induced osteoclastogenesis was partially abrogated. However, we were unable to find the abnormal bone phenotypes in

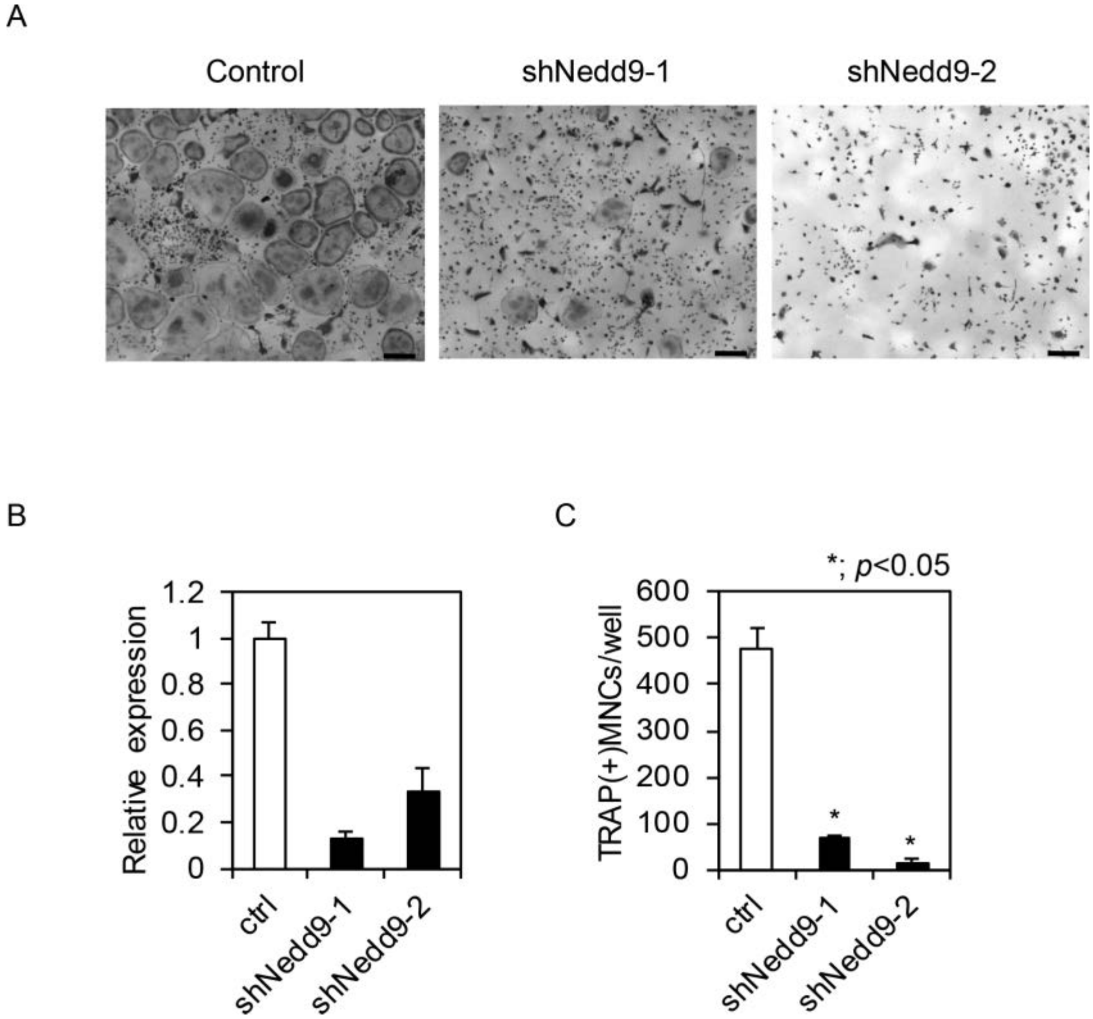

Fig 7. (A) Effects of knockdown of *Nedd9* gene by shRNA on osteoclastogenesis. BMMs infected with retrovirus vector carrying *shNedd9* were treated with 5 nM RANKL for 3 days and stained with TRAP. (B) Expression of *Nedd9* gene by realtime PCR. (C) The number of TRAP positive osteoclasts was significantly reduced by retroviral introduction of *shNedd9*. Bars = 100 μm. *$P < 0.05$.

doi:10.1371/journal.pone.0157992.g007

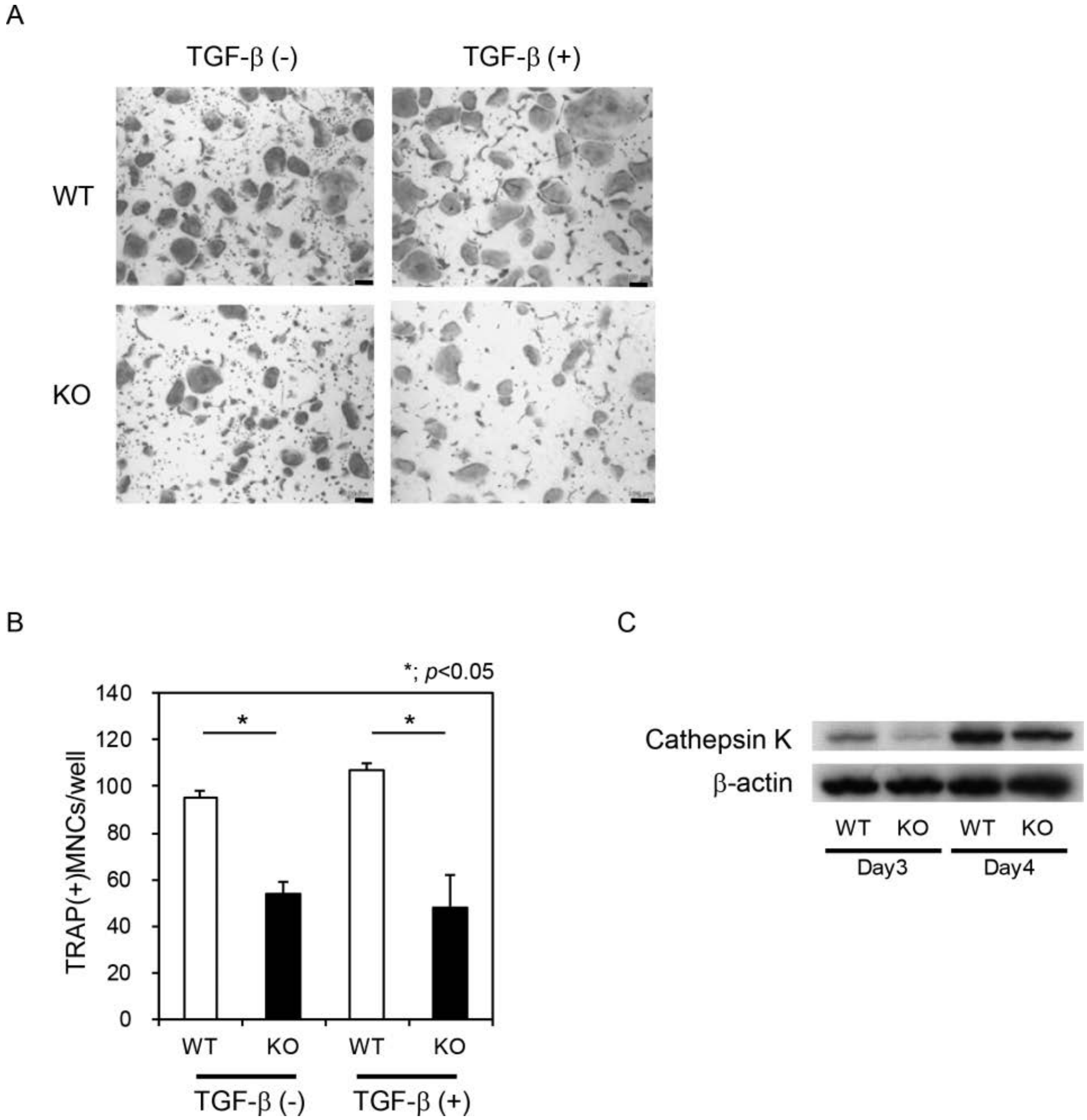

Fig 8. Impaired osteoclastogenesis in Nedd9-/- BMMs. (A) BMMs were isolated from *Nedd9* knockout (KO) and wild-type (WT) mice and cultured in the presence of RANKL with or without TGF-ß. Osteoclastogenesis was evaluated by TRAP staining (A), the number of multinuclear osteoclasts (B) and the expression of Cathepsin K protein (C).

doi:10.1371/journal.pone.0157992.g008

Nedd9-/- mice. This may be due to the effect of Nedd9 on other types of cells such as osteoblasts or osteocytes, or the effect of Nedd9 deficiency is only observed in mice under pathological conditions such as ovariectomy and arthritis, or those treated by TGF-ß. Further studies are required to fully understand the role of Nedd9 in the skeletal milieu.

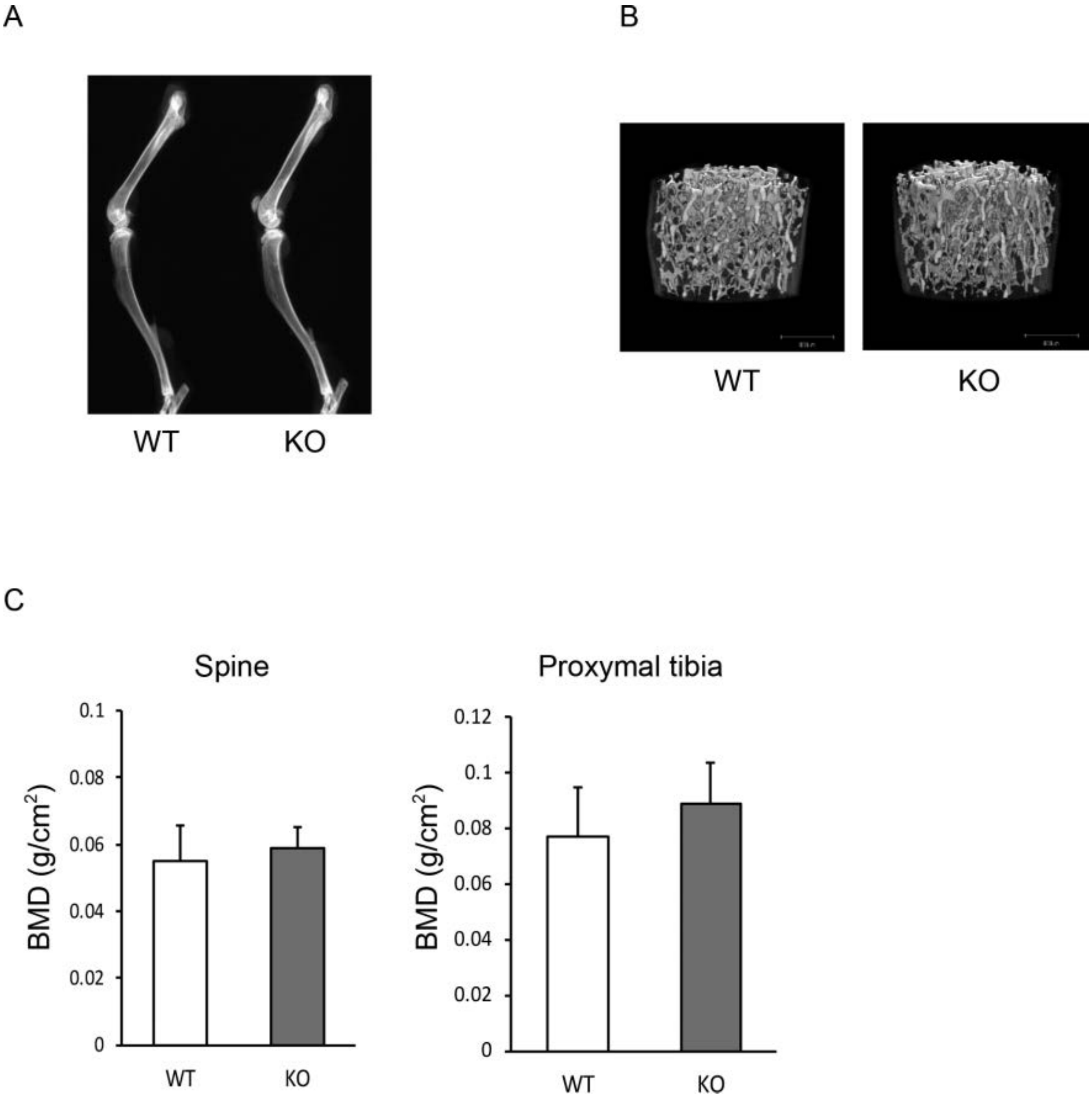

Fig 9. (A) Bone phenotypes of 12-week-old male *Nedd9*-/- and wild-type mice were evaluated using soft-X ray of the lower extremities. (B) micro CT in lumbar vertebral bodies (C) DEXA in lumbar vertebral bodies and proximal tibia.

doi:10.1371/journal.pone.0157992.g009

Materials and Methods

Reagents

Recombinant human M-CSF was purchased from R&D Systems (Minneapolis, MN, USA), and TGF-β and SB431542 were from Sigma-Aldrich (St Louis, MO, USA). GST-RANKL was purchased from Oriental Yeast Co., Ltd (Shiga, Japan). Alpha-minimum essential medium (α-MEM) and fetal bovine serum (FBS) were purchased from Life Technologies (Carlsbad, CA, USA). Smad2/3 antibody was purchased from BD Biosciences (Monoclonal antibody, Mouse, 610843, San Jose, CA, USA), anti-trimethyl-histone H3 lysine 4 was from Activemotif (Polyclonal antibody, Rabbit, 39159, Carlsbad, CA, USA), anti-trimethyl-histone H3 lysine 27 was from Millipore (Polyclonal antibody, Rabbit, 07–449, Billerica, MA, USA), anti-β-actin was from Sigma-Aldrich (Polyclonal antibody, Rabbit, A2066, St Louis, MO, USA).

Animals

Nedd9-/- mice with C57BL/6J (B6) genetic background were generated as previously reported [22]. In short, the exon 2 encoding the N-terminal SH3 domain in the Cas-L protein was replaced with EGFP and a neomycin resistance gene. All animal procedures were approved by the Animal Care and Use Committee of the University of Tokyo.

Cell Culture

Murine bone marrow cells were collected from the femur and tibia of male ddY mice at 4–5 weeks of age. To prepare BMMs, cells were cultured in α-MEM/10% FBS with 100 ng/ml M-CSF for 5 days. BMMs were further cultured in the presence of 10 ng/ml M-CSF and 100 ng/ml RANKL for 4 days to generate osteoclasts. To examine the effect of the TGF-β-Smad pathway on osteoclastogenesis, 1 ng/ml TGF-β or 10 μM SB431542 was added with RANKL. Cells were stained with tartrate-resistant acid phosphatase (TRAP), and TRAP-positive cells containing more than three nuclei were counted as osteoclasts32.

Real-time PCR analysis

Total RNA was extracted with ISOGEN (Wako Pure Chemical Industries, Ltd.), and a 1-μg aliquot was reverse transcribed using a QuantiTect Reverse Transcription kit (QIAGEN) to produce singlestranded cDNA. PCR was performed on an ABI Prism 7000 Sequence Detection System (Applied Biosystems) using QuantiTect SYBR Green

PCR Master Mix (QIAGEN) according to the manufacturer's instructions. All reactions were performed in triplicate. After data collection, the mRNA copy number of a specific gene was calculated with a standard curve generated with serially diluted plasmids containing PCR amplicon sequences and then normalized to rodent total RNA with mouse ß-actin serving as an internal control. Primer sequences were as follows: Nedd9 forward, 5′-CCACCCTCCTACC AGAATCA-3′; Nedd9 reverse, 5′-ATACCCCTTGAGTGCTGTGG-3′; *Cathepsin K*-forward, 5'-ACGGAGGCATTGACTCTGAAGATG-3'; *Cathepsin K*-reverse, 5'-GGAAGCACCAACG AGAGGAGAAAT-3'.

Expression constructs and gene transduction

For retrovirus construction, the full-length cDNAs were amplified by PCR using KODplus (Takara Bio Inc.), subcloned into Zero Blunt TOPO II vectors (Invitrogen), and inserted into pMX-puro vectors. A total of 2×10^6 BOSC23 packaging cells were transfected with 6 μg of vector using FuGENE 6 (Roche). After 24 h, the medium was replaced with fresh α-MEM/10% FBS, and cells were incubated for an additional 24 h. The supernatant was then collected as retroviral stock after centrifugation at 2,400 rpm for 3 min. A total of 5×10^6 BMMs were incubated with 8 ml of retroviral stock for 5 h in the presence of 6 μg/ml polybrene and 30 ng/ml recombinant mouse M-CSF. After 5 h of retroviral infection, the medium was changed to α-MEM/10% FBS and 100 ng/ml M-CSF, and cells were cultured for an additional 24 h. BMMs were recovered with trypsin, and puromycin-resistant cells were selected by incubation with α-MEM/10% FBS containing 2 μg/ml puromycin for 2 d and used for further experiments.

RNA interference (RNAi)

RNAi expression vectors were constructed with piGENEmU6 vector (iGENE Therapeutics; Tokyo, Japan) as described [32] [33], and the U6 promoter and inserts were cloned into pMx vectors. Retroviruses carrying specific genes were prepared by transfecting BOSC packaging cells with retrovirus vectors and collecting the supernatant after 2 days. For retroviral infection, after the first 2 days of culture, BMMs were incubated with retrovirus in the presence of 30 ng/ml M-CSF and 4 ng/ml polybrene (Sigma-Aldrich; St Louis, MO, USA) for 6 h and cultured overnight in the presence of 10 ng/ml M-CSF. To select the transduced BMMs, cells were detached with Trypsin/EDTA (Sigma-Aldrich; St Louis, MO, USA) and cultured with 10 ng/ml M-CSF and 2 μg/ml puromycin (Sigma-Aldrich) for 2 days. Primer sequences were as follows: shNedd9_1 (sense) 5′-gtttGCATTAGATCTTTGGTCGACAgtgtgctgtccTGTTGGCCAAAGGTCTGATGCttttt-3′, shNedd9_1 (antisense) 5′-atgcaaaaaGCATCAGACCTTTGGCCAACAggacagcacacTGTCGACCAAAGATCTAATGC-3′, shNedd9_2(sense) 5′-gtttGCAGTGCTAGGAGTGACATGTgtgtgctgtccACATGTTACTCCTGGTACTGCttttt-3′, shNedd9_2 (antisense) 5′-atgcaaaaaGCAGTACCAGGAGTAACATGTggacagcacacACATGTCACTCCTAGCACTGC-3′.

ChIP and ChIP-seq

Cells were cultured in 15-cm plates to approximately 80% confluency. Cells were fixed with 1% formaldehyde at room temperature and then neutralized with glycine. After cells were collected and re-suspended, samples were sonicated. Samples were incubated with protein A/G beads that had been pre-incubated with 4–10 μg of antibody. Immunoprecipitates were washed and reverse-crosslinked, and DNA was purified with a PCR purification kit (Qiagen, Germantown, MD, USA). DNA libraries were prepared for sequencing using the standard Illumina protocol. Purified DNA was applied for cluster generation and sequencing on the cBot Cluster Generation system and Genome Analyzer IIx system (Illumina; San Diego, CA, USA) following the manufacturer's instructions. Obtained sequences were mapped to the reference mouse genome. ChIP primer sequences were as follows: Nedd9 forward: 5′-AGAAGGCAGAGGCAGCATAA-3′, Nedd9 reverse: 5′-CCTGTGGCATCATCTCTAAGG-3′, Pdgfb forward: 5′- TTTCAAGGCGATGAGGTCAC-3′, Pdgfb reverse: 5′- GGAGAGTGCCCCAGACCT -3′, Smad6 forward: 5′-CATGCAGGGTGTCTCTAGCA-3′, Smad6 reverse: 5′-GGCTACATGGATCACGATGG-3′, Tmepai forward: 5′-AAACCTACTGCGACGACAGG-3′, Tmepai reverse: 5′-ATGAGAGGCACTTTGCAACC-3′, Ski forward: 5′-TGGAGAGGCTCTGCTCTAGG-3′, Ski reverse: 5′-CCTGCAGCTGGTTTGTGTAA-3′, Cdkn1a forward: 5′-TCTGT GTACGTGCGTGTGTG-3′, Cdkn1a reverse: 5′-TAAATTCCCGCCTATGTTGG-3′, Serpine1 forward: 5′-AGCCCAATAGAGAACTTCAAGTCC-3′, Serpine1 reverse: 5′-CAGTACACCTCAAAACCCAGCC-3′, Smad7 forward: 5′-TGCGAAACACAATCGCTTT-3′, Smad7 reverse: 5′-CTCTGCTCGGCTGGTTCC-3′, Ppib forward: 5′-ATGTGGTACGGAAGGTGGAGA-3′, Ppib reverse: 5′-AGCTGCTTAGAGGGATGAGG-3′, Hoxa13 forward: 5′-TGGCATGTTTTAGGGACCTC-3′, Hoxa13 reverse: 5′-CACATCCTTGGGAGGGTCTA-3.

Microarray expression array analysis

Total RNA was extracted with TRIzol and subjected to GeneChip (Affymetrix; Santa Clara, CA, USA) expression analysis according to the technical manual. Briefly, biotin-labeled cRNA synthesized from total RNA was hybridized to a GeneChip Mouse Genome MOE430 2.0 oligonucleotide array (Affymetrix; Santa Clara, CA, USA). The arrays were stained with streptavidin-phycoerythrin and image data was collected with an Affymetrix scanner. Microarray Suite software 5.0 was used to calculate the average difference (AD) for each gene probe set, shown as the gene expression intensity value. The AD values were normalized for each array so that the average of all AD values was 100. One array datum was obtained for each sample. Obtained data were verified by qPCRs for various transcripts, and we had no conflicting results between the array data and qPCR data. Affymetrix probe IDs were converted to gene symbols.

Statistical analyses

The results are expressed as mean±SD. Statistical analyses were performed using a two-tailed unpaired Student's *t* test for continuous variables and chi-square tests for categorical variables. A p value of less than 0.05 was considered to be statistically significant.

Acknowledgments

We thank Dr. M. Miyagishi (National Institute of Advanced Industrial Science and Technology) for providing advice for designing and cloning strategies for shRNA constructs. We also thank H. Kawahara, R. Yamaguchi and J. Sugita (Department of Orthopaedic Surgery, The University of Tokyo) for providing expert technical assistance.

Author Contributions

Conceived and designed the experiments: TY CM T. Miyamoto HA S. Tanaka. Performed the experiments: YO SN TK TY JH NI T. Matsumoto. Analyzed the data: YO TY NI YI S. Tsutsumi YK T. Miyamoto HA S. Tanaka. Contributed reagents/materials/analysis tools: SS MK S. Tsutsumi CM HA. Wrote the paper: YO TY T. Miyamoto S. Tanaka.

References

1. Tanaka S. Signaling axis in osteoclast biology and therapeutic targeting in the RANKL/RANK/OPG system. Am J Nephrol. 2007; 27(5):466–78. doi: 10.1159/000106484 PMID: 17652963.
2. Yasui T, Kadono Y, Nakamura M, Oshima Y, Matsumoto T, Masuda H, et al. Regulation of RANKL-induced osteoclastogenesis by TGF-beta through molecular interaction between Smad3 and Traf6. J Bone Miner Res. 2011; 26(7):1447–56. doi: 10.1002/jbmr.357 PMID: 21305609.
3. Omata Y, Yasui T, Hirose J, Izawa N, Imai Y, Matsumoto T, et al. Genomewide comprehensive analysis reveals critical cooperation between Smad and c-Fos in RANKL-induced osteoclastogenesis. J Bone Miner Res. 2015; 30(5):869–77. doi: 10.1002/jbmr.2418 PMID: 25431176.
4. Janssens K, ten Dijke P, Janssens S, Van Hul W. Transforming growth factor-beta1 to the bone. Endocr Rev. 2005; 26(6):743–74. doi: 10.1210/er.2004-0001 PMID: 15901668.
5. Tang SY, Alliston T. Regulation of postnatal bone homeostasis by TGFbeta. Bonekey Rep. 2013; 2:255. doi: 10.1038/bonekey.2012.255 PMID: 24404376; PubMed Central PMCID: PMCPMC3722719.
6. Ikushima H, Miyazono K. TGF-beta signal transduction spreading to a wider field: a broad variety of mechanisms for context-dependent effects of TGF-beta. Cell Tissue Res. 2012; 347(1):37–49. doi: 10.1007/s00441-011-1179-5 PMID: 21618142.
7. Massague J, Attisano L, Wrana JL. The TGF-beta family and its composite receptors. Trends Cell Biol. 1994; 4(5):172–8. PMID: 14731645.
8. Li MO, Flavell RA. TGF-beta: a master of all T cell trades. Cell. 2008; 134(3):392–404. doi: 10.1016/j.cell.2008.07.025 PMID: 18692464; PubMed Central PMCID: PMCPMC3677783.
9. Graff JM, Bansal A, Melton DA. Xenopus Mad proteins transduce distinct subsets of signals for the TGF beta superfamily. Cell. 1996; 85(4):479–87. PMID: 8653784.
10. Huang W, Drissi MH, O'Keefe RJ, Schwarz EM. A rapid multiparameter approach to study factors that regulate osteoclastogenesis: demonstration of the combinatorial dominant effects of TNF-alpha and TGF-ss in RANKL-mediated osteoclastogenesis. Calcif Tissue Int. 2003; 73(6):584–93. doi: 10.1007/s00223-003-0059-8 PMID: 14517717.
11. Margueron R, Trojer P, Reinberg D. The key to development: interpreting the histone code? Curr Opin Genet Dev. 2005; 15(2):163–76. doi: 10.1016/j.gde.2005.01.005 PMID: 15797199.

12. Zhang Y, Reinberg D. Transcription regulation by histone methylation: interplay between different covalent modifications of the core histone tails. Genes Dev. 2001; 15(18):2343–60. doi: 10.1101/gad.927301 PMID: 11562345.

13. Strahl BD, Ohba R, Cook RG, Allis CD. Methylation of histone H3 at lysine 4 is highly conserved and correlates with transcriptionally active nuclei in Tetrahymena. Proc Natl Acad Sci U S A. 1999; 96 (26):14967–72. PMID: 10611321; PubMed Central PMCID: PMCPMC24756.

14. Bernstein BE, Mikkelsen TS, Xie X, Kamal M, Huebert DJ, Cuff J, et al. A bivalent chromatin structure marks key developmental genes in embryonic stem cells. Cell. 2006; 125(2):315–26. doi: 10.1016/j.cell.2006.02.041 PMID: 16630819.

15. Yasui T, Hirose J, Tsutsumi S, Nakamura K, Aburatani H, Tanaka S. Epigenetic regulation of osteoclast differentiation: possible involvement of Jmjd3 in the histone demethylation of Nfatc1. Journal of bone and mineral research: the official journal of the American Society for Bone and Mineral Research. 2011; 26(11):2665–71. doi: 10.1002/jbmr.464 PMID: 21735477.

16. Giresi PG, Lieb JD. Isolation of active regulatory elements from eukaryotic chromatin using FAIRE (Formaldehyde Assisted Isolation of Regulatory Elements). Methods. 2009; 48(3):233–9. doi: 10.1016/j.ymeth.2009.03.003 PMID: 19303047; PubMed Central PMCID: PMCPMC2710428.

17. Subramanian A, Tamayo P, Mootha VK, Mukherjee S, Ebert BL, Gillette MA, et al. Gene set enrichment analysis: a knowledge-based approach for interpreting genome-wide expression profiles. Proc Natl Acad Sci U S A. 2005; 102(43):15545–50. doi: 10.1073/pnas.0506580102 PMID: 16199517; PubMed Central PMCID: PMCPMC1239896.

18. Minegishi M, Tachibana K, Sato T, Iwata S, Nojima Y, Morimoto C. Structure and function of Cas-L, a 105-kD Crk-associated substrate-related protein that is involved in beta 1 integrin-mediated signaling in lymphocytes. The Journal of experimental medicine. 1996; 184(4):1365–75. PMID: 8879209; PubMed Central PMCID: PMC2192828.

19. Tikhmyanova N, Little JL, Golemis EA. CAS proteins in normal and pathological cell growth control. Cell Mol Life Sci. 2010; 67(7):1025–48. doi: 10.1007/s00018-009-0213-1 PMID: 19937461; PubMed Central PMCID: PMCPMC2836406.

20. Tornillo G, Defilippi P, Cabodi S. Cas proteins: dodgy scaffolding in breast cancer. Breast Cancer Res. 2014; 16(5):443. PMID: 25606587; PubMed Central PMCID: PMCPMC4384296.

21. Law SF, Zhang YZ, Klein-Szanto AJ, Golemis EA. Cell cycle-regulated processing of HEF1 to multiple protein forms differentially targeted to multiple subcellular compartments. Mol Cell Biol. 1998; 18 (6):3540–51. PMID: 9584194; PubMed Central PMCID: PMCPMC108935.

22. Seo S, Asai T, Saito T, Suzuki T, Morishita Y, Nakamoto T, et al. Crk-associated substrate lymphocyte type is required for lymphocyte trafficking and marginal zone B cell maintenance. J Immunol. 2005; 175 (6):3492–501. PMID: 16148091.

23. Shagisultanova E, Gaponova AV, Gabbasov R, Nicolas E, Golemis EA. Preclinical and clinical studies of the NEDD9 scaffold protein in cancer and other diseases. Gene. 2015; 567(1):1–11. doi: 10.1016/j.gene.2015.04.086 PMID: 25967390; PubMed Central PMCID: PMCPMC4458429.

24. Barski A, Cuddapah S, Cui K, Roh TY, Schones DE, Wang Z, et al. High-resolution profiling of histone methylations in the human genome. Cell. 2007; 129(4):823–37. doi: 10.1016/j.cell.2007.05.009 PMID: 17512414.

25. Guenther MG, Levine SS, Boyer LA, Jaenisch R, Young RA. A chromatin landmark and transcription initiation at most promoters in human cells. Cell. 2007; 130(1):77–88. doi: 10.1016/j.cell.2007.05.042 PMID: 17632057; PubMed Central PMCID: PMC3200295.

26. Schwartz YB, Pirrotta V. Polycomb silencing mechanisms and the management of genomic programmes. Nature reviews Genetics. 2007; 8(1):9–22. doi: 10.1038/nrg1981 PMID: 17173055.

27. Liu X, Elia AE, Law SF, Golemis EA, Farley J, Wang T. A novel ability of Smad3 to regulate proteasomal degradation of a Cas family member HEF1. EMBO J. 2000; 19(24):6759–69. doi: 10.1093/emboj/19.24.6759 PMID: 11118211; PubMed Central PMCID: PMCPMC305889.

28. Zheng M, McKeown-Longo PJ. Regulation of HEF1 expression and phosphorylation by TGF-beta 1 and cell adhesion. J Biol Chem. 2002; 277(42):39599–608. doi: 10.1074/jbc.M202263200 PMID: 12189134.

29. Morimoto K, Tanaka T, Nitta Y, Ohnishi K, Kawashima H, Nakatani T. NEDD9 crucially regulates TGF-beta-triggered epithelial-mesenchymal transition and cell invasion in prostate cancer cells: involvement in cancer progressiveness. Prostate. 2014; 74(8):901–10. doi: 10.1002/pros.22809 PMID: 24728978.

30. Inamoto S, Iwata S, Inamoto T, Nomura S, Sasaki T, Urasaki Y, et al. Crk-associated substrate lymphocyte type regulates transforming growth factor-beta signaling by inhibiting Smad6 and Smad7. Oncogene. 2007; 26(6):893–904. doi: 10.1038/sj.onc.1209848 PMID: 16909115.

31. Katayose T, Iwata S, Oyaizu N, Hosono O, Yamada T, Dang NH, et al. The role of Cas-L/NEDD9 as a regulator of collagen-induced arthritis in a murine model. Biochemical and biophysical research communications. 2015; 460(4):1069–75. doi: 10.1016/j.bbrc.2015.03.156 PMID: 25847598.

32. Miyagishi M, Taira K. Strategies for generation of an siRNA expression library directed against the human genome. Oligonucleotides. 2003; 13(5):325–33. doi: 10.1089/154545703322617005 PMID: 15000823.

33. Miyagishi M, Taira K. RNAi expression vectors in mammalian cells. Methods Mol Biol. 2004; 252:483–91. doi: 10.1385/1-59259-746-7:483 PMID: 15017073.

Mizutani *et al. BMC Res Notes (2016) 9:324*
DOI 10.1186/s13104-016-2128-x

BMC Research Notes

RESEARCH ARTICLE

Open Access

Establishment of anti-mesothelioma monoclonal antibodies

Natsuko Mizutani[1,2], Masaaki Abe[2], Shuji Matsuoka[2*], Kazunori Kajino[2], Midori Wakiya[2,3], Naomi Ohtsuji[2], Ryo Hatano[4], Chikao Morimoto[4] and Okio Hino[2]

Abstract

Background: Mesotheliomas are aggressive, therapy-resistant tumors that are predicted to increase in incidence at least until 2020. The prognosis of patients with mesothelioma is generally poor because they are typically diagnosed at a late stage and their tumors are resistant to current conventional therapies. For these reasons, improved diagnosis and therapy are urgently required. To address these issues, the aim of our research was to develop novel mesothelioma-specific monoclonal antibodies (mAbs) as diagnostic and therapeutic agents.

Methods: To develop anti-mesothelioma mAbs useful for diagnosis and therapy, we repeatedly immunized a BALB/c mouse with viable mesothelioma cells, alternating between those from three mesothelioma cell lines. We hybridized the spleen cells from this immunized mouse with P3U1 myeloma cells. We then screened supernatants harvested from the hybridoma clones by assessing whether they bound to a mesothelioma cell line not used for immunization and altered its morphology. We designed this developmental strategy to reduce the risk of obtaining clonotypic mAbs against a single mesothelioma cell line.

Results: Our newly generated mouse anti-human mAbs immunostained clinical samples of mesotheliomas. One of the newly generated mAbs did not react with any other tumor cell line tested. Two other mAbs significantly inhibited the proliferation of mesothelioma cells.

Conclusion: These newly generated anti-mesothelioma mAbs are potentially useful as diagnostic and therapeutic agents for mesothelioma. Moreover, our novel strategy for establishing antitumor mAbs may facilitate the development of new diagnostic and therapeutic techniques for mesotheliomas and other malignancies.

Keywords: Monoclonal antibody, Mesothelioma, Diagnosis, Therapy, Method

Background

Mesothelioma is an aggressive tumor that develops from mesothelial cells, which line the pleural, peritoneal, and pericardial cavities. The development of mesothelioma is usually associated with chronic exposure to asbestos fibers [1, 2]. The worldwide incidence of mesothelioma is increasing and is expected to peak in approximately 2020 because of the long latent period between exposure to asbestos fibers and the appearance of disease [3]. Asbestos continues to be mined in Russia, China, Brazil, Kazakhstan and other countries [4]. Asbestos is still imported and used in brake pads, gaskets, etc., even in the US [4]. Diagnosis based on chest X-ray and computed tomography (CT) findings must be confirmed by cytologic serous effusion examination or biopsy [5–7].

Immunohistochemistry has significantly enhanced the accuracy of cytology, although reaching a diagnosis remains frequently difficult [8–10]. Although many diagnostic procedures are available, no single test unambiguously distinguishes mesothelioma from other carcinomas or even benign from malignant cells. The correct combination of antibodies used to detect positive or negative markers should be employed and a comprehensive assessment of the staining results must be conducted [11].

---

*Correspondence: matsuoka@juntendo.ac.jp
[2] Departments of Pathology and Oncology, Juntendo University School of Medicine, 2-1-1, Hongo, Bunkyo-ku, Tokyo 113-8421, Japan
Full list of author information is available at the end of the article

© 2016 The Author(s). This article is distributed under the terms of the Creative Commons Attribution 4.0 International License (http://creativecommons.org/licenses/by/4.0/), which permits unrestricted use, distribution, and reproduction in any medium, provided you give appropriate credit to the original author(s) and the source, provide a link to the Creative Commons license, and indicate if changes were made. The Creative Commons Public Domain Dedication waiver (http://creativecommons.org/publicdomain/zero/1.0/) applies to the data made available in this article, unless otherwise stated.

Mesothelioma is categorized histologically as epithelioid, sarcomatoid, biphasic, and desmoplastic, among others [9]. The histological subtypes help predict prognosis and the choice of treatment. Therefore, it is important to analyze pathological tissue using an appropriate combination of antibodies for diagnosis and classification. Nevertheless, many cases are difficult to diagnosis [12–16].

Although an anti-CD26 mAb is a promising candidate, no effective molecular target for therapy exists [17, 18]. Therefore, the development of novel anti-mesothelioma mAbs may facilitate diagnosis and serve as therapeutic agents. Subsequent to the development of mAbs by Köhler, Milstein, and Jerne in 1975 [19], excessively large number of mAbs were generated as diagnostic [20, 21] or therapeutic reagents [22].

Diagnostic or therapeutic mAbs are now typically generated by immunizing mice with synthetic peptides or target antigens that are purified to some extent [23, 24]. Except for nude or SCID mice, mice reject inoculated live malignant human tumor cells. During the first or second challenge, tumor cells may be primarily killed by NK and CD8 cytotoxic T cells or ingested by macrophages. However, during the course of repeated immunizations, mouse B cells are generated that produce antibodies against the tumor cells. These antibodies probably make a major contribution to the rejection of the tumor cells. This hypothesis served as the rationale for our experiments that were aimed at establishing anti-mesothelioma mAbs. We report here the generation of anti-human mesothelioma mAbs for diagnosis and treatment. This was accomplished by immunizing a mouse with live mesothelioma cell lines. The hybridomas were selected for their ability to produce antibodies that bound to mesothelioma cell lines not used for immunization. Some of these newly established mAbs reacted specifically with mesothelioma cells or inhibited their proliferation.

Methods

Mice

Female BALB/c mice (6–8 weeks of age) were purchased from Charles River Japan (Yokohama, Japan) and housed in a specific pathogen-free facility in micro-isolator cages. Animal experiments were conducted following protocols approved by the Animal Care Committee of Juntendo University of Medicine.

Cells

The human mesothelioma cell lines ACC-MESO-1 and ACC-MESO-4 were purchased from the RIKEN Cell Bank (Ibaraki, Japan), JMN was a kind gift from Dr. Brenda Gerwin and others (NCI-H226, MSTO-211H, NCI-H28 and NCI-H2452) were purchased from the American Type Culture Collection (ATCC) (Manassas, VA). The lung cancer cell lines (A549, PC9, Lu24, and WA-hT), and the HuH-7 (hepatocellular carcinoma), MKN1 (gastric cancer), OVK18 (ovarian cancer), VMRC-RCW (renal cell carcinoma) cell lines were purchased from the RIKEN Cell Bank. The MCF7 (breast cancer), KP3 (pancreatic cancer), and HCT 116 (colon cancer) cell lines were purchased from ATCC. All cells were cultured and maintained in RPMI-1640 medium (GIBCO, Grand Island, NY) supplemented with 10 % heat-inactivated fetal calf serum.

Antibodies

The mouse anti-HLA class I (HLA class-A, B, C) mAb (clone: W6/32) was purchased from Harlan Laboratories Inc. (IN). Alexa Flour® 488-conjugated goat anti-mouse IgG was purchased from Invitrogen (CA). Mouse IgG was purchased from Abcam (Cambridge UK). The mAbs for WT-1 (clone: 6F-H2), Calretinin (clone: DAK-Calret 1), Podoplanin (clone: D2-40), Cytokeratin 5/6 (clone: D5/16 B4), EMA (clone: E29), Carcinoembryonic Antigen (CEA) (clone: II-7), TTF-1 (clone: 8G7G3/1), and Epithelial-Related Antigen (clone: Moc-31) were purchased from DAKO. The mAb against Mesothelin (clone: 22A31) and anti-GLUT-1 polyclonal Ab were purchased from IBL (Japan). Anti-CD26 mAbs (clone 1F7, 5F8) were established in our laboratory [25].

Anti-CD25 mAb (clone: BC96) and mouse Ig G1 isotype control (MOPC-21) were purchased from TONBO biosciences (CA).

Generation of mAbs against mesothelioma cells

An eight-week-old female BALB/c mouse was immunized alternately using intraperitoneal injections of $2–5 \times 10^6$ living cells derived from the mesothelioma cell lines ACC-MESO4, MSTO-211H, and NCI-H226 every 2 weeks for 3 months. Three days after the last immunization, spleen cells were fused with P3U1-non-producing myeloma cells using polyethylene glycol 4000 (Merck, Darmstadt, Germany) and cultured in RPMI-1640 supplemented with 10 % fetal calf serum (FCS, Japan Bioserum, Fukuyama, Japan), 5 % BriClone (NICB, Dublin, Ireland), and HAT (Invitrogen, Tokyo, Japan) in the wells of 96-well flat-bottom plates (Costar, Corning Incorporated, Corning, NY). Hybridoma supernatants were screened for reactivity with the mesothelioma NCI-H2452 cells, which were not used for immunization. Light microscopy revealed morphological changes and an aggregation of target cells induced by incubation with supernatants of hybridoma clones after 72 h. The reactivity of hybridoma supernatants for the other mesothelioma cell lines was also determined. Four hybridomas, JMAM1–4, were selected and cloned using limiting dilution. The isotype of these mAbs was IgG1, and they cross-reacted widely with mesothelioma cell lines.

Flow cytometric (FACS) analysis

The expression of the molecular target(s) of the newly established mouse anti-human mesothelioma mAbs was determined using a BD LSRForessa™ cell analyzer (BD Bioscience, CA, USA). Briefly, the human mesothelioma cell lines and the cell lines derived from other tumors were incubated with the supernatants of hybridomas and then with Alexa Flour® 488-conjugated rat anti-mouse IgG (BD Bioscience) on ice.

Inhibition test

NCI-H226 cells were first incubated with already known existing Abs and further incubated with Alexa Flour® 488-labeled JMAM mAbs.

Immunocytochemistry

Samples of pleural effusions submitted to the Department of Pathology, Juntendo University, were used for immunohistochemistry and other histological staining procedures. Three representative cases of cytologically diagnosed mesothelioma were used for immunohistochemistry, and all cases were stained with positive and negative antibody panels of diagnostic antibodies to confirm the diagnosis of mesothelioma. Cell smears were fixed in 95 % ethanol for Papanicolaou and immunostaining, or air-dried for May-Grunwald-Giemsa staining. Cell sediments were fixed with ethanol and embedded in paraffin for immunostaining. Sections were deparaffinized using three changes of xylene and rehydrated with a graded series of ethanol concentrations. Endogenous peroxidase was inactivated with 0.3 % H_2O_2 in phosphate-buffered saline for 10 min. Samples were incubated with the novel anti-mesothelioma mAbs JMAM1–4 at 4 °C overnight in a humidified chamber, followed by the addition of EnVision™ + DualLink (DAKO) and 3.3′-diaminobenzidine (Dojindo Laboratories) as the chromogen. Cell smears and cell-block sections were counterstained to reveal nuclei using Mayer's hematoxylin. For all cases, we stained cell block sections using antibodies against EMA, Podoplanin, GLUT-1, Calretinin, WT-1, Cytokeratin 5/6, Mesothelin, CEA, TTF-1, and epithelial-related antigen to confirm the diagnosis of mesothelioma (Table 1).

In vitro proliferative assay of mesothelial cells incubated with mAbs

MSTO-211H cells (1 × 10^4 cells/well) were incubated with 10 % FCS-RPMI supplemented with 0.005–0.4 μg/ml of JMAM1–4 mAbs for 48 h at 37 °C in an atmosphere containing 5 % CO_2. The culture was pulsed with 0.5 μCi of tritiated thymidine, [^{3}H]-TdR, for the final 24 h. The incorporation of [^{3}H]-TdR was determined using scintillation counting. Data are expressed as the mean ± standard deviation (SD) of triplicate samples and represent three separate experiments.

Wound-healing assay

Mesothelioma NCI-H226 cells were seeded in 6-well plates (Corning) and grown to 90 % confluence in RPMI plus 10 % FCS. The cell monolayer was wounded with the tip of an Eppendorf P200 pipette. After wounding, the wells were washed with media to remove dead cells and debris. The wells were treated with either 3 μg/ml of anti-mesothelioma mAbs (JMAM1–4) or a control IgG (3 μg/ml) and cultured further. The wound closure was observed after 24 h.

Cell invasion assay

For the cell invasion test, a Corning Matrigel Invasion Chamber (8-μm pore size, coated with Matrigel; Discovery Labware Inc., Bedford, MA, USA) was placed into the wells of 24-well culture plates; RPMI-1640 medium with 10 % serum and JMAM1–4 mAbs (each 10 μM) were added into the lower chamber; then, 2 × 10^4 NCI-H226 cells in serum-free RPMI-1640 medium was added to the upper chamber and cultured at 37 °C. After 15 h of incubation, the cells on the upper surface of the filter membrane that had not migrated were gently scraped away with a cotton swab. The invading cells on the lower surface of the filter membrane were fixed with methanol, stained with Diff-Quick™ (Sysmex), and counted as described above. All tests were performed in triplicate.

Statistical analysis

The data were analyzed using Student's *t* test. The results are expressed as the mean ± SD and P values of <0.05 were considered significant. Statistical analyses were performed using SPSS 14.0 software (IBM, NY).

Results

Morphological changes of mesothelioma cell lines induced by the newly generated mAbs

We found that the newly generated four mAbs reproducibly induced morphological changes in a mesothelioma cell line that was not used for immunization. Light microscopy revealed that the morphology of the NCI-H2452 cells changed from spindle-shaped to round, and the numbers of these cells decreased after incubation with JMAM1–4 mAbs for 72 h compared with control mouse IgG (Fig. 1a, upper column). These morphological changes indicated that the mAbs bound the mesothelial cell lines. These findings were also reproduced using MSTO-211H cells that were used for immunization

Table 1 Antibodies used in this study and immunocytochemical reactivity

Antibody	Clone	Source	Dilution	Specimen	Case 1	Case 2	Case 3
JMAM1		Our labolatory	Undiluted cell supernatant	Cell smear	+	+	+
JMAM2		Our labolatory	Undiluted cell supernatant	Cell smear	+	+	+
JMAM3		Our labolatory	Undiluted cell supernatant	Cell smear	+	+	+
JMAM4		Our labolatory	Undiluted cell supernatant	Cell smear	+	+	+
WT-1	6F-H2	DAKO	1:200	Cell block	+	±	+
Carletnin	Dak-Calret 1	DAKO	1:100	Cell block	+	+	+
Mesothelin	22A31	IBL	1:1000	Cell block	+	+	+
Podoplanin	D2–40	DAKO	1:200	Cell block	+	+	+
CK5/6	D5/16B4	DAKO	1:50	Cell block	+	+	+
EMA	E29	DAKO	1:100	Cell block	+	+	+
GLUT-1	5B12.3	IBL	1:1000	Cell block	+	+	+
CEA	II-7	DAKO	1:50	Cell block	−	−	−
TTF-1	8G7G3/1	DAKO	1:100	Cell block	−	−	−
Epithelial-related antigen	Moc-31	DAKO	1:100	Cell block	−	−	−

(Fig. 1a, lower column). Furthermore, these mAbs aggregated MSTO-211H cells. Taken together, these findings indicate that the newly established mAbs reacted with the mesothelial cell lines.

Analysis of the binding of mAbs to the mesothelial cell lines

The reactivity of the mAbs against the mesothelial cell lines was determined using FACS analysis. JMAM1, JMAM2 and JMAM3 mAbs stained the epithelial (ACC-MESO-4, JMN) and sarcomatous (MSTO-211H, H2452, H28 and MESO-1) cell lines. In contrast, JMAM4 stained the epithelial cell lines but not the sarcomatous cell lines (Fig. 1b).

Competitive inhibition of JMAM mAbs with established mAbs

To determine whether the newly established JMAM mAbs bind to the same epitope of the already existing Abs, we performed an inhibition test by flow cytometry.

NCI-H226 cells were incubated with JMAM mAbs followed by staining with existing Abs already known to bind to mesothelioma [anti-calretinin, anti-podoplanin (D2-40), anti-GLUT-1, anti-CD25 (BC96), anti-CD26 (1F7, 5F8), anti-C-ERC/mesothelin (22A31)]. (Fig. 2).

Anti-calretinin was able to partially inhibit the staining of the NCI-H226 mesothelioma cell line with JMAM2 mAb. This result indicates that the JMAM2 determinant is strongly related to calretinin; however, the other JMAM mAbs have no relationship with already existing Abs, they may bind to mesothelioma cells.

Analysis of the binding of mAbs to other tumor cell lines

Using FACS analysis, we next determined whether the mAbs bound to lung cancer cell lines. Binding of JMAM1 to epithelial-type lung cancer cell lines (A549 and PC9) was not detectable. In contrast, it bound to the small-cell lung cancer cell lines WA-hT and Lu24. The extent of binding of JMAM2 and JMAM3 mAbs to lung cancer cell lines varied. The JMAM4 mAb did not bind to any of the lung cancer cell lines (Fig. 3a).

To determine the cross-reactivity of these novel anti-mesothelioma mAbs to cell lines derived from tumors other than those of the lung, we used FACS analysis to determine their ability to react with MCF7 (breast cancer), HuH-7 (liver cancer), KP3 (pancreatic cancer), MKN-1 (gastric cancer), HCT 116 (colon cancer), OVK18 (ovarian cancer), and VMRC-RCW (renal cell carcinoma) cell lines. The JMAM1 mAb only cross reacted with the VMRC-RCW cell line. JMAM4 mAbs did not react detectably with any of these carcinoma cell lines. The JMAM2 mAb slightly or significantly stained all carcinoma cell lines tested. The JMAM3 mAb did not stain the liver or pancreatic cancer cell lines; however, it lightly stained a gastric cancer cell line and strongly stained breast and colon cancer cell lines (Fig. 3b). Taken together, these data indicate that the JMAM1 mAb distinguished mesothelioma and small-cell lung cancer cells from epithelial lung cancer cells as well as any other cancer cells derived from these tissues except for renal cell carcinoma. These data also suggesting that JMAM4 mAb may distinguish epithelial mesotheliomas from all other cancers.

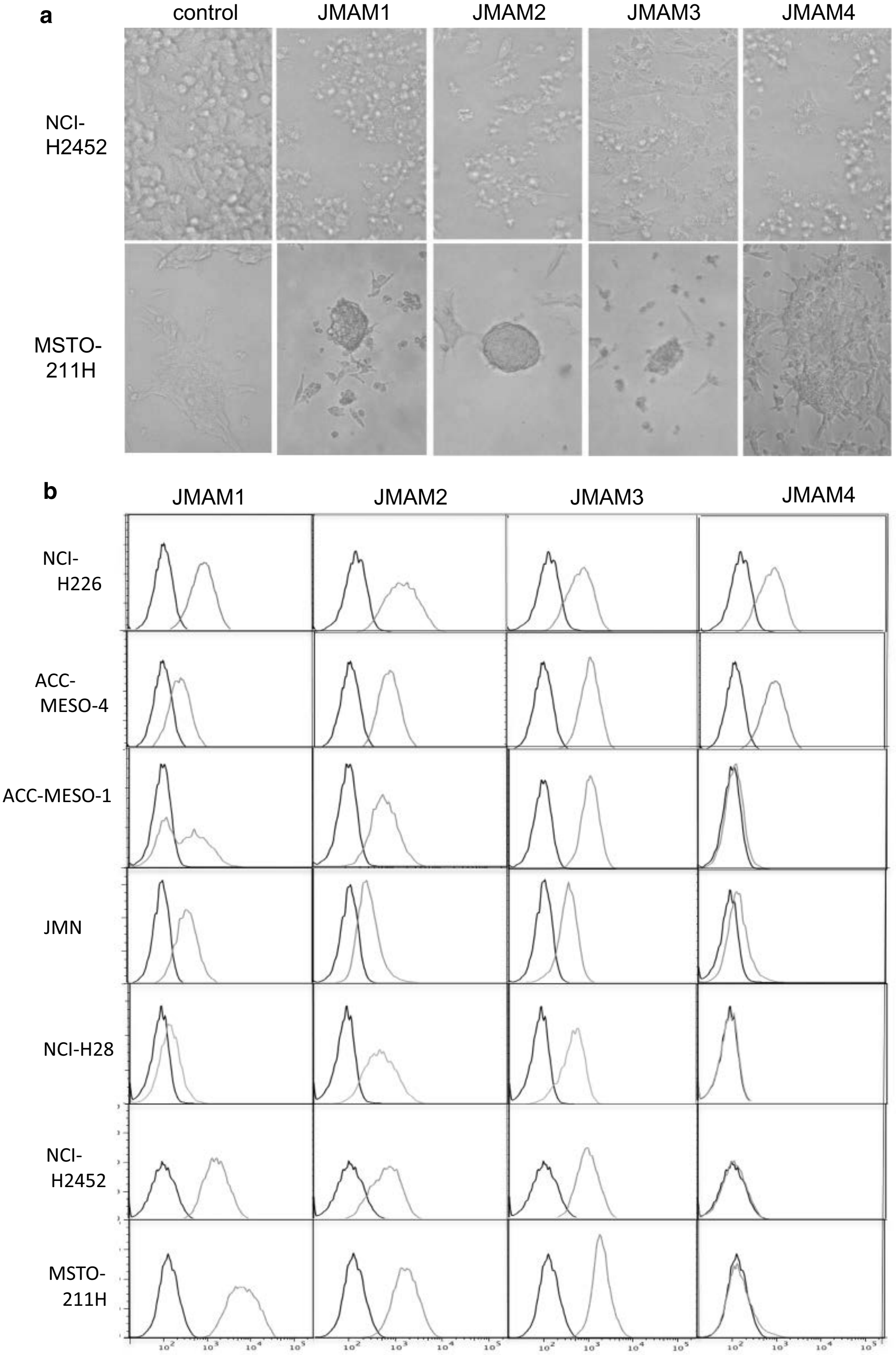

Fig. 1 Reactivity of JMAM mAbs with mesothelioma cell lines. **a** Morphological changes by JMAM mAbs. NCI-H2452 cells were incubated with hybridoma supernatants for 72 h and observed using visible light microscopy. RPMI-1640 medium with 10 % FCS served as the control (*upper column*). These findings were also reproduced using MSTO-211H cells (*lower column*). **b** Flow cytometry analysis of JMAM mAb reactivity. Mesothelioma cell lines were incubated with the hybridoma supernatant (*green* histogram) or control mouse IgG (*black* histogram), subsequently stained with Alexa Flour®-488 labeled anti-mouse IgG Ab and analyzed using flow cytometry

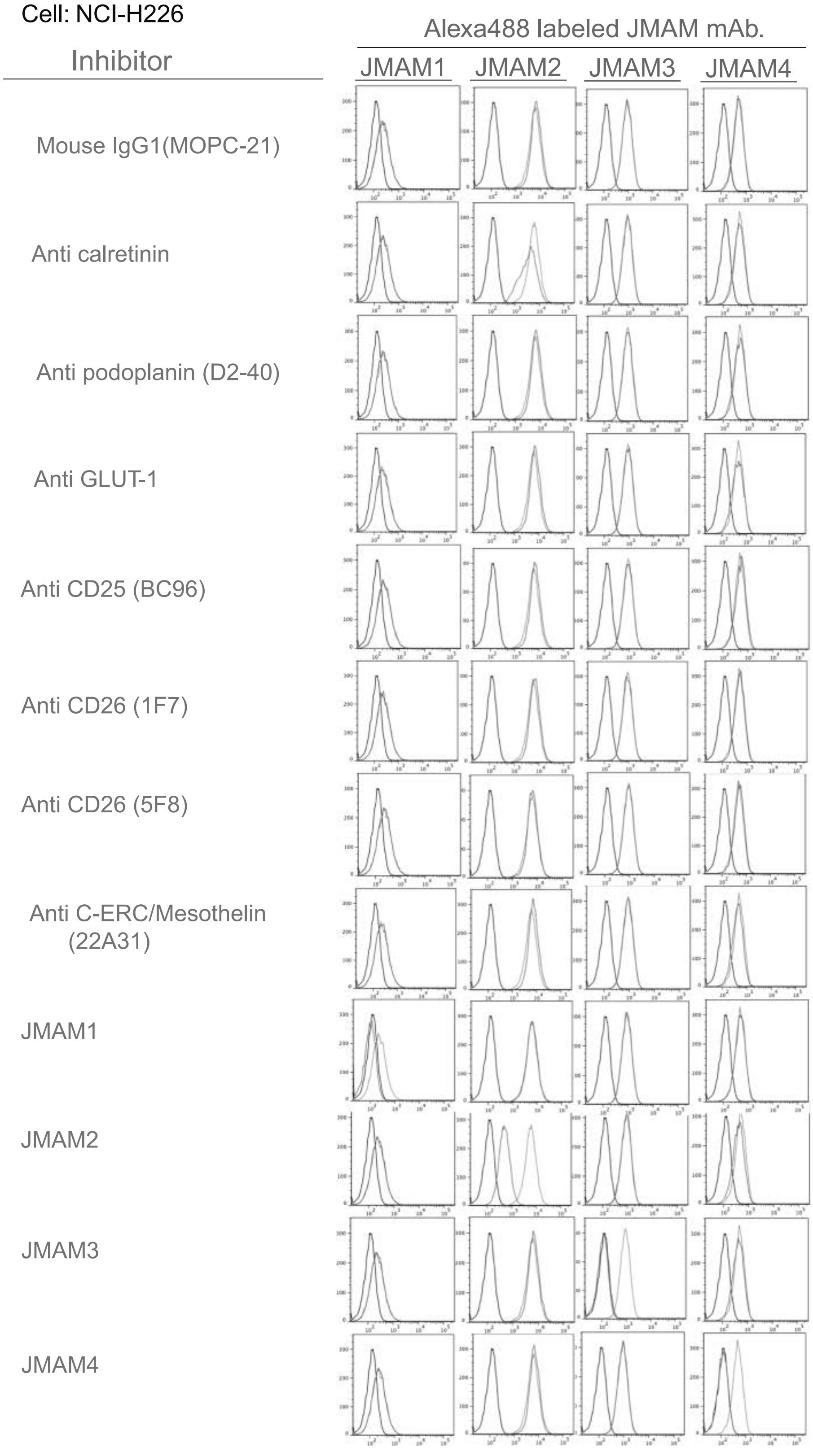

Fig. 2 Competitive inhibition of JMAM mAbs with established mAbs. Staining profiles of JMAM mAbs without or with already existent mAbs are shown by *green lines* or *red lines*, respectively

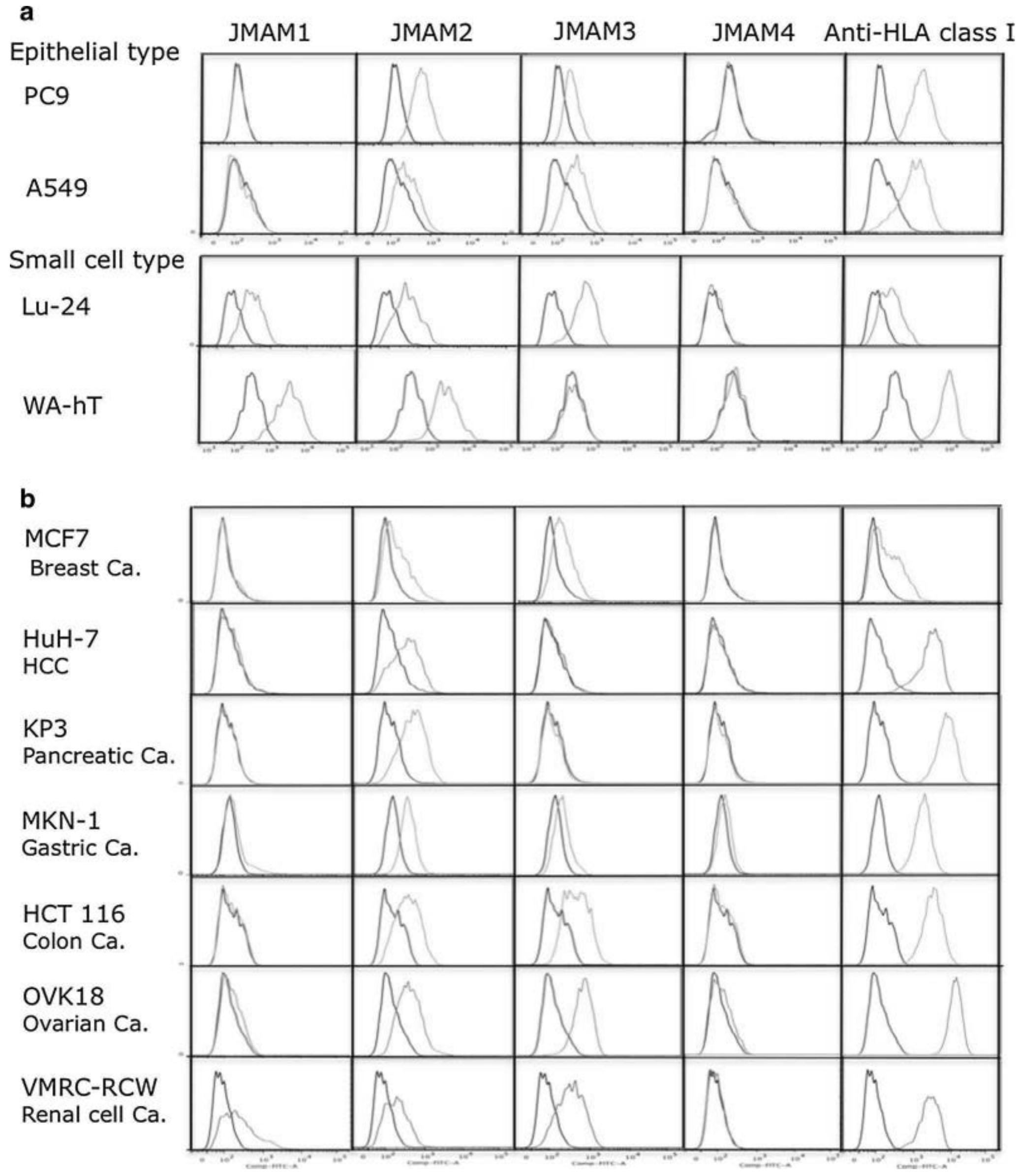

Fig. 3 Reactivity of JMAM mAbs with other cell lines. Epithelial-type and small-cell-type lung cancer (**a**) and other cancer cell lines (**b**) were incubated with hybridoma supernatants (*green* histogram) or control mouse IgG (*black* histogram), subsequently stained with Alexa Flour® 488-labeled anti-mouse IgG Ab and analyzed using flow cytometry

Analysis of mesotheliomas by mAbs

To determine whether these newly generated mAbs were suitable for immunohistochemical staining of formalin-fixed tissue sections, we used them to analyze surgically resected mesothelioma tissue specimens. Unfortunately, we did not detect staining of formalin-fixed paraffin-embedded tissue specimens (data not shown). The antigens recognized by the mAbs might have been masked or antigenically inactivated by formalin fixation.

Body fluid retention is one of the symptoms of many patients with malignant mesothelioma who are often diagnosed with mesothelioma by body fluid cytological examination. Therefore, we investigated whether the mAbs reacted with cytological samples using body fluid specimens that were fixed with ethanol. We analyzed specimens from three patients with malignant mesothelioma and those from patients suspected to have malignant mesothelioma (Fig. 4). All materials were prepared from pleural effusions.

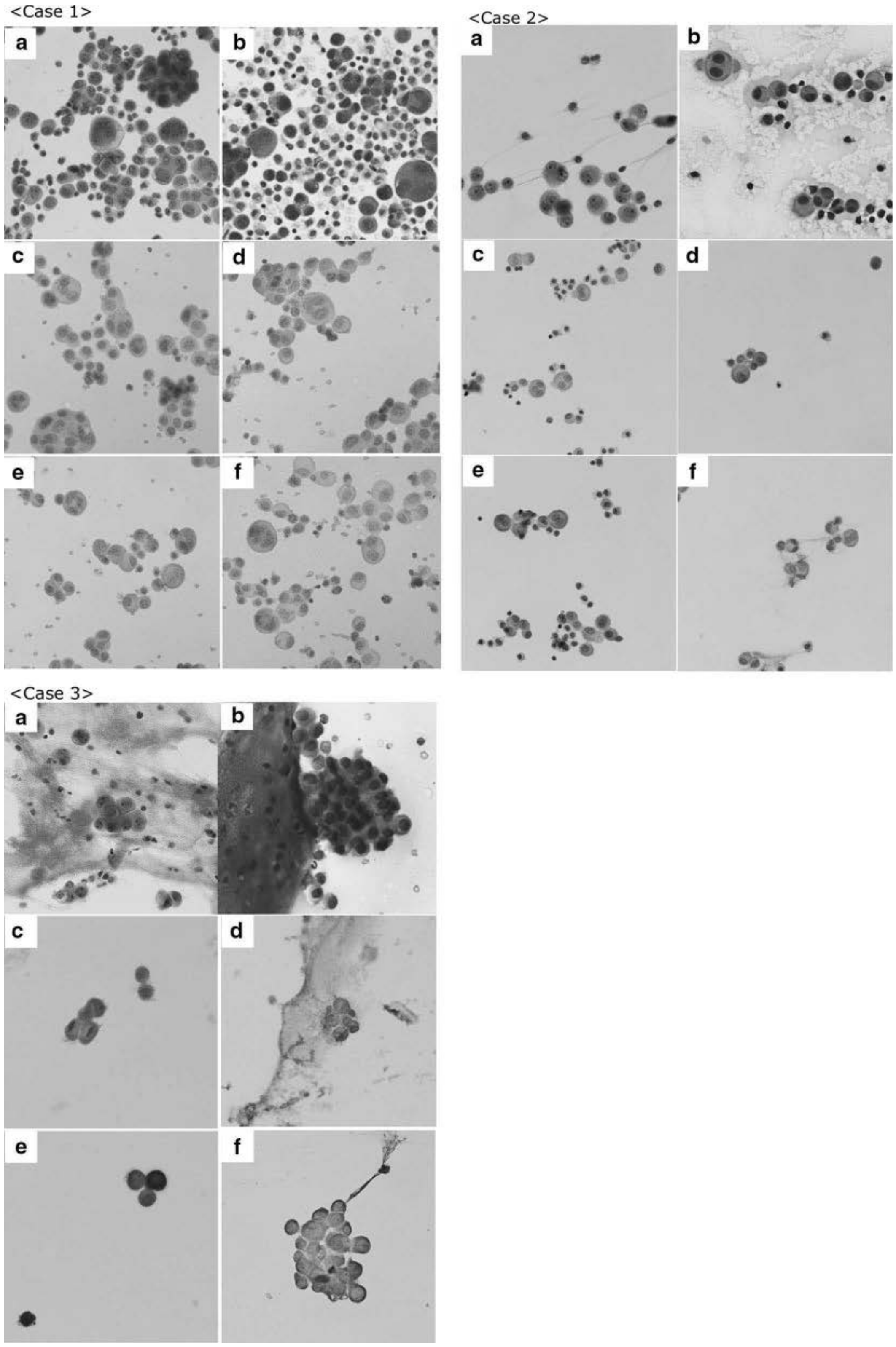
<Case 1>
a
b
c
d
e
f
<Case 2>
a
b
c
d
e
f
<Case 3>
a
b
c
d
e
f

(See figure on previous page.)

Fig. 4 Immunocytochemistry of clinical cases. **a** Papanicolaou; **b** Giemsa; **c** JMAM1; **d** JMAM2; **e** JMAM3; **f** JMAM4. Original magnification 400×. The malignant mesothelioma smear specimens, prepared from pleural effusions. *Case 1* JMAM1, JMAM2, JMAM3, and JMAM4 mAbs stained membranes. JMAM2 mAb stained membranes and the cytoplasm. *Case 2* All mAbs stained membranes. *Case 3* JMAM1 and JMAM4 mAbs stained membranes; JMAM2 and JMAM3 mAbs stained membranes and cytoplasm

Case 1 Many cell clusters were present, including tight and loose clusters with flattened cellular borders. Individual cells showed wide variation in shape and size, ranging from small to very large. The JMAM1–4 mAbs stained membranes, whereas the JMAM2 mAb stained the cytoplasm and the membrane.

Case 2 The few malignant cells present were judged Class III by Papanicolaou classification. All mAbs stained membranes clearly.

Case 3 Present were small to large clusters with knobby borders and a single-cell population. These cells had low nuclear: cytoplasmic ratios, but occasionally showed macronucleoli. The staining of membranes by mAbs JMAM1–4 was distinct. Antibodies against Podoplanin, Mesothelin, EMA, and GLUT-1 stained cell-block specimens, which confirmed these atypical cells as derived from mesothelioma (Table 1). Because JMAM1–4 mAbs stained the membranes of all mesothelioma specimens tested, they may be useful for the cytological testing of pleural effusions of patients with mesothelioma.

Histopathology and cytology of lung and mesothelial cells

Reactive normal pleura and lung immunoreactive features are shown in Fig. 5. Reactive pleural effusion mesothelial cells stained with JMAM mAbs (a); however, normal pleural mesothelium and lung tissue did not stain with JMAM mAbs (b, c).

Analysis of the effects of mAbs on the proliferation of mesothelioma cells

We next tested whether the mAbs inhibited the proliferation of the MSTO-211H mesothelioma cell line (Fig. 6). The JMAM1 and JMAM3 mAbs inhibited the proliferation of MSTO-211H cells as a function of their dose. Thus, proliferation was reduced by at least 50 and 40 % by 0.4 µg/ml of JMAM1 or JMAM3 mAbs, respectively.

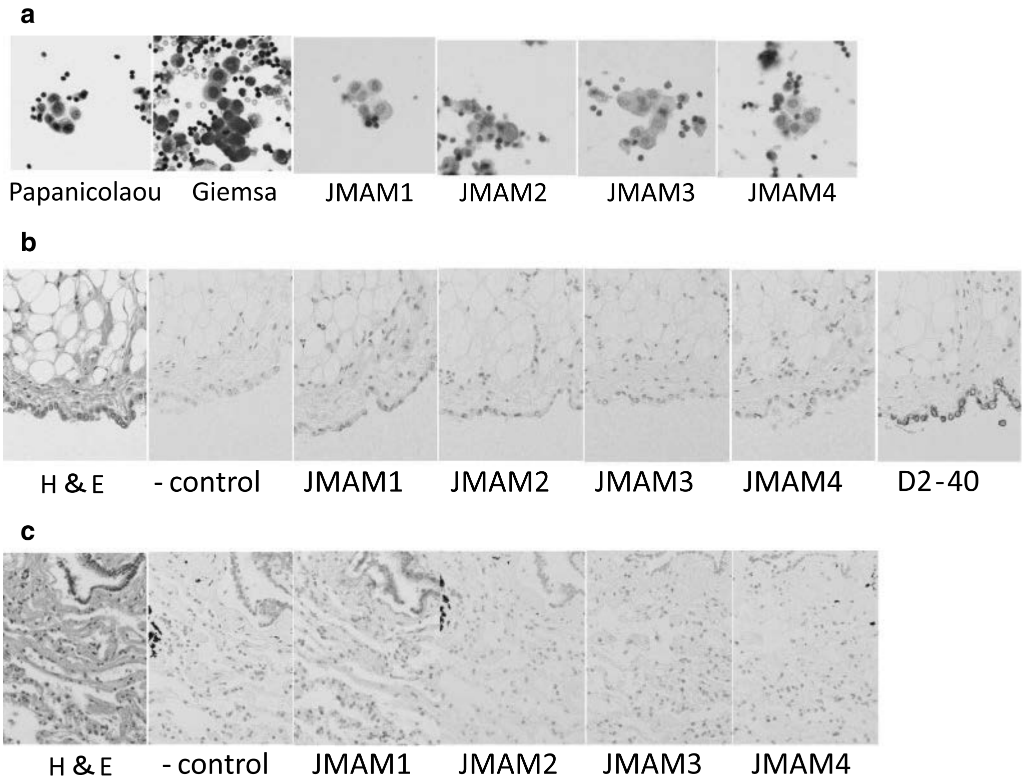

Fig. 5 Histopathology and cytological findings of reactive mesothelial cells, normal pleura and lung, with immunoreactive features. **a** Pleural effusion (reactive mesothelial cells, 1000×). **b** Normal pleura (400×). **c** Normal lung (400×)

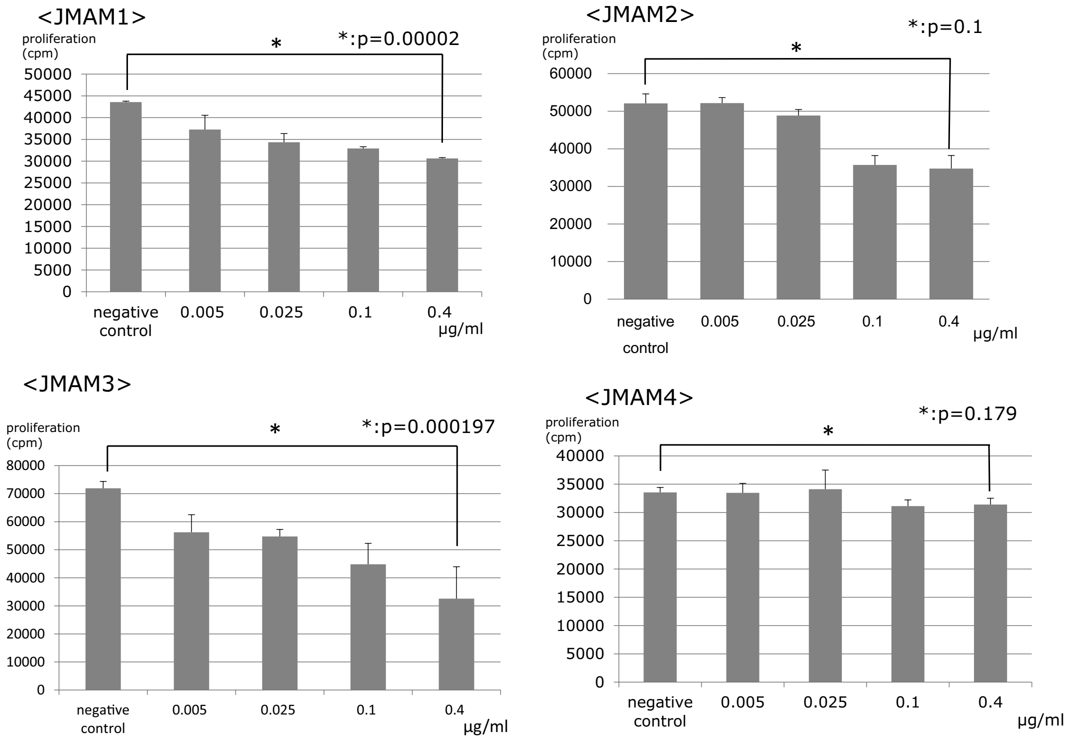

Fig. 6 Proliferation of MSTO-211H cells in the presence of JMAM1–4 mAbs. JMAM1–4 mAbs were added at the indicated concentrations to cultures of MSTO-211H mesothelioma cells. JMAM1, $P < 0.05$; JMAM2, $P = 0.1$; JMAM3, $P < 0.05$; JMAM4, $P = 0.18$

The JMAM2 mAb inhibited cell proliferation to some extent. The JMAM4 mAb did not inhibit the proliferation of MSTO-211H cells. These results indicate that JMAM1 and JMAM2 mAbs may be useful for treating patients with mesothelioma, at least those with the epithelioid phenotype.

Analysis of the effect of JMAM mAbs on migration of mesothelioma cells

Cell motility is an essential process of tumor metastasis and progression. Therefore, we investigated whether the mAbs would affect the migration of mesothelioma cells using a wound-healing assay. The anti-mesothelioma mAbs JMAM1, JMAM2, and JMAM3 significantly inhibited the ability of NCI-H226 cells to migrate to and close an experimentally induced wound (Fig. 7). These results show that the anti-mesothelioma mAbs inhibited the motility of mesothelioma cells and suggest that the JMAM1–4 mAbs may possess a remarkable ability to inhibit the progression of mesotheliomas.

Analysis of the effect of JMAM mAbs on invasion of mesothelioma cells

We assessed the cell invasion ability of mesothelioma NCI-H226 cells. Significant inhibition of invasion was observed by JMAM mAbs compared with control mouse IgG1 Ab (Fig. 8). JMAM1 mAb significantly decreased the trans membrane migration of NCI-H226 cells compared with cells treated with the mouse IgG1 isotype control.

Discussion

Differentiating between a mesothelioma and a papillary adenocarcinoma is sometimes very difficult [25]. Clinicians recommend that the definitive diagnosis of mesothelioma may be achieved using immunohistochemical analysis of cytological or histological specimens with currently available antibodies [8]. Many mAbs are developed for the diagnosis of and therapy for mesothelioma. Previously, we focused on CD26 as a novel therapeutic target for mesothelioma and have developed a humanized anti-CD26 mAb (clone: YS110), which is currently being evaluated in a phase I clinical trial for patients with malignant mesothelioma [26]. We also developed anti-human CD26 mAbs (clone: 1F7, 5F8) that clearly and reliably detect the denatured CD26 molecule in formalin-fixed paraffin-embedded tissue [27]. Although many antibodies are available to aid diagnosis, no single antibody can unambiguously distinguish mesotheliomas from other carcinomas. Anti-CD26 mAb reacts with epithelial and sarcomatoid mesotheliomas. However, anti-CD26 mAb also reacts with several other tumor cells and lymphocytes.

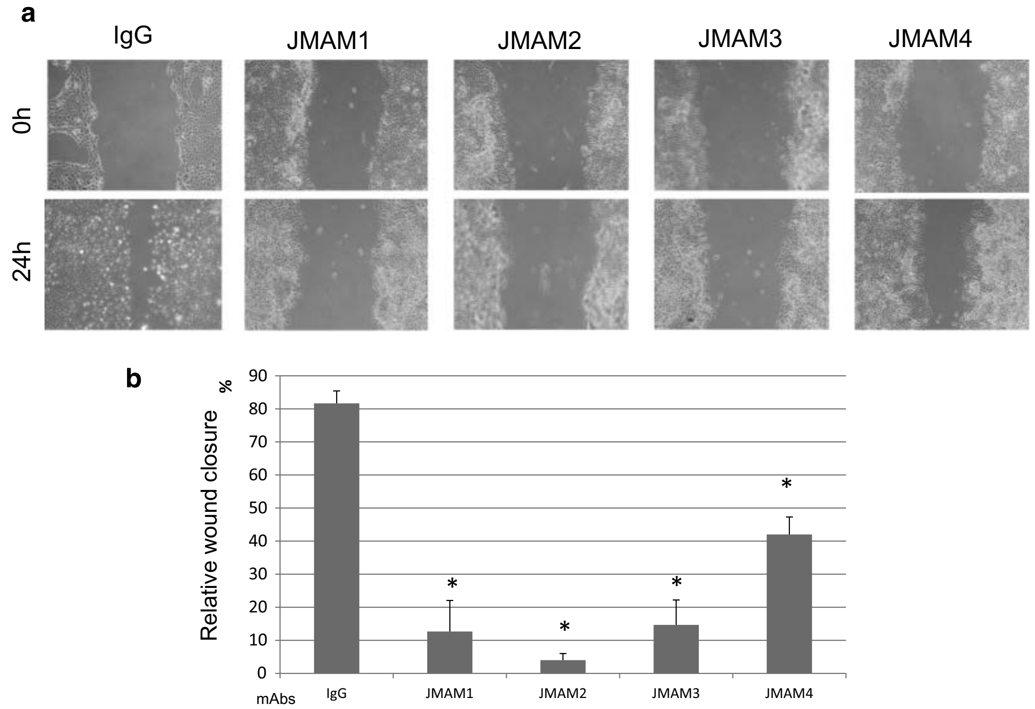

Fig. 7 Wound-healing assays. **a** Representative images of wound closure assays after NCI-H226 cells were incubated with anti-mesothelioma antibodies or control mouse IgG. **b** The extent of wound closure was calculated by analyzing the scratched area covered by the cells after 24 h using ImageJ software. The data were normalized to the control values. The data are represented as the mean ± SD of three independent experiments. *P < 0.05; treated versus IgG control

Anti-mesothelin mAbs react with epithelial but not sarcomatoid mesotheliomas [13]. In contrast, JMAM1, JMAM2, and JMAM3 mAbs react with both subtypes. Anti-mesothelin mAbs react with renal cell carcinomas and pancreatic and ovarian cancers [28–30], unlike the JMAM4 mAbs that did not react with lung, ovarian, or renal cell carcinomas or any of the other cancer cell lines tested. JMAM1 mAb did not cross-react with other carcinoma cell lines except for small-cell-type lung cancer cell lines and renal cell carcinoma cell lines. Taken together, our newly generated mAbs are more specific for mesothelioma than other diagnostic mAbs and may be helpful in the differential diagnosis of mesothelioma. Novel anti-mesothelioma mAbs may either serve as tools to diagnose mesotheliomas as stand-alone reagents or together with other diagnostic mAbs.

It is now commonly accepted that therapeutic mAbs dramatically improve the treatment of cancer patients. However, after repeated therapy, not all patients respond to therapeutic mAbs [31] because clones appear during the course of treatment those do not express the target. Therefore, additional therapeutic options are required to treat these patients. Common therapeutic mAbs against cell surface molecules exert their effects largely through immunological mechanisms, including complement-dependent cytotoxicity (CDC) and antibody-dependent cellular cytotoxicity (ADCC). ADCC and CDC may not be effective for treating patients with cancer because the patients may be immunocompromised due to radiation, chemotherapy, and the malignancy itself. However, in addition to indirectly inducing Fc-dependent cell death, several mAbs possess a direct antitumor effect that induces cell arrest or programmed cell death [32, 33].

Therefore, in this study, we investigated reactivity with mesothelioma cells as well as the direct antitumor effect of the newly generated anti-mesothelioma mAbs. We found that JMAM1 and JMAM3 mAbs inhibited the proliferation of the MSTO-211H mesothelial cell line, and JMAM1–4 mAbs inhibited wound closure by NCI-H226 cells to varying degrees. JMAM1–4 also inhibited invasion of NCI-H226 cells to various degrees. Unfortunately, we did not identify the target molecules of JMAM1–4 mAbs. Nevertheless, the promising anti-mesothelioma activities of these antibodies warrant continued studies in vitro and in vivo that will include efforts to identify their targets. Our strategy for generating diagnostic and therapeutic mAbs specific for tumor cells differs from those of conventional methods that employ immunization with peptides or DNA. Specifically, we

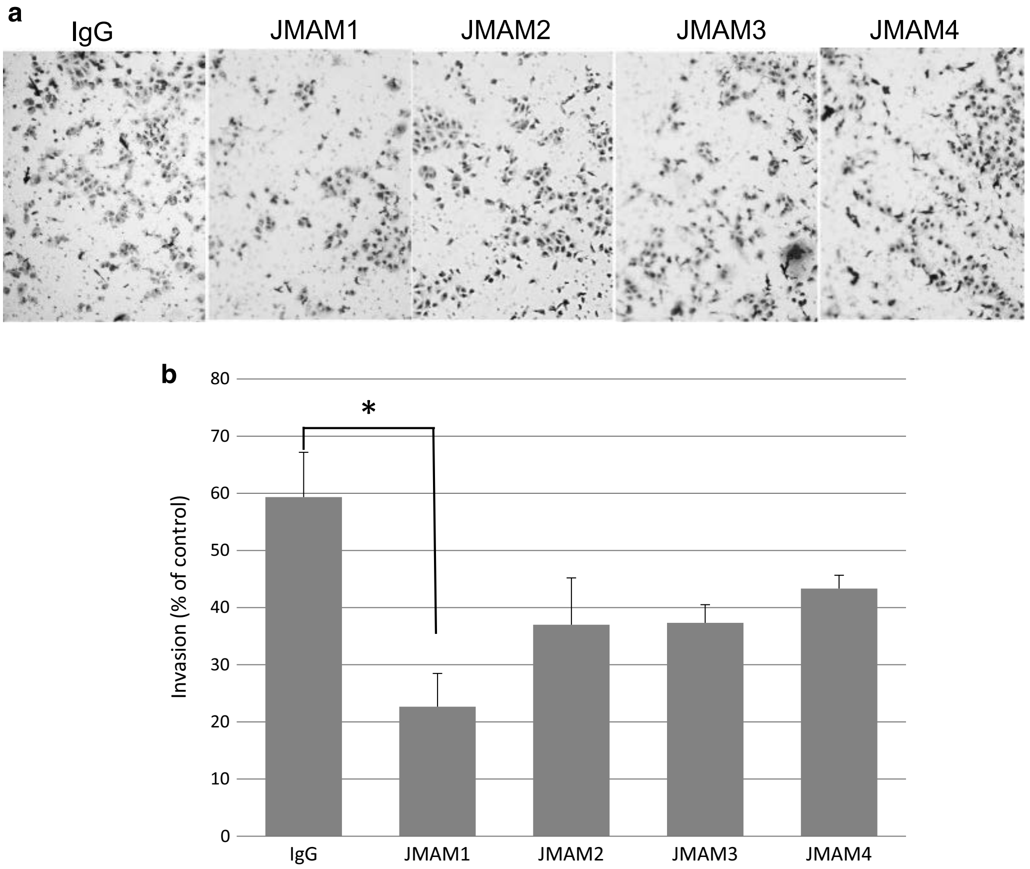

Fig. 8 Analysis of the effect of JMAM mAbs on invasion of mesothelioma cells. Cells (NCI-H226) were seeded into the *upper chamber* and the *lower chamber* was filled with medium as described in the "Methods" section. Photos were captured by a light microscope at ×200 (**a**). The migration of cells was measured by counting the migrating cells on the lower surface of the membrane in 3 fields (**b**). JMAM1, *$P < 0.05$; JMAM2, $P = 0.12$; JMAM3, $P = 0.08$; JMAM4, $P = 0.18$. Each mAb treated versus IgG control

immunized a mouse with three different mesothelioma cell lines and screened the antibodies using a different mesothelioma cell line to potentially obtain novel mAbs that react with unknown targets on the surface of mesothelioma cells.

Conclusion

Newly established anti-mesothelioma mAbs, JMAM1–4, are potentially useful as diagnostic and therapeutic agents for mesothelioma. Moreover, our novel strategy for establishing anti-tumor mAbs may facilitate the development of new diagnostic and therapeutic techniques for other malignancies as well as mesothelioma.

Authors' contributions

NM, SM, RO and MA designed and performed experiments and wrote the paper. MW, KK and NO performed experiments. CM and OH supervised part of the experiments. All authors read and approved the final manuscript.

Author details

[1] Department of Pathology, Kyorin University School of Medicine, 6-20-2, Shinkawa, Mitaka-shi, Tokyo 181-8611, Japan. [2] Departments of Pathology and Oncology, Juntendo University School of Medicine, 2-1-1, Hongo, Bunkyo-ku, Tokyo 113-8421, Japan. [3] Department of Pathology, Tokyo Medical University Hachioji Medical Center, 1163 Tatemachi, Hachioji-shi, Tokyo 193-0998, Japan. [4] Therapy Development and Innovation for Immune Disorders and Cancers, Juntendo University School of Medicine, 2-1-1, Hongo, Bunkyo-ku, Tokyo 113-8421, Japan.

Acknowledgements

We thank Dr. T Kamei for constructive discussions, the staff of the Animal Care Committee for animal care, and the staff of the Pathology Department for their assistance in collecting body fluid samples and for consultations.

Competing interests

The authors declare that they have no competing interests.

Ethics

This study has been performed according to the principles of Helsinki and was approved by the Ethics Committee at Juntendo University School of Medicine.

Funding

S. Matsuoka received a Grant from the Japan Society for the Promotion of Science (Web: https://kaken.nii.ac.jp/d/p/15K06880.en.html, Grant Number: 15K06880).

The funders had no role in the study design, data collection and analysis, decision to publish, or preparation of the manuscript.

Received: 20 August 2015 Accepted: 16 June 2016
Published online: 24 June 2016

References

1. Kazan-Allen L. Asbestos and mesothelioma: worldwide trends. Lung Cancer. 2005;49(Suppl 1):S3–8.
2. Robinson BW, Musk AW, Lake RA. Malignant mesothelioma. Lancet. 2005;5:397–408.
3. Carbone M, Ly BH, Dodson RF, Pagano I, Morris PT, Dogan UA, Gazdar AF, Pass HI, Yang H. Malignant mesothelioma: facts, myths and hypotheses. J Cell Physiol. 2012;227:44–58.
4. US Department of the Interior, US Geological Survey. Mineral commodity summaries 2015. 2015. p. 22–23.
5. Nguyen G, Akin MM, Villanueva RR, Slatnik J. Cytopathology of malignant mesothelioma of the pleura in fine-needle aspiration biopsy. Diagn Cytopathol. 1999;21:253–9.
6. Whitaker D. The cytology of malignant mesothelioma. Cytopathology. 2000;11:139–51.
7. Fassina A, Fedeli U, Corradin M, Da FM, Fabbris L. Accuracy and reproducibility of pleural effusion cytology. Leg Med. 2008;10:20–5.
8. Pu RT, Pang Y, Michael CW. Utility of WT-1, p63, MOC31, mesothelin, and cytokeratin (CK903 and CK5/6) immunostains in differentiating adenocarcinoma, squamous cell carcinoma, and malignant mesothelioma in effusions. Diagn Cytopathol. 2008;36:20–5.
9. Chung A, Inai K, Samet J. Tumor of the pleura. In: Travis WD, Muller BE, Hermelink HK, Harris CG, editors. Pathology and genetics. Tumours of the lung, pleura, thymus and heart. Lyon: IARC Press; 2004. p. 128–42.
10. Robinson BW, Lake RA. Advances in malignant mesothelioma. N Engl J Med. 2005;353:1591–603.
11. Inai K. Pathology of mesothelioma. Environ Health Prev Med. 2008;13:60–4.
12. Ordóñez NG. Immunohistochemical diagnosis of epithelioid mesotheliomas: a critical review of old markers, new markers. Hum Pathol. 2002;33:953–67.
13. Ordóñez NG. Value of mesothelin immunostaining in the diagnosis of mesothelioma. Mod Pathol. 2003;16:192–7.
14. Betta P, Magnani C, Bensi T, Trincheri FN, Oreccha S. Immunohistochemistry and molecular diagnostics of pleural malignant mesothelioma. Arch Pathol Lab Med. 2012;136:253–61.
15. Takeshima Y, Inai K, Amatha V, Gemba K, Aoe K, Fujimoto N, Kato K, Kishimoto T. Accurancy of pathological diagnosis of mesothelioma cases in Japan: clinicopathological analysis of 382 cases. Lung Cancer. 2009;66:191–7.
16. Kao CS, Vardy J, Chatfield M, Corte P, Pavlakis N, Clarke C, Zandwijk NV, Clarke S. Validation of prognostic factors in malignant pleural mesothelioma. Clin Lung Cancer. 2013;14:70–7.
17. Inamoto T, Yamada T, Ohnuma K, Kina S, Takahashi N, Yamochi T, Inamoto S, Katsuoka Y, Hosono O, Tanaka H, Dang NH, Morimoto C. Humanized Anto-CD26 monoclonal antibody as a treatment for malignant mesothelioma tumors. Clin Cancer Res. 2007;13:4191–200.
18. Yamada K, Hayashi M, Du W, Ohnuma K, Sakamoto M, Morimoto C. Yamada T. cc. Cancer Cell International. 2009;9:17.
19. Köhler G, Milstein C. Continuous cultures of fused cells secreting antibody of predefined specificity. Nature. 1975;256:495–7.
20. Koprowski H, Steplewski Z, Mitchell K, Herlyn M, Herlyn D, Fuhrer P. Colorectal carcinoma antigens detected by hybridoma antibodies. Somatic Cell Genet. 1979;5:957–72.
21. Bast CR, Feeney M, Lazarus H, Nadler LM, Colvin BR, Knapp CR. Reactivity of a monoclonal antibody with human ovarian carcinoma. J Clin Invest. 1981;68:1331–7.
22. Maloney DG, Grillo-López AJ, White CA, Bodkin D, Schilder RJ, Neidhart JA, Janakiraman N, Foon KA, Liles TM, Dallaire BK, Wey K, Royston I, Davis T, Levy R. IDEC-C2B8 (Rituximab) anti-CD20 monoclonal antibody therapy in patients with relapsed low-grade non-Hodgkin's lymphoma. Blood. 1997;90(6):2188–95.
23. Ishikawa K, Segawa T, Hagiwara Y, Maeda M, Abe M, Hino O. Establishment of novel monoclonal antibody to human ERC/mesothelin useful for study and diagnosis of ERC/mesothelin-expressing cancers. Pathol Int. 2009;59:161–6.
24. Lewis GD, Figari I, Fendly B, Wong WL, Carter P, Gorman C, Shepard HM. Differential responses of human tumor cell lines to anti-p185HER2 monoclonal antibodies. Cancer Immunol Immunother. 1993;37:255–63.
25. Kwee WS, Veldhuizen RW, Alons CA, Morawetz F, Boon ME. Quantitative and qualitative differences between benign and malignant mesothelial cells in pleural fluid. Acta Cytol. 1982;26:401–6.
26. Aoe K, Amatya VJ, Fujimoto N, Ohnuma K, Hosono O, Hiraki A, Fujii M, Yamada T, Dang NH, Takeshima Y, Inai K, Kishimoto T, Morimoto C. CD26 overexpression is associated with prolonged survival and enhanced chemosensitivity in malignant pleural mesothelioma. Clin Cancer Res. 2012;18:1447–56.
27. Hatano R, Yamada T, Matsuoka S, Iwata S, Yamazaki H, Komiya E, Okamoto T, Dang NM, Ohnuma K, Morimoto C. Establishment of monoclonal anti-human CD26 antibodies suitable for immunostaining of formalin-fixed tissue. Diagn Pathol. 2014. doi:10.1186/1746-1596-9-30.
28. Robinson BW, Creaney J, Lake R, Nowark A, Musk AW, de Klerk N, Winzell P, Hellstrom KE, Helstrom I. Mesothelin-family proteins and diagnosis of mesothelioma. Lancet. 2003;362:1612–6.
29. Hellstrom I, Raycraft J, Kanan S, Sardesai NY, Verch T, Yang Y, Hellstrom KH. Mesothelin variant 1 is released from tumor cells as a diagnostic marker. Cancer Epidemiol Biomark Prev. 2006;15:1014–20.
30. Scholler N, Fu N, Yang Y, Ye Z, Goodman GE, Hellstrom KE, Hellstrom I. Soluble member(s) of the mesothelin/megakaryocyte potentiating factor family are detectable in sera from patients with ovarian carcinoma. Proc Natl Acad Sci USA. 1999;6:11531–6.
31. O'Brien SM, Kantarjian H, Thomas DA, Giles FJ, Freireich EJ, Cortes J, Lemer S, Keating MJ. Rituximab dose-escalation trial in chronic lymphocytic leukemia. J Clin Oncol. 2001;19:2165–70.
32. Matsuoka S, Asano Y, Sano K, Kishimto H, Yamashita I, Yorifuji H, Utsuyama M, Hirokawa K, Tada T. A novel type of cell death of lymphocytes induced by a monoclonal antibody without participation of lymphocytes. J Exp Med. 1995;181:2007–15.
33. Yuniel FM, Alejandro LR. Lonely killers. mAbs. 2008;3:528–34.

Submit your next manuscript to BioMed Central and we will help you at every step:

- We accept pre-submission inquiries
- Our selector tool helps you to find the most relevant journal
- We provide round the clock customer support
- Convenient online submission
- Thorough peer review
- Inclusion in PubMed and all major indexing services
- Maximum visibility for your research

Submit your manuscript at
www.biomedcentral.com/submit

BioMed Central

Data in Brief 8 (2016) 1377–1380

Contents lists available at ScienceDirect

Data in Brief

journal homepage: www.elsevier.com/locate/dib

Data Article

Data on CUX1 isoforms in idiopathic pulmonary fibrosis lung and systemic sclerosis skin tissue sections

Tetsurou Ikeda [a,b,c,*,1], Maria Fragiadaki [b], Xu Shi-wen [a], Markella Ponticos [a], Korsa Khan [a], Christopher Denton [a], Patricia Garcia [a], George Bou-Gharios [b], Akio Yamakawa [c], Chikao Morimoto [c], David Abraham [a]

[a] *Royal Free and University College Medical School, London, UK*
[b] *Imperial College School of Medicine, London, UK*
[c] *University of Tokyo, Institute of Medical Science, Tokyo, Japan*

A R T I C L E I N F O

Article history:
Received 5 July 2016
Received in revised form
4 August 2016
Accepted 8 August 2016
Available online 10 August 2016

A B S T R A C T

This data article contains complementary figures related to the research article entitled, “Transforming growth factor-β-induced CUX1 isoforms are associated with fibrosis in systemic sclerosis lung fibroblasts” (Ikeda et al. (2016) [2], http://dx.doi.org/10.1016/j.bbrep.2016.06.022), which presents that TGF-β increased CUX1 binding in the proximal promoter and enhancer of the *COL1A2* and regulated COL1. Further, in the scleroderma (SSc) lung and diffuse alveolar damage lung sections, CUX1 localized within the α-smooth muscle actin (α-SMA) positive cells (Fragiadaki et al., 2011) [1], “High doses of TGF-beta potently suppress type I collagen via the transcription factor CUX1” (Ikeda et al., 2016) [2]. Here we show that CUX1 isoforms are localized within α-smooth muscle actin-positive cells in SSc skin and idiopathic pulmonary fibrosis (IPF) lung tissue sections. In particular, at the granular and prickle cell layers in the SSc skin sections, CUX1 and α-SMA are co-localized. In addition, at the fibrotic loci in the IPF lung tissue sections, CUX1 localized within the α-smooth muscle actin (α-SMA) positive cells.

DOI of original article: http://dx.doi.org/10.1016/j.bbrep.2016.06.022
[*] Corresponding author at: University of Tokyo, Institute of Medical Science, Tokyo, Japan.
E-mail address: ikedatetsurou@kochi-u.ac.jp (T. Ikeda).
[1] Present address: Kochi Medical School, Kochi, Japan.

http://dx.doi.org/10.1016/j.dib.2016.08.014
2352-3409/© 2016 The Authors. Published by Elsevier Inc. This is an open access article under the CC BY license (http://creativecommons.org/licenses/by/4.0/).

© 2016 The Authors. Published by Elsevier Inc. This is an open access article under the CC BY license (http://creativecommons.org/licenses/by/4.0/).

Specifications Table

Subject area	*Biology*
More specific subject area	*Fibrosis*
Type of data	*Image*
How data was acquired	*Confocal microscopy (Zeiss Axioscope light microscope, Carl Zeiss)*
Data format	*Analysed*
Experimental factors	For immunohistochemistry, sections were pretreated with methanol, followed by antigen retrieval in heated 10-mM citrate buffer (pH 6).
Experimental features	The primary antibodies were CUX1 antibody (0.2 mg/ml) and the monoclonal anti-α-SMA clone, 1a Cy3-conjugated antibody (0.7 mg/ml). Sections were sequentially incubated with a 1/200 dilution of an Alexa 488 secondary antibody.
Data source location	*London, United Kingdom*
Data accessibility	*Data presented in this article*

Value of the data

- The data provides the evidence that CUX1 isoforms localise within α-smooth muscle actin-positive cells in SSc skin tissue sections, especially in the granular and prickle cell layers.
- The data provides the evidence that CUX1 isoforms localise within α-smooth muscle actin-positive cells at the fibrotic loci in idiopathic pulmonary fibrosis (IPF) lung tissue sections.
- The data could further help research on the function of CUX1 isoforms in fibrosis-related diseases.

1. Data

Immunohistochemistry revealed the presence of α-SMA-positive fibrotic loci, which are characteristic in the lungs of patients with IPF and in the skin of patients with SSc. In the IPF tissue sections, CUX1 localised at alveolar cells and fibrotic loci. In addition, CUX1 localised within α-SMA-positive cells but was not observed in the normal lung section (Fig. 1). In the SSc skin tissue sections, CUX1 co-localised with α-SMA at the granular cell layer, prickle cell layer and fibrotic loci in the epidermis. In addition, CUX1 localised within α-SMA-positive cells. These were not observed at the epidermis in the normal skin sections (Fig. 2).

2. Experimental design, materials and methods

For formalin-fixed, paraffin-embedded specimens, the tissues were fixed and hydrated as described previously [1,2]. For immunohistochemistry, the sections were pretreated with methanol (VWR, Lutterworth, UK), followed by antigen retrieval in heated 10-mM citrate buffer (pH 6). The primary antibodies were CUX1 antibody (0.2 mg/ml) and the monoclonal anti-α-SMA clone, 1a Cy3-conjugated antibody (0.7 mg/ml). The sections were sequentially incubated with a 1/200 dilution of

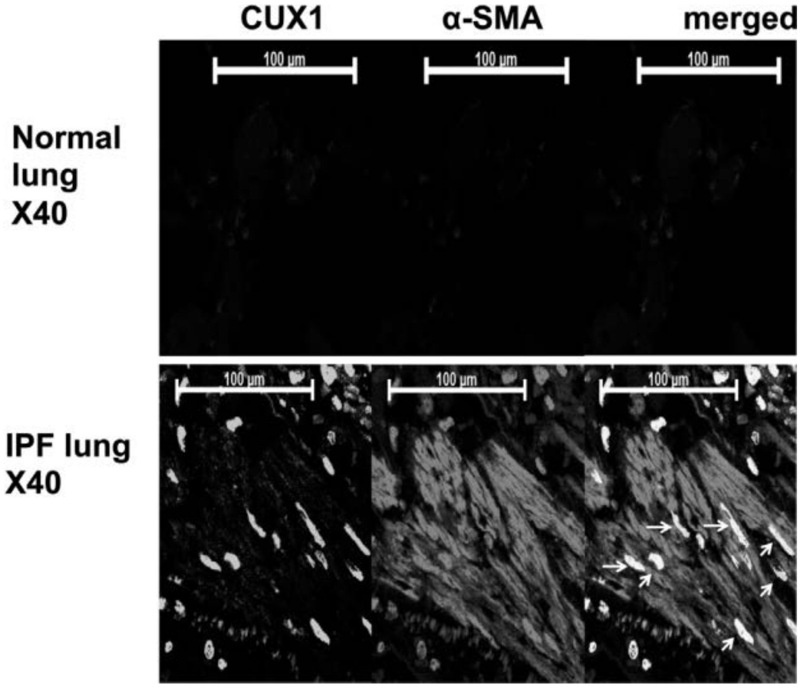
CUX1
α-SMA
merged
100 µm
100 µm
100 µm
Normal lung X40
100 µm
100 µm
100 µm
IPF lung X40

Fig. 1. Idiopathic pulmonary fibrosis (IPF) lung tissue sections stained with antibodies against CUX1 and α-smooth muscle actin (SMA). The figure shows fibrotic loci that were stained by CUX1 and α-SMA antibodies. Alveolar cells around the loci were positive for CUX1 and α-SMA. CUX1 localised within α-SMA-positive cells. Normal lung sections were used as negative control for CUX1 and α-SMA.

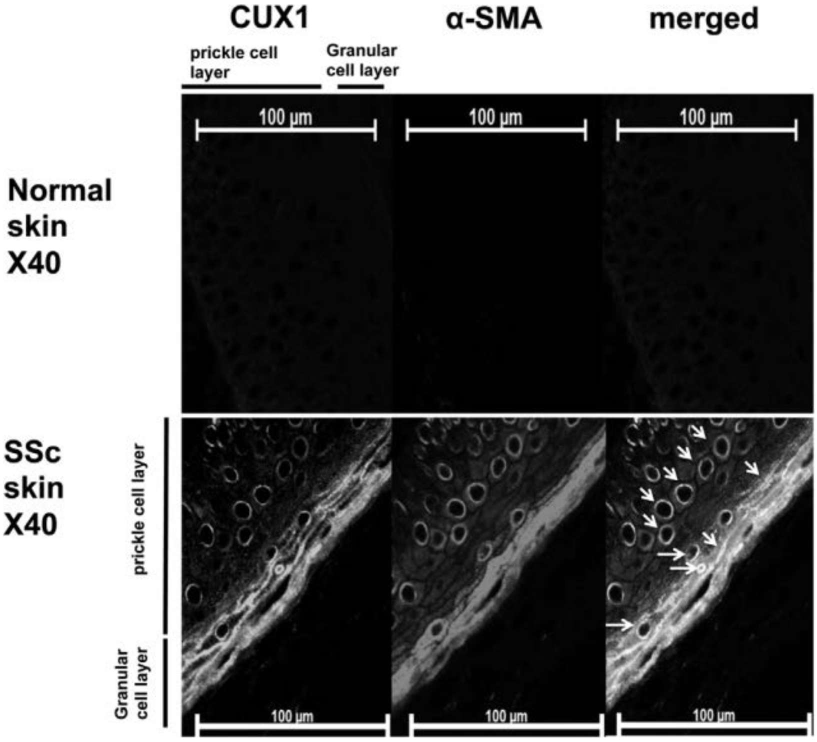
CUX1
α-SMA
merged
prickle cell layer
Granular cell layer
100 µm
100 µm
100 µm
Normal skin X40
SSc skin X40
prickle cell layer
Granular cell layer
100 µm
100 µm
100 µm

Fig. 2. Systemic sclerosis (SSc) skin tissue sections stained with antibodies against CUX1 and α-smooth muscle actin (SMA). The figure shows epidermis that were stained by CUX1 and α-SMA antibodies. The granular and prickle cells in the epidermis were positive for CUX1 and α-SMA. CUX1 localised within α-SMA-positive cells. Normal skin sections were used as negative control for CUX1 and α-SMA.

an Alexa 488 secondary antibody. The slides were viewed and photographed using a Zeiss Axioscope light microscope with Axiovision software.

Acknowledgments

This work was partly supported by a Grant from the Japanese Society for the Promotion of Science (Grant no. 17109011). Furthermore, this work was supported by the Global COE Program 'Center of Education and Research for the Advanced Genome-Based Medicine-For personalized medicine and the control of worldwide infectious disease,' MEXT Japan. The authors would like to thank Enago for the English language review.

Transparency document. Supplementary material

Transparency data associated with this article can be found in the online version at http://dx.doi.org/10.1016/j.dib.2016.08.014.

References

[1] M. Fragiadaki, T. Ikeda, A. Witherden, R.M. Mason, D. Abraham, G. Bou-Gharios, High doses of TGF-beta potently suppress type I collagen via the transcription factor CUX1, Mol. Biol. Cell 22 (2011) 1836–1844.

[2] T. Ikeda, M. Fragiadaki, X. Shi-wen, M. Ponticos, K. Khan, C. Denton, P. Garcia, G. Bou-Gharios, A. Yamakawa, C. Morimoto, D. Abraham, Transforming growth factor-β-induced CUX1 isoforms are associated with fibrosis in systemic sclerosis lung fibroblasts, Biochem. Biophys. Rep. 7 (2016) 246–252.

Critical Reviews™ in Immunology, 36(3):163–237 (2016)

Role of IL-26⁺CD26⁺CD4 T Cells in Pulmonary Chronic Graft-Versus-Host Disease and Treatment with Caveolin-1-Ig Fc Conjugate

Kei Ohnuma,[a,*] Ryo Hatano,[a] Takumi Itoh,[a] Noriaki Iwao,[b] Nam H. Dang,[c] Chikao Morimoto[a]

[a]Department of Therapy Development and Innovation for Immune Disorders and Cancers, Graduate School of Medicine, Juntendo University, 2-1-1, Hongo, Bunkyo-ku, Tokyo 113-8421, Japan; [b]Department of Hematology, Juntendo University Shizuoka Hospital, Nagaoka 1129, Izunokuni-city, Shizuoka 410-2295, Japan; [c]Division of Hematology/Oncology, University of Florida, 1600 SW Archer Road- Box 100278, Room MSB M410A, Gainesville, FL 32610, U.S.A.

*Address all correspondence to: Dr. K. Ohnuma, Department of Therapy Development and Innovation for Immune Disorders and Cancers, Graduate School of Medicine, Juntendo University, 2-1-1, Hongo, Bunkyo-ku, Tokyo 113-8421, Japan; Tel.: +81-3-3868-2310; Fax: +81-3-3868-2310: E-mail: kohnuma@juntendo.ac.jp.

ABSTRACT: Obliterative bronchiolitis is the primary noninfectious pulmonary complication after allogeneic hematopoietic cell transplantation and the only pathognomonic manifestation of pulmonary chronic graft-versus-host disease (cGVHD). In our recent study, we identified a novel effect of IL-26, which is absent in rodents, on transplant related-obliterative bronchiolitis. Sublethally irradiated NOD/Shi-*scid*IL2rγ^{null} mice transplanted with human umbilical cord blood gradually exhibited obliterative bronchiolitis with increased collagen deposition and predominant infiltration with human IL-26$^+$CD26$^+$CD4 T cells. Moreover, we showed that IL-26 increased collagen synthesis in fibroblasts *in vitro* and that collagen contents were increased in a murine GVHD model using *IL26* transgenic mice. *In vitro* analysis demonstrated a significant increase in IL-26 production by CD4 T cells following CD26 costimulation, while immunoglobulin Fc domain fused with the N-terminal of caveolin-1, the ligand for CD26, (Cav-Ig) effectively inhibited production of IL-26. Administration of Cav-Ig before or after onset of GVHD impeded the development of clinical and histologic features of GVHD without interrupting engraftment of donor-derived human cells, with preservation of the graft-versus-leukemia effect. We concluded that cGVHD of the lungs is caused in part by IL-26$^+$CD26$^+$CD4 T cells, and that treatment with Cav-Ig could be beneficial for cGVHD prevention and therapy.

Begell Author Proofs

KEY WORDS: CD26/dipeptidyl petidase IV; caveolin-1; chronic graft-versus-host diease; obliterative bronchiolitis; IL-26.

ABBREVIATIONS: A20-luc: luciferase-transfected A20 cell; **ADA:** adenosine deaminase; **aGVHD:** acute graft-versus-host disease; **alloHSCT:** allogeneic hematopoietic stem cell transplantation; **APC:** antigen presenting cell; **ATG:** antihuman T-lymphocyte immune globulin; **Cav-Ig:** soluble Fc fusion proteins containing the N-terminal domain of caveolin-1; **CB:** cord blood; **cGVHD:** chronic graft-versus-host disease; **DPPIV:** dipeptidyl petidase IV; **GVHD:** graft-versus-host disease; **GVL:** graft-versus-leukemia; **HSC:** hematopoietic stem cell; **HuCB:** human umbilical cord blood; **IBD:** inflammatory bowel diseases; **IFN:** interferon; **IL:** interleukin; **mAb:** monoclonal antibody; **NHLF:** normal human lung fibroblast; **NOG:** NOD/Shi-*scid*IL2rγ^{null}; **OB:** obliterative bronchiolitis; PBL: peripheral blood lymphocyte; **RA:** rheumatoid arthritis; **Tg:** transgenic; **TNF:** tumor necrosis factor.

I. I. INTRODUCTION

Graft-versus-host disease (GVHD) is a severe complication and major cause of morbidity and mortality following allogeneic hematopoietic stem cell transplantation (alloHSCT).[1] On the basis of differences in clinical manifestations and histopathology, GVHD can be divided into acute and chronic forms.[1] Acute GVHD (aGVHD) and chronic GVHD (cGVHD) are traditionally diagnosed primarily by time of onset, with cGVHD occurring after day 100 of transplantation.[2] However, cGVHD has distinct clinicopathologic features and is often diagnosed based on these features regardless of time of onset,

1040-8401/16/$35.00 © 2016 by Begell House, Inc.

being characterized by cutaneous fibrosis, involvement of exocrine glands, hepatic disease, and obliterative bronchiolitis (OB).[3,4] OB, characterized by airway blockade, peribronchiolar and perivascular lympho-fibroproliferation and obliteration of bronchioles, is a late-stage complication of cGVHD.[5] Patients diagnosed with OB have a 5-year survival rate of only 10 to 40%, compared to more than 80% in patients without OB.[6,7] Therefore, the establishment of a humanized murine model of cGVHD manifesting OB is urgently needed to develop novel therapeutic strategies for use in the clinical setting. Furthermore, while multiple strategies to control cGVHD involving T-cell depletion from the graft or global immunosuppression have been developed, cGVHD is still a common clinical outcome in many alloHSCT patients.[4,8] In addition, immunosuppression potentially abrogates the graft-versus-leukemia (GVL) effect, associated with increased relapses following alloHSCT.[9] Novel therapeutic approaches are thus needed to prevent cGVHD without eliminating the GVL effect.

GVHD is initiated when donor-derived T cells are primed by professional antigen presenting cells (APCs) to undergo clonal expansion and maturation.[1] Costimulatory pathways are required to induce T-cell proliferation, cytokine secretion, and effector function following antigen-mediated T-cell receptor activation,[10] and the important role of costimulatory pathways in transplant biology has been established.[1] CD26 is associated with T-cell signal transduction processes as a costimulatory molecule and is a marker of T-cell activation.[11–14] We previously showed that CD26-mediated costimulation in human CD4 T cells exerts an effect on production of T_H1-type proinflammatory cytokines such as interferon (IFN)-γ.[15] Moreover, CD26^{high}CD4 T cells respond maximally to recall antigens with a high competence for trafficking to inflammatory tissues and for antibody synthesis of B cells.[12,14,15] We also showed that CD26-caveolin-1 interaction leads to activation of both CD4 T cells and APCs.[16–18] More recently, we performed *in vitro* experiments to demonstrate that blockade of CD26-mediated T-cell costimulation by soluble Fc fusion proteins containing the N-terminal domain of caveolin-1 (Cav-Ig) diminished primary and secondary proliferative responses not only to recall antigen but also to unrelated allogeneic APC.[19] Other investigators recently reported that CD26^{high} T cells contain T_H17 cells and that CD26^{high} T_H17 cells are enriched in inflamed tissues including rheumatoid arthritis (RA) and inflammatory bowel diseases (IBD).[20] These accumulating data strongly suggest that CD26-mediated costimulation plays an important role in memory response to recall antigens and that blockade of CD26 costimulation may be an effective therapeutic strategy for immune disorders including GVHD and autoimmune diseases.

In this review, we summarize our recent work to establish a pulmonary cGVHD murine model induced by transplantation of human umbilical cord blood (HuCB), which exhibited obliterative bronchiolitis (OB) as well as sclerodermatous skin GVHD after HSCT, and to describe a novel effect of IL-26 produced by donor-derived human CD4 T cells on fibroproliferation of OB. We also showed that IL-26 of HuCB CD4 T cells was produced via CD26 costimulation by its ligand caveolin-1. Furthermore, abrogation of CD26 costimulation by Cav-Ig before or during the early onset of GVHD impeded the development of pulmonary cGVHD. These results provide proof of principle that human $\text{IL-26}^{+}\text{CD26}^{+}$CD4 T cells are involved in the pathophysiology of pulmonary cGVHD.

Begell Author Proofs

II. CURRENT ISSUES IN CHRONIC GVHD

A. Diagnosis

In the past, cGVHD included any clinical manifestations of GVHD that occurred beyond 100 days after hematopoietic cell transplantation.[21] According to the NIH consensus criteria published in 2005, the broad category of cGVHD includes classic cGVHD, presenting with manifestations that can be ascribed only to cGVHD. Moreover, cGVHD also includes the so-called overlap syndrome, which has diagnostic or distinctive cGVHD

TABLE 1: Signs and Symptoms of Chronic GVHD

Organ	Diagnostic (sufficinet for diagnosis)	Distinctive (insufficient alone for diagnosis)	Common (in both acute and chronic GVHD)
Skin	Poikiloderma, Lichen planus-like, Sclerosis or Morphea	Depigmentation	Erythema, Maculopapular rash, Pruritus
Nails		Dystrophy, Logitudinal ridging or brittle, Onycholysis, Nail loss*	
Scalp and body hair		Alopcia, Scaling	
Mouth	Lichen planus-like, Hyperkeratic plaques	Xerostomia, Mucocele, Ulcer*, Psuedomembrane*	Gingivitis, Erythema, Mucositis, Pain
Eyes		Keratoconjunctivitis**, Sicca syndrome	
Genitalia	Lichen planus-like, Vaginal scarring or stenosis	Erosion*, Fissures*, Ulcers*	
GI tract	Esophageal web, Stricture or stenosis*		Anorexia, Nausea, Vomiting, Diarrhea
Liver			Mixed hepatitis
Lung	OB by biopsy	OB by PFTs and radiology**	BOOP
Muscle, fascia, joints	Fasciitis, Joint contractures	Myositis or polymyositis**	
Hematopoietic and immune			Thrombocytopenia, Lymphopenia, Eosinophilia, Hypo or hypergammaglobulinemia, Autoantibody (ITP and AIHA)
Other			Effusions***

Begell Author Proofs

* In all cases, infection, malignancy and adverse effects of drugs must be excluded.
**Diagnosis of chronic GVHD requires biopsy or radiology confirmation (or Schrimer test for eyes).
***Pericardial, pleural effusions or ascites.
AIHA, autoimmune hemolytic anemia; BOOP, bronchiolitis obriterans with organizing pneumonia; GI, gastrointestinal; GVHD, graft-versus-host disease; ITP, idiopathic thrombocytopenic purpura; OB, obliterative bronchiolitis; PTFs, pulmonary function tests.

manifestations together with features typical of aGVHD.[21] Table 1 shows a summary of the signs and symptoms of cGVHD determined by the NIH consensus criteria.[3,21] However, several issues regarding the diagnosis of cGVHD have been raised recently: (1) The presentation of cGVHD can be very polymorphic, ranging from discrete lichenoid features in the mouth alone, to a multisystemic appearance resembling an aggressive lupus or scleroderma-like disease. (2) Although the NIH panel recommended that distinctive but not diagnostic features may require biopsy to confirm the diagnosis, this may not be easily available without risk for some diseases, including fasciitis or myositis. (3) The NIH criteria for lung involvement include only OB and organizing pneumonia (formally called bronchiolitis obliterans with organizing pneumonia), and the NIH scoring system includes both clinical signs and results of pulmonary function tests. Although the diagnosis of cGVHD is often based on clinical signs and symptoms, pathologic examination is warranted and clearly either helps confirm the diagnosis of cGVHD rather than aGVHD by using validated histologic changes specific for cGVHD (including skin, bronchioles, and salivary glands) or helps narrow down a differential diagnosis between cGVHD and carcinoma for mouth ulcerations.[22]

B. Pathophysiology and Clinical Translation

In recent years, significant advances in our understanding of human cGVHD have been made. It is now evident that the clinical manifestations of cGVHD are the result of a highly complex immune pathologic process involving both donor T and B cells as well as other cells.[4,23,24] Donor T cells clearly play an important role in the immune pathology of chronic GVHD; *in vivo* T-cell depletion is the only prophylactic measure that effectively decreases the incidence of cGVHD.[25,26] The immune response occurring in chronic lichenoid GVHD showed a mixed T_H1/T_H17 signature with upregulated T_H1/T_H17 cytokine/chemokine transcripts and elevated numbers of IFN-γ and interleukin (IL)-17-producing $CD8^+$ T cells.[27] Moreover, patients with active cGVHD have a lower frequency of $CD4^+$ regulatory T cells (T_{reg}) than patients without cGVHD.[28] Regarding B cells, it has been recognized since the early description of the disease that patients with cGVHD frequently have circulating antibodies that are reactive with recipient cells.[29] However, whether these antibodies are pathogenic or simply reflect a disturbed B-cell homeostasis is still unknown, although T-follicular helper cells (TfHs) may provide a link between the interacting T- and B-cell networks in cGVHD.[30] Only antihuman T-lymphocyte immune globulin (ATG) has been shown to lower the incidence of chronic GVHD after stem-cell transplantation from an unrelated donor and from an HLA-identical sibling.[31,32] ATG consists of antibodies exhibiting a direct effect on T cells through opsonization and lysis after complement activation. Because antigens such as CD19 or CD138 are also targeted by ATG, antitumor effects have been observed in B-cell cancers and to a lesser extent in myeloid cancers.[33] Taking into account the effect of donor T and B cells on the development of chronic GVHD,[23] the effect of ATG on APCs such as B cells and dendritic cells (DCs) and the induction of T_{reg} may have contributed to the significant reduction in chronic GVHD.[34,35]

C. Preclinical Models in cGVHD

Begell Author Proofs

Although many preclinical models mimicking human cGVHD including OB have been established,[36] control of OB after alloHSCT has not yet been achieved thoroughly.[37] The clinical application of murine data is limited because multiple yet limited schema have arisen to identify alloimmune reactions in cross-species comparisons. For instance, one extensively utilized model of cGVHD clearly exhibited immune-complex glomerulonephritis, which is rarely seen in human cGVHD.[38] Moreover, transfer of autoantibodies from mice with GVHD to normal mice failed to cause autoimmune pathology.[29] These limitations are due to preparative regimens, composition of donor graft, and genetic backgrounds of donor and recipient animals.[36] In addition, recent work has demonstrated multiple differences in immunological functions between humans and mice.[39,40] On the other hand, because *in vivo* T-cell depletion is the only prophylactic measure that effectively decreases the incidence of cGVHD,[4,41] donor T cells clearly play an important role in the immune pathology of cGVHD. In view of these findings, the development of novel therapeutic strategies for use in the clinical setting and the establishment of a humanized murine model of cGVHD are urgently needed.

III. HUMANIZED MURINE MODEL OF CHRONIC GVHD

A. Donor Source of the Newly Established cGVHD Model

We previously analyzed a humanized murine aGVHD model involving mice transplanted with human adult peripheral blood lymphocytes (PBL). We showed that liver and skin were predominantly involved as target organs in this model of aGVHD, which was clearly impeded by the administration of anti-CD26 monoclonal antibody (mAb).[42] Our data suggest that CD26$^+$ T cells play an effector role in this aGVHD model. However, because the mice studied in our previous work succumbed to aGVHD around 4 weeks after transplantation of human adult PBL, this early-onset model of aGVHD does not permit the assessment of longer-term consequences of interventional therapies such as the development of OB, a form of cGVHD of the lung. Similarly, contaminated PBLs caused aggressive xenogeneic reactions in mice transplanted with human bone marrow cells, while depletion of T cells in human bone marrow cells led to graft failure in a humanized murine model.[45] Therefore, an alternative source for human hematopoietic stem cells (HSC) is required for the establishment of a humanized murine model of cGVHD.

In contrast to adult PBL, the HuCB lymphocytes have been reported to be immature, predominantly consisting of CD45RA$^+$ naïve cells.[43,44] We previously showed that, while all HuCB CD4 T cells constitutively expressed CD26, CD26-mediated costimulation was considerably attenuated in HuCB CD4 T cells, compared to the robust activation via CD26 costimulation of adult PBL.[43] These findings provide further insights into the cellular mechanisms of the immature immune response of HuCB. Furthermore, humanized mice transplanted with human HSC isolated from HuCB exhibited human hematopoiesis reconstitution as well as B-cell engraftment with a similar antibody repertoire, as observed in human B cells.[45,46] Based on these findings, we hypothesized that HuCB naïve CD4 T cells gradually acquire a xenogeneic response via attenuated stimulatory signaling with indolent inflammation in the target organs, leading eventually to chronic inflammatory changes. We therefore sought to develop a humanized murine pulmonary cGVHD model utilizing HuCB donor cells and to overcome the limitations seen in the humanized murine aGVHD model, such as vigorous activation of all engrafted T cells and extensive loss of B-cell maturation and activation.[45]

B. Pathologic Findings of Humanized cGVHD Murine Model

As described above, the establishment of a humanized murine model of pulmonary cGVHD is needed to better understand and treat this serious and often fatal complication of alloHSCT. To determine whether pulmonary cGVHD is induced by human immune cells in a murine model, we first attempted to establish a humanized murine model utilizing NOD/Shi-*scid*IL2rγ^{null} (NOG) mice as recipients and HuCB as donor cells. To establish a control that did not develop GVHD following hematopoietic reconstitution, we used T-cell–depleted CD34$^+$ cells isolated from HuCB.[47-49] As shown in Figure 1A-i and ii, T-cell–depleted CD34$^+$ transplanted mice (CD34$^+$ transplant) survived for 5 months without any signs or symptoms of GVHD. Meanwhile, whole-CB–transplanted mice exhibited clinical signs/symptoms of GVHD as early as 4 weeks post transplant (Fig. 1A-ii) and demonstrated a significantly decreased survival rate (Fig. 1A-i). Human cells were engrafted similarly in both groups, as shown in Fig. 1A-iii. Previous work with other humanized murine models showed that reconstituted human CD45$^+$ cells were overcome by CD3$^+$ T cells after transplant due to reduced B-cell development,[45] which may impair the integrity of host immunity. In contrast, we confirmed that NOG mice transplanted with human HuCB maintained a stable number of T and B cells (Fig. 1B), consistent with previously reported results.[46,48–50] Therefore, the human immune system appeared to be effectively reconstituted in the present murine model involving whole CB as well as CD34$^+$ transplant.

We next conducted histological studies of GVHD

Begell Author Proofs

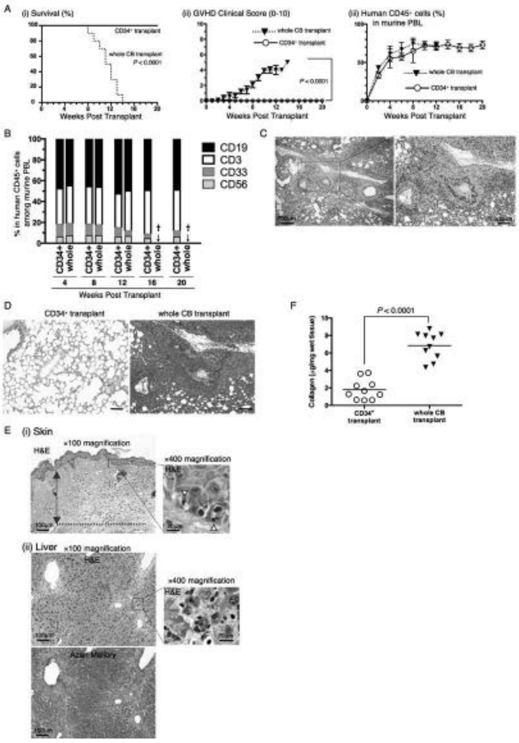

Begell Author Proofs

FIG. 1: Obliterative bronchiolitis in sublethally irradiated NOG mice transplanted with human umbilical cord blood cells (HuCB). NOG mice were irradiated at a sublethal dose (200cGy), the next day they were transplanted with 1X10^5 T-cell–depleted CD34$^+$ cells purified from HuCB (CD34$^+$ transplant) or with 1Ξ10^7 mononuclear cells isolated from HuCB (whole CB transplant). (A) (i) Survival curve. *P* value was calculated using the log-rank test. (ii) Clinical GVHD score (mean±SEM). *P* value was calculated using the log-rank test. (iii) Engraftment of human leukocytes in recipient mice. Peripheral blood of recipient mice was harvested at the indicated time points, and the population of human CD45$^+$ cells was analyzed using flow cytometry. Data are shown as mean±SEM of human CD45$^+$ cells among total peripheral blood leukocytes (PBLs). (B) Sustained composition of human leukocyte populations in recipient PBLs. PBLs harvested from each group were stained for human CD3, CD19, CD33, or CD56 among human CD45$^+$ cells. Data are presented as mean percentages of human CD45$^+$ cells. Cross indicates death of all mice in whole-CB–transplant group. (C) H&E staining of the lung of whole-CB–transplant (8 weeks post transplantation). The left panel shows lower magnification (40X) and the right panel shows higher magnification (100X). (D) Collagen deposition was evaluated in the lung tissues of CD34$^+$ or whole-CB–transplant (8 weeks post transplantation) with an Azan-Mallory staining. The histology shown in whole-CB–transplant is a sequential section of panel C. Dark blue areas indicating collagen deposition are clearly observed in whole-CB–transplant mice, compared to those in CD34$^+$ transplant mice. Original magnification is 100X. Scale bars indicate 100μm. (E) (i) Skin, H&E staining of the skin tissue of whole-CB–transplant mice (8 weeks post transplantation). The skin specimen shows homogenization (sclerosis) of most of the reticular dermis (blue two-way arrow) with fat loss and follicular drop-out (dotted line indicates the border between the hypodermis and muscle layer). In the stratum basale, vacuolar degeneration is presented with apoptotic bodies (yellow arrow heads). (ii) Liver, H&E and Azan-Mallory staining of the liver tissue of whole-CB–transplant mice (8 weeks post transplantation). Low-power magnification shows portal fibrosis and high-power magnification shows cholestasis. (F) Collagen contents in the lung were quantified by Sircol collagen assay. The mean number (±SEM) of total collagen contents (μg) per wet lung tissue weight (mg) was determined. Increased collagen contents were clearly observed in whole-CB–transplant mice, compared to those in CD34$^+$ transplant mice. Each dot indicates individual value and horizontal bars indicate mean value (reprinted with permission from The American Association of Immunologists, Inc., Copyright 2015).[51]

target organs. The lung of whole-CB–transplant mice showed perivascular and subepithelial inflammation and fibrotic narrowing of the bronchiole (Fig. 1C and right panel of Fig. 1D), while CD34$^+$ transplant control group displayed normal appearance of GVHD target organs such as the lung (left panel of Fig. 1D). For the diagnosis of pulmonary cGVHD, it is necessary to show concomitant active GVHD findings in other organs, including skin and liver.[21] Skin of whole-CB–transplant mice manifested fat loss, follicular drop-out and sclerosis of the reticular dermis in the presence of apoptosis of the basilar keratinocytes, whereas the liver exhibited portal fibrosis and cholestasis (Fig. 1E). These findings indicate that whole-CB–transplant mice develop pulmonary cGVDH as well as concomitant active GVHD in skin and liver. Because OB can be characterized as a fibroproliferative disease,[37] we also performed Mallory staining and lung collagen assays to quantify collagen contents as a measurement of the extent of disease. The lung of whole-CB–transplant mice displayed a significant increase in peribronchiolar and perivascular collagen deposition and in total lung collagen content, compared to CD34$^+$ transplant mice (Figs. 1D and 1F). Taken together, our data demonstrate that the lung of whole-CB–transplant mice exhibits OB as manifestation of pulmonary GVHD.

C. Pathophysiology of Pulmonary cGVHD in Our Model

To determine the potential cellular mechanisms involved in the pathogenesis of pulmonary GVHD, we next analyzed the composition of donor-derived human lymphocytes in the GVHD lung. In contrast to data demonstrating that recipient PBL contained donor-derived human CD19$^+$, CD33$^+$, or CD56$^+$ as well as CD3$^+$ cells (Fig. 1B), donor-derived human CD3$^+$ cells were the predominant cell type observed in the lung of whole-CB–transplant mice, comprising more than 99% of the lymphocyte population (Fig. 2A). Moreover, the human CD4 T-cell subset was the predominant population observed in the lung of whole-CB–transplant mice, not CD8 T cells (Fig. 2B). These findings were also confirmed by immunohistochemistry studies of the lung specimens (Fig. 2C). These data suggest that the development of OB found in whole-CB–transplant mice involves donor-derived human CD3 lymphocytes, particularly CD4 T cells.

We next analyzed the expression profile of mRNAs of various inflammatory cytokines in human CD4 T cells isolated from the lung of whole-CB–transplant mice. We found that *IFNG*, *IL17A, IL21,* and *IL26* significantly increased over the course of GVHD development following whole CB transplantation, while *IL2*, *TNF* (TNF-α), *IL4*, *IL6* and *IL10* decreased.[51] In addition, substantial increases were seen in the levels of *IFNG* and *IL26*, with *IL17A* and *IL21* remaining at a low level.[51] It has been reported that IFN-γ and IL-26 are produced by T$_H$1 cells,[52] while IFN-γ, IL-17A and IL-26 are produced by T$_H$17 cells.[53] Because both T$_H$1 and T$_H$17 cells strongly express CD26,[15,20] we next analyzed the expression level of CD26/DPP4, demonstrating that *DPP4* mRNA expression in human CD4 T cells infiltrating in the lung of mice with OB significantly increased.[51] These findings on expression levels of mRNA were also confirmed by examining protein levels in sera of recipient mice utilizing ELISA.[51]

To determine whether these cytokines were produced by the infiltrating human CD26$^+$CD4 T cells, we next conducted flow cytometric analysis of lymphocytes isolated from the lung of whole CB or CD34$^+$ transplant control mice. As shown in Fig. 2D, levels of human IFN-γ$^+$, and IL-26$^+$CD26$^+$CD4 T cells were significantly increased in whole-CB–transplant mice compared to CD34$^+$ transplant control mice, while levels of IL-17A$^+$CD26$^+$CD4 T cells were similarly very low in both groups. These findings were also confirmed by immunohistochemistry studies of the lung specimens (Fig. 2E). To determine whether CD26$^+$CD4 T cells produced IL-26, IFN-γ and/or IL17A, multicolor-staining flow cytometric studies were conducted. As shown in Fig. 2F-i, CD26$^+$CD4 T cells in the lung of whole-CB–transplant mice predominantly produced IL-26 rather than IFN-γ. In addition, while CD26$^+$IFN-γ$^+$CD4 cells exclusively expressed IL-26, CD26$^+$IL-26$^+$CD4 cells were pre-

Begell Author Proofs

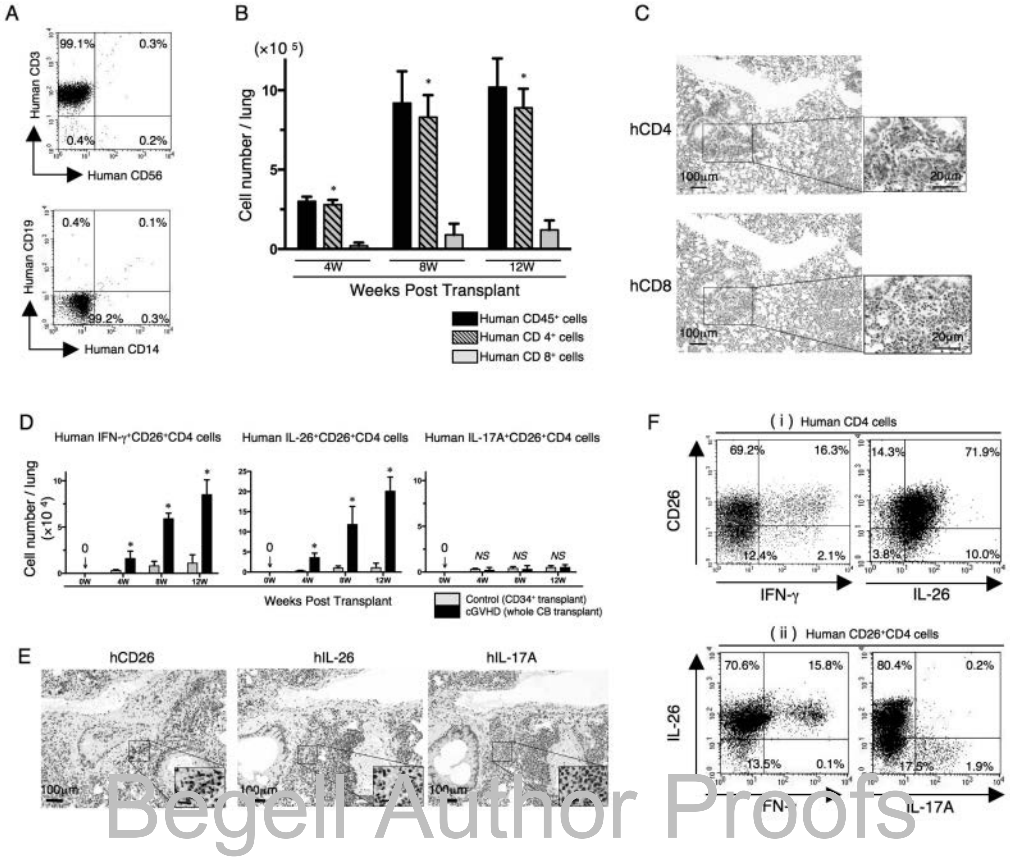

Begell Author Proofs

FIG. 2: Predominant infiltration of donor-derived CD4+ T cells in obliterative bronchiolitis of chronic GVHD. NOG mice were preconditioned and transplanted by the same method as in Fig. 1. (A) Representative 2-D dot plots of human lymphocyte composition in the lung of whole-CB–transplant mice (8 weeks post transplantation). Single-suspension cells isolated from the lung of whole-CB–transplant mice (8 weeks post transplantation) were sorted by human CD45$^+$ cells and then analyzed using flow cytometry. The upper panel shows representative human CD3 and/or CD56 staining, and the lower panel, representative human CD19 and/or CD14 staining. Numbers indicate relative percentages per quadrant. (B) Absolute cell numbers (mean±SEM) of human CD45$^+$, CD4$^+$, or CD8$^+$ cells per lung of whole-CB–transplant mice were quantified by flow cytometry. CD4$^+$ T cells were predominantly observed in the lung of whole-CB–transplant mice. $* P<0.0001$ versus CD8$^+$ cells. (C) Anti-human CD4 or CD8 immunohistochemistry of sequential sections of lung tissue of whole-CB–transplant mice (8 weeks post transplantation). Predominant infiltration of CD4$^+$ cells was observed, with similar results to those obtained by flow cytometry as shown in panel F. Original magnification is 100X or 400X (inset in each panel). (D) Absolute cell numbers of human IFN-γ^+CD26$^+$CD4, IL-26$^+$CD26$^+$CD4, or IL-17A$^+$CD26$^+$CD4 cells in the lung of CD34$^+$ transplant or whole-CB–transplant mice were quantified by flow cytometry. $* P<0.0001$ versus corresponding CD34$^+$ transplant group; NS, not significant. (E) Anti-human CD26, IL-26 or IL-17A immunohistochemical staining of sequential sections of the lung from whole-CB–transplant mice (8 weeks post transplantation). The lung of whole-CB–transplant mice was clearly infiltrated with human CD26 or IL-26 (brown stained cells) but not with IL-17A positive cells. Original magnification is 100X or 400X (inset in each panel). Scale bars in the inset indicate 20 μm. (F) Representative 2-D dot plots of human CD26 and IFN-γ or IL-26 cells by gating for human CD4$^+$ cells (panel i) and of human IFN-γ or IL-17A among IL-26$^+$ cells by gating for human CD26$^+$CD4$^+$ cells (panel ii). Single-suspension cells isolated from the lung of whole-CB–transplant mice (8 weeks post transplantation) were sorted by human CD45$^+$ cells then analyzed using flow cytometry. Numbers indicate relative percentages per quadrant [(B) – (F) reprinted with permission from The American Association of Immunologists, Inc., Copyright 2015].[51]

dominantly IFN-γ–negative cells, and IL-17A$^+$ cells were exclusively IL-26 negative (Fig. 2F-ii). These data suggest that CD26$^+$CD4 T cells in the lung of mice with OB express IL-26 as well as IFN-γ but do not belong to the $\mathrm{T_H}$17 cell population.

IV. ROLE OF IL-26 IN CHRONIC GVHD

A. IL-26 in Immune System: an Overview

Originally discovered in *Herpesvirus saimiri*–transformed T cells,[54] IL-26 is now classified as belonging to the IL-10 family of cytokines.[53] Human IL-26 is a 171-amino acid protein that belongs to the IL-10 family of cytokines, a family that includes IL-10, IL-19, IL-20, IL-22, and IL-24.[55] The IL-26 protein is encoded by the *IL26* gene located on chromosome 12q15 between genes for interferon IFN-γ and IL-22[52,56,57] and is conserved in several vertebrate species but not found in mice and rats.[52] IL-26 is a secreted protein produced by T, NK cells, or synoviocytes,[58,59] and binding of IL-26 to a distinct cell surface receptor consisting of IL-20RA and IL-10RB results in functional activation via STAT3 phosphorylation (Fig. 3).[56] Although IL-26 shares approximately 25% of its amino acid homology with IL-10 (and utilizes one of the IL-10 receptor subunits as a cell surface receptor),[56,60] a growing body of evidence indicates that the functional effects of IL-26 differ substantially from those of IL-10. Functional studies are compatible with IL-26 driving or sustaining inflammation rather than suppressing it. In addition, IL-26 gene expression or protein production has been analyzed in patients with systemic sclerosis, RA, inflammatory bowel diseases (IBD), and hepatitis C virus (HCV) infection.[59,61-64] IL-26 is evidently involved in chronic inflammatory disorders including autoimmune diseases (Fig. 4), but its role in acute inflammatory disorders and onset of chronic inflammatory disorders has yet to be established.

Because expression of IL-20RA, the key subunit of IL-26 receptor that mediates IL-26 signaling, is restricted to skin, intestine, and lungs, IL-26 is thought to promote defense mechanisms at mucosal surfaces by bridging immune cells and epithelia. IL-26 exhibits priming effects on various immune cells to boost antiviral and antimicrobial responses. IL-26 induces TNF-related apoptosis-inducing ligand (TRAIL) on human NK cells that kill HCV-infected hepatocytes.[64] Moreover, IL-26 derived from CD68$^+$ alveolar macrophages and $\mathrm{T_H}$17 cells propel antimicrobial responses by priming the recruitment of neutrophils toward bacteria and assembled effector immune cells in the lungs and by triggering the production of plasmacytoid DC–derived IFN-α.[65,66] Furthermore, it was reported that human $\mathrm{T_H}$17-cell–derived IL-26 mediates protective immunity by direct microbicidal action due to its functional similarity to naturally occurring antimicrobial peptides. IL-26 inhibited the growth of gram-negative or -positive bacteria, including *Pseudomonas aeruginosa*, *Escherichia coli*, *Klebsiella pneumonia,* and *Staphylococcus aureus,* by direct bactericidal action.[66] Therefore, even when the limitations of current knowledge are taken into account, IL-26 emerges as an important player in host defense and inflammation, with the potential to represent a therapeutic target in infections and chronic inflammatory disorders (Fig. 4).

Begell Author Proofs

B. IL-26 Contributes to Collagen Deposition in the cGVHD Lung

Because significant collagen deposition was observed in peribronchial blood vessels in the lung of aGVHD (Fig. 1C),[5,67] we sought to determine whether collagen production was induced by IFN-γ$^+$ and/or IL-26$^+$CD26$^+$CD4 T-cell infiltration in cGVHD lung. Although IFN-γ is a key regulator of cellular immunity, development of cGVHD lung has been reported to be independent of IFN-γ.[68] On the other hand, the effect of IL-26 on cGVHD pathophysiology has not yet been determined. We therefore focused on IL-26 as a potential effector cytokine for lung cGVHD. While the human IL-26 gene *IL26* is located adjacent to *IFNG* on chromosome 12q15, and the IL-26 gene is absent in rodents,[52,69] we cannot formally exclude the possibility that human IL-26 activates murine cells. We therefore conducted *in vitro* assays to determine the effect of human IL-26 on murine

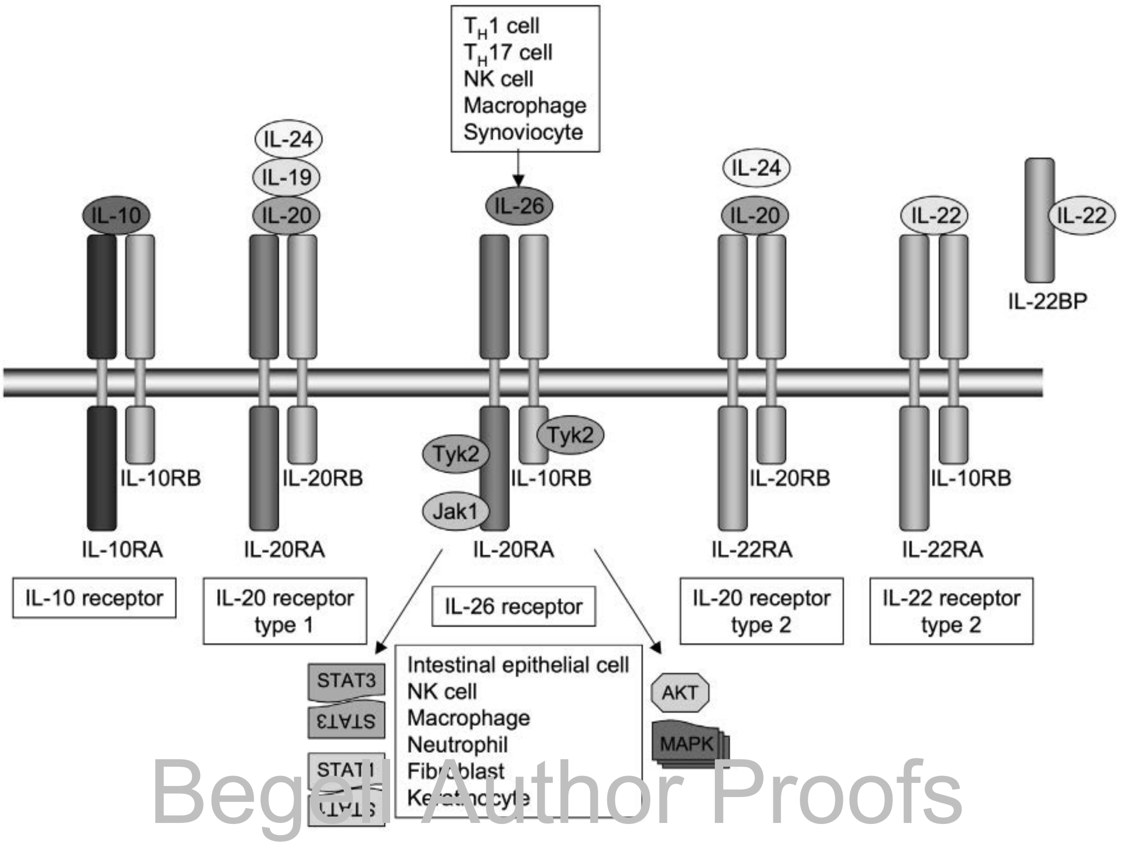
T_H1 cell
T_H17 cell
NK cell
Macrophage
Synoviocyte
IL-10
IL-24
IL-19
IL-20
IL-26
IL-24
IL-20
IL-22
IL-22
IL-22BP
IL-10RB
IL-20RB
Tyk2
Tyk2
IL-10RB
IL-20RB
IL-10RB
Jak1
IL-10RA
IL-20RA
IL-20RA
IL-22RA
IL-22RA
IL-10 receptor
IL-20 receptor type 1
IL-26 receptor
IL-20 receptor type 2
IL-22 receptor type 2
STAT3
STAT3
STAT1
STAT1
Intestinal epithelial cell
NK cell
Macrophage
Neutrophil
Fibroblast
Keratinocyte
AKT
MAPK

Begell Author Proofs

FIG. 3: Receptors and downstream signaling of IL-26 and other IL-10 family cytokines.

cells. We first showed that both IL-20RA and IL-10RB, a functional receptor complex for IL-26, were expressed in the murine fibroblast cell-line NIH3T3 as well as normal human lung fibroblast (NHLF).[51] We next showed that exogenous recombinant human IL-26 induced phosphorylation of STAT3 in both NHLF and NIH3T3.[51] These data indicate that human IL-26 is active not only in NHLF but also in murine fibroblasts. To examine a functional effect of IL-26 on murine fibroblast, we next conducted *in vitro* assays for collagen synthesis. We showed that an increase in collagen production in NIH3T3 as well as in NHLF was observed in a dose-dependent manner following the addition of exogenous IL-26 and that collagen production was inhibited by neutralizing anti-IL-20RA polyclonal antibody (pAb).[51] These results strongly suggest that human IL-26 activates both human and murine fibroblasts via IL-20RA, leading to increased collagen production.

To further extend the above *in vitro* results to an *in vivo* system, we analyzed the lung of murine alloreactive GVHD using human *IL26* transgenic (Tg) mice. For this purpose, we used mice carrying human *IFNG* and *IL26* transgene (190-*IFNG* Tg mice) or mice carrying human *IFNG* transgene with deleting *IL26* transcription (ΔCNS-77 Tg mice). 190-*IFNG* Tg mice exhibited production of IL-26 by CD4 T cells under T_H1- or T_H17-polarizing conditions, while expression of IL-26 was completely abrogated in ΔCNS-77 Tg mice.[52] In addition, production of IFN-γ by T or NK cells was equivalent in both 190-*IFNG* Tg and ΔCNS-77 Tg mice.[57] As shown in Fig. 5A, lung histology of recipient NOG mice deriving from parental C57BL/6 (B6 WT) mice

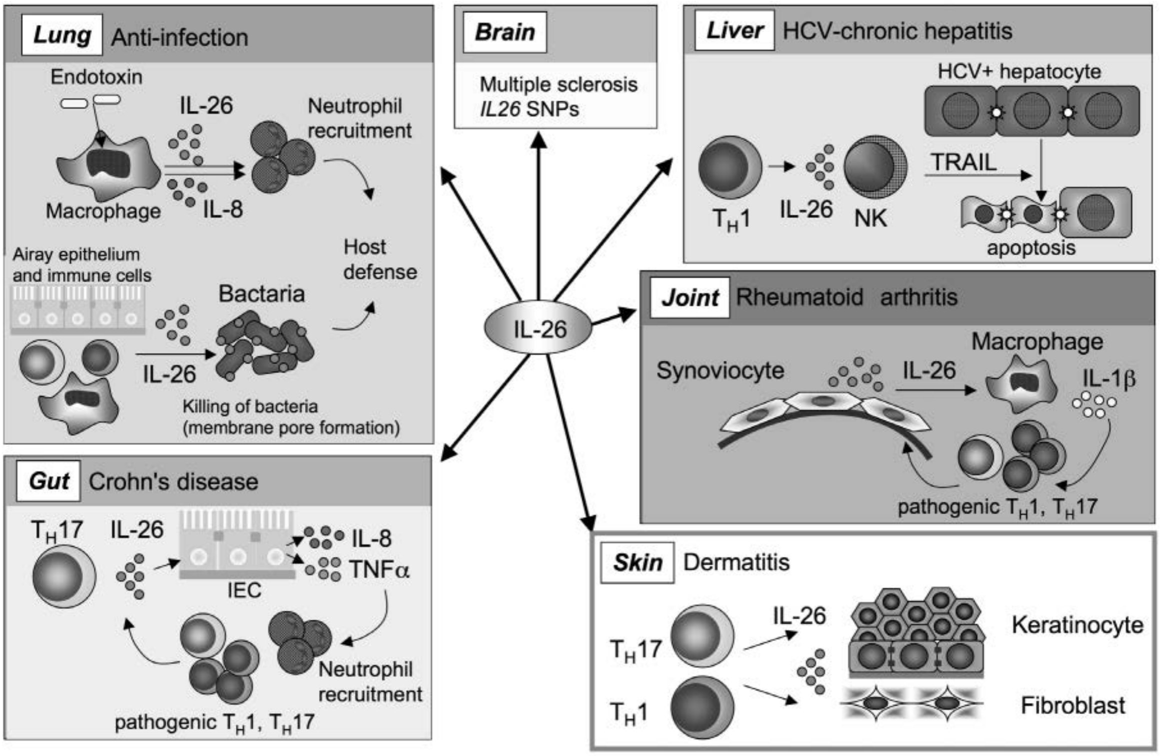
Lung
Anti-infection
Endotoxin
IL-26
Neutrophil recruitment
Macrophage
IL-8
Airay epithelium and immune cells
Host defense
Bactaria
IL-26
Killing of bacteria (membrane pore formation)
Brain
Multiple sclerosis
IL26 SNPs
Liver
HCV-chronic hepatitis
HCV+ hepatocyte
TRAIL
T_H1
IL-26
NK
apoptosis
IL-26
Joint
Rheumatoid arthritis
Macrophage
Synoviocyte
IL-26
IL-1β
pathogenic T_H1, T_H17
Gut
Crohn's disease
T_H17
IL-26
IL-8
TNFα
IEC
Neutrophil recruitment
pathogenic T_H1, T_H17
Skin
Dermatitis
IL-26
Keratinocyte
T_H17
T_H1
Fibroblast

FIG. 4: Multifaceted actions of IL-26 in host defense and autoimmune responses. Upon activation, various immune cells including T_H1, T_H17, NK cells and macrophages secrete IL-26. IL-26 exerts antibacterial and antiviral actions through direct killing of bacteria by forming membrane pores, and by priming immune cells such as neutrophils, NK cells and plasmacytoid dendritic cells. Other cytokines might act in synergy with IL-26 to enhance these host defense actions. IL-26 response requires tight regulation as increased expression of IL-26 has been reported in several autoimmune and inflammatory diseases.

Begell Author Proofs

or ΔCNS-77 Tg mice showed peribronchial infiltration and cuffing denoting GVHD (panels a or g), while collagen deposit was not detected by Mallory staining (panels b or h), and IL-26$^+$ cells were not detected (panels c or i). On the other hand, histology of recipient NOG mice deriving from 190-*IFNG* Tg mice showed peribronchial infiltration and cuffing denoting GVHD (panel d of Fig. 5A) with collagen deposition and IL-26$^+$ cell infiltration (panels e and f of Fig. 5A). Significant increase in collagen deposition in the lungs of recipient NOG mice deriving from 190-*IFNG* Tg mice was quantified by collagen assays and shown in Fig. 5B. These results suggest that human IL-26, but not human IFN-γ, plays a critical role in pulmonary fibrosis associated with lung cGVHD.

V. ROLE OF CD26 IN CHRONIC GVHD

A. Molecular Mechanisms of T-Cell Response via CD26

In 1979, a large-molecular-weight complex composed of adenosine deaminase (ADA) activity was found to be an ADA-binding protein (ADBP), also known as adenosine deaminase complexing protein-2 (ADCP2).[70] In 1992, this ADBP (or ADCP2) was determined to be identical to CD26, a T-cell activation molecule and a 110-kD glycoprotein that is present also on epithelial cells of various tissues including the liver, kidney, and intestine.[71–73] The human CD26 cDNA contains a 3,465 base-pair (bp) open reading frame that encodes a 766-amino-acid protein. The

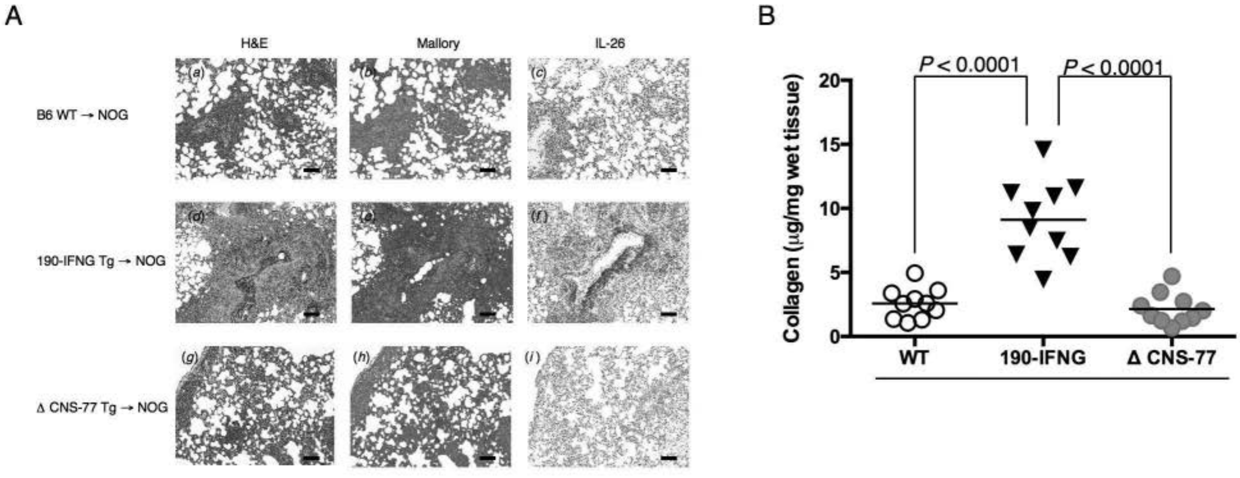

FIG. 5: Collagen deposition in cGVHD lung is induced in NOG mice receiving bone marrow (BM) cells and splenocytes of *IL26* transgenic (Tg) mice. (A) H&E, Azan-Mallory staining and anti-IL-26 immunohistochemistry of sequential sections of lung from NOG mice at 4 weeks after transplantation of BM and splenocytes isolated from parental B6 (WT) (*panels a-c*), 190-*IFNG* BAC Tg (*panels d-f*) or ΔCNS-77 Tg (*panels g-i*) mice. Lungs of recipients of 190-*IFNG* BAC Tg mice showed areas of collagen deposition and IL-26$^+$ cell infiltration, while recipients of WT or ΔCNS-77 Tg mice showed BO and septal infiltration without collagen deposition or IL-26$^+$ cells. Original magnification is 100X. Scale bars indicate 100μm. (B) Collagen contents in the lung were quantified by Sircol collagen assay. Each lung specimen was prepared from mice as shown in panel A. The mean number (±SEM) of total collagen contents (μg) per wet lung tissue weight (mg) was determined. Increased collagen contents were clearly observed in recipients of 190-IFNG Tg mice, compared to those in recipients of B6 WT or ΔCNS-77 Tg mice. Each dot indicates individual value and horizontal bars indicate mean value (reprinted with permission from The American Association of Immunologists, Inc., copyright 2015).[51]

Begell Author Proofs

human CD26 amino acid sequence has 85% amino acid identity with the mouse and rat CD26.[72,73] The 5'-flanking region does not contain a TATA box or CAAT box commonly found in housekeeping genes.[74,75] CD26 does contain a 300-bp G-C–rich region with potential binding sites for NF-κB, AP2, or Sp1.[76] CD26 expression is activated by IFNs and retinoic acid in chronic lymphocytic leukemia via Stat1α and the GAS (IFN-γ activation site) response element (TTCnnnGAA located at bp -35 to -27) in the CD26 promoter.[77]

Human CD26 is composed of 766 amino acids (Fig. 6), including a short cytoplasmic domain of 6 amino acids, a transmembrane region of 22 amino acids, and an extracellular domain with dipeptidyl peptidase activity that selectively removes the N-terminal dipeptide from peptides with proline or alanine at the penultimate position.[78] Analysis of single amino acid point mutations in the β-propeller motif identified Glu205 and Glu206 to be essential for DPPIV enzyme activity, and the central tunnel and α/β-hydrolase domains both participate in DPPIV inhibitor binding.[79–81] CD26/DPPIV was initially considered to cleave peptides only after a proline or alanine residue, but its substrates are now known include hydroxyproline, serine, glycine, valine, threonine, and leucine.[80,82,83] CD26 binds to caveolin-1 on APC, and residues 201 to 211 of CD26 along with the serine catalytic site at residue 630, which constitute a pocket structure of CD26/DPPIV, contribute to its binding to the caveolin-1 scaffolding domain.[18] This region in CD26 contains a caveolin-binding domain ($\Phi X \Phi XXXX \Phi XX \Phi$; Φ and X depict aromatic residue and any amino

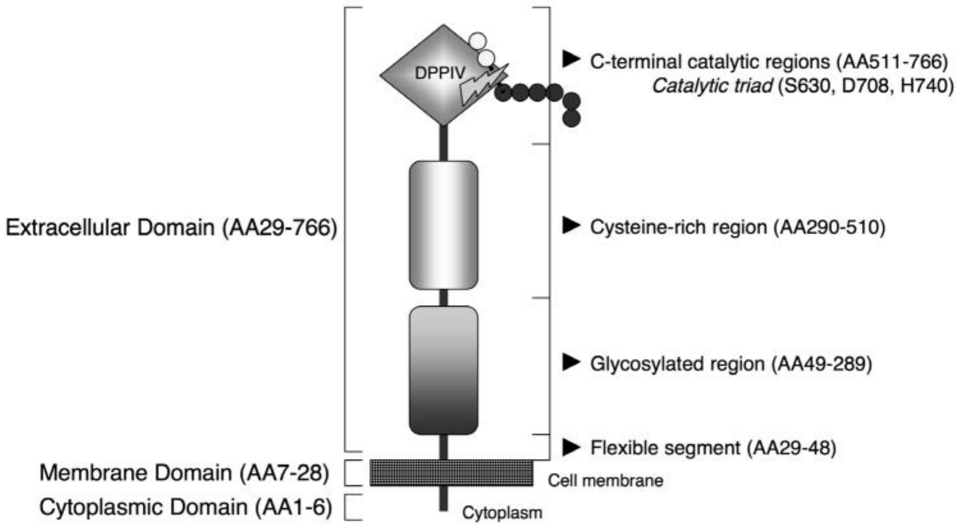
DPPIV
C-terminal catalytic regions (AA511-766)
Catalytic triad (S630, D708, H740)
Extracellular Domain (AA29-766)
Cysteine-rich region (AA290-510)
Glycosylated region (AA49-289)
Flexible segment (AA29-48)
Membrane Domain (AA7-28)
Cell membrane
Cytoplasmic Domain (AA1-6)
Cytoplasm

FIG. 6: Schematic diagrams of the amino acids of human CD26. Human CD26 cDNA is composed of 2,301 base pairs, translated to a 766-amino-acid protein. DDPIV catalyzes the hydrolysis of N-terminal dipeptides from polypeptides with proline or alanine in the penultimate position. See text for further details.

acid, respectively), specifically WVYEEEVFSAY in CD26. These observations strongly support the hypothesis that DPPIV enzyme activity is necessary for CD26-mediated T-cell costimulatory activation, as demonstrated in our previous work using CD26-targeted mAbs.[15,84] Single-amino-acid point-mutation analysis showed that His750 residue is responsible for dimerization,[85] which is required for T-cell costimulation signaling.[16]

In human peripheral blood, CD26 is found on $CD4^+$ T memory cells and $CD8^+$ effector/memory T cells.[12,86,87] It has been reported that 0–5% of freshly isolated $CD20^+$ B cells do express the CD26 antigen.[88] Following stimulation with phorbol 12-myristate 13-acetate (PMA) or *Streptococcus aureus* protein, the fraction of CD26-positive cells increased to 51%.[12,89] Meanwhile, CD26 is not expressed or is found only at low levels on monocytes of healthy adults.[90,91] Only a small fraction of peripheral NK cells was found to express CD26.[92]

CD26 is a costimulatory molecule for T-cell signal transduction. Whereas CD26 expression is enhanced following activation of resting T cells, $CD4^+CD26^{high}$ T cells respond maximally to recall antigens such as tetanus toxoid.[12] In addition, $CD4^+$ T cells with *in vitro* transendothelial migratory capacity appear to express high CD26.[93] Moreover, $CD26^{high}CD8^+$ T cells in humans belong to early effector memory T cells, and $CD26^{high}CD8^+$ T cells exhibit increased expression of granzyme B, TNF-α, IFN-γ and Fas ligand, and exert a cytotoxic effect with CD26-mediated costimulation.[87]

The cytoplasmic tail of CD26 is responsible for T-cell costimulation induced by anti-CD3 plus caveolin-1.[16] We found that CARMA1 binds to the cytoplasmic tail of dimeric CD26 and that a PDZ domain in CARMA1 is necessary for binding to CD26. Following its phosphorylation, CARMA1 functions as a signaling intermediate downstream of protein kinase θ (PKCθ) and upstream of IκB kinase (IKK) in the T-cell receptor (TCR) signaling transduction pathway, which leads eventually to NF-κB activation. Dimeric CD26, but not monomeric CD26, binds to CARMA1.[16] The enzymatic pocket structure of the DPPIV catalytic site is necessary for binding of CD26 to caveolin-1, which leads to the upregulation of CD86 expression on APC (Fig. 7).[17] Dimerization of CD26 is therefore not only

Begell Author Proofs

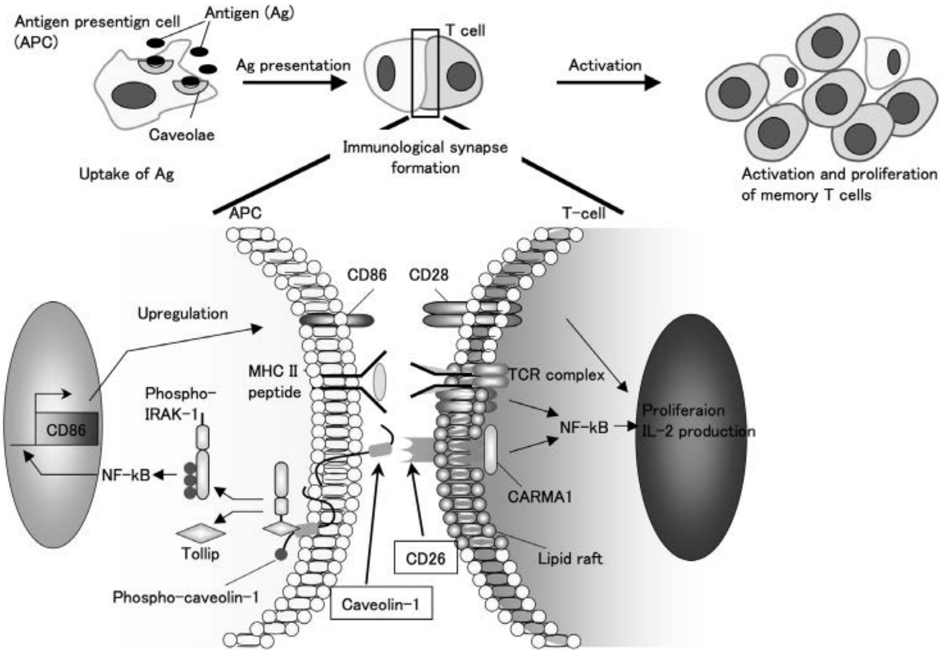
Antigen presentign cell
(APC)
Antigen (Ag)
Caveolae
Uptake of Ag
Ag presentation
T cell
Immunological synapse
formation
Activation
Activation and proliferation
of memory T cells
APC
T-cell
CD86
CD28
Upregulation
MHC II
peptide
Phospho-
IRAK-1
CD86
NF-kB
Tollip
Phospho-caveolin-1
Caveolin-1
CD26
TCR complex
NF-kB
CARMA1
Lipid raft
Proliferaion
IL-2 production

FIG. 7: Molecular mechanisms of CD26-caveolin-1 interaction in memory antigen response. Antigen-presenting cells (APC) take up recall antigens such as tetanus toxoid via caveolae. Following antigen uptake, a portion of caveolin-1 is exposed on the outer cell surface and aggregates in the APC–T-cell contact area in lipid rafts, presumably by homo-oligomerization. Aggregated caveolin-1 then binds to its specific ligand CD26, resulting in caveolin-1 phosphorylation. Phospho-caveolin-1 transduces a signal into the APC leading to dissociation of IRAK-1 and Tollip, followed by activation of NF-κB and finally resulting in CD86 upregulation and T-cell costimulation. On the T-cell side, binding by specific MHC-peptide complexes leads to TCR signal transduction. Additionally, caveolin-1 on the APC ligates CD26 dimers on the T-cell surface resulting in the recruitment of lipid rafts in the plasma membrane and the recruitment of CARMA1 to the cytosolic portion of CD26. Ultimately, these steps lead to the activation of NF-κB, and T-cell proliferation and IL-2 production.

Begell Author Proofs

necessary for binding to caveolin-1 but also serves as a scaffolding structure for the cytoplasmic signaling molecule CARMA1. Overall, CD26 ligation by caveolin-1 on APC recruits CD26-interacting CARMA1 to lipid rafts, resulting in the formation of a CARMA1-Bcl10-MALT1-IKK complex, and this membrane-associated Bcl10 complex then activates IKK through ubiquitination of NF-κB essential modulator (NEMO).[14]

B. IL-26 Production via CD26-Mediated T-Cell Costimulation

IL-26 is co-expressed with IFN-γ by T_H1 cells,[53] and CD26/DPPIV is preferentially expressed on T_H1 cells activated via CD26-mediated costimulation.[15] In addition, CD26$^+$CD4 T cells in the cGVHD lung predominantly produced IL-26 rather than IFN-γ (Fig. 2F). Thus, we hypothesize that human CD4 T cells produce IL-26 following CD26 costimulation. To test this hypothesis, we conducted *in vitro* costimulation experiments using HuCB CD4 T cells and analyzed expression of various inflammatory cytokines. We showed that levels of *IL26* and *DPP4* were significantly increased following CD26 costimulation compared with those in CD28 costimulation, while expression levels of *IL26* and *DPP4* were enhanced by CD28 or CD26 costimulation.[51] On the other hand, expression levels of *IL2*, *IFNG*, and *IL17A* were not increased following either CD26 costimulation

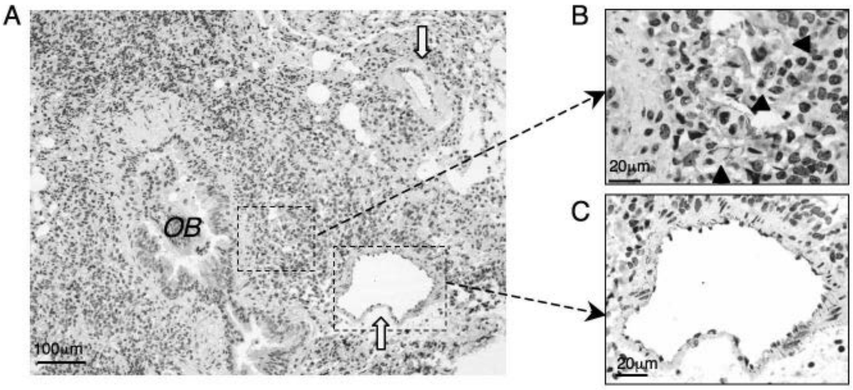

FIG. 8: Expression of caveolin-1 in the cGVHD lung of HuCB-NOG mice. Anti-caveolin-1 immunohistochemistry of the lung of whole-CB–transplant mice (8 weeks post transplantation). Caveolin-1 was detected on the epithelial cell surface (yellow arrows in *panel A*) and macrophage-like large cells (arrow heads in *panel B*) around inflammatory vessels (*panel C*) in obliterative bronchiolitis lesion (*OB* in panel A). Original magnification, 100X (A) and 400X (B, C).

or CD28 costimulation, due to the immaturity of HuCB T cells, as was previously reported.[43,94] We next conducted costimulation experiments evaluating dose and time kinetics using the CD26 costimulatory ligand Cav-Ig as well as anti-CD26 or anti-CD28 mAbs. We showed that production of IL-26 increased following CD26 costimulation with Cav-Ig or anti-CD26 mAb in dose- and time-dependent manners, while a slight increase in IL-26 level was observed following CD28 costimulation only at higher doses of mAb and longer stimulation periods.[51] Blocking experiments were then performed for further confirmation, showing that IL-26 production induced by Cav-Ig or anti-CD26 mAb was clearly inhibited by treatment with soluble Cav-Ig in a dose-dependent manner, while no change was observed with CD28 costimulation. These findings strongly suggest that production of IL-26 by HuCB CD4 T cells is regulated via CD26-mediated costimulation. Moreover, because the functional sequences of the N-terminal of caveolin-1 are highly conserved between human and mouse,[95] allowing for the capability to bind human CD26 as a costimulatory ligand, it is conceivable that donor HuCB T cells transferred into mice were activated via CD26 costimulation triggered by murine caveolin-1. In fact, using pAb recognizing the N-terminal of both human and murine caveolin-1, expression of caveolin-1 was detected in endothelial cells and macrophage-like cells of OB-like lesions in cGVHD lung (Fig. 8). Taken together, CD26-mediated IL-26 production triggered by caveolin-1 is identified as a possible therapeutic target in cGVHD using HuCB NOG mice.

VI. TARGETING CD26 IN CHRONIC GVHD

A. Prophylaxis of Lung cGVHD by Cav-Ig Administration

Given the role of CD26 costimulation in IL-26 production and IL-26 regulation of collagen production, we therefore sought to determine whether disruption of CD26 costimulation by a blocking reagent, Cav-Ig, prolonged survival of the recipient mice associated with a reduction in the incidence of OB. Recipients treated with Cav-Ig survived for 7 months without any clinical findings of GVHD (Figs. 9A and B). Meanwhile, the survival rate of recipient mice treated with control Ig was significantly reduced (Fig. 9A), with clinical signs/symptoms of GVHD (Fig. 9B). Human cells were engrafted similarly in both groups

Begell Author Proofs

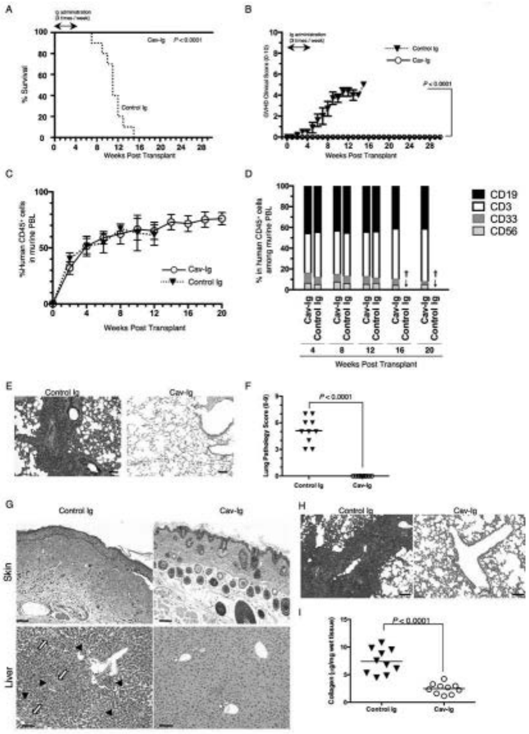

Begell Author Proofs

FIG. 9: Administration of Cav-Ig prevents obliterative bronchiolitis by reducing the level of IL-26$^+$CD26$^+$CD4 cells and collagen deposition. Sublethally irradiated NOG mice were transplanted with 1X10^7 mononuclear cells isolated from HuCB. Cav-Ig or control Ig (each 100µg/dose) was administered intraperitoneally thrice a week, beginning at day +1 after transplantation until day +28. (A) Overall survival and (B) clinical GVHD score (mean±SEM). (C) Engraftment of human leukocytes in recipient mice. Peripheral blood of recipient mice was harvested at the indicated time points, and human CD45$^+$ cell population was analyzed using flow cytometry. Data are shown as mean±SEM of human CD45$^+$ cells among total PBL. (D) Sustained composition of human leukocyte populations in recipient PBL. PBL harvested from each group were stained for human CD3, CD19, CD33 or CD56 among human CD45$^+$ cells. Data are presented as mean percentages of human CD45$^+$ cells. Cross indicates death of all mice in control Ig group. (E) H&E staining of the lung of recipients administered with control Ig or Cav-Ig group (6 weeks post transplantation). Original magnification is 100X. Scale bars indicate 100 µm. (F) Pathologic damage in the lung of recipients administered with Cav-Ig or control Ig was examined at 6 weeks post transplantation, using a semi-quantitative scoring system. Each dot indicates individual value and horizontal bars indicate mean value. (G) H&E staining of the skin and liver tissues for the control Ig group or Cav-Ig group evaluated at 6 weeks post transplantation. The skin specimen of the control Ig group showed sclerotic changes including acanthosis, loss of rete ridge, fat loss, follicular drop-out, and homogenized collagen deposition, in contrast to the normal appearance of the skin of the Cav-Ig group. The liver specimen of the control Ig group showed portal inflammation (arrow heads) and portal collagen deposition (yellow arrows), which were not observed in the Cav-Ig group. Original magnification is 100X. Scale bars indicate 100 µm. (H) Collagen deposition was determined in the lung tissues of recipients of Cav-Ig or control Ig group (6 weeks post transplantation) with an Azan-Mallory staining. Original magnification is 100X. Scale bars indicate 100µm. (I) Collagen contents in the lung of recipients of Cav-Ig or control Ig group (6 weeks post transplantation) were quantified by Sircol Collagen Assay. The mean number (±SEM) of total collagen contents (µg) per wet lung tissue weight (mg) was determined. Decreased collagen contents were clearly observed in recipients of Cav-Ig group. Each dot indicates individual value and horizontal bars indicate mean value (reprinted with permission from The American Association of Immunologists, Inc., copyright 2015).[51]

as shown in Figs. 9C and D. Histologic findings of the lung showed the development of OB in control Ig while appearing normal in Cav-Ig–recipient mice, with none having positive pathology scores (Figs. 9E and F). These effects of Cav-Ig were also observed in other GVHD-target organs such as the skin and liver (Fig. 9G). Moreover, collagen contents in the lung were reduced in Cav-Ig–administered recipients (Figs. 9H and I). Taken together, these results support the notion that Cav-Ig administration prevents the development of pulmonary GVHD in whole-CB–transplant mice by decreasing the number of IL-26$^+$CD26$^+$CD4 T cells.

B. Therapeutic Administration of Cav-Ig after Onset of GVHD

Because pulmonary GVHD progresses in an indolent manner over weeks and months, patients are often affected by the clinical findings prior to being diagnosed with cGVHD.[24] We therefore sought to determine whether blockade of caveolin-1/CD26 interaction effectively suppresses OB development following the appearance of clinical signs/symptoms. For this purpose, treatment began on day 29 following the appearance of an increase in GVHD scores, indicating the early stages of cGVHD development. Recipients treated with Cav-Ig survived for 7 months with remission of GVHD symptoms (Figs. 10A and B). Meanwhile, the survival rate of recipients treated with control Ig was significantly decreased (Fig. 10A), with progression of clinical signs/symptoms of GVHD (Fig. 10B). Human cells were engrafted similarly in both groups (Figs. 10C and D). In contrast to progressive OB of control Ig treated-recipients, peribrochial inflammation shown at post transplantation week 5 was attenuated at post transplantation week 10 in Cav-Ig–treated recipients (Fig. 10E). On the other hand, the pathologic scores of control Ig-treated recipients were significantly increased at 10 weeks compared to those at week 5 (Fig. 10F). Meanwhile, the pathologic scores of Cav-Ig treated recipients were significantly reduced at week 10 compared to those at week 5 (Fig. 10F), and these scores were clearly less than those of control Ig-treated recipients (Fig. 10F). These effects of Cav-Ig administration were also observed in the skin and liver (Figs. 10G, H, I and J). Moreover, levels of human IFN-γ$^+$ and IL-26$^+$CD26$^+$CD4 T cells in the lung of control Ig-treated recipients were significantly increased at 10 weeks compared to those at week 5 (∗ of Fig. 10K). On the other hand, levels of human IFN-γ$^+$ and IL-26$^+$CD26$^+$CD4 T cells in the lung of Cav-Ig–treated recipients were significantly reduced at week 10 compared to those at week 5 (∗∗ of Fig. 10K), and these levels were clearly less than those of control Ig treated-recipients (∗∗∗ of Fig. 10K). Furthermore, total collagen contents in the lung were significantly lower in Cav-Ig–treated recipients than control Ig-treated recipients (Fig. 10L). Taken together, these data suggest that Cav-Ig administration not only prevents the development of cGVHD but also represents a novel therapeutic approach for the early stages of cGVHD by regulating levels of IL-26$^+$CD26$^+$CD4 T cells.

C. Treatment with Cav-Ig Preserves GVL Capability

Begell Author Proofs

Because GVHD and GVL effect are highly linked immune reactions,[96] we evaluated the potential influence of Cav-Ig treatment on GVL effect. For this purpose, cohorts of Cav-Ig-treated or control Ig-treated whole-CB–transplant mice were irradiated at sublethal doses and then injected intravenously with luciferase-transfected A20 (A20-luc) cells 1 day prior to whole CB transplantation to allow for dissemination of tumor cells. In day 1 following transplantation, treatment with Cav-Ig or control Ig three times per week began and continued to day 28. Mice inoculated with A20 cells alone all died of tumor progression within 6 weeks (Figs. 11A and B). Recipients treated with control Ig exhibited clinical evidence of GVHD such as weight loss and ruffled fur and died of GVHD without tumor progression in 13 weeks (Figs. 11A and B). In contrast, recipient mice treated with Cav-Ig displayed significantly prolonged survival (Fig. 11A) without involvement of A20-luc cells (Fig. 11B). To better characterize the potency of the GVL effect, we

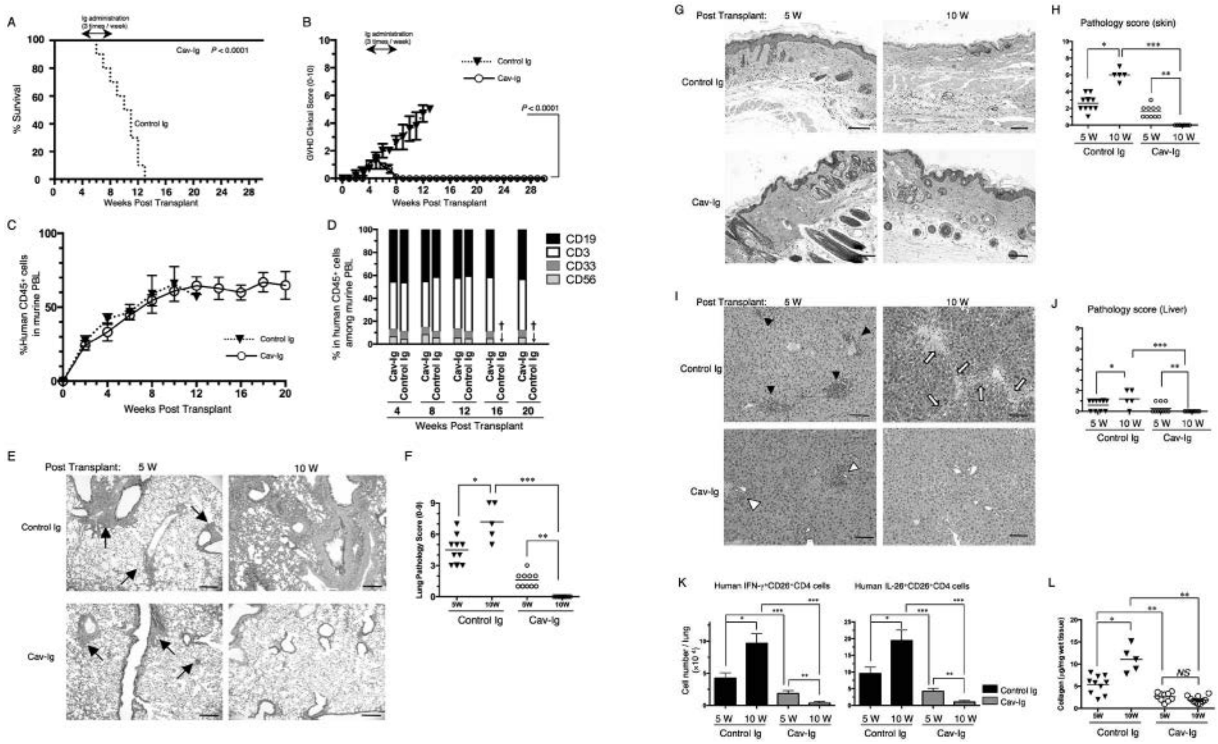

Begell Author Proofs

FIG. 10: Administration of Cav-Ig during early GVHD development impedes lethal GVHD by reducing the level of IL-26$^+$CD26$^+$CD4 cells and collagen deposition in the lung. Sublethally irradiated NOG mice were transplanted with 1X10^7 mononuclear cells isolated from HuCB. Cav-Ig or control Ig (each 100μg/dose) was administered intraperitoneally three times per week, beginning at day 29 after transplantation and continued until day 56. (A) Overall survival and (B) clinical GVHD score (mean±SEM). (C) Peripheral blood of recipients was harvested at the indicated time points, and populations of human CD45$^+$ cells were analyzed using flow cytometry. Data are shown as mean±SEM of human CD45$^+$ cells among total PBL. (D) Sustained composition of human leukocyte populations in recipient PBL. PBL harvested from each group were stained for human CD3, CD19, CD33, or CD56 among human CD45$^+$ cells. Data are presented as mean percentages of human CD45$^+$ cells. Cross indicates death of all mice in control Ig group. (E) H&E staining of the lung tissues of control Ig group and Cav-Ig group at 5 weeks or 10 weeks post transplantation. Arrows indicate perivascular and peribronchial inflammation of the small airway. Original magnification is 100X. Scale bars indicate 100 μm. (F) Pathologic damage in the lung of recipients administered with Cav-Ig or control Ig was examined at 5 and 10 weeks post transplantation using a semiquantitative scoring system. Each dot indicates individual value and horizontal bars indicate mean value. (G) H&E staining of the skin tissues of control Ig group or Cav-Ig group at 5 weeks or 10 weeks post transplantation. Normal skin histology was observed in recipient mice with Cav-Ig administration, in contrast to sclerodermatous changes developed in recipient mice with control Ig administration. Original magnification is 100X. Scale bars indicate 100μm. (H) Pathologic damage in the skin of recipients administered with Cav-Ig or control Ig was examined at 5 and 10 weeks post transplantation using a semiquantitative scoring system. Recipients of control Ig developed progression of GVHD pathology (*, $P<0.0001$). In contrast, recipients of Cav-Ig showed significant reduction in GVHD pathology at 10 weeks rather than at 5 weeks post transplantation (**, $P<0.0001$), and also as compared to recipients of control Ig group at 10 weeks (***, $P<0.0001$). Each dot indicates individual value and horizontal bars indicate mean value. (I) H&E staining of the liver tissues of control Ig group or Cav-Ig group at 5 weeks or 10 weeks post transplantation. In recipient mice with Cav-Ig administration, portal inflammation was observed at 5 weeks post transplantation (white arrow heads), with restoration to normal appearance at 10 weeks post transplantation. In contrast, portal inflammation was observed in recipient mice with control Ig administration at 5 post transplantation (black arrow heads) and portal

fibrosis, at 10 weeks post transplantation (yellow arrows). Original magnification is 100X. Scale bars indicate 100μm. (J) Pathologic damage in the livers of recipients administered with Cav-Ig or control Ig was examined at 5 and 10 weeks post transplantation using a semiquantitative scoring system. Recipients of control Ig developed progression of GVHD pathology (*, $P<0.05$). In contrast, recipients of Cav-Ig showed significant reduction in GVHD pathology at 10 weeks rather than at 5 weeks post transplantation (**, $P<0.0001$), and also as compared to recipients of control Ig group at 10 weeks (***, $P<0.0001$). Each dot indicates individual value and horizontal bars indicate mean value. (K) Absolute cell number of human IFN-γ^+ or IL-26$^+$CD26$^+$CD4 cells in the lung of recipients of Cav-Ig or control Ig group. *, **, or *** indicates $P<0.0001$. (L) Collagen contents in the lung of recipients of Cav-Ig or control Ig group (5 and 10 weeks post transplantation) were quantified by Sircol collagen assay. The mean number (±SEM) of total collagen contents (μg) per wet lung tissue weight (mg) was determined. Each dot indicates individual value and horizontal bars indicate mean value. * or ** indicates $P<0.0001$; NS, not significant [(A) – (F) reprinted with permission from The American Association of Immunologists, Inc., copyright 2015].[51]

repeated these studies with injection of A20-luc cells on day 28 after whole CB transplantation to allow for the acquisition of immunosuppression by Cav-Ig treatment. Mice inoculated with A20 cells alone all died of tumor progression within 2 weeks after tumor inoculation (Figs. 11C and D). Recipient mice treated with control Ig demonstrated clinical evidence of GVHD such as weight loss and ruffled fur and died of GVHD without tumor progression within 13 weeks after transplantation (Figs. 11C and D). In contrast, recipients treated with Cav-Ig exhibited significantly prolonged survival (Fig. 11C) without involvement of A20-luc cells (Fig. 11D). Collectively, these results demonstrate that Cav-Ig treatment of whole-CB–transplant mice was effective in reducing the symptoms of cGVHD without a concomitant loss of the GVL effect.

VII. PERSPECTIVES

While the human CD26 amino acid sequence has 85% amino acid identity with the mouse CD26,[72] the mouse CD26 has different biologic properties from the human CD26, including the fact that the mouse CD26 is not a T-cell activation marker and does not bind to ADA.[72,97] Therefore, humanized murine models need to be developed to explore the role of CD26-mediated costimulation in cGVHD. With relevance as a costimulatory ligand for human CD26, human caveolin-1 has 95% amino acid identity with the mouse caveolin-1,[95] and the binding regions of the mouse caveolin-1 for human CD26 are well conserved. Costimulatory activation of human T cells in NOG mice therefore can occur via CD26–caveolin-1 interaction. Moreover, the N-terminal domain is present in the outer cell surface during the antigen presenting process,[18] and caveolin-1 forms homodimer or homo-oligomer via its N-terminal domain.[95] These collective data suggest that the administered Cav-Ig binds to the N-terminal of caveolin-1 on the cell surface of APCs as well as to CD26 in T cells, leading to suppression of cGVHD in HuCB-NOG mice via blockade of CD26-caveolin-1 interaction.

In addition to the priming of donor-derived T cells by APCs, production of effector cytokines in the target organs plays an important role in cGVHD development.[1] In the present study, we found that donor-derived CD4 T cells predominantly infiltrated the OB lesions of HuCB-NOG mice and that IL-26 as well as IFN-γ levels were enhanced significantly in the infiltrating human CD26$^+$CD4 T cells. Although there has been little information available regarding the biological functions of IL-26 using animal models due to the absence of the IL-26 gene in mouse,[52,69] we demonstrated the role of IL-26 in lung fibrosis using a humanized murine cGVHD model. Moreover, our murine allogeneic transplantation model utilizing 190-*IFNG* Tg and ΔCNS-77 Tg mice demonstrated that human IL-26, not IFN-γ, induced pulmonary fibrosis. In both 190-*IFNG* Tg and ΔCNS-77 Tg mice, production of IFN-γ by T or NK cells is equivalent in both tissue culture studies and analysis of basal levels in various tissues including spleen, lymph

Begell Author Proofs

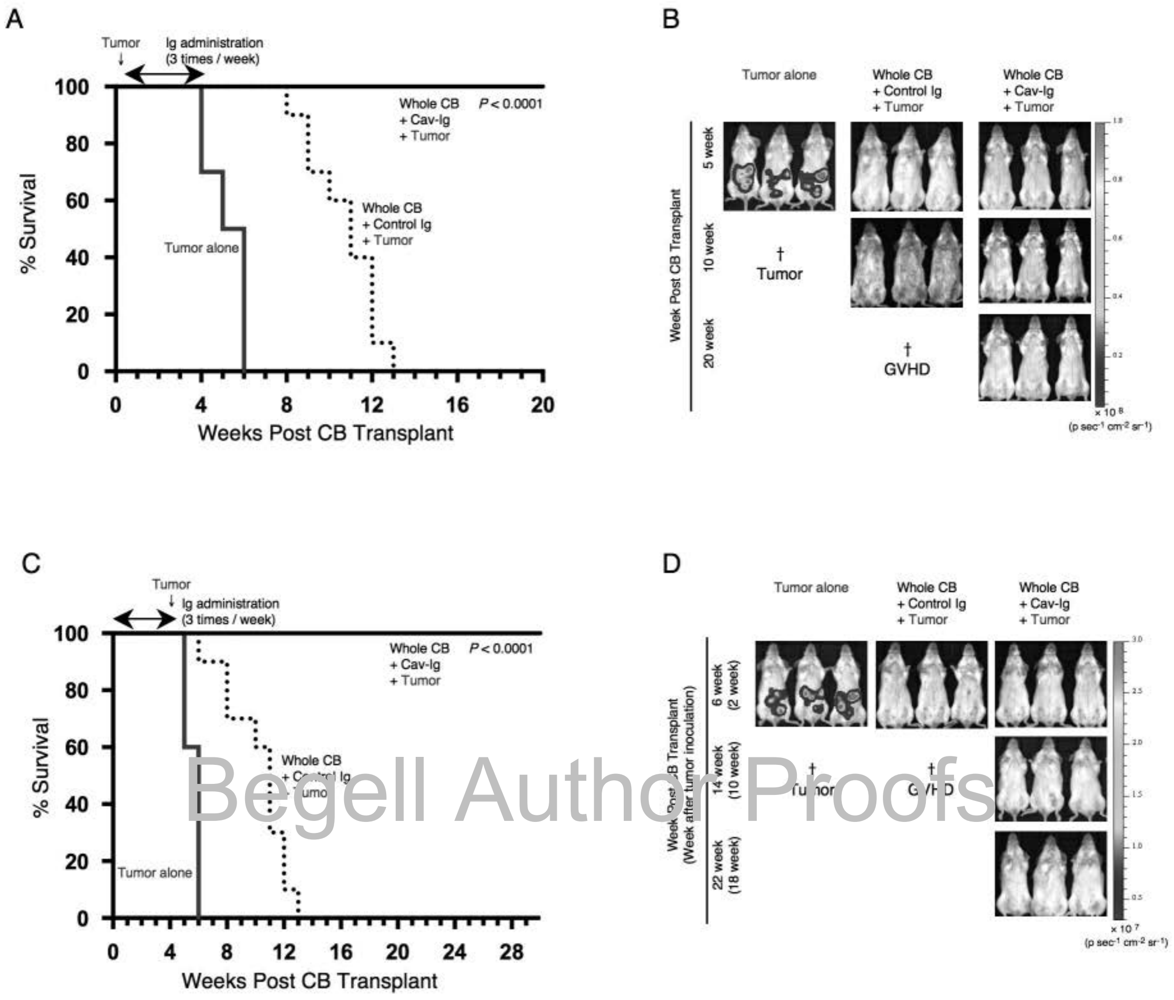

Begell Author Proofs

FIG. 11: Cav-Ig preserves GVL effect. (A) NOG mice were irradiated at a sublethal dose (200 cGy) and the next day were inoculated with 1X10^4 A20-luc cells via tail vein. The mice were then transplanted the following day with 1X10^7 mononuclear cells isolated from HuCB. Cav-Ig or control Ig (each 100μg/dose) was administered intraperitoneally thrice a week, beginning at day 1 after transplantation and continued until day +28. Overall survival is depicted. *P*<0.0001 versus recipients of control Ig by log-rank test. (B) *In vivo* bioluminescence imaging (BLI) was performed at the indicated time points after treatment as described in panel A. Representative mice are shown. Cross indicates death of all mice in the group of tumor alone or control Ig groups. Ruffled fur consistent with skin GVHD is shown in recipients of control Ig group at 10 weeks post transplant (middle panel). (C) Sublethally irradiated NOG mice were transplanted with mononuclear cells isolated from HuCB. Cav-Ig or control Ig was administered intraperitoneally three times per week, beginning at day 1 after transplantation and continued until day +28. 1X10^5 A20-luc cells were inoculated via tail vein on day +28 post transplantation. Overall survival is depicted. *P*<0.0001 versus recipients of control Ig by log-rank test. (D) *In vivo* BLI was performed at the indicated time points after treatment as described in panel C. Representative mice are shown. Cross indicates death of all mice in the group of tumor alone or control Ig groups. Slightly ruffled fur consistent with skin GVHD is shown in recipients of control Ig group at 6 weeks post transplant (middle panel).

node, and colon.[57] On the other hand, expression of IL-26 is observed in T_H1- or T_H17-polarizing CD4 cells of 190-*IFNG* Tg mice, whereas it is completely abrogated in ΔCNS-77 Tg mice.[52] Although human and murine IFN-γ share 40% amino acid identity, IFN-γ exhibits species specificity with respect to receptor binding and biological activity.[98,99] Taken together with the previous report that development of cGVHD lung is independent of IFN-γ,[68] the elevated human IFN-γ in HuCB-NOG did not likely function as an inflammatory cytokine but rather as a T_H1 and/or T_H17 cell marker of $CD26^+CD4$ T cells.[15,20,100] Regarding its specific receptor, IL-26 primarily binds to IL-20RA, followed by recruitment of IL-10RB.[56] Although IL-10RB is broadly expressed on most cell types and tissues, IL-20RA is not expressed in lymphoid organs but is expressed in the lung and skin.[101] It is thus conceivable that IL-26–related chronic inflammatory changes in HuCB-NOG mice occur in the lung and skin of cGVHD or autoimmune diseases, including systemic sclerosis.

Recent work with a murine model showed that donor-derived B-cell activation and maturation with the aid of TfH were necessary for cGVHD and that bronchiolitis obliterans syndrome was reversed by the abrogation of IL-21 signaling.[30] However, in our present model with OB, a substantial B-cell population was detected in the recipient PBL. In fact, no direct evidence for a causal relationship for autoantibodies or alloantibodies in the pathogenesis of organ manifestation of cGVHD has been observed in humans.[29] Furthermore, cGVHD of the visceral organs seemed to respond poorly to B-cell depletion therapy such as rituximab.[29,37] It is speculated that this observed discrepancy is due to differences in the B-cell maturation process between mice and human.[40] Despite these limitations of murine or humanized murine models, targeting CD4 T cells to control cGVHD is a reasonable therapeutic approach because T cell help plays a pivotal role in B-cell maturation and activation in cGVHD.[102] A related issue concerns the process of B-cell development in humanized mice. Given the fact that HuCB contains ample HSCs as well as naïve lymphocytes, the use of HuCB as donor cells led to sustained recovery of lymphocytes in the recipient PBL, as had also been reported by other investigators.[46,48,49,103] In addition, it has been demonstrated that specific antibodies in human B cells generated in the humanized mice transplanted with HSC isolated from HuCB were effectively synthesized.[45,46,48,50] Despite the limitations of cross-species comparisons, our study provides insights into the pathogenesis of clinical pulmonary cGVHD induced by human lymphocytes.

Begell Author Proofs

Because we previously showed an effect of anti-CD26 mAb on an aGVHD model using adult PBL,[42] we performed preliminary testing of anti-CD26 mAb effect on recipient mice of whole-CB–transplant, and found a high incidence of graft failure. Our speculation regarding the reason for this failure is this: We previously reported that HuCB CD4 T cells broadly express CD26,[43] and other investigators observed that $CD34^+CD38^{low/-}$ or $CD34^+CD38^+$ hematopoietic stem/progenitor cells in HuCB preferentially express CD26.[104] These findings suggest that treatment with anti-CD26 mAb in a HuCB transplant model may reduce the levels of hematopoietic stem/progenitor and/or CD4 T cells in the graft of HuCB, resulting in increased graft failure.

Importantly, there may be potential adverse events such as off-target effects associated with the proposed use of Cav-Ig therapy. Although caveolin-1 exists in the inner surface of most cell types,[95] its N-terminus is detected on endothelial cells as well as APCs following cellular activation.[105] Therefore, it is possible that Cav-Ig binds to cell surface caveolin-1, thereby affecting endothelial cell functions. Other issues relate to the GVL effects. Our data demonstrated that Cav-Ig clearly impeded GVHD in our model with preservation of GVL effects. We speculate that CD26-dependent xenogeneic priming of CD4 T cells is inhibited by Cav-Ig,[19,42] while CD28-dependent GVL effects are exerted after engraftment.[106]

Based on our study, it is conceivable that IL-26 may be another potential therapeutic target in the management of clinical cGVHD. We have already developed several clones of anti-IL-26 mAb that have been screened for inhibitory effects on various cells expressing IL-26 receptor. IL-26 has been reported to exhibit antibacterial and antiviral effects as part of a host defense mechanism.[66] We are currently actively investigating whether anti-IL-26 therapy exacerbates bacterial infections in the presence of GVHD following HSCT, and definitive data regarding the effects of IL-26-targeted therapy will be presented in the near future.

In conclusion, our present work demonstrates that caveolin-1 blockade controls cGVHD by suppressing the immune functions of donor-derived T cells and decreasing IL-26 production. Moreover, IL-26$^+$CD26$^+$CD4 T-cell infiltration appears to play a significant role in cGVHD of the lung and skin. While complete suppression of cGVHD with current interventional strategies represents a difficult challenge at the present time, our data demonstrate that control of cGVHD clinical findings can be achieved in a murine experimental system by regulating IL-26$^+$CD26$^+$CD4 T cells with Cav-Ig. Our work also suggests that Cav-Ig treatment may be a novel therapeutic approach for chronic inflammatory diseases, including RA and IBD, in which IL-26 plays an important role.

Begell Author Proofs

ACKNOWLEDGMENTS

This work was supported by JSPS KAKENHI (grant nos. 15H04879 and 15K15324 to K.O.); JSPS KAKENHI (grant no 16H05345 to C.M.); JPSP KAKENHI (grant no. 16K09878 to N.I.); JSPS Research Fellowships for Young Scientists (R.H.); a grant from the Ministry of Health, Labour, and Welfare, Japan (grant no. 150401-01 to C.M.); and a Grant-in-Aid from the Foundation of Strategic Research Projects in Private Universities from the Ministry of Education, Culture, Sports, Science, and Technology, Japan (grant no. S1311011 to K.O. and C.M).

REFERENCES

1. Blazar BR, Murphy WJ, Abedi M. Advances in graft-versus-host disease biology and therapy. Nat Rev Immunol. 2012;12:443–58.
2. Deeg HJ, Lin D, Leisenring W, Boeckh M, Anasetti C, Appelbaum FR, Chauncey TR, Doney K, Flowers M, Martin P, Nash R, Schoch G, Sullivan KM, Witherspoon RP, Storb R. Cyclosporine or cyclosporine plus methylprednisolone for prophylaxis of graft-versus-host disease: a prospective, randomized trial. Blood. 1997;89:3880–7.
3. Filipovich AH. Diagnosis and manifestations of chronic graft-versus-host disease. Best Pract Res Clin Haematol. 2008;21:251–7.
4. Socie G, Ritz J. Current issues in chronic graft-versus-host disease. Blood. 2014;124:374–84.
5. Chien JW, Duncan S, Williams KM, Pavletic SZ. Bronchiolitis obliterans syndrome after allogeneic hematopoietic stem cell transplantation-an increasingly recognized manifestation of chronic graft-versus-host disease. Biol Blood Marrow Transplant. 2010;16:S106–14.
6. Dudek AZ, Mahaseth H, DeFor TE, Weisdorf DJ. Bronchiolitis obliterans in chronic graft-versus-host disease: analysis of risk factors and treatment outcomes. Biol Blood Marrow Transplant. 2003;9:657–66.
7. Nakasone H, Kanda J, Yano S, Atsuta Y, Ago H, Fukuda T, Kakihana K, Adachi T, Yujiri T, Taniguchi S, Taguchi J, Morishima Y, Nagamura T, Sakamaki H, Mori T, Murata M: GVHD Working Group of the Japan Society for Hematopoietic Cell Transplantation. A case–control study of bronchiolitis obliterans syndrome following allogeneic hematopoietic stem cell transplantation. Transplant Intl. 2013;26:631–9.
8. Zeiser R, Blazar BR. Preclinical models of acute and chronic graft-versus-host disease: how predictive are they for a successful clinical translation? Blood. 2016;127:3117–26.
9. Champlin R, Khouri I, Giralt S. Graft versus malignancy with allogeneic blood stem cell transplantation: a potential primary treatment modality. Pediatr Transplant. 1999;3 Suppl 1:52–8.
10. Rudd CE. T-cell signaling and immunopathologies. Semin Immunopathol. 2010;32:91–4.
11. Fox DA, Hussey RE, Fitzgerald KA, Acuto O, Poole C, Palley L, Daley JF, Schlossman SF, Reinherz EL. Ta1, a novel 105 KD human T cell activation antigen defined by a monoclonal antibody. J Immunol. 1984;133:1250–6.
12. Morimoto C, Torimoto Y, Levinson G, Rudd CE, Schrieber M, Dang NH, Letvin NL, Schlossman SF. 1F7, a novel cell surface molecule, involved in helper function of CD4 cells. J Immunol. 1989;143:3430–9.
13. Dang NH, Torimoto Y, Deusch K, Schlossman SF, Morimoto C. Comitogenic effect of solid-phase immobilized anti-1F7 on human CD4 T cell activation via CD3 and CD2 pathways. J Immunol. 1990;144:4092–100.
14. Ohnuma K, Dang NH, Morimoto C. Revisiting an old acquaintance: CD26 and its molecular mechanisms in T cell function. Trends Immunol. 2008;29:295–301.
15. Morimoto C, Schlossman SF. The structure and function of CD26 in the T-cell immune response. Immunol Rev. 1998;161:55–70.
16. Ohnuma K, Uchiyama M, Yamochi T, Nishibashi K, Hosono O, Takahashi N, Kina S, Tanaka H, Lin X, Dang NH, Morimoto C. Caveolin-1 triggers T-cell activation

via CD26 in association with CARMA1. J Biol Chem. 2007;282:10117–31.

17. Ohnuma K, Yamochi T, Uchiyama M, Nishibashi K, Iwata S, Hosono O, Kawasaki H, Tanaka H, Dang NH, Morimoto C. CD26 mediates dissociation of Tollip and IRAK-1 from caveolin-1 and induces upregulation of CD86 on antigen-presenting cells. Mol Cell Biol. 2005;25:7743–57.
18. Ohnuma K, Yamochi T, Uchiyama M, ishibashi K, Yoshikawa N, Shimizu N, Iwata S, Tanaka H, Dang NH, Morimoto C. CD26 up-regulates expression of CD86 on antigen-presenting cells by means of caveolin-1. Proc Natl Acad Sci U S A. 2004;101:14186–191.
19. Ohnuma K, Uchiyama M, Hatano R, Takasawa W, Endo Y, Dang NH, Morimoto C. Blockade of CD26-mediated T cell costimulation with soluble caveolin-1-Ig fusion protein induces anergy in CD4$^+$ T cells. Biochem Biophys Res Commun. 2009;386:327–32.
20. Bengsch B, Seigel B, Flecken T, Wolanski J, Blum HE, Thimme R. Human Th17 cells express high levels of enzymatically active dipeptidylpeptidase IV (CD26). J Immunol. 2012;188:5438–47.
21. Filipovich AH, Weisdorf D, Pavletic S, Socie G, Wingard JR, Lee SJ, Martin P, Chien J, Przepiorka D, Couriel D, Cowen EW, Dinndorf P, Farrell A, Hartzman R, Henslee-Downey J, Jacobsohn D, McDonald G, Mittleman B, Rizzo JD, Robinson M, Schubert M, Schultz K, Shulman H, Turner M, Vogelsang G, Flowers ME. National Institutes of Health consensus development project on criteria for clinical trials in chronic graft-versus-host disease. I. Diagnosis and staging working group report. Biol Blood Marrow Transplant. 2005;11:945–56.
22. Shulman HM, Cardona DM, Greenson JK, Hingorani S, Horn T, Huber E, Kreft A, Longerich T, Morton T, Myerson D, Prieto VG, Rosenberg A, Treister N, Washington K, Ziemer M, Pavletic SZ, Lee SJ, Flowers ME, Schultz KR, Jagasia M, Martin PJ, Vogelsang GB, Kleiner DE. NIH Consensus Development Project on Criteria for Clinical Trials in Chronic Graft-versus-Host Disease: II. The 2014 Pathology Working Group Report. Biol Blood Marrow Transplant. 2015;21:589–603.
23. Shlomchik WD. Graft-versus-host disease. Nat Rev Immunol. 2007;7:340–52.
24. Soiffer R. Immune modulation and chronic graft-versus-host disease. Bone Marrow Transplant. 2008;42 Suppl 1:S66–9.
25. Champlin RE. T-cell depletion for bone marrow transplantation: effects on graft rejection, graft-versus-host disease, graft-versus-leukemia, and survival. Cancer Treat Res. 1990;50:99–111.
26. Ho VT, Soiffer RJ. The history and future of T-cell depletion as graft-versus-host disease prophylaxis for allogeneic hematopoietic stem cell transplantation. Blood. 2001;98:3192–204.
27. Broady R. Cutaneous GVHD is associated with the expansion of tissue-localized Th1 and not Th17 cells. Blood. 2010;116:5748–751.
28. Matsuoka K, Kim HT, McDonough S, Bascug G, Warshauer B, Koreth J, Cutler C, Ho VT, Alyea EP, Antin JH, Soiffer RJ, Ritz J. Altered regulatory T cell homeostasis in patients with CD4$^+$ lymphopenia following allogeneic hematopoietic stem cell transplantation. J Clin Invest. 2010;120:1479–93.
29. Shimabukuro-Vornhagen A, Hallek MJ, Storb RF, von Bergwelt-Baildon MS. The role of B cells in the pathogenesis of graft-versus-host disease. Blood. 2009;114:4919–27.
30. Flynn R, Du J, Veenstra RG, Reichenbach DK, Panoskaltsis-Mortari A, Taylor PA, Freeman GJ, Serody JS, Murphy WJ, Munn DH, Sarantopoulos S, Luznik L, Maillard I, Koreth J, Cutler C, Soiffer RJ, Antin JH, Ritz J, Dubovsky JA, Byrd JC, Macdonald KP, Hill GR, Blazar BR. Increased T follicular helper cells and germinal center B cells are required for chronic GVHD and bronchiolitis obliterans. Blood. 2014;123:3988–998.
31. Finke J, Bethge WA, Schmoor C, Ottinger HD, Stelljes M, Zander AR, Volin L, Ruutu T, Heim DA, Schwerdtfeger R, Kolbe K, Mayer J, Maertens JA, Linkesch W, Holler E, Koza V, Bornhauser M, Einsele H, Kolb HJ, Bertz H, Egger M, Grishina O, Socie G. Standard graft-versus-host disease prophylaxis with or without anti-T-cell globulin in haematopoietic cell transplantation from matched unrelated donors: a randomised, open-label, multicentre phase 3 trial. Lancet Oncol. 2009;10:855–64.
32. Kröger N, Solano C, Wolschke C, Bandini G, Patriarca F, Pini M, Nagler A, Selleri C, Risitano A, Messina G, Bethge W, Pérez de OJ, Duarte R, Carella AM, Cimminiello M, Guidi S, tefanoFinke J, Mordini N, Ferra C, Sierra J, Russo D, Petrini M, Milone G, Benedetti F, Heinzelmann M, Pastore D, Jurado M, Terruzzi E, Narni F, Vöp A, Ayuk F, Ruutu T, Bonifazi F. Antilymphocyte globulin for prevention of chronic graft-versus-host disease. N Engl J Med. 2016;374:43–53.
33. Ayuk FA, Fang L, Fehse B, Zander AR, Kroger N. Antithymocyte globulin induces complement-dependent cell lysis and caspase-dependent apoptosis in myeloma cells. Exp Hematol. 2005;33:1531–6.
34. Fang L, Fehse B, Engel M, Zander A, Kroger N. Antithymocyte globulin induces *ex vivo* and *in vivo* depletion of myeloid and plasmacytoid dendritic cells. Transplantation. 2005;79:369–71.
35. Shimony O, Nagler A, Gellman YN, Refaeli E, Rosenblum N, Eshkar-Sebban L, Yerushalmi R, Shimoni A, Lytton SD, Stanevsky A, Or R, Naor D. Anti-T lymphocyte globulin (ATG) induces generation of regulatory T cells, at least part of them express activated CD44. J Clin Immunol. 2011;32:173–88.
36. Chu YW, Gress RE. Murine models of chronic graft-versus-host disease: insights and unresolved issues. Biol Blood Marrow Transplant. 2008;14:365–78.
37. Barker AF, Bergeron A, Rom WN, Hertz MI. Obliterative bronchiolitis. N Engl J Med. 2014;370:1820–8.
38. Reddy P, Johnson K, Uberti JP, Reynolds C, Silver S, Ayash L, Braun TM, Ratanatharathorn V. Nephrotic syndrome

Begell Author Proofs

associated with chronic graft-versus-host disease after allogeneic hematopoietic stem cell transplantation. Bone Marrow Transplant. 2006;38:351–7.

39. Seok J, Warren HS, Cuenca AG, Mindrinos MN, Baker HV, Xu W, Richards DR, McDonald-Smith GP, Gao H, Hennessy L, Finnerty CC, Lopez CM, Honari S, Moore EE, Minei JP, Cuschieri J, Bankey PE, Johnson JL, Sperry J, Nathens AB, Billiar TR, West MA, Jeschke MG, Klein MB, Gamelli RL, Gibran NS, Brownstein BH, Miller-Graziano C, Calvano SE, Mason PH, Cobb JP, Rahme LG, Lowry SF, Maier RV, Moldawer LL, Herndon DN, Davis RW, Xiao W, Tompkins RG. Genomic responses in mouse models poorly mimic human inflammatory diseases. Proc Natl Acad Sci U S A. 2013;110:3507–12.
40. Benitez A, Weldon AJ, Tatosyan L, Velkuru V, Lee S, Milford TA, Francis OL, Hsu S, Nazeri K, Casiano CM, Schneider R, Gonzalez J, Su RJ, Baez I, Colburn K, Moldovan I, Payne KJ. Differences in mouse and human nonmemory B cell pools. J Immunol. 2014;192:4610–19.
41. Antin JH, Bierer BE, Smith BR, Ferrara J, Guinan EC, Sieff C, Golan DE, Macklis RM, Tarbell NJ, Lynch E, Reichert TA, Blythman H, Bouloux C, Rappeport JM, Burakoff SJ, Weinstein HJ. Selective depletion of bone marrow T lymphocytes with anti-CD5 monoclonal antibodies: effective prophylaxis for graft-versus-host disease in patients with hematologic malignancies. Blood. 1991;78:2139–49.
42. Hatano R, Ohnuma K, Yamamoto J, Dang NH, Yamada T, Morimoto C. Prevention of acute graft-versus-host disease by humanized anti-CD26 monoclonal antibody. Br J Haematol. 2013;162:263–77.
43. Kobayashi S, Ohnuma K, Uchiyama M, Iino K, Iwata S, Dang NH, Morimoto C. Association of CD26 with CD45RA outside lipid rafts attenuates cord blood T-cell activation. Blood. 2004;103:1002–10.
44. Sato K, Nagayama H, Takahashi TA. Aberrant CD3- and CD28-mediated signaling events in cord blood T cells are associated with dysfunctional regulation of Fas ligand-mediated cytotoxicity. J Immunol. 1999;162:4464–71.
45. Shultz LD, Brehm MA, Garcia-Martinez JV, Greiner DL. Humanized mice for immune system investigation: progress, promise and challenges. Nat Rev Immunol. 2012;12:786–98.
46. Tezuka K, Xun R, Tei M, Ueno T, Tanaka M, Takenouchi N, Fujisawa J. An animal model of adult T-cell leukemia: humanized mice with HTLV-1-specific immunity. Blood. 2014;123:346–55.
47. Ito M, Hiramatsu H, Kobayashi K, Suzue K, Kawahata M, Hioki K, Ueyama Y, Koyanagi Y, Sugamura K, Tsuji K, Heike T, Nakahata T. NOD/SCID/γ_c^{null} mouse: an excellent recipient mouse model for engraftment of human cells. Blood. 2002;100:3175–82.
48. Matsumura T, Kametani Y, Ando K, Hirano Y, Katano I, Ito R, Shiina M, Tsukamoto H, Saito Y, Tokuda Y, Kato S, Ito M, Motoyoshi K, Habu S. Functional CD5$^+$ B cells develop predominantly in the spleen of NOD/SCID/γ_c^{null} (NOG) mice transplanted either with human umbilical cord blood, bone marrow, or mobilized peripheral blood CD34$^+$ cells. Exp Hematol. 2003;31:789–97.
49. Yahata T, Ando K, Nakamura Y, Ueyama Y, Shimamura K, Tamaoki N, Kato S, Hotta T. Functional human T lymphocyte development from cord blood CD34$^+$ cells in nonobese diabetic/Shi-*scid*, IL-2 receptor γ null mice. J Immunol. 2002;169:204–9.
50. Ito R, Takahashi T, Katano I, Ito M. Current advances in humanized mouse models. Cell Mol Immunol. 2012;9:208–14.
51. Ohnuma K, Hatano R, Aune TM, Otsuka H, Iwata S, Dang NH, Yamada T, Morimoto C. Regulation of pulmonary graft-versus-host disease by IL-26$^+$CD26$^+$CD4 T lymphocytes. J Immunol. 2015;194:3697–712.
52. Collins PL, Henderson MA, Aune TM. Lineage-specific adjacent *IFNG* and *IL26* genes share a common distal enhancer element. Genes Immun. 2012;13:481–8.
53. Donnelly RP, Sheikh F, Dickensheets H, Savan R, Young HA, Walter MR. Interleukin-26: an IL-10-related cytokine produced by Th17 cells. Cytokine Growth Factor Rev. 2010;21:393–401.
54. Knappe A, Hor S, Wittmann S, Fickenscher H. Induction of a novel cellular homolog of interleukin-10, AK155, by transformation of T lymphocytes with herpesvirus saimiri. J Virol. 2000;74:3881–7.
55. Kotenko SV. The family of IL-10-related cytokines and their receptors: related, but to what extent? Cytokine Growth Factor Rev. 2002;13:223–40.
56. Hor S, Pirzer H, Dumoutier L, Bauer F, Wittmann S, Sticht H, Renauld JC, de Waal Malefyt R, Fickenscher H. The T-cell lymphokine interleukin-26 targets epithelial cells through the interleukin-20 receptor 1 and interleukin-10 receptor 2 chains. J Biol Chem. 2004;279:33343–51.
57. Collins PL, Chang S, Henderson M, Soutto M, Davis GM, McLoed AG, Townsend MJ, Glimcher LH, Mortlock DP, Aune TM. Distal regions of the human *IFNG* locus direct cell type-specific expression. J Immunol. 2010;185:1492–501.
58. Wilson NJ, Boniface K, Chan JR, McKenzie BS, Blumenschein WM, Mattson JD, Basham B, Smith K, Chen T, Morel F, Lecron JC, Kastelein RA, Cua DJ, McClanahan TK, Bowman EP, de Waal Malefyt R. Development, cytokine profile and function of human interleukin 17-producing helper T cells. Nat Immunol. 2007;8:950–7.
59. Corvaisier M, Delneste Y, Jeanvoine H, Preisser L, Blanchard S, Garo E, Hoppe E, Barre B, Audran M, Bouvard B, Saint-Andre JP, Jeannin P. IL-26 is overexpressed in rheumatoid arthritis and induces proinflammatory cytokine production and Th17 cell generation. PLoS Biol. 2012;10:e1001395.
60. Sheikh F, Baurin VV, Lewis-Antes A, Shah NK, Smirnov SV, Anantha S, Dickensheets H, Dumoutier L, Renauld JC, Zdanov A, Donnelly RP, Kotenko SV. Cutting edge: IL-26 signals through a novel receptor complex composed of IL-20 receptor 1 and IL-10 receptor 2. J Immunol. 2004;172:2006–10.
61. Goris A, Marrosu MG, Vandenbroeck K. Novel

Begell Author Proofs

polymorphisms in the IL-10 related AK155 gene (chromosome 12q15). Genes Immun. 2001;2:284–6.

62. Vandenbroeck K, Cunningham S, Goris A, Alloza I, Heggarty S, Graham C, Bell A, Rooney M. Polymorphisms in the interferon-γ/interleukin-26 gene region contribute to sex bias in susceptibility to rheumatoid arthritis. Arthritis Rheum. 2003;48:2773–8.
63. Silverberg MS, Cho JH, Rioux JD, McGovern DP, Wu J, Annese V, Achkar JP, Goyette P, Scott R, Xu W, Barmada MM, Klei L, Daly MJ, Abraham C, Bayless TM, Bossa F, Griffiths AM, Ippoliti AF, Lahaie RG, Latiano A, Pare P, Proctor DD, Regueiro MD, Steinhart AH, Targan SR, Schumm LP, Kistner EO, Lee AT, Gregersen PK, Rotter JI, Brant SR, Taylor KD, Roeder K, Duerr RH. Ulcerative colitis-risk loci on chromosomes 1p36 and 12q15 found by genome-wide association study. Nat Genet. 2009;41:216–20.
64. Miot C, Beaumont E, Duluc D, Le Guillou-Guillemette H, Preisser L, Garo E, Blanchard S, Hubert Fouchard I, Creminon C, Lamourette P, Fremaux I, Cales P, Lunel-Fabiani F, Boursier J, Braum O, Fickenscher H, Roingeard P, Delneste Y, Jeannin P. IL-26 is overexpressed in chronically HCV-infected patients and enhances TRAIL-mediated cytotoxicity and interferon production by human NK cells. Gut. 2014;64:1466–75.
65. Che KF, Tengvall S, Levanen B, Silverpil E, Smith ME, Awad M, Vikstrom M, Palmberg L, Qvarfordt I, Skold M, Linden A. Interleukin-26 in antibacterial host defense of human lungs. Effects on neutrophil mobilization. Am J Respir Crit Care Med. 2014;190:1022–31.
66. Meller S, Di Domizio J, Voo KS, Friedrich HC, Chamilos G, Ganguly D, Conrad C, Gregorio J, Le Roy D, Roger T, Ladbury JE, Homey B, Watowich S, Modlin RL, Kontoyiannis DP, Liu YJ, Arold ST, Gilliet M. T_H17 cells promote microbial killing and innate immune sensing of DNA via interleukin 26. Nat Immunol. 2015;16:970–9.
67. Shulman HM, Kleiner D, Lee SJ, Morton T, Pavletic SZ, Farmer E, Moresi JM, Greenson J, Janin A, Martin PJ, McDonald G, Flowers ME, Turner M, Atkinson J, Lefkowitch J, Washington MK, Prieto VG, Kim SK, Argenyi Z, Diwan AH, Rashid A, Hiatt K, Couriel D, Schultz K, Hymes S, Vogelsang GB. Histopathologic diagnosis of chronic graft-versus-host disease: National Institutes of Health Consensus Development Project on Criteria for Clinical Trials in Chronic Graft-versus-Host Disease: II. Pathology Working Group Report. Biol Blood Marrow Transplant. 2006;12:31–47.
68. Yi T, Chen Y, Wang L, Du G, Huang D, Zhao D, Johnston H, Young J, Todorov I, Umetsu DT, Chen L, Iwakura Y, Kandeel F, Forman S, Zeng D. Reciprocal differentiation and tissue-specific pathogenesis of Th1, Th2, and Th17 cells in graft-versus-host disease. Blood. 2009;114:3101–12.
69. Fickenscher H, Pirzer H. Interleukin-26. Int Immunopharmacol. 2004;4:609–13.
70. Daddona PE, Kelley WN. Human adenosine deaminase. Stoichiometry of the adenosine deaminase-binding protein complex. Biochim Biophys Acta. 1979;580:302–11.
71. Hopsu-Havu VK, Glenner GG. A new dipeptide naphthylamidase hydrolyzing glycyl-prolyl-β-naphthylamide. Histochemie. 1966;7:197–201.
72. Marguet D, Bernard AM, Vivier I, Darmoul D, Naquet P, Pierres M. cDNA cloning for mouse thymocyte-activating molecule. A multifunctional ecto-dipeptidyl peptidase IV (CD26) included in a subgroup of serine proteases. J Biol Chem. 1992;267:2200–8.
73. Tanaka T, Camerini D, Seed B, Torimoto Y, Dang NH, Kameoka J, Dahlberg HN, Schlossman SF, Morimoto C. Cloning and functional expression of the T cell activation antigen CD26. J Immunol. 1992;149:481–6.
74. Abbott CA, Baker E, Sutherland GR, McCaughan GW. Genomic organization, exact localization, and tissue expression of the human CD26 (dipeptidyl peptidase IV) gene. Immunogenetics. 1994;40:331–8.
75. Bohm SK, Gum JR, Jr., Erickson RH, Hicks JW, Kim YS. Human dipeptidyl peptidase IV gene promoter: tissue-specific regulation from a TATA-less GC-rich sequence characteristic of a housekeeping gene promoter. Biochem J. 1995;311 (Pt 3):835–43.
76. Erickson RH, Lai RS, Lotterman CD, Kim YS. Identification of upstream stimulatory factor as an activator of the human dipeptidyl peptidase IV gene in Caco-2 cells. Gene. 2000;258:77–84.
77. Bauvois B, Djavaheri-Mergny M, Rouillard D, Dumont J, Wietzerbin J. Regulation of CD26/DPPIV gene expression by interferons and retinoic acid in tumor B cells. Oncogene. 2000;19:265–72.
78. Heins J, Welker P, Schonlein C, Born I, Hartrodt B, Neubert K, Tsuru D, Barth A. Mechanism of proline-specific proteinases: (I) Substrate specificity of dipeptidyl peptidase IV from pig kidney and proline-specific endopeptidase from Flavobacterium meningosepticum. Biochim Biophys Acta. 1988;954:161–9.
79. David F, Bernard AM, Pierres M, Marguet D. Identification of serine 624, aspartic acid 702, and histidine 734 as the catalytic triad residues of mouse dipeptidyl-peptidase IV (CD26). A member of a novel family of nonclassical serine hydrolases. J Biol Chem. 1993;268:17247–52.
80. Abbott CA, Yu DM, Woollatt E, Sutherland GR, McCaughan GW, Gorrell MD. Cloning, expression and chromosomal localization of a novel human dipeptidyl peptidase (DPP) IV homolog, DPP8. Eur J Biochem. 2000;267:6140–50.
81. Rasmussen HB, Branner S, Wiberg FC, Wagtmann N. Crystal structure of human dipeptidyl peptidase IV/CD26 in complex with a substrate analog. Nat Struct Biol. 2003;10:19–25.
82. Yaron A, Naider F. Proline-dependent structural and biological properties of peptides and proteins. Crit Rev Biochem Mol Biol. 1993;28:31–81.
83. Bjelke JR, Kanstrup AB, Rasmussen HB. Selectivity among dipeptidyl peptidases of the S9b family. Cell Mol Biol.

Begell Author Proofs

2006;52:3–7.

84. Tanaka T, Kameoka J, Yaron A, Schlossman SF, Morimoto C. The costimulatory activity of the CD26 antigen requires dipeptidyl peptidase IV enzymatic activity. Proc Natl Acad Sci U S A. 1993;90:4586–90.
85. Chien CH, Huang LH, Chou CY, Chen YS, Han YS, Chang GG, Liang PH, Chen X. One site mutation disrupts dimer formation in human DPP-IV proteins. J Biol Chem. 2004;279:52338–45.
86. Dang NH, Torimoto Y, Sugita K, Daley JF, Schow P, Prado C, Schlossman SF, Morimoto C. Cell surface modulation of CD26 by anti-1F7 monoclonal antibody. Analysis of surface expression and human T cell activation. J Immunol. 1990;145:3963–71.
87. Hatano R, Ohnuma K, Yamamoto J, Dang NH, Morimoto C. CD26-mediated co-stimulation in human CD8$^+$ T cells provokes effector function via pro-inflammatory cytokine production. Immunology. 2013;138:165–72.
88. Buhling F, Junker U, Reinhold D, Neubert K, Jager L, Ansorge S. Functional role of CD26 on human B lymphocytes. Immunol Lett. 1995;45:47–51.
89. Fujimaki W, Takahashi N, Ohnuma K, Nagatsu M, Kurosawa H, Yoshida S, Dang NH, Uchiyama T, Morimoto C. Comparative study of regulatory T cell function of human CD25CD4 T cells from thymocytes, cord blood, and adult peripheral blood. Clin Dev Immunol. 2008;2008:305859.
90. Stohlawetz P, Hahn P, Koller M, Hauer J, Resch H, Smolen J, Pietschmann P. Immunophenotypic characteristics of monocytes in elderly subjects. Scand J Immunol. 1998;48:324–6.
91. Ohnuma K, Munakata Y, Ishii T, Iwata S, Kobayashi S, Hosono O, Kawasaki H, Dang NH, Morimoto C. Soluble CD26/dipeptidyl peptidase IV induces T cell proliferation through CD86 up-regulation on APCs. J Immunol. 2001;167:6745–55.
92. Buhling F, Kunz D, Reinhold D, Ulmer AJ, Ernst M, Flad HD, Ansorge S. Expression and functional role of dipeptidyl peptidase IV (CD26) on human natural killer cells. Nat Immunol. 1994;13:270–9.
93. Masuyama J, Berman JS, Cruikshank WW, Morimoto C, Center DM. Evidence for recent as well as long term activation of T cells migrating through endothelial cell monolayers *in vitro*. J Immunol. 1992;148:1367–74.
94. Kloosterboer FM, van Luxemburg-Heijs SA, Willemze R, Falkenburg JH. Similar potential to become activated and proliferate but differential kinetics and profiles of cytokine production of umbilical cord blood T cells and adult blood naive and memory T cells. Hum Immunol. 2006;67:874–83.
95. Engelman JA, Zhang X, Galbiati F, Volonte D, Sotgia F, Pestell RG, Minetti C, Scherer PE, Okamoto T, Lisanti MP. Molecular genetics of the caveolin gene family: implications for human cancers, diabetes, Alzheimer disease, and muscular dystrophy. Am J Hum Genet. 1998;63:1578–87.
96. Wu CJ, Ritz J. Revealing tumor immunity after hematopoietic stem cell transplantation. Clin Cancer Res. 2009;15:4515–17.
97. Yan S, Marguet D, Dobers J, Reutter W, Fan H. Deficiency of CD26 results in a change of cytokine and immunoglobulin secretion after stimulation by pokeweed mitogen. Eur J Immunol. 2003;33:1519–27.
98. Fidler IJ, Fogler WE, Kleinerman ES, Saiki I. Abrogation of species specificity for activation of tumoricidal properties in macrophages by recombinant mouse or human interferon-gamma encapsulated in liposomes. J Immunol. 1985;135:4289–96.
99. Gibbs VC, Williams SR, Gray PW, Schreiber RD, Pennica D, Rice G, Goeddel DV. The extracellular domain of the human interferon gamma receptor interacts with a species-specific signal transducer. Mol Cell Biol. 1991;11:5860–6.
100. Zielinski CE, Mele F, Aschenbrenner D, Jarrossay D, Ronchi F, Gattorno M, Monticelli S, Lanzavecchia A, Sallusto F. Pathogen-induced human T$_H$17 cells produce IFN-γ or IL-10 and are regulated by IL-1β. Nature. 2012;484:514–18.
101. Wolk K, Kunz S, Asadullah K, Sabat R. Cutting edge: immune cells as sources and targets of the IL-10 family members? J Immunol. 2002;168:5397–402.
102. Zhang C, Todorov I, Zhang Z, Liu Y, Kandeel F, Forman S, Strober S, Zeng D. Donor CD4$^+$ T and B cells in transplants induce chronic graft-versus-host disease with autoimmune manifestations. Blood. 2006;107:2993–3001.
103. Ishikawa F, Yasukawa M, Lyons B, Yoshida S, Miyamoto T, Yoshimoto G, Watanabe T, Akashi K, Shultz LD, Harada M. Development of functional human blood and immune systems in NOD/SCID/IL2 receptor γ chain^{null} mice. Blood. 2005;106:1565–73.
104. Campbell TB, Hangoc G, Liu Y, Pollok K, Broxmeyer HE. Inhibition of CD26 in human cord blood CD34$^+$ cells enhances their engraftment of nonobese diabetic/severe combined immunodeficiency mice. Stem Cells Dev. 2007;16:347–54.
105. Ohnuma K, Inoue H, Uchiyama M, Yamochi T, Hosonno O, Dang NH, Morimoto C. T-cell activation via CD26 and caveolin-1 in rheumatoid synovium. *Mod. Rheumatol.* 2006;16:3–13.
106. Blazar BR, Taylor PA, Boyer MW, Panoskaltsis-Mortari A, Allison JP, Vallera DA. CD28/B7 interactions are required for sustaining the graft-versus-leukemia effect of delayed post-bone marrow transplantation splenocyte infusion in murine recipients of myeloid or lymphoid leukemia cells. J Immunol. 1997;159:3460–73.

Q1: Please provide running title

Begell Author Proofs

Hayashi *et al. Cancer Cell Int (2016) 16:35*
DOI 10.1186/s12935-016-0310-9

Cancer Cell International

PRIMARY RESEARCH

Open Access

A humanized anti-CD26 monoclonal antibody inhibits cell growth of malignant mesothelioma via retarded G2/M cell cycle transition

Mutsumi Hayashi[1,2], Hiroko Madokoro[1], Koji Yamada[3], Hiroko Nishida[1], Chikao Morimoto[4], Michiie Sakamoto[1] and Taketo Yamada[1,5*]

Abstract

Background: Malignant Mesothelioma (MM) is a highly aggressive tumor with poor prognosis. Multimodal treatments and novel molecular targeted therapies against MM are in high demand in order treat this disease effectively. We have developed a humanized monoclonal antibody YS110 against CD26 expressed in 85 % of MM cases. CD26 is thought to be involved in tumor growth and invasion by interacting with collagen and fibronectin, or affecting signal transduction processes.

Methods: We evaluated the direct anti-tumor effect of YS110 against MM cell lines, NCI-H2452 and JMN, and investigated its effects on cell cycle and on the cell cycle regulator molecules. In addition, we investigated synergistic effects of YS110 and anti-tumor agent pemetrexed (PMX) against MM cell line both in vitro and in vivo.

Results: YS110 suppressed the proliferation of NCI-H2452 cells by approximately 20 % in 48 h. Based on cell cycle analysis, percentage of cells in G2/M phase increased 8.0 % on the average after YS110 treatment; in addition, cell cycle regulator p21 cip/waf1 was increased and cyclin B1 was decreased after YS110 treatment. Inhibitory phosphorylation of both cdc2 (Tyr15) and cdc25C (Ser216) were elevated. Furthermore, activating phosphorylation of p38 MAPK (Thr180/Tyr182) and ERK1/2 (Thr202/Tyr204) were augmented at 24 h after YS110 treatment. PMX rapidly induced CD26 expression on cell surface and the treatment with both YS110 and PMX inhibited in vivo tumor growth accompanied by a synergistic reduction in the MIB-1 index.

Conclusion: This is a first report of a novel anti-proliferative mechanism of the humanized anti-CD26 monoclonal antibody YS110, which resulted in G2/M cell cycle delay through regulation of quantity and activity of various cell cycle regulating molecules.

Keywords: Mesothelioma, CD26, Monoclonal antibody, G2/M transition, Pemetrexed

Background

Malignant mesothelioma (MM) is an aggressive cancer of the pleura, peritoneal cavity, pericardium, and scrotum and has a poor prognosis. MM is associated with occupational exposure to asbestos and, despite legislation introduced by many industrialized countries, the incidence is not expected to peak until 2020 due to the long latency between initial exposure and disease expression [1]. As single modality approach to treatment has failed to extend survival, multimodal treatment and novel molecular targeted therapies are highly sought after. Although extrapleural pneumonectomy (EPP) is a preferred treatment option, median survival among patients receiving EPP alone is less than 10 months [2]. EPP followed by high-dose radiation therapy (RT) has

---

*Correspondence: taketo@saitama-med.ac.jp
[5] Department of Pathology, Saitama Medical University, 38 Morohongo, Saitama, Moroyama-machi 350-0495, Japan
Full list of author information is available at the end of the article

© 2016 Hayashi et al. This article is distributed under the terms of the Creative Commons Attribution 4.0 International License (http://creativecommons.org/licenses/by/4.0/), which permits unrestricted use, distribution, and reproduction in any medium, provided you give appropriate credit to the original author(s) and the source, provide a link to the Creative Commons license, and indicate if changes were made. The Creative Commons Public Domain Dedication waiver (http://creativecommons.org/publicdomain/zero/1.0/) applies to the data made available in this article, unless otherwise stated.

been shown to prolong median survival to 33.8 months in patients with Stage 1 and Stage 2 MM but survival remained 10 months in patients with Stage 3 and Stage 4 MM [2]. A Phase 3 trial showed that combination of pemetrexed and cisplatin improved survival over cisplatin alone for inoperable patients [3]. According to recent multicenter trials of trimodality treatment that consisted of neoadjuvant chemotherapy (cisplatin and pemetrexed), EPP, and adjuvant RT led in the USA [2] and Europe [4], median survival of patients who completed the therapy was 29.1 months compared to 18.4 months in controls. Since the trimodality approach seems to be limited and because not all patient can tolerate aggressive therapies, novel molecular targeted therapies are highly desirable. To date, a number of molecular targeted agents have been evaluated in MM. While tyrosine kinase inhibitors against epidermal growth factor receptor (EGFR) and platelet-derived growth factor receptor (PDGFR) did not show clinically significant effects, histone deacetylase inhibitor (HDACI) and anti-angiogenic agents showed some clinical benefits and are undergoing Phase 3 trials [5]; however, none of these agents have been incorporated into clinical practice and efforts must continue in the area of both clinical research and search for novel target molecules.

CD26 is an 110 kD glycoprotein anchored in the cellular membrane with dipeptidyl peptidase IV activity. CD26 is also known as a co-stimulatory molecule of the T lymphocyte. CD26 binds to caveolin-1 on antigen-presenting cells and the interaction triggers signal transduction process leading to T cell proliferation and cytokine production [6]. Several recent studies have shown that CD26 is highly expressed in several malignancies, including MM, lung adenocarcinoma, hepatocellular carcinoma, prostate cancer, and thyroid cancer [7]. CD26 expression evaluated by immunohistochemistry was positive in 85 % of tested MM cases [8, 9]. Moreover, CD26 is thought to be involved in tumor growth and invasion through its interaction with collagen and fibronectin or by regulating activity of chemotactic peptides through its DPPIV activity. Furthermore, CD26 has been reported to be involved in signal transduction processes, including the p38 MAPK pathway. Though the mechanisms of action of CD26 have not been clarified, its enzymatic activity does not appear essential for its role in signal transduction process [10]. Considering its high rate of overexpression in MM and suspected function in tumor progression, we have developed a humanized an anti-CD26 antibody, designated YS110, as a targeted therapy against CD26-positive malignancies, including MM. We have previously reported the anti-tumor effects of YS110 against MM cells [11]. In addition to the anti-tumor effect via antibody-dependent-cell-mediated-cytotoxicity, YS110 showed direct anti-tumor effect via $p27^{kip1}$ accumulation [11]; however, the molecular mechanism of direct anti-tumor effect of YS110 against MM cell lines remains unknown.

The molecular mechanisms underlying the direct anti-tumor effect of several monoclonal antibodies have been investigated; for example, the anti-HER-2 antibody (Trastuzumab) and anti-EGFR antibody (Cetuximab) result in G1/S cell cycle arrest by upregulating the CDK inhibitor $p27^{kip1}$ via multiple signaling pathways [12, 13]. The anti-CD20 antibody (rituximab) can induce cell death of malignant B cell lymphoma cells in vitro via inhibition of the p38 MAPK, ERK1/2, and AKT anti-apoptotic survival pathways [14]. Most therapeutic antibodies against cancers that affect the cell cycle, including antibodies mentioned above, result in G1/S arrest. So far, only one anti-cancer antibody, the anti-human type 1 insulin-like growth factor receptor (IGF-IR) antibody A12 against androgen-independent prostate cancer cell line LuCaP 35 V, has been reported to cause G2/M cell cycle delay although its molecular mechanism is not yet understood [15].

In this study, we focused on evaluating the direct in vitro effect of the humanized anti-CD26 monoclonal antibody YS110 against the MM cell line NCI-H2452 and investigated its effect on the cell cycle and on cell cycle-regulating molecules. YS110 inhibited growth of YS110 with G2/M cell cycle arrest and altered the expression or phosphorylation state of cell cycle molecules. Furthermore, pemetrexed (PMX), a standard reagent against mesothelioma, rapidly induced CD26 expression on the cell surface and treatment with both YS110 and PMX inhibited in vivo tumor growth in a synergistic manner. This is the first report describing a novel anti-proliferative mechanism of the humanized anit-CD26 monoclonal antibody YS110, which resulted in G2/M cell cycle delay, through regulation of quantity and activity of various cell cycle-regulating molecules.

Results

YS110 inhibits mesothelioma cell proliferation

YS110 inhibits proliferation of the mesothelioma cell line NCI-H2452 in a concentration-dependent manner (Fig. 1). Maximum of growth inhibition was 18.3 % at 250 μg/mL of YS110. Based on this result, we used YS110 at 2 μg/mL, which showed 11.2 % of growth inhibition, in the following experiments.

YS110 induced G2/M cell cycle delay in mesothelioma cells

To investigate the mechanism responsible for the growth inhibition caused by YS110, cell-cycle distribution was determined by flow cytometry analysis. At 24 h after YS110 treatment, the percentage of cells in

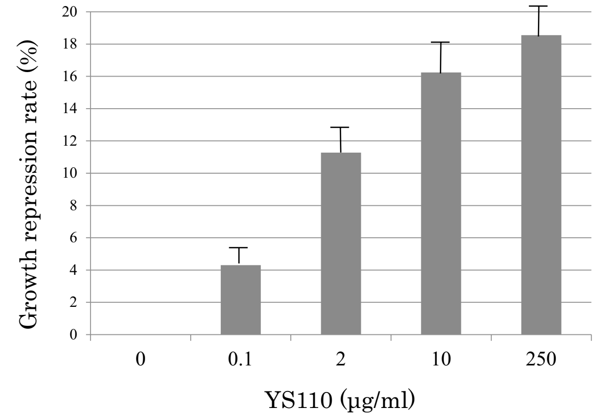

Fig. 1 YS110 inhibits NCI-H2452 cell proliferation. WST-1 assay revealed inhibition of NCI-H2452 cell proliferation with YS110 treatment in a concentration-dependent manner up to 18.6 %. The experiment was performed using 96 multi-well plates

the G2/M phase increased compared to the control. The representative experiment is shown (Fig. 2a). On the average of ten experiments, the percentage of G2/M phase cells were significantly increased after YS110 treatment ($p < 0.05$) (Fig. 2b). This cell cycle delay may be compatible with repression of cell proliferation. Furthermore, in another CD26 positive MM cell line NCI-H28, the percentage of cells in G2/M phase increased by 5 % on the average after YS110 treatment though its significance could not be proved statistically (data not shown).

YS110 alters cell cycle regulators

We investigated the alterations caused by YS110 treatment in the quantity and activation state of cell cycle regulators responsible for G2/M transition. At 24 h after YS110 treatment, the cell cycle regulator p21 increased while the positive regulatory subunit cyclin B1 decreased. Inhibitory phosphorylation of cdc2 on Tyr15 and inhibitory phosphorylation of cdc25C on Ser216, an upstream inhibitory regulator of cdc2, was elevated (Fig. 3a). Cdc25C phosphorylated on Ser216 is known to be sequestrated into cytoplasm and refrained from contact with cdc2 [16]. After YS110 treatment for 24 h, cytoplasmic whole cdc25C was elevated while nuclear whole cdc25C was decreased, as confirmed by densitometry analysis (Fig. 3b). At 6 h and 12 h after YS110 treatment, the amount of phosphorylated cdc2 and phosphorylated cdc25C were varied among experiments despite consistent increase at 24 h. No significant change in cdc25A and cdc25B was observed (data not shown).

YS110 elevates activating phosphorylation of p38 MAPK and ERK1/2

In order to determine the upstream regulator of cdc25C phosphorylation caused by YS110 treatment, expression and activation status of several molecules known to regulate cell cycle through cdc25C phosphorylation were examined. Activating phosphorylation of p38 MAPK (Thr180/Tyr182) and ERK1/2 (Thr202/Tyr204) were elevated 24 h after YS110 treatment (Fig. 4a). No significant change in chk1, chk2, or c-TAK1 was observed (data not shown). While the p38 inhibitor SB203580 failed to block G2/M arrest caused by YS110 (data not shown), the MEK1/2 inhibitor U0126 blocked G2/M arrest caused by YS110 according to cell cycle analysis using flowcytometry (Fig. 4b).

Pemetrexed (PMX) increased CD26 expression in mesothelioma cells in vitro

CD26 expression on the cell surface of JMN cells increased 15 % from 6 to 6.5 % 24 h after treatment with 10 μM of PMX based on flowcytometry analysis (Fig. 5a). In order to confirm the augmented expression of CD26 in JMN cells, Western blot analysis was performed. CD26 protein expression was rapidly induced in whole cell lysates by treatment with 10 μM of PMX at 1 h after PMX treatment; most augmentation of CD26 expression at 6 h and then this augmented expression continued to 24 h after PMX treatment (Fig. 5b). In order to examine the altered expression of CD26 in NCI-H2452 cells, Western blot analysis was performed. CD26 protein expression in NCI-H2452 cells was also rapidly induced in whole cell lysates by treatment with 10 μM of PMX at 1 h after PMX treatment; most augmentation of CD26 expression at 6 h and then this augmented expression continued to 24 h after PMX treatment (Fig. 5b).

Effective inhibition of in vivo *mesothelioma cell growth by combined treatment with both YS110 and PMX*

Combination effects of YS110 and PMX were examined using xenograft models with JMN cells transplanted into NOG mice subcutaneously. Mice were then monitored for the development and progression of tumors and the tumor size was determined by caliper measurement. Tumor size in mice treated with both YS110 and PMX was smaller than mice treated with only YS110 or PMX (data not shown). The weight of tumors with YS110 treatment was insignificantly reduced (Fig. 6A). PMX treatment induced a significant reduction in tumor weight ($p < 0.05$); the combination of YS110 and PMX treatment synergistically reduced tumor weight compared with YS110 single treatment and PMX single treatment ($p < 0.05$).

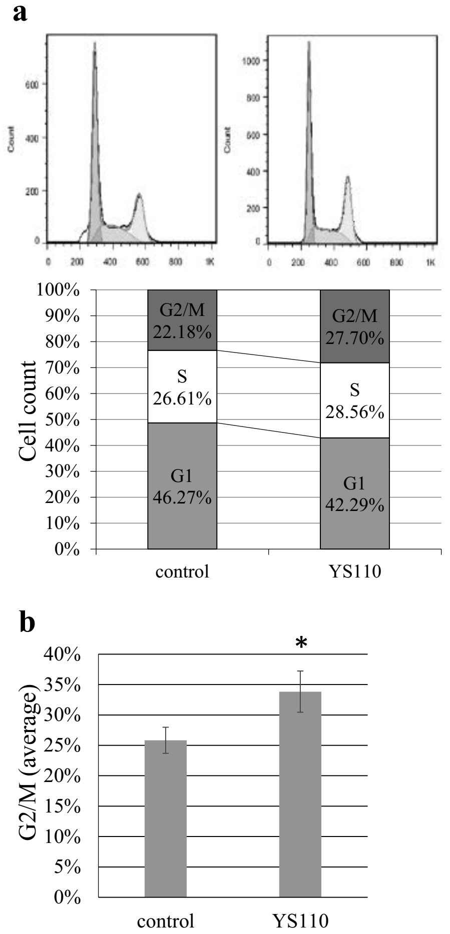

Fig. 2 YS110 induces G2/M cell cycle delay in NCI-H2452 cells. **a** Flowcytometry analysis using propidium iodide staining revealed that the percentage of G2/M phase cells increased while the percentage of G1 phase cells was reduced in NCI-H2452 cells treated 24 h with 2 μg/mL of YS110. A representative experiment is shown. **b** The average percentage of G2/M phase cells in NCI-H2452 cells treated 24 h with 2 μg/mL of YS110 was significantly increased (*$p < 0.05$)

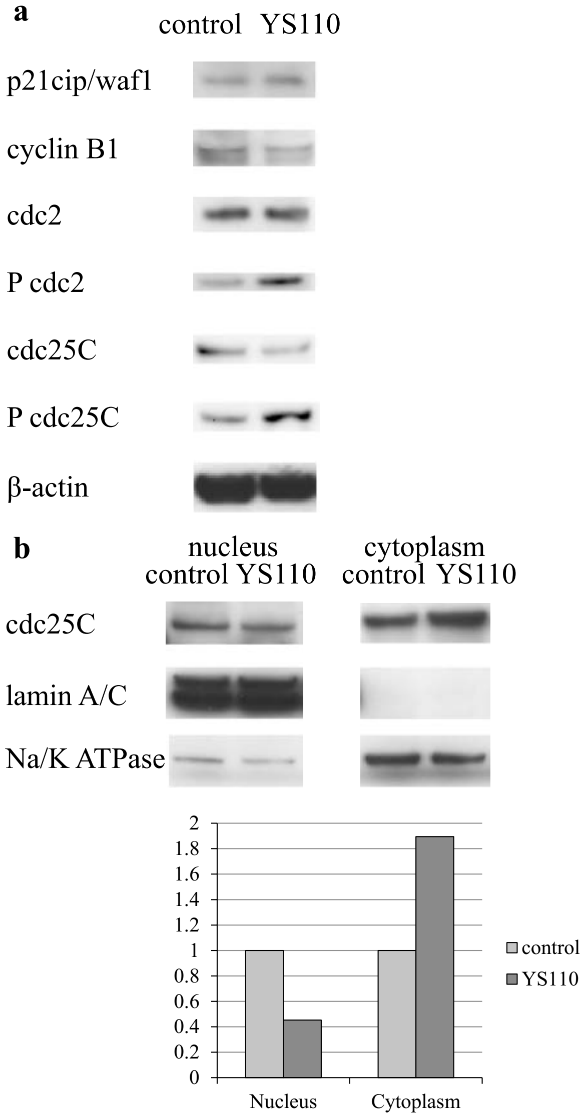

Fig. 3 YS110 alters expressions and phosphorylation of cell cycle regulators. **a** At 24 h after treatment with 2 μg/mL of YS110, p21 protein expression increased while cyclinB1 protein expression decreased. Inhibitory phosphorylation of cdc2 Tyr15 and cdc25C Ser216 were elevated while there was no significant change in whole cdc2 and cdc25C protein. β-actin was used as an internal control. **b** Alteration in subcellular distribution of whole cdc25C by YS110 treatment is shown. At 24 h after treatment with 2 μg/mL of YS110, nuclear cdc25C protein decreased while cytoplasmic cdc25C protein increased. LaminA/C was used as a nuclear marker and Na–K ATPase was used as a cytoplasmic marker. The *bar graph* demonstrates the densitometric analysis of a Western blot of whole cdc25C. Results are normalized by the densitometry of control cells. All experiments were performed in triplicate and a representative experiment is shown

Combination effects of tumor growth in vivo were examined by measuring the MIB-1 index histologically. The MIB-1 index was significantly decreased in tumors after YS110 or PMX single treatment compared with controls ($p < 0.05$; Fig. 6B, C). Combinatory treatment with YS110 and PMX significantly reduced the MIB-1 index compared to single treatment ($p < 0.05$; Fig. 6B, C).

Histology of the tumor derived from JMN cells in the xenograft model is shown in Fig. 6C. Sarcomatous mesothelioma is shown in HE staining (Fig. 6C-a) and stained with anti-CD26 polyclonal antibody (R&D) (Fig. 6C-b). The MIB-1 index was measured by immunohistochemistry using the anti-Ki-67 (MIB-1) monoclonal antibody. Staining of Ki-67 antigens in nucleus was shown in tumors treated with control IgG (Fig. 6C-c), YS110 (Fig. 6C-d), and both YS110 and PMX (Fig. 6C-e). The number of Ki-67 positive nuclei was decreased after combined treatment of YS110 and PMX and the necrotic area is indicated by an asterisk (Fig. 6C-e).

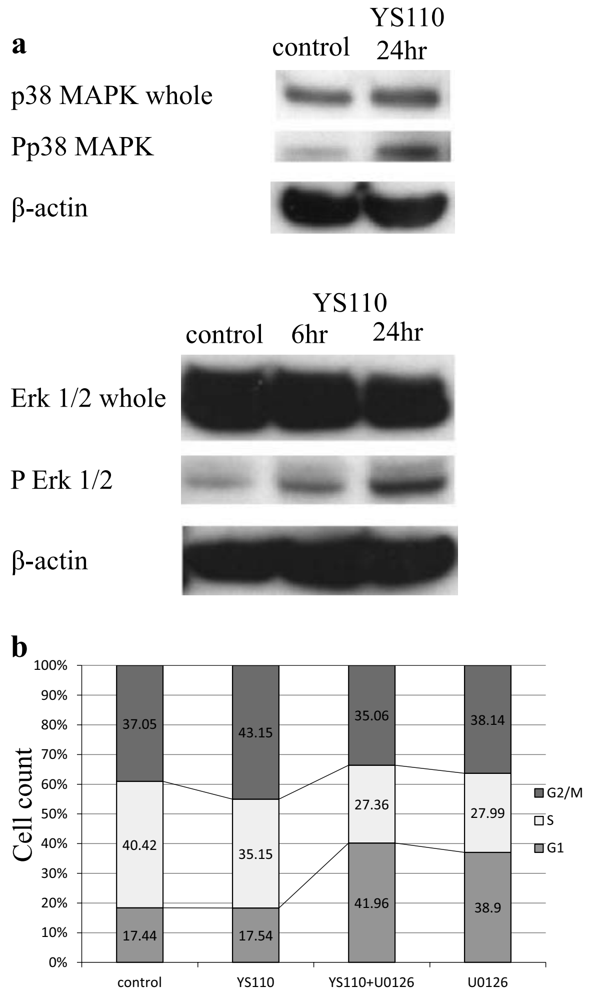

Fig. 4 YS110 augments phosphorylation of p38MAPK and ERK1/2. **a** Activating phosohorylation of p38 (Thr180/Tyr182) and ERK1/2 (Thr202/Tyr204) were elevated by 24 h after treatment with YS110 while no substantial changes of whole p38 and ERK1/2 protein were observed. β-actin was used as an internal control. **b** G2/M arrest caused by YS110 treatment was reversed by ERK1/2 activation inhibitor U0126 (10 μM). A proportion (43.15 %) of G2/M was elevated in cells with YS110 treatment compared with in cells without YS110 (control, 37.05 %) and the proportion of G2/M decreased in cells with both YS110 and U0126 treatment (35.06 %). All experiments were performed in triplicate and a representative experiment is shown

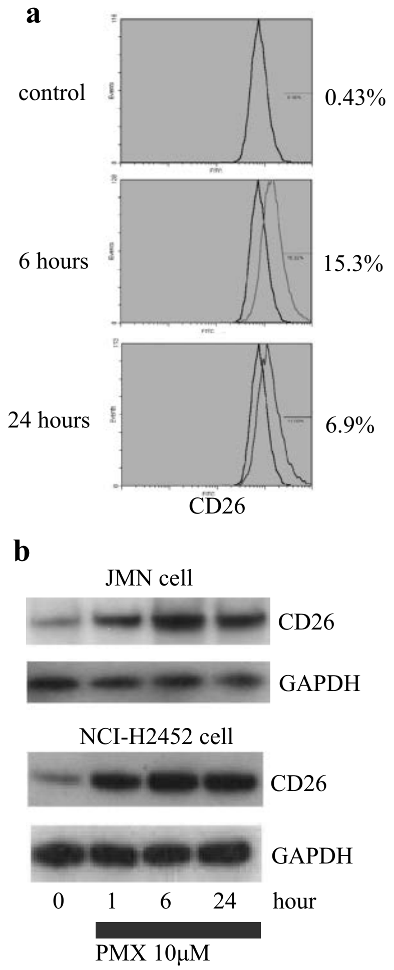

Fig. 5 Pemetrexed (PMX) increased CD26 expression in vitro. **a** Based on flowcytometry analysis, cell surface CD26 expression on JMN cells increased 6-24 h after treatment with 10 μM of PMX. **b** Based on Western blot analysis, the expression of CD26 protein was rapidly induced in whole cell lysates by treatment with 10 μM of PMX at 1–24 h. GAPDH was used as an internal control. All experiments were performed in triplicate and a representative experiment is shown

Discussion

Novel molecular targeted therapies are in high demand since the aggressive trimodality approach against MM has been proved to be limited. We developed a humanized monoclonal antibody against CD26, designated as YS110, a molecular targeted therapy against MM [11]. We expected YS110 to cause ADCC to eliminate CD26 positive MM cells. In addition to the ADCC effect, YS110 demonstrated direct anti-proliferative effects in vitro against CD26-positive MM cell lines. We proposed that investigation into the molecular mechanisms of the direct anti-proliferative effect against MM cells would be beneficial for both understanding anti-tumor effect of YS110, as well as uncover the underlying mechanism its proliferation and progression. Although the direct anti-proliferative effect of YS110 is limited to a repression rate of approximately 20 % in vitro, the molecular mechanism was associated with the proliferative signal transduction system and cell cycle. Cell cycle analysis revealed that YS110 caused significant delay of the G2/M transition. To our knowledge, only one anti-cancer MoAb, anti-IGF-IR antibody A12 against the androgen-independent prostate

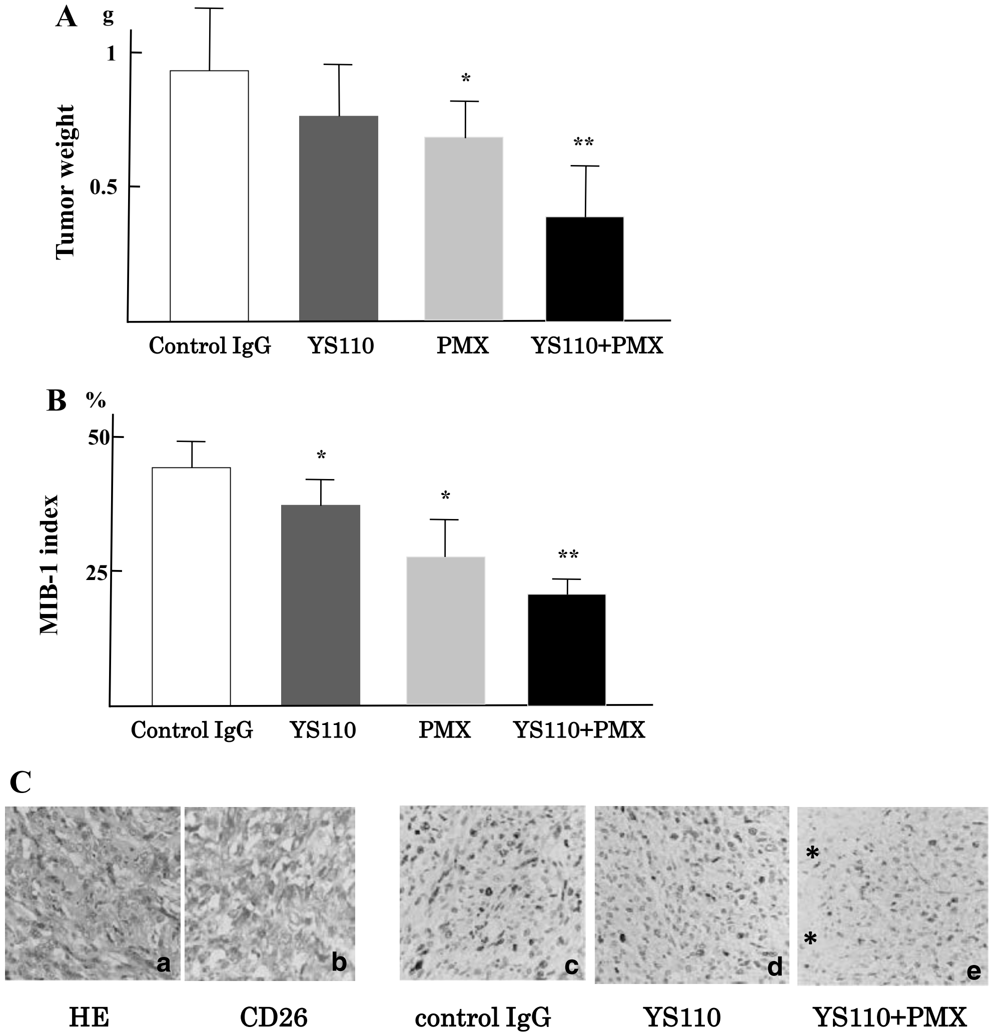

Fig. 6 Effective inhibition of mesothelioma cell growth in vivo. **A** Combination effects of YS110 and PMX were examined using xenograft models with JMN cells transplantation subcutaneously. The weight of tumors treated with YS110 was insignificantly reduced but PMX treatment induced a significantly reduced tumor weight ($*p < 0.05$). A combination of YS110 and PMX treatment reduced tumor weight compared with the weight of tumors with YS110 single treatment and PMX single treatment synergistically ($**p < 0.05$). **B** Combination effects of tumor growth in vivo were examined using a measurement of MIB-1 index histologically. MIB-1 index was significantly reduced with YS110 or PMX single treatment compared with control IgG treatment ($*p < 0.05$). The MIB-1 index after combinatory treatment with YS110 and PMX was significantly reduced compared with YS110 or PMX single treatment ($**p < 0.05$). **C** Sarcomatous mesothelioma is shown in HE staining (*a*) and stained with anti-CD26 polyclonal antibody (R&D) (*b*) MIB-1 index was measured by immunohistochemistry using the anti-Ki-67 monoclonal antibody (DAKO, clone MIB-1). Staining of Ki-67 antigens in nucleus is seen in tumors treated with control IgG (*c*), YS110 (*d*), and both YS110 and PMX (*e*). The number of Ki-67 positive nucleus was reduced after combinatory treatment of YS110 and PMX and the necrotic area is indicated by an *asterisk* (*e*)

cancer cell line LaCaP 35 V, has been reported to result in G2/M delay although its molecular mechanism is not yet understood [15]. Therefore, we are the first to report results on the molecular mechanisms underlying G2/M delay from a cancer targeted-antibody. In order to elucidate the mechanism of G2/M delay mediated by YS110, we analyzed the quantities and phosphorylation status of G2/M regulators using Western blot analysis. At 24 h after treatment with YS110, inhibitory phosphorylation of cdc2 and its upstream regulator cdc25C were elevated. Phosphorylation of Cdc25C on Ser216 is sequestrated into the cytoplasm and therefore restrained from contact with nuclear cdc2. Increased levels of cytoplasmic whole cdc25 protein and decreased levels of nuclear whole cdc25C protein at 24 h occurred after YS110 treatment, confirming sequestration. Western blot analysis also revealed an increased amount of cell cycle inhibitor p21 and decreased amount of cyclinB1 promotes

G2/M progression at 24 h after YS110 treatment. These alterations may be compatible with the retarded G2/M transition.

To determine the upstream regulator of the altered cdc25C phosphorylation state caused by YS110, we investigated several molecules known to regulate cdc25C. 24 h after YS110 treatment, activated phosphorylation levels of p38 MAPK (Thr180/Thy182) and ERK 1/2 (Thr202/Tyr204) were elevated. Inhibitor assays indicated that YS110 treatment activated the ERK signal pathway, but not the p38MAPK pathway, which induced G2/M delay.

MAPK activation results in many different biological responses, including proliferation, differentiation, and cell death. Although ERK1/2 activation is associated with cell survival and proliferation, a number of studies have shown that activation of ERK1/2 can mediate cell cycle arrest and cell death depending on the stimuli and cell types involved [17]. A number of anti-cancer reagents and an anti-cancer antibodies have been reported to induce G2/M cell cycle arrest and/or apoptosis mediated by ERK1/2 activation [18, 19]. These reagents, like YS110, cause G2/M cell cycle delay by inhibiting phosphorylation of cdc2 and cdc25C and by activating phosphorylation of ERK1/2. The G2/M delay caused by these drugs is antagonized by MEK inhibitors. Among monoclonal antibodies that have been investigated for their anti-cancer characteristics, the anti-CD40 antibody has been reported to cause apoptosis of diffuse large B-cell lymphoma cell lines with ERK1/2 activation through CD40 signaling [20]. In these reported cases, as well as our findings of YS110-CD26 interaction, the mechanisms underlying G2/M delay or apoptosis through ERK1/2 activation is still unknown. As for G1/S cell cycle regulation, a report has indicated that HER2 signaling related to trastuzumab treatment had effects on CDC25A protein stability [21]. The involvement of cell cycle regulators on the effect of anti-tumor antibodies should be further investigated.

Previously, we reported that YS110 induces intranuclear transportation of CD26. When bound to YS110, CD26 is translocated to the nucleus via caveolin-dependent endocytosis. This translocation suppresses transcription of the POLR2A gene, which encodes a large subunit of RNA polymerase, in MM cell lines [22, 23]. The relationship between POLR2A suppression and G2/M cell cycle delay also requires further investigation.

The NCI-H2452 cell line is derived from the epithelioid type of MM and its growth rate is lower than the sarcomatoid type of MM, the JMN cell line [24]. Profiles of cell cycling for synchronization assay in S-phase by thymidine block are available for NCI-H2452 cells but not for JMN cells. NCI-H2452 cells have no tumorigenicity in immunodeficient mice but JMN cells form subcutaneous tumors or diffuse and spread into the thorax [11, 22, and 23]; therefore, after YS110 treatment, we examined the in vitro cell cycle using NCI-H2452 cells and in the in vivo xenograft model using JMN cells.

Pemetrexed (PMX) induced augmented CD26 expression in both NCI-H2452 cells and JMN cells rapidly (Fig. 5b); this induction of cell surface CD26 on MM cells may be useful for anti-CD26 MoAb therapy against MM. The combination of YS110 and PMX therapy against xenografted MM tumors was applied using JMN cell transplanted immunodeficient mice. As a result, anti-tumor effects were significantly shown in xenografted tumors with YS110 and PMX combined treatment compared to tumors with single treatment of YS110 or PMX, which was accompanied by a significantly reduced MIB-1 index. The combined treatment with YS110 and PMX showed a tendency to retard both G1/S and G2/M transition; however, significant differences of G1/S or G2/M proportion were not seen between YS110 plus PMX treatment and YS110 or PMX single treatment (data not shown).

There have been many anti-cancer monoclonal antibodies (MoAbs) developed and their anti-cancer mechanisms are highly variable. Investigations into each molecular mechanism of an anti-cancer MoAb are significant because it is valuable for the optimization of antibody therapies against cancer and contributes to elucidating the mechanisms of oncogenesis and cancer proliferation. This is the first report of a novel anti-proliferative mechanism of a humanized anti-CD26 monoclonal antibody YS110 causing G2/M cell cycle delay through ERK1/2 phosphorylation and identifying PMX as a CD26 inducer.

Conclusions

Humanized anti-CD26 monoclonal antibody YS110 suppressed proliferation of CD26 positive MM cell lines through a novel mechanism causing G2/M cell cycle delay through ERK1/2 phosphorylation. Anti-tumor agent PMX was identified as a CD26 inducer.

Methods

Reagents and antibodies

The humanized anti-CD26 antibody YS110 was constructed from the anti-CD26 mouse monoclonal antibody 14D10 coding sequence as previously described [11] and normal human IgG1 (Southern Biotech, Birmingham, AL) was used as a control. Rabbit monoclonal antibody to cyclinB1, p21cip/waf1, cdc2, phospho-cdc2 (Tyr15), cdc25c, phospho-cdc25c (Ser216), Erk1/2, phospho-Erk1/2(Thr202/Tyr204), p38MAPK, and phosphor-p38MAPK (Thr180/Tyr182) were from Cell Signaling Technology Inc. (Danvers, MA) and the mouse monoclonal antibody against β-actin or Glyceraldehyde

3-phosphate dehydrogenase (GAPDH) was from DAKO (Glostrup, Denmark). The goat anti-CD26 polyclonal antibody and MEK 1/2 inhibitor U0126 was from Cell Signaling Technology Inc. (Danvers, MA).

Cell culture

NCI-H2452, NCI-H28 and JMN, CD26-positive cell lines established from malignant mesothelioma, were kind gifts from Dr. Chikao Morimoto (Departement of Therapy Development and Innovation for Immune Disorders and Cancers, Juntendo University). Both cell lines were grown in RPMI medium (Sigma-Aldrich, Tokyo, Japan) supplemented with 10 % heat-inactivated fetal bovine serum (FBS), ABPC (100 unit/mL), Streptomycin (100 μg/mL), and 5 % CO_2 at 37 °C.

Cell proliferation assay

The effect of YS110 on the proliferation of NCI-H2452 cells was measured using a colorimetric cell proliferation kit WST-1 (Roche Diagnostics, Tokyo, Japan) based on the colorimetric detection of a formazan salt. In brief, 5×10^3 NCI-H2452 cells were seeded in RPMI1640 medium supplemented with 10 % heat inactivated FBS on 96-well plate with or without 2 μg/mL YS110. After 48 h of incubation at 37 °C in 5 % CO_2, a reading at 450 nm was carried out according to the manufacturer's instructions. Background absorbance of each sample at 630 nm was subtracted from the readings at 450 nm. The experiment was performed in triplicate and a representative experiment is shown.

Cell cycle assay and flowcytometry

For the cell cycle study, NCI-H2452 and NCI-H28 cells were synchronized in the S-phase by a repeated thymidine block. In brief, 5×10^5 cells seeded in RPMI1640 medium supplemented with 10 % heat inactivated fetal bovine serum on 10 cm culture dishes were treated with 0.56 mM thymidine for 18 h, released for 10 h by three washes, and then treated again with 0.56 mM thymidine for 15 h. Synchronized cells were then returned to thymidine free medium with or without 2 μg/mL YS110 and incubated for 24 h. Cell cycle profiles were performed by flowcytometry using a procedure for propidium iodide staining of nuclei. Acquisition was performed using an EPICS XL/XL-MCL version 3.0 (Beckman Coulter, Brea, CA, USA) and data were analyzed using Flowjo software (TreeStar, Ashland, OR, USA). The experiment was performed in triplicate and a representative experiment is shown.

Western blotting

For total cell lysate preparation, NCI-H2452 cells or JMN cells cultured with or without 2 μg/mL YS110 for 24 h were lysed at 4 °C by lysis buffer with phosphatase inhibitors (50 mM Tris–HCl, 150 mM NaCl, 1 % NP-40, 0.25 % deoxycholate, 500 μM NaVO3, 50 mM NaF). For the preparation of nuclear and cytoplasmic extracts, NCI-H2452 cells were processed using NE-PER Nuclear and Cytoplasmic Extraction Reagents (Thermo scientific, Waltham, LA) according to the manufacturer's instruction. For Western blot analyses, 30 μg of each cell lysate was separated on an SDS–polyacrylamide gel and transferred to a PVDF membrane Hybond-P (GE Healthcare, Little Chalfont, UK). The membranes were blocked in blocking buffer [5 % dry milk and 0.2 % Tween 20 in Tris buffered saline (TBS)] for 2 h at room temperature, and incubated with the primary antibodies in antibody dilution buffer (5 % bovine serum albumin, 0.2 % Tween 20 in TBS) overnight at 4 °C. Dilutions of primary antibodies were 1:200, except anti p21cip/waf1 antibody, which was diluted at 1:100. After three washes, the blots were incubated with secondary antibodies (goat anti-rabbit polyclonal antibody and rabbit anti-mouse polyclonal antibody) diluted 1:1000 with dilution buffer for 1 h at room temperature and developed using the ECL Western Blotting Detection Reagents (GE Healthcare, Little Chalfont, UK). Quantification of relative band densities was performed using standard densitometry scanning techniques using ImageQuant 350 and ImageQuant TL software (GE Healthcare, Little Chalfont, UK). All the experiments performed in triplicate and a representative experiment is shown.

Xenograft model using human mesothelioma cell lines

NOD/Shi-scid, IL-2 receptor gamma null (NOG) mice were obtained from the Central Institute for Experimental Animals. JMN cells (1×10^6) were implanted subcutaneously in the back flank of NOG mice. Mice were injected intratumorally with control human IgG_1 ($n = 3$) or YS110 ($n = 3$) at doses of 5 mg/kg body weight. JMN cells expressing CD26 were inoculated into the thoracic cavities of NOG mice. Thereafter, mice were intraperitoneally injected with control human IgG_1 ($n = 3$) or YS110 (5 μg per injection; $n = 3$), and/or pemetrexed (PMX, purchased from Eli Lilly; 100 mg/kg body weight) commencing on the day of cancer cell injection. Each antibody was administered three times per week. Mice were then monitored for the development and progression of tumors. Tumor weight was measured by scale. All experiments were approved by the Animal Care and Use Committee of Keio University and were performed in accordance with the institute guidelines.

Histology and immunohistochemistry

Tumor tissues were fixed in 10 % neutral buffered formalin, embedded in paraffin, and sectioned at a thickness of 5 μm. Sections were paraffin depleted and rehydrated in a graded series of ethanol solutions. For histology, sections were stained with hematoxylin and eosin. For immunohistochemistry, sections were washed with PBS, subjected to antigen retrieval by heating at 100 °C in 0.01 M sodium citrate (pH 6.0) for 10 min, then treated with 3 % H_2O_2, before incubation with the following primary antibodies: goat anti-CD26 pAb (AF1180, R&D Systems, Minneapolis, MN) (1:100) and mouse anti-Ki-67 mAb (MIB-1, DAKO Japan) (1:100). Immune complexes were detected by using an ImmPRESS REAGENT KIT (Vector Laboratories, Burlingame, CA) with 3, 3′-diaminobenzidine, and sections were counterstained with hematoxylin

Statistical analyses

Statistical analyses were assessed using SPSS version 17.0 (SPSS Inc., Chicago, IL). The *p* value, from which statistical significance was assumed, was set to $p < 0.05$.

Abbreviations

MM: malignant mesothelioma; PMX: pemetrexed; NOG mouse: NOD/Shi-scid, IL-2 receptor gamma null mouse.

Authors' contributions

MH and TY designed and performed the research; HN and CM provided reagents and cells and examined protein expressions; HM, MS and TY analyzed the data; MH and TY wrote the manuscript. All authors read and approved the final manuscript.

Author details

[1] Department of Pathology, Keio University School of Medicine, 35 Shinanomachi, Tokyo, Shinjuku-ku 160-8582, Japan. [2] Department of Pediatrics, Keio University School of Medicine, 35 Shinanomachi, Tokyo, Shinjuku-ku 160-8582, Japan. [3] Laboratory of Nuclear Transport Dynamics, National Insititute of Biomedical Innovation, 7-6-8 Saito-Asagi, Ibaraki City, Osaka Prefecture 567-0085, Japan. [4] Department of Therapy Development and Innovation for Immune Disorders and Cancers, Juntendo University, 2-1-2 Hongo, Tokyo, Bunkyo-ku 113-8421, Japan. [5] Department of Pathology, Saitama Medical University, 38 Morohongo, Saitama, Moroyama-machi 350-0495, Japan.

Acknowledgements

We thank H. Suzuki for technical assistance and A. Sato and K. Tsutsumi for animal care and support of tumorigenicity assay.

Competing interests

YS110 was provided by Y's therapeutics. TY and CM are possessing non-listed stock of Y's therapeutics. MH and HN are paid by the consignment study cost of Y's therapeutics. TY and CM are advisers for Kissei Pharmaceutical Co., Ltd, which carried out the Phase I clinical trial for YS110 against CD26 positive cancers. HM, KY, and MS have no competing interests.

Ethical approval

All animal experiments were approved by the Animal Care and Use Committee of Keio University and were performed in accordance with the institute guidelines.

Funding

This study was supported by the Program for Promotion of Fundamental Studies in Health Sciences of the National Institute of Biomedical Innovation (07–17 to TY and CM), a Grant-in-Aid for Scientific Research (B) (23390086 and 16H04714 to TY and 22790355 to MH) and Global COE Program "Education and Research Center for Stem Cell Medicine" (to KY) from the Ministry of Education, Culture, Sports, Science and Technology of Japan, and a Grant-in-Aid for Drug Design Biomarker Research (H24-B10-003 to TY and CM) from the Ministry of Health, Labor and Welfare and a Grant-in-Aid for Industrial Accident Clinical Research (H27-150401-01 to TY and CM) from the Ministry of Health, Labor and Welfare.

Received: 23 December 2015 Accepted: 24 April 2016
Published online: 30 April 2016

References

1. Sugarbaker DJ. Multimodality management of malignant pleural mesothelioma: introduction. Semin Thorac Cardiovasc Surg. 2009;21:95–6.
2. Krug LM, Pass HI, Rusch VW, Kindler HL, Sugarbaker DJ, Rosenzweig KE, Flores R, Friedberg JS, Pisters K, Monberg M, Obasaju CK, Vogelzang NJ. Multicenter phase II trial of neoadjuvant pemetrexed plus cisplatin followed by extrapleural pneumonectomy and radiation for malignant pleural mesothelioma. J Clin Oncol. 2009;27:3007–13.
3. Vogelzang NJ, Rusthoven JJ, Symanowski J, Denham C, Kaukel E, Ruffie P, Gatzemeier U, Boyer M, Emri S, Manegold C, Niyikiza C, Paoletti P. Phase III study of pemetrexed in combination with cisplatin versus cisplatin alone in patients with malignant pleural mesothelioma. J Clin Oncol. 2003;21:2636–44.
4. Van Schil PE, Baas P, Gaafar R, Maat AP, Van de Pol M, Hasan B, Klomp HM, Abdelrahman AM, Welch J, van Meerbeeck JP. Trimodality therapy for malignant pleural mesothelioma: results from an EORTC phase II multicentre trial. Eur Respir J. 2010;36:1362–9.
5. Greillier L, Marco S, Barlesi F. Targeted therapies in malignant pleural mesothelioma: a review of clinical studies. Anticancer Drugs. 2011;22:199–205.
6. Ohnuma K, Uchiyama M, Yamochi T, Nishibashi K, Hosono O, Takahashi N, Kina S, Tanaka H, Lin X, Dang NH, Morimoto C. Caveolin-1 triggers T-cell activation via CD26 in association with CARMA1. J Biol Chem. 2007;282:10117–31.
7. Bauvois B. Transmembrane proteases in cell growth and invasion: new contributors to angiogenesis? Oncogene. 2004;23:317–29.
8. Aoe K, Amatya VJ, Fujimoto N, Ohnuma K, Hosono O, Hiraki A, Fujii M, Yamada T, Dang NH, Takeshima Y, Inai K, Kishimoto T, Morimoto C. CD26 overexpression is associated with prolonged survival and enhanced chemosensitivity in malignant pleural mesothelioma. Clin Cancer Res. 2012;18:1447–56.
9. Amatya VJ, Takeshima Y, Kushitani K, Yamada T, Morimoto C, Inai K. Overexpression of CD26/DPPIV in mesothelioma tissue and mesothelioma cell lines. Oncol Rep. 2011;26:1369–75.
10. Antczak C, De Meester I, Bauvois B. Ectopeptidases in pathophysiology. Bio Essays. 2001;23:251–60.
11. Inamoto T, Yamada T, Ohnuma K, Kina S, Takahashi N, Yamochi T, Inamoto S, Katsuoka Y, Hosono O, Tanaka H, Dang NH, Morimoto C. Humanized anti-CD26 monoclonal antibody as a treatment for malignant mesothelioma tumors. Clin Cancer Res. 2007;13:4191–200.
12. Le X-F, Pruefer F, Bast RC. HER2-targeting antibodies modulate the cyclin-dependent kinase inhibitor p27Kip1 via multiple signaling pathways. Cell Cycle. 2005;4:87–95.
13. Vincenzi B, Schiavon G, Silletta M, Santini D, Tonini G. The biological properties of cetuximab. Crit Rev Oncol Hematol. 2008;68:93–106.
14. Weiner GJ. Rituximab: mechanism of action. Semin Hematol. 2010;47:115–23.
15. Wu JD, Odman A, Higgins LM, Haugk K, Vessella R, Ludwig DL, Plymate SR. In vivo effects of the human type I insulin-like growth factor receptor antibody A12 on androgen-dependent and androgen-independent xenograft human prostate tumors. Clin Cancer Res. 2005;11:3065–74.
16. Takizawa CG, Morgan DO. Control of mitosis by changes in the subcellular location of cyclin-B1-Cdk1 and Cdc25C. Curr Opin Cell Biol. 2000;12:658–65.
17. Mebratu Y, Tesfaigzi Y. How ERK1/2 activation controls cell proliferation and cell death: is subcellular localization the answer? Cell Cycle. 2009;8:1168–75.
18. Zhang Z, Miao L, Lv C, Sun H, Wei S, Wang B, Huang C, Jiao B. Wentilactone B induces G2/M phase arrest and apoptosis via the Ras/Raf/MAPK signaling pathway in human hepatoma SMMC-7721 cells. Cell Death Dis. 2013;4:e657.

19. Chuang M-J, Wu S-T, Tang S-H, Lai X-M, Lai H-C, Hsu K-H, Sun K-H, Sun G-H, Chang S-Y, Yu D-S, Hsiao P-W, Huang S-M, Cha T-L. The HDAC inhibitor LBH589 induces ERK-dependent prometaphase arrest in prostate cancer via HDAC6 inactivation and down-regulation. PLoS One. 2013;8:e73401.
20. Hollmann CA, Owens T, Nalbantoglu J, Hudson TJ, Sladek R. Constitutive activation of extracellular signal-regulated kinase predisposes diffuse large B-cell lymphoma cell lines to CD40-mediated cell death. Cancer Res. 2006;66:3550–7.
21. Brunetto E, Ferrara AM, Rampoldi F, Talarico A, Cin ED, Grassini G, Spagnuolo L, Sassi I, Ferro A, Cuorvo LV, Barbareschi M, Piccinin S, Maestro R, Pecciarini L, Doglioni C, Cangi MG. CDC25A protein stability represents a previously unrecognized target of HER2 signaling in human breast cancer: implication for a potential clinical relevance in trastuzumab treatment. Neoplasia. 2013;15:579–90.
22. Yamada K, Hayashi M, Du W, Ohnuma K, Sakamoto M, Morimoto C, Yamada T. Localization of CD26/DPPIV in nucleus and its nuclear translocation enhanced by anti-CD26 monoclonal antibody with anti-tumor effect. Cancer Cell Int. 2009;9:17.
23. Yamada K, Hayashi M, Madokoro H, Nishida H, Du W, Ohnuma K, Sakamoto M, Morimoto C, Yamada T. Nuclear localization of CD26 induced by a humanized monoclonal antibody inhibits tumor cell growth by modulating of POLR2A transcription. PLoS ONE. 2013;8:e62304.
24. Penno MB, Askin FB, Ma H, Carbone M, Vargas MP, Pass HI. High CD44 expression on human mesotheliomas mediates association with hyaluronan. Cancer J Sci Am. 1995;1:196–203.

Submit your next manuscript to BioMed Central and we will help you at every step:

- We accept pre-submission inquiries
- Our selector tool helps you to find the most relevant journal
- We provide round the clock customer support
- Convenient online submission
- Thorough peer review
- Inclusion in PubMed and all major indexing services
- Maximum visibility for your research

Submit your manuscript at
www.biomedcentral.com/submit

BioMed Central

Effects of obesity and diabetes on alpha and beta cell mass in surgically resected human pancreas

Jun Inaishi[1], Yoshifumi Saisho[1], Seiji Sato[1], Kinsei Kou[1], Rie Murakami[1], Yuusuke Watanabe[1], Minoru Kitago[2], Yuko Kitagawa[2], Taketo Yamada[3,4], and Hiroshi Itoh[1]

[1] Department of Internal Medicine, Keio University School of Medicine, Tokyo, Japan; [2] Department of Surgery, Keio University School of Medicine, Tokyo, Japan; [3] Department of Pathology, Keio University School of Medicine, Tokyo, Japan; [4] Department of Pathology, Saitama Medical University, Saitama, Japan Original article

Context: The ethnic difference in beta cell regenerative capacity in response to obesity may be attributable to different phenotypes of type 2 diabetes among ethnicities.

Objective: This study aimed to clarify the effects of diabetes and obesity on beta (BCM) and alpha cell mass (ACM) in the Japanese population.

Design, Setting and Participants: We obtained the pancreases of 99 individuals who underwent pancreatic surgery and whose resected pancreas sample contained adequate normal pancreas for histological analysis. Questionnaires on family history of diabetes and history of obesity were conducted in 59 patients. Pancreatic sections were stained for insulin or glucagon, and fractional beta and alpha cell area were measured. Islet size and density as well as beta cell turnover were also quantified.

Results: In patients with diabetes, BCM was decreased by 46% compared with age- and BMI-matched non-diabetic patients (1.48 ± 1.08% vs. 0.80 ± 0.54%, $P < 0.001$), while there was no difference in ACM between the groups. There was no effect of obesity or history of obesity on BCM and ACM irrespective of the presence or absence of diabetes. There was a negative correlation between BCM, but not ACM, and HbA1c before and after pancreatic surgery. In addition, reduced BCM was observed in patients with pancreatic cancer compared with those with other pancreatic tumors.

Conclusions: These findings suggest that the increase in BCM in the face of insulin resistance is extremely limited in Japanese, and BCM rather than ACM has a major role in regulating blood glucose level in humans.

Both type 1 (T1DM) and type 2 diabetes (T2DM) are characterized by a deficit of beta cell mass (BCM) (1). Preservation or recovery of BCM is therefore an important therapeutic strategy for both T1DM and T2DM. On the other hand, the paradoxical increase in glucagon secretion in subjects with diabetes suggests an increase in alpha cell mass (ACM), which was shown in rodent studies to occur through the mechanism of dedifferentiation of beta cells to alpha cells (2). However, since it is not yet possible to measure BCM as well as ACM in vivo in humans, the physiological and pathological changes in BCM and ACM in the face of obesity and diabetes in humans remain to be established.

As plasma insulin level is increased approximately 2 to 3-fold with obesity to compensate insulin resistance (3), it is widely believed that BCM increases with obesity. In

---

ISSN Print 0021-972X ISSN Online 1945-7197
Printed in USA
Copyright © 2016 by the Endocrine Society
Received February 13, 2016. Accepted April 7, 2016.

Abbreviations: ACA; alpha cell area, ACM; alpha cell mass, BCA; beta cell area, BCM; beta cell mass, CPR; C-peptide immunoreactivity, GA; glycated albumin, GAD; glutamic acid decarboxylase, IPMN; intraductal papillary mucinous neoplasm, PC; pancreatic cancer, PARP; poly(ADP-ribose) polymerase-1, ssDNA; single-stranded DNA, T2DM; type 2 diabetes

doi: 10.1210/jc.2016-1374

The Endocrine Society. Downloaded from press.endocrine.org by [${individualUser.displayName}] on 14 April 2016. at 06:14 For personal use only. No other uses without permission. . All rights reserved.

adult humans, we and others have shown that BCM increases by approximately 20 to 50% in obese nondiabetic individuals in the Caucasian population (4, 5). However, a meta-analysis of the insulin secretion-sensitivity relationship among different ethnic groups has shown higher insulin sensitivity and lower insulin secretion in Asians compared with Caucasians and African Americans (6), suggesting ethnic differences in insulin secretory ability.

We have recently reported that no significant increase in BCM was observed in obese nondiabetic adults and those treated with corticosteroids in the Japanese population (7, 8). These findings suggest that beta cell regenerative capacity, as well as beta cell functional capacity, may differ between Japanese and Caucasians. These studies were however based on autopsy pancreas where it was not possible to completely exclude the effects of confounding factors, such as underlying diseases leading to death, nutritional change and intensive medical treatment prior to death, and postmortem changes on pancreas morphology.

Therefore, in this study, to overcome these limitations and complement autopsy studies, we sought to address the following questions by using surgically resected pancreas samples in the Japanese population where we were able to obtain detailed medical information and history of obesity: 1) Is there any interaction between the effects of diabetes and obesity on BCM and ACM? 2) Is there any correlation between history of obesity and BCM and ACM? 3) Is there any correlation between BCM or ACM, and pre- and postoperative glycemic control?

Materials and Methods

Patients

The study was approved by the Ethics Committee of Keio University School of Medicine. A total of 99 Japanese individuals (61 men and 38 women) who underwent pancreatic surgery and whose resected pancreas sample contained adequate normal pancreas for histological analysis were included in the study (Table 1 and Supplemental Figure 1). Written informed consent was obtained from each patient, while it was waived for patients who had discontinued hospital visits at the time of study enrollment (N = 40).

Of these, 41 patients had been diagnosed with type 2 diabetes before the diagnosis of pancreatic tumors, and eight patients were diagnosed with pancreatic cancer (PC) and diabetes at the same time. There was no case of type 1 diabetes or case in which glutamic acid decarboxylase (GAD) antibody was positive.

Measurements and questionnaire

Information on each patient including HbA1c, glycated albumin (GA), plasma glucose and serum C-peptide immunoreactivity (CPR) levels were obtained from the medical records. HbA1c was measured by HPLC and expressed as NGSP and IFCC values. GA and CPR were measured by an enzymatic method and chemiluminescent enzyme immunoassay (EIA), respectively. Beta cell function was assessed by serum CPR to plasma glucose ratio (CPR index) calculated as CPR (nmol/l)/plasma glucose (mmol/l), as previously reported (9).

In addition, a questionnaire on family history of diabetes and history of obesity was conducted in 59 patients. The questionnaire consisted of the following categories: 1) history of obesity in childhood and adolescence, 2) body weight at age 20 years and every decade thereafter, 3) maximum body weight in life, and 4)

Table 1. Characteristics of subjects.

	Patients without diabetes (NDM)			Patients with diabetes (DM)			
	Total	Lean	Obese	Total	Lean	Obese	**Total**
N (male/female)	50 (26/24)	40 (17/23)	10 (9/1)	49 (35/14)	40 (28/12)	9 (7/2)	99 (61/38)
Age (years)	64 ± 14	64 ± 14	63 ± 13	67 ± 9	67 ± 8	67 ± 13	65 ± 12
BMI (kg/m^2)	22.5 ± 2.7	21.5 ± 1.9	26.4 ± 1.2*	21.9 ± 3.5	20.7 ± 2.4	27.6 ± 1.6*	22.2 ± 3.1
HbA1c (%)1)	5.6 ± 0.5	5.7 ± 0.5	5.6 ± 0.6	7.8 ± 1.6#	7.8 ± 1.8#	7.5 ± 0.9#	6.7 ± 1.6
HbA1c (mmol/mol)1)	38 ± 6	38 ± 6	37 ± 6	61 ± 18#	62 ± 19#	58 ± 10#	50 ± 18
GA (%)2)	14.8 ± 1.8	14.8 ± 1.8	N/A	21.2 ± 4.4#	21.6 ± 4.9#	20.1 ± 2.7#	20.1 ± 4.7
PG (mmol/liter)3)	6.24 ± 1.20	6.21 ± 1.21	6.37 ± 1.23	8.33 ± 2.52#	8.44 ± 2.71#	7.83 ± 1.41#	7.27 ± 2.22
CPR (nmol/liter)3)4)	0.57 (0.37–0.96)	0.56 (0.36–0.69)	1.036)	0.51 (0.34–0.71)	0.54 (0.31–0.71)	0.50 (0.39–0.80)	0.56 (0.36–0.73)
CPR index ([nmol/liter]/[mmol/liter])4)	0.101 (0.060–0.155)	0.085 (0.058–0.115)	0.1746)	0.063 (0.045–0.086)	0.056 (0.044–0.085)	0.066 (0.055–0.102)	0.065 (0.047–0.103)
Duration of DM (years)	-	-	-	8 ± 9	7 ± 9	9 ± 6	-
Medication for diabetes, n (%)							
Diet only	-	-	-	14 (28)	13 (33)	1 (11)	-
OHA	-	-	-	20 (41)	13 (33)	7 (78)	-
Insulin ± OHA	-	-	-	15 (31)	14 (35)	1 (11)	-
Clinical diagnosis, n (%)							
Neuroendocrine tumor	13 (26)	10 (25)	3 (30)	7 (14)	7 (18)	0 (0)	20 (20)
Pancreatic cancer	28 (56)	24 (60)	4 (40)	34 (70)	28 (70)	6 (67)	62 (63)
IPMN	9 (18)	6 (15)	3 (30)	7 (14)	5 (12)	2 (22)	16 (17)
Others5)	0 (0)	0 (0)	0 (0)	1 (2)	0 (0)	1 (11)	1 (1)
Operative procedure, n (%)							
Distal pancreatectomy	40 (80)	31 (78)	9 (90)	33 (68)	29 (73)	4 (44)	73 (74)
Pancreatoduodenectomy	6 (12)	6 (15)	0 (0)	12 (24)	7 (17)	5 (56)	18 (18)
Total pancreatectomy	4 (8)	3 (7)	1 (10)	4 (8)	4 (10)	0 (0)	8 (8)

Data with normal distribution are expressed as mean ± SD, and non-normally distributed data are expressed as median (interquartile range). * $P <$ 0.05 *vs.* Lean. # $P < 0.05$ *vs.* NDM. 1) HbA1c was obtained in 93 subjects. 2) GA was obtained in 35 subjects. 3) Timing of blood sampling (i.e. fasting or postprandial) was not determined. 4) CPR and CPR index were obtained in 56 subjects. 5) Disseminated sarcoma originating from small intestine. 6) $n = 2$. CPR index was calculated as CPR (nmol/liter)/PG (mmol/liter). N/A: not available. OHA: oral hypoglycemic agent. IPMN: intraductal papillary mucinous neoplasm.

The Endocrine Society. Downloaded from press.endocrine.org by [${individualUser.displayName}] on 14 April 2016. at 06:14 For personal use only. No other uses without permission. . All rights reserved.

first-degree family history of diabetes. Duration of obesity was calculated from the responses to the questionnaire.

The cases were classified into four groups according to the presence or absence of diabetes and obesity. Obesity was defined as BMI ≥ 25 kg/m^2 (10).

Pancreatic tissue processing

The surgically resected pancreas was immediately fixed in formaldehyde and embedded in paraffin for subsequent analysis. In eight cases that underwent total pancreatectomy, pancreas samples were obtained from the head in three cases and the body or tail in five cases. Five-micrometer sections were cut from the tumor-free region and stained for light microscopy as follows: 1) with hematoxylin-eosin, 2) for insulin (peroxidase staining) with hematoxylin, 3) for glucagon with hematoxylin, 4) for insulin and Ki67 for assessment of beta cell replication, and 5) for insulin and single-stranded DNA (ssDNA) or cleaved poly(ADP-ribose) polymerase-1 (PARP) for assessment of beta cell apoptosis, as previously described (7, 8).

Morphometric analysis

To quantify fractional beta cell area (BCA), the entire pancreatic section was imaged at the original magnification x200 (x20 objective) using a Mirax Scan and Mirax Viewer (Carl Zeiss MicroImaging GmbH, Goettingen, Germany). The ratio of BCA to total pancreas area was digitally measured using Image Pro Plus software (Media Cybernetics, Silver Springs, MD), as previously reported (7, 8). Likewise, the ratio of alpha cell area to total pancreas area (ACA) was also digitally measured, and the ratio of ACA to BCA was determined in each case. All measurements were conducted by a single investigator (J.I.), and the intraobserver coefficient of variance was 7%. All measurements were conducted twice, and the mean of the two measurements was used. At the time of measurement, the investigator was blinded to both the glycemic and obesity status for each specimen.

To conduct further morphometric analysis, size and density of islets, density of scattered beta cells and insulin-positive duct cells were quantified in randomly selected areas of the pancreas that contained approximately 100 islets in each case (106 ± 6 islets, total 10 491 islets) using a Mirax Viewer (7, 8). Scattered beta cells were defined as a cluster of three or fewer beta cells in acinar tissue. In addition, beta cell replication and apoptosis were quantified and expressed as percentage of islets.

Statistical analysis

Data are presented as mean ± SD or, if non-normally distributed, median (interquartile range) in the text and tables. Mann-Whitney U test was used to assess difference between two groups, and Spearman correlation coefficient was used to assess the correlation between two parameters. ANCOVA and multivariate regression were used to adjust for covariates. Statistical analyses were performed using SPSS 22 software (IBM, Armonk, NY). A P value of < 0.05 was considered statistically significant.

Results

Change in islet morphology in patients with diabetes

Representative photomicrographs of the pancreas of patients with and without diabetes are shown in Figure 1. In patients with diabetes (DM group), BCA was decreased by 46% compared with age- and BMI-matched nondiabetic patients (NDM group) (1.48 ± 1.08% vs. 0.80 ± 0.54%, $P < .001$, Supplemental Figure 2). There was no difference in ACA between the two groups (0.49 ± 0.44% vs. 0.35 ± 0.31%, $P = .09$). ACA to BCA ratio in the DM group was thus increased compared with that in the NDM group (0.35 ± 0.18 vs. 0.46 ± 0.30, $P = .045$).

Mean islet size (5297 ± 2115 vs. 4486 ± 1990 μm^2, $P = .03$) and islet density (4.52 ± 3.05 vs. 3.09 ± 2.04 /mm^2, $P = .003$) were both decreased in the DM group compared with the NDM group. On the other hand, there was no difference in the density of scattered beta cells, density of insulin-positive duct cells and beta cell replication between the two groups. Beta cell apoptosis (ie, ssDNA and/or cleaved PARP-positive beta cells) was not found in either group (Supplemental Figure 2).

Reduced BCA in the DM group was also observed when patients diagnosed with PC and diabetes at the same time (N = 8) were excluded from the analysis (0.81 ± 0.55%, $P < .001$ vs. NDM). Furthermore, a similar reduction in

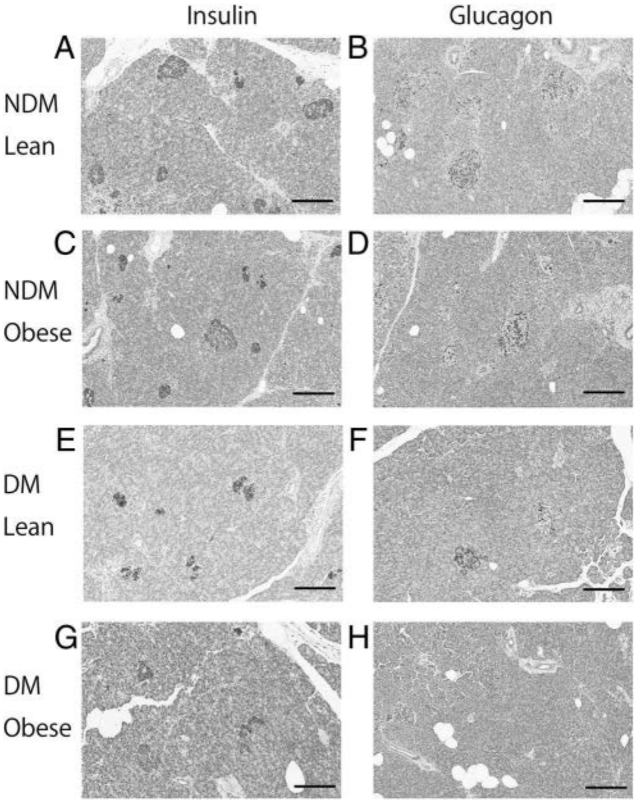

Figure 1. Representative photomicrographs of pancreas immunostained for insulin (brown) (A, C, E, G) or glucagon (brown) (B, D, F, H) and with hematoxylin (x20 objective). Examples of lean (65-year-old woman, BMI 21.5, HbA1c 5.7% (38 mmol/mol)) (A and B) and obese (63-year-old man, BMI 26.0, HbA1c 5.6% (37 mmol/mol)) (C and D) subjects without diabetes, and lean (63-year-old woman, BMI 19.6, HbA1c 8.2% (66 mmol/mol)) (E and F) and obese (70-year-old man, BMI 29.0, HbA1c 7.7% (60 mmol/mol)) (G and H) subjects with diabetes. Scale bar, 200 μm.

The Endocrine Society. Downloaded from press.endocrine.org by [${individualUser.displayName}] on 14 April 2016. at 06:14 For personal use only. No other uses without permission. . All rights reserved.

BCA was observed in patients with diabetes duration > 3 years and those with diabetes duration ≤ 3 years (*P* = .65, Supplemental Figure 3A). There was no difference in BCA among patients treated with different medications (Supplemental Figure 3D).

There was no difference in either BCA or ACA according to the pancreas regions from where the samples had been obtained (ie, pancreas head vs. body or tail, Supplemental Figure 4D-I). However, BCA of subjects with PC was significantly lower than that of those with other tumors, irrespective of the presence or absence of diabetes (Supplemental Figure 4A).

Effects of obesity on islet morphology

Patients with or without diabetes were further classified according to presence or absence of obesity (Table 1). In the NDM group, there was no difference in BCA (1.42 ± 1.09% vs. 1.71 ± 1.07%, *P* = .21), ACA (0.48 ± 0.46% vs. 0.55 ± 0.37%, *P* = .33) and ACA to BCA ratio (0.33 ± 0.16 vs. 0.41 ± 0.26, *P* = .56) between lean and obese subjects (Figure 2). Similarly, no differences in BCA, ACA and ACA to BCA ratio between lean and obese subjects were observed in the DM group. Accordingly, BCA was similarly decreased with diabetes in the lean and obese groups (*P* = .001 and *P* = .04, respectively). There were no correlations between BMI and BCA, ACA or ACA/BCA ratio in either the NDM or DM group (Figure 2D-I). No increase in BCA in obese subjects was also confirmed by the ANCOVA model including age, sex, diabetes and PC (adjusted mean (95% confidence interval (CI)) 1.20% (1.01–1.40) vs. 1.20% (0.77–1.62) in lean vs. obese, respectively).

In the DM group, but not the NDM group, mean islet size in obese subjects was increased compared with that in lean subjects (6220 ± 2219 vs. 4096 ± 1736 μm^2, *P* = .01, Supplemental Figure 5A), and was positively correlated with BMI (R = 0.43, *P* = .002, Supplemental Figure 5H). In both the NDM and DM groups, there was no difference in islet density and beta cell turnover between the lean and obese groups (Supplemental Figure 5B-F).

Effect of history of obesity and family history of diabetes on islet morphology

To examine the effect of history of obesity on islet morphology, cases that answered the questionnaire on history of obesity (N = 59) were divided into three groups according to the duration of obesity (lean (ie, no history of obesity), ≤10 years and > 10 years, Supplemental Table 1). Among the three groups, no difference in BCA and ACA was found in either the NDM or DM group (Figure 3). Neither BCA nor ACA was correlated with maximum BMI in life (Figure 3E-H). In the DM group, there was a

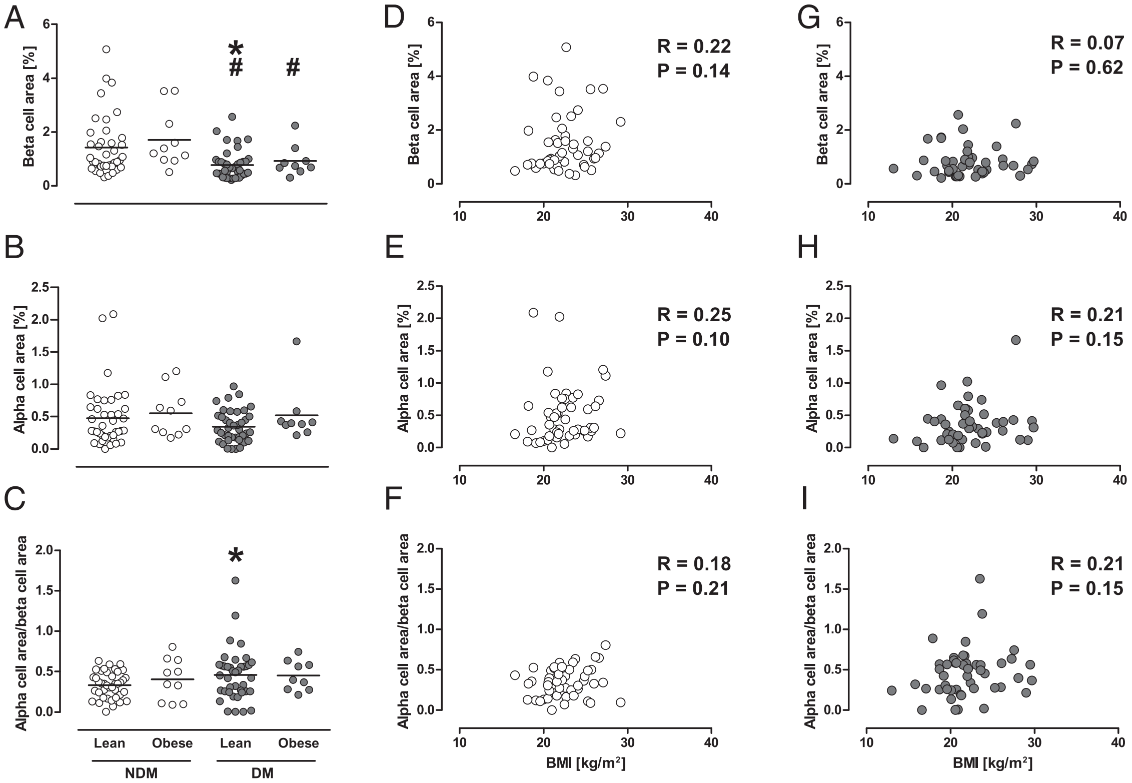

Figure 2. A, B and C: Effects of obesity on beta cell area (BCA), alpha cell area (ACA) and ACA to BCA ratio in cases with and without diabetes. Gray and white circles show cases with and without diabetes, respectively. Bars indicate mean. * $P < .05$ vs. lean cases without diabetes. # $P < .05$ vs. obese cases without diabetes. D-I: Correlations between BMI and BCA, ACA or ACA to BCA ratio in cases with and without diabetes.

The Endocrine Society. Downloaded from press.endocrine.org by [${individualUser.displayName}] on 14 April 2016. at 06:14 For personal use only. No other uses without permission. . All rights reserved.

positive correlation between mean islet size and maximum BMI (R = 0.48, $P = .003$).

Among the 59 patients, three subjects in the NDM group (12%) and 11 subjects in the DM group (33%) had a first-degree family history of diabetes. Although there was no significant difference in BCA and ACA between patients with and without a family history of diabetes, in the DM group islet density was significantly decreased and mean islet size was increased with borderline significance in patients with a family history compared with those without (Figure 4).

Association between beta cell mass and pre- and postsurgery glycemic markers

BCA was negatively correlated with HbA1c and GA before surgery (R = −0.42, $P < .001$ and R = −0.49, $P = .003$, respectively, Figure 5A and B), while ACA was not (R = −0.15, $P = .15$ and R = 0.20, $P = .25$, respectively). The relationship between BCA and HbA1c remained significant after adjustment for age, sex, BMI and presence of PC ($\beta = -0.21$, $P = .04$). BCA was correlated with CPR index before surgery (R = 0.37, $P = .005$, Supplemental Figure 6C).

A negative correlation between BCA and HbA1c or GA was also observed at 3 and 6 months after surgery (Figure 5C-D and Supplemental Figure 6A-B). In contrast, ACA was not correlated with postoperative HbA1c or GA at any time point (data not shown). The same results were observed when only cases with distal pancreatectomy were included in the analysis (data not shown).

Discussion

In this study, we report that 1) BCA in individuals with diabetes was decreased by ~45% compared with that in those without diabetes, while there was no difference in ACA, 2) there was little effect of obesity or history of obesity on BCA and ACA irrespective of the presence or absence of diabetes, and 3) BCA, but not ACA, was significantly correlated with preoperative and postoperative glycemic control. The findings of this study extend the current knowledge on the pathophysiological changes in BCM and ACM in humans, as discussed below.

First, the reduction in BCA by ~45% in Japanese patients with T2DM was consistent with our prior report using autopsy pancreas (8). Although it is often difficult to distinguish T2DM and PC-associated diabetes in patients with PC, we confirmed the same results in patients with diabetes duration > 3 years, in whom T2DM was likely to have preceded the development of pancreatic tumors (11). A recent study suggested that beta cell loss in patients with T2DM is overestimated due to the presence of degranulated beta cells (12); however, the comparable reduction in islet size and density in this study supports the idea that the number of beta cells is indeed reduced in those with T2DM, as reported by prior observations (5, 8, 13–15).

Reduced insulin secretion and a paradoxical increase in glucagon secretion is a hallmark of T2DM (16); however, the change in ACM in patients with diabetes is controversial. ACM has been reported to increase in patients with T2DM (14), but this was not found in other studies (8, 17, 18). A recent rodent study has suggested beta cell to alpha cell transdifferentiation as a mechanism of increased ACM in diabetes (2). In the present study, we observed no significant increase in ACA in patients with T2DM, although the relative proportion of ACA to BCA was significantly increased compared with that in nondiabetic patients. Thus, the present study indicates that the relative increase in ACM compared to BCM in patients with T2DM is mainly driven by reduced BCM, but not an increase in ACM. The reduced islet size and density observed in patients with diabetes also reflect reduced total endocrine cells in patients with diabetes.

The second objective of this study was to clarify the effects of obesity on BCM and ACM in patients with and without diabetes. We have previously reported no increase in BCM in Japanese obese nondiabetic individuals compared with lean controls by using autopsy samples (7). In contrast, in the Caucasian population, autopsy studies have shown that BCM is increased by ~20 to 50% in obese nondiabetic individuals (4, 5). A recent study in the Caucasian population using surgically resected pancreas has also shown a significant increase in BCA in nondiabetic individuals with insulin resistance (19). These inconsistent findings suggest the possibility that the adaptive change in BCM in response to obesity differs among ethnicities.

In this study, using surgically resected pancreas, we confirmed no increase in BCA in Japanese obese individuals with or without diabetes, in line with recent Japanese studies (20, 21). Since it has been reported that beta cell replication rapidly decreases postmortem (22, 23), beta cell turnover might be underestimated in autopsy pancreas. Here, we found that beta cell replication and surrogate markers of beta cell neogenesis in the surgically resected pancreas were also not changed in obese individuals. Furthermore, we here showed that there was no effect of either duration of obesity or maximum BMI in life on BCA in these subjects. Similarly to BCA, ACA was also not changed in obese individuals irrespective of the presence or absence of diabetes. Although studies have shown that beta cell function adjusted for insulin sensitivity is comparable between Japanese and Caucasians (24, 25), con-

The Endocrine Society. Downloaded from press.endocrine.org by [${individualUser.displayName}] on 14 April 2016. at 06:14 For personal use only. No other uses without permission. . All rights reserved.

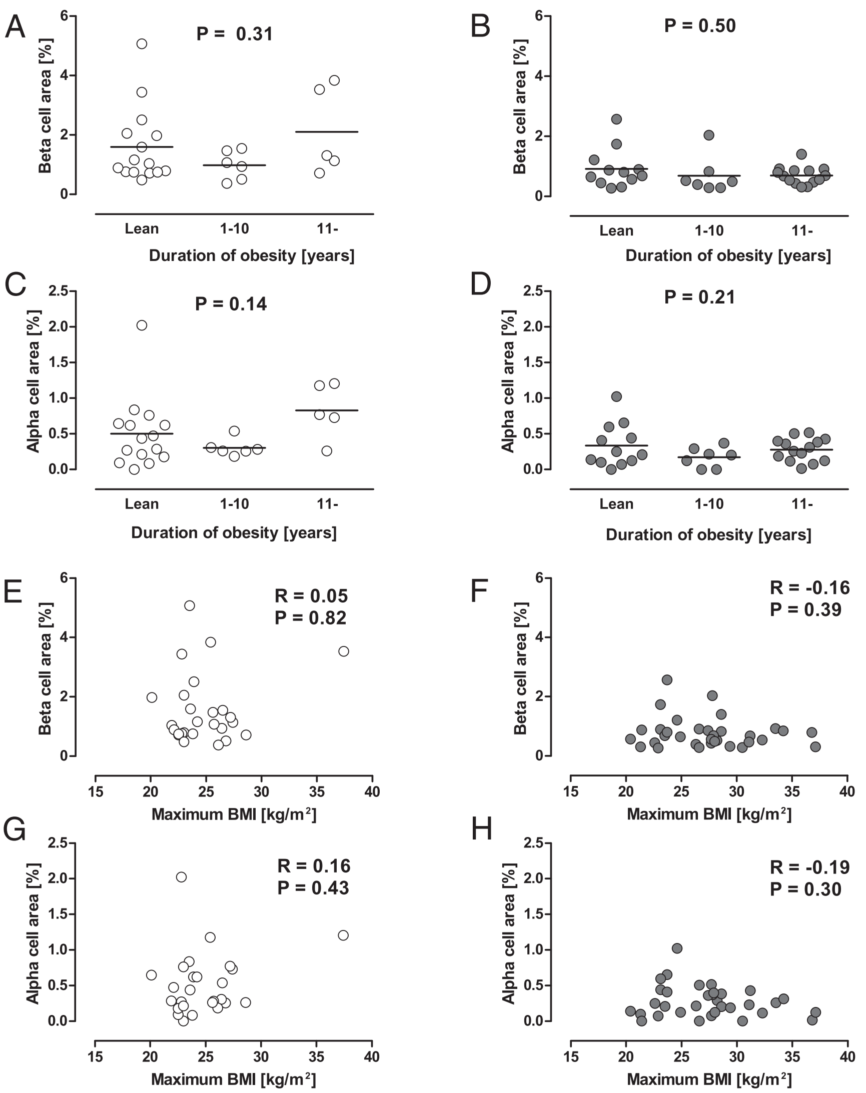

Figure 3. A-D: Effects of history of obesity on beta cell area (BCA) and alpha cell area (ACA). Cases that answered the questionnaire (N = 59) were divided into three groups according to the duration of obesity (lean (ie, no history of obesity), ≤10 years and > 10 years). Bars indicate mean. E-H: Correlations between maximum BMI in life and BCA or ACA in cases with and without diabetes. Gray and white circles show cases with and without diabetes, respectively.

sidering the similar incidence of T2DM despite less degree of obesity in Japanese compared with Caucasians (26), our results suggest that the ethnic difference in BCM could be attributable to lower maximum insulin secretory ability in Asians compared with Caucasians. Further studies are needed to determine genetic and environmental factors regulating BCM in humans and clarify the underlying mechanisms of the ethnic difference in beta cell change in response to obesity.

While mean islet size was reduced in patients with T2DM compared with nondiabetic subjects, there was a positive correlation between mean islet size and BMI in patients with T2DM. Considering the lack of significant change in BCA or ACA with obesity, the increase in islet size possibly resulted from an increase in other endocrine cells, amyloid deposits or other components. It has been reported that islet amyloid deposition is positively correlated with BMI in patients with T2DM (27). It would be of interest to clarify the underlying mechanism of islet remodeling with obesity in patients with T2DM, which may cause further beta cell loss in these patients.

It is also of note that we assessed the effect of a first-degree family history of diabetes on BCM. As a result, in patients with diabetes, reduced islet density with greater islet size was observed in patients with a family history of diabetes. We have previously reported that islet number rather than islet size is a major determinant of BCM, and islet density was negatively correlated with plasma glucose level in nondiabetic humans (28). Reduced islet density with greater islet size has also been reported in nondiabetic subjects with the TCF7L2 polymorphism who are susceptible to T2DM (29). Together with these prior studies, the present study suggests that a genetic factor is associated with T2DM susceptibility through reduced islet number.

Finally, we investigated the clinical significance of BCM, ie, the relationship between BCA and plasma glucose level, and found a negative correlation between BCA and HbA1c, consistent with our and prior reports (8, 14, 30, 31). We also confirmed the association between BCA and plasma glucose level using another glycemic index, GA. Intriguingly, the relationships between BCA and glycemic markers remained significant even 6 months after surgery in patients with pancreatoduodenectomy or distal pancreatectomy where a half of the pancreas had been resected, indicating that BCA predicts glycemic control before and after surgery. The present study and others have also observed a significant correlation between BCA and endogenous insulin secretion assessed by CPR or CPR index (21, 31), which have been shown to predict future glycemic control (32). These findings underpin the importance of BCM rather than ACM in regulation of glucose metabolism in humans.

Another unexpected and novel finding of this study was

The Endocrine Society. Downloaded from press.endocrine.org by [${individualUser.displayName}] on 14 April 2016. at 06:14 For personal use only. No other uses without permission. . All rights reserved.

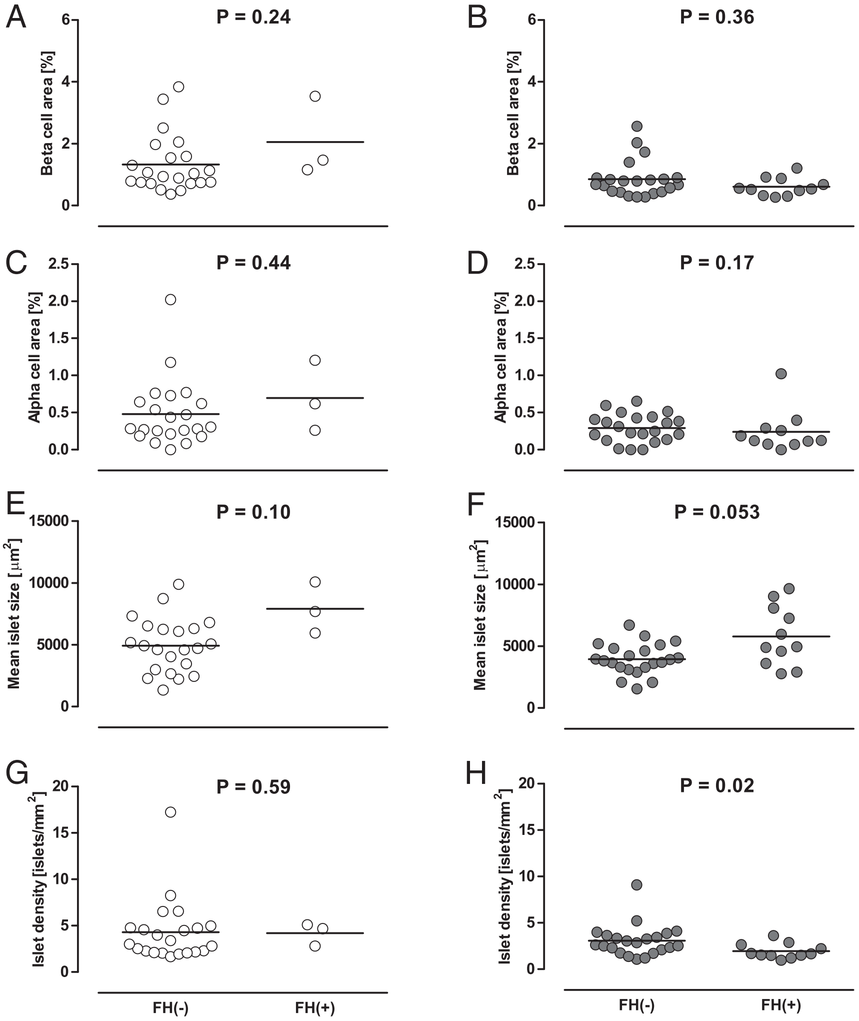

Figure 4. Effects of first-degree family history of diabetes (FH) on beta cell area (BCA) (A and B), alpha cell area (ACA) (C and D) and islet morphology (E-H). Gray and white circles show cases with and without diabetes, respectively. Bars indicate mean.

the reduced BCA in patients with PC compared with those with other pancreatic tumors. It is known that PC is associated with new-onset or worsening of diabetes (33). However, the mechanisms by which PC causes deterioration of glucose metabolism remain largely unknown. It has been reported that beta cell function is impaired in patients with PC (34). One study reported reduced BCA in patients with PC and diabetes (35), while others did not (21, 31). These inconsistent results might have been due to the small sample size in these studies. In this study, reduced BCA in patients with PC was observed irrespective of the presence or absence of diabetes, suggesting that the reduction in BCM is independent of the effect of diabetes. The reduced BCA in the tumor-free region supports the concept that PC may affect endocrine cells indirectly through humoral factors such as adrenomedullin (36). Further study will be needed to clarify the underlying mechanisms by which PC induces glucose intolerance through a reduction in endocrine cells.

The strengths of the present study include 1) the relatively large sample size with well-matched controls, 2) detailed medical information before and after surgery and 3) detailed information on history of obesity and family history of diabetes obtained by questionnaire. The major limitation of this study was that the cases had pancreatic diseases which might have affected pancreatic morphology. However, we confirmed the same results in cases with and without PC, and the findings of this study were consistent with our prior report using autopsy pancreas in which cases with pancreatic disease were excluded (7, 8, 28). Second, the pancreas samples were obtained from different portions of the pancreas according to the operative procedures. However, it has been reported that the proportion of endocrine cells is constant throughout the pancreas with the exception of the ventral portion of the pancreatic head (37), and we confirmed that there was no difference in either BCA or ACA between samples from the head and those from the body or tail. Another limitation of the study was that we evaluated BCA as a surrogate for BCM. Thus, the different pancreas mass in each case might have affected our findings, although it was difficult to determine pancreas mass because of the presence of pancreatic tumors. Nonetheless, estimates of BCM based on reference data (38) did not change our conclusion (data not shown), and an increase in BCA in obese subjects has been observed in both autopsy and surgically resected pancreas in the Caucasian population (4, 19), supporting our conclusion that the change in BCA in response to obesity is limited in Japanese. Finally, although we evaluated the history of obesity, none of the cases had a history of childhood obesity. Since postnatal beta cell replication is more frequently observed in the first 5 years of life (39, 40), we were not able to exclude the possibility that childhood obesity may promote BCM expansion in the Japanese population.

In conclusion, there was no increase in BCM in Japanese obese individuals who underwent pancreatic surgery, and BCM was not related to BMI, history of obesity or maximum BMI. These findings suggest that the increase in

The Endocrine Society. Downloaded from press.endocrine.org by [${individualUser.displayName}] on 14 April 2016. at 06:14 For personal use only. No other uses without permission. . All rights reserved.

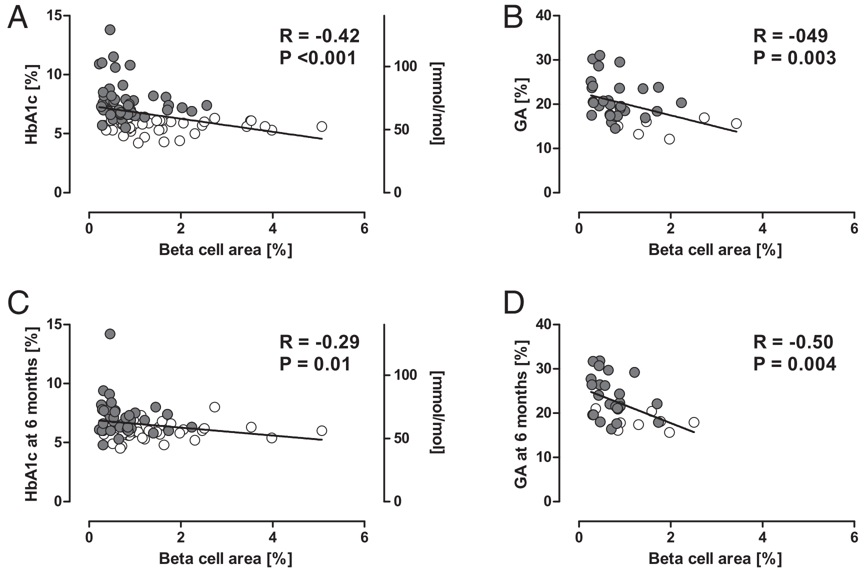

Figure 5. A and B: Correlations between BCA and preoperative HbA1c (N = 93) or glycated albumin (GA) (N = 35). C and D: Correlations between BCA and HbA1c (N = 77) or GA (N = 32) at 6 months after surgery. Gray and white circles show cases with and without diabetes, respectively. C and D: Cases that underwent total pancreatectomy were excluded.

BCM in the face of insulin resistance is extremely limited in Japanese. BCM was reduced by ~45% in patients with T2DM, and BCM, but not ACM, was associated with preoperative and postoperative glycemic control. These findings support the concept that BCM rather than ACM has a major role in regulating blood glucose level in humans.

Acknowledgments

We thank Yuko Madokoro, Department of Pathology, Keio University School of Medicine, for technical assistance and Dr. Wendy Gray, self-employed, for editing the manuscript.

Address all correspondence and requests for reprints to: Yoshifumi Saisho, MD, PhD, Department of Internal Medicine, Keio University School of Medicine, 35 Shinanomachi, Shinjuku-ku, Tokyo 160–8582, Japan, TEL: +81–3-3353–1211 (x62383), FAX: +81–3-3359–2745, E-mail: ysaisho@keio.jp.

This work was supported by Funding: Japan Diabetes Foundation, the Keio Gijuku Academic Development Funds, and a Grant-in-Aid for Scientific Research (15K09399) from the Ministry of Education, Culture, Sports, Science and Technology (MEXT) (Y.S.).

Disclosure statement: The authors have no conflict of interest. Y.S. is the guarantor of this work and, as such, had full access to all the data in the study and takes responsibility for the integrity of the data and the accuracy of the data analysis.

Author contributions: J.I. and Y.S. researched data and wrote the manuscript. S.S., K.K., R.M. and Y.W. contributed to discussion and reviewed/edited the manuscript. M.K. and Y.K. researched data and reviewed/edited the manuscript. T.Y. researched data, contributed to discussion and reviewed/edited the manuscript. H.I. contributed to discussion and reviewed/edited the manuscript.

References

1. **Saisho Y.** Beta cell dysfunction: Its critical role in prevention and management of type 2 diabetes. *World J Diabetes*. 2015;6:109–124.
2. **Talchai C, Xuan S, Lin HV, Sussel L, Accili D.** Pancreatic beta cell dedifferentiation as a mechanism of diabetic beta cell failure. *Cell*. 2012;150:1223–1234.
3. **Polonsky KS, Given BD, Van Cauter E.** Twenty-four-hour profiles and pulsatile patterns of insulin secretion in normal and obese subjects. *J Clin Invest*. 1988;81:442–448.
4. **Saisho Y, Butler AE, Manesso E, Elashoff D, Rizza RA, Butler PC.** β-cell mass and turnover in humans: Effects of obesity and aging. *Diabetes Care*. 2013;36:111–117.
5. **Rahier J, Guiot Y, Goebbels RM, Sempoux C, Henquin JC.** Pancreatic beta-cell mass in European subjects with type 2 diabetes. *Diabetes Obes Metab 10 Suppl*. 2008;4:32–42.
6. **Kodama K, Tojjar D, Yamada S, Toda K, Patel CJ, Butte AJ.** Ethnic differences in the relationship between insulin sensitivity and insulin response: A systematic review and meta-analysis. *Diabetes Care*. 2013;36:1789–1796.
7. **Kou K, Saisho Y, Satoh S, Yamada T, Itoh H.** Change in beta-cell mass in Japanese nondiabetic obese individuals. *J Clin Endocrinol Metab*. 2013;98:3724–3730.
8. **Sato S, Saisho Y, Inaishi J, Kou K, Murakami R, Yamada T, Itoh H.** Effects of glucocorticoid treatment on beta- and alpha-cell mass in Japanese adults with and without diabetes. *Diabetes*. 2015;64:2915–2927.
9. **Saisho Y, Kou K, Tanaka K, Abe T, Kurosawa H, Shimada A, Meguro S, Kawai T, Itoh H.** Postprandial serum C-peptide to plasma glucose ratio as a predictor of subsequent insulin treatment in patients with type 2 diabetes. *Endocr J*. 2011;58:315–322.
10. **Kanazawa M, Yoshiike N, Osaka T, Numba Y, Zimmet P, Inoue S.** Criteria and classification of obesity in Japan and Asia-Oceania. *Asia Pac J Clin Nutr 11 Suppl*. 2002;8:S732–S737.
11. **Chari ST, Leibson CL, Rabe KG, Timmons LJ, Ransom J, de Andrade M, Petersen GM.** Pancreatic cancer-associated diabetes mellitus: prevalence and temporal association with diagnosis of cancer. *Gastroenterology*. 2008;134:95–101.
12. **Marselli L, Suleiman M, Masini M, Campani D, Bugliani M, Syed F, Martino L, Focosi D, Scatena F, Olimpico F, Filipponi F, Masiello P, Boggi U, Marchetti P.** Are we overestimating the loss of beta cells in type 2 diabetes? *Diabetologia*. 2014;57:362–365.
13. **Butler AE, Janson J, Bonner-Weir S, Ritzel R, Rizza RA, Butler PC.** Beta-cell deficit and increased beta-cell apoptosis in humans with type 2 diabetes. *Diabetes*. 2003;52:102–110.
14. **Mizukami H, Takahashi K, Inaba W, Tsuboi K, Osonoi S, Yoshida T, Yagihashi S.** Involvement of oxidative stress-induced DNA damage, endoplasmic reticulum stress, and autophagy deficits in the decline of beta-cell mass in Japanese type 2 diabetic patients. *Diabetes Care*. 2014;37:1966–1974.
15. **Butler AE, Dhawan S, Hoang J, Cory M, Zeng K, Fritsch H, Meier JJ, Rizza RA, Butler PC.** Beta-cell deficit in obese type 2 diabetes, a minor role of beta-cell dedifferentiation and degranulation. *J Clin Endocrinol Metab*. 2016;101:523–532.

The Endocrine Society. Downloaded from press.endocrine.org by [${individualUser.displayName}] on 14 April 2016. at 06:14 For personal use only. No other uses without permission. . All rights reserved.

16. **Muller WA, Faloona GR, Aguilar-Parada E, Unger RH.** Abnormal alpha-cell function in diabetes. Response to carbohydrate and protein ingestion. *N Engl J Med*. 1970;283:109–115.
17. **Henquin JC, Rahier J.** Pancreatic alpha cell mass in European subjects with type 2 diabetes. *Diabetologia*. 2011;54:1720–1725.
18. **Kilimnik G, Zhao B, Jo J, Periwal V, Witkowski P, Misawa R, Hara M.** Altered islet composition and disproportionate loss of large islets in patients with type 2 diabetes. *PLoS One*. 2011;6:e27445.
19. **Mezza T, Muscogiuri G, Sorice GP, Clemente G, Hu J, Pontecorvi A, Holst JJ, Giaccari A, Kulkarni RN.** Insulin resistance alters islet morphology in nondiabetic humans. *Diabetes*. 2014;63:994–1007.
20. **Mizukami H, Takahashi K, Inaba W, Osonoi S, Kamata K, Tsuboi K, Yagihashi S.** Age-associated changes of islet endocrine cells and the effects of body mass index in Japanese. *J Diabetes Invest*. 2014; 5:38–47.
21. **Fujita Y, Kozawa J, Iwahashi H, Yoneda S, Uno S, Yoshikawa A, Okita K, Eguchi H, Nagano H, Imagawa A, Shimomura I.** Increment of serum C-peptide measured by glucagon test closely correlates with human relative beta-cell area. *Endocr J*. 2015;62:329–337.
22. **Sullivan BA, Hollister-Lock J, Bonner-Weir S, Weir GC.** Reduced Ki67 staining in the postmortem state calls into question past conclusions about the lack of turnover of adult human beta-cells. *Diabetes*. 2015;64:1698–1702.
23. **Caballero F, Siniakowicz K, Hollister-Lock J, Duran L, Katsuta H, Yamada T, Lei J, Deng S, Westermark GT, Markmann J, Bonner-Weir S, Weir GC.** Birth and death of human beta-cells in pancreases from cadaver donors, autopsies, surgical specimens, and islets transplanted into mice. *Cell Transplant*. 2014;23:139–151.
24. **Jensen CC, Cnop M, Hull RL, Fujimoto WY, Kahn SE.** Beta-cell function is a major contributor to oral glucose tolerance in high-risk relatives of four ethnic groups in the U.S. *Diabetes*. 2002;51:2170–2178.
25. **Moller JB, Pedersen M, Tanaka H, Ohsugi M, Overgaard RV, Lynge J, Almind K, Vasconcelos NM, Poulsen P, Keller C, Ueki K, Ingwersen SH, Pedersen BK, Kadowaki T.** Body composition is the main determinant for the difference in type 2 diabetes pathophysiology between Japanese and Caucasians. *Diabetes Care*. 2014;37: 796–804.
26. **Hsia DS, Larrivee S, Cefalu WT, Johnson WD.** Impact of lowering BMI cut points as recommended in the revised American Diabetes Association's Standards of Medical Care in Diabetes—2015 on diabetes screening in Asian Americans. *Diabetes Care*. 2015;38: 2166–2168.
27. **Kamata K, Mizukami H, Inaba W, Tsuboi K, Tateishi Y, Yoshida T, Yagihashi S.** Islet amyloid with macrophage migration correlates with augmented β-cell deficits in type 2 diabetic patients. *Amyloid*. 2014;21:191–201.
28. **Kou K, Saisho Y, Sato S, Yamada T, Itoh H.** Islet number rather than islet size is a major determinant of beta- and alpha-cell mass in humans. *J Clin Endocrinol Metab*. 2014;99:1733–1740.
29. **Le Bacquer O, Kerr-Conte J, Gargani S, Delalleau N, Huyvaert M, Gmyr V, Froguel P, Neve B, Pattou F.** TCF7L2 rs7903146 impairs islet function and morphology in non-diabetic individuals. *Diabetologia*. 2012;55:2677–2681.
30. **Ritzel RA, Butler AE, Rizza RA, Veldhuis JD, Butler PC.** Relationship between beta-cell mass and fasting blood glucose concentration in humans. *Diabetes Care*. 2006;29:717–718.
31. **Meier JJ, Menge BA, Breuer TG, Muller CA, Tannapfel A, Uhl W, Schmidt WE, Schrader H.** Functional assessment of pancreatic beta-cell area in humans. *Diabetes*. 2009;58:1595–1603.
32. **Saisho Y, Kou K, Tanaka K, Abe T, Shimada A, Kawai T, Itoh H.** Association between beta cell function and future glycemic control in patients with type 2 diabetes. *Endocr J*. 2013;60:517–523.
33. **Pannala R, Basu A, Petersen GM, Chari ST.** New-onset diabetes: a potential clue to the early diagnosis of pancreatic cancer. The Lancet. *Oncology*. 2009;10:88–95.
34. **Chari ST, Zapiach M, Yadav D, Rizza RA.** Beta-cell function and insulin resistance evaluated by HOMA in pancreatic cancer subjects with varying degrees of glucose intolerance. *Pancreatology*. 2005; 5:229–233.
35. **Katsumichi I, Pour PM.** Diabetes mellitus in pancreatic cancer: is it a causal relationship? *Am J Surg*. 2007;194:S71–75.
36. **Aggarwal G, Ramachandran V, Javeed N, Arumugam T, Dutta S, Klee GG, Klee EW, Smyrk TC, Bamlet W, Han JJ, Rumie Vittar NB, de Andrade M, Mukhopadhyay D, Petersen GM, Fernandez-Zapico ME, Logsdon CD, Chari ST.** Adrenomedullin is up-regulated in patients with pancreatic cancer and causes insulin resistance in beta cells and mice. *Gastroenterology*. 2012;143:1510–1517 e1511.
37. **Sakuraba H, Mizukami H, Yagihashi N, Wada R, Hanyu C, Yagihashi S.** Reduced beta-cell mass and expression of oxidative stress-related DNA damage in the islet of Japanese Type II diabetic patients. *Diabetologia*. 2002;45:85–96.
38. **Saisho Y, Butler AE, Meier JJ, Monchamp T, Allen-Auerbach M, Rizza RA, Butler PC.** Pancreas volumes in humans from birth to age one hundred taking into account sex, obesity, and presence of type-2 diabetes. *Clin Anat*. 2007;20:933–942.
39. **Meier JJ, Butler AE, Saisho Y, Monchamp T, Galasso R, Bhushan A, Rizza RA, Butler PC.** Beta-cell replication is the primary mechanism subserving the postnatal expansion of beta-cell mass in humans. *Diabetes*. 2008;57:1584–1594.
40. **Gregg BE, Moore PC, Demozay D, Hall BA, Li M, Husain A, Wright AJ, Atkinson MA, Rhodes CJ.** Formation of a human beta-cell population within pancreatic islets is set early in life. *J Clin Endocrinol Metab*. 2012;97:3197–3206.

The Endocrine Society. Downloaded from press.endocrine.org by [${individualUser.displayName}] on 14 April 2016. at 06:14 For personal use only. No other uses without permission. . All rights reserved.

Nogami *et al. BMC Medical Imaging* (2016) 16:31
DOI 10.1186/s12880-016-0134-z

BMC Medical Imaging

CASE REPORT Open Access

Anisakiasis mimics cancer recurrence: two cases of extragastrointestinal anisakiasis suspected to be recurrence of gynecological cancer on PET-CT and molecular biological investigation

Yuya Nogami[1], Yoko Fujii-Nishimura[2], Kouji Banno[1*], Atsushi Suzuki[1], Nobuyuki Susumu[1], Taizo Hibi[3], Koji Murakami[4], Taketo Yamada[5,7], Hiromu Sugiyama[6], Yasuyuki Morishima[6] and Daisuke Aoki[1]

Abstract

Background: We report two cases of anisakiasis lesions that were initially suspected to be recurrence of gynecological cancer by positron emission tomography-computed tomography (PET-CT). Both cases were extragastrointestinal anisakiasis that is very rare.

Case presentation: The first case was a patient with endometrial cancer. At 19 months after surgery, a new low density area of 2 cm in diameter in liver segment 4 was found on follow-up CT. In PET-CT, the lesion had abnormal ^{18}fluoro-deoxyglucose (FDG) uptake with elevation in the delayed phase, with no other site showing FDG uptake. Partial liver resection was performed. A pathological examination revealed no evidence of malignancy, but showed necrotic granuloma with severe eosinophil infiltration and an irregular material with a lumen structure in the center. Parasitosis was suspected and consultation with the National Institute of Infectious Diseases (NIID) showed the larvae to be *Anisakis simplex* sensu stricto by genetic examination.
The second case was a patient with low-grade endometrial stromal sarcoma (LG-ESS). At 8 months after surgery, swelling of the mediastinal lymph nodes was detected on CT and peripheral T-cell lymphoma was diagnosed by biopsy. A new peritoneal lesion with abnormal FDG uptake was detected on pre-treatment PET-CT and this lesion was increased in size on post-treatment PET-CT. Tumorectomy was performed based on suspected dissemination of LG-ESS recurrence. The findings in a pathological examination were similar to the first case and we again consulted the NIID. The larvae was identified as *Anisakis pegreffi*, which is a rare pathogen in humans.
Having experienced these rare cases, we investigated the mechanisms of FDG uptake in parasitosis lesions by immunohistochemical staining using antibodies to glucose transporter type 1 (GLUT-1) and hexokinase type 2 (HK-2). While infiltrated eosinophils were negative, macrophages demonstrated positive for both antibodies. Therefore, mechanisms behind FDG uptake may involve macrophages, which is common among various granulomas. This is the first report to investigate parasitosis in such a way.

Conclusion: These cases suggest that anisakiasis is a potential differential diagnosis for a lesion with FDG uptake in PET-CT, and that it is difficult to distinguish this disease from a recurrent tumor using PET-CT alone.

Keywords: Extragastrointestinal anisakiasis, *Anisakis*, PET-CT, Gynecological cancer, Genetic examination, PCR, Glucose transporter type 1, Hexokinase type 2

---

* Correspondence: kbanno@z7.keio.jp
[1]Department of Obstetrics and Gynecology, Keio University School of Medicine, Shinanomachi 35 Shinjuku-ku, Tokyo 160-8582, Japan
Full list of author information is available at the end of the article

© 2016 Nogami et al. **Open Access** This article is distributed under the terms of the Creative Commons Attribution 4.0 International License (http://creativecommons.org/licenses/by/4.0/), which permits unrestricted use, distribution, and reproduction in any medium, provided you give appropriate credit to the original author(s) and the source, provide a link to the Creative Commons license, and indicate if changes were made. The Creative Commons Public Domain Dedication waiver (http://creativecommons.org/publicdomain/zero/1.0/) applies to the data made available in this article, unless otherwise stated.

Background

Positron emission tomography (PET)-computed tomography (CT) is increasingly commonly used for various cancers, especially for detection of a metastasis or recurrent lesion. For gynecological cancers, PET-CT is used for examination of possible malignancy of lesions detected by CT or MRI in postoperative follow-up [1]. A lesion with abnormal uptake indicates possible recurrence, and PET-CT is believed to have better accuracy for determining malignancy compared to CT or MRI [2–4]. Surgery is rarely performed for postoperative recurrence, but an exact diagnosis is difficult without a pathological examination. Thus, a lesion that mimics tumor recurrence can lead to unnecessary surgery, chemotherapy, and radiotherapy.

Anisakiasis is relatively common in East Asia due to consumption of raw fish. Anisakiasis often presents with acute abdominal symptoms caused by an allergic reaction in the gastric mucosa. Anisakisis usually infect gastric or intestinal walls, and the feature of the images including PET-CT have been reported [5, 6]. Extragastrointestinal anisakiasis is less common, but such cases have been reported [7–9]. After penetrating the bowel wall, *Anisakis* produce a granuloma as their bodies collapse with time. Incidental detection of this lesion is difficult to distinguish from recurrence in patients with a history of malignancy. This may result in unnecessary resection, and in some cases the collapsing worm body may make the final diagnosis difficult, even after resection.

We experienced two cases of extragastrointestinal anisakiasis in which a recurrent gynecological tumor was initially suspected on imaging. PET-CT showed that the lesions had abnormal uptake in both cases. Even PET-CT could not distinguish between anisakiasis and a tumor metastasis, and diagnosis in the second case was further complicated by collapse of the worm body. A polymerase chain reaction (PCR) using a specific primer for an *Anisakis*-specific region confirmed anisakiasis in both cases.

Besides, we investigated the mechanism of FDG uptake to granuloma of parasitosis. These cases are rare but reported already, however, the mechanisms are still unknown. We investigated it by immunostaining using anti-bodies to glucose transporter type 1 (GLUT-1) and hexokinase type 2 (HK-2), which are recognized as the key factors of FDG uptake in PET.

We describe these two cases with a literature review and molecular biological investigation. We suggest that anisakiasis should be a differential diagnosis for a solitary lesion detected on PET-CT, and we show the utility of PCR for diagnosis of anisakiasis.

Case presentation

Case 1

The patient was a 44-year-old woman who had been diagnosed with endometrial cancer. She underwent semi-radical hysterectomy, bilateral salpingo-oophorectomy, pelvic and paraaortic lymph node dissection, and partial omentectomy. A pathological examination revealed that the tumor was grade 2 endometrioid adenocarcinoma with more than 50 % myometrial invasion, and clinical stage Ic (FIGO 1988). Given the intermediate risk of recurrence based on the pathological result, she received adjuvant chemotherapy of 6 cycles of a cyclophosphamide-adriamycin-cisplatin (CAP) regimen.

Follow-up CT performed 19 months after surgery detected a new low density area of 15 mm in diameter in segment 4 of the liver (Fig. 1). Serum tumor markers including CA125 and CA19-9 were not elevated, and were similar to the levels before initial therapy. Data from blood tests are shown in Table 1. MRI showed a liver tumor with a high intensity signal in diffusion-weighted imaging (DWI). In a dynamic study using gadolinium ethoxybenzyl diethylenetriaminepentaacetic acid (Gd-EOB-DTPA), early staining in the arterial phase was unclear and the lesion gave a low intensity signal in the hepatobiliary phase (Fig. 2). These findings were compatible with a metastatic tumor.

PET-CT was performed to confirm the presence of a malignant liver tumor and to search for other metastases. The liver lesion had no specific ^{18}fluoro-deoxyglucose (FDG) uptake compared with normal liver tissue in the early phase, and this was elevated in the delayed phase (standardized uptake value (SUV) max: 2.52 in the early phase, 3.61 in the delayed phase) (Fig. 3). No other metastasis was detected. Recurrence of endometrial cancer was suspected and partial resection of the liver was planned for the solitary metastasis.

The resected liver sample included a white nodule of 17 mm in diameter with a regular border macroscopically (Fig. 4). Microscopic examination showed clear eosinophil infiltration and granuloma with an

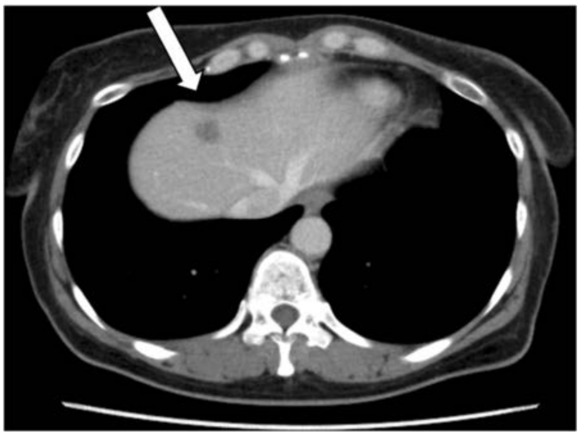

Fig. 1 Axial slice on enhanced CT in the equilibrium phase. A low density area was detected in segment 4 of the liver (*arrow*)

Table 1 Data from blood test of case 1. Eosinophilia was not shown and no tumor marker was elevated

TB	0.8	mg/dl	(0.4–1.2)	WBC	6000	/µl	(3600–8900)	AFP	1	ng/ml	(<20)
AST	17	U/L	(5–37)	Neutro	55.2	%	(37–72)	PIVKA-II	12	mAU/ml	(<40)
ALT	15	U/L	(6–43)	Lymph	37.6	%	(25–48)	CA19-9	<1	U/ml	(<35)
ALP	245	U/L	(110–348)	Mono	3.7	%	(2–12)	CA125	16	U/ml	(<37)
γGTP	13	U/L	(0–75)	Eosino	3.7	%	(1–9)				
BUN	11.6	mg/dl	(9–21)	Baso	2.2	%	(0–2)				
Cr	0.62	mg/dl	(0.5–0.8)	Hb	13.9	g/dl	(11.2–15.2)				
				HCT	42	%	(35.6–45.4)				
				Plt	2.43	10^6/µl	(1.53 - 3.46)				

TB total bilirubin, *AST* aspartate aminotransferase, *ALT* alanine aminotransferase, *ALP* alkaline phosphatase, *gGTP* γ glutamyl transpeptidase, *BUN* blood urea nitrogen, *Cr* creatinine, *WBC* white blood cell, *Neutro* neutrophil, *Lymph* lymphocyte, *Mono* monocyte, *Eosino* eosinophil, *Baso* basophil, *Hb* hemogrobin, *HCT* haematocrit, *Plt* platelet, *AFP* alpha-fetoprotein, *PIVKA-II* protein induced by vitamin K absence or antagonist-II

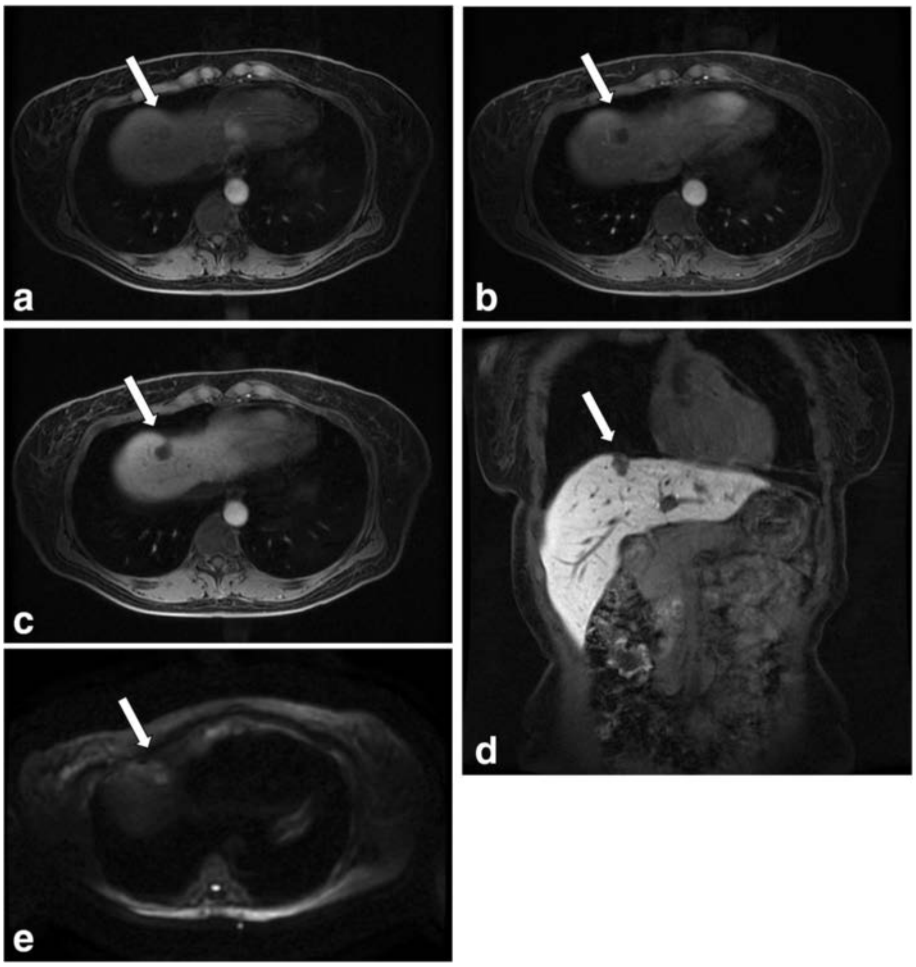

Fig. 2 Axial slices of liver acquisition with volume acceleration flex on dynamic MRI in pre-contrast phase (**a**), arterial phase (**b**) and the hepatobiliary phase (**c**). Coronal slice on enhanced MRI in the hepatobiliary phase (**d**). The lesion (*arrows*) gave a low intensity signal in all phases and a high intensity signal in DWI (**e**)

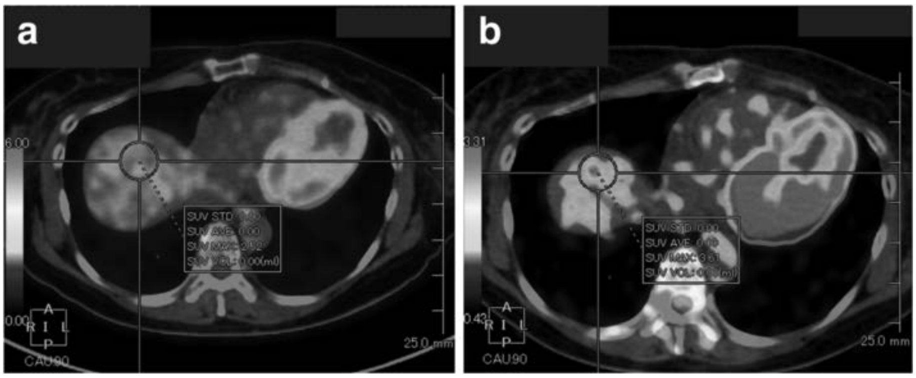

Fig. 3 Axial slice on PET-CT showing the liver lesion in the early (**a**) and delayed phase (**b**). FDG uptake was undetectable among physiological uptake of the liver in the early phase; however, uptake elevated (SUVmax: 2.52 to 3.61) and was detectable in the delayed phase

exogenous material in the center. There were no findings consistent with malignancy. The exogenous material had a lumen structure which was suspected to be due to larva migrans. The slide was sent to the National Institute of Infectious Diseases (NIID) to identify the larvae. A detailed microscopic examination revealed that the larvae had Y-shape lateral cords and renette cells, which are specific to *Anisakis* (Fig. 5).

A PCR method using a specific primer pair was performed for identification of the *Anisakis* species. The methods of DNA amplification and sequencing are described under a separate heading. This search revealed that the larvae were *Anisakis simplex* sensu stricto (Fig. 6).

These findings showed that the liver lesion was not due to recurrence of endometrial cancer. The patient has had no recurrence for 4 years.

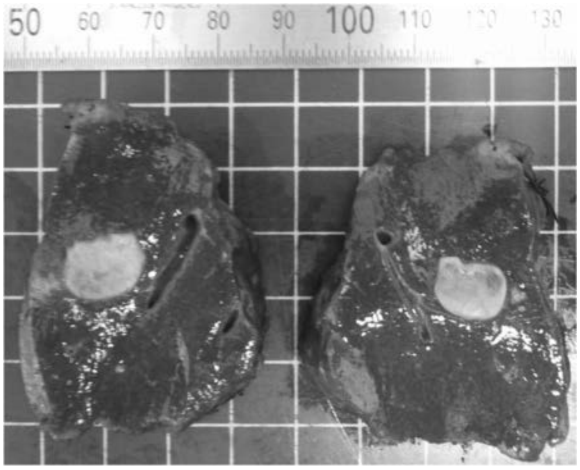

Fig. 4 Macroscopic findings in the resected liver, showing a white node with a regular border of about 2 cm in diameter

Case 2

The patient was a 33-year-old woman who had been diagnosed with low-grade endometrial stromal sarcoma (LG-ESS). She underwent extended total hysterectomy and bilateral salpingo-oophorectomy. Pathological examination revealed clinical stage IB (FIGO 2008). High-dose medroxyprogesterone acetate (400 mg/day) was administered as adjuvant therapy.

Follow-up CT 8 months after surgery indicated swelling of mediastinal lymph nodes. Biopsy of these nodes performed by a respiratory surgeon revealed peripheral T-cell lymphoma (PTCL), rather than recurrence of LG-ESS. She was referred to the department of hematology. PET-CT performed for pretreatment staging showed abnormal FDG uptake in a nodule of 10 mm in diameter in the peritoneum just below the lower median abdominal wall, in addition to uptakes in mediastinal lymph nodes. The nodule was located clearly extragastrointestinally. The patient was treated with 3 cycles of a cyclophosphamide-adriamycin-vincristin-prednisolone (CHOP) regimen. Post-treatment PET-CT showed that the nodule in the peritoneum increased in size to 16 mm with abnormal FDG uptake (SUVmax: 4.02 in the early phase, 4.21 in the delayed phase) (Fig. 7), despite a marked effect of the therapy on other lesions. Data from blood tests before chemotherapy are shown in Table 2.

The PET-CT findings for the nodule were not compatible with PTCL; therefore, exploratory laparotomy was performed to examine possible dissemination of LG-ESS. The nodule was on the omentum and partial omentectomy was performed (Fig. 8). No other macroscopic lesion in the abdomen was found. Pathological examination revealed that the nodule had an abscess with clear eosinophil infiltration. An exogenous material that appeared to be a larva was found in the center of the abscess. The larva body had collapsed, but the specific Y-shape lateral cord was recognizable (Fig. 9). Based on the experience of the first case, we sent the slide to the NIID. The PCR method revealed that the worm was *Anisakis pegreffi* (Fig. 6), which is

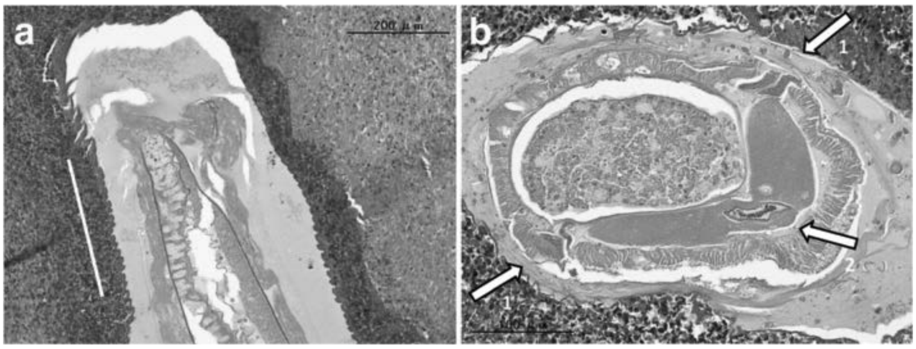

Fig. 5 **a** Sagittal slice of the larva, showing a wave-shaped (cross-striated) border (*white line*). **b** Axial slice of the larva, showing a Y-shaped lateral cord (*arrows 1*) and a renette cell (*arrow 2*). These findings are characteristics of *Anisakis*

rare as an infectious pathogen in human. These findings showed that the patient did not have recurrent LG-ESS. The patient has had no recurrence of LG-ESS for 2 years and that of PTCL for a year.

Imaging parameters of CT, MRI, and PET-CT

CT: The device is an Acquilion ONE (Toshiba Medical Systems, Otawara, Japan) by using a tube voltage of 120 kVp and tube current varied between 96 mA and 160 mA. Slice thickness is 5 mm for abdominal scanning as a post-operative follow up in a cancer patient.

MRI: The device is a Discovery MR750 3.0 T (GEHealthcare, Waukesha, Wisconsin, USA) using 32-channel torso coil as a receiver. Liver acquisition with volume acceleration flex (LAVA-Flex) is practiced with EOB dynamic MRI in our institute. The acquisition sequence is LAVA Flex with parameters as follows: Time of repectition (TR)/time of echo (TE) = 3.9/1.7 msec, flip angle = 12 o, slice thickness/gap = 3.6/1.8 mm, matrices = 256 × 256, acquisition time = 19 s. Gd-EOB-DTPA: Primovist® (Bayer Healthcare AG, Berlin, Germany)-enhanced images in the hepatobiliary phase are taken at 15 min after contrast injection.

PET-CT: Biograph mCT (Siemens Medical Solutions, Knoxville, TN, USA). In our institute, patients routinely receive DPS for differentiation. Patients were administered 3.7 MBq/kg of FDG and received routine PET-CT DPS at 1 and 2 h after administration. Data were analyzed on an AZE workstation (AZE Ltd, Tokyo, Japan).

Molecular investigation

Identification of anisakid nematodes (DNA amplification and sequencing)

The worm body was scratched from the deparaffinized slide under stereoscopic microscopy and placed in a

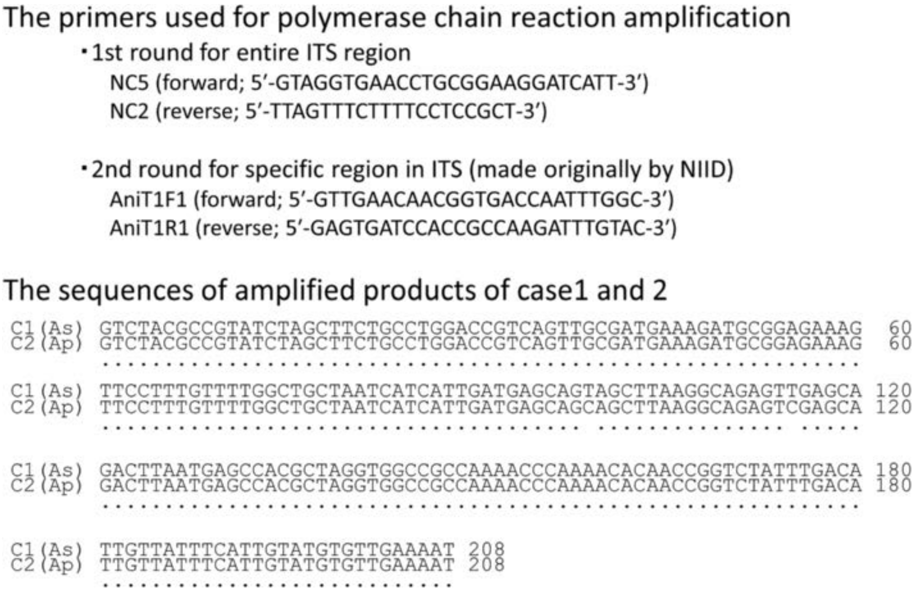

The primers used for polymerase chain reaction amplification

- 1st round for entire ITS region
  NC5 (forward; 5′-GTAGGTGAACCTGCGGAAGGATCATT-3′)
  NC2 (reverse; 5′-TTAGTTTCTTTTCCTCCGCT-3′)

- 2nd round for specific region in ITS (made originally by NIID)
  AniT1F1 (forward; 5′-GTTGAACAACGGTGACCAATTTGGC-3′)
  AniT1R1 (reverse; 5′-GAGTGATCCACCGCCAAGATTTGTAC-3′)

The sequences of amplified products of case1 and 2

```
C1(As)  GTCTACGCCGTATCTAGCTTCTGCCTGGACCGTCAGTTGCGATGAAAGATGCGGAGAAAG  60
C2(Ap)  GTCTACGCCGTATCTAGCTTCTGCCTGGACCGTCAGTTGCGATGAAAGATGCGGAGAAAG  60
        ............................................................

C1(As)  TTCCTTTGTTTTGGCTGCTAATCATCATTGATGAGCAGTAGCTTAAGGCAGAGTTGAGCA 120
C2(Ap)  TTCCTTTGTTTTGGCTGCTAATCATCATTGATGAGCAGCAGCTTAAGGCAGAGTCGAGCA 120
        ...................................... ............... .....

C1(As)  GACTTAATGAGCCACGCTAGGTGGCCGCCAAAACCCAAAACACAACCGGTCTATTTGACA 180
C2(Ap)  GACTTAATGAGCCACGCTAGGTGGCCGCCAAAACCCAAAACACAACCGGTCTATTTGACA 180
        ............................................................

C1(As)  TTGTTATTTCATTGTATGTGTTGAAAAT 208
C2(Ap)  TTGTTATTTCATTGTATGTGTTGAAAAT 208
        ............................
```

Fig. 6 Primers used for genetic identification of *Anisakis* and sequences obtained

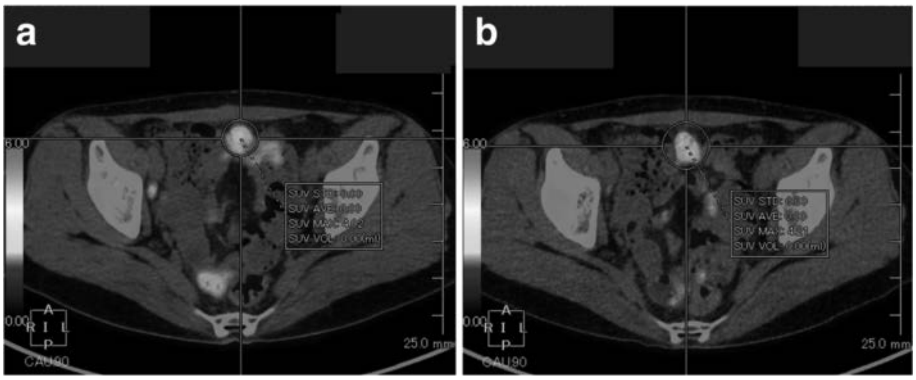

Fig. 7 Axial slice on PET-CT after CHOP therapy in the early (**a**) and delayed phase (**b**). The lesion had increased in size compared with pre-treatment and showed FDG uptake (SUVmax: 4.02 to 4.21)

plastic tube. DNA was extracted using proteinase K (Qiagen) and SDS (Sigma-Aldrich) [10]. The entire internal transcribed spacer (ITS) region (ITS1, 5.8S rDNA and ITS2) was amplified by PCR using the primers NC5 and NC2 in the first round. Then nested PCR was performed in the second round to amplify a specific region in the ITS1 using the following primers that were originally constructed: AniT1F1: 5′-GTTGAACAACGGTGA CCAATTTGGC-3′, and AniT1R1: 5′-. PCR was conducted by the method indicated in reference [10]. An amplification product of 208 bp was obtained. Sequence similarities were determined by a BLAST search of the DNA Data Bank of Japan (DDBJ) (http://www.ddbj.nig.ac.jp/index-e.html). Sequence alignment and comparison was facilitated by the GENETYX-WIN program (ver. 7.0, Software Development Co, Tokyo, Japan).

Investigation for the mechanism of FDG uptake (immunochemical staining using anti-bodies to GLUT-1 and HK-2)

Once FDG is uptaken to cells through the GLUT-1 and phosphorylated by HK-2, FDG is unable to pass out of cells unless dephosphorylated by glucose-6-phosphatase (G6P). Because malignant cells have a high ratio of HK-2/G6P, they present an elevation of FDG uptake in delayed phase in dual-phase scanning (DPS) of PET-CT. Since both cases indicated the elevation, recurrence was a stronger consideration among other differential diagnoses.

Cases of parasitosis suspected as malignancy in PET have been previously reported but are very rare [11–13]. There are no reports investigating the mechanisms of FDG uptake in parasitosis granuloma. We researched them to develop ways to differentiate them by investigating overexpression of GLUT-1 and HK-2.

GLUT-1 expression was evaluated immunohistochemically using rabbit polyclonal anti-Glucose Transporter GLUT1 antibody (ab652, Abcam, Cambridge, UK) at a dilution of 1:500. HK-2 expression was evaluated with rabbit polyclonal anti-Hexokinase Type II (AB3279, Chemicon International, Temecula, USA) diluted at 1:500. Immunohistochemical staining was performed using the Leica Bond-Max automatic immunostainer and the Bond Polymer Refine Detection kit (Leica).

In both cases, only macrophages were positive for both antibodies; GLUT-1 and HK-2. The eosinophils, which

Table 2 Data from blood test of case 2. Eosinophilia was not shown and sIL2R was elevated due to lymphoma

TB	0.5	mg/dl	(0.4–1.2)	WBC	5400	/μl	(3600–8900)	sIL2R	381	U/ml	(<20)
AST	13	U/L	(5–37)	Neutro	53.3	%	(37–72)	CA125	11	U/ml	(<37)
ALT	7	U/L	(6–43)	Lymph	34.9	%	(25–48)				
ALP	237	U/L	(110–348)	Mono	5.8	%	(2–12)				
LDH	184	U/L	(0–75)	Eosino	5.4	%	(1–9)				
BUN	10.4	mg/dl	(9–21)	Baso	0.6	%	(0–2)				
Cr	0.6	mg/dl	(0.5–0.8)	Hb	13	g/dl	(11.2–15.2)				
				HCT	39.1	%	(35.6–45.4)				
				Plt	2.5	10^6/μl	(1.53–3.46)				

TB total bilirubin, *AST* aspartate aminotransferase, *ALT* alanine aminotransferase, *ALP*, alkaline phosphatase, *LDH* lactate dehydrogenase, *BUN* blood urea nitrogen, *Cr* creatinine, *WBC* white blood cell, *Neutro* neutrophil, *Lymph* lymphocyte, *Mono* monocyte, *Eosino* eosinophil, *Baso* basophil, *Hb* hemogrobin, *HCT* haematocrit, *Plt* platelet, *sIL-2R* soluble interleukin-2 receptor

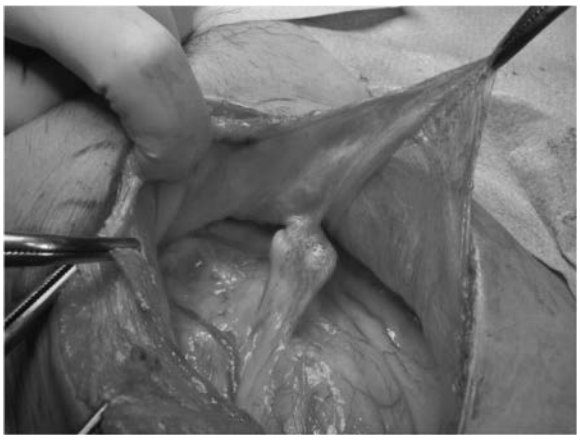

Fig. 8 Intra-abdominal findings in exploratory laparotomy. The lesion was located on the omentum with adhesion to the parietal peritoneum

were infiltrated around worm bodies, were negative for them (Figs. 10, 11). These results suggest that eosinophil infiltration may not boost FDG uptake or have any specific roles. Instead, the reason for FDG uptake to parasitosis granuloma may be the macrophages, which is commonly seen in granulomas.

Discussion

Extragastrointestinal anisakiasis accounts for 0.45 % of cases of anisakiasis in Japan [14]. The condition is caused by an *Anisakis* worm penetrating the bowel wall and forming an intra-abdominal colony. Cases in the omentum have been described in Japan and Italy [7, 15]. Occurrence as a solitary liver lesion is particularly rare, with the only examples found in eight cases reported in Japan [16, 17]. Most cases of extragastrointestinal anisakiasis are asymptomatic and detected incidentally.

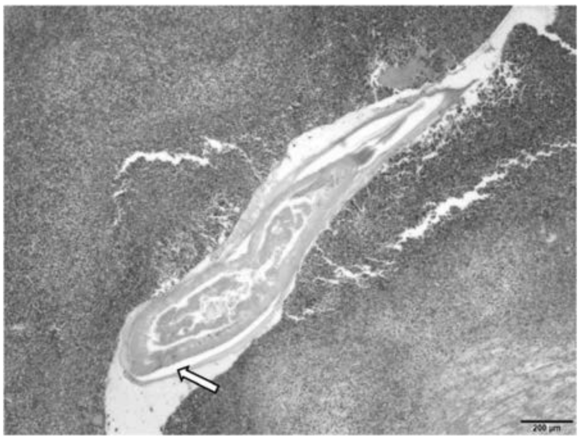

Fig. 9 The nodule had an abscess with clear eosinophil infiltration. The larva body had collapsed, but the specific Y-shaped lateral cord was recognizable (arrow)

In the present two cases, malignant metastatic tumor was indicated as first choice of differential diagnosis by two imaging modalities. Dynamic MRI using contrast agent is often performed as the detailed examination for hepatic tumor, as in case 1. Low signal in hepatobilliary phase without early enhancement is compatible with metastatic tumor. However, because Gd-EOB-DTPA contrasting is dependent on expression of OATP1B1/3 [18], and parasitic granuloma does not necessarily show expression of OATP1B1/3, Gd-EOB-DTPA may not be useful for differentiating between metastatic tumor and parasitic granuloma. Using Gd-EOB-DTPA contrast benefits in clarifying the tumor location. The diagnostic efficacy of PET-CT for extragastrointestinal anisakiasis has not been examined because of the rarity of the disease. Our cases indicated that lesions of extragastrointestinal anisakiasis present with abnormal FDG uptake and were difficult to distinguish from a malignant tumor. *Anisakis* cannot live in the human body and die immediately, and thus FDG uptake was not directly associated with the worm body, but with inflammatory cells around the body. Dual-phase scanning is a well-known method for distinguishing between inflammation and malignancy [19–22], based on the observation that malignant lesions have elevated FDG uptake in the delayed phase compared with the early phase. However, the lesions in both of our cases showed elevation in delayed phases, especially in case 1. Without previous CT or MRI, the tumor might not have been detected using only the early phase scan. There has been a report of an anisakiasis case without FDG uptake [16] and the uptake decreased with time in our second case, suggesting that FDG uptake in anisakiasis lesions may decrease with time. This may help to distinguish it from malignancy, but it remains difficult to observe without therapy for cases in which malignancy is suspected.

Anisakiasis occurs due to eating of infected raw fish, such as mackerel, and horse mackerel. Consumption of raw fish is common in Asia, including Japan, and Northern Europe [23], and there is a recent trend to expansion of this behavior in the United States [24]. Food and drug administration in the United States and European Food Safety Authority in Europe recommend the frozen stock required for raw fish to prevent parasitosis. Increased use of imaging modalities such as MRI and PET-CT is likely to lead to more incidental findings of asymptomatic lesions [25], and this may lead to an increase in cases similar to those in this report. This is a concern because differential diagnosis from a malignant tumor is difficult for these lesions. The difficulty was provided by time lag. There is a time lag between infection and detection of a lesion, since generating a granuloma or an abscess in anisakiasis takes 2 months to 2 years [26].

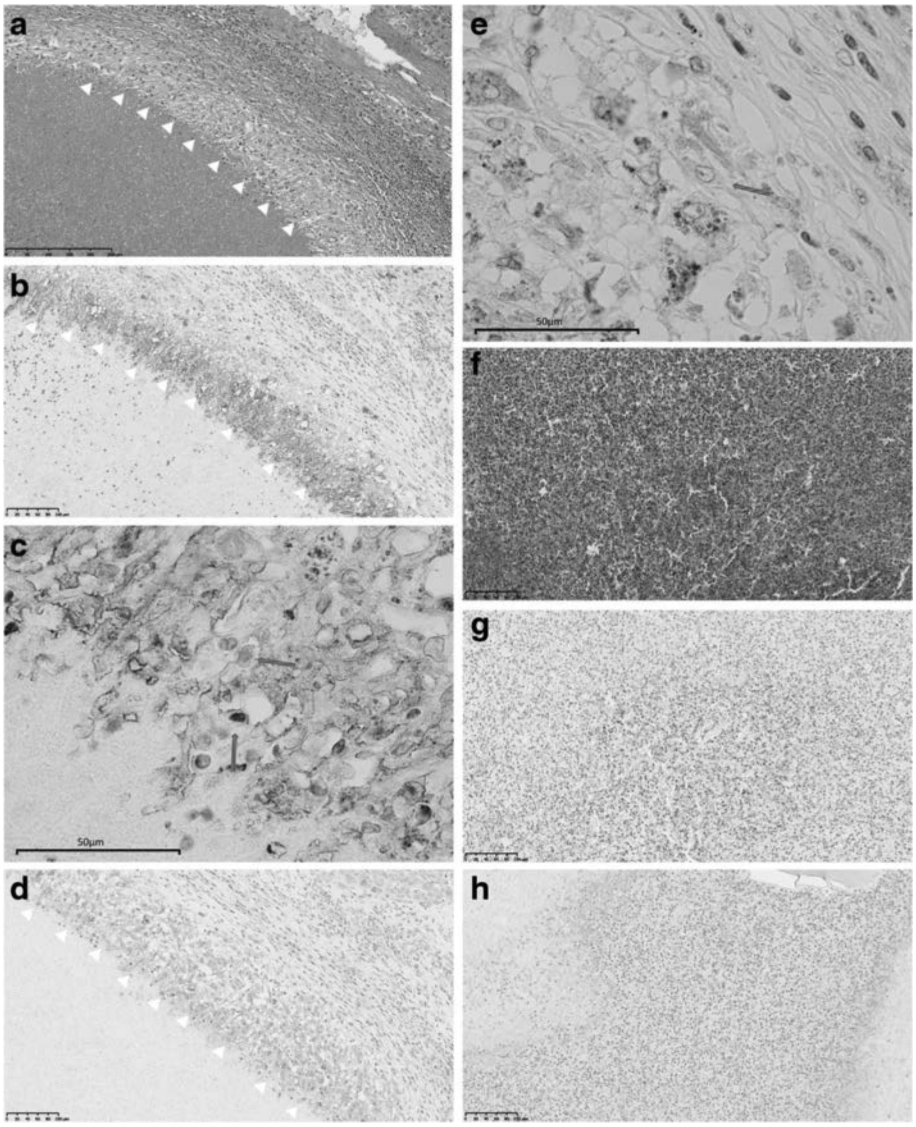

Fig. 10 In case 1, macrophages around abscess (**a** HE, *arrows*) were positive for GLUT-1 on the cell membrane (**b**, **c**, *arrows*) and HK-2 in the cytoplasm (**d**, **e**, *arrows*). Extensive eosinophil infiltrate (**f** HE, throughout the whole figure) were negative for GLUT-1 (**g**) and HK-2 (**h**)

The prior imaging to the detection of the tumor was 10 months in case 1, and 2 months in case 2. It is suspected that the patients were infected and granuloma formation occurred during this interval. The hematological or serological acute reaction of infection and the patient's memory of symptoms or food consumption can be lost due to this time lag. In this situation, a test for eosinophilia, a specific antibody test and history taking, which are important in diagnosis of parasitosis, are less useful. In fact, eosinophilia was not seen in either of our cases and a specific antibody for *Anisakis* was negative in the first case. And we retook the patients' history retrospectively after surgery, neither of the patients remembered a characteristic dietary history. The difficulty of diagnosing is not only because of the vagueness of memory, but is also related to the existence of asymptomatic cases. Our two cases were also asymptomatic cases and there were no imaging findings on contrast CT. Generally, *Anisakis* larvae bite the intestinal wall, which causes acute severe abdominal pain. The pain is caused mainly by allergic reaction, rather than mechanical stimulus. Even in extragastrointestinal anisakiasis, which larvae penetrate the wall of the gastrointestinal tract, many cases are detected incidentally. There seems to be many asymptomatic cases.

The risk of recurrence of a primary malignancy should also be considered. In our first case, the risk of recurrence of endometrial cancer was intermediate, at about 10 % at 20 months after initial therapy [27]. In the

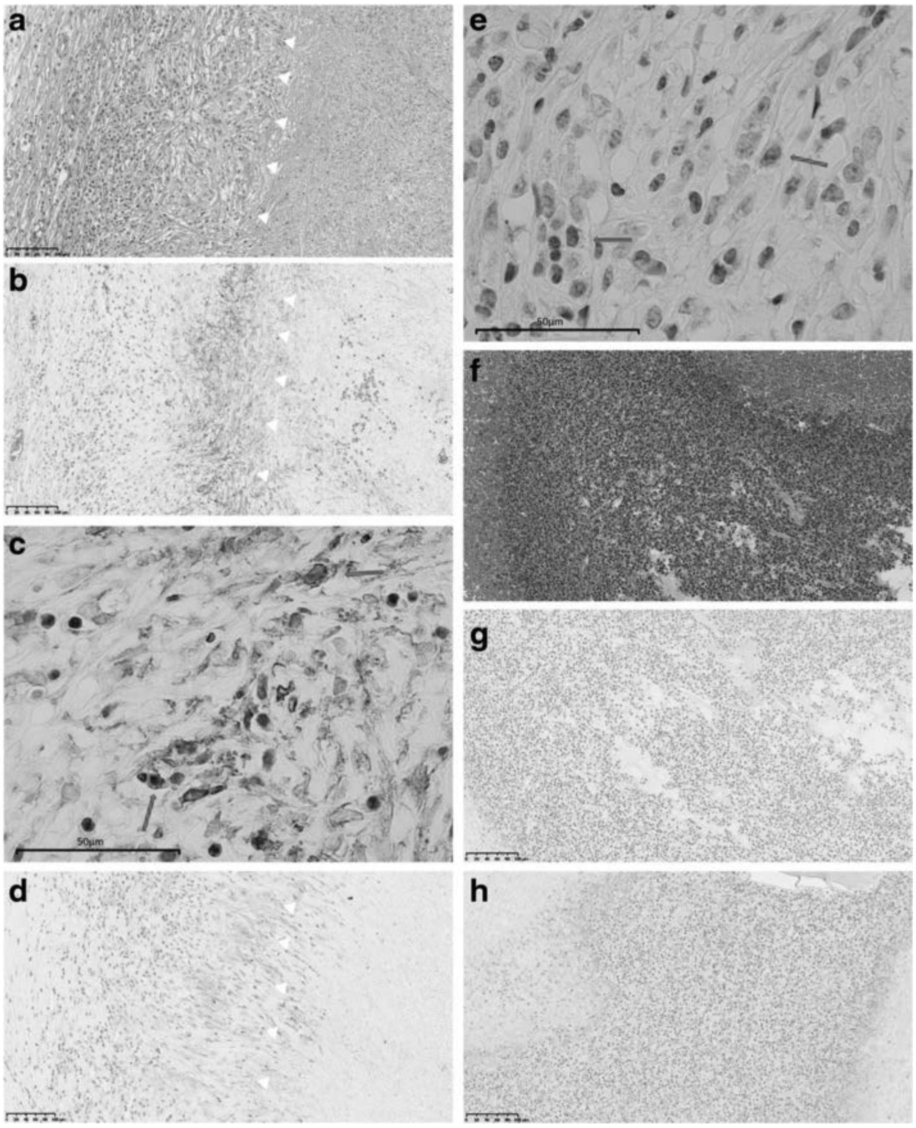

Fig. 11 In case 2, macrophages around abscess (**a** HE, *arrows*) were positive for GLUT-1 on the cell membrane (**b**, **c**, *arrows*) and HK-2 in the cytoplasm (**d**, **e**, *arrows*). Extensive eosinophil infiltrate (**f** HE, throughout the whole figure) were negative for GLUT-1 (**g**) and HK-2 (**h**)

second case, the patient had stage I LG-ESS. The recurrence risk for this cancer is over 30 %, even in stage I, although the period of progression-free LG-ESS is generally longer than 8 months [28]. Therefore, both cases had a relatively low risk of recurrence, but this information was difficult to include in the diagnosis with certainty. In addition to the complexity of FDG uptake in PET-CT, the lesion location may also increase the difficulty of diagnosis. If a lesion is detected in the intestinal wall or intramesentery, in which anisakiasis is relatively common, recurrence of gynecological cancer is less likely. However, a lesion in the peritoneum or liver is less likely to be due to extragastrointestinal anisakiasis, and this is also a common site of tumor recurrence. Cases of extragastrointestinal anisakiasis in the uterus [29, 30] and ovary [31] have also been reported, indicating that differential diagnosis of such lesions is also required.

Generally, inflammatory lesions such as pneumonia and abscess, which need to be differentiated with malignancy, include macrophages and neutrophils. These cells increase the glucose uptake, but the changes seen in the delayed phase in DPS differs with cancer cells because of the difference of HK-2/G6P ratio. The two cases we report had eosinophilic granuloma. We speculated that the elevation of SUV in the delayed phase may be caused by eosinophils, and investigated their feature by immunochemical straining using anti-GLUT-1 and anti-HK-2 antibodies. However, against our expectation, eosinophils showed negative expression of GLUT-1 and HK-2, and only macrophages were strained. Although we have not investigated the expression of G6P, the expression HK-2 in macrophages may cause the elevation of uptake in inflammatory lesion in is the delayed phase. Thus, DPS is not necessarily superior to other modalities in distinguishing malignancy and inflammation. New imaging modalities such as PET-CT allow an "abnormality" to be detected incidentally. It is important to determine whether a lesion found on PET-CT is truly abnormal, and this limitation of new technologies should be recognized.

In our cases, a genetic test was used to define the pathogen. The *Anisakis* worm collapses in the human body and this may cause difficulty with diagnosis, as in our second case. The PCR methods described here are useful in these cases. In addition, improved definition of species among *Anisakis* larvae might bring new insights. No studies have been reported about the frequency of species in extragastrointestinal anisakiasis. However, Umehara A. et al. reported that 99 % of all human anisakiasis are due to *Anisakis simplex* sensu stricto [32]. *Anisakis pegreffi* is relatively common among fish that are landed [33]. This discrepancy is explained by the difference of the larvae's ability to penetrate to the fish muscle, thus causing ingested by human [34–36]. In both cases included in the present study, it is thought that the larvae penetrated the gastrointestinal wall. Thus, the case of extragastrointestinal anisakiasis of *Anisakis pegreffi* is very rare and interesting. Accumulation of cases are required to clarify the epidemiology of extragastrointestinal anisakiasis and identify routes of infection.

Conclusion

We experienced two cases of anisakiasis that were initially suspected to be recurrence of gynecological cancer on PET-CT. These cases suggest that anisakiasis should be a differential diagnosis for a lesion presenting with FDG uptake on PET-CT. Our results also indicate that it is difficult to distinguish anisakiasis from a recurrent tumor using PET-CT and there is no specific mechanism of FDG uptake in parasitosis granuloma. These findings are important because current dietary habits and use of imaging modalities suggest that similar cases will increase worldwide.

Consent for publication

Written informed consent was obtained from the patients for publication of this case series and any accompanying images.

Availability of data and materials

The dataset supporting the conclusions of this article is included within the article.

Abbreviations

CT: computed tomography; PET: positron emission tomography; FDG: ^{18}fluoro-deoxyglucose; NIID: the National Institute of Infectious Diseases; LG-ESS: low-grade endometrial stromal sarcoma; PCR: polymerase chain reaction; GLUT-1: glucose transporter type 1; HK-2: hexokinase type 2; CAP: cyclophosphamide-adriamycin-cisplatin; FIGO: International federation of gynecology and obstetrics; Gd-EOB-DTPA: gadolinium ethoxybenzyl diethylenetriaminepentaacetic acid; DWI: diffusion-weighted imaging; SUV: standardized uptake value; PTCL: peripheral T-cell lymphoma; CHOP: cyclophosphamide-adriamycin-vincristin- prednisolone; ITS: internal transcribed spacer; DDBJ: DNA Data Bank of Japan; G6P: glucose-6-phosphatase; DPS: dual-phase scanning.

Competing interests

The authors declare that they have no competing interests.

Authors' contributions

YN is first author and has performed the entire management of this work which has various parts. Majority of this manuscript has been written by the first author. YFN is second author, and she and TY diagnosed anisakiasis by pathological examination. YFN also performed immunochemical staining and interpreted the result. KB is the corresponding author and was involved in establishing the study concept and conferred with YN and DA about additional investigations like immunochemical straining. AS, NS and TH were the doctors in charge for cases and they decided medical options in patient's clinical course and performed surgery. They also submitted tissues to NIID for genetic diagnosis after conference with YFN and TY. KM made diagnoses by PET-CT and reviewed the image retrospectively and calculated SUV and the elevation in delayed phase of DPS. HS and YM performed genetic examination using PCR method to identify the type of larvae. Especially, they prepared shorter primer only for these cases. YFN and HS reviewed the part of manuscript referring experimental methods. All authors read and approved the final manuscript.

Funding

This report received no funding.

Author details

[1]Department of Obstetrics and Gynecology, Keio University School of Medicine, Shinanomachi 35 Shinjuku-ku, Tokyo 160-8582, Japan. [2]Department of Pathology, Keio University School of Medicine, Shinanomachi 35 Shinjuku-ku, Tokyo 160-8582, Japan. [3]Department of Surgery, Keio University School of Medicine, Shinanomachi 35 Shinjuku-ku, Tokyo 160-8582, Japan. [4]Department of Radiology, Keio University School of Medicine, Shinanomachi 35 Shinjuku-ku, Tokyo 160-8582, Japan. [5]Division of Diagnostic Pathology, Keio University School of Medicine, Shinanomachi 35 Shinjuku-ku, Tokyo 160-8582, Japan. [6]Department of Parasitology, National Institute of Infectious Diseases, Toyama 1-23-1 Shinjuku-ku, Tokyo 162-8640, Japan. [7]Department of Pathology, Saitama Medical University, Moroyama-machi 38, Iruma-gun, Saitama 350-0495, Japan.

Received: 17 November 2015 Accepted: 21 April 2016
Published online: 26 April 2016

References

1. Nogami Y, Iida M, Banno K, Kisu I, Adachi M, Nakamura K, et al. Application of FDG-PET in cervical cancer and endometrial cancer: utility and future prospects. Anticancer Res. 2014;34:585–92.
2. Chu Y, Zheng A, Wang F, Lin W, Yang X, Han L, et al. Diagnostic value of 18 F-FDG-PET or PET-CT in recurrent cervical cancer: a systematic review and meta-analysis. Nucl Med Commun. 2014;35:144–50.
3. Gu P, Pan LL, Wu SQ, Sun L, Huang G. CA 125, PET alone, PET-CT, CT and MRI in diagnosing recurrent ovarian carcinoma: a systematic review and meta-analysis. Eur J Radiol. 2009;71:164–74.
4. Antunovic L, Cimitan M, Borsatti E, Baresic T, Sorio R, Giorda G, et al. Revisiting the clinical value of 18 F-FDG PET/CT in detection of recurrent epithelial ovarian carcinomas: correlation with histology, serum CA-125 assay, and conventional radiological modalities. Clin Nucl Med. 2012;37:e184–8.
5. Abe K, Yoshikai T, Baba S, Isoda T, Honda H. PET/CT findings in acute gastric anisakiasis. Clin Nucl Med. 2014;39:e340–2.

6. Shibata E, Ueda T, Akaike G, Saida Y. CT findings of gastric and intestinal anisakiasis. Abdom Imaging. 2014;39:257–61.
7. Kagei N, Orikasa H, Hori E, Sannomiya A, Yasumura Y. A case of hepatic anisakiasis with a literal survey for extra-gastrointestinal anisakiasis. Jpn J Parasitol. 1995;44:346–51.
8. Cancrini G, Magro G, Giannone G. [1st case of extra-gastrointestinal anisakiasis in a human diagnosed in Italy]. Parassitologia. 1997;39:13–7. In Italy.
9. Takekawa Y, Kimura M, Sakakibara M, Yoshii R, Yamashita Y, Kubo A, et al. Two cases of parasitic granuloma found incidentally in surgical specimens. Jpn J Clin Pathol. 2004;52:28–31 (In Japanese).
10. Sugiyama H, Singh TS, Rangsiruji A. Paragonimus. In: Liu D, editor. Molecular Detection of Human Parasitic Pathogens. Boca Raton: CRC press; 2013. p. 421–33.
11. Yoo Ie R, Park HJ, Hyun J, Chung YA, Sohn HS, Chung SK, et al. Two cases of pulmonary paragonimiasis on FDG-PET CT imaging. Ann Nucl Med. 2006;20:311–5.
12. Chen CJ, Chou SC, Chen HJ, Chen HY. Solitary necrotic nodule with larval infestation in the liver on F-18 FDG PET/CT. Clin Nucl Med. 2010;35:724–5.
13. Cheng W, Li F, Zhuang H, Zhong D, Wu C, Zhu Z. Hepatic paragonimiasis revealed by FDG PET/CT. Clin Nucl Med. 2010;35:726–8.
14. Ishikura H, Kikuchi H, Sato N, Ohtani S, Yagi K, Ishikura H, et al. [Changing larva migrans caused by anisakidae larvae]. Clin Parasitol. 1992;3:70–3. In Japanese.
15. Pampiglione S, Rivasi F, Criscuolo M, De Benedittis A, Gentile A, Russo S, et al. Human anisakiasis in Italy: a report of eleven new cases. Pathol Res Pract. 2002;198:429–34.
16. Ishida M, Sano S, Terada T, Mitsui T, Sudoh Y, Yamaguchi A. A case of hepatic anisakiasis. J Jpn Surg Assoc. 2013;74:2557–61. in Japanese.
17. Morita M, Soyama A, Takatuki M, Kuroki T, Abe K, Hayashi T, et al. A case of hepatic mass induced by extra-gastrointestinal anisakiasis. J Jpn Surg Assoc. 2013;74:483–7 (in Japanese).
18. Leonhardt M, Keiser M, Oswald S, Kuhn J, Jia J, Grube M, et al. Hepatic uptake of the magnetic resonance imaging contrast agent Gd-EOB-DTPA: role of human organic anion transporters. Drug Metab Dispos. 2010;38:1024–8.
19. Zhuang H, Pourdehnad M, Lambright ES, Yamamoto AJ, Lanuti M, Li P, et al. Dual time point 18 F-FDG PET imaging for differentiating malignant from inflammatory processes. J Nucl Med. 2001;42:1412–7.
20. Shen G, Hu S, Deng H, Jia Z. Diagnostic value of dual time-point 18 F-FDG PET/CT versus single time-point imaging for detection of mediastinal nodal metastasis in non-small cell lung cancer patients: a meta-analysis. Acta Radiol. 2014;56:681–7.
21. Mochizuki Y, Omura K, Nakamura S, Harada H, Shibuya H, Kurabayashi T. Preoperative predictive model of cervical lymph node metastasis combining fluorine-18 fluorodeoxyglucose positron-emission tomography/computerized tomography findings and clinical factors in patients with oral or oropharyngeal squamous cell carcinoma. Oral Surg Oral Med Oral Pathol Oral Radiol. 2012;113:274–82.
22. Nogami Y, Banno K, Irie H, Iida M, Masugi Y, Murakami K, et al. Efficacy of 18-FDG PET-CT Dual-phase Scanning for Detection of Lymph Node Metastasis in Gynecological Cancer. Anticancer Res. 2015;35:2247–53.
23. EFSA Panel on Biological Hazards. Scientific Opinion on assessment of epidemiological data in relation to the health risks resulting from the presence of parasites in wild caught fish from fishing grounds in the Baltic Sea. EFSA Journal. 2011;9:2320.
24. Fein SB, Lando AM, Levy AS, Teisl MF, Noblet C. Trends in U.S. consumers' safe handling and consumption of food and their risk perceptions, 1988 through 2010. J Food Prot. 2011;74:1513–23.
25. Organisation for Economic Co-operation and Development, OECD Health Statistics 2014. 2014. http://www.oecd.org/health. Accessed 20 May 2015.
26. Kojima K, Koyanagi T, Shiraki K. Pathological analysis of anisakiasis. Jpn J Clin Med. 1966;24:134–43 (in Japanese).
27. Susumu N, Sagae S, Udagawa Y, Niwa K, Kuramoto H, Satoh S, et al. Randomized phase III trial of pelvic radiotherapy versus cisplatin-based combined chemotherapy in patients with intermediate- and high-risk endometrial cancer: a Japanese Gynecologic Oncology Group study. Gynecol Oncol. 2008;108:226–33.
28. Li AJ, Giuntoli 2nd RL, Drake R, Byun SY, Rojas F, Barbuto D, et al. Ovarian preservation in stage I low-grade endometrial stromal sarcomas. Obstet Gynecol. 2005;106:1304–8.
29. Takao Y, Fukuma T, Shigeki M, Shyono Y, Tokunaga K, Uchiyama A. [An Anisakis larva observed in the utero-cervix]. Clin Parasitol. 1993;4:200–2. in Japanese.
30. Shiozaki Y, Kudo M, Adachi T, Takizawa K, Iguchi T, Takeda Y. A case of anisakiasis by the histological examination after the operation of uterus. Clin Parasitol. 1993;4:205–6 (in Japanese).
31. Mori H, Hirata M, Kase Y, Takagi Y, Sekine I, Aoki Y, et al. A case of ovarian anisakiasis. Sankatofujinka. 1982;49:1361–3 (in Japanese).
32. Umehara A, Kawakami Y, Araki J, Uchida A. Molecular identification of the etiological agent of the human anisakiasis in Japan. Parasitol Int. 2007;56:211–5.
33. Umehara A, Kawakami Y, Ooi HK, Uchida A, Ohmae H, Sugiyama H. Molecular identification of Anisakis type I larvae isolated from hairtail fish off the coasts of Taiwan and Japan. Int J Food Microbiol. 2010;143:161–5.
34. Suzuki J, Murata R, Hosaka M, Araki J. Risk factors for human Anisakis infection and association between the geographic origins of Scomber japonicus and anisakid nematodes. Int J Food Microbiol. 2010;137:88–93.
35. Arizono N, Yamada M, Tegoshi T, Yoshikawa M. Anisakis simplex sensu stricto and Anisakis pegreffii: biological characteristics and pathogenetic potential in human anisakiasis. Foodborne Pathog Dis. 2012;9:517–21.
36. del Carmen RM, Valero A, Navarro-Moll MC, Martin-Sanchez J. Experimental comparison of pathogenic potential of two sibling species Anisakis simplex s.s. and Anisakis pegreffii in Wistar rat. Trop Med Int Health. 2013;18:979–84.

Submit your next manuscript to BioMed Central and we will help you at every step:

- We accept pre-submission inquiries
- Our selector tool helps you to find the most relevant journal
- We provide round the clock customer support
- Convenient online submission
- Thorough peer review
- Inclusion in PubMed and all major indexing services
- Maximum visibility for your research

Submit your manuscript at
www.biomedcentral.com/submit

BioMed Central

ANTICANCER RESEARCH
International Journal of Cancer Research and Treatment
ISSN: 0250-7005

Computed Tomographic Features of Malignant Peritoneal Mesothelioma

KATSUYA KATO[1§], KENICHI GEMBA[2], NOBUKAZU FUJIMOTO[2], KEISUKE AOE[4],
YUKIO TAKESHIMA[5], KOUKI INAI[5] and TAKUMI KISHIMOTO[3]

[1]Department of Radiology, Okayama University Hospital, Shikatacho, Okayama, Japan;
Departments of [2]Respiratory Medicine and [3]Internal Medicine,
Okayama Rosai Hospital, Chikkomidorimachi, Okayama, Japan;
[4]Department of Medical Oncology, National Hospital Organization Yamaguchi-Ube Medical Center,
Higashikiwa, Ube, Japan;
[5]Department of Pathology, Graduate School of Biomedical Sciences,
Hiroshima University, Minamiku, Hiroshima, Japan

Reprinted from
ANTICANCER RESEARCH *36*: 1067-1072 (2016)

ANTICANCER RESEARCH
International Journal of Cancer Research and Treatment

HighWire Press STANFORD UNIVERSITY

ISSN (print): 0250-7005
ISSN (online): 1791-7530

Editorial Board

P. A. ABRAHAMSSON, *Malmö, Sweden*
B. B. AGGARWAL, *Houston, TX, USA*
T. AKIMOTO, *Kashiwa, Chiba, Japan*
P. Z. ANASTASIADIS, *Jacksonville, FL, USA*
A. ARGIRIS, *San Antonio, TX, USA*
J. P. ARMAND, *Toulouse, France*
V. I. AVRAMIS, *Los Angeles, CA, USA*
R. C. BAST, *Houston, TX, USA*
D.-T. BAU, *Taichung, Taiwan, ROC*
G. BAUER, *Freiburg, Germany*
E. E. BAULIEU, *Le Kremlin-Bicetre, France*
E. J. BENZ, Jr., *Boston, MA, USA*
J. BERGH, *Stockholm, Sweden*
F. T. BOSMAN, *Lausanne, Switzerland*
G. BROICH, *Monza, Italy*
Ø. S. BRULAND, *Oslo, Norway*
J. M. BUATTI, *Iowa City, IA, USA*
M. M. BURGER, *Basel, Switzerland*
M. CARBONE, *Honolulu, HI, USA*
C. CARLBERG, *Kuopio, Finland*
J. CARLSSON, *Uppsala, Sweden*
A. F. CHAMBERS, *London, ON, Canada*
P. CHANDRA, *Frankfurt am Main, Germany*
L. CHENG, *Indianapolis, IN, USA*
J.-G. CHUNG, *Taichung, Taiwan, ROC*
E. DE CLERCQ, *Leuven, Belgium*
W. DEN OTTER, *Amsterdam, The Netherlands*
E. P. DIAMANDIS, *Toronto, ON, Canada*
G. TH. DIAMANDOPOULOS, *Boston, MA, USA*
D. W. FELSHER, *Stanford, CA, USA*
J. A. FERNANDEZ-POL, *Chesterfield, MO, USA*
I. J. FIDLER, *Houston, TX, USA*
A. P. FIELDS, *Jacksonville, FL, USA*
B. FUCHS, *Zurich, Switzerland*
D. FUCHS, *Innsbruck, Austria*
G. GABBIANI, *Geneva, Switzerland*
R. GANAPATHI, *Charlotte, NC, USA*
A. F. GAZDAR, *Dallas, TX, USA*
J. H. GESCHWIND, *Baltimore, MD, USA*
A. GIORDANO, *Philadelphia, PA, USA*
G. GITSCH, *Freiburg, Germany*
R. H. GOLDFARB, *Guilford, CT, USA*
L. HELSON, *Quakertown, PA, USA*
R. M. HOFFMAN, *San Diego, CA, USA*
S. C. JHANWAR, *New York, NY, USA*
J. V. JOHANNESSEN, *Oslo, Norway*
B. KAINA, *Mainz, Germany*
P. -L. KELLOKUMPU-LEHTINEN, *Tampere, Finland*
D. G. KIEBACK, *Marl, Germany*
R. KLAPDOR, *Hamburg, Germany*
S. D. KOTTARIDIS, *Athens, Greece*
G. R. F. KRUEGER, *Köln, Germany*
Pat M. KUMAR, *Manchester, UK*
Shant KUMAR, *Manchester, UK*
O. D. LAERUM, *Bergen, Norway*
F. J. LEJEUNE, *Lausanne, Switzerland*
L. F. LIU, *Piscataway, NJ, USA*
D. M. LOPEZ, *Miami, FL, USA*
E. LUNDGREN, *Umeå, Sweden*
Y. MAEHARA, *Fukuoka, Japan*
J. MAHER, *London, UK*
J. MARESCAUX, *Strasbourg, France*
J. MARK, *Skövde, Sweden*
S. S. MARTIN, *Baltimore, MD, USA*
S. MITRA, *Houston, TX, USA*
S. MIYAMOTO, *Fukuoka, Japan*
M. MUELLER, *Villingen-Schwenningen, Germany*
F. M. MUGGIA, *New York, NY, USA*
M. NAMIKI, *Kanazawa, Ishikawa, Japan*
R. NARAYANAN, *Boca Raton, FL, USA*
K. NILSSON, *Uppsala, Sweden*
S. PATHAK, *Houston, TX, USA*
J.L. PERSSON, *Malmö, Sweden*
G. J. PILKINGTON, *Portsmouth, UK*
C. D. PLATSOUCAS, *Norfolk, VA, USA*
A. POLLIACK, *Jerusalem, Israel*
M. RIGAUD, *Limoges, France*
U. RINGBORG, *Stockholm, Sweden*
M. ROSELLI, *Rome, Italy*
A. SCHAUER, *Göttingen, Germany*
M. SCHNEIDER, *Wuppertal, Germany*
A. SETH, *Toronto, ON, Canada*
G. V. SHERBET, *Newcastle-upon-Tyne, UK*
G.-I. SOMA, *Kagawa, Japan*
G. S. STEIN, *Burlington, VT, USA*
T. STIGBRAND, *Umeå, Sweden*
T. M. THEOPHANIDES, *Athens, Greece*
P. M. UELAND, *Bergen, Norway*
H. VAN VLIERBERGHE, *Ghent, Belgium*
R. G. VILE, *Rochester, MN, USA*
M. WELLER, *Zurich, Switzerland*
B. WESTERMARK, *Uppsala, Sweden*
Y. YEN, *Duarte, CA, USA*
M.R.I. YOUNG, *Charleston, SC, USA*
B. ZUMOFF, *New York, NY, USA*

J. G. DELINASIOS, *Athens, Greece*
Managing Editor

G. J. DELINASIOS, *Athens, Greece*
Assistant Managing Editor and Executive Publisher

E. ILIADIS, *Athens, Greece*
Production Editor

Editorial Office: International Institute of Anticancer Research, 1st km Kapandritiou-Kalamou Rd., Kapandriti, P.O. Box 22, Attiki 19014, Greece. Tel / Fax: +30-22950-53389.

U.S. Branch: Anticancer Research USA, Inc., 111 Bay Avenue, Highlands, NJ 07732, USA.

E-mails: Editorial Office: journals@iiar-anticancer.org
Managing Editor: editor@iiar-anticancer.org

ANTICANCER RESEARCH supports: (a) the establishment and the activities of the INTERNATIONAL INSTITUTE OF ANTICANCER RESEARCH (IIAR; Kapandriti, Attiki, Greece); and (b) the organization of the International Conferences of Anticancer Research. The IIAR is a member of UICC. For more information about ANTICANCER RESEARCH, IIAR and the Conferences, please visit the IIAR website: www.iiar-anticancer.org

Publication Data: ANTICANCER RESEARCH (AR) is published monthly from January 2009. Each annual volume comprises 12 issues. Annual Author and Subject Indices are included in the last issue of each volume. ANTICANCER RESEARCH Vol. 24 (2004) and onwards appears online with Stanford University HighWire Press from April 2009.

Copyright: On publication of a manuscript in AR, which is a copyrighted publication, the legal ownership of all published parts of the paper passes from the Author(s) to the Journal.

Annual Subscription Rates 2016 per volume: Institutional subscription US$ 1,898.00 (online) or US$ 2,277.00 (print & online). Personal subscription US$ 897.00 (online) or US$ 1,277.00 (print & online). Prices include rapid delivery and insurance. The complete previous volumes of Anticancer Research (Vol. 1-35, 1981-2015) are available at 50% discount on the above rates.

Subscription Orders: Orders can be placed at agencies, bookstores, or directly with the Publisher. (e-mail: subscriptions@iiar-anticancer.org)

Advertising: All correspondence and rate requests should be addressed to the Editorial Office.

Book Reviews: Recently published books and journals should be sent to the Editorial Office. Reviews will be published within 2-4 months.

Articles in ANTICANCER RESEARCH are regularly indexed in all bibliographic services, including Current Contents (Life Sciences), Science Citation Index, Index Medicus, Biological Abstracts, PubMed, Chemical Abstracts, Excerpta Medica, University of Sheffield Biomedical Information Service, Current Clinical Cancer, AIDS Abstracts, Elsevier Bibliographic Database, EMBASE, Compendex, GEOBASE, EMBiology, Elsevier BIOBASE, FLUIDEX, World Textiles, Scopus, Progress in Palliative Care, Cambridge Scientific Abstracts, Cancergram (International Cancer Research Data Bank), MEDLINE, Reference Update - RIS Inc., PASCAL-CNRS, Inpharma-Reactions (Datastar, BRS), CABS, Immunology Abstracts, Telegen Abstracts, Genetics Abstracts, Nutrition Research Newsletter, Dairy Science Abstracts, Current Titles in Dentistry, Inpharma Weekly, BioBase, MedBase, CAB Abstracts/Global Health Databases, Investigational Drugs Database, VINITI Abstracts Journal, Leeds Medical Information, PubsHub, Sociedad Iberoamericana de Información Científica (SIIC) Data Bases.

Authorization to photocopy items for internal or personal use, or the internal or personal clients, is granted by ANTICANCER RESEARCH, provided that the base fee of $2.00 per copy, plus 0.40 per page is paid directly to the Copyright Clearance Center, 27 Congress Street, Salem, MA 01970, USA. For those organizations that have been granted a photocopy license by CCC, a separate system of payment has been arranged. The fee code for users of the Transactional Reporting Service is 0250-7005/2016 $2.00 +0.40.

The Editors and Publishers of ANTICANCER RESEARCH accept no responsibility for the opinions expressed by the contributors or for the content of advertisements appearing therein.

Copyright© 2016, International Institute of Anticancer Research
(Dr. John G. Delinasios), All rights reserved.

D.T.P. BY IIAR
PRINTED BY ENTYPO, ATHENS, GREECE. PRINTED ON ACID-FREE PAPER

ANTICANCER RESEARCH *36*: 1067-1072 (2016)

Computed Tomographic Features of Malignant Peritoneal Mesothelioma

KATSUYA KATO[1§], KENICHI GEMBA[2], NOBUKAZU FUJIMOTO[2], KEISUKE AOE[4],
YUKIO TAKESHIMA[5], KOUKI INAI[5] and TAKUMI KISHIMOTO[3]

[1]Department of Radiology, Okayama University Hospital, Shikatacho, Okayama, Japan;
Departments of [2]Respiratory Medicine and [3]Internal Medicine,
Okayama Rosai Hospital, Chikkomidorimachi, Okayama, Japan;
[4]Department of Medical Oncology, National Hospital Organization Yamaguchi-Ube Medical Center,
Higashikiwa, Ube, Japan;
[5]Department of Pathology, Graduate School of Biomedical Sciences,
Hiroshima University, Minamiku, Hiroshima, Japan

Abstract. *Aim: The objective of this study was to determine the computed tomographic (CT) features of malignant peritoneal mesothelioma (MPM). Patients and Methods: We analyzed CT features of MPM cases and compared them to those of other malignant conditions (non-MPM). Results: Multiple nodular lesions occurred more frequently in the MPM group compared to non-MPM cases (p=0.013). Thickening of the mesentery was detected more frequently in MPM cases than in non-MPM cases (56% vs. 18%, p=0.029). Pleural plaques were detected in 13 cases (45%) in the MPM group but were not detected in the non-MPM group. The MPM-CT index score, determined in each case as the sum of the findings which are potentially characteristic of MPM, was significantly higher in MPM than in non-MPM cases (p=0.001). Conclusion: MPM presented characteristic CT findings, and the MPM-CT index may be useful for differential diagnosis of MPM.*

Malignant mesothelioma (MM) is an aggressive tumor that develops from mesothelial cells of the pleura, peritoneum, pericardium, or testicular *tunica vaginalis*. It is generally associated with a history of asbestos exposure (1) and has a very poor prognosis (2). Once rare, the incidence of MM has increased worldwide as a result of past wide-spread exposure to asbestos. Malignant peritoneal mesothelioma (MPM) represents the second most common site of MM, accounting for 10-20% of MM (3, 4).

A diagnosis of MPM should be based on the histology of an adequate specimen of the peritoneum or cytological analyses of ascites, but this is often difficult. Paracentesis with fluid cytology has a variable sensitivity of 32-76%, with the major limitation being difficulty in distinguishing benign from malignant lesions (4, 5). In particular, the differential diagnosis between MPM and peritoneal carcinomatosis is a critical issue. Radiological analysis is essential for this differential diagnosis; computed tomographic (CT) imaging is the most common initial imaging modality and can reveal moderate to extensive ascites with peritoneal, visceral, or omental involvement. Magnetic resonance imaging may more accurately quantify the extent of disease; however, its routine use is not yet supported (6). The role of positron-emission tomography is not well defined in detection of this disease (7).

In the current study, we retrospectively examined the CT features for patients with MPM.

Patients and Methods

Study approval. All procedures performed in the current study were in accordance with the Helsinki declaration. This study was performed in accordance with the Ethical Guidelines for Epidemiological Research of the Japanese Ministry of Education, Culture, Sports, Science and Technology, and Ministry of Health, Labour and Welfare and was approved by the Japan Labour Health and Welfare Organization and the Institutional Review Boards of Okayama Rosai Hospital. Patient confidentiality was strictly maintained. As described below, informed consent was provided by the closest living relatives of each patient.

Patients. This study was a part of our previous nationwide survey of MM. Methods of the retrospective survey have been described

---

[§]*Present address:* Department of Diagnostic Radiology 2, Kawasaki Medical School, Nakasange, Kitaku, Okayama, Japan.

Correspondence to: Nobukazu Fujimoto, MD, Ph.D., Department of Respiratory Medicine, Okayama Rosai Hospital, 1-10-25 Chikkomidorimachi, Okayama 7028055, Japan. Tel: 81-86-2620131, Fax: 81-86-2623391, e-mail: nobufujimot@gmail.com

Key Words: Asbestos, peritoneum, mesothelioma, CT image.

previously (1, 8). In brief, we requested and received authorization to view the death records from the Vital Statistics database in Japan. We then extracted all cases of death due to MM between 2003 and 2005. There were 2,742 deaths due to MM (Figure 1). We contacted the closest living relatives of each patient to obtain consent for our study by postal mail. As a result, informed consent was obtained by postal mail for 1,153 cases. Based on authorization from relatives, we contacted the patients' medical institutions to obtain medical information, including medical records, X-ray and CT images by postal mail. These data were obtained in 743 cases. Among them, we found 105 cases in which the clinical diagnosis of MPM had been made. Pathological specimens were provided in 53 out of the 105 cases. We reviewed the pathological specimen of these cases according to World Health Organization criteria (9), and analyzed the radiological features of the cases.

CT analysis of MPM. The items examined on the CT images were as follows: (i) degree of accumulation of ascites, (ii) location of the lesion, (iii) maximum dimensions of the nodular lesion, (iv) number of tumor masses, (v) extent of peritoneal thickening, (vi) extent of thickening of the mesentery, (vii) stellate pattern findings in the mesentery, and (viii) pleural plaques. These items were examined according to the criteria listed in Table I.

Statistical analysis. Comparisons between independent groups were performed using the Chi-square test and non-parametric analysis was performed with the Mann–Whitney *U*-test. Average values were compared by *t*-test. Areas under the receiver operating characteristic (ROC) curves (AUCs) were calculated using standard techniques. Statistical calculations were performed with SPSS statistical package, version 11.0 (SPSS Inc., Chicago, IL, USA).

Results

Pathological review of the cases. As shown in Figure 2, pathological diagnosis of MPM was confirmed in 34 cases. Among the 34 cases, there were 27 (79.0%) cases of epithelioid, four (12.0%) cases of biphasic, and three (9%) cases of sarcomatous sub-types. There were 16 cases ultimately diagnosed as other conditions (non-MPM), including six cases of serous papillary adenocarcinoma, four cases of adenocarcinoma, two cases each of carcinosarcoma and unclassified sarcoma, and one case each of peritoneal metastasis of renal cell carcinoma and rhabdomyosarcoma. Differentiation between the epithelioid sub-type of mesothelioma and poorly differentiated adenocarcinoma was impossible in one case. In another case, a confirmed pathological diagnosis could not be made as to whether it was an epithelioid sub-type of mesothelioma, another malignant condition, or reactive mesothelium. In addition, there was one case in which a malignant condition was highly suspected from CT images, but only reactive mesothelium was demonstrated in the pathological specimen. These three cases were finally categorized as "diagnosis could not be made," and they were excluded from further analyses. The MPM group included 30 (88.2%) males and 4 (11.8%) females and the non-MPM group included two (12.5%) males and 14 (87.5%) females.

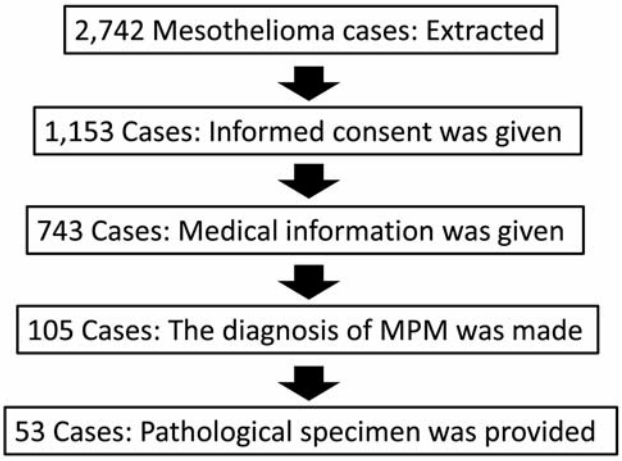
2,742 Mesothelioma cases: Extracted
1,153 Cases: Informed consent was given
743 Cases: Medical information was given
105 Cases: The diagnosis of MPM was made
53 Cases: Pathological specimen was provided

Figure 1. *The schema of the case collection of this study.*

Radiological analyses. Among the 50 cases, abdominal and pelvic CT scans were available in 32 MPM cases and 11 non-MPM cases (three cases of serous papillary adenocarcinoma, two cases each of adenocarcinoma, carcinosarcoma and unclassified sarcoma, and one case each of peritoneal metastasis of renal cell carcinoma and rhabdomyosarcoma). Chest CT images were available in 40 cases (29 MPM and 11 non-MPM). CT findings of the MPM and non-MPM groups are shown in Table I.

There were 19/32 (59%) cases of moderate to massive accumulation of ascites in the MPM group, and 3/11 (27%) cases in the non-MPM group. Although the proportion was higher in the MPM compared to non-MPM group, the difference did not reach statistical significance (p=0.066). We analyzed the location of MPM. For this purpose, the existence or non-existence of MPM in the parahepatic space, great omentum, paracolic gutter, mesentery proper, rectovesical pouch, and perisplenic space was determined. There was no difference concerning the location of the disease between the MPM and non-MPM groups.

We next categorized the maximum dimension of the nodular lesion as <1 cm, 1-3 cm, >3-5 cm, or >5 cm based on the abdominal CT images (Figure 3A). As shown in Table I, the proportion of cases with a maximum dimension of <1 cm was higher in the MPM group than in the non-MPM group, but this difference was not statistically significant (47% *vs.* 18%, p=0.097).

In the MPM group, there were multiple nodular lesions in 30 cases (94%), which was significantly more frequent in MPM than in non-MPM cases (p=0.013).

Thickening of the peritoneum was categorized as none, mild, irregular, or massive (defined as ≥1 cm, Figure 3B). As shown in Table I, MPM cases had a higher proportion of irregular or massive thickening compared to non-MPM cases, although this

Table I. *Computed tomographic findings of malignant peritoneal mesothelioma (MPM) and finding of cases ultimately diagnosed as other conditions (non-MPM).*

Characteristic		Proportion of cases with the finding (%)		
	Findings	MPM	Non-MPM	*p*-Value
Ascites accumulation	None	2 (6.3)	2 (18.2)	
	Small	11 (34.4)	6 (54.5)	
	Moderate	12 (37.5)	2 (18.2)	
	Massive	7 (21.9)	1 (9.1)	0.066
Maximum dimension of nodular lesion	<1 cm	15 (46.9)	2 (18.2)	
	1-3 cm	6 (18.8)	2 (18.2)	
	>3-5 cm	2 (6.3)	3 (27.3)	
	>5 cm	9 (28.1)	4 (36.4)	0.097
Location of MPM				
Parahepatic space	Yes	18 (56.3)	5 (45.5)	
	No	14 (43.8)	6 (54.5)	0.536
Great omentum	Yes	29 (90.6)	8 (72.7)	
	No	3 (9.4)	3 (27.3)	0.139
Paracolic gutter	Yes	18 (56.3)	5 (45.5)	
	No	14 (43.8)	6 (54.5)	0.536
Mesentery proper	Yes	25 (78.1)	8 (72.7)	
	No	7 (21.9)	3 (27.3)	0.715
Rectovesical pouch	Yes	18 (56.3)	9 (81.8)	
	No	14 (43.8)	2 (18.2)	0.13
Perisplenic space	Yes	14 (43.8)	3 (27.3)	
	No	18 (56.3)	8 (72.7)	0.668
Nodular lesions	Solitary	2 (6.3)	4 (36.4)	
	Multiple	30 (93.8)	7 (63.6)	0.013
Thickening of the peritoneum	None	3 (9.4)	3 (27.3)	
	Slight thickening	15 (46.9)	6 (54.5)	
	Irregular thickening	6 (18.8)	2 (18.2)	
	Massive thickening	8 (25.0)	0 (0.0)	0.066
Thickening of the mesentery	None	14 (43.8)	9 (81.8)	
	Slight thickening	12 (37.5)	2 (18.2)	
	Irregular thickening	4 (12.5)	0 (0.0)	
	massive thickening	2 (6.3)	0 (0.0)	0.029
Stellate pattern findings	Yes	11(34.4)	3 (27.3)	
	No	21(65.6)	8 (72.7)	0.665
Pleural plaques	Yes	13 (44.8)	0 (0.0)	
	No	16 (55.2)	11(100.0)	0.007

difference was not statistically significant (44% *vs*. 18%, *p*=0.066).

Thickening of the mesentery was categorized as none, mild, irregular thickening, or massive thickening (defined as ≥3 mm, Figure 3C). Thickening of the mesentery was detected more frequently in MPM cases than in non-MPM cases (56% *vs*. 18%, *p*=0.029).

We examined stellate pattern findings as an indicator of mesenteric vascular enlargement (Figure 3D). Stellate patterns were detected in 11 cases (34%) in the MPM group and in three cases (27%) in the non-MPM group. This difference was not statistically significant (*p*=0.665).

Finally, pleural plaques were examined in chest CT images, which were available for 29 out of the 32 MPM

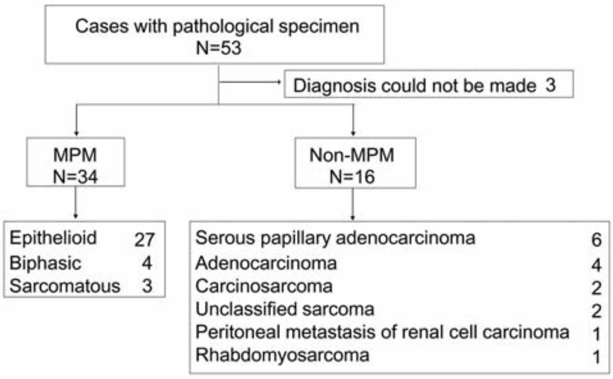
Cases with pathological specimen
N=53
Diagnosis could not be made 3
MPM
N=34
Non-MPM
N=16
Epithelioid 27
Biphasic 4
Sarcomatous 3
Serous papillary adenocarcinoma 6
Adenocarcinoma 4
Carcinosarcoma 2
Unclassified sarcoma 2
Peritoneal metastasis of renal cell carcinoma 1
Rhabdomyosarcoma 1

Figure 2. *The breakdown of the confirmed pathological diagnosis of enrolled patients.*

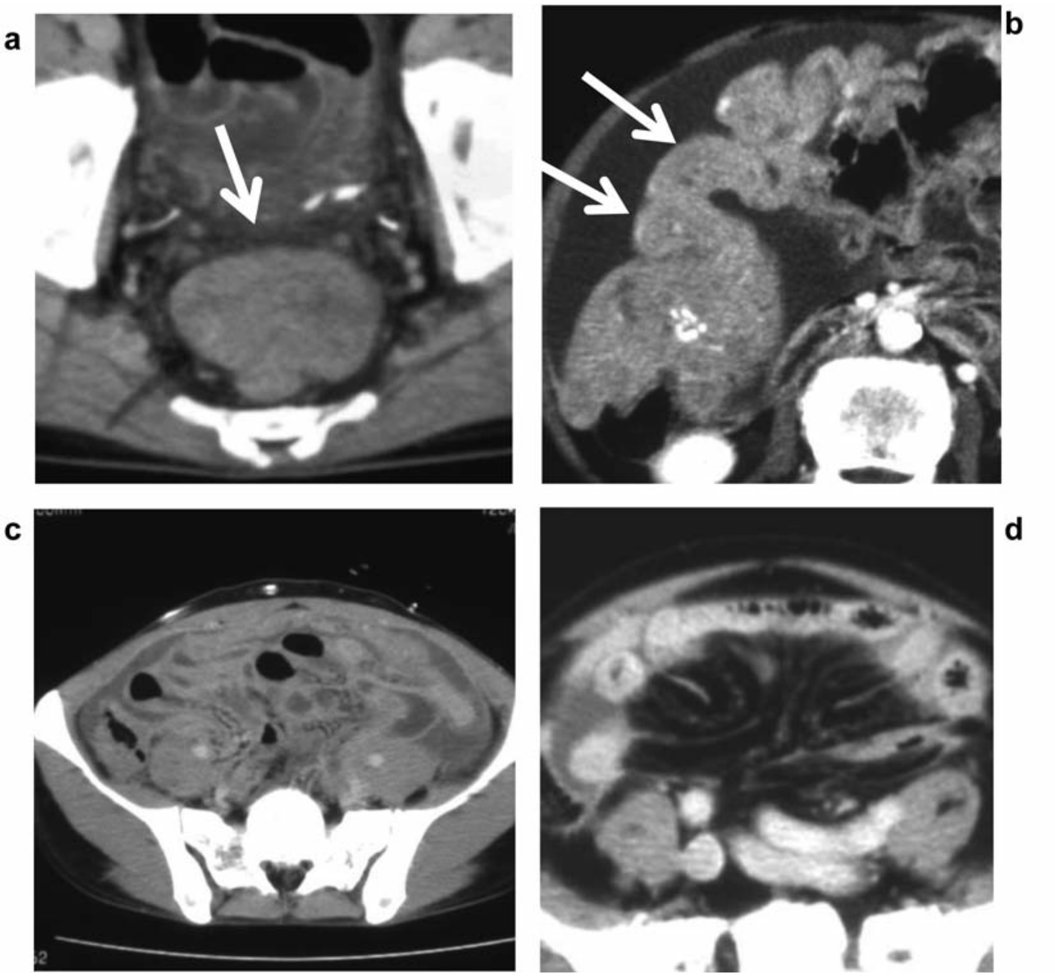

Figure 3. *Examples of computed tomographic images of malignant peritoneal mesothelioma with maximum dimension of the nodular lesion >5 cm (A), massive thickening of the peritoneum (B), massive thickening of the mesentery (C), and stellate structure findings (D).*

cases and 11 of the non-MPM cases. Pleural plaques were detected in 13 cases (45%) in the MPM group. None were detected among the non-MPM cases.

Proposal of an MPM-CT index. Among the findings analyzed above, we selected six findings that were detected more frequently in MPM than in non-MPM with a *p*-value of <0.100: degree of accumulation of ascites, maximum dimension of the nodular lesion, number of tumor masses, extent of peritoneal thickening, extent of thickening of the mesentery, and pleural plaques. In each case, CT findings were scored as 1 in the case of (i) moderate to massive accumulation of ascites, (ii) maximum dimension of nodular lesion <1 cm, (iii) multiple nodular lesions, (iv) irregular to massive thickening of the peritoneum, and (v) mild to massive thickening of the mesentery. The MPM-CT index was determined in each case as the sum of these six findings. As shown in Figure 4A, the index was significantly higher in MPM than in non-MPM cases (*p*=0.001). To evaluate the utility of the index for differentiation between MPM and non-MPM cases, we performed an ROC analysis. The AUC value for the differential diagnosis between the two groups was 0.821 (95% confidence interval=0.694-0.945) (Figure 4B). Based on a cutoff value of 3, sensitivity was 53% and specificity was 100%.

Discussion

MPM is poorly described and the knowledge of its natural history is very limited. In previous reports, at least 70% of cases of MPM were associated with chronic exposure to asbestos (10, 11); however, it is not clear how inhaled asbestos induces peritoneal neoplasms.

It is often difficult to make a pathological distinction between MPM and peritoneal metastatic adenocarcinoma (12, 13), although some immunohistochemical markers, such

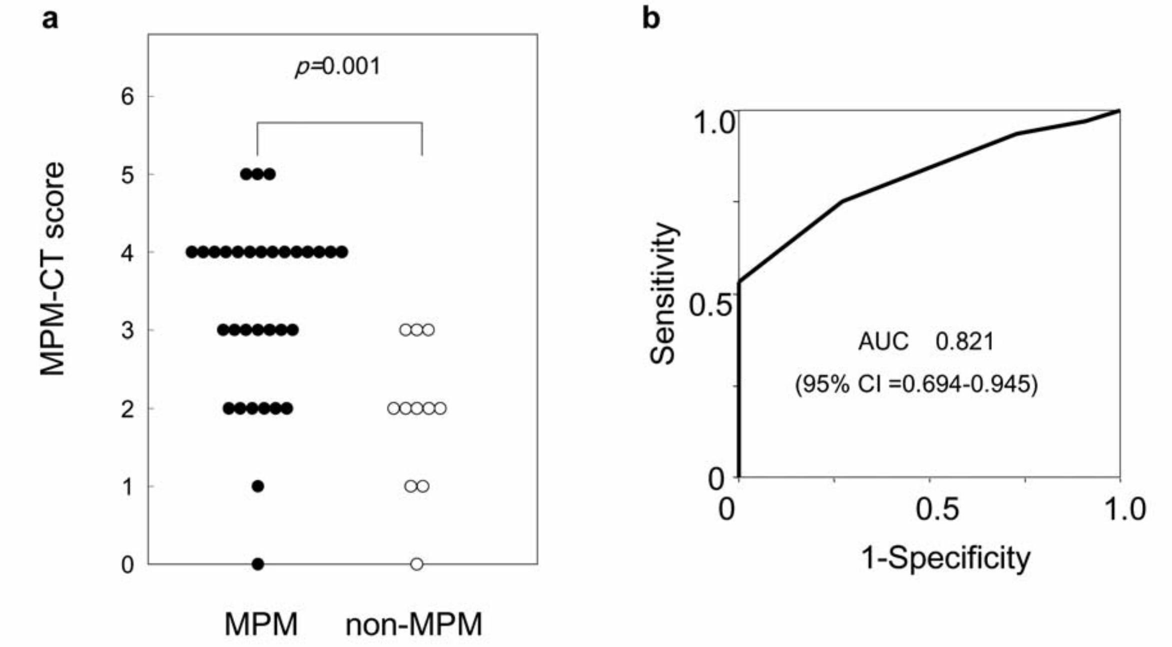

Figure 4. *A: Comparison of malignant peritoneal mesothelioma (MPM)–computed tomography (CT) index between MPM and non-MPM groups. B: Receiver operating characteristic curves to evaluate the usefulness of the MPM-CT index for the differentiation between MPM and non-MPM.*

as calretinin, thrombomodulin, and cytokeratin 5/6, could facilitate this (14, 15). In the current study, we reviewed the pathological specimens of 53 cases that had been diagnosed as MPM, and confirmed a diagnosis of MPM in only 34 cases (64.2%). The difficulty involved in making a clinical and pathological differential diagnosis often results in a diagnostic delay. Factors contributing to the diagnostic delay include the rarity of this entity, the long latent period from the exposure to asbestos, and the non-specific clinical features of the disease. Biochemistry and tumor markers are of limited assistance in this regard.

In the current study, we analyzed CT features of MPM. For this purpose, we extracted all cases of death due to MM between 2003 and 2005 based on death records from the Vital Statistics in Japan. A strength of our study is that it contained many cases of MPM. To the best of our knowledge, this is the largest study of radiological analysis of MPM. We tried to analyze 105 cases in which the clinical diagnosis of MPM had been made, and after the pathological review of the provided specimens, we determined there were 34 MPM cases. We had to accept the low collection rate of the study based on the postal mail method. However, there is no selection bias throughout the process of data collection.

There is a wide spectrum of imaging findings in MPM, the most common of which include a thickening of the mesentery and peritoneum. Findings on CT images are highly variable; therefore differentiating MPM from other intra-abdominal malignancies is difficult (12, 16-18). Based on the results of the current study, we proposed the use of an MPM-CT index that comprises accumulation of ascites, maximum dimension of the nodular lesion, number of tumor masses, extent of peritoneal thickening, extent of mesenteric thickening, and pleural plaques. We found marked differences in these findings between the MPM and non-MPM groups. With a cut-off score of 3, diagnostic sensitivity was 53% and specificity of 100%, while ROC analysis revealed an AUC value of 0.821. These results indicate the clinical utility of this MPM-CT index for the differential diagnosis of MPM. In fact, the sensitivity is around 50%; however, the high specificity would contribute to the differentiation.

A limitation of the current study is that this was a retrospective analysis. A validation study to confirm the utility of the index is warranted, with a new patient cohort that includes pathologically confirmed MPM cases and other peritoneal malignant conditions.

Conclusion

MPM is a rare tumor that is difficult to diagnose and treat. An accurate diagnosis of MPM is essential in order to determine the prognosis, and occupation-related compensation claims following asbestos exposure. MPM demonstrates characteristic radiological findings, and the MPM-CT index may be useful for the differential diagnosis of MPM.

Conflicts of Interest

None.

Acknowledgements

This study was supported by the Research and Development and the Dissemination of Projects Related to the Nine Fields of Occupational Injuries and Illnesses of the Japan Labour Health and Welfare Organization. This work is also supported by grants-in-aid from the Ministry of Health, Labor and Welfare, Japan. These study sponsors had no involvement in in study design, writing of the manuscript, the collection of data, and decision to submit the manuscript for publication.

References

1 Gemba K, Fujimoto N, Kato K, Aoe K, Takeshima Y, Inai K and Kishimoto T: National survey of malignant mesothelioma and asbestos exposure in Japan. Cancer Sci *103*: 483-490, 2012.

2 Gemba K, Fujimoto N, Aoe K, Kato K, Takeshima Y, Inai K and Kishimoto T: Treatment and survival analyses of malignant mesothelioma in Japan. Acta Oncol *52*: 803-808, 2013.

3 Blackham AU and Levine EA: Cytoreductive surgery with hyperthermic intraperitoneal chemotherapy for malignant peritoneal mesothelioma. European J Clin Med Oncol *4*: 25-32, 2012.

4 Kindler HL: Peritoneal mesothelioma: the site of origin matters. Am Soc Clin Oncol Educ Book 2013, 182-188, 2013.

5 Turner KM, Varghese S and Alexander HR Jr.: Surgery for peritoneal mesothelioma. Curr Treat Options Oncol *12*: 189-200, 2011.

6 Low RN, Sebrechts CP, Barone RM and Muller W: Diffusion-weighted MRI of peritoneal tumors: comparison with conventional MRI and surgical and histopathologic findings – a feasibility study. AJR *193*: 461-470, 2009.

7 Cao Q, Lu M, Heath J, Hausner PF, Alexander HR, Dilsizian V and Chen W: 18F-FDG PET/CT in a recurrent diffuse malignant peritoneal mesothelioma. Clin Nucl Med *37*: 492-494, 2012.

8 Takeshima Y, Inai K, Amatya VJ, Gemba K, Aoe K, Fujimoto N, Kato K and Kishimoto T: Accuracy of pathological diagnosis of mesothelioma cases in Japan: clinicopathological analysis of 382 cases. Lung Cancer *66*: 191-197, 2009.

9 Churg A, Cagle PT and Roggli VL: Tumors of the serosal membrane. AFIP atlas of tumor pathology. Series *4*. 48-49, 2006.

10 D'Albuquerque LA, Padilla JM, Rodrigues AL, Souza MV, Quireze Junior C, Meniconi MT, Copstein JL, dos Santos Junior ED, de Melo CR, Santo GC and de Oliveira e Silva A: Diffuse primary malignant mesothelioma in abdominal cavity. Arq Gastroenterol *34*: 163-168, 1997.

11 Cocco P and Dosemeci M: Peritoneal cancer and occupational exposure to asbestos: results from the application of a job-exposure matrix. Am J Ind Med *35*: 9-14, 1999.

12 Clark JR and Ross WB: An unusual case of ascites: pitfalls in diagnosis of malignant peritoneal mesothelioma. Aust NZ J Surg *70*: 384-388, 2000.

13 Mohamed F and Sugarbaker PH: Peritoneal mesothelioma. Curr Treat Options Oncol *3*: 375-386, 2002.

14 Ordonez NG: Role of immunohistochemistry in distinguishing epithelial peritoneal mesotheliomas from peritoneal and ovarian serous carcinomas. Am J Surg Pathol *22*: 1203-1214, 1998.

15 Attanoos RL, Webb R, Dojcinov SD and Gibbs AR: Value of mesothelial and epithelial antibodies in distinguishing diffuse peritoneal mesothelioma in females from serous papillary carcinoma of the ovary and peritoneum. Histopathology *40*: 237-244, 2002.

16 Ros PR, Yuschok TJ, Buck JL, Shekitka KM and Kaude JV: Peritoneal mesothelioma. Radiologic appearances correlated with histology. Acta Radiol *32*: 355-358, 1991.

17 Smith TR: Malignant peritoneal mesothelioma: marked variability of CT findings. Abdom Imaging *19*: 27-29, 1994.

18 Gupta S, Gupta RK, Gujral RB, Agarwal D, Saxena R and Tandon P: Peritoneal mesothelioma simulating pseudomyxoma peritonei on CT and sonography. Gastrointest Radiol *17*: 129-131, 1992.

Received November 21, 2015
Revised January 24, 2016
Accepted February 2, 2016

Instructions for Authors 2016

General Policy. ANTICANCER RESEARCH (AR) will accept original high quality works and reviews on all aspects of experimental and clinical cancer research. The Editorial Policy suggests that priority will be given to papers advancing the understanding of cancer causation, and to papers applying the results of basic research to cancer diagnosis, prognosis, and therapy. AR will also accept the following for publication: (a) Abstracts and Proceedings of scientific meetings on cancer, following consideration and approval by the Editorial Board; (b) Announcements of meetings related to cancer research; (c) Short reviews (of approximately 120 words) and announcements of newly received books and journals related to cancer, and (d) Announcements of awards and prizes.

The principal aim of AR is to provide prompt publication (print and online) for original works of high quality, generally within 1-2 months from final acceptance. Manuscripts will be accepted on the understanding that they report original unpublished works in the field of cancer research that are not under consideration for publication by another journal, and that they will not be published again in the same form. All authors should sign a submission letter confirming the approval of their article contents. All material submitted to AR will be subject to review, when appropriate, by two members of the Editorial Board and by one suitable outside referee. The Editors reserve the right to improve manuscripts on grammar and style.

The Editors and Publishers of AR accept no responsibility for the contents and opinions expressed by the contributors. Authors should warrantee due diligence in the creation and issuance of their work.

NIH Open Access Policy. The journal acknowledges that authors of NIH funded research retain the right to provide a copy of the final manuscript to the NIH four months after publication in ANTICANCER RESEARCH, for public archiving in PubMed Central.

Copyright. Once a manuscript has been published in ANTICANCER RESEARCH, which is a copyrighted publication, the legal ownership of all published parts of the paper has been transferred from the Author(s) to the journal. Material published in the journal may not be reproduced or published elsewhere without the written consent of the Managing Editor or Publisher.

Format. Two types of papers may be submitted: (i) Full papers containing completed original work, and (ii) review articles concerning fields of recognisable progress. Papers should contain all essential data in order to make the presentation clear. Reasonable economy should be exercised with respect to the number of tables and illustrations used. Papers should be written in clear, concise English. Spelling should follow that given in the "Shorter Oxford English Dictionary".

Manuscripts. Submitted manuscripts should not exceed fourteen (14) pages (approximately 250 words per double - spaced typed page), including abstract, text, tables, figures, and references (corresponding to 4 printed pages). Papers exceeding four printed pages will be subject to excess page charges. All manuscripts should be divided into the following sections:
(a) *First page* including the title of the presented work [not exceeding fifteen (15) words], full names and full postal addresses of all Authors, name of the Author to whom proofs are to be sent, key words, an abbreviated running title, an indication "review", "clinical", "epidemiological", or "experimental" study, and the date of submission. (Note: The order of the Authors is not necessarily indicative of their contribution to the work. Authors may note their individual contribution(s) in the appropriate section(s) of the presented work); (b) *Abstract* not exceeding 150 words, organized according to the following headings: Background/Aim - Materials and Methods/Patients and Methods - Results - Conclusion; (c) *Introduction;* (d) *Materials and Methods/Patients and Methods;* (e) *Results;* (f) *Discussion;* (g) *Acknowledgements;* (h) *References.* All pages must be numbered consecutively. Footnotes should be avoided. Review articles may follow a different style according to the subject matter and the Author's opinion. Review articles should not exceed 35 pages (approximately 250 words per double-spaced typed page) including all tables, figures, and references.

Figures. All figures should appear at the end of the submitted document file. Once a manuscript is accepted all figures and graphs should be submitted separately in either jpg, tiff or pdf format and at a minimum resolution of 300 dpi. Graphs must be submitted as pictures made from drawings and must not require any artwork, typesetting, or size modifications. Symbols, numbering and lettering should be clearly legible. The number and top of each figure must be indicated. Pages that include color figures are subject to color charges.

Tables. All tables should appear at the end of the submitted document file. Once a manuscript is accepted, each table should be submitted separately, typed double-spaced. Tables should be numbered with Roman numerals and should include a short title.

References. Authors must assume responsibility for the accuracy of the references used. Citations for the reference sections of submitted works should follow the standard form of "Index Medicus" and must be numbered consecutively. In the text, references should be cited by number. Examples: 1 Sumner AT: The nature of chromosome bands and their significance for cancer research. Anticancer Res 1: 205-216, 1981. 2 McGuire WL and Chamnes GC: Studies on the oestrogen receptor in breast cancer. In: Receptors for Reproductive Hormones (O' Malley BW, Chamnes GC (eds.). New York, Plenum Publ Corp., pp 113-136, 1973.

Nomenclature and Abbreviations. Nomenclature should follow that given in "Chemical Abstracts", "Index Medicus", "Merck Index", "IUPAC –IUB", "Bergey's Manual of Determinative Bacteriology", The CBE Manual for Authors, Editors and Publishers (6th edition, 1994), and MIAME Standard for Microarray Data. Human gene symbols may be obtained from the HUGO Gene Nomenclature Committee (HGNC) (http://www.gene.ucl.ac.uk/). Approved mouse nomenclature may be obtained from http://www.informatics.jax.org/. Standard abbreviations are preferable. If a new abbreviation is used, it must be defined on first usage.

Clinical Trials. Authors of manuscripts describing clinical trials should provide the appropriate clinical trial number in the correct format in the text.
For International Standard Randomised Controlled Trials (ISRCTN) Registry (a not-for-profit organization whose registry is administered by Current Controlled Trials Ltd.) the unique number must be provided in this format: ISRCTNXXXXXXXX (where XXXXXXXX represents the unique number, always prefixed by "ISRCTN"). Please note that there is no space between the prefix "ISRCTN" and the number. Example: ISRCTN47956475.

For Clinicaltrials.gov registered trials, the unique number must be provided in this format: NCTXXXXXXXX (where XXXXXXXX represents the unique number, always prefixed by 'NCT'). Please note that there is no space between the prefix 'NCT' and the number. Example: NCT00001789.

Ethical Policies and Standards. ANTICANCER RESEARCH agrees with and follows the "Uniform Requirements for Manuscripts Submitted to Biomedical Journals" established by the International Committee of Medical Journal Editors in 1978 and updated in October 2001 (www.icmje.org). Microarray data analysis should comply with the "Minimum Information About Microarray Experiments (MIAME) standard". Specific guidelines are provided at the "Microarray Gene Expression Data Society" (MGED) website. Presentation of genome sequences should follow the guidelines of the NHGRI Policy on Release of Human Genomic Sequence Data. Research involving human beings must adhere to the principles of the Declaration of Helsinki and Title 45, U.S. Code of Federal Regulations, Part 46, Protection of Human Subjects, effective December 13, 2001. Research involving animals must adhere to the Guiding Principles in the Care and Use of Animals approved by the Council of the American Physiological Society. The use of animals in biomedical research should be under the careful supervision of a person adequately trained in this field and the animals must be treated humanely at all times. Research involving the use of human foetuses, foetal tissue, embryos and embryonic cells should adhere to the U.S. Public Law 103-41, effective December 13, 2001.

Submission of Manuscripts. Please follow the Instructions for Authors regarding the format of your manuscript and references.
Manuscripts must be submitted only through our online submission system at: http://www.iiar-submissions.com/login.html
In case a submission is incomplete, the corresponding Author will be notified accordingly.
Questions regarding difficulties in using the online submission system should be addressed to: email: journals@iiar-anticancer.org

Galley Proofs. Unless otherwise indicated, galley proofs will be sent to the corresponding Author of the submission. Corrections of galley proofs should be limited to typographical errors. Reprints, PDF files, and/or Open Access may be ordered after the acceptance of the paper. Authors of online open access articles published in 2015 are entitled to a complimentary online subscription to Anticancer Research 2015. Requests should be addressed to the Editorial Office. Galley proofs should be returned corrected to the Editorial Office by email within two days.

Copyright© 2016 - International Institute of Anticancer Research (J.G. Delinasios). All rights reserved (including those of translation into other languages). No part of this journal may be reproduced, stored in a retrieval system, or transmitted in any form or by any means, electronic, mechanical, photocopying, microfilming, recording or otherwise, without written permission from the Publisher.

Specific information and additional instructions for Authors

1. Anticancer Research (AR) closely follows the new developments in all fields of experimental and clinical cancer research by (a) inviting reviews on topics of immediate importance and substantial progress in the last three years, and (b) providing the highest priority for rapid publication to manuscripts presenting original results judged to be of exceptional value. Theoretical papers will only be considered and accepted if they bear a significant impact or formulate existing knowledge for the benefit of research progress.

2. Anticancer Research will consider the publication of conference proceedings and/or abstracts provided that the material submitted fulfils the quality requirements and instructions of the journal, following the regular review process by two suitable referees. (For further information please click here)

3. An acknowledgement of receipt, including the article number, title and date of receipt is sent to the corresponding author of each manuscript upon receipt. If this receipt is not received within 20 days from submission, the author should call or write to the Editorial Office to ensure that the manuscript (or the receipt) was not lost in the mail or during electronic submission.

4. Each manuscript submitted to AR is sent for review in confidence to two suitable referees with the request to return the manuscript with their comments to the Editorial Office within 12 days from receipt. If reviewers need a longer time or wish to send the manuscript to another expert, the manuscript may be returned to the Editorial Office with a delay. All manuscripts submitted to AR, are treated in confidence, without access to any person other than the Managing Editor, the journal's secretary, the reviewers and the printers.

5. All accepted manuscripts are peer-reviewed and carefully corrected in style and language, if necessary, to make presentation clear. (There is no fee for this service). Every effort is made (a) to maintain the personal style of the author's writing and (b) to avoid change of meaning. Authors will be requested to examine carefully manuscripts which have undergone language correction at the pre-proof or proof stage.

6. Authors should pay attention to the following points when writing an article for AR:
   - The Instructions to Authors must be followed in every detail.
   - The presentation of the experimental methods should be clear and complete in every detail facilitating reproducibility by other scientists.
   - The presentation of results should be simple and straightforward in style. Results and discussion should not he combined into one section, unless the paper is short.
   - Results given in figures should not be repeated in tables.
   - Figures (graphs or photographs) should be prepared at a width of 8 or 17 cm with legible numbers and lettering.
   - Photographs should be clear with high contrast, presenting the actual observation described in the legend and in the text. Each legend should provide a complete description, being self-explanatory, including technique of preparation, information about the specimen and magnification.
   - Statistical analysis should be elaborated wherever it is necessary. Simplification of presentation by giving only numerical or % values should be avoided.
   - Fidelity of the techniques and reproducibility of the results, should be points of particular importance in the discussion section. Authors are advised to check the correctness of their methods and results carefully before writing an article. Probable or dubious explanations should be avoided.
   - Authors should not cite results submitted for publication in the reference section. Such results may be described briefly in the text with a note in parenthesis (submitted for publication by... authors, year).
   - The References section should provide as complete a coverage of the literature as possible including all the relevant works published up to the time of submission.
   - By following these instructions, Authors will facilitate a more rapid review and processing of their manuscripts and will provide the readers with concise and useful papers.

7. Following review and acceptance, a manuscript is examined in language and style, and galley proofs are rapidly prepared. Second proofs are not sent unless required.

8. Authors should correct their galley proofs very carefully and preferably twice. An additional correction by a colleague always proves to be useful. Particular attention should be paid to chemical formulas, mathematical equations, symbols, medical nomenclature etc. Any system of correction marks can be used in a clear manner, preferably with a red pen. Additions or clarifications are allowed provided that they improve the presentation but do not bring new results (no fee).

9. Articles submitted to AR may be rejected without review if:
   - they do not fall within the journal's policy.
   - they do not follow the instructions to authors.
   - language is unclear.
   - results are not sufficient to support a final conclusion.
   - results are not objectively based on valid experiments.
   - they repeat results already published by the same or other authors before the submission to AR.
   - plagiarism is detected by plagiarism screening services.

   (Rejection rate (2015): 64%).

10. Authors who wish to prepare a review should contact the Managing Editor of the journal in order to get confirmation of interest in the particular topic of the review. The expression of interest by the Managing Editor does not necessarily imply acceptance of the review by the journal.

11. Authors may inquire information about the status of their manuscript(s) by calling the Editorial Office at +30-22950-53389, Monday to Friday 9.00-16.00 (Athens time), or by sending an e-mail to journals@iiar-anticancer.org

12. Authors who wish to edit a special issue on a particular topic should contact the Managing Editor.

13. Authors, Editors and Publishers of books are welcome to submit their books for immediate review in AR. There is no fee for this service.

(This text is a combination of advice and suggestions contributed by Editors, Authors, Readers and the Managing Editor of AR).

Copyright © 2016 IIAR (J.G. Delinasios)

Fatal pleural mesothelioma in Japan (2003–2008): evaluation of computed tomography findings

Katsuya Kato, Kenichi Gemba, Nobukazu Fujimoto, Keisuke Aoe, Yukio Takeshima, Kouki Inai & Takumi Kishimoto

Japanese Journal of Radiology
(formerly: Radiation Medicine)

ISSN 1867-1071

Jpn J Radiol
DOI 10.1007/s11604-016-0539-1

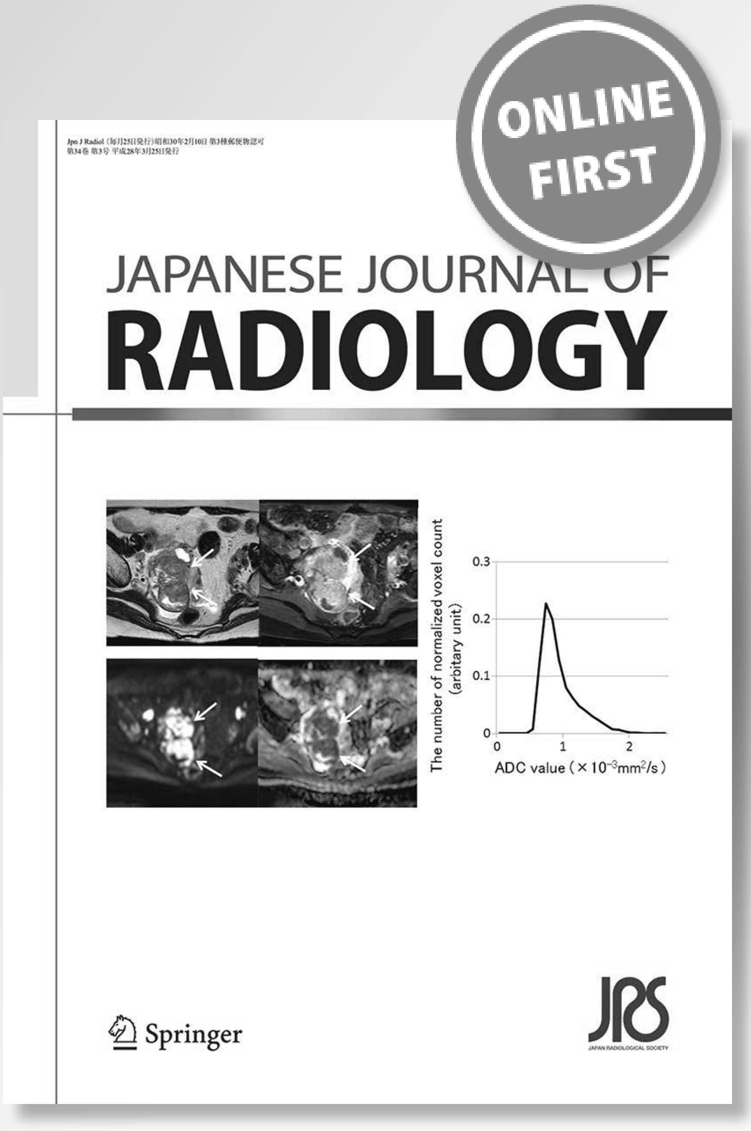

ONLINE FIRST

Jpn J Radiol（毎月25日発行）昭和30年2月10日 第3種郵便物認可
第34巻 第3号 平成28年3月25日発行

JAPANESE JOURNAL OF
RADIOLOGY

Springer

JRS
JAPAN RADIOLOGICAL SOCIETY

The number of normalized voxel count (arbitary unit)
0.3
0.2
0.1
0
0
1
2
ADC value（× 10^{-3}mm^2/s）

Springer

Your article is protected by copyright and all rights are held exclusively by Japan Radiological Society. This e-offprint is for personal use only and shall not be self-archived in electronic repositories. If you wish to self-archive your article, please use the accepted manuscript version for posting on your own website. You may further deposit the accepted manuscript version in any repository, provided it is only made publicly available 12 months after official publication or later and provided acknowledgement is given to the original source of publication and a link is inserted to the published article on Springer's website. The link must be accompanied by the following text: "The final publication is available at link.springer.com”.

Springer

Author's personal copy

Jpn J Radiol
DOI 10.1007/s11604-016-0539-1

ORIGINAL ARTICLE

Fatal pleural mesothelioma in Japan (2003–2008): evaluation of computed tomography findings

Katsuya Kato[1,6] · **Kenichi Gemba**[2,7] · **Nobukazu Fujimoto**[2] · **Keisuke Aoe**[3] · **Yukio Takeshima**[4] · **Kouki Inai**[4,8] · **Takumi Kishimoto**[5]

Received: 4 February 2016 / Accepted: 14 March 2016
© Japan Radiological Society 2016

Abstract

Purpose The purpose of this study was to clarify the characteristic findings of mesothelioma at the time of diagnosis, and determine precautions and guidelines for diagnosing mesothelioma early in imaging studies.

Materials and methods Overall, 327 patients with pleural mesothelioma were selected from 6030 patients who died of mesothelioma between 2003 and 2008 in Japan. Their imaging findings were examined retrospectively.

Results Plaques were found in 35 % of computed tomography (CT) scans. Asbestosis, diffuse pleural thickening, and rounded atelectasis were found in only seven (2 %), five (2 %), and two cases (1 %), respectively. Pleural thickening findings on CT scans were classified into four stages: no irregularity, mild irregularity, high irregularity, and mass formation. Overall, 18 % of cases did not show a clear irregularity. Localized thickening was observed in the mediastinal (77 %) and basal (76 %) pleura and in the interlobar fissure (49 %). Eight percent of cases did not have any thickening in these three areas.

Conclusions Upon examination of the CT scans at diagnosis, 18 % of mesothelioma cases did not show a clear irregularity. When diagnosing pleural effusion of unknown etiology, it is necessary to consider the possibility of mesothelioma even when no plaque and pleural irregularity are observed.

Keywords Mesothelioma · Computed tomography · Japan

Introduction

Mesothelioma is a rare, asbestos-related disease [1, 2] with a poor prognosis [3]. Asbestos was used extensively in Japan for construction and industrial products owing to its useful characteristics; however, since the discovery of its carcinogenic potential, alternative products have been introduced and the manufacture and use of asbestos is now prohibited. It takes 30–40 years of incubation to develop mesothelioma or lung cancer originating from asbestos [4–7], and the number of patients with mesothelioma has been increasing over recent years; this has become a problem in many countries. The United States prohibited asbestos usage earlier compared to other countries, and the number of patients developing asbestos-related problems reached a peak there in 2004, with the number now decreasing. In Europe, the peak is expected be around 2015–2020, and in Japan, where the

✉ Katsuya Kato
kato-rad@med.kawasaki-m.ac.jp

[1] Department of Radiology, Okayama University Hospital, 2-1-1 Shikatacho, Okayama 7008558, Japan

[2] Department of Medical Oncology, Okayama Rosai Hospital, 1-10-25 Chikkomidorimachi, Okayama 7028055, Japan

[3] Department of Medical Oncology, National Hospital Organization Yamaguchi-Ube Medical Center, 685 Higashikiwa, Ube 7550241, Japan

[4] Department of Pathology, Hiroshima University Graduate School of Medicine, 1-2-3 Kasumi, Hiroshima 7340037, Japan

[5] Department of Internal Medicine, Okayama Rosai Hospital, 1-10-25 Chikkomidorimachi, Okayama 7028055, Japan

[6] Present Address: Department of Diagnostic Radiology 2, Kawasaki Medical School, 2-1-80 Nakasange, Kita-ku, Okayama 7008505, Japan

[7] Present Address: Department of Respiratory Medicine, Chugoku Chuo Hospital, 148-13 Miyukicho Oaza Kamiiwanari, Fukuyama 7200001, Japan

[8] Present Address: Pathologic Diagnostic Center, Inc., 11-28 Hacchobori, Naka-ku, Hiroshima 7300013, Japan

Published online: 25 March 2016

Author's personal copy

prohibition occurred later, the peak will be around 2025, which implies that the number of patients will keep increasing until this time [6]. In accordance with Japanese law, crocidolite and amosite usage was stopped in 1995; chrysotile usage was stopped in 2004. The country's recent discontinuation is evidence of the delay in asbestos regulations in our country, and the damage caused by these delays is apparent. A newspaper article published in June 2005 reported that five residents who lived near the now-closed asbestos cement pipe plant in Amagasaki, Japan, developed pleural mesothelioma [8]. Since this report, asbestos-related problems have raised significant social concern. We performed a nationwide retrospective survey to evaluate all cases of mesothelioma in Japan. As a result, we analyzed more than 6000 cases of mesothelioma that were registered in the Vital Statistics yearly survey performed by the Japanese Ministry of Health, Labour, and Welfare between 2003 and 2008. To the best of our knowledge, this is the largest study of Japanese cases of mesothelioma. Our study used images, mainly computed tomography (CT) and plain radiography, from deceased patients with pleural mesothelioma that were acquired with family and institutional permissions. In a review of the literature, we found no other reports examining the number of cases with mesothelioma and their images. The clinical features of the cases with mesothelioma in this study have already been reported [9]. The purpose of the current study was to clarify the characteristics of the imaging findings obtained at the time of the diagnosis of pleural mesothelioma, and determine precautions and guidelines for diagnosing mesothelioma early in imaging studies.

Subjects and methods

Study approval

This study was conducted according to the Ethical Guidelines for Epidemiological Research by the Japanese Ministry of Education, Culture, Sports, Science and Technology, and the Ministry of Health, Labor, and Welfare. The study was approved by the relevant institutional ethical review boards.

Patient selection and imaging studies

The methods of this retrospective survey have been previously described [9]. In brief, we requested and received authorization to view the death records in the Vital Statistics register in Japan, and we extracted all cases of death due to malignant mesothelioma between 2003 and 2008; in total, 6030 deaths were found to be due to mesothelioma. We contacted the closest living relatives of each patient to obtain consent for our study by postal mail. As a result, informed consent was obtained by mail from the relatives of 2069 patients (34.3 %). Subsequently, we contacted the patients' respective medical institutions to obtain the following information by mail: medical records, radiographs, and/or CT images. Different institutions had different types of CT images. We accepted both digital and film CT scans for review to examine as many cases as possible. We also reviewed the medical records and radiological images to confirm the clinical and pathological diagnoses of malignant mesothelioma.

Image interpretation

All patients underwent CT and plain radiography at the time of diagnosis of pleural mesothelioma. CT images were obtained using various CT scanners and a range of scan protocols at each institution. CT scans with a 5-mm thickness were the most common, but other slice thicknesses were found, ranging from 1 to 10 mm. Plain radiographs and CT images were retrospectively reviewed with consensus by three co-researchers: one chest radiologist and two pulmonologists. The chest radiologist (K.K.) had 24 years of experience and the two respiratory physicians (T.K. and K.G.) had 28 and 20 years of experience, respectively. Additionally, all three co-researchers had worked in a hospital that specialized in occupational respiratory disease for more than 10 years, and they were members of the official pneumoconiosis examination committee for laborers in the Okayama prefecture.

Evaluating items

First, pleural plaque and its calcification were evaluated on CT images. Pleural plaques were also assessed on plain chest radiographs of the same cases. Additionally, the images were checked for pleural effusion, lung asbestosis, diffuse pleural thickening, and rounded atelectasis.

Next, the pleural findings from the CT images were classified into four stages: no irregularity, mild irregularity, high irregularity, and mass formation. The four stages are shown in Fig. 1. No irregularity indicated that there was no pleural thickening found or that the thickening was ≤3 mm with no irregular surface. Mild irregularity indicated a regular surface with a thickening >3 mm but ≤5 mm; this stage also included cases of slight asperity with no clear nodular irregularity. Clinically, this was non-specific thickening due to either a benign or a malignant lesion. Mild irregular findings on CT may indicate benign pleural lesions such as pleurisy. High irregularity indicated a thickening >5 mm. Clear nodular thickening was required for this classification, and clinically, a malignancy was strongly suspected. Mass formation indicated that the irregularity was even more severe and that

Author's personal copy

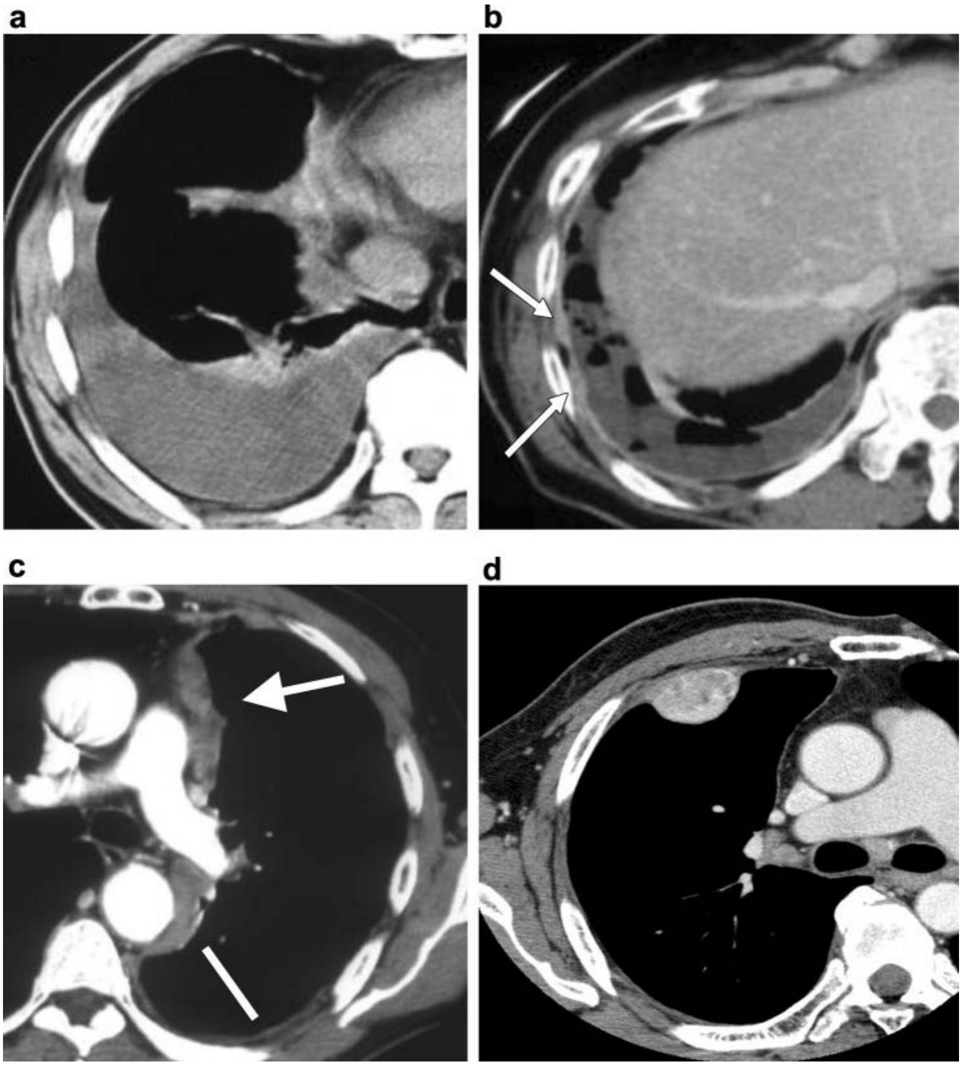

Fig. 1 **a** No irregularity: pleural effusion but no irregularity of the pleura. **b** Mild irregularity: a slight irregularity of the pleura; however, the irregularity does not indicate a severe irregularity, such as a malignancy. **c** High irregularity: severe irregular thickening of the pleura; a malignant lesion is suspected. **d** Mass formation: severe irregular thickening of the pleura, with clear mass formation; this finding suggests a malignant lesion

a partial mass with a diameter of >1 cm was clearly formed. We did not include massive irregularity in mass formation; we included only the CT findings that identified a clearly formed mass. We examined the entire pleura very carefully, because the grading of pleural irregularity changes even with a localized pleural thickening. Both multiple and isolated masses were defined as a mass formation; clinically, this indicated a malignant lesion.

When we considered the tumor (T) part of the tumor node metastasis classification of malignant tumors staging system, used by the International Mesothelioma Interest Group, for pleural mesothelioma, it was difficult to distinguish between T1 and T2 by using CT alone; therefore, T1 and T2 were considered a single group. Thus, our examination was based on three groups: T1–2, T3, and T4.

Following the staging classification, localization of the pleural lesions was examined; we evaluated for signs of mediastinal pleural lesions, which are characteristic of mesothelioma [10]. The interlobar pleura, where pleural lesions are more easily identified, and the basal lung, which frequently has lesions, were also examined for the presence of abnormalities (Fig. 2).

Statistical analysis

Statistical analysis was performed using the chi-squared test to analyze the correlation of each CT finding with the pathological diagnoses that were divided into the epithelial type and non-epithelial type. We considered $p < 0.05$ significant. Statistical calculations were performed using the SPSS statistical package, version 22.0 (IBM Corp., Armonk, NY, USA).

Results

Data from 1111 patients were obtained. We confirmed the clinical diagnosis of mesothelioma in 929 patients,

Author's personal copy

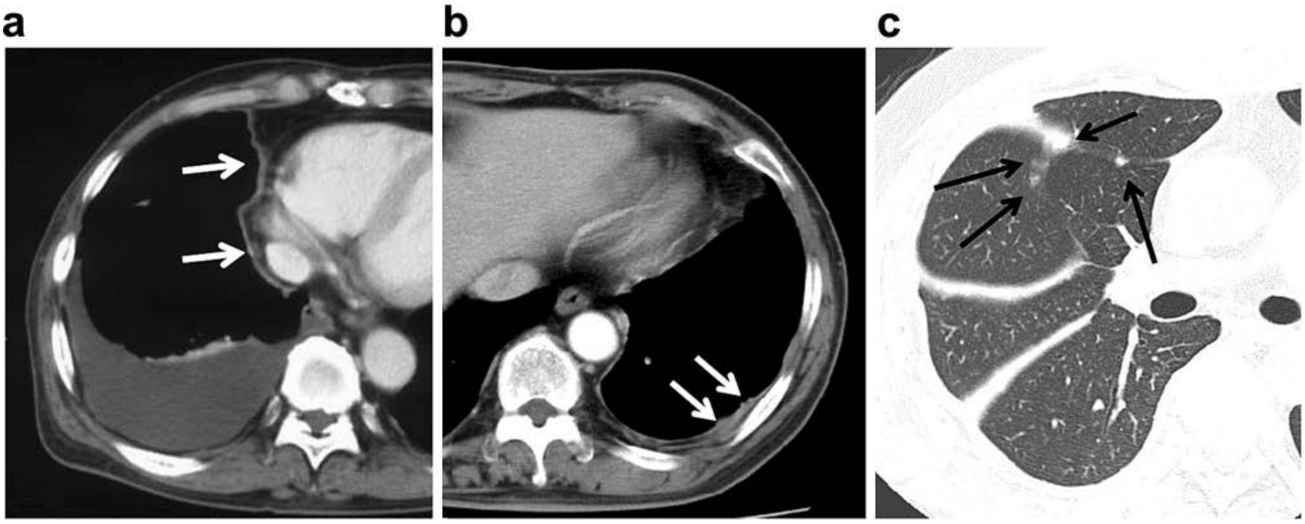

Fig. 2 **a** Mediastinal pleural irregularity: a thickened pleura with a slight irregularity in a broad area of the mediastinal pleura. The thickness is not severe in this classification, but if broad thickening is found in this area, a high potential for mesothelioma can be suspected. **b** Pleura irregularity in the base of the lungs: Tuberous irregular pleural thickening at the base of the left lung. A malignant pleural lesion can be suspected. **c** Irregular interlobar pleura: Tuberous thickening begins in the right interlobar pleura. The interlobar pleural layer is surrounded by lung parenchyma; therefore, the pleura can be easily evaluated on the images. High-resolution computed tomography (CT) can provide clearer images, but evaluation of the interlobar pleural irregularities is also possible using average CT scans, if carefully examined

including 753 men (81.1 %) and 176 women (18.9 %). The median age at diagnosis was 67.0 years (range, 16–94 years). The origin of mesothelioma was the pleura in 794 patients (85.5 %), peritoneum in 123 (13.2 %), pericardium in seven (0.8 %), and testicular tunica vaginalis in five (0.5 %). Of those 794 patients, 327 (273 men, 54 women; mean age, 68 years) had chest CT images obtained at the time of diagnosis; we examined those images (Fig. 3).

The histological subtypes of mesothelioma were determined in 327 cases based on the World Health Organization's criteria [11]: 176 (54 %) with epithelioid mesothelioma, 75 (23 %) with sarcomatoid mesothelioma, 59 (18 %) with biphasic mesothelioma, and 17 (5 %) with other types.

Pleural plaque was found on chest CT images of 114/327 patients (35 %), and 56 of those (49 %) had calcification. Plain chest radiographs showed that only 36 (11 %) of 327 patients had plaque.

Pleural effusion was found in 304 patients (93 %), but lung asbestosis, diffuse pleural thickening, and rounded atelectasis were only found in seven (2 %), five (2 %), and two patients (1 %), respectively.

Table 1 shows the classification of pleural findings into the four stages. Table 1 compares these four stages with the T classification system. Among the 327 cases of pleural mesothelioma, seven were classified with no irregularity (2 %); 53 with a mild irregularity that included a possible benign lesion (16 %); 140 with a high irregularity that included seemingly malignant lesions (43 %); and 127 with a mass formation that indicated a malignant lesion. Thus, 82 % of cases showed severe pleural irregularities on CT images that were indicative of a potential malignancy, and 18 % of cases did not have irregularities that were indicative of malignant lesions. All the cases with no irregularity were classified as T1–2; 49 cases (92 %) with a mild irregularity were also classified as T1–2. Cases with a mild pleural irregularity progressed slowly. However, cases with a high irregularity and mass formation had a high malignant potential; 78 % of cases with a high irregularity and 84 % of cases with a mass formation were classified as T3–4.

Lesion localization was as follows: the mediastinal pleura in 251 patients (77 %), base of the lungs in 250 (76 %), and interlobular pleura in 159 (49 %) (Table 2). Only 27 cases (8 %) had no lesions in the mediastinal and interlobular pleurae.

Statistically, there was no significant correlation between the CT findings and pathological subtypes (Table 2).

Discussion

Eighty percent of patients with pleural malignant mesothelioma are men [6, 12]. In the present study, 273 patients (83 %) were men. The high percentage of men in our study is similar to the finding of a previous report [6]. The age range of our study was extremely wide, ranging from 16–94 years at diagnosis. This wide age range indicates that cases of mesothelioma caused by environmental

Author's personal copy

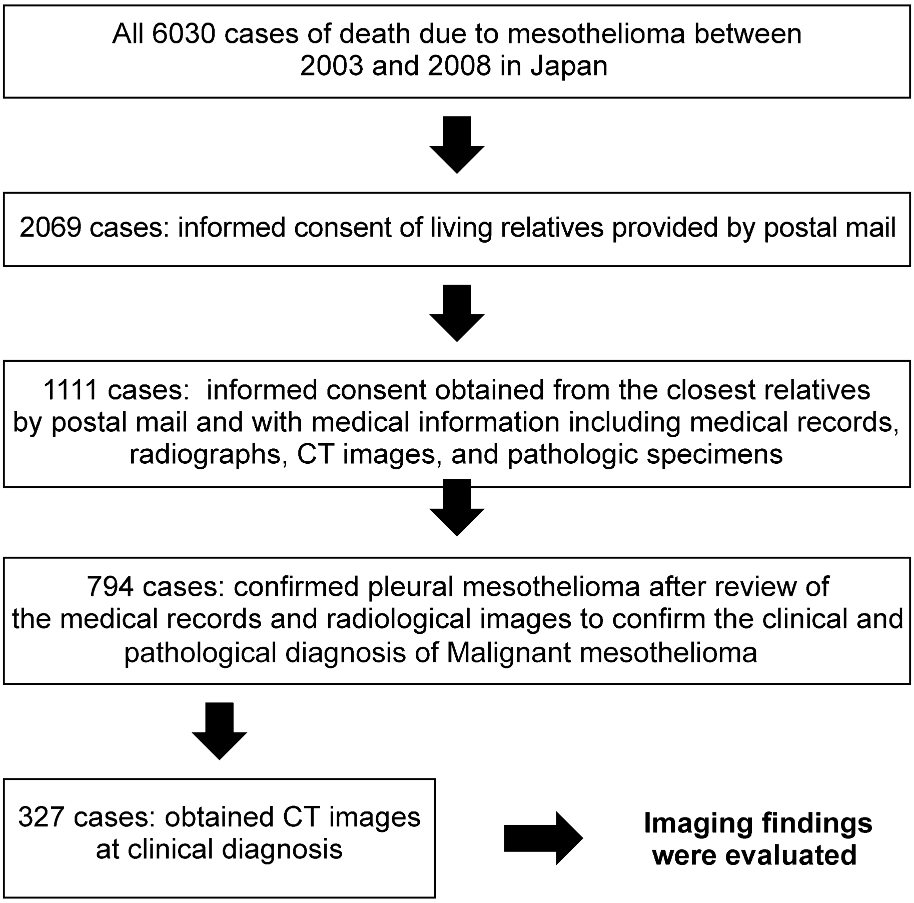
All 6030 cases of death due to mesothelioma between 2003 and 2008 in Japan
2069 cases: informed consent of living relatives provided by postal mail
1111 cases: informed consent obtained from the closest relatives by postal mail and with medical information including medical records, radiographs, CT images, and pathologic specimens
794 cases: confirmed pleural mesothelioma after review of the medical records and radiological images to confirm the clinical and pathological diagnosis of Malignant mesothelioma
327 cases: obtained CT images at clinical diagnosis
Imaging findings were evaluated

Fig. 3 Procedures used to select computed tomography images of the cases with pleural mesothelioma

Table 1 CT images at the time of the diagnosis of pleural mesothelioma and pleural findings from CT images at the time of the diagnosis pleural mesothelioma compared to the T classification system in 327 cases

Pleural findings	No irregularity	Mild irregularity	High irregularity	Mass formation
No. of cases	7	53	140	127
Percentage	2	16	43	39
T1–2	7	49	31	20
T3	0	4	89	58
T4	0	0	20	49

CT computed tomography, *no.* number

exposure were included in this study. The average latency period (i.e., the time interval between the first asbestos exposure and death) for mesothelioma development is 30–40 years [13]. Bianchi et al. [7] reported that the latency period ranges from 14–75 years (mean 48.8 years, median 51.0 years). This suggests that if the onset is diagnosed at 16 years old, the patient must have been exposed to the attributing environmental conditions since birth. This could be the case, for example, if the patient was born in a neighborhood with an asbestos factory. Due to this environmental exposure, juvenile mesothelioma would occur; these cases were also included in our study.

The image findings, mainly CT results, of 327 patients with pleural mesothelioma were selected from 6030 patients who died of mesothelioma between 2003 and 2008. Although there are a number of previous studies that have described the findings of pleural mesothelioma on CT scans [10, 13–16], no reports have evaluated the CT scans of as many as 327 patients by using uniform criteria. Therefore, the results of our study are of interest, as we present the first broad report on the results of mesothelioma on CT scans obtained at the time of the initial diagnosis.

Pleural plaque was observed in 35 % of the CT scans but in only 11 % of plain chest radiographs. Previous studies that used CT have shown pleural plaque in 12.1–78 % of cases [10, 14–16]. Additionally, only one-third of cases that had plaque on CT scans also had plaque on radiographs; this result is similar to that of a previous study [17]. Only

Author's personal copy

Table 2 Results of the statistical evaluation of the difference in CT findings between the epithelial type and non-epithelial type of mesothelioma

		Epithelial	Non-epithelial	*p* value (χ^2-test)
CT findings				
Asbestosis	+	3	4	0.523
	−	176	144	
Plaque	+	119	94	0.575
	−	60	54	
Rounded atelectasis	+	1	1	0.893
	−	178	147	
Diffuse pleural thickening	+	1	4	0.116
	−	178	144	
Pleural effusion	+	167	137	0.798
	−	12	11	
CT stages				
No irregularity		5	2	0.370
Mild irregularity–mass formation		174	146	
No irregularity–mild irregularity		36	24	0.365
High irregularity–mass formation		143	124	
No irregularity–high irregularity		75	52	0.212
Mass formation		104	96	

CT computed tomography, + positive, − negative

2 % of cases had pulmonary fibrosis equivalent to asbestosis in the current study. Asbestosis results from high-dose asbestos exposure. This examination was a national investigation that included patients who did not work with asbestos and those who worked in asbestos-related industries. Plaque was observed in only 35 % of cases. Therefore, we believe that the ratio of persons with a high concentration of asbestos exposure among the target cases was low.

Regarding pleural irregularities, 18 % of cases had either no irregularity (no clear malignancy on the image) or a mild irregularity (these cases were mainly T1–2). Although previous reports have described the pleural effusion occurrence rate [5, 18], to our knowledge, no reports to date have described the difficulties in diagnosing malignancy based on CT images among the more than 300 known cases. To make a successful early diagnosis, it is necessary to be aware that there could be cases with no irregularities among T1–2 cases. It is necessary to pay extra attention to the possibility of a mild pleural irregularity. According to the International Mesothelioma Interest Group staging system, the median overall survival (OS) rates for patients with stages I and II (T1–2 and N0), stage III, and stage IV tumors were 11.2 months (9.4–13.0 months), 7.9 months (7.1–8.7 months), and 3.9 months (3.0–4.6 months) (95 % confidence interval), respectively. The OS was significantly shorter for stage III patients than for stages I and II patients ($p < 0.001$); the OS was significantly shorter for stage IV patients than for stage III patients ($p < 0.001$) [8].

Regarding lesion localization, the mediastinal pleura was the most common site (77 % of cases). Abnormal findings were also observed in the basal lung and interlobular pleurae. Overall, lesions in these three sites encompassed 82 % of all cases. Mediastinal pleural lesions can be considered to have a relatively high specificity as malignant pleural lesions, and the basal lung and interlobar pleura are surrounded by lung parenchyma, which makes the evaluation of microlesions easier. Therefore, focusing on these three locations on CT images during diagnosis could improve the sensitivity and potential for diagnosing mesothelioma earlier.

There was no significant correlation between each CT finding and the pathological subtypes. Although the epithelial type of mesothelioma is associated with a better prognosis than the sarcomatous and biphasic subtypes [19], less irregularity subtype groups are not significantly correlated with the epithelial subtype of mesothelioma.

There are a number of limitations in our study. First, our study was retrospective, and the cases were collected from many institutions. Therefore, a variety of imaging devices and methods for both CT and plain radiography were used. However, because we evaluated CT images obtained with various scanners, our image evaluation process was simple; the principal objective was to identify irregular findings that the mesothelioma expert believed to be malignant. In Japan, there is a wide range of CT imaging techniques, but in most cases, an evaluable image was obtained. However, an advantage of this multi-center study was the large number of cases we were able to collect and examine. Secondly, the ability to diagnose mesothelioma differed among the hospitals. As the timing of the mesothelioma diagnosis varied according to the diagnostic ability of each institution, this may have introduced bias into our study; the progression of the mesothelioma lesion could be associated with a delay in diagnosis. Therefore, we speculate that the number of cases with mesothelioma with less severe irregularity findings would increase if each institution had made the diagnosis at an appropriate time. Additionally, in our study, we did not evaluate interobserver variation, thus this was a limitation too. However, all observers were adequately experienced with asbestos-related diseases, and thus good evaluation for radiologic images was performed.

In conclusion, 18 % of cases with mesothelioma in our study did not display a clear irregularity on CT images, and these cases were classified as low T-stage at the time of diagnosis. Therefore, when diagnosing pleural effusion of unknown etiology, the possibility of pleural mesothelioma

Author's personal copy

must be considered even in cases with no identifiable plaque. When the findings do not indicate a malignant lesion, we can still suspect potential mesothelioma when slight changes are observed in the mediastinal or interlobar pleura. Images of early-stage mesothelioma need to be interpreted accurately.

Acknowledgements This research was funded primarily by grants from the research foundation of the Ministry of Health, Labor, and Welfare of Japan (200500129A, 200635021A, 200733015A, 200733015B, 200836010A, 200938007A, and 201032004B) and by the Industrial Disease Clinical Research Grants from the Ministry of Health, Labor, and Welfare of Japan (1403101). This study is one of the research and development and dissemination projects related to the 13 fields of occupational injuries and illnesses of the Japan Health, Labor, and Welfare Organization. The sponsors had no involvement in the study design, collection, and analysis and interpretation of the data; writing of the manuscript; or decision to submit the manuscript for publication. We thank the living relatives of the patients with mesothelioma who provided consent; medical institutions that provided the medical information on the patients with mesothelioma; and Mrs. Rie Sugimoto, Mrs. Keiko Fujimura, Miss Naomi Ogura, and Miss Shiori Sato for collecting data.

Compliance with ethical standards

Conflict of interest The authors declare that they have no conflicts of interest.

Funding This research was funded primarily by grants from the research foundation of the Ministry of Health, Labor, and Welfare of Japan (200500129A, 200635021A, 200733015A, 200733015B, 200836010A, 200938007A, and 201032004B) and by Industrial Disease Clinical Research Grants from the Ministry of Health, Labor, and Welfare of Japan (1403101).

Ethical statement This study was conducted according to the Ethical Guidelines for Epidemiological Research by the Japanese Ministry of Education, Culture, Sports, Science and Technology, and the Ministry of Health, Labor, and Welfare. This study was approved by the Japan Health, Labor, and Welfare Organization and the institutional review boards of each institution. Patient confidentiality was strictly maintained. Informed consent was obtained from the closest living relatives of each patient.

References

1. Wagner JC, Sleggs CA, Marchand P. Diffuse pleural mesothelioma and asbestos exposure in the North Western Cape Province. Br J Ind Med. 1960;17:260–71.
2. Prazakova S, Thomas PS, Sandrini A, Yates DH. Asbestos and the lung in the 21st century: an update. Clin Respir J. 2014;8:1–10.
3. Muers MF, Stephens RJ, Fisher P, Darlison L, Higgs CM, Lowry E, et al. Active symptom control with or without chemotherapy in the treatment of patients with malignant pleural mesothelioma (MS01): a multicentre randomised trial. Lancet. 2008;371:1685–94.
4. Rusch VW. A proposed new international TNM staging system for malignant pleural mesothelioma from the International Mesothelioma Interest Group. Lung Cancer. 1996;14:1–12.
5. Metintas M, Ucgun I, Elbek O, Erginel S, Metintas S, Kolsuz M, et al. Computed tomography features in malignant pleural mesothelioma and other commonly seen pleural diseases. Eur J Radiol. 2002;41:1–9.
6. Robinson BW, Lake RA. Advances in malignant mesothelioma. New Engl J Med. 2005;353:1591–603.
7. Bianchi C, Brollo A, Ramani L, Bianchi T, Giarelli L. Asbestos exposure in malignant mesothelioma of the pleura: a survey of 557 cases. Ind Health. 2001;39:161–7.
8. Oshima H. 51 death asbestos-related illness in ten years. Mainichi Newspapers. 2005;1.
9. Gemba K, Fujimoto N, Aoe K, Kato K, Takeshima Y, Inai K, et al. Treatment and survival analyses of malignant mesothelioma in Japan. Acta Oncol. 2013;52:803–8.
10. Leung AN, Muller NL, Miller RR. CT in differential diagnosis of diffuse pleural disease. AJR Am J Roentgenol. 1990;154:487–92.
11. Churg A, Cagle PT, Roggli VL. Separation of benign and malignant mesothelial proliferations. In: AFIP Atlas of tumor pathology. Series 4. Tumors of the serosal membrane. Silver Springs: ARP Press; 2006. p. 83–101.
12. Roe OD, Stella GM. Malignant pleural mesothelioma: history, controversy and future of a manmade epidemic. Eur Respir Rev. 2015;24:115–31.
13. Erzen C, Eryilmaz M, Kalyoncu F, Bilir N, Sahin A, Baris YI. CT findings in malignant pleural mesothelioma related to nonoccupational exposure to asbestos and fibrous zeolite (erionite). J Comput Assist Tomogr. 1991;15:256–60.
14. Kawashima A, Libshitz HI. Malignant pleural mesothelioma: CT manifestations in 50 cases. AJR Am J Roentgenol. 1990;155:965–9.
15. Senyiğit A, Bayram H, Babayiğit C, Topcu F, Nazaroglu H, Bilici A, et al. Malignant pleural mesothelioma caused by environmental exposure to asbestos in the Southeast of Turkey: CT findings in 117 patients. Respiration. 2000;67:615–22.
16. Seely JM, Nguyen ET, Churg AM, Müller NL. Malignant pleural mesothelioma: computed tomography and correlation with histology. Eur J Radiol. 2009;70:485–91.
17. Staples CA. Computed tomography in the evaluation of benign asbestos-related disorders. Radiol Clin North Am. 1992;30:1191–207.
18. Okten F, Koksal D, Onal M, Ozcan A, Simsek C, Erturk H. Computed tomography findings in 66 patients with malignant pleural mesothelioma due to environmental exposure to asbestos. Clin Imaging. 2006;30:177–80.
19. Meyerhoff RR, Yang CF, Speicher PJ, Gulack BC, Hartwig MG, D'Amico TA, et al. Impact of mesothelioma histologic subtype on outcomes in the surveillance, epidemiology, and end results database. J Surg Res. 2015;196:23–32.

Drug Discoveries & Therapeutics. 2016; 10(2):114-116.

Case Report

DOI: 10.5582/ddt.2016.01005

Angiosarcoma of the thoracic wall responded well to nanoparticle albumin-bound paclitaxel: A case report

Naofumi Hara[1], Nobukazu Fujimoto[2,*], Yosuke Miyamoto[1], Tomoko Yamagishi[1], Michiko Asano[1], Yasuko Fuchimoto[1], Sae Wada[1], Shinji Ozaki[1], Hideyuki Nishi[3], Takumi Kishimoto[4]

[1] *Department of Respiratory Medicine, Okayama Rosai Hospital, Okayama, Japan;*
[2] *Department of Medical Oncology, Okayama Rosai Hospital, Okayama, Japan;*
[3] *Department of Surgery, Okayama Rosai Hospital, Okayama, Japan;*
[4] *Department of Internal Medicine, Okayama Rosai Hospital, Okayama, Japan.*

Summary **An 81-year-old woman visited a local clinic due to chest pain and a skin induration on the right precordia. She had a history of right breast cancer, and she had undergone a mastectomy and radiation therapy 10 years prior. Computed tomography (CT) imaging of the chest demonstrated a lobular mass that involved the right anterior thoracic wall and partially extruded from the thoracic cavity into the subcutaneous tissue. The tumor was surgically excised, and pathological analyses yielded a diagnosis of angiosarcoma. Five months after the operation, CT imaging showed multiple masses on the right pleura, indicating a local relapse and pleural dissemination of the angiosarcoma. Systemic chemotherapy composed of nanoparticle albumin-bound paclitaxel (nab-PTX) (80 mg/m^2) was delivered weekly. After 4 courses of chemotherapy, the tumors regressed remarkably. Nab-PTX may be an effective treatment option for recurrent or metastatic angiosarcoma.**

Keywords: Angiosarcoma, paclitaxel, chemotherapy

1. Introduction

Angiosarcoma is an extremely rare malignant vessel tumor that comprises 1% of all soft tissue sarcomas (*1*). It develops in subcutaneous tissue at many sites in the body, and a previous medical history of trauma, breast cancer, and/or radiotherapy are considered risk factors for the disease. Localized tumors are treated with surgical removal. However, for recurrent and unresectable conditions, there is limited evidence to support chemotherapy regimens. Here, we describe a patient with angiosarcoma that developed in the thoracic wall, which responded well to systemic chemotherapy composed of nanoparticle albumin-bound paclitaxel (nab-PTX).

2. Case report

An 81-year-old woman was referred to our hospital for an examination due to right chest pain. She had a history of right breast cancer and had undergone a mastectomy and adjuvant radiotherapy 10 years prior. Upon examination, a skin induration with tenderness was found on the right precordia. Computed tomography (CT) imaging of the chest demonstrated right pleural effusion and a lobular mass that involved the right anterior thoracic wall; this mass had partially extruded from the thoracic cavity into the subcutaneous tissue (Figure 1A). On enhanced CT images, the mass showed a contrast effect in the early stages of the arterial phase. The tumor was surgically excised. Pathological analyses of the tumor showed disarrayed growth of hyperchromatic and vasoformative mesenchymal tumor cells with abnormal mitosis (Figure 2A). Immunohistochemical analyses revealed that the cells were positive for CD31 (Figure 2B) and CD34 (Figure 2C), but negative for epithelial markers, S-100 (Figure 2D) and D2-40 (Figure 2E). Based on these findings, the diagnosis was confirmed as angiosarcoma. Five months after the operation, CT images showed

---

Released online in J-STAGE as advance publication February 15, 2016.

**Address correspondence to:*
Dr. Nobukazu Fujimoto, Department of Medical Oncology, Okayama Rosai Hospital, 1-10-25 Chikkomidorimachi, Okayama 702-8055, Japan.
E-mail: nobufujimot@gmail.com

multiple masses on the right pleura, indicating a local relapse and pleural dissemination of the angiosarcoma (Figure 1B). Systemic chemotherapy composed of nab-PTX (80 mg/m^2) was delivered weekly. After 4 courses of chemotherapy, the masses in the pleura regressed remarkably (Figure 1C). The only adverse event was alopecia, no myelosuppression or neurotoxicity was observed. After a total of 14 courses of chemotherapy, multiple tumors reappeared, and the patient died at 18 months after the initial diagnosis. Autopsy was not allowed.

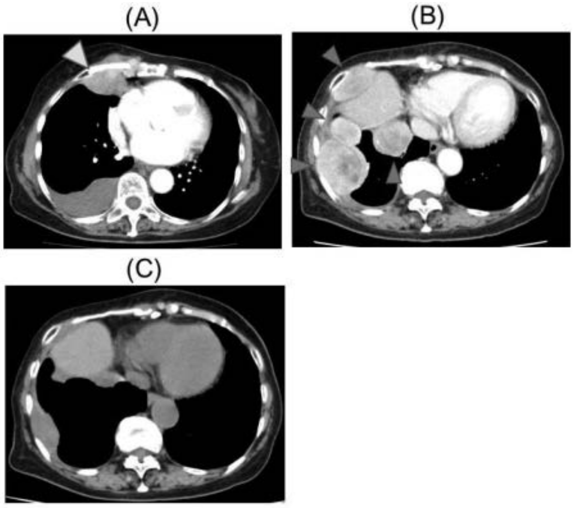

Figure 1. Computed tomography images of the chest. (A) Right pleural effusion and a lobular mass (white arrowhead) were observed at the initial examination. **(B)** Multiple masses on the right pleura (red arrowheads) appeared 5 months after the operation. **(C)** Regressed masses on the pleura after 4 courses of chemotherapy.

3. Discussion

Angiosarcoma is an uncommon malignant vessel tumor. Angiosarcoma can develop in the subcutaneous tissue in almost all parts of the body, but the most common sites are the head and neck, followed by the breast and liver (*2*). Angiosarcoma of the pleura is extremely rare (*3*). A history of breast cancer and radiation therapy are known risk factors for this disease (*4,5*), and both these factors were present in the current case study. There is limited evidence to support chemotherapy regimens for unresectable and recurrent angiosarcomas; however, a few reports have suggested that anthracyclines, ifosfamide, and taxanes are potential treatment options. A retrospective study showed that, when paclitaxel was used to treat unresectable angiosarcomas, progression-free survival was achieved for 6.8 months for scalp angiosarcoma and 2.8 months for sites below the clavicle (*6*). Nab-PTX is a novel, soluble, polyoxyethylated, castor oil-free, biologically interactive form of paclitaxel, which allows shorter infusion times and requires no premedication for hypersensitive reactions. Nab-PTX has been approved for breast cancer (*7*), non-small cell lung cancer (*8*), and gastric cancer (*9*) in Japan. Moreover, in the future, it will be used in more patients as an alternative to PTX. In the current case, nab-PTX was delivered to an aged patient with recurrent angiosarcoma that had disseminated in the pleura. This

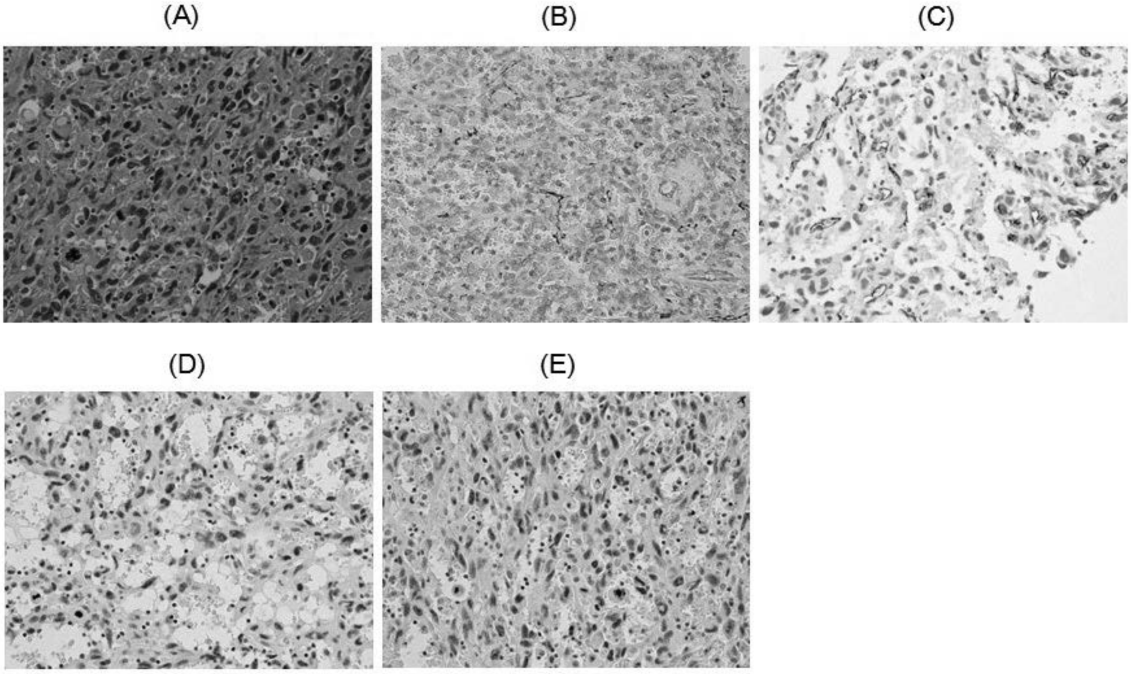

Figure 2. Pathological analyses. (A) Resected tumor specimen showed disarrayed growth of hyperchromatic and vasoformative mesenchymal tumor cells with abnormal mitosis (×40). Immunohistochemical analyses revealed that the cells were positive for CD31 **(B)** and CD34 **(C)**, but negative for epithelial markers, S-100 **(D)** and D2-40 **(E)** (×40).

treatment elicited a favorable response and few adverse events, though the tumor acquired resistance eventually. To our knowledge, the current case was the first to show that angiosarcoma significantly responded to nab-PTX. Our results suggested that weekly administration of nab-PTX may be an effective treatment option for recurrent angiosarcoma.

In conclusion, we described a case of angiosarcoma in the pleura, which showed a significant response to nab-PTX.

Acknowledgements

Supported by "The research, development, and dissemination of projects related to nine fields of occupational injuries and illnesses" of the Japan Labour Health and Welfare Organization and by grants-in-aid from the Ministry of Health, Labor and Welfare, Japan.

References

1. Wanebo HJ, Koness RJ, MacFarlane JK, Eilber FR, Byers RM, Elias EG, Spiro RH. Head and neck sarcoma: report of the Head and Neck Sarcoma Registry. Society of Head and Neck Surgeons Committee on Research. Head Neck. 1992; 14:1-7.
2. Albores-Saavedra J, Schwartz AM, Henson DE, Kostun L, Hart A, Angeles-Albores D, Chable-Montero F. Cutaneous angiosarcoma. Analysis of 434 cases from the Surveillance, Epidemiology, and End Results Program, 1973-2007. Ann Diagn Pathol. 2011; 15:93-97.
3. Zhang S, Zheng Y, Liu W, Yu X. Primary epithelioid angiosarcoma of the pleura: a case report and review of literature. Int J Clin Exp Pathol. 2015; 8:2153-2158.
4. Karlsson P, Holmberg E, Johansson KA, Kindblom LG, Carstensen J, Wallgren A. Soft tissue sarcoma after treatment for breast cancer. Radiother Oncol. 1996; 38:25-31.
5. Blanchard DK, Reynolds C, Grant CS, Farley DR, Donohue JH. Radiation-induced breast sarcoma. Am J Surg. 2002; 184:356-358.
6. Fury MG, Antonescu CR, Van Zee KJ, Brennan MF, Maki RG. A 14-year retrospective review of angiosarcoma: clinical characteristics, prognostic factors, and treatment outcomes with surgery and chemotherapy. Cancer J. 2005; 11:241-247.
7. Gradishar WJ, Tjulandin S, Davidson N, Shaw H, Desai N, Bhar P, Hawkins M, O'Shaughnessy J. Phase III trial of nanoparticle albumin-bound paclitaxel compared with polyethylated castor oil-based paclitaxel in women with breast cancer. J Clin Oncol. 2005; 23:7794-7803.
8. Rizvi NA, Riely GJ, Azzoli CG, Miller VA, Ng KK, Fiore J, Chia G, Brower M, Heelan R, Hawkins MJ, Kris MG. Phase I/II trial of weekly intravenous 130-nm albumin-bound paclitaxel as initial chemotherapy in patients with stage IV non-small-cell lung cancer. J Clin Oncol. 2008; 26:639-643.
9. Koizumi W, Morita S, Sakata Y. A randomized Phase III trial of weekly or 3-weekly doses of nab-paclitaxel versus weekly doses of Cremophor-based paclitaxel in patients with previously treated advanced gastric cancer (ABSOLUTE Trial). Jpn J Clin Oncol. 2015; 45:303-306.

(Received January 5, 2016; Revised February 8, 2016; Accepted February 9, 2016)

European Journal of Radiology 85 (2016) 1594–1600

Contents lists available at ScienceDirect

European Journal of Radiology

journal homepage: www.elsevier.com/locate/ejrad

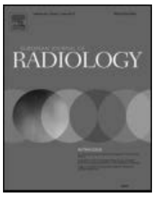

Pleural irregularities and mediastinal pleural involvement in early stages of malignant pleural mesothelioma and benign asbestos pleural effusion

Katsuya Kato[a,*], Kenichi Gemba[b,1], Nobukazu Fujimoto[b], Keisuke Aoe[c],
Yukio Takeshima[d], Kouki Inai[d,2], Takumi Kishimoto[e]

[a] *Department of Radiology, Okayama University Hospital, 2-1-1 Shikatacho, Okayama 7008558, Japan*
[b] *Department of Medical Oncology, Okayama Rosai Hospital, 1-10-25 Chikkomidorimachi, Okayama 7028055, Japan*
[c] *Department of Medical Oncology, National Hospital Organization Yamaguchi-Ube Medical Center, 685 Higashikiwa, Ube 7550241, Japan*
[d] *Department of Pathology, Hiroshima University Graduate School of Medicine, 1-2-3 Kasumi, Hiroshima 7340037, Japan*
[e] *Department of Internal Medicine, Okayama Rosai Hospital, 1-10-25 Chikkomidorimachi, Okayama 7028055, Japan*

ARTICLE INFO

Article history:
Received 8 March 2016
Received in revised form 23 May 2016
Accepted 19 June 2016

Keywords:
Mesothelioma
Benign asbestos pleural effusion
CT scan

ABSTRACT

Objective: To elucidate differences in the level and localization of pleural irregularities in early malignant pleural mesothelioma (eMPM) and benign asbestos pleural effusion (BAPE) using CT.

Study design: Retrospective assessment of CT findings of consecutive patients with BAPE at a single centre and patients with eMPM reported in Japanese vital statistics.

Methodology: Thirty-six patients with confirmed diagnoses of BAPE and sixty-six patients with confirmed diagnoses of eMPM (mesothelioma stages T1 or T2) were included. Informed consent, CT scans, and clinical and pathologic details were obtained for all patients and were reviewed by one radiologist, two pathologists, and two pulmonologists. Asbestosis, pleural plaque, rounded atelectasis, and diffuse pleural thickening were assessed in all patients.

Results: Prevalence of asbestosis, pleural plaque, rounded atelectasis, and diffuse pleural thickening was significantly higher in the BAPE group. Low-level irregularity was more common in the BAPE group ($p < 0.001$), whereas high-level irregularity, mediastinal localization, and interlobar fissure were more prevalent in the eMPM group ($p < 0.001$). Interlobar pleural irregularity was not observed in any patients in the BAPE group, although 55% of patients in the eMPM group showed interlobar pleural irregularity. Mediastinal pleural involvement was observed in 74% of patients in the eMPM group and had a positive predictive value of 89%.

Conclusion: This study demonstrates that the level and localization of plural irregularities significantly differed between patients with BAPE and eMPM. Large-scale prospective studies are needed to fully establish the diagnostic utility of such differences.

© 2016 Elsevier Ireland Ltd. All rights reserved.

1. Introduction

Malignant pleural mesothelioma (MPM) is a neoplasm of mesodermal origin and is associated with exposure to asbestos [1]. MPM has a poor prognosis, but detection in early stages can significantly increase patient survival, as distant metastasis occurs at considerably later stages. Unfortunately, however, the diagnosis of MPM is often delayed, either because of nonspecific symptoms or the unreliability of radiological imaging and pleural biopsy techniques [2]. In particular, the variability of pleural findings makes features of anatomical imaging modalities complicated [3], leading to poor differential diagnosis with benign tumours and with other malignant tumours, such as sarcomas and adenocarcinomas [4–6].

Benign asbestos pleural effusion (BAPE) is a complication of chronic exposure to asbestos. It is generally classified as the accumulation of pleural fluid and may be asymptomatic or associated with pain, fever, and dyspnoea. Differentiation of BAPE from early stages of MPM is difficult, due to several overlapping radiological features [7,8]. Considerable work has been conducted to discern

---

[*] Corresponding author at: Department of Diagnostic Radiology 2, Kawasaki Medical School, 2-1-80 Nakasange, Kita-ku, Okayama 700-8505, Japan.
E-mail address: kato-rad@med.kawasaki-m.ac.jp (K. Kato).

[1] Present address: Department of Respiratory Medicine, Chugoku Chuo Hospital, Fukuyama, Japan.

[2] Present address: Pathologic Diagnostic Center, Inc., Hiroshima, Japan.

http://dx.doi.org/10.1016/j.ejrad.2016.06.013
0720-048X/© 2016 Elsevier Ireland Ltd. All rights reserved.

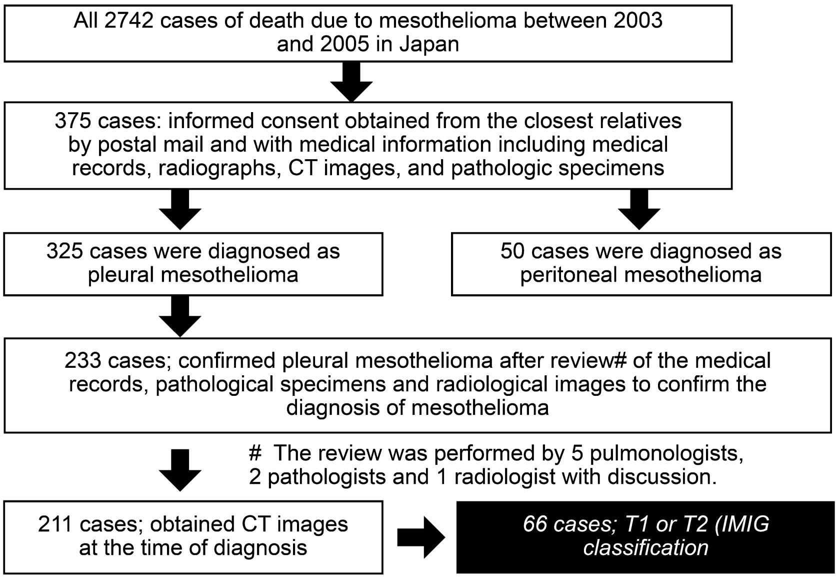
All 2742 cases of death due to mesothelioma between 2003 and 2005 in Japan
375 cases: informed consent obtained from the closest relatives by postal mail and with medical information including medical records, radiographs, CT images, and pathologic specimens
325 cases were diagnosed as pleural mesothelioma
50 cases were diagnosed as peritoneal mesothelioma
233 cases; confirmed pleural mesothelioma after review# of the medical records, pathological specimens and radiological images to confirm the diagnosis of mesothelioma
# The review was performed by 5 pulmonologists, 2 pathologists and 1 radiologist with discussion.
211 cases; obtained CT images at the time of diagnosis
66 cases; T1 or T2 (IMIG classification

Fig. 1. Flow chart summarizing enrolment of patients in eMPM group.

distinct features of MPM and BAPE, using different diagnostic modalities including X-ray, PET, MRI, and CT [9–11]. However, confirmatory diagnoses of MPM mostly still depend on histopathologic evaluations of biopsy specimens, even though the procedure is associated with complications [12].

In Japan, the production and application of asbestos have been prohibited since 2004. However, since asbestos-related diseases have long latency periods, the number of mesothelioma patients has increased in recent years [13–15]. Evidence suggests that it takes 30–40 years of incubation to develop mesothelioma after exposure to asbestos. It has therefore been postulated that the number of MPM patients in Japan will peak in 2025. The trend is in line with other advanced countries, as in the past, asbestos was used extensively for construction and industrial products [16,17]. We researched the Vital Statistics survey carried out by the Japanese Ministry of Health, Labour, and Welfare and found more than 6000 mesothelioma cases [17]. These statistics, along with the diagnostic issues outlined above, clearly stress an immediate need for efficient strategies for the early diagnosis and management of MPM.

Computed tomography (CT) has been used as a non-invasive tool for diagnosing, staging, and following-up MPM. Asbestos exposure may lead to pleural effusion, pleural thickening, and pleural plaques, which can be effectively diagnosed using CT scans [18]. However, the differences between the CT features of benign and malignant pleural diseases are poorly understood [3,4,19]. The purpose of this study was to evaluate the differences between the CT findings of patients diagnosed with stage I and II MPM and patients diagnosed with BAPE. We also attempted to assess changes in the grade of pleural irregularity, localization of pleural irregularity, and changes in CT scan features during follow-up.

2. Subjects and methods

2.1. BAPE group

Thirty-six patients who were referred to the Okayama Rosai Hospital between Mar 1, 2005 and Apr 30, 2008 and who had a definitive diagnosis of BAPE were included. BAPE was indicated by symptoms including chronic cough, abnormal pulmonary function tests, chest pain, breathlessness, hoarseness of the voice, and CT scan results. All patients had a history of asbestos exposure. Pleural biopsy was performed in all cases. All pathologic specimens were reviewed by a pathologist, and the histological assessment of malignancy was made on the basis of standard cytological tests. BAPE was defined on the basis of four criteria: (a) history of asbestos exposure, (b) radiologic or thoracentesis confirmation of pleura, (c) absence of another cause for the pleural effusion, and (d) no malignant tumour developing within one year [20–22]. Follow-up was conducted through routine visits. Informed consent was obtained from all patients, and the Institutional Ethical Review Board of Okayama Rosai Hospital approved the study.

The CT scans were obtained using X-vigor in 6 cases and Aquilion$^{\mathrm{TM}}$32 (Toshiba Medical Systems, Otawara, Tochigi, Japan) in 30 cases. Patients were screened in the supine position with or without injection of contrast media, depending on the radiologists' judgment; 9 cases were screened without contrast media, while 24 cases used it and 3 cases were screened both with and without contrast media. A slice thickness of 5 mm and mediastinal and lung parenchymal window settings were used. The window width was 1500 HU for parenchymal imaging and 350 HU for soft tissues. Parenchymal and soft tissue images were reconstructed with sharp and smooth filters, respectively. Intravenous iodinated contrast medium was used to determine lymph node enlargement and pleural irregularities. The CT scans and accompanying chest radiographs were reviewed by one radiologist and two pulmonologists (K. K., T. K., and N. F.) who were familiar with asbestos-related disease and who were members of the official pneumoconiosis examination committee for labourers in the Okayama prefecture. The observers were unaware of the pathologic diagnosis; a conclusion was reached by consensus.

2.2. Early MPM (eMPM) group

Sixty-six patients were included in the early MPM group. The subjects were selected from mesothelioma death cases in the Japanese Vital Statistics (2003–2005). The detailed method for patient selection and data collection has been described elsewhere [23]. In brief, we extracted all cases of death due to malignant mesothelioma in the Vital Statistics register in Japan (2003–2005). Informed consent was obtained from living relatives, and complete medical records, radiographs, and/or CT images were obtained from the respective medical institutions. We reviewed medical records and radiological images with clinically and pathologically confirmed diagnoses of malignant mesothelioma based on ICD CD46.

Table 1
Characteristics of patients in BAPE and eMPM groups.

Characteristic	Total (n = 102)	BAPE (n = 36)	eMPM (n = 66)	P value
Age, years (Mean ± SD)	69.3 ± 9.3	72.0 ± 7.2	67.8 ± 10.1	0.0297
Sex (M/F)	92/10	36/0	56/10	0.0133
History of asbestos exposure, years (Mean ± SD)	24.1 ± 15.9	28.1 ± 14.7	16.6 ± 17.0	0.0009
Latency, years (Mean ± SD)	31.3 ± 21.6	46.3 ± 11.5	24.0 ± 21.6	0.0001
eMPM histological subtype				
Epithelioid			41 (62.12%)	
Sarcomatoid			8 (12.12%)	
Biphasic			12 (18.18%)	
Unknown			5 (7.58%)	

Table 2
Clinical imaging characteristics in BAPE and eMPM groups.

	BAPE (n = 36)	eMPM (n = 66)	P value	
Asbestosis		6 (17%)	1 (2%)	< 0.05
PR classification	PR1	4	1	
	PR2	1	0	
	PR3	1	0	
Pleural plaque		33 (92%)	23 (35%)	<0.001
Calcification (+)		25	10	
Rounded atelectasis		16 (44%)	0 (0%)	<0.001
Diffuse pleural thicknesses		9 (25%)	1 (2%)	<0.001
Pleural effusion		36 (100%)	64 (97%)	0.291

PR: profusion rate.

Thirty-four cases were screened without contrast media, while 27 cases used contrast media, and 5 cases were screened both with and without contrast media. Patients with incomplete CT findings were excluded. All CT scans were retrospectively reviewed at our institution by one radiologist and two pulmonologists (K. K., T. K., and K. G.) who were familiar with asbestos-related disease and who were members of the official pneumoconiosis examination committee for labourers in the Okayama prefecture. The TNM Classification of Malignant Tumors staging system used by the International Mesothelioma Interest Group (IMIG) for pleural mesothelioma was used to stage MPM [24]. Only patients with stage T1 and T2 tumours were included in the analysis (Fig. 1).

2.3. *Pleural findings*

The images were analysed to identify pleural plaques and calcification, pleural effusion, lung asbestosis, diffuse pleural thickening, and rounded atelectasis. Pleural plaques were defined as circumscribed, pleural areas of opacity with well-demarcated edges [25]. The pleural findings from the CT images were classified into four stages: “no irregularity”,” low-level irregularity”, “high-level-irregularity”, and” mass formation”. These four stages are shown in Supplementary Figs. 1–4. “No irregularity” indicated complete absence of pleural thickening or thickening ≤3 mm with no irregular surface. “Low-level irregularity” indicated a regular surface with a thickening >3 mm but ≤1 cm; this stage also included cases of slight asperity with no clear nodular irregularity <5 mm. Clinically, this was non-specific thickening due to either a benign or a malignant lesion. Mild irregular findings on CT may indicate benign pleural lesions such as pleurisy. “High-level-irregularity” indicated a regular thickening >1 cm, an irregular thickening >5 mm, and clear nodularity >3 mm but not “mass formation”. For an irregular thickening, slight asperity was required for this classification. Clinically “high–level irregularities” have a high index of suspicion for malignancy. “Mass formation” indicated a clearly formed partial mass with a diameter of >1 cm. We examined the entire pleura very carefully, to ensure careful grading of pleural irregularity changes, even with localized pleural thickening. Both multiple and isolated masses were defined as mass formation; clinically, this indicated a malignant lesion [17]. Metintas et al. showed that thicknesses >1 cm were not a meaningful variable in univariate analyses [9]. In this work, we therefore proposed criteria based on much lower pleural thickening (no irregularities ≤3 mm; low-level irregularities >3 mm but ≤5 mm, high-level >5 mm, and mass formation was noted at >1 cm). We believe that these criteria can be useful for the diagnosis of the early stages of MPM (I & II) [26]. In the case of the BAPE and eMPM groups, all pleural thickenings were measured on the monitor with electronic callipers in the DICOM medical image viewer at an appropriate digital magnification. In the BAPE group, all measurements were made with the Synapse medical imaging and information management system (Fuji Medical, Tokyo, Japan). In the eMPM group, when digital data were available, measurements were performed in the POP-net system (Image ONE, Tokyo, Japan). When digital images were not available, we measured the numbers of pixels in a 1 cm scale on the scanned film and used the pixels in the pleura to calculate the thickness of the pleura. All cases where diffuse pleural thickening was observed involved contrast CT, and we could differentiate thickened pleura from the collapsed lung.

2.4. *Statistical analysis*

Statistical analysis was carried out using the SPSS 20 software. Descriptive statistical tests were used for analysis of data. Unpaired *t*-tests and Mann-Whitney tests were used to compare differences. P values less than 0.05 were considered to be statistically significant.

3. Results

Thirty-six patients (all males), with a mean age of 72.0 years, were included in the BAPE group, and sixty-six patients, with a mean age 67.8 years, were included in the eMPM group. In the BAPE group, histopathological results indicated chronic inflammation in the majority of cases; the average history of exposure to asbestos was 28.1 years and the mean latency (the gap between exposure to asbestos and diagnosis) was 46.3 years. In the eMPM group, complete data and informed consent were obtained from

Table 3
Grade of pleural irregularity in BAPE and eMPM groups.

	BAPE (n = 36)	eMPM (n = 66)	P value
No irregularity	8 (22%)	6 (9%)	<0.001#
Low-level irregularity	26 (72%)	36 (54%)	
High-level irregularity	2 (5%)	15 (23%)	<0.001*
Mass formation	0 (0%)	9 (14%)	

Low-level irregularity" indicated a regular surface with a thickening >3 mm but ≤1 cm, and "High-level-irregularity" indicated a regular thickening >1 cm, or an irregular thickening >5 mm, and clear nodularity >3 mm but not "mass formation".
#No- and low-level pleural irregularity together (BAPE vs. eMPM: 94.4% vs. 63.6%; P < 0.001).
*High-level pleural irregularity and mass formation together (BAPE vs. eMPM: 5.5% vs. 36.4%; P < 0.001 (χ^2 test).

Table 4
Localization of pleural irregularity in BAPE and eMPM groups.

	BAPE (n = 36)	eMPM (n = 66)	P value
Mediastinal	8 (22%)	49 (74%)	<0.001
Basal	32 (91%)	51 (77%)	0.150
Interlobar fissure	0 (0%)	36 (55%)	<0.001

1111 patients, and thoracoscopic biopsy, pleural biopsy, and pleural fluid cytology confirmed the diagnosis of stage I and stage II MPM in 66 patients. The mean age at diagnosis was 67.8 years, and the origin of eMPM was epithelioid in 41 cases, sarcomatoid in 8 cases, biphasic in 12 cases, and unknown in 5 cases. Of the eMPM subjects, 60.6% had an occupational exposure to asbestos, with a mean duration of exposure of 16.6 years and a mean latency of 24.0 years (Table 1).

Asbestosis was found in 6 patients in the BAPE group, and the incidence was higher than that observed in the eMPM group. The prevalence of pleural plaque was notably higher in the BAPE group. Rounded atelectasis and diffuse pleural thickening were also significantly more common in the BAPE group, although there was no significant difference in pleural effusion (Table 2).

The grades of pleural irregularity are presented in Table 3. No irregularity was found in 22% of the BAPE group and 9% of the eMPM group. No mass formation was observed in the BAPE group, but it was found in 14% of patients in the eMPM group. Interestingly, no- or low-level pleural irregularity together were more prevalent in the BAPE group and high-level pleural irregularity and mass formation together were more prevalent in the eMPM group

Table 4 presents the locations of pleural irregularity. Mediastinal and interlobar fissure were found to be statistically different between the two groups. Interlobar pleural fissure was not observed in any of the patients in the BAPE group, although 55% of patients in the eMPM group had interlobar pleural fissure (P < 0.001). Mediastinal pleural involvement was observed in 74% of patients in the eMPM group and just 22% in the BAPE group (P < 0.001); notably, mediastinal involvement had a sensitivity of 79.5%, specificity of 81%, positive predictive value of 89%, and negative predictive value of 68% for eMPM diagnosis. Basal irregularities were higher in the BAPE group (91% vs. 77%), although the difference did not reach statistical significance.

In addition to differences in pleural irregularity, location, and plaques in the BAPE and eMPM groups, a significant difference was observed in the pleural parameters during follow-up. In patients diagnosed with BAPE, pleural irregularities either regressed or remained unchanged, whereas in patients diagnosed with eMPM, pleural irregularities were found to worsen or remain unchanged during follow-up. Fig. 2 presents a representative case of a patient in the BAPE group who had shown high-level unilateral pleural irregularities at diagnosis. During the 5-year follow-up period, the level of pleural irregularities remained high, with little change in features. Fig. 3(A–D) shows changes in the CT scan features during follow-up of two patients in the BAPE group. One patient showed bilateral mediastinal pleural thickening at diagnosis, which significantly regressed within two months in both axial and coronal CT scans. In another patient (Fig. 3C,D), unilateral mediastinal pleural thickening and effusion in the right thorax was observed at presentation and significantly regressed before the CT scan recorded 3 months later. Fig. 4 shows a CT scan of a patient in the eMPM group at presentation and follow-up; CT findings did not indicate any regression of pleural irregularities. Fig. 5 shows a CT scan of another patient diagnosed with eMPM at presentation and at follow-up; it was evident that pleural irregularities rapidly worsened within a period of few months.

4. Discussion

Our results indicate that CT imaging features can aid early diagnosis of MPM. One distinct feature was the involvement of mediastinal pleura, which was found to be significantly more prevalent in patients with eMPM than in patients with BAPE. Metintas et al. reviewed the CT findings of patients with MPM and benign pleural disease [9]. They concluded that circumferential lung encasement by multiple nodules and pleural thickening with irregular pleuropulmonary margins were more prevalent in patients with MPM. They also reported mediastinal pleural involvement as an independent factor that could be used for differentiation of MPM from benign pleural diseases; in our work, mediastinal pleural involvement was observed in 74% of patients with eMPM and just 22% of patients with BAPE (P < 0.001), highlighting the mediastinal pleural involvement even in early stages of MPM. Leung et al. investigated differential diagnoses of benign and malignant pleural diseases using CT scans and also reported mediastinal pleural involvement [25]. In our work, asbestosis was found more frequently in the BAPE group, which supports the belief that asbestosis is probably not involved in the initial stages of asbestos-induced lung carcinogenesis, though it might increase the risk of lung cancer [1,19,27].

Ökten et al. reported pleural effusion in 83% of patients with MPM [28]; they cautioned that no CT scan findings were pathognomonic for MPM, although such findings may provide clues for differential diagnosis. In another study, plural effusion was observed in almost 80% of the cases, but an independent association was not established [29]. In our work, we found 97% and 100% pleural effusion in the BAPE and eMPM groups, respectively, without any statistical difference. This observation supports the findings of Ökten et al. and indicates that pleural effusion should be used with caution for the diagnosis of MPM, especially in the early stages. Interestingly, we found that pleural plaques were more prevalent in the BAPE group than in the eMPM group (92% vs. 35%, P < 0.001), undermining the diagnostic utility of pleural plaques for the diagnosis of eMPM. This finding is of particular importance since pleural plaques are reported in some studies to have strong association with mesothelioma [27], even after adjustment for time since first exposure to asbestos and cumulative exposure index. Conversely, out of 13 identified studies on the association of pleural plaques with lung cancer, only three have reported such correlations [19,27,30]. In spite of disagreement among different studies on association of pleural plaques with MPM, the markedly higher prevalence of pleural plaques observed in patients with BAPE in this work provides strong evidence for the poor utility of pleural plaques for the diagnosis of early stages of MPM.

Our results suggest that pleural irregularity grade and location have different features in BAPE and eMPM patients. Patients with BAPE showed a high prevalence of low-level pleural irregularity, whereas MPM patients had high-level pleural irregularity and mass formation. We defined irregularities on the basis of pleural

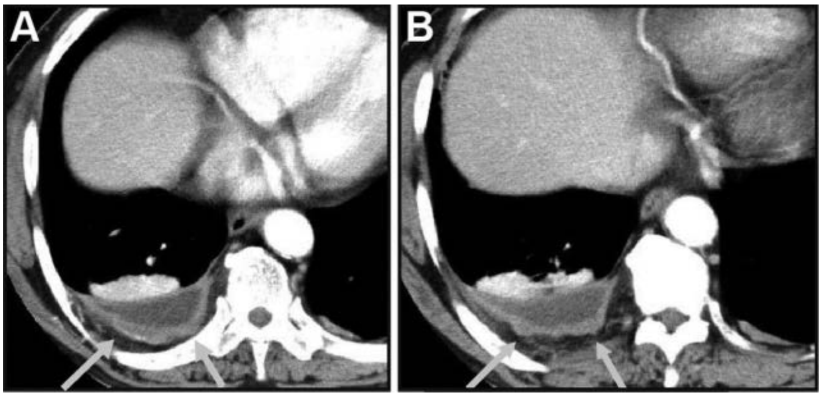

Fig. 2. Changes in the CT scan features of a patient in the BAPE group (male, 70 years) with a 21-year history of asbestos exposure. (A) Axial CT scan at diagnosis, showing high-level irregular pleural thickening (arrows). (B) Axial CT scan after five years of follow-up; a similar level irregular pleural thickening persists.

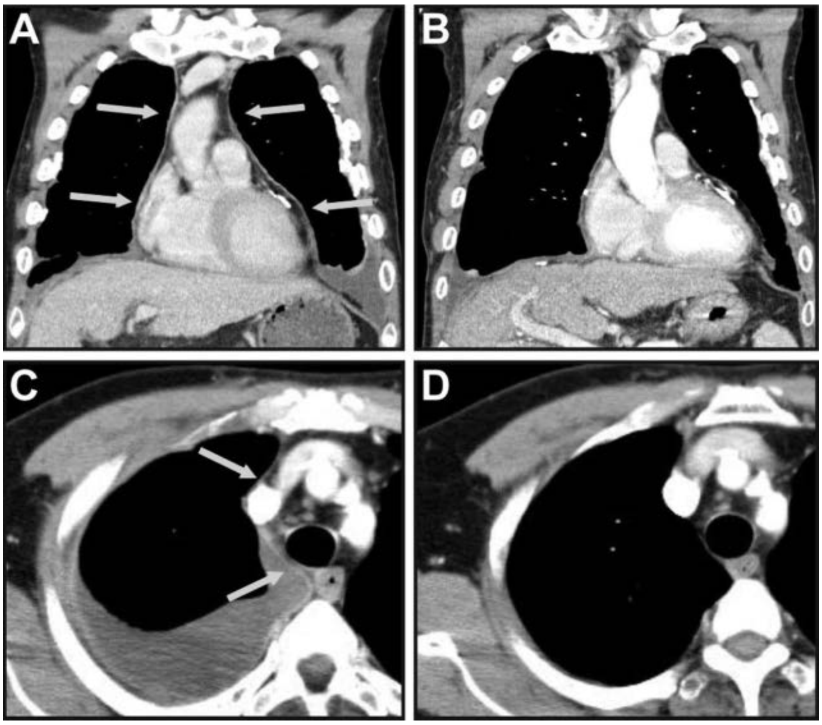

Fig. 3. Changes in the contrast-enhanced CT scan features of a patient in the BAPE group (male, 64 years) with a 39-year history of asbestos exposure. (A) Coronal view of the patient at diagnosis, with visible bilateral mediastinal pleural thickening and left pleural effusion. (B) Coronal view of the same patient after two months, showing regression. (C) Another patient (male, 69 years) with a 42-year history of asbestos exposure. Axial CT scan at diagnosis, showing unilateral mediastinal pleural thickening and effusion in the right thorax (arrows). (D) Axial CT scan after three months of follow-up, showing regression.

thickening. Leung et al. reported that parietal pleural thickening greater than 1 cm was helpful in distinguishing benign cases from malignant ones, although they also used criteria such as circumferential and nodular pleural thickening [28]. MPM is generally locally aggressive, with frequent invasion of the chest wall, mediastinum, and diaphragm, which might complicate CT scan. In the analysis of follow-up CT scans, it was evident that in cases of BAPE, pleural effusion either regressed or remained constant, whereas in cases of eMPM, pleural effusion either advanced or remained constant. Mavi et al. used dual time point 18F-fluorodeoxyglucose positron emission tomography to differentiate between benign and malignant plural diseases [31]. They showed that, in MPM, 18F-FDG uptake increased with time. Conversely, in benign pleural disease, the uptake of 18F-FDG decreased with time. Our results indicated that changes in pleural irregularities during follow-up might be useful for eMPM and BAPE diagnosis, although a more extensive study is needed to clearly establish the suitability of follow-up CT scans for differential diagnosis.

Our study had certain limitations. First, as the eMPM group used retrospective data collection from multiple centres, there was an inhomogeneity in the CT scan parameters and protocols used. However, the multicentre nature of the eMPM group helped us avoid any regional biases. Furthermore, adding to the strength of this work, obtaining a prospective group with this much sample size is practically difficult considering the rarity of the disease, and all CT scan image analyses were done by a team of independent reviewers who were blinded to the histopathologic results. The other limitation was that the BAPE group was another unique group and was single centre based. There is therefore a possibility that the patients were representative only of a particular region in Japan. Another limitation is that there could be an effect of contrast media in CT scan images; however, being a retrospective and registry-based

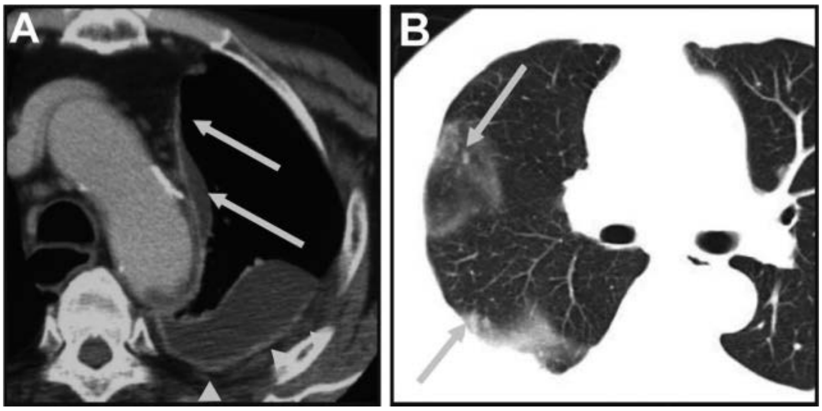

Fig. 4. A representative axial CT scan showing mediastinal pleural thickening and interlobar fissural pleural thickening of patients in eMPM group. (A) Male, 75 years old, with a 33-year history of asbestos exposure, showing unilateral mediastinal pleural thickening. (B) Posterior pleural thickening in the same patient. Mediastinal pleural thickening (arrows) and basal pleural thickening (arrow heads).

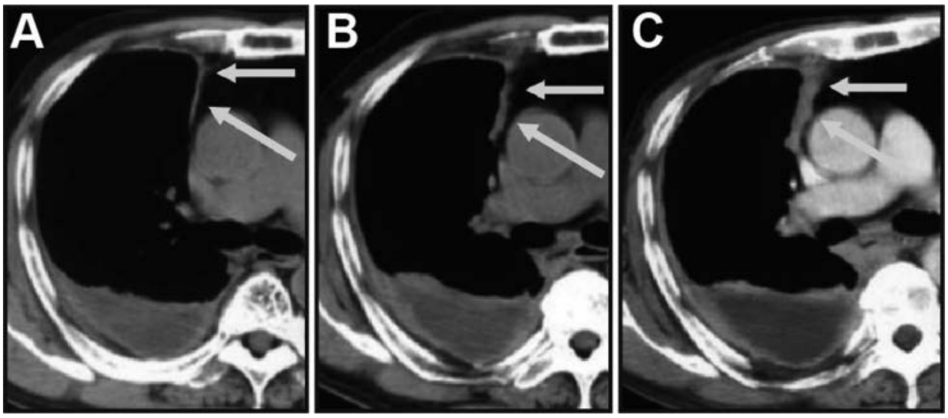

Fig. 5. A representative axial CT scan depicting changes during follow-up in a male, 78 years old, with a 35-year history of asbestos exposure. (A) Unilateral mediastinal and posterior pleural thickening and pleural effusion. (B) Progressed irregular pleural thickening after two months. (C) Progressed irregular pleural thickening after 8 months.

study, we could not investigate the effect of contrast media on pleural irregularities in all cases. Nevertheless, in 8 cases (3 BAPE and 5 eMPM) we could obtain CT scans both with and without contrast media. Our analysis indicated no difference between CT scans with or without contrast media. Despite this, a dedicated independent study with a large sample size is needed to further strengthen the effect of contrast media. Additionally, in this study, to avoid ambiguity, decisions on CT findings were made by relying on the agreement within a team of one radiologist and two pulmonologists. Inter-rater reliability and independent association between parameters should to be taken in future studies.

However, in spite of these limitations, this work clearly underscores the significance of level and localization of pleural irregularities, which could provide important clues for the diagnosis of early stages of MPM. More large-scale, multicentre studies with long-term follow-up are needed to establish a diagnostic standard for eMPM and to fully elucidate pleural irregularities in the early stages of MPM. This study serves as a basis for such studies.

5. Conclusion

This study indicated that the level and location of pleural irregularities could be of potential help in the differential diagnosis between BAPE and eMPM. There was no significant difference between the two groups in term of prevalence of pleural effusion. However, mediastinal pleural involvement was found more frequently in patients with early MPM. Large-scale multicentre prospective studies with long-term follow-up are needed to fully establish a standard protocol.

Conflict of interest

The authors declare that they have no conflicts of interest to disclose.

Funding

This research was funded primarily by grants from the research foundation of the Ministry of Health, Labour, and Welfare of Japan (200500129A, 200635021A, 200733015A, 200733015B, 200836010A, 200938007A, and 201032004B) and by Industrial disease clinical research grants from the Ministry of Health, Labour, and Welfare of Japan (150401).

Role of funding

The funding source had no role in study design and concept, data acquisition, data analysis and interpretation, and manuscript preparation and submission.

Author contribution

Katsuya Kato: image reading/interpretation (BAPE, eMPM), analysis of imaging results.

Kenichi Gemba; image reading/interpretation (eMPM), statistical analysis, clinical analysis.

Nobukazu Fujimoto: image reading/interpretation (BAPE), gathering cases, clinical analysis.

Keisuke Aoe: gathering and management of cases, clinical analysis.

Yukio Takeshima: pathological investigation.

Kouki Inai: pathological investigation.

Takumi Kishimoto: image reading/interpretation (BAPE, eMPM), gathering and management of cases, research supervision.

All authors have approved the final article.

Appendix A. Supplementary data

Supplementary data associated with this article can be found, in the online version, at http://dx.doi.org/10.1016/j.ejrad.2016.06.013.

References

[1] S. Prazakova, P.S. Thomas, A. Sandrini, D.H. Yates, Asbestos and the lung in the 21st century: an update, Clin. Resp. J. 8 (2014) 1–10.

[2] L.T. Nickell, J.P. Lichtenberger, L. Khorashadi, G.F. Abbott, B.W. Carter, Multimodality imaging for characterization classification, and staging of malignant pleural mesothelioma, Radiographics 34 (2014) 1692–1706.

[3] M.B. Gotway, Pleural abnormalities and volume loss: imaging considerations, Clin. Pulm. Med. 16 (2009) 346–349.

[4] S.G. Armato III, A.K. Nowak, R.J. Francis, M. Kocherginsky, M.J. Byrne, Observer variability in mesothelioma tumor thickness measurements: defining minimally measurable lesions, J. Thorac. Oncol. 9 (2014) 1187–1194.

[5] K.H. Lee, et al., Mesenchymal tumours of the thorax: CT findings and pathological features, Clin. Radiol. 58 (2003) 934–944.

[6] R. Maeda, N. Isowa, H. Onuma, et al., Minute localized malignant pleural mesothelioma coexisting with multiple adenocarcinomas, Gen. Thorac. Cardiovasc. Surg. 58 (2010) 91–94.

[7] M. Metintas, I. Ucgun, O. Elbek, et al., Computed tomography features in malignant pleural mesothelioma and other commonly seen pleural diseases, Eur. J. Radiol. 41 (2002) 1–9.

[8] C.S. Ng, R.F. Munden, H.I. Libshitz, Malignant pleural mesothelioma: the spectrum of manifestations on CT in 70 cases, Clin. Radiol. 54 (1999) 415–421.

[9] A.M. Khan, K. Tlemcani, N. Shanmugam, A localized pleural based mass with intense uptake on positron emission tomography scan, Chest 131 (2007) 294–299.

[10] J.M. Seely, E.T. Nguyen, A.M. Churg, et al., Malignant pleural mesothelioma: computed tomography and correlation with histology, Eur. J. Radiol. 70 (2009) 485–491.

[11] T. Terada, C. Tabata, R. Tabata, et al., Clinical utility of 18-fluorodeoxyglucose positron emission tomography/computed tomography in malignant pleural mesothelioma, Exp. Ther. Med. 4 (2012) 197–200.

[12] N.A. Maskell, F.V. Gleeson, R.J.O. Davies, Standard pleural biopsy versus CT-guided cutting-needle biopsy for diagnosis of malignant disease in pleural effusions: a randomised controlled trial, Lancet 361 (2003) 1326–1330.

[13] A. Iyoda, T. Yusa, C. Kadoyama, et al., Diffuse malignant pleural mesothelioma: a multi-institutional clinicopathological study, Surg. Today 38 (2008) 993–998.

[14] N. Fujimoto, K. Aoe, K. Gemba, et al., Clinical investigation of malignant mesothelioma in Japan, J. Cancer Res. Clin. Oncol. 136 (2010) 1755–1759.

[15] K. Gemba, N. Fujimoto, K. Aoe, et al., Treatment and survival analyses of malignant mesothelioma in Japan, Acta Oncol. 52 (2013) 803–808.

[16] T. Kishimoto, K. Morinaga, S. Kira, The prevalence of pleural plaques and/or pulmonary changes among construction workers in Okayama, Japan, Am. J. Ind. Med. 37 (2000) 291–295.

[17] C. Bianchi, A. Brollo, L. Ramani, T. Bianchi, L. Giarelli, Asbestos exposure in malignant mesothelioma of the pleura: a survey of 557 cases, Ind. Health 39 (2001) 161–167.

[18] K. Chaisaowong, T. Aach, P. Jäger, et al., Computer-assisted diagnosis for early stage pleural mesothelioma: towards automated detection and quantitative assessment of pleural thickenings from thoracic CT images, Methods Inf. Med. 46 (2007) 324–331.

[19] J. Ameille, P. Brochard, M. Letourneux, C. Paris, J.C. Pairon, Asbestos-related cancer risk in patients with asbestosis or pleural plaques, Rev. Mal. Respir. 28 (2011) e11–e17.

[20] G.R. Epler, T.C. McLoud, E.A. Gaensler, Prevalence and incidence of benign asbestos pleural effusion in a working population, JAMA 247 (1982) 617–622.

[21] T.L. Guidotti, C.A. Brodkin, D. Christiani, et al., Diagnosis and initial management of nonmalignant diseases related to asbestos, Am. J. Resp. Crit. Care Med. 170 (2004) 691–715.

[22] D.W. Henderson, et al., Asbestos, asbestosis, and cancer: the Helsinki criteria for diagnosis and attribution, Scand. J. Work Environ. Health 23 (1997) 311–316.

[23] T. Kishimoto, K. Gemba, N. Fujimoto, et al., Clinical study on mesothelioma in Japan: relevance to occupational asbestos exposure, Am. J. Ind. Med. 53 (2010) 1081–1087.

[24] V.W. Rusch, A proposed new international TNM staging system for malignant pleural mesothelioma: from the international mesothelioma interest group, Lung Cancer 14 (1996) 1–12.

[25] A.N. Leung, N.L. Muller, R.R. Miller, CT in differential diagnosis of diffuse pleural disease, Am. J. Roentgenol. 154 (1990) 487–492.

[26] A. Orki, O. Akin, A.E. Tasci, et al., The role of positron emission tomography/computed tomography in the diagnosis of pleural diseases, Thorac. Cardiovasc. Surg. 57 (2009) 217–221.

[27] J.C. Pairon, F. Laurent, M. Rinaldo, et al., Pleural plaques and the risk of pleural mesothelioma, J. Natl. Cancer Inst. 105 (2013) 293–301.

[28] F. Ökten, D. Köksal, M. Onal, et al., Computed tomography findings in 66 patients with malignant pleural mesothelioma due to environmental exposure to asbestos, Clin. Imaging 30 (2006) 177–180.

[29] O. Tamer Dogan, I. Salk, F. Tas, et al., Thoracic computed tomography findings in malignant mesothelioma, Iran. J. Radiol. 9 (2012) 209–211.

[30] U. Elboga, M. Yılmaz, M. Uyar, et al., The role of FDG PET-CT in differential diagnosis of pleural pathologies, Rev. Esp. Med. Nucl. Imagen Mol. 31 (2012) 187–191.

[31] A. Mavi, S. Basu, T.F. Cermik, et al., Potential of dual time point FDG-PET imaging in differentiating malignant from benign pleural disease, Mol. Imaging Biol. 11 (2009) 369–378.

Histopathology 2016 DOI: 10.1111/his.13073

Utility and pitfalls of immunohistochemistry in the differential diagnosis between epithelioid mesothelioma and poorly differentiated lung squamous cell carcinoma

Kei Kushitani,[1] Vishwa J Amatya,[1] Yasuko Okada,[2] Yuya Katayama,[2] Amany S Mawas,[1,3] Yoshihiro Miyata,[4] Morihito Okada,[4] Kouki Inai,[1,5] Takumi Kishimoto[6] & Yukio Takeshima[1]
[1]*Department of Pathology, Institute of Biomedical and Health Sciences, Hiroshima University, Hiroshima, Japan,* [2]*Faculty of Medicine, Hiroshima University, Hiroshima, Japan,* [3]*Department of Pathology and Clinical Pathology, Faculty of Veterinary Medicine, South Valley University, Qena, Egypt,* [4]*Department of Surgical Oncology, Research Centre for Radiation Casualty Medicine, Research Institute for Radiation Biology and Medicine, Hiroshima University, Hiroshima, Japan,* [5]*Pathologic Diagnostic Centre, Inc., Hiroshima, Japan, and* [6]*Department of Internal Medicine, Okayama Rosai Hospital, Okayama, Japan*

Date of submission 30 June 2016
Accepted for publication 30 August 2016
Published online *Article Accepted* 2 September 2016

Kushitani K, Amatya V J, Okada Y, Katayama Y, Mawas A S, Miyata Y, Okada M, Inai K, Kishimoto T & Takeshima Y
(2016) *Histopathology*. DOI: 10.1111/his.13073

Utility and pitfalls of immunohistochemistry in the differential diagnosis between epithelioid mesothelioma and poorly differentiated lung squamous cell carcinoma

Aims: The aims of this study were to clarify the usefulness of immunohistochemistry in the differential diagnosis of epithelioid mesothelioma with a solid growth pattern [solid epithelioid mesothelioma (SEM)] and poorly differentiated squamous cell carcinoma (PDSCC), and to confirm the validity of a specific type of antibody panel. Additionally, we aimed to clarify the pitfalls of immunohistochemical analyses.

Methods and results: Formalin-fixed paraffin-embedded specimens from 36 cases of SEM and 38 cases of PDSCC were immunohistochemically examined for calretinin, podoplanin (D2-40), Wilms' tumour gene product (WT1), cytokeratin (CK) 5/6, p40, p63, carcinoembryonic antigen (CEA), epithelial-related antigen (MOC31), claudin-4, thyroid transcription factor-1 (TTF-1), and napsin A. WT1 showed the highest diagnostic accuracy (85.1%) as a mesothelial marker, and CEA, p40 and claudin-4 showed higher diagnostic accuracies (95.9%, 94.6%, and 93.2%, respectively) as carcinoma markers. Calretinin (diagnostic accuracy: 75.7%), D2-40 (diagnostic accuracy: 67.6%), CK5/6 (diagnostic accuracy: 63.5%), TTF-1 (diagnostic accuracy: 55.4%) and napsin A (diagnostic accuracy: 52.7%) could not differentiate between SEM and PDSCC. Among these markers, the combination of calretinin and WT1 showed the highest diagnostic accuracy (86.5%) as a positive marker, and the combination of p40 and CEA showed the highest diagnostic accuracy (97.3%) as a negative marker. The combination of CEA and claudin-4 also showed relatively high diagnostic accuracy (94.6%) as a negative marker.

Conclusions: We recommend the combination of WT1 and calretinin as a positive maker, and the combination of CEA and claudin-4 as a negative marker, for differential diagnoses of SEM and PDSCC.

Keywords: calretinin, carcinoembryonic antigen, claudin-4, immunohistochemistry, mesothelioma, p40, squamous cell carcinoma, WT1 protein

Address for correspondence: Yukio Takeshima, MD, PhD, 1-2-3 Kasumi, Minami-ku, Hiroshima 734-8551, Japan. e-mail: ykotake@hiroshima-u.ac.jp

© 2016 John Wiley & Sons Ltd.

Introduction

Malignant mesothelioma (MM) is a rare, aggressive malignant neoplasm that most commonly arises from pleural mesothelial cells. MM is correlated with occupational and environmental asbestos exposure.[1–5] As the incidence of MM has increased in many countries, pathologists encounter this disease frequently. In Japan, the death toll from MM has been increasing since the 1990s, and it is predicted to peak in the 2030s.[6]

A diffuse pleurotropic growth pattern is characteristic of MM.[7,8] However, a number of non-mesotheliomatous neoplasms showing diffuse pleurotropic growth patterns (described as 'pseudomesotheliomatous growth') have been reported, and most of these tumours are peripheral lung carcinomas.[9–13] Although the majority of pseudomesotheliomatous lung carcinomas are adenocarcinomas (ACs), a few pseudomesotheliomatous pulmonary squamous cell carcinoma (SCC) cases have also been reported.[14] Lately, the incidence of peripheral-type pulmonary SCC, but not central SCC, has been increasing.[15,16] Thus, the chance of encountering 'pseudomesotheliomatous' SCCs might increase. Additionally, MM may occur as a localized mass similar to peripheral lung cancer and other pleural tumours; it is then classified as 'localized MM' according to the new World Health Organization (WHO) classification.[7] Therefore, the histopathological differential diagnosis of MM and SCC will become crucial in the future.

Malignant mesotheliomas are divided into three major histological subtypes: epithelioid, sarcomatoid, and biphasic. Among these, epithelioid mesothelioma (EM) shows a wide range of histological and cytological patterns, such as papillary, tubular, solid, clear cell, deciduoid, rhabdoid, and pleomorphic.[17] Poorly differentiated SCC (PDSCC) shows a nested, sheet-like or cord-like histological pattern, and lacks obvious keratinization and/or intercellular bridges in some parts of or throughout the tumour.[18] Therefore, the differential diagnosis between EM showing a solid histological pattern [solid EM (SEM)] and PDSCC can be challenging with conventional light microscopy (haematoxylin and eosin-stained specimen) alone.

The role of immunohistochemistry in distinguishing pleural EM from pulmonary AC has received much attention. Currently, many immunohistochemical markers are available for distinguishing pleural EM from pulmonary AC. Among these, calretinin, cytokeratin (CK) 5/6, podoplanin (D2-40) and Wilms' tumour gene product (WT1) are regarded as the best positive markers for EM, and carcinoembryonic antigen (CEA), MOC31 [epithelial-related antigen (ERA)], Ber-EP4, BG-8, thyroid transcription factor-1 (TTF)-1, and napsin A are regarded as the best positive markers for lung AC.[19–22]

However, there are only a few reports on the immunohistochemical differential diagnosis of EM and lung SCC. Ordonez *et al.* have reported the immunohistochemical analyses of 30 EMs showing a solid pattern and 30 pulmonary non-keratinizing SCCs, and have recommended the combination of two positive (WT1 and calretinin/mesothelin) and two negative (p63 and ERA) markers for differentiating EM from lung SCC.[23]

Here, we examined 11 commercially available immunohistochemical markers in histological specimens of SEM and PDSCC obtained from Japanese cases. We aimed to evaluate the usefulness of immunohistochemistry in differentiating SEM from PDSCC, and to recommend the best antibody panel for use in pathological laboratories, after considering the pitfalls of immunohistochemical analyses.

Materials and methods

PATIENTS AND HISTOLOGICAL SAMPLES

We used formalin-fixed paraffin-embedded (FFPE) specimens from 36 patients with a definite histological diagnosis of SEM who had undergone pleural biopsy, pleurectomy/decortication, extrapleural pneumonectomy or autopsy between 2000 and 2014.

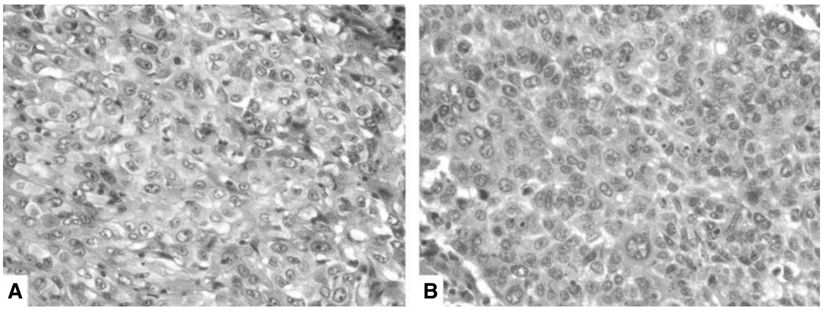

Figure 1. Representative histological images of solid epithelioid mesothelioma and poorly differentiated squamous cell carcinoma. (**A**) Solid epithelioid mesothelioma. (**B**) Poorly differentiated squamous cell carcinoma.

© 2016 John Wiley & Sons Ltd, *Histopathology*

SEM was defined as 'EM consisting of mainly solid, sheet-like or cord-like proliferations of cuboidal or polygonal epithelioid cells' (Figure 1A). All SEM cases used in this study were comprehensively diagnosed according to a combination of clinical history (e.g. occupational asbestos exposure), radiographic examination (e.g. diffuse pleurotropic growth pattern, lack of intrapulmonary mass, or the presence of pleural plaques), and histopathological findings. In all cases, we performed immunohistochemical investigation with 15–20 markers, including the 11 markers examined in this study.

Formalin-fixed paraffin-embedded histological samples of the surgical specimens from 38 patients with a histological diagnosis of primary pulmonary PDSCC were obtained by surgical resection (wedge resection, segmentectomy, lobectomy, or pneumonectomy) from 2000 to 2014. PDSCC included keratinizing SCC with minimal squamous differentiation (keratinization and/or intercellular bridge) and non-keratinizing SCC, as defined in the WHO 2015 criteria (Figure 1B).[24] The samples were collected from the archives of the Department of Pathology at Hiroshima University. Among 38 PDSCCs that we examined, 34 were of the peripheral type, and four were of the central type. Ten cases showed invasion to the visceral pleura but not right through and exposed on the surface of the pleura, seven cases showed focal invasion to the parietal pleura or chest wall, and 21 cases were intrapulmonary lesions without pleural invasion. There was no case showing diffuse pleurotropic growth.

Each tumour specimen was reviewed by three pathologists (K.K., V.J.A., and Y.T.); all of the cases were rediagnosed on the basis of the currently accepted histological criteria.[17,18]

This study was performed in accordance with the Ethics Guidelines for Human Genome/Gene Research enacted by the Japanese government for the collection of tissue specimens, and was approved by the institutional ethics review committee (Hiroshima University E-48).

IMMUNOHISTOCHEMICAL PROCEDURES

Immunohistochemical staining of sections from the FFPE tissue samples was performed with Ventana BenchMark GX (Roche Diagnostics, Basel, Switzerland), by use of the Ventana ultraView Universal DAB Detection Kit; the staining procedure is based on the indirect biotin-free system. Protocols involving heat induction-based or protease digestion-based antigen retrieval were performed as recommended by the manufacturer, with some modifications. Table 1 shows the list of primary antibodies, clones, sources, and antibody dilutions.

Table 1. Primary antibodies used in this study

Marker	Clone	Manufacturer	Dilution	Location of evaluation
Calretinin	SP65	Ventana	Prediluted	Nucleus
Podoplanin	D2-40	Nichirei Bioscience	Prediluted	Membrane
WT1	6F-H2	Ventana	Prediluted	Nucleus
CK5/6	D5/16 B4	Dako	1:25	Membrane and/or cytoplasm
p40	BC28	Biocare Medical	1:100	Nucleus
p63	DAK-p63	Dako	1:25	Nucleus
CEA	COL-1	Nichirei Bioscience	Prediluted	Membrane and/or cytoplasm
ERA	MOC31	Dako	1:25	Membrane
Claudin-4	3E2C1	Life Technologies	1:100	Membrane
TTF-1	SPT24	Nichirei Bioscience	Prediluted	Nucleus
Napsin A	MRQ-60	Ventana	Prediluted	Cytoplasm

CEA, carcinoembryonic antigen; CK, cytokeratin; ERA, epithelial-related antigen; TTF-1, thyroid transcription factor-1; WT1, Wilms' tumour gene product.

Immunoreactivity was scored as either negative (no immunostaining) or positive. Cells showing nuclear staining for calretinin, WT1, p40, p63, and TTF-1, membranous staining for podoplanin, ERA, and claudin-4, cytoplasmic staining for napsin A or membranous and/or cytoplasmic staining for CK5/6 and CEA were regarded as 'positive'. The immunoreactivity grade was semiquantified as follows: 0, 0% positive cells or trace staining; 1+, 1–10% positive cells; 2+, 11–50% positive cells; and 3+, >51% positive cells.

EVALUATION OF UTILITY OF EACH MARKER AND COMBINATIONS OF TWO MARKERS

Sensitivity, specificity, positive predictive values (PPVs), negative predictive values (NPVs) and diagnostic accuracies were calculated for each marker and combination of two markers.

Results

IMMUNOREACTIVITY OF ANTIBODIES FOR SEM AND PDSCC

The detection rates of each antibody in SEM and PDSCC are shown in Table 2. Representative immunohistochemical staining images for SEM and PDSCC are shown in Figures 2 and 3, respectively. The staining pattern for each antibody for the two tumour types is described in the following paragraphs.

CALRETININ

Thirty-three of 36 SEMs (91.7%) and 15 of 38 PDSCCs (39.5%) were positive for calretinin. In SEMs, immunoreactivity was generally strong and diffuse (grade 3+). In contrast, in PDSCCs, the staining grade was distributed from 1+ to 3+ approximately equally.

D2-40

Thirty-five of 36 SEMs (97.2%) and 23 of 28 PDSCCs (60.5%) were positive for D2-40. In the majority of SEMs, immunoreactivity was strong and diffuse (grade 3+), whereas the majority of PDSCCs showed a focal or multifocal positive pattern (grade 1+/2+).

WT1

Twenty-six of 36 SEMs (72.2%) were positive for WT1, with most of them showing grade 3+, whereas only one PDSCC (2.6%) was focally positive (grade 1+) for WT1.

CK5/6

Twenty-six of 36 (72.2%) of SEMs and 37 of 38 (97.4%) of PDSCCs were positive for CK5/6. For both tumours, the majority of cases showed diffuse and strong immunoreactivity (grade 3+).

P40

Only two SEMs (5.6%) were positive for p40, and staining was observed in an extremely confined area (grade 1+). In contrast, 36 of 38 PDSCCs (94.7%) were positive for p40, and most cases showed diffuse and strong immunoreactivity (grade 3+).

Table 2. Immunohistochemical findings for solid epithelioid mesothelioma (SEM) and poorly differentiated squamous cell carcinoma (PDSCC) for various antibodies

		SEM staining grade					PDSCC staining grade			
Marker	SEM, *n* (%)	0	1+	2+	3+	PDSCC, *n* (%)	0	1+	2+	3+
Calretinin	33/36 (91.7)	3	0	2	31	15/38 (39.5)	23	7	4	4
D2-40	35/36 (97.2)	1	3	2	30	23/38 (60.5)	15	5	12	6
WT1	26/36 (72.2)	10	5	3	18	1/38 (2.6)	37	1	0	0
CK5/6	26/36 (72.2)	10	5	6	15	37/38 (97.4)	1	2	6	29
p40	2/36 (5.6)	34	2	0	0	36/38 (94.7)	2	0	4	32
p63	6/36 (16.7)	30	5	0	1	37/38 (97.4)	1	1	2	34
CEA	0/36 (0)	36	0	0	0	35/38 (92.1)	3	14	13	8
ERA	12/36 (33.3)	24	8	3	1	34/38 (89.5)	4	5	11	18
Claudin-4	2/36 (5.6)	34	2	0	0	35/38 (92.1)	3	3	17	15
TTF-1	0/36 (0)	36	0	0	0	5/38 (13.2)	33	5	0	0
Napsin A	0/36 (0)	36	0	0	0	3/38 (7.9)	35	3	0	0

CEA, carcinoembryonic antigen; CK, cytokeratin; ERA, epithelial-related antigen; TTF-1, thyroid transcription factor-1; WT1, Wilms' tumour gene product.

The grade of immunoreactivity was semiquantified as follows: 0, 0% positive cells or trace staining; 1+, 1–10% positive cells; 2+, 11–50% positive cells; 3+, >51% positive cells.

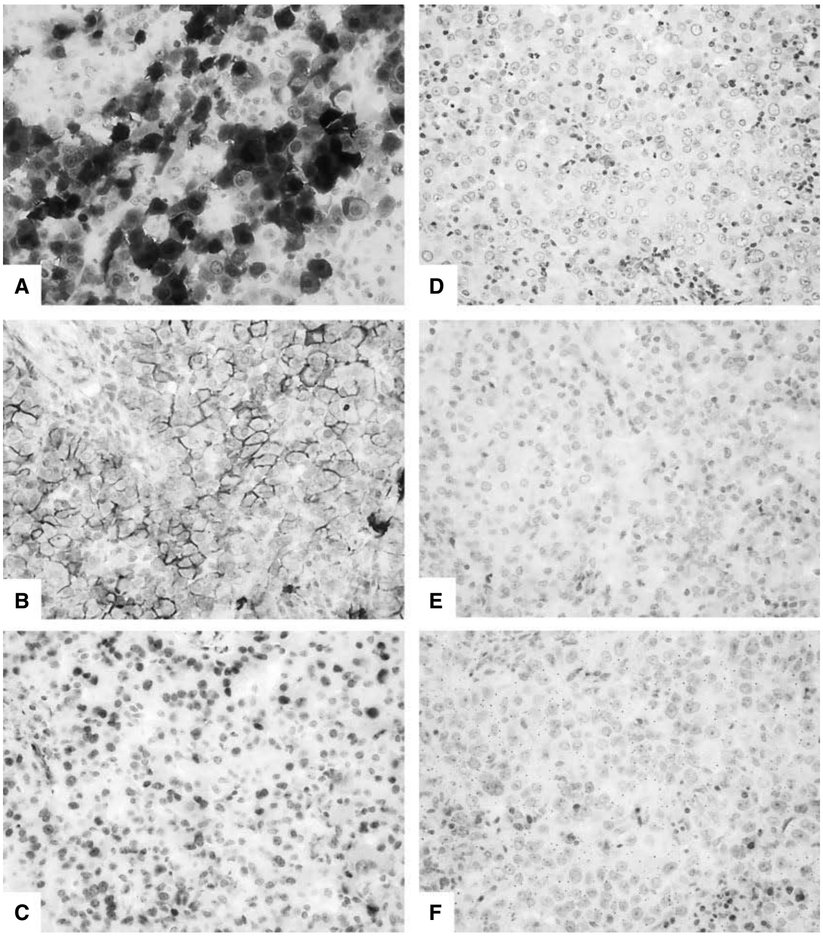

Figure 2. Representative immunohistochemical staining panel for solid epithelioid mesothelioma. The mesothelioma cells showed positivity for calretinin (nuclear) (**A**), D2-40 (membranous) (**B**), and Wilms' tumour gene product (nuclear) (**C**), but were negative for carcinoembryonic antigen (**D**), p40 (**E**), and claudin-4 (**F**).

P63

Six of 36 SEMs (16.7%) were positive for p63, and most of them showed staining in an extremely confined area (grade 1+). However, one SEM showed diffuse and strong immunoreactivity (grade 3+). In contrast, 37 of 38 PDSCCs (97.4%) were positive for p63, and most of them showed diffuse and strong immunoreactivity (grade 3+).

CEA

None of the SEMs were positive CEA. In contrast, 92.1% of PDSCCs were positive for CEA. However, in the majority of the CEA-positive PDSCCs, staining was limited to ≤50% of the tumour cells (grades 1+ and 2+).

ERA

Approximately 33.3% of SEMs and 89.5% of PDSCCs were positive for ERA. In the majority of the ERA-positive SEMs, staining was limited to ≤50% of the tumour cells (grades 1+ and 2+). In contrast, approximately half of the ERA-positive PDSCCs showed diffuse and strong immunoreactivity (grade 3+).

CLAUDIN-4

Only two SEMs (5.6%) were positive for claudin-4, and staining was observed in an extremely confined area (grade 1+). In contrast, 35 of 38 PDSCCs (92.1%) were positive for claudin-4, and, in most of them, staining was observed in ≥10% of the tumour cells (grade 2+ or 3+).

TTF-1 AND NAPSIN A

None of the SEMs were positive for TTF-1 or napsin A; five PDSCCs that were positive for TTF-1 and three PDSCCs that were positive for napsin A showed focal immunoreactivity (grade 1+).

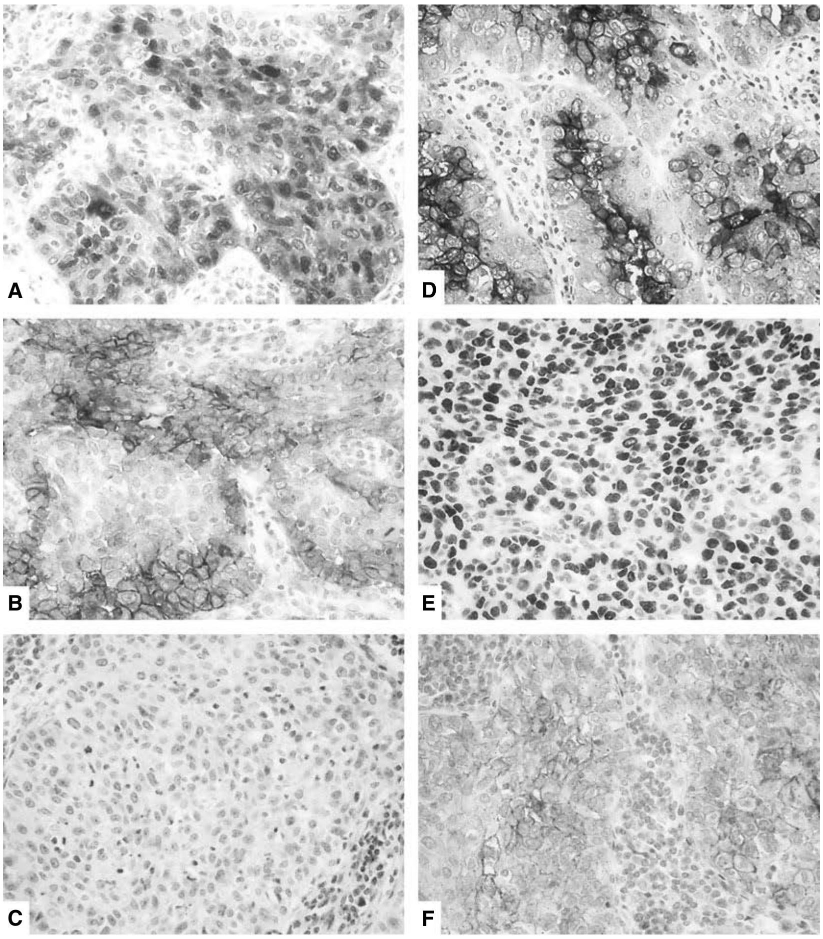

Figure 3. Representative immunohistochemical staining panel for poorly differentiated squamous cell carcinoma. The carcinoma cells were positive for calretinin (nuclear) (**A**), D2-40 (membranous) (**B**), carcinoembryonic antigen (cytoplasmic) (**D**), p40 (nuclear) (**E**), and claudin-4 (membranous) (**F**), but negative for Wilms' tumour gene product (**C**).

SENSITIVITY, SPECIFICITY, PPVS, NPVS AND DIAGNOSTIC ACCURACIES OF EACH ANTIBODY FOR DIFFERENTIAL DIAGNOSIS BETWEEN SEM AND PDSCC

The sensitivity, specificity, PPVs, NPVs and diagnostic accuracies of each marker and combination of two markers for the differential diagnosis between SEM and PDSCC are shown in Tables 3–5.

For SEM, WT1 as a positive marker and p40, p63, CEA and claudin-4 as negative markers showed relatively high diagnostic accuracy (>80%). Among the 11 antibodies evaluated, that for CEA showed the highest sensitivity, NPV and diagnostic accuracy (Table 3).

Among the combinations of two markers, the combination of calretinin and WT1 (both calretinin positivity and WT1 positivity) showed the highest specificity, PPV and diagnostic accuracy as a positive marker (Table 4), and the combination of p40 and CEA (both p40 negativity and CEA negativity) showed the highest specificity, PPV and diagnostic accuracy as a negative marker (Table 5).

Discussion

Here, we used various commercially available markers to differentiate SEM with a solid growth pattern from PDSCC showing minimal or no keratinization, and attempted to identify the best antibody panel for differentiating SEM and PDSCC, with their pitfalls in interpretation. We found that WT1 had the highest diagnostic accuracy as a positive marker, and that CEA, p40, p63 and claudin-4 showed high diagnostic accuracies as negative markers (>90%).

Wilms' tumour gene product encodes a zinc-finger transcription factor that controls the expression of many growth factors and their receptors.[25] Nuclear immunoreactivity for WT1 has been reported in 43–100% of EMs,[20–22,26] whereas it is negligibly expressed in pulmonary ACs and SCCs.[20,21,23,27] In

Table 3. Sensitivity, specificity, positive predictive values (PPVs), negative predictive values (NPVs) and diagnostic accuracies of each antibody for the differential diagnosis between solid epithelioid mesothelioma and non-keratinizing squamous cell carcinoma

Immunohistochemical findings	Sensitivity (%)	Specificity (%)	PPV (%)	NPV (%)	Diagnostic accuracy (%)
Calretinin-positive	91.7	60.5	68.8	88.5	75.7
D2-40-positive	97.2	39.5	60.3	93.8	67.6
WT1-positive	72.2	97.4	96.3	78.7	85.1
CK5/6-positive	72.2	2.6	41.3	9.1	36.5
p40-negative	94.4	94.7	94.4	94.7	94.6
p63-negative	83.3	97.4	96.8	86.0	90.5
CEA-negative	100	92.1	92.3	100	95.9
ERA-negative	66.7	89.5	85.7	73.9	78.4
Claudin-4-negative	94.4	92.1	91.9	94.6	93.2
TTF-1-negative	100	13.2	52.2	100	55.4
Napsin A-negative	100	7.9	50.7	100	52.7

CEA, carcinoembryonic antigen; CK, cytokeratin; WT1, TTF-1, thyroid transcription factor-1; Wilms' tumour gene product.

Table 4. Sensitivity, specificity, positive predictive values (PPVs), negative predictive values (NPVs) and diagnostic accuracies of combinations of two positive markers for the differential diagnosis between solid epithelioid mesothelioma and non-keratinizing squamous cell carcinoma

Combination of two markers	Sensitivity (%)	Specificity (%)	PPV	NPV	Diagnostic accuracy
Calretinin-positive and D2-40-positive	88.9	73.7	76.2	87.5	81.1
Calretinin-positive or D2-40-positive	100	26.3	56.3	100	62.2
Calretinin-positive and WT1-positive	72.2	100	100	79.2	86.5
Calretinin-positive or WT1-positive	91.7	57.9	67.3	88	74.3
D2-40-positive and WT1-positive	72.2	97.4	96.3	78.7	85.1
D2-40-positive or WT1-positive	97.2	39.5	60.3	93.8	67.6

WT1, Wilms' tumour gene product.

this study, although the sensitivity of WT1 (72.2%) was the lowest among the positive markers, its high specificity (97.4%) and the fact that it showed the highest diagnostic accuracy (85.1%) among three positive markers (calretinin, D2-40, and WT1) for differentiating SEM from PDSCC led us to consider WT1 as the best positive marker. Previously, Ordonez *et al.* had reported WT1 positivity in 93% (28 of 30 cases) of the EMs studied.[23] In this study, 72.2% of EMs tested positive for WT1, which is lower than the positivity percentage reported by Ordonez *et al.* Differences in the source of the primary antibody or staining system might explain this discrepancy. The positivity rate for WT1 in SEMs in this study was similar to that observed in our previous studies on EMs with a tubulopapillary pattern,[20,21] indicating that the WT1 positivity rate is not different between tubulopapillary and solid EMs. Additionally, we

© 2016 John Wiley & Sons Ltd, *Histopathology*

Table 5. Sensitivity, specificity, positive predictive values (PPVs), negative predictive values (NPVs) and diagnostic accuracies of combinations of two negative markers for the differential diagnosis between solid epithelioid mesothelioma and non-keratinizing squamous cell carcinoma

Combination of two markers	Sensitivity (%)	Specificity (%)	PPV (%)	NPV (%)	Diagnostic accuracy (%)
p40-negative and CEA-negative	94.4	100	100	95	97.3
p40-negative or CEA-negative	100	86.8	87.8	100	93.2
p40-negative and claudin-4-negative	91.7	100	100	92.7	95.9
p40-negative or claudin-4-negative	100	86.8	87.8	100	93.2
CEA-negative and claudin-4-negative	94.4	94.7	94.4	94.7	94.6
CEA-negative or claudin-4-negative	100	89.5	90	100	94.6

CEA, carcinoembryonic antigen.

detected positivity in the endothelium of blood vessels in the same sections of SEM, which excludes the possibility of false-negative results.

Calretinin is a 29-kDa, calcium-binding protein involved in calcium signalling, and is strongly expressed in the neurons of the retina and sensory pathways.[28,29] Immunoreactivity for calretinin has been reported in 55–100% of EM cases.[22] In this study, calretinin showed relatively high sensitivity (91.7%) as a positive marker for SEM. However, the specificity (60.5%) and diagnostic accuracy (75.7%) were not sufficiently high, although the distribution of the reactive grade in PDSCC was lower than that in EM. Therefore, the utility of calretinin for differentiation between SEM and PDSCC is limited. However, the combination of calretinin and WT1 antibodies would be helpful for elevating the low sensitivity of WT1 (72.2%) for practical application and detection of mesothelial origin. D2-40 is not useful for differentiating SEM from PDSCC; although D2-40 showed the highest sensitivity (97.2%) as a positive marker for SEM, its specificity (39.5%) and diagnostic accuracy (67.6%) were the lowest among the three positive markers for mesothelioma (calretinin, D2-40, and WT1).

p40 (ΔNp63), a non-transactivating isoform of p63, is a squamous/basal-type biomarker.[30] p63 and p40 are expressed in most SCCs, but are rarely expressed in EMs; p40 shows higher sensitivity and specificity than p63.[30,31] In addition, Bishop *et al.* reported that p63 was expressed in various proportions of ACs and large-cell lymphomas, and p40 showed much higher specificity for SCC.[32] In this study, both p40 and p63 showed high sensitivity, specificity, and diagnostic accuracy, but the sensitivity and diagnostic accuracy of p40 were higher than those of p63, suggesting that p40 is a useful negative marker for distinguishing SEM from PDSCC. However, a small number of EMs showed positivity for p40 and/or p63 (most cases were graded as 1+); this phenomenon must be kept in mind when p40 is used in practical pathological diagnosis.

Claudin-4 is a major component of tight junctions, and is widely expressed in most epithelial and carcinoma cells.[33–35] Membranous immunoreactivity for claudin-4 has been reported in 88–100% of carcinomas of various origins and in 0–29% of EMs.[33,34,36,37] Therefore, claudin-4 is considered to be a useful immunohistochemical marker for distinguishing EM from various carcinomas. In this study, claudin-4 showed high sensitivity (94.4%), specificity (92.1%), and diagnostic accuracy (93.2%), implying that claudin-4 is a useful negative marker for distinguishing SEM from PDSCC.

Carcinoembryonic antigen was the first accepted immunohistochemical marker for differentiating EM from lung AC;[38] because of its high sensitivity and specificity, it is still considered to be one of the best markers.[39] Ordonez reported that CEA is also useful for differentiating EM from lung SCC.[23] In this study, CEA showed the best sensitivity (100%) and diagnostic accuracy (95.9%) among all 11 evaluated markers, suggesting that CEA is the best negative marker for distinguishing SEM from PDSCC.

Ordnez *et al.* and the IMIG2012 update recommend MOC31 (ERA) as a negative marker (positivity rate: EM, 2–10%; SCC, 97–100%).[17,23] However, on the basis of the results of the present study, we cannot recommend the use of MOC31 as a negative maker (positivity rate: EM, 33.3; SCC, 89.5). This discrepancy may be attributable to the different clones of antibodies and differences in the antigen detection systems used.

The IMIG2012 guideline recommended consideration of two mesothelial and two carcinoma markers, on the basis of morphology at initial workup,[17] and the new WHO classification recommends calretinin, CK5/6, WT1 and D2-40 as the best mesothelial markers.[7] However, the choice of markers for differentiating SEM from poorly differentiated non-small cell carcinoma requires attention. Calretinin, D2-40 and CK5/6 are useful mesothelial markers for differentiating EM from AC. However, these markers are not useful for distinguishing SEM from PDSCC, because of their low sensitivity or specificity. Therefore, when two of these three markers are chosen as mesothelial markers, there is some possibility of misdiagnosing PDSCC as SEM. Similarly, although TTF-1 and napsin A are useful carcinoma markers for differentiating EM from pulmonary AC, they are not useful for differentiating EM from SCC. Therefore, the use of TTF-1 and napsin A as carcinoma markers may also lead to misdiagnosis of PDSCC as SEM.

In this study, the combination of calretinin and WT1 showed the highest diagnostic accuracy as a positive marker panel, and the combination of p40 and CEA showed the highest diagnostic accuracy (97.3%) as a negative marker panel. From these results, the combination of calretinin, WT1, p40 and CEA seems to be the best immunohistochemical marker panel for distinguishing SEM from PDSCC. However, when p40 is chosen as one of the carcinoma markers, there is some possibility of misdiagnosing solid AC as SEM, because p40 is rarely expressed in AC.[30–32] In contrast, claudin-4 is widely expressed in both AC and SCC,[33–35] and the diagnostic accuracy of the combination of CEA and claudin-4 (94.6%) was comparable to that of p40 and CEA (97.3%). On the basis of these considerations, claudin-4 should be used as a carcinoma marker instead of p40, in the histopathological differential diagnosis of pleural tumours consisting of solid, sheet-like or cord-like proliferations of epithelioid cells, which require differentiation from PDSCC or solid AC.

In conclusion, we conducted immunohistochemical analyses for differentiating SEM from PDSCC, using 11 commercially available antibodies. On the basis of our results, we recommend the use of a combination of WT1 and calretinin as a positive maker, and a combination of CEA and claudin-4 as a negative marker, to overcome the weaknesses of the individual markers to some extent. In the future, there should be an emphasis on the identification and utilization of new markers, especially mesothelial-specific positive markers.

Conflicts of interest

The authors have no conflicts of interest to declare.

Author contributions

K. Inai, T. Kishimoto and Y. Takeshima designed the research study. K. Kushitani, Y. Miyata, M. Okada and Y. Takeshima contributed to the collection of cases. K. Kushitani, Y. Okada and Y. Katayama performed the research. K. Kushitani wrote the first draft of the manuscript. V. J. Amatya, A. S. Mawas and Y. Takeshima contributed to the final approval of the manuscript.

Acknowledgements

The authors thank the Technical Centre, Hiroshima University, for technical assistance, and thank Editage (www.editage.jp) for English-language editing. This study was funded in part by the Japanese Ministry of Health, Labour and Welfare.

References

1. Gemba K, Fujimoto N, Aoe K *et al.* Treatment and survival analyses of malignant mesothelioma in Japan. *Acta Oncol.* 2013; **52**; 803–808.
2. Gemba K, Fujimoto N, Kato K *et al.* National survey of malignant mesothelioma and asbestos exposure in Japan. *Cancer Sci.* 2012; **103**; 483–490.
3. Prazakova S, Thomas PS, Sandrini A, Yates DH. Asbestos and the lung in the 21st century: an update. *Clin. Respir. J.* 2014; **8**; 1–10.
4. Robinson BW, Musk AW, Lake RA. Malignant mesothelioma. *Lancet* 2005; **366**; 397–408.
5. Roggli VL, Sharma A, Butnor KJ, Sporn T, Vollmer RT. Malignant mesothelioma and occupational exposure to asbestos: a clinicopathological correlation of 1445 cases. *Ultrastruct. Pathol.* 2002; **26**; 55–65.
6. Murayama T, Takahashi K, Natori Y, Kurumatani N. Estimation of future mortality from pleural malignant mesothelioma in Japan based on an age-cohort model. *Am. J. Ind. Med.* 2006; **49**; 1–7.
7. Galateau-Salle F, Churg A, Roggli V *et al.* Tumours of the pleura. In Travis WD, Brambilla E, Burke AP, Marx A, Nicholson AG eds. *World Health Organization classification of tumours of the lung, pleura, thymus and heart*. Lyon: IARC Press, 2015; 153–181.
8. Churg A, Cagle P, Roggli V. *Tumors of the serosal membranes.* Washington, DC: American Registry of Pathology, 2006; 147.

9. Harwood TR, Gracey DR, Yokoo H. Pseudomesotheliomatous carcinoma of the lung. A variant of peripheral lung cancer. *Am. J. Clin. Pathol.* 1976; **65**; 159–167.
10. Koss MN, Fleming M, Przygodzki RM, Sherrod A, Travis W, Hochholzer L. Adenocarcinoma simulating mesothelioma: a clinicopathologic and immunohistochemical study of 29 cases. *Ann. Diagn. Pathol.* 1998; **2**; 93–102.
11. Mayall FG, Gibbs AR. 'Pleural' and pulmonary carcinosarcomas. *J. Pathol.* 1992; **167**; 305–311.
12. Oka K, Otani S, Yoshimura T *et al.* Mucin-negative pseudomesotheliomatous adenocarcinoma of the lung: report of three cases. *Acta Oncol.* 1999; **38**; 1119–1121.
13. Shah IA, Salvatore JR, Kummet T, Gani OS, Wheeler LA. Pseudomesotheliomatous carcinoma involving pleura and peritoneum: a clinicopathologic and immunohistochemical study of three cases. *Ann. Diagn. Pathol.* 1999; **3**; 148–159.
14. Attanoos RL, Gibbs AR. 'Pseudomesotheliomatous' carcinomas of the pleura: a 10-year analysis of cases from the Environmental Lung Disease Research Group, Cardiff. *Histopathology* 2003; **43**; 444–452.
15. Funai K, Yokose T, Ishii G *et al.* Clinicopathologic characteristics of peripheral squamous cell carcinoma of the lung. *Am. J. Surg. Pathol.* 2003; **27**; 978–984.
16. Sakurai H, Asamura H, Watanabe S, Suzuki K, Tsuchiya R. Clinicopathologic features of peripheral squamous cell carcinoma of the lung. *Ann. Thorac. Surg.* 2004; **78**; 222–227.
17. Husain AN, Colby T, Ordonez N *et al.* Guidelines for pathologic diagnosis of malignant mesothelioma: 2012 update of the consensus statement from the International Mesothelioma Interest Group. *Arch. Pathol. Lab. Med.* 2013; **137**; 647–667.
18. Travis WD, Brambilla E, Nicholson AG *et al.* The 2015 World Health Organization classification of lung tumors: impact of genetic, clinical and radiologic advances since the 2004 classification. *J. Thorac. Oncol.* 2015; **10**; 1243–1260.
19. Galateau-Salle F, Churg A, Roggli V, Travis WD; World Health Organization Committee for Tumors of the Pleura. The 2015 World Health Organization classification of tumors of the pleura: advances since the 2004 classification. *J. Thorac. Oncol.* 2016; **11**; 142–154.
20. Kushitani K, Takeshima Y, Amatya VJ, Furonaka O, Sakatani A, Inai K. Immunohistochemical marker panels for distinguishing between epithelioid mesothelioma and lung adenocarcinoma. *Pathol. Int.* 2007; **57**; 190–199.
21. Amatya VJ, Takeshima Y, Kohno H *et al.* Caveolin-1 is a novel immunohistochemical marker to differentiate epithelioid mesothelioma from lung adenocarcinoma. *Histopathology* 2009; **55**; 10–19.
22. Ordonez NG. Application of immunohistochemistry in the diagnosis of epithelioid mesothelioma: a review and update. *Hum. Pathol.* 2013; **44**; 1–19.
23. Ordonez NG. The diagnostic utility of immunohistochemistry in distinguishing between epithelioid mesotheliomas and squamous carcinomas of the lung: a comparative study. *Mod. Pathol.* 2006; **19**; 417–428.
24. Tsao M-S, Brambilla E, Nicholson AG *et al.* Squamous cell carcinoma. In Travis WD, Brambilla E, Burke AP, Marx A, Nicholson AG eds. *World Health Organization classification of tumours of the lung, pleura, thymus and heart*. Lyon: IARC Press, 2015; 51–55.
25. Hohenstein P, Hastie ND. The many facets of the Wilms' tumour gene, WT1. *Hum. Mol. Genet.* 2006; **15**(Spec. No. 2); R196–R201.
26. Takeshima Y, Amatya VJ, Kushitani K, Inai K. A useful antibody panel for differential diagnosis between peritoneal mesothelioma and ovarian serous carcinoma in Japanese cases. *Am. J. Clin. Pathol.* 2008; **130**; 771–779.
27. Ordonez NG. The immunohistochemical diagnosis of mesothelioma: a comparative study of epithelioid mesothelioma and lung adenocarcinoma. *Am. J. Surg. Pathol.* 2003; **27**; 1031–1051.
28. Rogers JH. Calretinin: a gene for a novel calcium-binding protein expressed principally in neurons. *J. Cell Biol.* 1987; **105**; 1343–1353.
29. Doglioni C, Dei Tos AP, Laurino L *et al.* Calretinin: a novel immunocytochemical marker for mesothelioma. *Am. J. Surg. Pathol.* 1996; **20**; 1037–1046.
30. Pelosi G, Rossi G, Cavazza A *et al.* Deltanp63 (p40) distribution inside lung cancer: a driver biomarker approach to tumor characterization. *Int. J. Surg. Pathol.* 2013; **21**; 229–239.
31. Tatsumori T, Tsuta K, Masai K *et al.* P40 is the best marker for diagnosing pulmonary squamous cell carcinoma: comparison with p63, cytokeratin 5/6, desmocollin-3, and SOX2. *Appl. Immunohistochem. Mol. Morphol.* 2014; **22**; 377–382.
32. Bishop JA, Teruya-Feldstein J, Westra WH, Pelosi G, Travis WD, Rekhtman N. P40 (DeltaNp63) is superior to p63 for the diagnosis of pulmonary squamous cell carcinoma. *Mod. Pathol.* 2012; **25**; 405–415.
33. Facchetti F, Lonardi S, Gentili F *et al.* Claudin 4 identifies a wide spectrum of epithelial neoplasms and represents a very useful marker for carcinoma versus mesothelioma diagnosis in pleural and peritoneal biopsies and effusions. *Virchows Arch.* 2007; **451**; 669–680.
34. Soini Y, Kinnula V, Kahlos K, Paakko P. Claudins in differential diagnosis between mesothelioma and metastatic adenocarcinoma of the pleura. *J. Clin. Pathol.* 2006; **59**; 250–254.
35. Lodi C, Szabo E, Holczbauer A *et al.* Claudin-4 differentiates biliary tract cancers from hepatocellular carcinomas. *Mod. Pathol.* 2006; **19**; 460–469.
36. Lonardi S, Manera C, Marucci R, Santoro A, Lorenzi L, Facchetti F. Usefulness of claudin 4 in the cytological diagnosis of serosal effusions. *Diagn. Cytopathol.* 2011; **39**; 313–317.
37. Ordonez NG. Value of claudin-4 immunostaining in the diagnosis of mesothelioma. *Am. J. Clin. Pathol.* 2013; **139**; 611–619.
38. Wang NS, Huang SN, Gold P. Absence of carcinoembryonic antigen-like material in mesothelioma: an immunohistochemical differentiation from other lung cancers. *Cancer* 1979; **44**; 937–943.
39. Ordonez NG. What are the current best immunohistochemical markers for the diagnosis of epithelioid mesothelioma? A review and update *Hum. Pathol.* 2007; **38**; 1–16.

Modern Pathology (2017), 1–10

© 2017 USCAP, Inc All rights reserved 0893-3952/17 $32.00

MUC4, a novel immunohistochemical marker identified by gene expression profiling, differentiates pleural sarcomatoid mesothelioma from lung sarcomatoid carcinoma

Vishwa Jeet Amatya[1], Kei Kushitani[1], Amany Sayed Mawas[1,2], Yoshihiro Miyata[3], Morihito Okada[3], Takumi Kishimoto[4], Kouki Inai[1,5] and Yukio Takeshima[1]

[1]Department of Pathology, Hiroshima University Graduate School of Biomedical and Health Sciences, Hiroshima, Japan; [2]Department of Pathology and Clinical Pathology, South Valley University, Qena, Egypt; [3]Department of Surgical Oncology, Research Institute for Radiation Biology and Medicine, Hiroshima University, Hiroshima, Japan; [4]Department of Internal Medicine, Okayama Rosai Hospital, Okayama, Japan and [5]Pathologic Diagnostic Center, Inc., Hiroshima, Japan

Sarcomatoid mesothelioma, a histological subtype of malignant pleural mesothelioma, is a very aggressive tumor with a poor prognosis. Histological diagnosis of sarcomatoid mesothelioma largely depends on the histomorphological feature of spindled tumor cells with immunohistochemical reactivity to cytokeratins. Diagnosis also requires clinico-radiological and/or macroscopic evidence of an extrapulmonary location to differentiate it from lung sarcomatoid carcinoma. Although there are promising immunohistochemical antibody panels to differentiate mesothelioma from lung carcinoma, a consensus on the immunohistochemical markers that distinguish sarcomatoid mesothelioma from lung sarcomatoid carcinoma has not been reached and requires further study. We performed whole gene expression analysis of formalin-fixed paraffin-embedded tissue from sarcomatoid mesothelioma and lung sarcomatoid carcinoma and observed significant differences in the expression of MUC4 and other genes between sarcomatoid mesothelioma and lung sarcomatoid carcinoma. Immunohistochemistry demonstrated that MUC4 was expressed in the spindled tumor cells of lung sarcomatoid carcinoma (21/29, 72%) but was not expressed in any sarcomatoid mesothelioma (0/31, 0%). To differentiate sarcomatoid mesothelioma from lung sarcomatoid carcinoma, negative MUC4 expression showed 100% sensitivity and 72% specificity and accuracy rate of 87%, which is higher than immunohistochemical markers such as calretinin, D2-40 and Claudin-4. Therefore, we recommend to include MUC4 as a novel and useful negative immunohistochemical marker for differentiating sarcomatoid mesothelioma from lung sarcomatoid carcinoma.

Modern Pathology advance online publication, 27 January 2017; doi:10.1038/modpathol.2016.181

Malignant pleural mesothelioma, a highly aggressive tumor with a poor prognosis, is strongly associated with asbestos exposure; its incidence is increasing in Japan and Western countries and is expected to increase in developing countries.[1] It is histologically classified into three subtypes: epithelioid, biphasic, and sarcomatoid mesothelioma.[2] The International Mesothelioma Interest Group (IMIG) has published guidelines for the differential diagnosis of epithelioid mesothelioma from lung adenocarcinoma and squamous cell carcinoma using immunohistochemical antibody panels of mesothelioma markers (calretinin, D2-40, WT1, cytokeratin 5/6), lung adenocarcinoma markers (CEA, TTF-1, Napsin-A, MOC-31, BerEP4, BG8, B72.3) and lung squamous carcinoma markers (p63, p40, MOC-31, Ber-EP4, cytokeratin 5/6).[3]

However, a consensus on the immunohistochemical markers that differentiate sarcomatoid mesothelioma from lung sarcomatoid carcinoma

---

Correspondence: Dr Y Takeshima, MD, PhD, Department of Pathology, Hiroshima University Graduate School of Biomedical and Health Sciences, 1-2-3 Kasumi, Minami-ku, Hiroshima 734-8551, Japan.
E-mail: ykotake@hiroshima-u.ac.jp

Received 15 June 2016; revised 3 September 2016; accepted 6 September 2016; published online 26 January 2017

has not been reached and requires further study. The histological diagnosis of sarcomatoid mesothelioma largely depends on the histomorphological feature of spindled tumor cells supported by immunohistochemical cytokeratin reactivity; it also requires clinico-radiological and/or macroscopic evidence of an extrapulmonary location. The immunohistochemical markers for lung adenocarcinoma and squamous carcinoma are not useful for diagnosing lung sarcomatoid carcinoma. To date, D2-40 and calretinin are two commonly used positive mesothelial markers expressed in sarcomatoid mesothelioma.[4–7] However, without convincing calretinin and D2-40 positivity, it is difficult to differentiate sarcomatoid mesothelioma from sarcomatoid carcinoma. In previous reports, including ours, high D2-40 sensitivity has been reported to differentiate sarcomatoid mesothelioma from lung sarcomatoid carcinoma; however, D2-40 specificity is not perfect.[6,7] Therefore, the clinico-radiological identification of tumor location at the extrapulmonary site remains essential to differentiate between these two diseases.

In recent decades, gene expression profiling has been used in many cancers to identify the pathways involved in malignant transformation and to identify novel candidate diagnostic and prognostic markers. We have recently reported the application of gene expression analysis to identify novel markers differentiating epithelioid mesothelioma from reactive mesothelial hyperplasia by PCR array.[8] Although gene expression analysis requires specimens with a high proportion of tumor cells containing good quality RNA, we successfully analyzed the RNA extracted from formalin-fixed paraffin-embedded samples.

The aim of this study was to perform gene expression analysis on spindled tumor cells dissected from formalin-fixed paraffin-embedded tissue of sarcomatoid mesothelioma and lung sarcomatoid carcinoma. Our gene expression microarray data identified several novel genes that are differentially expressed between sarcomatoid mesothelioma and lung sarcomatoid carcinoma, and of these, we validated MUC4 as a novel and useful negative immunohistochemical marker differentiating sarcomatoid mesothelioma from lung sarcomatoid carcinoma.

Materials and methods

Formalin-Fixed Paraffin-Embedded Tissue Samples

Sarcomatoid mesothelioma and lung sarcomatoid carcinoma cases were retrieved from surgical pathology archives of our department during 2005–2014. The clinical details were also reviewed from the patient record files. The location of tumor was confirmed by reviewing clinical information (especially chest computed tomography findings to confirm the tumor localization), gross findings and reviewing histological sections stained with H&E and Elastica van Gieson. All lung sarcomatoid carcinoma cases in this study were located in the pulmonary parenchyma, which was confirmed by radiological, thoracoscopic and operative findings. None of the lung sarcomatoid carcinoma showed diffuse pleurotropic growth pattern described as 'pseudomesotheliomatous growth'. Sarcomatoid mesothelioma was located in extrapulmonary site showing dominant pleurotrophic growth pattern without obvious tumor mass in lung parenchyma. Pathological diagnosis of each case was confirmed by histological findings and immunohistochemical marker panel recommended by Guidelines for Pathologic Diagnosis of Malignant Mesothelioma-2012 Update of the Consensus Statement from the International Mesothelioma Interest Group[3] and current 2015 WHO histological classification of tumours of the lung, pleura, thymus and heart.[9] Sarcomatoid mesothelioma is characterized by a proliferation of spindle cells arranged in fascicles or having a haphazard distribution involving adjacent adipose tissue, parietal pleura or lung parenchyma.[9] Lung sarcomatoid carcinoma is a poorly differentiated non-small cell lung carcinoma that contains a component of sarcoma or sarcoma-like (spindle and/or giant cell) differentiation. Lung sarcomatoid carcinoma is a group of five types of carcinomas based on specific histological criteria and described as giant cell carcinoma, pleomorphic carcinoma, carcinosarcoma, spindle cell carcinoma and pulmonary blastoma. Of these, spindle cell carcinoma and pleomorphic carcinoma with predominant spindle cell component requires the differentiation from sarcomatoid mesothelioma. The number of patients who were diagnosed as sarcomatoid mesothelioma and lung sarcomatoid carcinoma after surgical resection and/or autopsy examination in Hiroshima University Hospital during 2005–2014 were 35 and 34 respectively, suggesting similar frequencies of their incidence. Localization of four cases of sarcomatoid mesothelioma and five cases of lung sarcomoid carcinoma could not be confirmed and thus were excluded from this study. Finally, 31 cases of sarcomatoid mesothelioma and 29 cases of lung sarcomatoid carcinoma were analyzed in the present study. Sarcomatoid mesothelioma included 25 cases of pure sarcomatoid growth (pure sarcomatoid mesothelioma) and 6 cases of biphasic mesothelioma showing predominantly sarcomatoid growth. Lung sarcomatoid carcinoma included 5 cases of spindle cell carcinoma and 24 of pleomorphic carcinoma with predominant spindle cell carcinoma component. Minor foci of squamous cell carcinoma and adenocarcinoma component were present in 5 and 19 cases of pleomorphic carcinoma. Carcinosarcoma, giant cell carcinoma and pulmonary blastema were not included in this study.

The anonymized (unlinkable) tissue samples were provided by the Department of Pathology for gene expression analysis and immunohistochemical study. This study is in accordance with the Ethics Guidelines for Human Genome/Gene Research enacted by the Japanese Government for the collection of tissue specimens and was approved by the institutional ethics review committee (Hiroshima University E-48).

Gene Expression Analysis

Formalin-fixed paraffin-embedded sections from six cases of sarcomatoid mesothelioma and six cases of lung sarcomatoid carcinoma were used for gene expression analysis. RNA extraction for gene expression analysis was performed from the spindled tumor cells of these cases. Five 10-μm-thick formalin-fixed paraffin-embedded tissue sections containing >90% spindled tumor tissue were processed for total RNA extraction using the Maxwell 16 LEV RNA FFPE Purification Kit (Promega, Tokyo, Japan) according to the manufacturer's protocol. After deparaffinization and lysis with proteinase K treatment, the samples were treated with a DNase cocktail for 15 min at room temperature, followed by RNA purification using a MAXWELL 16 instrument according to the manufacturer's protocol (Promega).

RNA quality was analyzed with an RNA StdSens Analysis kit using an Experion automated electrophoresis system (Bio-Rad Laboratories, Hercules, CA, USA). RNA quantity was estimated with a Qubit RNA HS Kit using a Qubit Fluorometer 2.0 (Molecular Probes/Life Technologies, Carlsbad, CA, USA). The Almac Xcel Array GeneChip (Affymetrix, Santa Clara, CA, USA) contains probe sets of >97 000 transcripts and was used to analyze gene expression profiles. Total RNA was amplified and labeled with a 3′ IVT Labeling Kit (Affymetrix) before hybridization onto the GeneChip. Briefly, 100 ng total RNA was amplified with a SensationPlus FFPE Amplification Kit (Affymetrix) to generate 30 μg of SenseRNA according to the manufacturer's protocol. Twenty-five micrograms of SenseRNA was labeled with a 3′ IVT Labeling Kit (Affymetrix) and hybridized to a Almac Xcel Array GeneChip (Affymetrix) at 45 °C for 16 h using a GeneChip Hybridization Oven 645 (Affymetrix). The hybridized GeneChip was washed, stained using GeneChip Fluidic Station 450 (Affymetrix) and scanned with a GeneChip Scanner 3000 7G (Affymetrix) using the GeneChip Operating Software (Affymetrix). The data were analyzed using the Gene Expression Console Software (Affymetrix), and further statistical analyses were performed using the Subio Software Platform (Subio, Amami-shi, Japan) to calculate plot graphs, fold change of expression and hierarchical clustering.

Validation of Gene Expression Analysis

The same 12 cases of sarcomatoid mesothelioma and lung sarcomatoid carcinoma that were analyzed for gene expression profiling were used to validate the microarray expression data. The relative mRNA expression of *MUC4*, a highly expressed gene in lung sarcomatoid carcinoma, and *IGF2*, highly expressed in sarcomatoid mesothelioma, was assessed with SYBR Green-based real-time RT-PCR using GAPDH as a control. A total of 100 ng RNA was used for mRNA expression with a one-step SYBR Green RT-PCR Kit (Takara-Bio, Tokyo, Japan) using a MX3000P real-time PCR thermal cycler (Stratagene, Agilent Technologies, Tokyo, Japan). The primer pairs used were *MUC4*-F: CAGGCCACCAACTTCA TCG; *MUC4*-R: ACACGGATTGCGTCGTGAG; *IGF2*-F: GTGGCATCGTTGAGGAGTG; *IGF2*-R: CACGTCC CTCTCGGACTTG; *GAPDH*-F: ACAACTTTGGTATC GTGGAAGG; and *GAPDH*-R: GCCATCACGCCA CAGTTTC. Data analysis was performed using the δδCT method for relative quantification. Briefly, threshold cycles (CT) for *GAPDH* (reference) and *MUC4*, *IGF2* (samples) were determined in triplicate. The relative expression (rI) was calculated using the formula: $rI = 2^{-(\text{CT sample} - \text{CT normal})}$.

Immunohistochemistry

Immunohistochemistry was performed using 3-μm tissue sections from the best representative formalin-fixed paraffin-embedded sarcomatoid mesothelioma and lung sarcomatoid carcinoma tissue blocks. All of the immunohistochemical staining was performed with a Benchmark GX automated immunohistochemical station (Ventana, Roche Diagnostics, Tokyo, Japan) using the ultraView Universal DAB Detection Kit (Ventana, Roche Diagnostic, Tokyo, Japan). The antigen retrieval methods and antibodies used in this study are summarized in Table 1. Immunoreactivity was scored as negative (0, no immunostaining) or positive. Positive immunoreactivity was graded as +1 for up to 10% of tumor cells showing positive immunostaining, +2 for >10–50% of the tumor cells, and +3 for >50% of the tumor cells. Only spindled tumor cells from sarcomatoid mesothelioma and lung sarcomatoid carcinoma were evaluated for the immunoreactivity of various markers. Statistical analyses were performed using Fisher's exact test. Sensitivity, specificity, positive predictive value, negative predictive value and accuracy rate were calculated using a simple 2 × 2 table.

Results

Differential Gene Expression and Validation in Sarcomatoid Mesothelioma and Lung Sarcomatoid Carcinoma

Out of the 97 000 analyzable transcripts on the Almac Xcel Array GeneChip, 2099 statistically significant mRNA transcripts were differentially expressed between sarcomatoid mesothelioma and lung sarcomatoid carcinoma by a more than a two-fold difference (Figure 1, plot graph). The

Table 1 List of antibodies with their clone, commercial source and reaction conditions

Antibody to	*Clone*	*Provider*	*Dilution*	*Antigen retrieval*
MUC4	8G7	Santa Cruz Biotechnology	× 25	CC1, 60 min
Calretinin	SP65	Ventana	Prediluted	CC1, 30 min
Podoplanin	D2-40	Nichirei	Prediluted	CC1, 60 min
WT1	6F-H2	Dako	× 25	CC1, 60 min
Pancytokeratin	AE1/AE3	Ventana	Prediluted	Protease 8 min
Cytokeratin	CAM5.2	Ventana	Prediluted	Protease 8 min
p40	BC28	Biocare Medical	× 50	CC1, 60 min
TTF-1	SP141	Ventana	Prediluted	CC1, 60 min
Claudin-4	3E2C1	Life Technologies	× 50	CC1, 60 min

Abbreviation: CC1, cell conditioning buffer 1 (Tris-based buffer, pH 8.5 from Ventana).

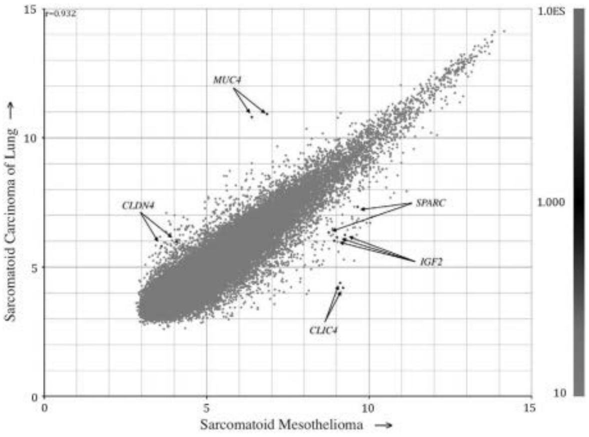

Figure 1 Scatter plot of raw data from the microarray experiments demonstrating MUC4 and CLDN4 with lower expression and IGF2, CLIC4 and SPARC4 with higher expression in sarcomatoid mesothelioma compared with that of lung sarcomatoid carcinoma.

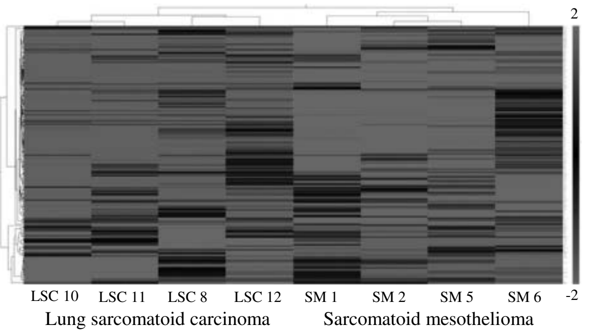

Figure 2 The hierarchical clustering of RNA transcripts with more than five-fold differential expression between sarcomatoid mesothelioma and lung sarcomatoid carcinoma revealed 156 upregulated mRNA transcripts, including *IGF2*, *MEG3*, *CLIC4* and *SPARC*, in sarcomatoid mesothelioma and 46 upregulated mRNA transcripts, including *MUC4* and *Claudin4*, in lung sarcomatoid carcinoma.

hierarchical clustering of mRNAs with more than a five-fold difference in expression revealed 156 upregulated mRNA transcripts, including *IGF2*, *MEG3*, *CLIC4* and *SPARC*, in sarcomatoid mesothelioma and 46 upregulated mRNA transcripts, including *MUC4* and *Claudin4*, in lung sarcomatoid carcinoma (Figure 2, hierarchical clustering; Supplementary Table S1). The mRNA expression hits were validated by real-time RT-PCR of *MUC4* and *IGF2*. *MUC4* mRNA expression was negligible in all six sarcomatoid mesothelioma, and the expression was observed in five of the six lung sarcomatoid carcinoma samples. *IGF2* mRNA was expressed in all of the sarcomatoid mesothelioma samples, although it was also expressed in three of the six lung sarcomatoid carcinoma samples (detailed data not shown).

Immunohistochemical Profiles of Sarcomatoid Mesothelioma and Lung Sarcomatoid Carcinoma

The percentage of positivity and immunohistochemical score for MUC4, mesothelioma markers (calretinin, D2-40, WT1) and lung carcinoma markers (TTF-1, p40, Claudin-4) along with the cytokeratins AE1/AE3 and CAM5.2 are shown in Table 2.

MUC4 Expression

MUC4 expression was observed in the cytoplasm of tumor cells, and the positivity of spindled tumor cells alone was evaluated. MUC4 was also observed in the surrounding normal lung tissue, particularly in bronchial tissue, and was considered an internal positive marker. It was expressed in spindled tumor cells of 21 lung sarcomatoid carcinoma (21/29, 72%; Figure 3b) but none in sarcomatoid mesothelioma (0/31, 0%; Figure 4b). In addition to spindled tumor cells of lung sarcomatoid carcinoma, MUC4 was also expressed in the non-small cell carcinoma component consisting of adenocarcinoma or squamous cell carcinoma in pleomorphic carcinoma. Among lung sarcomatoid carcinoma, 3 cases showed expression in >50% of tumor cells, 9 cases in 10–50% of tumor cells and 9 cases in <10% of tumor cells. Out of the 21 lung sarcomatoid carcinoma cases with MUC4

Table 2 Potential immunohistochemical markers for sarcomatoid mesothelioma and lung sarcomatoid carcinoma

	Sarcomatoid mesothelioma						*Lung sarcomatoid carcinoma*							
			Immunohistochemical score[a]						*Immunohistochemical score*[a]					
Antibody	*Positive cases*	*(%)*	*0*	*1+*	*2+*	*3+*	*Positive cases*	*(%)*	*0*	*1+*	*2+*	*3+*	P-*value*[b]	P-*value*[c]
MUC4	0/31	0	31	0	0	0	21/29	72	8	9	9	3	< 0.01	< 0.01
Calretinin	23/31	74	8	7	11	5	13/29	45	16	5	6	2	< 0.05	< 0.05
D2-40	22/31	71	9	9	12	1	9/29	31	20	9	0	0	< 0.01	< 0.01
WT1	6/31	19	25	5	1	0	1/29	3	28	1	0	0	NS	NS
AE1/AE3	29/31	94	2	2	8	19	29/29	100	0	5	2	22	NS	NS
CAM5.2	28/31	90	3	1	8	19	28/29	97	1	6	5	17	NS	NS
TTF-1	0/31	0	31	0	0	0	15/29	52	14	0	4	11	< 0.01	< 0.01
p40	2/31	7	29	2	0	0	6/29	21	23	0	3	3	NS	NS
Claudin-4	0/31	0	31	0	0	0	13/29	45	16	4	5	4	< 0.01	< 0.01

Abbreviations: NA, not available; NS, not significant; TTF-1, thyroid transcription factor; WT1, Wilms' tumor gene product.

[a] Calculated by Fisher's exact test of the positive rate between two groups.

[b] Calculated by the Mann–Whitney *U*-test of reactivity scores of the markers between two groups.

[c] Immunohistochemical score was semiquantified as follows: 0: 0%; 1+: 1–10%; 2+: 11–50%; 3+: > 51% of spindled tumor cells.

expression, p40 expression was observed only in 3 cases, TTF-1 in 12 cases and Claudin-4 in 10 cases. Of the nine lung sarcomatoid carcinoma cases without MUC4 expression, p40 expression was observed in three cases, TTF-1 in three cases and Claudin-4 in three cases.

Calretinin, D2-40 and WT1

Calretinin was expressed in the nucleus and cytoplasm of spindled tumor cells of 23 (74%) sarcomatoid mesothelioma and 13 (45%) lung sarcomatoid carcinoma samples, and D2-40 was expressed in the spindled tumor cells of 21 (71%) sarcomatoid mesothelioma and 9 (31%) lung sarcomatoid carcinoma. The immunohistochemical scoring pattern for calretinin expression was not different between sarcomatoid mesothelioma and lung sarcomatoid carcinoma. However, the immunohistochemical scoring pattern for D2-40 expression showed a higher score in sarcomatoid mesothelioma than in lung sarcomatoid carcinoma. WT1 nuclear expression was present in only 6 (19%) sarcomatoid mesothelioma and 1 (3%) lung sarcomatoid carcinoma, revealing it to be a poor immunohistochemical marker to differentiate sarcomatoid mesothelioma from lung sarcomatoid carcinoma.

TTF-1, p40, Claudin-4

Nuclear expression of TTF-1 and P40 was observed in 15 (52%) and 6 (21%) cases of lung sarcomatoid carcinoma, respectively. TTF-1 expression was not observed in sarcomatoid mesothelioma, but p40 expression was observed in 2 (7%) sarcomatoid mesothelioma cases. TTF-1 and/or p40 immunoreactivity was present in 19 of the 29 (66%) cases of lung sarcomatoid carcinoma and 2 of the 31 (7%) cases of sarcomatoid mesothelioma. Claudin-4 and/or TTF-1/p40 immunoreactivity was present in 25 of the 29 (86%) of lung sarcomatoid carcinoma and 2 of the 31 (7%) cases of sarcomatoid mesothelioma. However, p40 expression in sarcomatoid mesothelioma was focal and heterogeneous with an immunohistochemical score of 1.

Cytokeratins, AE1/AE3, CAM5.2

Cytokeratin AE1/AE3 and CAM5.2 expression was present in > 90% of both lung sarcomatoid carcinoma and sarcomatoid mesothelioma samples. The majority of sarcomatoid mesothelioma and lung sarcomatoid carcinoma cases showed the expression of both cytokeratins, and the remaining two lung sarcomatoid carcinoma cases and one sarcomatoid mesothelioma case expressed at least one of the two cytokeratins.

Sensitivity and Specificity of Each Marker to Differentially Diagnose Sarcomatoid Mesothelioma and Lung Sarcomatoid Carcinoma

The sensitivity, specificity, positive predictive value, negative predictive value and accuracy rate of each marker differentiating sarcomatoid mesothelioma from lung sarcomatoid carcinoma are shown in Table 3. The negative expression of the carcinoma markers TTF-1 and Claudin-4 showed 100% sensitivity, whereas p40 showed 94%; however, their specificity was restricted around or below 50%. The positive expression of calretinin showed 74% sensitivity and 55% specificity, and D2-40 showed 71% sensitivity and 69% specificity. Although WT1 showed the highest specificity of 97%, its sensitivity

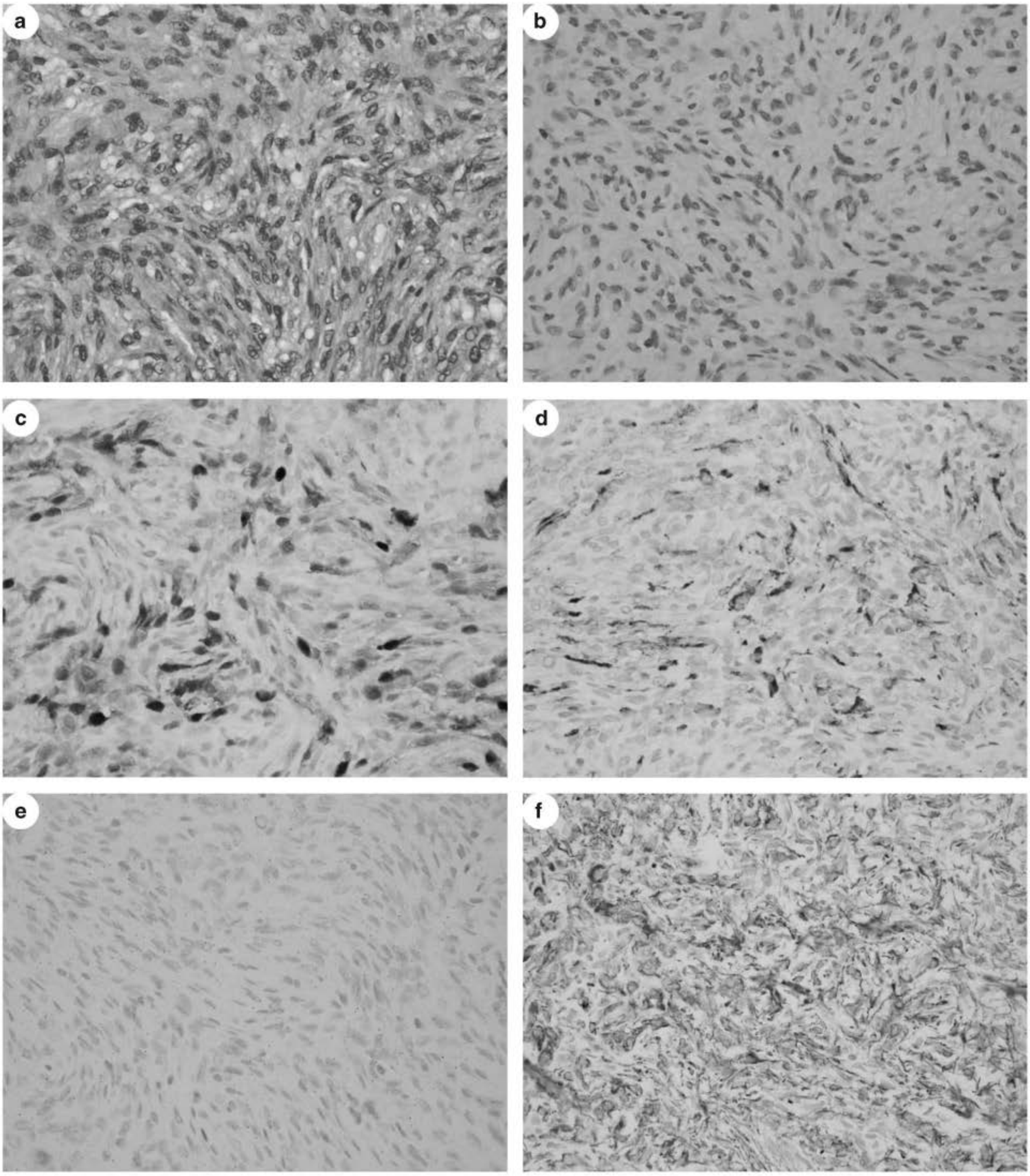

Figure 3 Representative pictures of immunohistochemical expression of MUC4 (**b**), Calretinin (**c**), D2-40 (**d**), Claudin-4 (**e**) and AE1/AE3 (**f**) from sarcomatoid mesothelioma (**a**). None of the sarcomatoid mesotheliomas showed immunohistochemical MUC4 expression.

was < 20%. AE1/AE3 and CAM5.2 showed high 94 and 90% sensitivities and near 0% specificity. In comparison to all of these known immunohistochemical markers, negative expression of MUC4 showed 100% sensitivity and 72% specificity, making the accuracy rate of 87%, the highest among these immunohistochemical markers.

Value of Immunohistochemical Marker Panel to Differentially Diagnosis Sarcomatoid Mesothelioma and Lung Sarcomatoid Carcinoma

MUC4 showed the highest sensitivity and specificity among the immunohistochemical markers for differentiatiation of sarcomatoid mesothelioma from lung

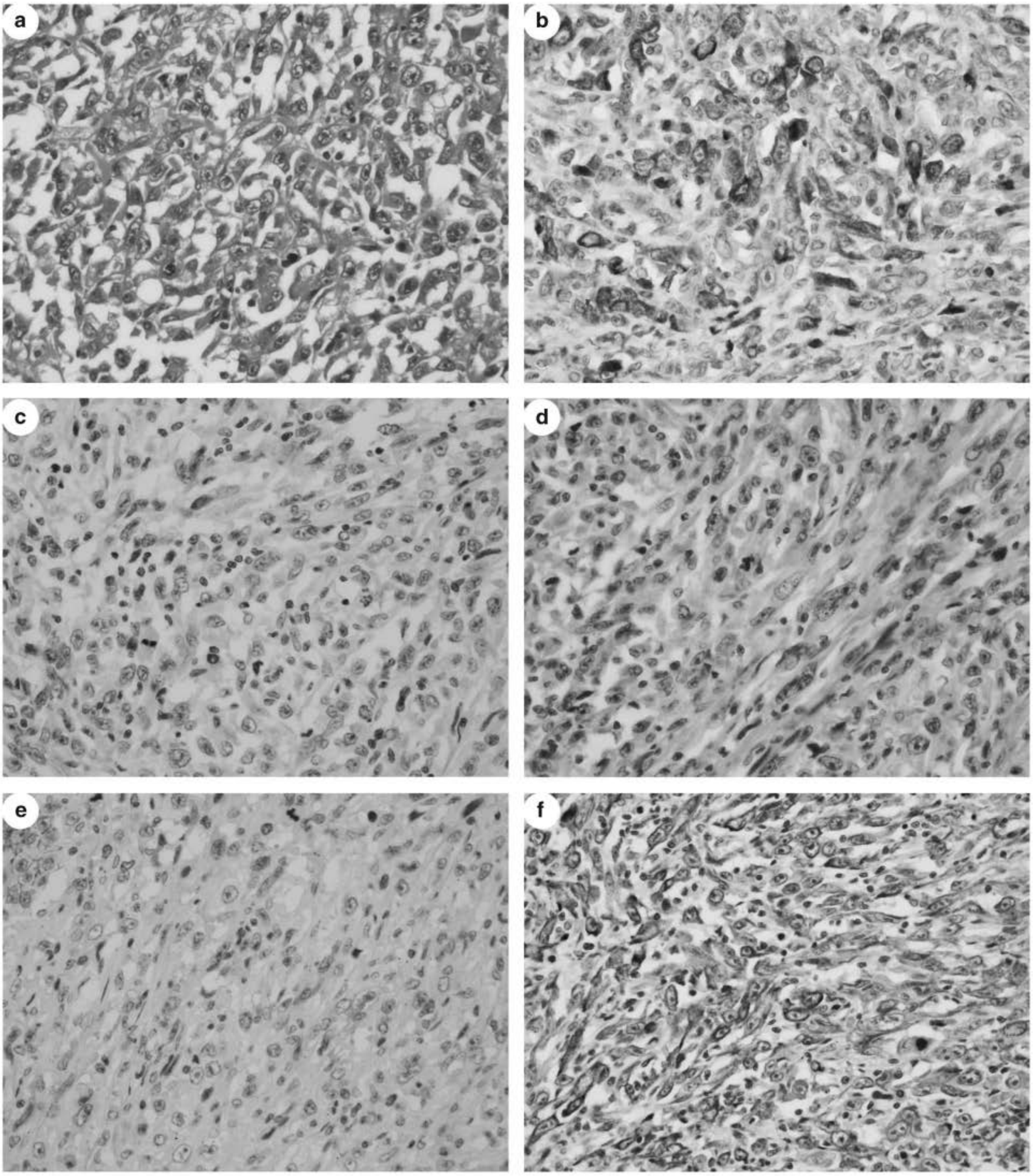

Figure 4 Representative pictures of immunohistochemical MUC4 expression (**b**), Calretinin (**c**), D2-40 (**d**), Claudin-4 (**e**) and AE1/AE3 (**f**) of lung sarcomatoid carcinoma (**a**). Twenty-one of the 29 (72%) lung sarcomatoid carcinomas exhibited cytoplasmic expression of MUC4.

sarcomatoid carcinoma. However, the specificity was 72%. Therefore, a combination of various markers was considered. Various combinations of immunohistochemical markers are shown in Table 4. Among the negative immunohistochemical markers, combination of MUC4, TTF-1 and p40 was observed in 26 of the 29 lung sarcomatoid carcinoma cases (90% specificity) and 2 of the 31sarcomatoid mesothelioma cases (93% sensitivity). Combination of MUC4 and Claudin-4 expression was found in 24 of the 29 lung sarcomatoid carcinoma cases (83% specificity) and none of the sarcomatoid

Table 3 Sensitivity, specificity, PPV, NPV and accuracy rate of each antibody to differentially diagnose sarcomatoid mesothelioma from lung sarcomatoid carcinoma

Findings	*Sensitivity (%)*	*Specificity (%)*	*PPV (%)*	*NPV (%)*	*Accuracy rate (%)*	P-*value*
MUC4 (−)	100	72	80	100	87	< 0.01
Calretinin (+)	74	55	64	67	65	< 0.05
D2-40 (+)	71	69	71	69	70	< 0.01
WT1 (+)	19	97	86	53	57	NS
AE1/AE3 (+)	94	0	50	0	48	NS
CAM5.2 (+)	90	3	50	25	48	NS
TTF-1 (−)	100	52	69	100	77	< 0.01
p40 (−)	94	21	56	75	58	NS
Claudin-4 (−)	100	45	66	100	73	< 0.01

Abbreviations: NPV, negative predictive value; NS, not significant; PPV, positive predictive value.

Table 4 Sensitivity, specificity, PPV, NPV and accuracy rate of two or more markers to differentially diagnose sarcomatoid mesothelioma from lung sarcomatoid carcinoma

Immunohistochemical markers	*Sensitivity (%)*	*Specificity (%)*	*PPV (%)*	*NPV (%)*	*Accuracy rate (%)*	P-*value*
p40 (−)/TTF-1 (−)	94	66	74	91	80	< 0.01
Claudin-4 (−)/TTF-1 (−)/p40 (−)	94	90	91	93	92	< 0.01
Claudin-4 (−)/TTF-1 (−)	100	83	86	100	92	< 0.01
MUC4 (−)/TTF-1 (−)/p40 (−)	94	93	94	93	93	< 0.01
MUC4 (−)/Claudin-4 (−)	100	83	86	100	92	< 0.01
MUC4 (−)/TTF-1 (−)/Claudin-4 (−)	100	90	91	100	95	< 0.01
MUC4 (−)/TTF-1 (−)/p40 (−)/Claudin-4 (−)	94	97	97	93	95	< 0.01

Abbreviations: NPV, negative predictive value; PPV, positive predictive value.

mesothelioma cases (100% sensitivity). The combination of MUC4, TTF-1 and Claudin-4 was observed in 26 of the 29 lung sarcomatoid carcinoma cases (90% specificity) and 0 of the 31 sarcomatoid mesothelioma cases (100% sensitivity).

Discussion

Sarcomatoid mesothelioma has the histomorphological feature of spindled tumor cells and resembles many tumors with spindled cells, including true sarcoma or sarcomatoid carcinomas. The immunohistochemical reactivity to cytokeratin remains critical to differentiate it from true sarcomas. However, differentiating sarcomatoid mesothelioma from lung sarcomatoid carcinoma is challenging, as the histomorphological and immunohistochemical characteristics are extremely similar. For this reason, clinical and/or gross evidence of an extrapulmonary location is indispensable for its diagnosis. Although the mesothelioma markers calretinin and D2-40 have been utilized to differentiate sarcomatoid mesothelioma from lung sarcomatoid carcinoma, they are not absolute, as their sensitivity and specificity are not sufficiently high. Although we previously reported the sensitivity of calretinin (78%) and D2-40 (87%), specificity was not high for calretinin (41%) and D2-40 (74%).[7] Our past and present data on calretinin and D2-40 were similar to reports by Ordonez *et al*[4] and Padgett *et al.*[6] Considering the low specificity of calretinin, D2-40 is considered the single most important immunohistochemical marker for its differentiation. However, in our practical experience, it is still very difficult to interpret the reactivity of D2-40 in these tumors, particularly in cases showing prominent fibro-collagenous proliferation.

TTF-1, a lung adenocarcinoma marker, and p40, a squamous cell carcinoma marker, have emerged as useful markers for non-small cell lung carcinoma[10,11] and are thus supposed to be expressed in pleomorphic lung carcinoma. TTF-1 might be identified as a novel marker differentiating pleomorphic carcinoma from sarcomatoid mesothelioma because of its low expression in sarcomatoid mesothelioma. However, in this study, despite their specificity of 100 or 94%, the sensitivity of TTF-1 (51%) and p40 (21%) are not good to distinguish sarcomatoid mesothelioma and lung sarcomatoid carcinoma. Though p40 expression is good marker of squamous cell carcinoma, it has been also reported in a few mesothelioma cases.[12] In this study too, we observed p40 expression in two sarcomatoid mesothelioma cases but very focal and heterogeneous, unlike its expression in squamous cell carcinoma. Claudin-4, which is reported to be a very reliable universal carcinoma marker differentiating epithelioid mesothelioma from various carcinomas,[13,14] showed limited value in lung sarcomatoid carcinoma cases. In this study, only half of lung sarcomatoid carcinoma expressed Claudin-4, and its punctate expression in the cytoplasm of spindled cells of lung sarcomatoid carcinoma resembled that of the punctate expression in the cytoplasm of sarcomatoid mesothelioma. TTF-1, p40 and Claudin-4 expression can be reliable markers for pleomorphic carcinomas with a prominent carcinoma component, such as adenocarcinoma or squamous cell carcinoma.

In this study, we analyzed all of the genes expressed in sarcomatoid mesothelioma and lung sarcomatoid carcinoma with the aim of identifying novel markers for their differential diagnosis. Although frozen tissue yields better and less degradable RNA for gene expression analysis, we preferred formalin-fixed paraffin-embedded tissue samples because they included the microscopically identifiable spindle cell tumor tissue. For this analysis, we have to amplify the small amount of RNA extracted from the formalin-fixed paraffin-embedded tissue before hybridization to the GeneChip. The Almac Xcel GeneChip from Affymetrix, which we used here, has been reported to produce identical results to the GeneChip using RNA derived from frozen tissue samples. In addition, it contains proprietary Almac-sequenced data and filtered public data for biomarker discovery and the validation of oncogene-related transcripts for a much higher detection rate in degraded samples.

From the differential expression analysis, a more than five-fold expression change in *IGF2*, *CLIC4* and *SPARC* was observed in sarcomatoid mesothelioma, and IGF2 expression was validated by real-time RT-PCR. We did not uncover significant differential expression of IGF2 between sarcomatoid mesothelioma and lung sarcomatoid carcinoma (data not shown). The discrepancy between the microarray data and real-time RT-PCR data can be explained because *IGF2* mRNA expression on a microarray chip is the relative expression between both lung sarcomatoid carcinoma and sarcomatoid mesothelioma but in a different quantity. We later investigated the immunohistochemical expression IGF2, CLIC4 and SPARC proteins in sarcomatoid mesothelioma and lung sarcomatoid carcinoma. However, there was no significant differential expression of these proteins between lung sarcomatoid carcinoma and sarcomatoid mesothelioma, limiting their applicability as an immunohistochemical positive marker of sarcomatoid mesothelioma.

In contrast, microarray gene expression analysis showed increased expression of *MUC4* in lung sarcomatoid carcinoma compared with that of sarcomatoid mesothelioma, and we found negligible *MUC4* mRNA expression in sarcomatoid mesothelioma at the mRNA level. MUC4 stands for member of mucin protein of high molecular weight glycoprotein.[15] It is expressed in various normal epithelium of the respiratory tract, particularly in the trachea and bronchi[16] and in the epithelium of the digestive and urogenital tracts.[17] MUC4 expression has been reported in various human carcinomas, including pancreatic,[18] breast[19] and lung adenocarcinoma.[20] Llinares *et al*[21] reported the diagnostic value of MUC4 expression in distinguishing epithelioid mesothelioma and lung adenocarcinoma. They found that MUC4 was expressed in 0 of the 41 epithelioid mesotheliomas and in 32 of the 35 (91%) lung adenocarcinoma. To our knowledge, this report has not been validated by other laboratories, as the antibody to MUC4 was not commercially available in the past. We observed MUC4 expression in lung adenocarcinoma and lung squamous cell carcinoma and observed no expression in epithelioid mesothelioma using a commercially available anti-MUC4 antibody. The current study is the first report to describe MUC4 expression in lung sarcomatoid carcinoma and no MUC4 expression in sarcomatoid mesothelioma. We observed a high specificity (72%) and absolute sensitivity (100%) for negative MUC4 expression to differentiate sarcomatoid mesothelioma from lung sarcomatoid carcinoma, with an accuracy rate of 87%. These values are far better than any previously identified immunohistochemical markers differentiating sarcomatoid mesothelioma from lung sarcomatoid carcinoma.

The sensitivity of MUC4 expression as a negative marker was the highest of the immunohistochemical markers in this study. Lung sarcomatoid carcinoma cases showing MUC4 expression (21 cases) also demonstrated co-expression of TTF-1 in 12 cases, Claudin-4 in 10 cases and p40 in 3 cases. Furthermore, lung sarcomatoid carcinoma cases without MUC4 expression showed TTF-1 expression in three cases, p40 in three cases and Claudin-4 in three cases. Therefore, MUC4 expression has better additional value of the immunohistochemical markers for the differential diagnosis of sarcomatoid mesothelioma from lung sarcomatoid carcinoma. The sensitivity of these markers can be improved by combining two or more, and the addition of TTF-1 and Claudin-4 to MUC4 expression improved the accuracy rate up to 95% for the differential diagnosis of sarcomatoid mesothelioma from lung sarcomatoid carcinoma.

In conclusion, we identified a novel immunohistochemical marker MUC4 that differentiates sarcomatoid mesothelioma from lung sarcomatoid carcinoma by applying whole gene expression analysis. The combination of MUC4 with TTF-1/p40 and Claudin-4 improved the sensitivity and specificity for differential diagnosis. Therefore, we propose including MUC4 as an additional negative marker to the immunohistochemical marker panel to differentiate sarcomatoid mesothelioma from lung sarcomatoid carcinoma.

Acknowledgments

We thank Ms Naomi Fukuhara for her administrative assistance. This work was supported in part by the

Japan Society for the Promotion of Science, Grants-in-Aid Scientific Research No. JP26460452 (YT) from the Ministry of Education, Science, Sports and Culture. Part of this study was performed at the Analysis Center of Life Science, Hiroshima University.

Disclosure/conflict of interest

The authors declare no conflict of interest.

References

1 Delgermaa V, Takahashi K, Park EK, *et al.* Global mesothelioma deaths reported to the World Health Organization between 1994 and 2008. Bull World Health Organ 2011;89:716–724, 24A–24C.
2 Roggli V, Churg A, Chirieac LR, *et al.* Sarcomatoid, desmoplastic, and biphasic mesothelioma. In: Travis WD, Brambilla E, Burke S, *et al.* (eds). WHO Classification of Tumours of the Lung, Pleura, Thymus, and Heart. IARC: Lyon, France, 2015, pp 165–168.
3 Husain AN, Colby T, Ordonez N, *et al.* Guidelines for pathologic diagnosis of malignant mesothelioma: 2012 update of the consensus statement from the International Mesothelioma Interest Group. Arch Pathol Lab Med 2013;137:647–667.
4 Ordonez NG. D2-40 and podoplanin are highly specific and sensitive immunohistochemical markers of epithelioid malignant mesothelioma. Hum Pathol 2005;36:372–380.
5 Chu AY, Litzky LA, Pasha TL, *et al.* Utility of D2-40, a novel mesothelial marker, in the diagnosis of malignant mesothelioma. Mod Pathol 2005;18:105–110.
6 Padgett DM, Cathro HP, Wick MR, *et al.* Podoplanin is a better immunohistochemical marker for sarcomatoid mesothelioma than calretinin. Am J Surg Pathol 2008;32:123–127.
7 Takeshima Y, Amatya VJ, Kushitani K, *et al.* Value of immunohistochemistry in the differential diagnosis of pleural sarcomatoid mesothelioma from lung sarcomatoid carcinoma. Histopathology 2009;54:667–676.
8 Kushitani K, Amatya VJ, Mawas AS, *et al.* Use of anti-Noxa antibody for differential diagnosis between epithelioid mesothelioma and reactive mesothelial hyperplasia. Pathobiology 2016;83:33–40.
9 Kerr KM, Pelosi G, Austin JHM, *et al.* Pleomorphic, spindle cell, and giant cell carcinoma. In: Travis WD, Brambilla E, Burke AP, *et al.* (eds). WHO Classification of Tumours of the Lung, Pleura, Thymus and Heart, 4th edn. IARC: Lyon, France, 2015, pp 88–90.
10 Travis WD, Noguchi M, Yatabe Y, *et al.* Adenocarcinomal. In: Travis WD, Brambilla E, Burke AP, *et al.* (eds). WHO Classification of Tumours of the Lung, Pleura, Thymus and Heart, 4th edn. IARC: Lyon, France, 2015, pp 26–37.
11 Tsao M-S, Brambilla E, Nicholson AG, *et al.* Squamous cell carcinoma. In: Travis WD, Brambilla E, Burke AP, *et al.* (eds). WHO Classification of Tumours of the Lung, Pleura, Thymus and Heart, 4th edn. IARC: Lyon, France, 2015, pp 51–55.
12 Tatsumori T, Tsuta K, Masai K, *et al.* p40 is the best marker for diagnosing pulmonary squamous cell carcinoma: comparison with p63, cytokeratin 5/6, desmocollin-3, and sox2. Appl Immunohistochem Mol Morphol 2014;22:377–382.
13 Ordonez NG. Value of claudin-4 immunostaining in the diagnosis of mesothelioma. Am J Clin Pathol 2013;139: 611–619.
14 Facchetti F, Lonardi S, Gentili F, *et al.* Claudin 4 identifies a wide spectrum of epithelial neoplasms and represents a very useful marker for carcinoma versus mesothelioma diagnosis in pleural and peritoneal biopsies and effusions. Virchows Arch 2007;451: 669–680.
15 Chaturvedi P, Singh AP, Batra SK. Structure, evolution, and biology of the MUC4 mucin. FASEB J 2008;22: 966–981.
16 Copin MC, Devisme L, Buisine MP, *et al.* From normal respiratory mucosa to epidermoid carcinoma: expression of human mucin genes. Int J Cancer 2000;86: 162–168.
17 Audie JP, Janin A, Porchet N, *et al.* Expression of human mucin genes in respiratory, digestive, and reproductive tracts ascertained by in situ hybridization. J Histochem Cytochem 1993;41: 1479–1485.
18 Moniaux N, Chaturvedi P, Varshney GC, *et al.* Human MUC4 mucin induces ultra-structural changes and tumorigenicity in pancreatic cancer cells. Br J Cancer 2007;97:345–357.
19 Rakha EA, Boyce RW, Abd El-Rehim D, *et al.* Expression of mucins (MUC1, MUC2, MUC3, MUC4, MUC5AC and MUC6) and their prognostic significance in human breast cancer. Mod Pathol 2005;18: 1295–1304.
20 Kwon KY, Ro JY, Singhal N, *et al.* MUC4 expression in non-small cell lung carcinomas: relationship to tumor histology and patient survival. Arch Pathol Lab Med 2007;131:593–598.
21 Llinares K, Escande F, Aubert S, *et al.* Diagnostic value of MUC4 immunostaining in distinguishing epithelial mesothelioma and lung adenocarcinoma. Mod Pathol 2004;17:150–157.

Supplementary Information accompanies the paper on Modern Pathology website (http://www.nature.com/modpathol)

Cancer Chemother Pharmacol (2016) 78:769–774
DOI 10.1007/s00280-016-3135-2

ORIGINAL ARTICLE

A phase II study of topotecan and cisplatin with sequential thoracic radiotherapy in elderly patients with small-cell lung cancer: Okayama Lung Cancer Study Group 0102

Toshio Kubo[1] · Keiichi Fujiwara[2] · Katsuyuki Hotta[3,4] · Toshiaki Okada[5,7] · Shoichi Kuyama[6,7] · Shingo Harita[7] · Takashi Ninomiya[3,8] · Haruhito Kamei[8,9] · Shinobu Hosokawa[10] · Akihiro Bessho[10] · Tadashi Maeda[9] · Toshiyuki Kozuki[11] · Nobukazu Fujimoto[12] · Kiichiro Ninomiya[3] · Mitsuhiro Takemoto[13,14] · Susumu Kanazawa[14] · Nagio Takigawa[15] · Masahiro Tabata[1] · Mitsune Tanimoto[16] · Hiroshi Ueoka[7,9] · Katsuyuki Kiura[3]

Received: 16 June 2016 / Accepted: 11 August 2016 / Published online: 20 August 2016
© Springer-Verlag Berlin Heidelberg 2016

Abstract

Purpose The treatment outcome in elderly patients with limited-disease small-cell lung cancer (LD-SCLC) remains poor. We carried out a phase II trial of split topotecan and cisplatin (TP) therapy and sequential thoracic radiotherapy for elderly LD-SCLC patients as a follow-up to our previous phase I trial.

Methods In total, 30 patients aged 76 years or older, with untreated LD-SCLC were enrolled. Four courses of topotecan (1.0 mg/m^2, days 1–3) and cisplatin (20 mg/m^2, days 1–3) were administered, followed by thoracic radiotherapy (1.8 Gy/day, total of 45 Gy). The primary end point was the overall response rate (ORR).

Results The trial was terminated early with 22 patients because of slow accrual. Their median age was 79 years. The median number of courses of chemotherapy administered was three, and the actual completion rate of the entire treatment course was 41 %. The ORR was 68 % with a 95 % confidence interval of 47–89 % (15/22 cases). The median progression-free survival and overall survival were 9.1 and 22.2 months, respectively. The main toxicity was myelosuppression, with grades 3–4 neutropenia (96 %), thrombocytopenia (50 %), and febrile neutropenia (32 %).

Conclusions This regimen produced a favorable survival outcome, despite moderate-to-severe toxicity profiles.

Electronic supplementary material The online version of this article (doi:10.1007/s00280-016-3135-2) contains supplementary material, which is available to authorized users.

✉ Katsuyuki Hotta
khotta@okayama-u.ac.jp

[1] Center for Clinical Oncology, Okayama University Hospital, Okayama, Japan

[2] Department of Respiratory Medicine, Okayama Medical Center, Okayama, Japan

[3] Department of Respiratory Medicine, Okayama University Hospital, Okayama, Japan

[4] Center for Innovative Clinical Medicine, Okayama University Hospital, 2-5-1 Shikata-cho, Kita-ku, Okayama 700-8558, Japan

[5] Department of Respiratory Medicine, Fukuyama Medical Center, Fukuyama, Japan

[6] Department of Respiratory Medicine, Iwakuni Medical Center, Iwakuni, Japan

[7] Department of Respiratory Medicine, Chugoku Central Hospital, Fukuyama, Japan

[8] Department of Clinical Oncology, Sumitomo Besshi Hospital, Niihama, Japan

[9] Department of Medical Oncology, Yamaguchi-Ube Medical Center, Ube, Japan

[10] Department of Respiratory Medicine, Japanese Red Cross Okayama Hospital, Okayama, Japan

[11] Department of Thoracic Oncology and Medicine, Shikoku Cancer Center, Matsuyama, Japan

[12] Department of Respiratory Medicine, Okayama Rosai Hospital, Okayama, Japan

[13] Department of Radiotherapy, Japanese Red Cross Society Himeji Hospital, Himeji, Japan

[14] Department of Radiology, Okayama University Hospital, Okayama, Japan

[15] Department of General Internal Medicine 4, Kawasaki Medical School, Okayama, Japan

[16] Department of Hematology and Oncology, Okayama University Hospital, Okayama, Japan

Further efforts are necessary to define an optimal regimen for elderly patients with limited SCLC.

Keywords Lung cancer · Elderly patient · Chemotherapy · Topotecan

Introduction

The standard treatment for patients with limited-disease small-cell lung cancer (LD-SCLC) is a combination of early concurrent twice-daily thoracic radiotherapy (TRT) and chemotherapy, consisting of etoposide (ETP) and cisplatin (CDDP) [1]. For extensive disease (ED)-SCLC, chemotherapy consisting of CDDP and ETP (PE) [2, 3] or CDDP and irinotecan (CPT-11) (PI) has widely been investigated [4].

However, elderly patients were excluded from these previous trials [4]. PE with early concurrent twice-daily TRT in elderly patients was effective, but highly toxic [5]. A combination of carboplatin and CPT-11 caused a high incidence of diarrhea (grade 2 or greater: 40 % [6]). Also, a combination of carboplatin and VP-16 is now often used for elderly patients [7], but no standard regimen has been established. Thus, there is ongoing need to further develop treatment strategies for the elderly.

Topotecan (TOP) is a promising drug for relapsed SCLC patients. TOP monotherapy produced better survival than best supportive care in a phase III trial [8]. In previously untreated SCLC patients, TOP monotherapy showed a 39 % overall response rate (ORR) [9]. Non-hematological toxicities were mild. In particular, diarrhea, which is the dose-limiting toxicity (DLT) of CPT-11, is reportedly rare [10, 11]. However, its utility in a first-line setting in the elderly remains unclear.

In a prior phase I trial, we demonstrated the safety profile of split TOP and CDDP (TP) therapy; the DLTs were febrile neutropenia (FN), persistent neutropenia, hyponatremia, and hepatic toxicity [12]. In that study, the ORR was 60 % in LD-SCLC patients and 55 % in ED-SCLC patients, with median survival times of 16.0 and 11.0 months, respectively. Based on these findings, we subsequently conducted a phase II trial of split TP therapy, with the primary end point of ORR and secondary end points of 1-year survival rate and toxicity.

Patients and methods

Eligibility

The eligibility criteria are listed in Supplemental Table 1. The baseline pretreatment evaluations included a complete history, physical examination, laboratory tests, a chest radiograph, computed tomography (CT) scans of the chest and abdomen, bronchoscopy, magnetic resonance imaging of the brain, and a radionuclide bone scan, if medically indicated.

Written informed consent was obtained from each patient before any screening or inclusion procedure. This study was conducted in compliance with the principles of the Declaration of Helsinki. The protocol was approved by the institutional review board of each participating institution.

Treatment schedule

The dose and schedule of the investigational regimen were intended to be the same as in the phase I trial [12]. TOP (1 mg/m^2, days 1–3), diluted in 100 mL of physiological saline, was administered intravenously for 30 min on days 1–3. After completion of the TOP infusion, CDDP (20 mg/m^2, days 1–3), diluted in 300 mL of physiological saline, was administered intravenously over 1 h on the same days. The treatment was repeated every 3 weeks until PD or a maximum of four cycles. Each patient was pre-medicated with dexamethasone and 5-HT3 inhibitor.

Initiation of the next cycle of chemotherapy was delayed until recovery of the white blood cell count to $\geq$3000/mm^3, the neutrophil count to $\geq$1500/mm^3, the platelet count to $\geq 10 \times 10^4$/mm^3, hemoglobin to $\geq$8.0 g/dL, and serum creatinine to $\leq$1.5 mg/dL. If grade 4 leukopenia, neutropenia, or FN was noted, the use of granulocyte colony-stimulating factor (G-CSF) was permitted.

Patients with LD-SCLC received thoracic irradiation at a total of 45 Gy in 25 fractions after the completion of chemotherapy. Prophylactic cranial irradiation was not planned.

Assessments of toxicity and antitumor activity

All toxicities were graded according to National Cancer Institute Common Terminology Criteria for Adverse Events (ver. 2). The standard Response Evaluation Criteria in Solid Tumors (ver. 1) was used to evaluate responses. A CT scan to assess target and nontarget lesions was designed to be done every 3 weeks during treatment. After the planned treatment, a CT scan was done at least every 6 months.

Statistical considerations

The efficacy of this combination therapy was assessed separately for LD- and ED-SCLC. In the LD group, assuming that an ORR of 90 % in eligible patients would indicate potential utility, whereas a rate of 70 % would be the lower limit of interest, with $\alpha = 0.05$ and $1 - \beta = 0.8$, and the estimated accrual number was 30 patients. An interim

Table 1 Clinical demographics of the 22 patients with LD-SCLC

Age, years (median, range)	79 (76–84)
Gender (male/female)	19 (86 %)/3 (14 %)
Staging (I/II/IIIA/IIIB)	3 (14 %)/3 (14 %)/7 (32 %)/9 (41 %)
ECOG PS (0–1/2)	20 (91 %)/2 (9 %)
Smoking (never/ever)	4 (18 %)/18 (82 %)
Median Charlson score (range)	3 (2–6)

LD-SCLC limited-disease small-cell lung cancer, *ECOG* Eastern Cooperative Oncology Group, *PS* performance status

analysis was preplanned, so that the regimen would be rejected if 19 or fewer of the first 23 patients had an objective response with Simon's minimax design. The primary end point would be considered to be met if 22 or more patients had an overall response at the final analysis.

In the ED group, assuming that an ORR of 85 % would indicate potential utility, whereas a rate of 60 % would be the lower limit of interest, with $\alpha = 0.05$ and $1 - \beta = 0.8$, and the estimated accrual number was 25 patients. This regimen would be rejected if three or fewer of the first five patients showed an objective response. The primary end point would be considered to be met if 18 or more patients had an overall response at the final analysis.

Results

Patient characteristics

Enrollment in this study began in December 2004. In the ED group, the trial was terminated at the time of the interim analysis for ED-SCLC (performed in 2007) because only three of the first five patients had an objective response (Supplemental Table 2). Therefore, further investigations were not evaluated in ED group. For LD-SCLC patients, the trial was also terminated early with 22 of the planned 30 patients because of slow accrual. The demographics of the 22 patients are listed in Table 1. The median age was 79 years (range 76–84), and 86 % of the patients were male (19/3). Most patients were ever smokers (82 %) had a performance status of 0–1 (91 %) and had a median Charlson score of 3 (range 2–6). Treatment delivery is shown in Fig. 1. Ultimately, 9 of 22 (41 %) patients completed the planned treatment.

Efficacy

With an intention to treat analysis, the ORR was 68 % (15/22, 95 % confidence interval [CI] 47–89 %) with no complete response; this did not meet the primary end point. The disease control rate, defined as the percentage of patients with partial responses and stable disease, was 77 % (95 % CI 58–96 %; Table 2).

For the survival analysis, with a median follow-up time for surviving patients of 17.9 months, 19 (86 %) patients experienced disease progression or died. The median progression-free survival (PFS) was 9.1 (95 % CI 4.7–14.9) months (Fig. 2a), and the median overall survival (OS) was 22.2 (95 % CI 9.8–35.4) months (Fig. 2b). The 1-year survival rate was 72 % (95 % CI 49–87 %).

Toxicity

We assessed toxicity in 22 patients. The main grade 3 or 4 toxicities are listed in Table 3. The most common adverse event was neutropenia (96 %, 21/22), followed

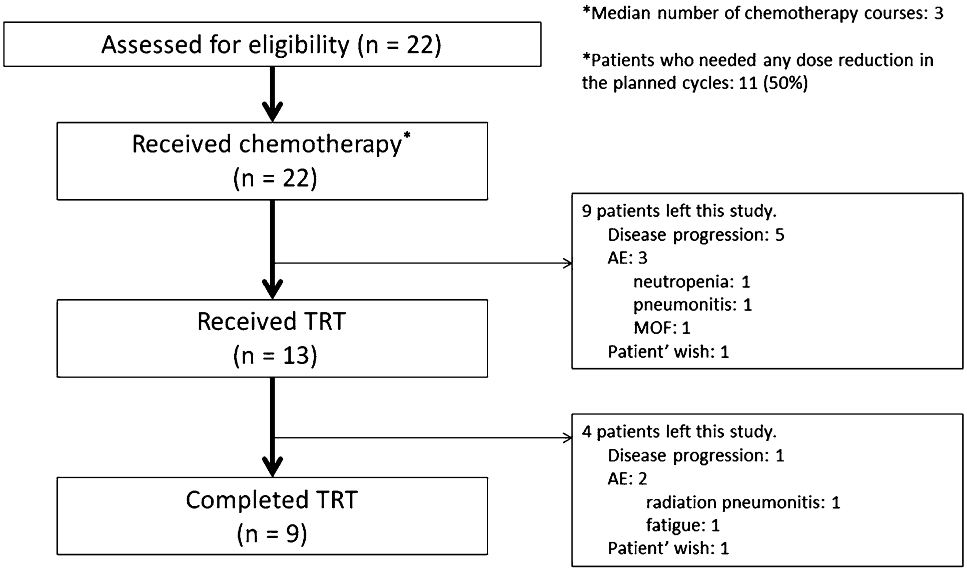
*Median number of chemotherapy courses: 3
*Patients who needed any dose reduction in the planned cycles: 11 (50%)
Assessed for eligibility (n = 22)
Received chemotherapy*
(n = 22)
9 patients left this study.
Disease progression: 5
AE: 3
neutropenia: 1
pneumonitis: 1
MOF: 1
Patient' wish: 1
Received TRT
(n = 13)
4 patients left this study.
Disease progression: 1
AE: 2
radiation pneumonitis: 1
fatigue: 1
Patient' wish: 1
Completed TRT
(n = 9)

Fig. 1 Study flow. *TRT* thoracic radiotherapy, *AE* adverse event, *MOF* multiple organ failure

Table 2 Overall response rate ($n = 22$)

	No. of patients	%
Response rate	15	68
Disease control rate	17	77
Partial response	15	68
Complete response	0	0
Stable disease	2	9
Progressive disease	4	18
Not evaluated	1	4.5

Disease control rate was defined as the proportion of partial response, complete response, and stable disease

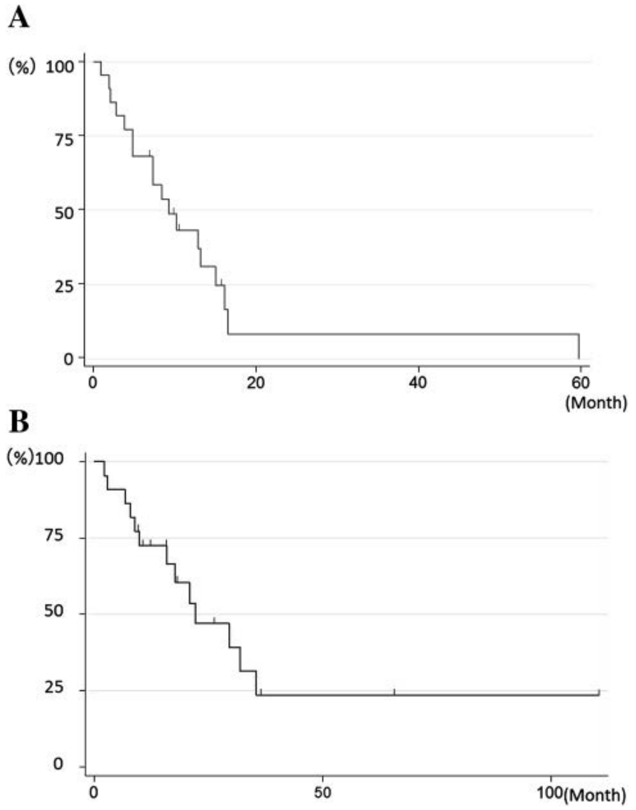

Fig. 2 **a** Progression-free survival curve ($n = 22$). **b** Overall survival curve ($n = 22$)

by thrombocytopenia (50 %, 11/22), and anemia (36 %, 8/22). These hematological adverse events were tolerable with an appropriate treatment or dose reduction of the protocol treatment. Other common adverse events were FN (32 %, 7/22), pneumonitis (18 %, 4/22), and nausea (14 %, 3/22). One treatment-related death during cycle 4 was observed, due to multiple organ failure, followed by hepatotoxicity.

Table 3 Adverse events ($n = 22$)

Toxicity	No. of patients			
Grades	Any grades	3	4	5
Hematological				
Neutropenia	22 (100 %)	5 (23 %)	16 (73 %)	0 (0 %)
Thrombocytopenia	18 (82 %)	7 (32 %)	4 (18 %)	0 (0 %)
Anemia	17 (77 %)	7 (32 %)	1 (4.5 %)	0 (0 %)
Non-hematological				
Febrile neutropenia	7 (32 %)	7 (32 %)	0 (0 %)	0 (0 %)
Creatinine elevation	5 (23 %)	1 (4.5 %)	0 (0 %)	0 (0 %)
AST/ALT increased	10 (45.5 %)	0 (0 %)	0 (0 %)	1 (5 %)
Nausea/vomiting	12 (54 %)	3 (13 %)	0 (0 %)	0 (0 %)
Diarrhea	6 (27 %)	0 (0 %)	0 (0 %)	0 (0 %)
Esophagitis	8 (36 %)	0 (0 %)	0 (0 %)	0 (0 %)
Pneumonitis	11 (50 %)	4 (18 %)	0 (0 %)	0 (0 %)

Subsequent treatments

At the time of the analysis, 17 (77 %) patients showed recurrence, 7 (41 %) developed distant metastases, 8 (47 %) had loco-regional disease, and 2 (12 %) developed both loco-regional disease and distant metastases. Brain metastases were observed in 2 patients (12 %). Of the 17 patients, 13 (76 %) received subsequent treatment (Table 4).

Response and survival stratified by clinical factors

The efficacy stratified by several clinical factors is shown in Supplemental Table 3. No significant difference in ORR or survival time was evident between the groups.

Discussion

We conducted a phase II trial of split TP therapy in elderly SCLC patients. In the ED group, the ORR was 68 %, which did not meet the primary end point. The survival outcome was somewhat favorable with a median PFS time of 9.1 months and median OS of 22.2 months, but moderate-to-severe toxicities were observed with one treatment-related death, leading to a low completion rate of the whole treatment (41 %).

Regarding ORR (the primary end point), it did not satisfy the preplanned criterion. Although this study was terminated early, the registered number of 22 patients was sufficient to determine whether the ORR did meet the end point in the interim analysis. The ORR of 68 % in this

Table 4 Subsequent treatments ($n = 17$)

Chemotherapy	7 (41 %)
CBDCA + ETP	4
CPT-11 + AMR	1
ETP	1
AMR	1
Chemotherapy + TRT	4 (24 %)
AMR followed by TRT	2
CBDCA + ETP followed by TRT	1
ETP + TRT	1
Palliative RT	2 (12 %)
Best supportive care	4 (24 %)

CBDCA carboplatin, *ETP* etoposide, *CPT-11* irinotecan, *AMR* amrubicin, *TRT* thoracic radiotherapy, *RT* radiotherapy

phase II trial was consistent with our phase I trial result—2 of 3 (67 %) patients at the recommended dose responded to treatment [12]. This reproducibility suggests that the current negative result was attributable simply to the predefined statistical consideration that was too strict in this phase II trial, and, possibly, to the moderate-to-severe toxicity profile and low completion rate of the planned treatment.

The median survival time of 22.2 months was favorable. It was not inferior to those noted in previous trials (Supplemental Table 4) [6, 7, 13, 14]. This was partly attributable to the high proportion of subsequent treatment after progression. This might mean that TP therapy is a regimen that can easily be transitioned to a subsequent treatment. Another reason might be patient selection; in fact, the median Charlson score was 3, meaning that the patients who participated in this trial were in good general condition.

In terms of safety, the main toxicity was myelosuppression, especially neutropenia (Table 3). Thus, several of the toxicities that occurred with this regimen may be preventable using prophylactic PEGylated G-CSF administration. In fact, it can reduce the proportion of FN by 6–68 % [15, 16], and 6–22 % in elderly patients. In total, the toxicities were more severe than those in previous trials, although there was no severe diarrhea, which is an advantage of TOP versus CPT-11 (Supplemental Table 4). Of note, severe pneumonitis was observed in 4 (18 %) patients, while its severity in TOP and radiotherapy has rarely been reported. The reason for this high proportion is unclear, but it might be due to patient selection. Careful patient follow-up is needed with our regimen, even though there was no treatment-related death due to pneumonitis.

This study has several limitations. The time period of accrual was too long, and factors other than the investigational regimen itself potentially affected the outcome, including the starting situation and any change in supportive care. Unfortunately, we could not obtain information about the actual number of patients who underwent a positron emission tomography scan. Also, we did not have detailed information as to how large the volume of lung receiving at least 20 Gy (V20) was and how the radiotherapy field was set in each patient, although these might have affected the efficacy, including PFS and OS. Thus, our results should be interpreted cautiously. Furthermore, we did not have any biomarker of this regimen for efficient patient selection, as is often the case with other cytotoxic agents.

In summary, split TP therapy and sequential thoracic radiation therapy did not meet the primary outcome criteria, with moderate-to-severe toxicities. The regimen is not useful and further efforts are necessary to define an optimal regimen for elderly patients with limited SCLC.

Acknowledgments We thank the patients and their families for participating in this trial. We also thank Yasunari Nakata, Masafumi Fujii, Hiroshi Date (Kyoto University Hospital), Masahiro Osawa, Daisuke Morichika, Tomoki Tamura (Okayama University Hospital), Hiromasa Takeda (Tsuyama Central Hospital), Nobuhiro Honda (Kawasaki Hospital), and Toshi Murakami (Japanese Red Cross Society Himeji Hospital), for cooperating in this trial. This study has been conducted with support from the Center for Innovative Clinical Medicine, Okayama University Hospital.

Author contributions TK, KH, and KN had full access to all of the data and take responsibility for the integrity of the data and accuracy of the data analysis. KF, NT, KH, and KK contributed to the study design. TK, KH, and KN contributed to data collection and analysis. All of the authors contributed to the writing of the manuscript and provided final approval of the version to be published.

Compliance with ethical standards

Conflict of interest K.H. has received honoraria from AstraZeneca, Eli Lilly Japan, Daiichi-Sankyo Pharmaceutical, Boehringer-Ingelheim, Nihon Kayaku, Taiho Pharmaceutical, and Chugai Pharmaceutical. KH also has received research funding from Eli Lilly Japan, MSD, and Chugai Pharmaceutical. J.S. has received honoraria from Pfizer, Eli Lilly, Taiho Pharmaceutical, Chugai Pharmaceutical, Boehringer-Ingelheim, AstraZeneca, and Kyowa Kirin. N.T. has received honoraria from Eli Lilly Japan, AstraZeneca, Daiichi-Sankyo Pharmaceutical, Chugai Pharmaceutical, Taiho Pharmaceutical, Pfizer Japan Inc, and Boehringer-Ingelheim in Japan. K.K. has received honoraria from Eli Lilly Japan, Nihon Kayaku, AstraZeneca, Daiichi-Sankyo Pharmaceutical, Chugai Pharmaceutical, Taiho Pharmaceutical, and Sanofi-Aventis. The remaining authors have stated that they have no conflicts of interest.

References

1. Socinski MA, Bogart JA (2008) Limited-stage small-cell lung cancer: the current status of combined-modality therapy. J Clin Oncol 25:4137–4145
2. Roth BJ, Johnson DH, Einhorn LH, Schacter LP, Cherng NC, Cohen HJ, Crawford J, Randolph JA, Goodlow JL, Broun GO et al (1992) Randomized study of cyclophosphamide,

doxorubicin, and vincristine versus etoposide and cisplatin versus alternation of these two regimens in extensive small-cell lung cancer: a phase III trial of the Southeastern Cancer Study Group. J Clin Oncol 10:282–291

3. Fukuoka M, Furuse K, Saijo N, Nishiwaki Y, Ikegami H, Tamura T, Shimoyama M, Suemasu K (1991) Randomized trial of cyclophosphamide, doxorubicin, and vincristine versus cisplatin and etoposide versus alternation of these regimens in small-cell lung cancer. J Natl Cancer Inst 83:855–861
4. Noda K, Nishiwaki Y, Kawahara M, Negoro S, Sugiura T, Yokoyama A, Fukuoka M, Mori K, Watanabe K, Tamura T, Yamamoto S, Saijo N (2002) Irinotecan plus cisplatin compared with etoposide plus cisplatin for extensive small-cell lung cancer. N Engl J Med 346:85–91
5. Okamoto K, Okamoto I, Takezawa K, Tachibana I, Fukuoka M, Nishimura Y, Nakagawa K (2010) Cisplatin and etoposide chemotherapy combined with early concurrent twice-daily thoracic radiotherapy for limited-disease small cell lung cancer in elderly patients. Jpn J Clin Oncol 40:54–59
6. Murata Y, Hirose T, Yamaoka T, Shirai T, Okuda K, Sugiyama T, Kusumoto S, Nakashima M, Ohmori T, Adachi M (2011) Phase II trial of the combination of carboplatin and irinotecan in elderly patients with small-cell lung cancer. Eur J Cancer 47:1336–1342
7. Okamoto H, Watanabe K, Nishiwaki Y, Mori K, Kurita Y, Hayashi I, Masutani M, Nakata K, Tsuchiya S, Isobe H, Saijo N (1999) Phase II study of area under the plasma-concentration-versus-time curve-based carboplatin plus standard-dose intravenous etoposide in elderly patients with small-cell lung cancer. J Clin Oncol 17:3540–3545
8. O'Brien ME, Ciuleanu TE, Tsekov H, Shparyk Y, Cuceviá B, Juhasz G, Thatcher N, Ross GA, Dane GC, Crofts T (2006) Phase III trial comparing supportive care alone with supportive care with oral topotecan in patients with relapsed small-cell lung cancer. J Clin Oncol 24:5441–5447
9. Schiller JH, Kim K, Hutson P, DeVore R, Glick J, Stewart J, Johnson D (1996) Phase II study of topotecan in patients with extensive-stage small-cell carcinoma of the lung: an Eastern Cooperative Oncology Group Trial. J Clin Oncol 14:2345–2352
10. Masuda N, Fukuoka M, Kusunoki Y, Matsui K, Takifuji N, Kudoh S, Negoro S, Nishioka M, Nakagawa K, Takada M (1992) CPT-11: a new derivative of camptothecin for the treatment of refractory or relapsed small-cell lung cancer. J Clin Oncol 10:1225–1229
11. Negoro S, Fukuoka M, Masuda N, Takada M, Kusunoki Y, Matsui K, Takifuji N, Kudoh S, Niitani H, Taguchi T (1991) Phase I study of weekly intravenous infusions of CPT-11, a new derivative of camptothecin, in the treatment of advanced non-small-cell lung cancer. J Natl Cancer Inst 83:1164–1168
12. Fujiwara K, Ueoka H, Kiura K, Tabata M, Takigawa N, Hotta K, Umemura S, Sugimoto K, Shibayama T, Kamei H, Harita S, Okimoto N, Tanimoto M (2006) A phase I study of 3-day topotecan and cisplatin in elderly patients with small-cell lung cancer. Cancer Chemother Pharmacol 57:755–760
13. Inoue A, Ishimoto O, Fukumoto S, Usui K, Suzuki T, Yokouchi H, Maemondo M, Kanbe M, Ogura S, Harada T, Oizumi S, Harada M, Sugawara S, Fukuhara T, Nukiwa T (2009) A phase II study of amrubicin combined with carboplatin for elderly patients with small-cell lung cancer: North Japan Lung Cancer Study Group Trial 0405. Ann Oncol 21:800–803
14. Tada A, Ueoka H, Kiura K, Tabata M, Takemoto M, Yamane H, Hiyama J, Aoe K, Shibayama T, Kamei H, Kawahara S, Harita S, Sato T, Kobayashi M, Eguchi K, Hiraki S, Hiraki Y, Tanimoto M (2002) Combination chemotherapy with carboplatin and etoposide for elderly patients aged 76 years or older with small cell lung cancer. Gan To Kagaku Ryoho 29:751–756
15. Kosaka Y, Rai Y, Masuda N, Takano T, Saeki T, Nakamura S, Shimazaki R, Ito Y, Tokuda Y, Tamura K (2015) Phase III placebo-controlled, double-blind, randomized trial of pegfilgrastim to reduce the risk of febrile neutropenia in breast cancer patients receiving docetaxel/cyclophosphamide chemotherapy. Support Care Cancer 23:1137–1143
16. Balducci L, Al-Halawani H, Charu V, Tam J, Shahin S, Dreiling L, Ershler WB (2007) Elderly cancer patients receiving chemotherapy benefit from first-cycle pegfilgrastim. Oncologist 12:1416–1424

臨床リウマチ医のための基礎講座
CD26分子に基づくトランスレーショナルリサーチ

順天堂大学大学院医学研究科
免疫病・がん先端治療学講座
森本幾夫

はじめに

我が国の生命科学分野の基礎研究成果はNatureやScience等の主要科学雑誌に掲載されるなど，国際的にも高い評価を受けている．しかし我が国においては臨床研究，特に臨床でのトランスレーションリサーチに対する支援体制などが十分に整備されていないため研究成果が，医療，製薬等の臨床現場に届いておらず，国民に成果が還元されていないと指摘されている．更に免疫病やがん領域の新薬はほとんど欧米発で占められ，日本発の創薬は非常に数少ない．一個の薬が世に出るまでには約500億円から1000億円の費用がかかるといわれている．従来は製薬会社が創薬の中心的役割を果たしていたが，大学等のアカデミアの基礎研究成果を産学共同体制で効率よく創薬に結びつけていくという気運が欧米諸国，日本ともに高まっている．このような背景で，日本政府は2007年から東京大学，京都大学など旧帝大系を中心として全国7カ所の大学及び神戸先端医療振興財団に「トランスレーショナルリサーチ」（橋渡し研究）施設整備のための研究資金援助をスタートした．

トランスレーショナルリサーチとは

トランスレーショナルリサーチ（橋渡し研究）（以下TR）という「ことば」は耳慣れないと思われるが最近医学界で頻回に聞く．要は，医学研究における研究室での基礎研究成果を臨床応用していく探索的な研究をいい，早期の臨床試験にまでもっていくことを指す．

医学研究に従事している者は，誰しもがその研究成果を患者の病気の治癒，改善あるいは早期診断のために応用したいと思っている．ベンチ（研究成果）からベッド（臨床応用）ということばはこのことに相当する．TRのことばの定義について早期の臨床試験を行うことなどもTRを施行していると表現する場合もあり，その定義が混乱している面もある．

これに関して，Dr. BirminghamがNature Medicine（2002年）にて以下のように定義している[1]．つまりアカデミアで医学研究，特に病気の原因究明やヒト検体を用いて研究を行なっている研究者は誰しもが自分はそうだと思っている．しかし彼は「自からの仕事が以下を試みる研究者」の研究を指すと定義する．つまり1. 患者の病気の診断または予後を改善する．2. 患者の病気の予防を向上させる．3. 患者における新しい治療を着想し実行する．更に上記に加えて通常基礎研究は個人で行う研究であるがTRはむしろチームで行うものとしている．要は，その構成メンバーとして，研究室ベースの研究者，患者の治療を行ったり，イメージングなどの評価を行う放射線や病理診断医，更に看護師，データマネージャー，薬剤師などから成っており，お互いに協力してTRを施行するのである．筆者もこの定義に同意している．

Translational research based on CD26 molecule.
Chikao Morimoto.
Department of Therapy Development and Innovation for Immune disorders and Cancers, Graduate School of Medicine, Juntendo University.
DOI: 10.14961/cra.28.91

CD26分子の構造と機能

CD26は細胞表面分子で，dipeptidyl peptidase IV(DPPIV)酵素を含む110KDaの膜蛋白でT細胞共刺激分子であり，関節リウマチなどの炎症局所でCD26強陽性T細胞が集積しており，炎症のエフェクターT細胞といわれている．またコラーゲン，フィブロネクチン，Adenosine deaminase (ADA)の結合蛋白であるなど多彩な機能を有している[2-4]．DPPIV酵素阻害薬はすでに糖尿病治療薬として幅広く臨床現場で用いられている（図１）．

CD26陽性T細胞リンパ腫株やヒトT細胞クローンを用いて試験管でCD26抗体で処理するとcyclin dependent kinase inhibitor（CDKI）のp21が誘導され細胞周期が止まることを見出し，T細胞リンパ腫株を移植した免疫不全マウスの系でも，抗体投与マウスは長期生存した．この結果はCD26抗体がT細胞異常を示す免疫病やT細胞腫瘍の治療に利用できる可能性を示した[4]．そこでCD26抗体の抗原結合部位のアミノ酸及び遺伝子配列解析を施行し，米国Abmaxis社と伴にインシリコ法にて良質なヒト化CD26抗体を開発した（図２）．

CD26と悪性中皮腫

アスベストは石綿とも呼ばれ，耐久性，耐熱性に優れ，幅広い用途に使用されてきた．しかし肺に吸入されると約30-40年の潜伏期間を経て悪性中皮腫などを引き起こす[5]．

日本では高度成長期に建築物などにアスベストが大量に消費されており，その潜伏期間が終わる21世紀に入りアスベストが原因で発生したと思われる悪性中皮腫による死亡者数が増加し，2030年をピークとして益々増加すると予測されており，大きな社会問題となっている．さらに悪性中皮腫は有効な化学療法剤に乏しく，予後はきわめて不良で，新規かつ有効な治療法開発は急務である．

ヒトT細胞共刺激分子のCD26がなぜ悪性中皮腫に関連しているのかという点であるが，著者らはCD26はコラーゲンの結合蛋白であることを報告している[6]．この研究過程でCD26は免疫系細胞だけでなく悪性中皮腫由来株JMNにも発現することを発見した．悪性中皮腫の患者組織でCD26発現を検討したところ，正常中皮では全く発現しないのに悪性中皮腫では8割以上が強く発現していることを見出し，ヒト化CD26抗体が新規治療法になり得るのではと考えた[7]．膠原病の臨床に携わっている筆者としては，ヒト化CD26抗体をまず膠原病などの免疫病の新規治療法にという考えがよぎった．2005年にヒト化CD26抗体を開発したがこの頃クボタショックといってアスベスト工場の周辺の人々にも悪性中皮腫が多発し，連日新聞にアスベストと中皮腫の記事が報道されていた．悪性中皮腫は全く有効な治療法が存在しないことに鑑み，悪性中皮腫の治療に使用できないかと考えた．CD26分子の遺伝子をCD26陰性中皮腫株に発現させたところ，親株と比して細胞遊走能，滲潤能ともに亢進が認められCD26そのものが悪性中皮腫の細胞増殖，滲潤に関与していることも明らかになった[7]．また，胸腔内でびまん性に中皮腫細胞が浸潤する中皮腫モデルマウスを作製し，このモデルマウスに抗体を投与して本抗体が有効である結果も得て，ヒトCD26抗体は悪性中皮腫の新規治療法として有望な可能性が示唆された．

ヒト化CD26抗体のFirst in Man第1相臨床試験

ヒト化CD26抗体は悪性中皮腫細胞株を用いたin vitroの実験でcyclin dependent kinase inhibitor (CDKI)のp21,p27などを誘導し，S期の細胞を減少させるとともにG2/M期で細胞周期を遅延させることが明らかになった．また本抗体はIgGであり，Antibody dependent cellular cytotoxicity (ADCC)により腫瘍細胞の腫瘍破壊をもたらす[7]．

ヒト化CD26抗体をヒトに投与するためにサルを用いた前臨床反復毒性試験を行い，その安全性を確認している．そこでフランスにおいて化学療法抵抗性の悪性中皮腫及びその他CD26陽性固形癌をターゲットとして第Ⅰ/Ⅱ相臨床試験をスタートした．

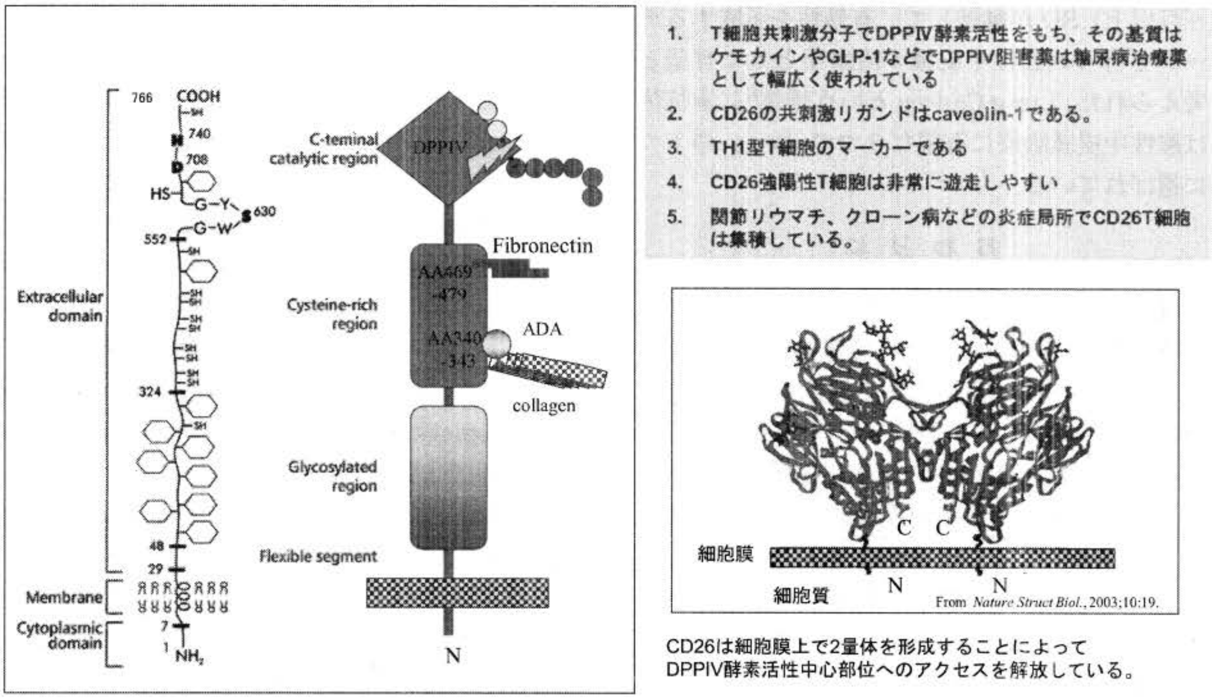
766
COOH
SH
740
708
HS
G-Y
S 630
G-W
552
SH
324
48
29
7
1
NH₂
Extracellular domain
Membrane
Cytoplasmic domain
C-teminal catalytic region
DPPIV
Fibronectin
AA469 -479
Cysteine-rich region
ADA
AA340 -343
collagen
Glycosylated region
Flexible segment
N
C
C
細胞膜
細胞質
N
N

1. T細胞共刺激分子でDPPⅣ酵素活性をもち、その基質はケモカインやGLP-1などでDPPIV阻害薬は糖尿病治療薬として幅広く使われている
2. CD26の共刺激リガンドはcaveolin-1である。
3. TH1型T細胞のマーカーである
4. CD26強陽性T細胞は非常に遊走しやすい
5. 関節リウマチ、クローン病などの炎症局所でCD26T細胞は集積している。

From *Nature Struct Biol.*, 2003;10:19.

CD26は細胞膜上で2量体を形成することによって
DPPIV酵素活性中心部位へのアクセスを解放している。

図1　CD26分子の構造と機能

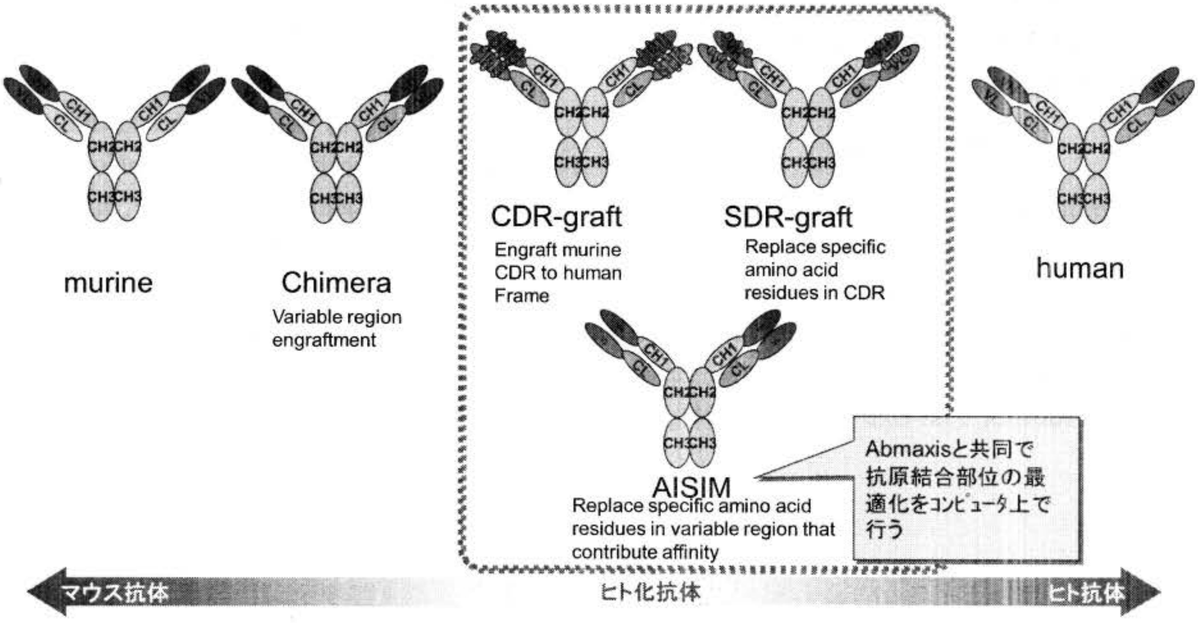
VL
VH
CH1
CL
CH2
CH3
murine
Chimera
Variable region engraftment
CDR-graft
Engraft murine CDR to human Frame
SDR-graft
Replace specific amino acid residues in CDR
human
AISIM
Replace specific amino acid residues in variable region that contribute affinity
Abmaxisと共同で抗原結合部位の最適化をｺﾝﾋﾟｭｰﾀ上で行う
マウス抗体
ヒト化抗体
ヒト抗体

図2　ヒト化抗体作成技術

平成26年9月に第Ⅰ相臨床試験は終了し，安全性を確認でき，また統計33例中評価ができた症例26症例中13例が Stable Disease（SD），13例が Progress Disease（PD）という結果を得た．特に治療抵抗性悪性中皮腫では19例中10例が SD となり，しかもその内6例が3ヶ月以上（5例は6

ヶ月以上）SD が継続して，有効性を示唆するデータも得られ悪性中皮腫の治療薬として有望と考えられた．Lung Cancer という雑誌[8]に本抗体は悪性中皮腫治療に有望な 3 つの Drug の 1 つに選ばれている．

おわりに

本稿ではトランスレーショナルリサーチについて概説して，その具体例として筆者が現在取り組んでいるヒト化 CD26抗体の悪性中皮腫への新規治療法開発について説明した．

現在 CTLA-4や PD-1への抗体が免疫チェックポイント阻害薬として癌免疫領域において非常にポピュラーになっているが最近 CD26分子も免疫チェックポイント機能が存在することが示唆され，この分子は自己免疫制御のみならず癌免疫にも深く係わっていることが示唆されている[9]．

ヒト化 CD26抗体は2016年に本邦においても悪性中皮腫をターゲットに第 I 相臨床試験をスタートする予定で近い将来，悪性中皮腫以外の癌のみならず関節リウマチなど膠原病領域にもその適応を拡大させていく予定であり，今後の更なる発展に努力したい．

文　　献

1）Birmingham K: What is translational research?. Nat Med. 2002, 8:647.

2）Morimoto C, Schlossman SF: Human naive and memory T cells revisited: new markers (CD31 and CD27) that help define CD4+ T cell subsets. Clin Exp Rheum, 11:241-247, 1993.

3）Morimoto C, Schlossman SF: The structure and function of CD26 in The T-cell immune response. Immunol Review, 161:55-70, 1998.

4）Ohnuma K, Dang NH, Morimoto C: Revising an old acquaintance: CD26 and its molecular mechanisms in T cell function. Trend Immunol, 29:296-301, 2008.

5）Robinson BW, Lake RA: Advances in malignant mesothelioma. N Engl J Med, 13;353:1591-603, 2005.

6）Dang NH, Torimoto Y, Schlossman SF, et al: Human CD4 helper T cell activation: functional involvement of two distinct collagen receptors, 1F7, and VLA integrin family. J Exp Med, 172:649-652, 1990.

7）Inamoto T, Yamada T, Morimoto C, et al: Humanized Anti-CD26 monoclonal antibody as a treatment for malignant mesothelioma tumors. Clin Cancer Res, 13:4191-200, 2007.

8）Raphael J, Le Teuff G, Hollebecque A, et al: Efficacy of phase 1 trials in malignant pleural mesothelioma: description of a series of patients at a single institution. Lung Cancer, 85:251-257, 2014.

9）Ohnuma K, Hatano R, Morimoto C: DPP4 in anti-tumor immunity: going beyond the enzyme. Nat Immunol, 16:791-792, 2015.

● 特別寄稿 ●

CD26分子に基づく悪性中皮腫への新治療法開発

森本　幾夫　大沼　圭*

〔*Jpn J Cancer Chemother* 43(7): 855-862, *July*, 2016〕

Development of New Therapy for Malignant Mesothelioma Based on CD26 Molecule: Chikao Morimoto and Kei Ohnuma (*Dept. of Therapy Development and Innovation for Immune Disorders and Cancers, Graduate School of Medicine, Juntendo University*)

Summary

CD26 is a 110 kDa, type Ⅱ transmembrane glycoprotein with dipeptidyl peptidase Ⅳ activity and is capable of cleaving N-terminal dipeptides with either L-proline or L-alanine at the penultimate position. Malignant mesothelioma (MM) is an aggressive malignancy arising from the mesothelial cells. It is generally associated with a history of asbestos exposure and has a very poor prognosis. Due to lack of efficacy of conventional treatments, novel therapeutic strategies are urgently needed to improve outcomes. Recently we showed that CD26 is preferentially expressed on epithelial type of MM cells but not on normal mesothelial cells. We have developed a highly biological active humanized anti-CD26 monoclonal antibody (mAb) and have published previously extensive *in vivo* data demonstrating the anti-tumor activity of humanized anti-CD26 mAb (YS110) in mouse xenograft models. The use of a humanized anti-CD26 mAb may therefore be a rational therapy for patients with MM. The first-in-human (FIH) phase Ⅰ study performed in France demonstrates that humanized anti-CD26 therapy is generally well-tolerated with preliminary evidence of activity in patients with advanced/refractory CD26-expressing cancers, particularly refractory malignant mesothelioma. From the above results, the phase Ⅰ clinical trial for malignant mesothelioma in Japan is to be started in the very near future. **Key words**: CD26, DPPⅣ, Malignant mesothelioma

要旨　CD26分子は110 kDaの膜蛋白質でdipeptidyl peptidase Ⅳ（DPPⅣ）酵素活性をもち，N末端から二つ目のプロリンやアラニンを切断する酵素である。悪性中皮腫（MM）は胸膜中皮細胞から発生する非常に攻撃的な腫瘍で一般的にはアスベスト曝露により発生し，非常に予後が悪い。有効な標準治療法は存在しないことから，新規かつ有効な治療法開発は急務とされている。最近われわれは，CD26分子は正常中皮細胞には発現しないが，上皮型中皮腫の約80％に発現することを報告した。さらに，非常に生物学的活性の強い良質なヒト化CD26抗体を開発してヒト癌細胞移植モデルマウスを用いて本抗体が強い抗腫瘍効果を有するという広範なデータを示してきた。本結果から，ヒト化CD26抗体は悪性中皮腫の新規治療法として臨床応用できる有望な可能性を強く示唆した。本抗体を用いて初めてヒトに投与する（first-in-human: FIH）第Ⅰ相臨床試験をフランスにて行い，ヒト化CD26抗体は良好な耐容性およびCD26陽性腫瘍，特に治療抵抗性悪性中皮腫に対して有効性を示す予備的な証拠も得ることができた。これらの結果を踏まえて，日本でも悪性中皮腫をターゲットとして第Ⅰ相臨床試験が近々開始される予定である。

はじめに

CD26分子はdipeptidyl peptidase Ⅳ（DPPⅣ）酵素を含むT細胞活性化分子で，われわれは単クローンCD26抗体の開発，CD26 cDNAの単離を世界に先駆けて行い，当分野の研究では世界の最先端にいる[1]。この研究過程で悪性中皮腫細胞株JMNがCD26を発現していることを発見し[2]，高親和性，高生物学活性の高いヒト化CD26抗体を開発した。本抗体は*in vitro*で中皮腫細胞株の増殖および浸潤を抑制し，中皮腫株移植マウスで腫瘍縮小，生存延長を来し，正常中皮では発現のないCD26が悪性中皮腫，特に上皮型では80％以上に発現していることを見いだした[3]。CD26は悪性中皮腫の増殖，浸潤に重要な役割を果たし，本抗体がその機能を抑制することから悪

---

* 順天堂大学大学院医学研究科・免疫病・がん先端治療学講座

連絡先: 〒113-8421 東京都文京区本郷2-1-1　順天堂大学大学院医学研究科・免疫病・がん先端治療学講座
森本　幾夫

Presented by Medical*Online

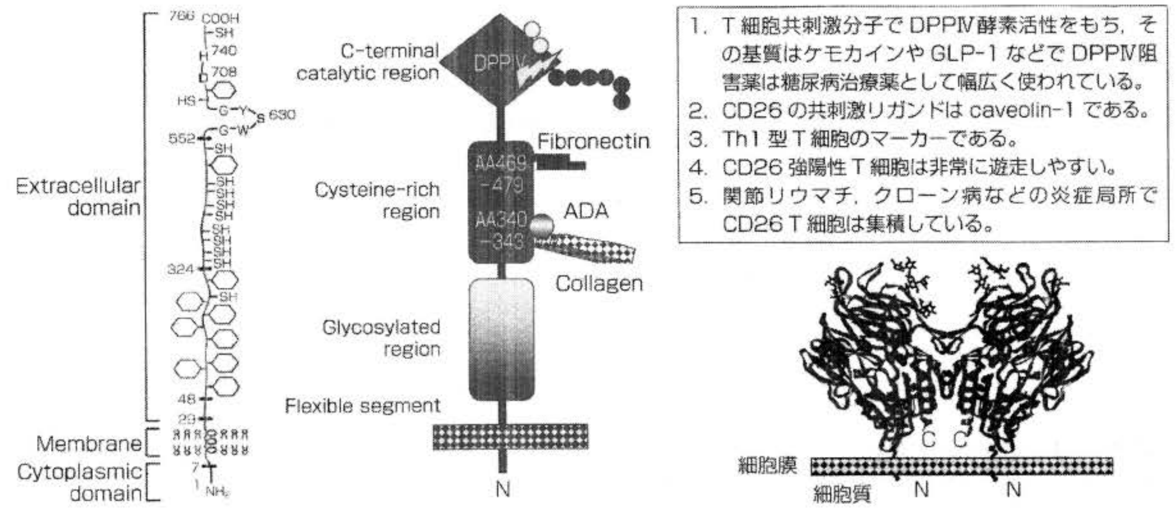
766 COOH
SH
740
H
708
D
HS
G Y S 630
552 G W
SH
SH
324
48
29
7
1 NH₂
Extracellular domain
Membrane
Cytoplasmic domain
C-terminal catalytic region
DPPⅣ
Cysteine-rich region
AA469 -479
AA340 -343
Fibronectin
ADA
Collagen
Glycosylated region
Flexible segment
N
C C
細胞膜
細胞質
N N

1．T 細胞共刺激分子で DPPⅣ酵素活性をもち，その基質はケモカインや GLP-1 などで DPPⅣ阻害薬は糖尿病治療薬として幅広く使われている。
2．CD26 の共刺激リガンドは caveolin-1 である。
3．Th1 型 T 細胞のマーカーである。
4．CD26 強陽性 T 細胞は非常に遊走しやすい。
5．関節リウマチ，クローン病などの炎症局所で CD26 T 細胞は集積している。

(From *Nature Struct Biol* 10(1): 19-25, 2003)
CD26 は細胞膜上で二量体を形成することによって
DPPⅣ酵素活性中心部位へのアクセスを解放している。

図 1 CD26 分子の構造と機能

性中皮腫の新規治療法として有望な可能性が強く示唆された[4,5]。

アスベストは潜伏期 20～40 年を経て悪性中皮腫を引き起こすため，今後ますます患者数が増加し 2030 年にピークを迎え，死亡者数も 2013 年には 1,425 人に上り，東日本大震災のがれきにもアスベストが混入しているといわれ，大きな社会問題となっている。多くの患者は最初の症状発現から 10～17 か月以内に死亡している。現時点では悪性中皮腫に対する有効な治療法はなく，新規かつ有効な治療法開発は急務である。

本稿では CD26 分子について概説して，ヒト化 CD26 抗体の悪性中皮腫移植マウスでの成績，作用機序および first-in-human (FIH) 第Ⅰ相臨床試験の成績について紹介したい。

Ⅰ．CD26 分子の構造と機能

CD26 は 110 kDa の膜糖蛋白で Ta1 という単クローン抗体と反応するヒト T 細胞表面抗原分子として報告され，活性化 T 細胞に強発現することから T 細胞活性化抗原として確立された[6,7]。一方，以前から肝臓や腸管粘膜表面にペプチダーゼ酵素活性が存在することが知られており DPPⅣとして研究されていたが，1992 年われわれによる遺伝子クローニングにより，DPPⅣ酵素と CD26 分子が同一のものであることが明らかとなった[8,9]。図 1 に示すように CD26 は 766 個のアミノ酸よりなり，N 末端が細胞質内，C 末端が細胞外に存在するⅡ型膜蛋白質である。細胞質部分は六つのアミノ酸からなり，既存のシグナル関連モチーフ構造は存在しない。

アミノ酸配列から予想される CD26 の平均分子量は 88 kDa であるが，48～324 番目の残基領域は糖鎖修飾を受けるため，生体では 110 kDa の糖蛋白として検出される[1]。さらに，630 番目のセリン残基を中心としてセリンプロテアーゼである DPPⅣ酵素活性をもっている[1]。CD26 の構造は種を越えて強く保存されており，種の間で高いホモロジーを示す[10]。ヒト CD26 とラット DPPⅣおよびマウス CD26 との相同性はそれぞれ 85%，86% である[9,11]。しかし，ヒト CD26 はアデノシンデアミナーゼ (adenosine deaminase: ADA) の結合蛋白であるがラット，マウス CD26 は ADA に結合しない[10,11]。

Ⅱ．CD26 陽性 T 細胞の生物学的機能

末梢血リンパ球における CD26 を静止 T 細胞での flow cytometry で検討すると 3 相性のパターンを示す[6,7]。CD26 強陽性の T 細胞集団 (CD26$^{\mathrm{bright}}$ T 細胞) は CD45RO 陽性メモリー T 細胞サブセットである[6]。CD26$^{\mathrm{bright}}$ T 細胞は IL-2 や IFN-γ などのサイトカインを分泌する Th1 型のリンパ球とされている[6]。最近になり Th17 T 細胞に CD26 は強く発現しているという報告もある[12]。このように CD26$^{\mathrm{bright}}$ T 細胞は炎症のエフェクター細胞として関節リウマチやバセドウ病などの自己免疫疾患の末梢血 T 細胞でその発現が増加し，これら疾患の炎症局所でも CD26$^{\mathrm{bright}}$ T 細胞の集簇が認められる[13]。一方，マウス CD26 分子は当初 thymocyte activating molecule (THAM) として報告され，胸腺細胞の CD4$^-$CD8$^-$ double nagative 細胞に強発現しており，静止期，活性化 T 細胞，B 細胞，NK 細胞はともに弱陽性である[11]。ヒト CD26 は胸腺においてはマウスと異なり，medullary thymocyte (髄質胸腺) から発現し，活性化さ

Presented by Medical*Online

]

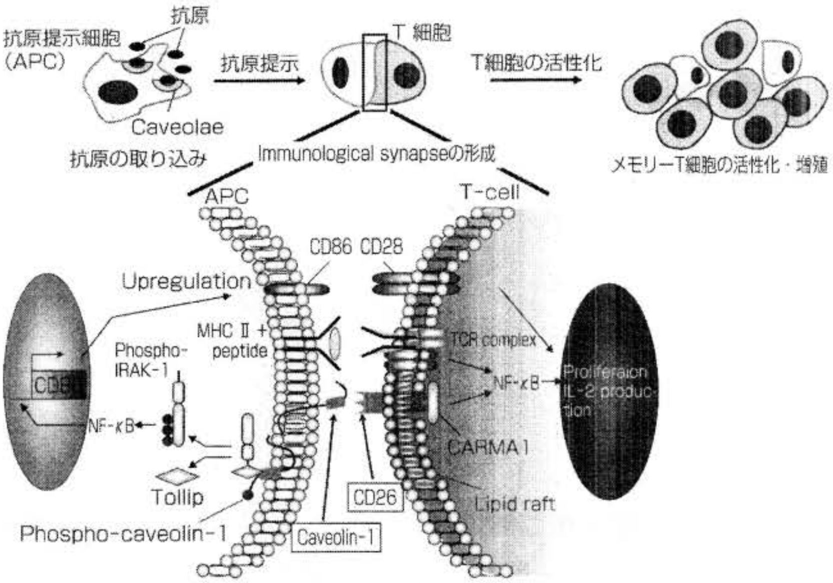
抗原
抗原提示細胞
（APC）
Caveolae
抗原の取り込み
抗原提示
T 細胞
T細胞の活性化
メモリーT細胞の活性化・増殖
Immunological synapseの形成
APC
T-cell
CD86 CD28
Upregulation
CD86
MHC II + peptide
Phospho-IRAK-1
NF-κB
Tollip
Phospho-caveolin-1
Caveolin-1
CD26
TCR complex
NF-κB
CARMA 1
Lipid raft
Proliferaion
IL-2 production

図 2　CD26 共刺激シグナルについて

れると末梢T 細胞はその発現は上昇し，また共刺激分子である[6]。しかし，マウス CD26 にはこの機能はなく，ヒト CD26 とマウス CD26 の免疫系での役割は異なっている。C57BL/6 バックグラウンドをもつ CD26 ノックアウトマウス（$CD26^{-/-}$KO マウス）は正常表現型で生存するが脾臓では CD4T 細胞の減少と NK 細胞の増加を認め，末梢血中では CD4 陽性 NKT 細胞が著明に減少し，IL-2，IFN-γ の産生減少が認められる[14]。

Ⅲ．CD26 共刺激シグナル伝達機構

図 2 に CD26 共刺激シグナルについて模式図を示した。われわれは，長らく不明であった T 細胞上 CD26 共刺激シグナル伝達の分子メカニズムを解明した。また，CD26 陽性 T 細胞のメモリー応答における共刺激リガンドとして抗原提示細胞（antigen presenting cell: APC）上の caveolin-1 を同定し，CD26 および caveolin 直下のシグナル分子を解明し CD26-caveolin 系が T 細胞のメモリー応答において新たな共刺激系であることを提示した[15]。すなわち，CD26 が抗原を取り込んだ APC 上の caveolin-1 と結合して caveolin-1 がリン酸化され，APC 上の CD28 リガンドである CD86 の発現を誘導する[15]。この際，caveolin-1 の 82～101 番目のアミノ酸残基が CD26 の DPP Ⅳ酵素活性中心（DPPⅣポケット構造）との結合に関与している[15]。CD26 の DPPⅣ酵素活性部位の 630 番目のセリン残基をアラニンに置換して酵素活性を失活させると，caveolin-1 は CD26 に結合できなくなる[15]。T 細胞の CD26 のメモリー抗原に曝露された APC の caveolin-1 が互いに接触して immunological synapse を形成し，メモリー T 細胞に対する増殖反応がもたらされる。CD26 によって APC 内で惹起される caveolin-1 下流のシグナル伝達機構として caveolin-1，Tollip，IRAK-1 複合体が NK-κB を活性化して CD86 の発現増強が誘発されるという CD26-caveolin という新たな免疫活性化経路を解明した[16]。さらに caveolin-1 が T 細胞上の CD26 と結合し，CD26 の細胞質ドメインに結合する CARMA1 が scaffolding protein として刺激シグナル伝達をつかさどり，T 細胞増殖や IFN-γ 産生などが誘導されることも明らかとなった[17]。

CD26 と caveolin-1 の免疫病態での意義を解明するため，関節リウマチ患者の罹患関節から得られた増殖滑膜の手術検体を病理組織学的に検討したところ，滑膜炎症部位に集積するリンパ球は CD26 を強く発現しており，これらのリンパ球に隣接した胚中心を形成する APC や増殖滑膜細胞，血管内皮細胞に caveolin-1 が強く発現していることが連続切片による解析で明らかとなった[18]。

Ⅳ．CD26 分子と悪性中皮腫

CD26 陽性 T 細胞腫瘍株やヒト細胞クローンを用いて *in vitro* で CD26 抗体で処理すると細胞増殖を抑制し，この時に cyclin dependent kinase inhibitor（CDKI）の p21 が誘導され細胞周期を止めることを見いだした[19]。

さらに，T 細胞腫瘍株を用いた系でも *in vitro* で CD26 抗体で処理すると p21 が誘導され細胞増殖を抑制し，この細胞株を移植した免疫不全マウスの系でも CD26 抗体の *in vivo* 投与で腫瘍細胞は壊死に陥り，抗体投与マウスは長期生存した[20]。この結果より，CD26 抗体は T 細胞異常を示す免疫病や CD26 陽性 T 細胞リンパ腫などの治療に有効な可能性を示した。そこで，自ら

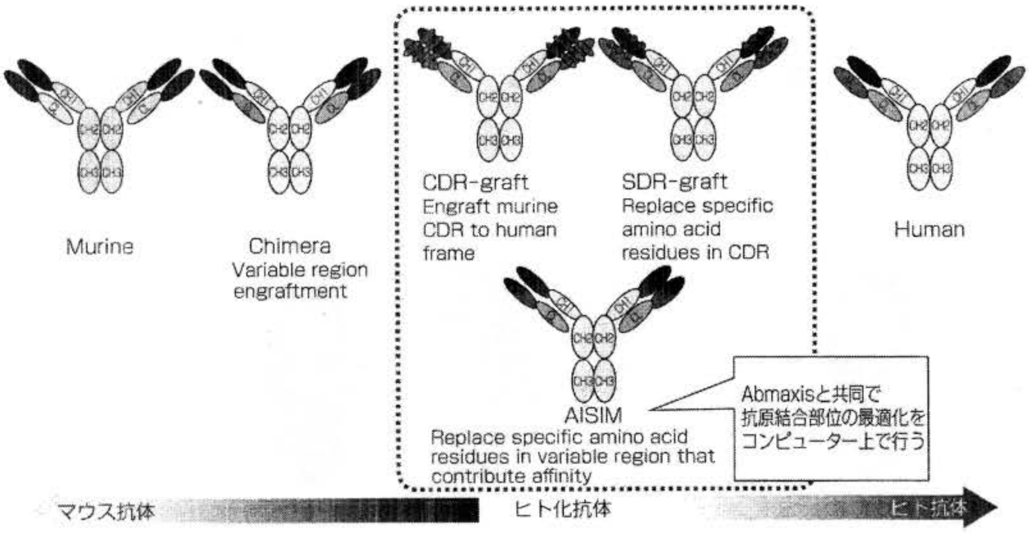
CH1
CL
CH2
CH3
Murine
Chimera
Variable region engraftment
CDR-graft
Engraft murine CDR to human frame
SDR-graft
Replace specific amino acid residues in CDR
Human
AISIM
Replace specific amino acid residues in variable region that contribute affinity
Abmaxisと共同で
抗原結合部位の最適化を
コンピューター上で行う
マウス抗体
ヒト化抗体
ヒト抗体

図 3 ヒト化抗体作製技術

開発したマウス由来 CD26 抗体から最も活性が強いと思われるものを選択して CD26 抗体の抗原結合部位のアミノ酸および遺伝子配列解析を施行し，米国アブマキシス社と共同でインシリコ法にて良質なヒト化 CD26 抗体を開発した（図 3)。

また，このヒト化抗体はもとのマウス型抗体と比しても親和性も高く，生物学活性はより強く，ヒトに用いる前に前臨床素性試験を行うサルの組織とも交叉反応性を示し良効な生産性も示した。

本ヒト抗体を開発した 2005 年にクボタショックという事件が話題に上った。つまりクボタショックとは，2005 年 6 月 29 日に毎日新聞が兵庫県尼崎市の大手機械メーカー・クボタの旧工場の周辺住民にアスベスト疾患が発生していると報告したのを契機として，社会的なアスベスト健康被害の問題が急浮上してきた現象をいい，その後連日のようにマスメディアにアスベストと中皮腫などアスベスト疾患の記事が報道された。

CD26 はコラーゲンの結合蛋白であり，われわれは T 細胞上の CD26 とコラーゲンの相互作用の研究を行っていたが，上皮型の細胞においてもその相互作用の解析を行う目的で種々癌細胞株の CD26 発現をスクリーニングする過程で偶然悪性中皮腫由来株である JMN が CD26 陽性であることを同定した[2]。

CD26 が特殊な JMN という悪性中皮腫細胞株にのみ発現している可能性があるため，慶應義塾大学医学部病理学 山田健人准教授（現埼玉医大病理学教授）に予備的に中皮腫患者の病理組織での CD26 発現を解析していただいたところ，反応性中皮では CD26 は発現していないのに悪性中皮腫では 9 例中 7 例に強発現することを見いだした。

さらに *in vivo* でヒト化 CD26 抗体は JMN 細胞株の増殖を抑制し，移植した免疫不全マウスの系においてもヒト化 CD26 抗体投与により，腫瘍縮小，生存延長，肺への転移抑制などをもたらすことを見いだし，CD26 分子が悪性中皮腫の治療ターゲットになる可能性が示唆された[4]。

V．CD26 の悪性中皮腫における発現およびその機能とヒト化 CD26 抗体の有効性について

悪性中皮腫はその病理組織型により上皮型，混合型，肉腫型の三つに分けることができる[21]。広島大学医学部病理学 井内康輝教授との共同研究で 152 症例の悪性中皮腫患者病理組織での CD26 発現を検討したところ，正常中皮ではまったく発現せず，上皮型では約 80％が陽性，混合型では約 40％が陽性，肉腫型ではほとんど発現せず，上皮型悪性中皮腫に有意に CD26 が発現することが明らかとなった[3]（図 4)。

JMN 以外の悪性中皮腫細胞株において CD26 の発現を検討したところ，9 種類の中皮腫株中 1 種類の MSTO 株のみが CD26 陰性で，他はすべて陽性であった。

この陰性株の MSTO 株に CD26 遺伝子を導入して CD26 を発現させたところ *in vitro* で親株に比して，ラミニン，Ⅳ型コラーゲン，フィブロネクチンをコートしたプレートに対して細胞遊走能，浸潤能ともに亢進が認められた[22,23]。

さらに，CD26 発現 MSTO 細胞株を免疫不全マウスへの胸腔内投与により，胸腔内でびまん性に中皮腫細胞が進展し，胸壁に浸潤するとともに心嚢や対側胸壁にも転移浸潤するヒト中皮腫浸潤・増殖モデルマウスの作製に成功した。このモデルマウスにヒト化 CD26 抗体を週 2

Membranous expression		Total No. of cases	(+)	(−)
Epithelioid mesothelioma	Well differentiated	48	40 (84%)	8
	Less differentiated	32	23 (72%)	9
Biphasic mesothelioma	Epithelioid component	21	16 (76%)	5
	Sarcomatoid component	21	0	21
Sarcomatoid mesothelioma		30	1 (3%)	29
Non-neoplastic mesothelial cells		32	0	32

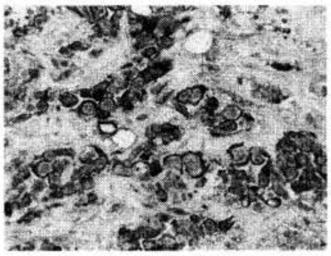

（広島大学 井内康輝教授グループ）

CD26 expressed on the mesothelioma cells

図4 悪性中皮腫のCD26分子の免疫組織染色

回，4週間腹腔内投与したところ，コントロールIgG投与群と比して，心外膜，対側胸壁への転移浸潤が著明に抑制され，さらに原発腫瘍そのものもほとんど消失した。このようにヒト化CD26抗体は本モデルにおいても有効性を示したことから，悪性中皮腫での新規治療法として臨床応用できる可能性を強く示唆した。

また，CD26分子と悪性中皮腫患者の予後との関係について解析したところ，悪性中皮腫組織のCD26発現そのものは予後との関係は認められなかったが，悪性中皮腫組織上のCD26発現をペメトレキセド，シスプラチンなど現行の悪性中皮腫の化学療法施行症例に限ると，その有効率と予後に有意な関連が認められた[24]。すなわち，CD26陽性発現度が高いほど化学療法の奏効率が高い傾向にあった。このように，CD26は化学療法剤治療反応性予測のバイオマーカーとなる可能性も示唆され，CD26陽発現性中皮腫症例には積極的に化学療法を施行すべきであると考えられた。

Ⅵ．ヒト化CD26抗体のFIH第Ⅰ相臨床試験

ヒト化CD26抗体のFIH第Ⅰ相臨床試験をスタートにするに当たって，サルを用いた前臨床毒性試験を行う必要がある。カニクイザルを用いて10〜100 mg/kgの単回静脈内点滴投与において特記すべき副作用と思われる変化は認められず，さらに毎週1回3か月間に及ぶ反復投与長期毒性試験においてもその安全性が確認された。

そこで，フランスのGustave-Roussy Institute Hospital，Cochin Hospital，Lyon Hospital，Caen Hospital，Dijon Hospitalの5施設で，化学療法抵抗性の悪性中皮腫およびその他CD26陽性悪性腫瘍をターゲットにした第Ⅰ相臨床試験がスタートした。0.1 mg/kg，0.4 mg/kg，1.0 mg/kg，2.0 mg/kg，4.0 mg/kg，6.0 mg/kgの6用量・3例または6例/コホートからなり，第4コホートの途中までは隔週投与で1か月間計3回の投与，その後ヒト化CD26抗体の血中濃度をさらに上げるためプロトコールを変更して1か月間ごと週計5回投与を行い，投与終了2週後にmodified RECISTにてその有効性を評価した。

化学療法剤抵抗性悪性腫瘍141症例のCD26発現をスクリーニングして，20%以上病理組織標本においてCD26陽性の場合にその対象症例とした。総計33例の化学療法抵抗性の固形癌で，22例が進行性悪性中皮腫，10例が腎癌および1例が尿路上皮癌であった。ヒト化CD26抗体投与の成績であるが，13例がprogressive disease（PD），13例がstabilized disease（SD），7例が評価できずであった。さらに，悪性中皮腫の評価可能例19例中10例がSDと評価され，5例が6か月以上SDを継続し，1例が3か月以上SDが継続し，有効性を示唆するデータも得られた。安全性に関して注射後反応が認められるcaseはあったが，免疫不全をはじめとして特記すべき有害事象は認められず，安全性も確認できた[25]フランスのGustave-Roussy Institute Hospitalは悪性中皮腫をターゲットにして様々な抗体を含む薬剤の第Ⅰ臨床試験を行っていたが，*Lung Cancer*という雑誌にこのグループが悪性中皮腫の第Ⅰ相臨床試験に使用された薬剤25種類についてその評価を報告し，そのなかで本抗体は三つの有望な薬剤の一つに選ばれた（後の二つとしては，FAK inhibitorおよびckit inhibitorである）[5]。

Presented by Medical*Online

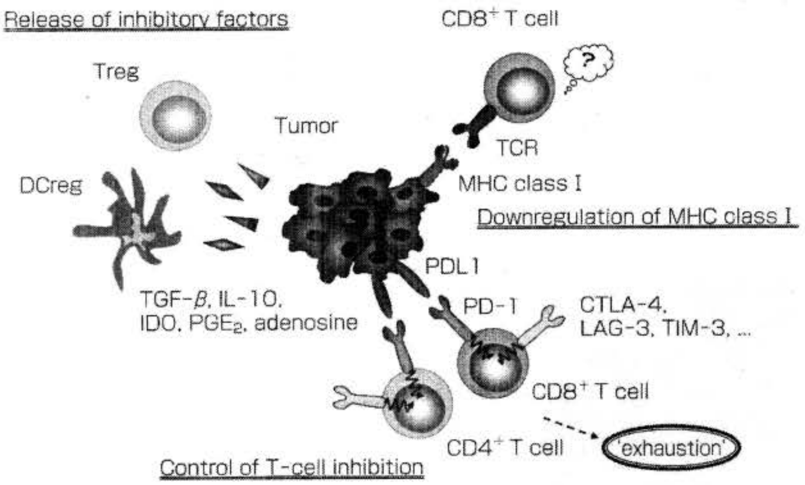
Release of inhibitory factors
Treg
Tumor
DCreg
TGF-β, IL-10,
IDO, PGE2, adenosine
CD8+ T cell
?
TCR
MHC class I
Downregulation of MHC class I
PDL1
PD-1
CTLA-4,
LAG-3, TIM-3, ...
CD8+ T cell
CD4+ T cell
exhaustion
Control of T-cell inhibition

図 5 癌細胞の免疫系からの攻撃を逃れる様々な機構について
IDO: indoleamine-2,3-dioxygenase, PGE_2: prostaglandin E_2

Ⅶ. ヒト化CD26抗体の作用機構

われわれはこれまでにヒト化CD26抗体の抗腫瘍作用メカニズムとして，本抗体はIgG1であるのでNK細胞やmacrophageのFcR受容体に抗体が結合することで抗体医薬特有の抗体依存性細胞傷害（ADCC）活性などの間接的作用に加えて，CD26陽性腫瘍に抗体が結合することによる直接的な作用があることを明らかにしてきた[4]。癌細胞の細胞膜上のCD26にヒト化CD26抗体が結合すると，CDKIであるp21やp27の発現が上昇し，S期の細胞を減少させるとともにG_2/M期で細胞周期を遅延させることが明らかになっている[4,19,20]。さらに，CD26抗体とCD26の複合体が膜から細胞質，さらに核内へと移行し，RNA polymeraseであるPOLR2A遺伝子の転写領域下流に結合することでPOLR2Aの転写を抑制し増殖を抑制する[26]。このように，細胞増殖や生存プログラムに重要な役割を果たすPOLR2A遺伝子機能を抑制することで，細胞増殖を抑制することを明らかにした。また，CD26はcollagenやfibronectinとの結合蛋白であるが，CD26抗体が結合することでそれらの蛋白への接着が阻害され[4]，このことからCD26抗体が$CD26^+$腫瘍の浸潤・転移の抑制にも働くことが示唆された。

CD26はヒトT細胞に活性化シグナルを伝達するT細胞共刺激分子であり，CD26抗体はCD26のリガンドであるcaveolin-1のCD26への結合をブロックする[15,17,27]。また，CD26の機能の一つにDPPⅣ酵素活性があり，N末端から2番目にプロリンまたはアラニンを有するペプチドの2アミノ酸を切断する[8]。生体内で様々な生理活性物質がその基質となることが知られているが，いくつかのケモカインもDPPⅣによる切断を受けその細胞遊走活性が不活性化される[10,13]。最近担癌マウスにDPPⅣ阻害薬のシタグリプチンを混ぜたエサを食べさせることにより，ケモカインCXCL10のDPPⅣ酵素による分解を抑えることによりCXCR3陽性T細胞の腫瘍微小環境への遊走を促進し，その結果腫瘍の増殖抑制をもたらすことが報告されている[28]。CD26抗体はDPPⅣ酵素活性自体に直接は影響しないが，フランスでの第Ⅰ相臨床試験の結果から，ヒト化CD26抗体の投与により血中の可溶性CD26の量が顕著に低下し，DPPⅣ酵素活性も同様に低下することが示されている。DPPⅣ酵素活性の低下によりCXCL10のケモカインの切断と不活性化が抑えられ，特にCXCR3陽性細胞が腫瘍組織に遊走しやすくなり，腫瘍細胞を破壊する可能性が考えられる[29]。これらの知見から，CD26抗体は免疫系にも影響する可能性が強く示唆される。

Ⅷ. CD26と免疫チェックポイント機構

さて，癌細胞には免疫系からの攻撃を逃れる様々な機構が備わっている（図5）。たとえばTreg細胞，regulatory dendritic cellsなどからTGF-β，IL-10産生がされて免疫系を抑制したり，腫瘍細胞上のMHCクラスⅠの発現低下が生じて腫瘍特異的キラーT細胞機能が発揮できなかったり，さらにCTLA-4，PD-1，LAG-3などの分子がT細胞表面に発現誘導され，その結果T細胞機能が抑制されるというものである[30]。

現在臨床現場では，特にメラノーマや非小細胞性肺癌の領域でCTLA-4抗体やPD-1/PDL1抗体を投与して免疫チェックポイント阻害により抗腫瘍免疫効果を亢進させ，ある患者集団ではとても有効であるとの報告がある[31]。

現在，腫瘍免疫エスケープを改善させるため様々な種

類の癌に対してCTLA-4，PD-1/PDL1抗体，さらにLAG-3抗体およびそれら抗体の組み合わせなどの臨床試験が行われており[32]，すでにCTLA-4抗体やPD-1/PDL1抗体はメラノーマや肺癌において臨床現場に届いている[33]。

CD26分子と免疫チェックポイント機構について，われわれはヒトCD4 T細胞をCD3とCD26抗体およびCD3とCD28抗体で刺激して様々なサイトカイン産生および細胞表面分子の発現を検討した。その結果，CD26刺激ではIL-10およびLAG-3分子の発現上昇が認められた[34]。しかし，CD28刺激では認められなかった。また，IL-10およびLAG-3ともにCD26刺激の強さが増加するにつれ，その産生量および発現もますます高くなったがCD28刺激ではこれらは認められなかった[34]。しかし，CTLA-4やFOX3の発現はCD26，CD28刺激ともに差は認められなかった[34]。

最近，他のグループもヒトCD4 regulatory T細胞におけるCD26陽性サブセットはCD3刺激において最もIL-10を強産生する細胞集団であることを報告し，われわれの結果を支持するデータをだしている[35]。このように，ヒトCD4 T細胞に強いCD26共刺激シグナルが伝達すると代表的抑制性サイトカインのIL-10の強産生および免疫チェックポイント分子のLAG-3分子の発現が誘導されることが明らかとなり，癌微小環境においてCD26分子は，IL-10高産生，LAG-3分子の高発現を通じて免疫チェックポイントとして機能している可能性が示唆され，ヒト化CD26抗体の投与によりこれら免疫チェックポイントが阻害され腫瘍免疫を亢進している可能性が考えられる[29,31]。

おわりに

CD26分子の免疫系および癌，特に悪性中皮腫での機能，さらにヒト化CD26抗体の前臨床でのデータおよびフランスでの第Ⅰ相臨床試験の結果を説明した。本抗体は本邦でも近々，治療抵抗性の悪性中皮腫を対象として第Ⅰ相臨床試験がスタートされる予定である。

CD26分子は悪性中皮腫以外にも非小細胞性肺癌，肝癌，大腸癌，腎癌など幅広く発現しており，これらの細胞株においても担癌マウスの系でヒト化抗体の有効性を確認しており，さらに化学療法剤との相乗作用の結果も得ている。

CD26抗体は直接的な抗癌作用以外にも免疫チェックポイント阻害など非常にユニークな機能を有しており，今後その対象を拡大させていく予定で癌に苦しむ患者に少しでも役立つことを願っている。

文　献

1) Ohnuma K, Dang NH and Morimoto C: Revisiting an old acquaintance: CD26 and its molecular mechanisms in T cell function. *Trends Immunol* **29**(5): 295-301, 2008.
2) Dang NH, Torimoto Y, Schlossman SF, *et al*: Human CD4 helper T cell activation: functional involvement of two distinct collagen receptors, 1F7 and VLA integrin family. *J Exp Med* **172**(2): 649-652, 1990.
3) Amatya VJ, Takeshima Y, Kushitani K, *et al*: Overexpression of CD26/DPPⅣ in mesothelioma tissue and mesothelioma cell lines. *Oncol Rep* **26**(6): 1369-1375, 2011.
4) Inamoto T, Yamada T, Ohnuma K, *et al*: Humanized anti-CD26 monoclonal antibody as a treatment for malignant mesothelioma tumors. *Clin Cancer Res* **13**(14): 4191-4200, 2007.
5) Raphael J, Le Teuff G, Hollebecque A, *et al*: Efficacy of phase 1 trials in malignant pleural mesothelioma: description of a series of patients at a single institution. *Lung Cancer* **85**(2): 251-257, 2014.
6) Morimoto C and Schlossman SF: The structure and function of CD26 in the T-cell immune response. *Immunol Rev* **161**(1): 55-70, 1998.
7) Morimoto C, Torimoto Y, Levinson G, *et al*: 1F7, a novel cell surface molecule, involved in helper function of CD4 cells. *J Immunol* **143**(11): 3430-3439, 1989.
8) Hopsu-Havu VK and Glenner GG: A new dipeptide naphthylamidase hydrolyzing glycyl-prolyl-beta-naphthylamide. *Histochemie* **7**(3): 197-201, 1966.
9) Tanaka T, Camerini D, Seed B, *et al*: Cloning and functional expression of the T cell activation antigen CD26. *J Immunol* **149**(2): 481-486, 1992.
10) Ohnuma K and Morimoto C: DPP4（dipeptidyl-peptidase 4）. *Atlas Genet Cytogenet Oncol Haematol* **17**(5): 301-312, 2013.
11) Marguet D, Bernard AM, Vivier I, *et al*: cDNA cloning for mouse thymocyte-activating molecule. A multifunctional ecto-dipeptidyl peptidase Ⅳ（CD26）included in a subgroup of serine proteases. *J Biol Chem* **267**(4): 2200-2208, 1992.
12) Bengsch B, Seigel B, Flecken T, *et al*: Human Th17 cells express high levels of enzymatically active dipeptidyl-peptidase Ⅳ(CD26). *J Immunol* **188**(11): 5438-5447, 2012.
13) Ohnuma K, Hosono O, Dang NH, *et al*: Dipeptidyl peptidase in autoimmune pathophysiology. *Adv Clin Chem* **53**: 51-84, 2011.
14) Yan S, Marguet D, Dobers J, *et al*: Deficiency of CD26 results in a change of cytokine and immunoglobulin secretion after stimulation by pokeweed mitogen. *Eur J Immunol* **33**(6): 1519-1527, 2003.
15) Ohnuma K, Yamochi T, Uchiyama M, *et al*: CD26 up-regulates expression of CD86 on antigen-presenting cells by means of caveolin-1. *Proc Natl Acad Sci USA* **101**(39): 14186-14191, 2004.
16) Ohnuma K, Yamochi T, Uchiyama M, *et al*: CD26 mediates dissociation of Tollip and IRAK-1 from caveolin-1 and induces upregulation of CD86 on antigen-presenting cells. *Mol Cell Biol* **25**(17): 7743-7757, 2005.
17) Ohnuma K, Uchiyama M, Yamochi T, *et al*: Caveolin-1 triggers T-cell activation via CD26 in association with CARMA1. *J Biol Chem* **282**(13): 10117-10131, 2007.
18) Ohnuma K, Inoue H, Uchiyama M, *et al*: T-cell activation via CD26 and caveolin-1 in rheumatoid synovium. *Mod Rheumatol* **16**(1): 3-13, 2006.
19) Ohnuma K, Ishii T, Iwata S, *et al*: G1/S cell cycle arrest provoked in human T cells by antibody to CD26. *Immunology* **107**(3): 325-333, 2002.

Presented by Medical*Online

20) Ho L, Aytac U, Stephens LC, *et al*: *In vitro* and *in vivo* antitumor effect of the anti-CD26 monoclonal antibody 1F7 on human CD30+ anaplastic large cell T-cell lymphoma Karpas 299. *Clin Cancer Res* **7**(7): 2031-2040, 2001.

21) Ismail-Khan R, Robinson LA, Williams CC, *et al*: Malignant pleural mesothelioma: a comprehensive review. *Cancer Control* **13**(4): 255-263, 2006.

22) Okamoto T, Iwata S, Yamazaki H, *et al*: CD9 negatively regulates CD26 expression and inhibits CD26-mediated enhancement of invasive potential of malignant mesothelioma cells. *PLoS One* **9**(1): e86671, 2014.

23) Yamamoto J, Ohnuma K, Hatano R, *et al*: Regulation of somatostatin receptor 4-mediated cytostatic effects by CD26 in malignant pleural mesothelioma. *Br J Cancer* **110**(9): 2232-2245, 2014.

24) Aoe K, Amatya VJ, Fujimoto N, *et al*: CD26 overexpression is associated with prolonged survival and enhanced chemosensitivity in malignant pleural mesothelioma. *Clin Cancer Res* **18**(5): 1447-1456, 2012.

25) Angevin E, Isambert N, Trillet-Lenoir VN, *et al* First-in-human phase I administration of YS 110, a monoclonal antibody directed against CD26 immunostimulatory molecule in advanced cancer patients. *J Clin Oncol* **33**(15): abstr 2519, 2015.

26) Yamada K, Hayashi M, Du W, *et al*: Localization of CD26/DPPⅣ in nucleus and its nuclear translocation enhanced by anti-CD26 monoclonal antibody with anti-tumor effect. *Cancer Cell Int* **9**: 17, 2009.

27) Ohnuma K, Uchiyama M, Hatano R, *et al*: Blockade of CD26-mediated T cell costimulation with soluble caveolin-1-Ig fusion protein induces anergy in $CD4^+$ T cells. *Biochem Biophys Res Commun* **386**(2): 327-332, 2009.

28) Barreira da Silva R, Laird ME, Yatim N, *et al*: Dipeptidylpeptidase 4 inhibition enhances lymphocyte trafficking, improving both naturally occurring tumor immunity and immunotherapy. *Nat Immunol* **16**(8): 850-858, 2015.

29) Ohnuma K, Hatano R and Morimoto C: DPP4 in anti-tumor immunity: going beyond the enzyme. *Nat Immunol* **16**(8): 791-792, 2015.

30) Palucka AK and Coussens LM: The basis of oncoimmunology. *Cell* **164**(6): 1233-1247, 2016.

31) Hamanishi J, Mandai M, Matsumura N, *et al*: PD-1/PD-L1 blockade in cancer treatment: perspectives and issues. *Int J Clin Oncol*: 2016. [Epub ahead of print]

32) Spranger S: Mechanisms of tumor escape in the context of the T cell-inflamed and the non-T-cell-inflamed tumor microenvironment. *Int Immunol*: 2016. [Epub ahead of print].

33) Nguyen LT and Ohashi PS: Clinical blockade of PD1 and LAG3—potential mechanisms of action. *Nat Rev Immunol* **15**(1): 45-56, 2015.

34) Hatano R, Ohnuma K, Otsuka H, *et al*: CD26-mediated induction of EGR2 and IL-10 as potential regulatory mechanism for CD26 costimulatory pathway. *J Immunol* **194**(3): 960-972, 2015.

35) Hua J, Davis SP, Hill JA, *et al*: Diverse gene expression in human regulatory T cell subsets uncovers connection between regulatory T cell genes and suppressive function. *J Immunol* **195**(8): 3642-3653, 2015.

Presented by Medical*Online

● 特 集 ● 希少がんの病理と診療

胸膜中皮腫の病理と診断（治療）

岸本 卓巳　藤本 伸一　西 英 行*

〔*Jpn J Cancer Chemother* **43**(5): 513-517, *May*, 2016〕

Clinical Pathological Diagnosis, and Treatment for Pleural Mesothelioma: Takumi Kishimoto, Nobukazu Fujimoto and Hideyuki Nishi (*Research Center for Asbestos-Related Diseases, Okayama Rosai Hospital*)

Summary

For the differential diagnosis between fibrous pleuritis and other malignancies such as lung cancer, multiple immunostaining is essential to diagnose pleural mesothelioma. For cytological diagnosis of pleural effusions, differentiation between mesothelioma cells and reactive mesothelial cells is very difficult. Therefore, histological diagnoses of tumor tissues obtained via biopsy are essential. To diagnose epthelioid mesothelioma, more than 2 positive and negative markers must be consistent with those known for mesothelioma. To diagnose sarcomatoid mesothelioma, keratin is usually positive, differentiating the diagnosis from that for real sarcoma. For surgical treatment for pleural mesothelioma, extrapleural pneumonectomy (EPP) and pleurectomy/decortication (P/D) are usually performed. The proportion of P/D increases because of the low death rates with surgery and similar survivals. However, a trimodal approach, such as EPP with chemotherapy and radiotherapy, is best for longer survival and expected to be curative. For chemotherapy, only cisplatin (CDDP) combined with pemetrexed (PEM) is effective, and no other agents have been identified for this disease. Nowadays, clinical immunotherapy trials start with phase II study. **Key words**: Pleural mesothelioma, Asbestos exposure, Immunostaining, **Corresponding author**: Takumi Kishimoto, Research Center for Asbestos-Related Diseases, Okayama Rosai Hospital, 1-10-25 Chikko midori-machi, Minami-ku, Okayama 702-8055, Japan

要旨 中皮腫の病理診断では，細胞診における中皮腫細胞と反応性中皮細胞の鑑別が難しいため腫瘍組織生検による鑑別が必須である。確定診断のためには複数の免疫染色を行い，線維性胸膜炎や肺癌との鑑別を行う。上皮型中皮腫の診断には陽性，陰性抗体が各2種類以上中皮腫に一致する必要がある。また，肉腫型中皮腫では真の肉腫との鑑別でケラチン陽性が重要である。中皮腫の治療法では外科手術として extrapleural pneumonectomy（EPP）と pleurectomy/decortication（P/D）が行われるが，周術期の死亡率が高い EPP に対して P/D は比較的低く，生存期間がほぼ同様であるため P/D の施行頻度が増加している。しかし，治癒をめざすためには，EPP に化学療法と放射線療法を加えた trimodality が望まれる。化学療法としては cisplatin (CDDP)＋pemetrexed (PEM) のみが有効であり，その他の治療法として免疫療法が試みられるようになってきた。

◆◆◆

はじめに

胸膜中皮腫は壁側胸膜の中皮細胞が腫瘍性増殖する疾病で，ほとんどが悪性腫瘍である。欧米では本疾患の約80％以上がアスベスト曝露によるが，日本においても73.7％が職業性アスベスト曝露により，その他環境曝露などを加えると約80％であることが明らかとなった1)。また，日本における中皮腫による死亡者数は1995年に500人であったものが増加傾向を示し，2013年には1,410人となった。そのうち増加しているのは男性の胸膜中皮腫であり，女性の胸膜中皮腫と腹膜中皮腫には増加傾向はみられない。一方，その診断は難しく，厚生労働省人口動態統計上中皮腫であると診断された症例において，男性の胸膜中皮腫のうち26％が中皮腫以外の疾患であったことも報告2)されている。

I．画像診断

進行期胸膜中皮腫の特徴像は胸膜がびまん性に不整な

---

* 岡山労災病院・アスベスト研究センター

連絡先: 〒702-8055 岡山市南区築港緑町1-10-25 岡山労災病院・アスベスト研究センター
岸本 卓巳

Presented by Medical*Online

肥厚を示す環状胸膜肥厚像（pleural rind）を呈するが，早期病変では胸膜肥厚をまったく呈さず胸水貯留のみのこともある。また，縦隔側胸膜肥厚のみや，胸膜炎の際に認められる不整のない軽度胸膜肥厚像を呈することも少なくない。肺癌と鑑別を要する胸膜上の単発腫瘤形成像や転移性腫瘍を示唆する多発腫瘤形成型もあることから，胸膜上に腫瘍性病変が存在する場合には鑑別診断として胸膜中皮腫を念頭に置く必要がある。

Ⅱ．血清あるいは胸水補助診断

胸膜中皮腫の血液マーカーとして，米国の FDA や日本の厚生労働省に認可されているのは soluble mesothelin related peptides（SMRP）のみである。本マーカーは治療経過のマーカーとしては有用であるが，Helsinki Criteria 2014[3] では中皮腫診断上推奨される血液マーカーはないとしており，血清 SMRP も必ずしも有用な診断マーカーであるとはいえない。

一方，胸水マーカーとして胸水ヒアルロン酸値が 100,000 ng/mL 以上であれば中皮腫の可能性が高いとする報告があり，有用性が高い。しかし，中皮腫のうち約半数以上は 100,000 ng/mL 未満である[4]。これを補完するマーカーとして前述の SMRP が 8 ng/mL 以上であれば，ヒアルロン酸に近い有用性がある[5]。

また，胸膜中皮腫の除外マーカーとして結核性胸膜炎の際に高値を示す adenosine deaminase（ADA）があるが，胸膜中皮腫の際にも高値を示すので注意を要する。肺癌や癌性胸膜炎において増加するマーカーとして CEA，CYFRA21-1 があげられる。CYFRA21-1 はサイトケラチン中間径フィラメントの可溶性フラグメントであり，胸膜中皮腫でも増加するが，肺癌でも増加するので特異的ではない。

Ⅲ．病理診断

1．胸水細胞診

胸膜中皮腫では，その 80％以上で胸水を伴うので胸水細胞診が有用であることもある。しかし，胸水に中皮腫細胞が認められるのは初回胸水貯留から間もない時期であり，腫瘍細胞が認められないことも少なくない。また，中皮細胞が出現していても中皮腫細胞ではなく，胸膜炎の際に増加する反応性中皮細胞であることも多く，この両者の鑑別が極めて難しい。

中皮腫細胞の特徴は，通常 long slender microvilli を有することから細胞辺縁の輪部がぼやけ，核が大型で核小体が目立ち，2 核以上の多核細胞，相互封入像や hump 様細胞質突起が認められることである[6]。反応性中皮細胞と比較すると，中皮腫細胞では EMA が膜表面に染色されるとともに GLUT-1，insulin-like growth factor Ⅱ mRNA-binding protein 3（IMP3），CD146 が陽性を示し，desmin が陰性を示すことが鑑別に有用である[7]。

表 1　中皮腫組織型別の抗体選択

	上皮型	肉腫型
陽性マーカー	Calretinin	CK（AE1/AE3）
	WT1	CAM5.2
	D2-40	D2-40
	Thrombomodulin	WT1
	Mesothelin	EMA
陰性マーカー	CEA	S-100
	TTF-1	Desmin
	BerEP-4	CD34
	MOC31	
	ER, PgR, etc	

しかし WHO 第 4 版には，両者の鑑別は難しく不可能であると記載されている[8]。一方，原発性あるいは転移性肺癌や胸膜あるいは胸壁原発の肉腫などとの鑑別には，以下に述べる病理組織におけるマーカーを使用する[8]。

2．病理組織診断

病理診断のためには胸腔鏡下生検が望ましく，脂肪織も含めた十分な大きさの組織を複数箇所から採取することが推奨される。

WHO 第 4 版は，中皮腫をびまん性悪性中皮腫，限局性中皮腫，高分化型乳頭状中皮腫，アデノマトイド腫瘍に分類した。アデノマトイド腫瘍は良性腫瘍であるが，その他は悪性で，大半はびまん性である。びまん性悪性中皮腫は上皮型，肉腫型，二相型に分類され，豊富な膠原線維を伴う線維形成型中皮腫は肉腫型の亜型とされる。組織型別では上皮型が約 60％，二相型が約 25％，肉腫型が約 15％である。

上皮型で最も多いパターンは solid type，tubulo-papillary type，trabecular type であり，特殊型として pleomorphic type，clear cell type，deciduoid type，lymphohistiocytoid type などのパターンや，細胞形成態を呈する型も知られている[8]。中皮腫の組織診断では中皮由来であることの確認が必要で，上皮型中皮腫の確定診断には主に腺癌との鑑別のため，表 1 にあげられる陽性マーカーが二つ以上，かつ陰性マーカーが二つ以上であることの確認が必要である（表 2）。扁平上皮癌ではカルレチニン（calretinin）の陽性率が比較的高いので，その鑑別には p40，p63 が陰性であることを確認する[9]。さらに，claudin 4 は中皮腫と癌腫の鑑別に有用である。一方，肉腫型の診断では真の肉腫を否定するため，上皮由来であることを示すサイトケラチン（CK）（AE1/AE3，CAM5.2 など）が陽性であることを確認する（表 2）。CK 陰性

表2　胸膜中皮腫の鑑別診断

鑑別要件	中皮腫	その他の疾患
中皮腫の陽性抗体，陰性抗体	上皮型中皮腫	肺癌
	2種類以上中皮腫に一致	中皮腫に一致しない
CK（AE1/AE3，CAM5.2）	肉腫型中皮腫	肉腫
	陽性	陰性
画像所見	肉腫型中皮腫	肉腫様癌
	胸膜病変	肺内病変
FISH法（homozygous deletion）	線維形成型中皮腫	線維性胸膜炎
	陽性	陰性
融合遺伝子	二相型中皮腫	滑膜肉腫
	陰性	陽性

の肉腫型中皮腫の存在も報告されているが，肉腫との鑑別は画像の他に総合的な診断を必要とする。また，肉腫型中皮腫と肉腫様癌の鑑別には現在のところ鑑別マーカーがないことから，画像所見における腫瘍の首座が肺か胸膜かによって鑑別を行う。

肉腫型中皮腫，特に線維形成型中皮腫の診断では線維性胸膜炎（良性石綿胸水）との鑑別が重要である。線維形成型では組織学的に細胞配列の乱れや肥厚の程度に不均一性があり，FISH法によるp16遺伝子のhomozygous deletionが高頻度に認められる（表2）。一方，線維性胸膜炎ではhomozygous deletionはなく，胸膜表面から垂直に伸びる血管増生と胸膜表層から深部に向かうにつれて細胞密度や異型度が低下する（zonation）ことが特徴である。p16遺伝子のhomozygous deletionは良性病変との鑑別に有用で，その特異度は100％であるが他の悪性腫瘍との鑑別にはならない[10]。

二相型中皮腫では，二相性を示す頻度の高い滑膜肉腫との鑑別が必要である。滑膜肉腫では転座t（X；18）（p11；q11）に伴う融合遺伝子が必ず認められるので，最終診断はこの融合遺伝子の存在を確認する（表2）。

Ⅳ. 治　療

米国のNational Comprehensive Cancer Network（NCCN）のガイドライン[11]では，その推奨グレードはカテゴリー2A「比較的低レベルのエビデンスに基づく」推奨である。

1．外科治療法

外科治療の目的は肉眼的完全切除であるが，術後の局所再発が極めて高率である。そのため，化学療法あるいは放射線療法と組み合わせた集学治療が必要である。肉腫型では術後再発の頻度が極めて高く，予後不良であることから手術は避けるべきであるとされている。

1）胸膜肺全摘出術（extrapleural pneumonectomy: EPP）

胸膜，肺，横隔膜，心膜を胸膜外側から一括して切除する方法である。手術関連死亡が比較的多く，術後のQOL低下などのリスクのある手術ではあるが，治療がうまくいけば生存期間の延長が期待される。IMIG分類のstage Ⅰ，Ⅱまでの早期病変が適応となる。特に左胸膜原発はよい適応である。EPPを行う場合には，まずcisplatin（CDDP）＋pemetrexed（PEM）による化学療法を2コース施行後にEPPを行い，術後に胸腔内に60 Gyの放射線療法を行う（trimodality）ことが標準とされ，遂行可能例では予後良好で5年生存も認められている[12]。

2）胸膜切除・肺剥皮術（pleurectomy/decortication: P/D）

肺を温存する縮小手術であり，手術関連死亡率が低い。しかし術式は様々で，腫瘤を切除する目的のdebulking P/D，壁側および臓側胸膜を広範囲に切除するいわゆるP/D，心膜・横隔膜の合併切除を行うextended P/Dがあるため一括した評価は難しいが，P/Dとextended P/Dには統計的に有意差があるという報告がある[13]。肺が残存するため術後の管理が比較的容易であり，右胸膜原発，合併症のある症例などリスクをもつ症例に施行されている。

EPPの場合には高い合併症の発生があるため，化学療法単独との比較試験（mesothelioma and radical surgery: MARS試験）ではEPPのMST 14.4か月vs化学療法単独のMST 19.5か月と，その有益性が証明されなかった[14]。

また，これら手術に対するメタアナリシス[15]からEPPの周術期死亡率は2.9％でOSは2～22か月（P/D: 6.8％，12～29か月）であったことから，2014年のNCCNのガイドライン[11]あるいはThe International Association for the Study of Lung Cancer（IASLC）の集計結果[16]では，stage Ⅱ以上には治療関連死亡の少ないP/Dを選択することを推奨している。しかし，P/Dを行った場合には患者側に肺が残存するため，放射線療法により根治療法が行えないという欠点がある。現在，EPPとP/

Presented by Medical*Online

表 3　胸膜中皮腫手術別治療成績（prospective study）

EPP

著者	年	症例数	併用療法	死亡率（%）	OS（M）
Pagan	2006	44	術後 CT+RT	4.5	20
Rea	2007	17	導入 CT+RT	0	25.5
Weder	2007	45	CT+RT	2.2	23
de Perrot	2009	45	CT+RT	6.7	14
Krug	2009	54	CT+RT	3.7	21.9
Van Schil	2010	42	導入 CT+RT	6.5	18.4

P/D

著者	年	症例数	併用療法	死亡率（%）	OS（M）
Richards	2006	44	CT	11	13
Bölükbus	2011	35	CT, RT	0	25
Nakas	2012	67	CT	3	13.4
Laug-Lazdunski	2012	54	CT	0	23
Fiedberg	2012	38	CT	2.6	31.7

D の比較試験は施行されていないので，どちらの手術療法を選択するかについては病変が左右のどちらか，患者の stage，PS，年齢や基礎疾患の有無などに応じて慎重に決定されるべきである17)（表 3）。

2．化 学 療 法

標準初回療法は CDDP と PEM 併用療法である。CDDP 単独投与を対象とした第Ⅲ相比較試験18)で奏効率 41.3%，PFS 5.7 か月，MST 12.1 か月であったことから米国の FDA で認可され，日本でも 2007 年 1 月に保険適応となった。carboplatin+PEM も無作為化比較試験はないが同様と評価されているため，CDDP が使用できない高齢者や腎機能障害のある症例に対して使用されている。second-line として vinorelbine や gemcitabine が用いられるが，有意な効果は認められておらず，現在その他にも治療効果が認められている薬剤はない。

最近の臨床第Ⅲ相試験において CDDP+PEM に bevacizumab を追加することにより，PFS 2 か月，OS は 2.75 か月の有意な延長が認められ，毒性は増加するものの管理可能であることが報告された19)。同じく最近の第Ⅱ相試験で，amatuximab（抗メソテリン・キメラ型抗体）の CDDP+PEM への上乗せ効果として PFS 6.1 か月，OS は 14.8 か月であったと報告されている20)。また，抗 cytotoxic T-lymphocyte antigen 4（CTLA4）抗体である tremelimumab を用いた第Ⅱ相試験が施行され，PFS 6.2 か月，OS が 10.7 か月と報告されている21)。これらの成績は有望であるが，治療効果の評価は今後の臨床試験にゆだねられている。また，抗 PD-1 抗体も効果があることが報告されており22)，今後の臨床試験が期待される。その他，抗 CD26 ヒト化抗体や遺伝子治療が開始されているが，まだ第Ⅰ相試験の段階である。

文　献

1) Gemba K, Fujimoto N, Kato K, *et al*: National survey of malignant mesothelioma and asbestos exposure in Japan. *Cancer Sci* **103**(3): 483-490, 2012.
2) Takeshima Y, Inai K, Amatya VJ, *et al*: Accuracy of pathological diagnosis of mesothelioma cases in Japan: clinicopathological analysis of 382 cases. *Lung Cancer* **66**(2): 191-197, 2009.
3) Wolff H, Vehmas T, Oksa P, *et al*: Asbestos, asbestosis, and cancer, the Helsinki criteria for diagnosis and attribution 2014: recommendations. *Scand J Work Environ Health* **41**(1): 5-15, 2015.
4) 藤本伸一，青江啓介，大泉聡史・他: 胸膜中皮腫を中心とした胸水ヒアルロン酸に関する症例調査．肺癌 **54**(6): 767-771, 2014.
5) Fujimoto N, Gemba K, Asano M, *et al*: Soluble mesothelin-related protein in pleural effusion from patients with malignant pleural mesothelioma. *Exp Ther Med* **1**(2): 313-317, 2010.
6) 亀井敏昭: 石綿関連疾患での中皮腫診断への体腔液細胞診の意義と検証．平成 24 年度石綿関連疾患に係る医学的所見の解析調査業務（体腔液細胞診による中皮腫診断の在り方に関する調査編）報告書, 2013, pp1-21.
7) 廣島健三: 悪性胸膜中皮腫～病理診断の困難さ～．日職災医誌 **63**(4): 215-218, 2015.
8) Galateau-Salle F, Churg A, Roggli V, *et al*: Epithelioid mesothelioma. Pathology and Genetics, Tumours of the lung, pleura, thymus and heart（eds by Travis WD, Brambilla E, Müller-Hermelink K, *et al*）, International Agency for Research on Cancer, Lyon, 2015, pp156-164.
9) Husain AN, Colby T, Ordonez N, *et al*: Guidelines for pathologic diagnosis of malignant mesothelioma: 2012 update of the consensus statement from the International Mesothelioma Interest Group. *Arch Pathol Lab Med* **137**(5): 647-667, 2013.
10) 鍋島一樹，濱崎　慎，松本慎二・他: 中皮腫と p16 遺伝子の欠失．呼吸 **33**(8): 754-761, 2014.
11) NCCN Clinical Practice Guidelines in Oncology（NCCN Guidelines）, Malignant Pleural Mesothelioma, version 1, 2014.
12) Sugarbaker DJ, Flores RM, Jaklitsch MT, *et al*: Resection margins, extrapleural nodal status, and cell type determine postoperative long-term survival in trimodality therapy of malignant pleural mesothelioma: results in 183 patients. *J Thorac Cardiovasc Surg* **117**(1): 54-63,

Presented by Medical*Online

1999.

13) Bedirhan MA, Cansever L, Demir A, *et al*: Which type of surgery should become the preferred procedure for malignant pleural mesothelioma: extrapleural pneumonectomy or extended pleurectomy? *J Thorac Dis* **5**(4): 446-454, 2013.

14) Treasure T, Lang-Lazdunski L, Waller D, *et al*: Extra-pleural pneumonectomy versus no extra-pleural pneumonectomy for patients with malignant pleural mesothelioma: clinical outcomes of the Mesothelioma and Radical Surgery (MARS) randomised feasibility study. *Lancet Oncol* **12**(8): 763-772, 2011.

15) Cao C, Tian D, Park J, *et al*: A systematic review and meta-analysis of surgical treatments for malignant pleural mesothelioma. *Lung Cancer* **83**(2): 240-245, 2014.

16) Rusch VW, Giroux D, Kennedy C, *et al*: Initial analysis of the international association for the study of lung cancer mesothelioma database. *J Thorac Oncol* **7**(11): 1631-1639, 2012.

17) Opitz I: Management of malignant pleural mesothelioma—The European experience. *J Thorac Dis* **6**(*Suppl* 2): S238-S252, 2014.

18) Vogelzang NJ, Rusthoven JJ, Symanowski J, *et al*: Phase Ⅲ study of pemetrexed in combination with cisplatin versus cisplatin alone in patients with malignant pleural mesothelioma. *J Clin Oncol* **21**(14): 2636-2644, 2003.

19) Zalcman G, Mazières J, Margery J, *et al*: Bevacizumab 15 mg/kg plus cisplatin-pemetrexed (CP) triplet versus CP doublet in malignant pleural mesothelioma (MPM): results of the IFCT-GFPC-0701 MAPS randomized phase 3 trial. *J Clin Oncol* **33**(15s): abstr 7500, 2015.

20) Hassan R, Kindler HL, Jahan T, *et al*: Phase Ⅱ clinical trial of amatuximab, a chimeric antimesothelin antibody with pemetrexed and cisplatin in advanced unresectable pleural mesothelioma. *Clin Cancer Res* **20**(23): 5927-5936, 2014.

21) 中野孝司，栗林康造: 胸膜中皮腫の治療．臨と研　**92**(7): 899-906, 2015.

22) Alley EW, Molife LR, Santoro A, *et al*: Pembrolizumab safe, with signs of clinical benefit, for patients with malignant pleural mesothelioma. AACR annual meeting in Philadelphia, 2015.

Presented by Medical*Online

厚生労働省
労災疾病臨床研究事業費補助金

悪性中皮腫に対するヒト化抗CD26抗体を基盤とする安全かつ有効な新規併用療法の確立

平成28年度　総括・分担研究報告書

平成29年3月31日発行

発行：研究代表者　森本　幾夫
〒113-8421　東京都文京区本郷2-1-1
順天堂大学大学院医学研究科　免疫病・がん先端治療学講座
TEL：03-3868-2310